Novel Tailor-Made Externally Triggerable Single-Molecular Switches for Molecular Electronics

Inaugural Dissertation

Zur

Erlangung der Würde eines Doktors der Philosophie

vorgelegt der

Philosophisch-Naturwissenschaftlichen Fakultät

der Universität Basel

von

Gero Dominik Harzmann

aus

Oldenburg (Oldb), Deutschland

Basel 2015

Genehmigt von der Philosophisch-Naturwissenschaftlichen Fakultät der Universität Basel auf Antrag von

Prof. Dr. Marcel Mayor
Prof. Dr. Oliver Wenger

Basel, den 17. Februar 2015

Prof. Dr. Jörg Schibler
Dekan

für Sophie, Lea und meine Eltern

Acknowledgements

First of all I would like to express my utmost gratitude to my supervisor Prof. Dr. Marcel Mayor. Marcel I deeply thank you for giving me the opportunity to work on such interesting and challenging projects, as well as for you constant support and guidance concerning the chemical aspects of this work, your openness for discussion and the freedom you gave me during my research. Furthermore, I want to thank you also for your support during the difficult times of my PhD. In summary it was simply a great pleasure to work in your group.

I further would like to thank Prof Dr. Dirk Kurth and Prof. Dr. Oliver Wenger for the co-examination of this PhD thesis, and Prof. Dr. Catherine Housecroft for chairing the oral exam.

In nanotechnology no progress is possible without the extensive collaboration between the various disciplines linked to this field. Therefore my special thanks go to all the collaborators with whom I closely cooperated during the last four years. First of all, I thank Prof. Dr. Herre van der Zant and especially his group member Riccardo Frisenda from the TU Delft for the fruitful collaboration and for performing the mechanically controllable break junction experiments of so many of the target compounds presented throughout this thesis. I further thank Herre and Riccardo for the numerous meetings and discussions we had during the last years. Secondly I would like to thank Prof. Dr. Richard Berndt and his group member Thomas Knaak from the Christian-Albrechts University Kiel for performing the STM experiments, discussed within this thesis and for the helpful discussions Thomas and I had throughout this time.

A special thanks goes to Dr. Sophie Harzmann, Dr. Michal Juríček, Dr. Pascal Hess, and Kevin Weiland for proofreading this thesis and to Michel Rickhaus for his valuable help providing the wonderful artworks displayed throughout this thesis as well as in the publications arising from this work.

Moreover, I would like to thank all present and former members of the Mayor group for the fruitful discussions, as well as for the fun we had on group retreats and outside of work. Herein, I owe a special thanks to all my former lab mates in the AC enclave of the Mayor group, namely, Dr. Nicolas Weibel, Dr. Elisabeth Kapatsina, Dr. Thomas Eaton, Dr. Marcel Müri, Dr. Kathiresan Murugavel, Dr. Loïc Le Pleux, Viktor Hoffmann, and Mario Lehmann for the nice working atmosphere in our labs over the years. I further thank Dr. Pascal Hess and Lukas Jundt for the funny times we had at so many conferences over the last years. Furthermore, I am especially obliged to Pascal Hess for the many days and nights we spent, sometimes discussing chemistry, but moreover for his friendship and for being my best man.

Furthermore, I would like to acknowledge Dr. Daniel Häussinger, Heiko Gsellinger and Kaspar Zimmermann for performing the more sophisticated NMR experiments presented during this work, Dr. Markus Neuburger for measuring numerous solid state structures, Dr. Heinz Nadig for performing extensive mass spectrometric analyses, and finally Werner Kirsch and Sylvie Mittelheisser for elemental analyses.

Additionally, I would like to thank the technical staff from the “Werkstatt Team”, namely, Alois Schäuble, Andreas Koller, Francis Cabrera, Markus Ast and Manuel Hermida, as well as Roy Lips from the “Materialausgabe” and the secretaries Brigitte Howald, Marina Mambelli and Beatrice Erismann. A special thanks goes to Markus Hauri for his help in so many ways, but also for the fun times we had visiting soccer games.

The Swiss National Science Foundation (NSF) and the National Center of Competence in Research for Nano-Scale Science (NCCR “Nano-Scale Science”) are acknowledged for financial support.

Furthermore, I am of course especially obliged to my parents and my brother for their constant support and love, without which I would not have been able to achieve the goals I achieved during my PhD and my whole life.

Last, but certainly not least, I would like to express my greatest possible thanks to the two most important persons in my life, my beautiful wife Sophie and my wonderful daughter Lea Zoey, the sunshine of both of our lives. Sophie, I thank you so much for your everlasting support, patience, and the love you gave me over the past 10 years.

Abstract

Molecular electronics marks a highly interdisciplinary scientific field, in which physicists, chemists, and biologist jointly investigate electronic phenomena on a molecular level. Herein, the foremost task of the chemist is the design and synthesis of novel, tailor-made model compounds bearing externally addressable or controllable functions, which are predominantly of electronic nature.

This present PhD thesis mainly focusses on the synthetic aspects towards innovative metalorganic coordination complexes, in particular those containing iron(II) species as the central metal ion. One of the very unique properties of iron(II) ions is their potential capability of switching their spin state between a low-spin and a high-spin form. It represents the general, overall target of this work to externally address and control these potential spin switching properties of the incorporated iron(II) centers and to, therefore, create molecular switching entities addressable on a single molecular level. On the pathway towards the ultimate miniaturization of electronic components such single molecular spin switching entities represent one of the inevitable key components.

Chapter 1 provides an introduction of the variety of scientific fields, which are of relevance to the work described within this thesis. Herein, at first the field of molecular electronics is introduced by addressing methods used to contact single molecules, important features of molecular charge transport, properties and important previous examples of single molecular switches, and finally by giving a sufficient background about the spin crossover phenomenon. Hereafter, syntheses and applications of terpyridines and their metal complexes are discussed, prior to giving a brief introduction about aryl-aryl bond formation reactions, representing a key task of the synthetic work described throughout this thesis. Finally, with regard to one of the main objectives of this work an introduction is given about azobenzenes and their incorporation into macrocyclic assemblies.

Chapter 2 plainly delivers a profound description of the main aims of this PhD work.

Chapter 3 describes the molecular design, synthesis, and physical investigation of a new class of electrically addressable, single molecular spin switches relying on the coordination sphere dependent spin state of hexa-coordinate iron(II) bis(terpyridine) complexes.

Chapter 4 describes molecular design, synthesis, and physical investigation of a mechanically addressable, single molecular spin switch once more relying on the coordination sphere dependent spin state of hexa-coordinate iron(II) bis(terpyridine) complexes.

Chapter 5 describes the conceptual design and synthesis towards optically addressable, molecular switching metalloazobenzenophanes, representing macrocycles including a photosensitive azobenzene moiety in the molecular backbone in addition to a potentially spin-switching iron(II) core ion.

Chapter 6 summarizes the present work and gives a brief outlook.

Chapter 7 provides experimental details as well as a full characterization of all the compounds described throughout this thesis.

Individual Projects

Voltage-Triggered Single Molecular Spin Switches

A variety of iron(II)-based electrically addressable single molecular spin switches was synthesized. The molecular design allots the incorporation of two different terpyridine ligands into these hexa-coordinate iron(II) target complexes. Herein, the first symmetric thiol-terminated ligand conduces to the complexes' immobilization into a molecular break junction and furthermore, guarantees electronic transport through the central metal ion, due to the tailor-made 4,4´´-disubstitution pattern at the terpyridine core. The second ligand exhibits electron-donating and electron-withdrawing substituents resulting in an intrinsic dipole moment due to an overall asymmetric electron distribution. The resulting electric addressability of the core ion's spin state could be shown for a variety of different target complexes by the according molecular conductance measurements and further validated by the investigation of a multitude of suitable reference compounds. These reference compounds can be distinguished between two classes, being either non-addressable by the applied electric fields, or being electrically addressable, but incapable of undergoing a spin crossover.

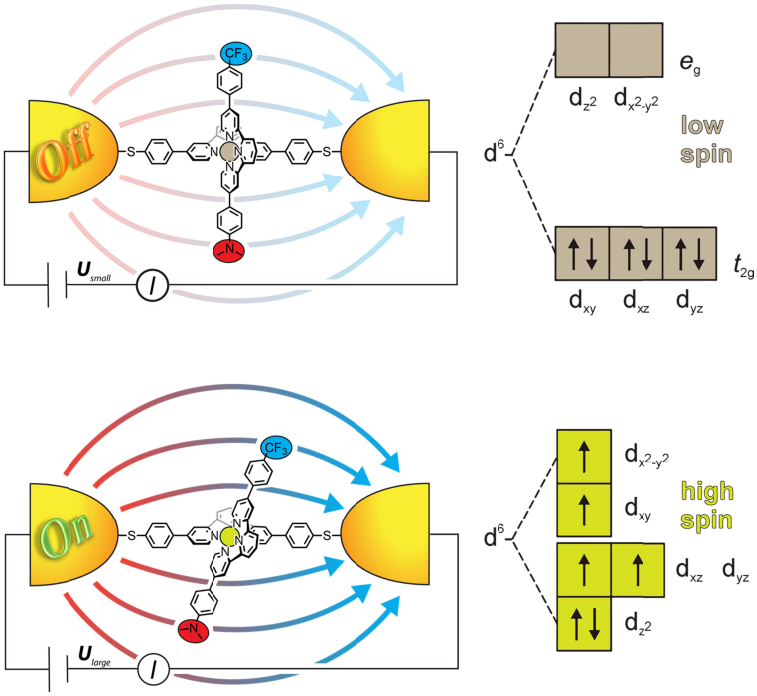

Furthermore, the bias-dependent spin crossover phenomena of related dipolar, homoleptic iron(II) bis(terpyridine) structures immobilized onto Au(111) surfaces have been investigated using scanning tunneling microscopy.

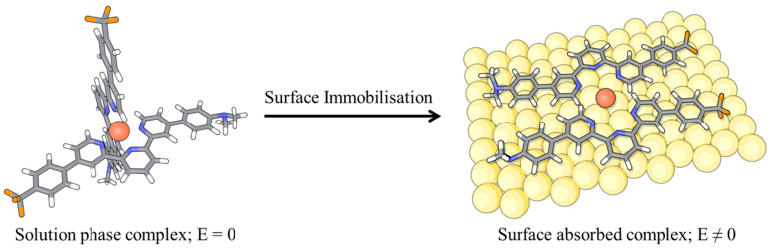

Mechanically Triggered Single Molecular Spin Switches

An iron(II)-based, mechanically addressable single molecular spin switch, based on the same terpyridine core moiety as the electrically addressable single molecular spin switches, was synthesized. Once the homoleptic target complex was immobilized into a molecular break junction, the geometrical distortion of the target structure, going along with the mechanical increase of the relative displacement of the nanoelectrodes, evokes a spin transition from the low-spin to the high-spin form at the coordination sphere dependent spin state of the hexa-coordinated iron(II) core ion. Apart from a clear distance-dependent bista-bility ($G_{final}/G_{start} \approx 10^2$ $G_{0)}$ observed for the iron(II) complex in the range of the performed conductance measurements, also the negative results observed for the Ru(II)-based reference compound, being incapable of undergoing any spin crossover, insistently underline the envisaged switching mechanism.

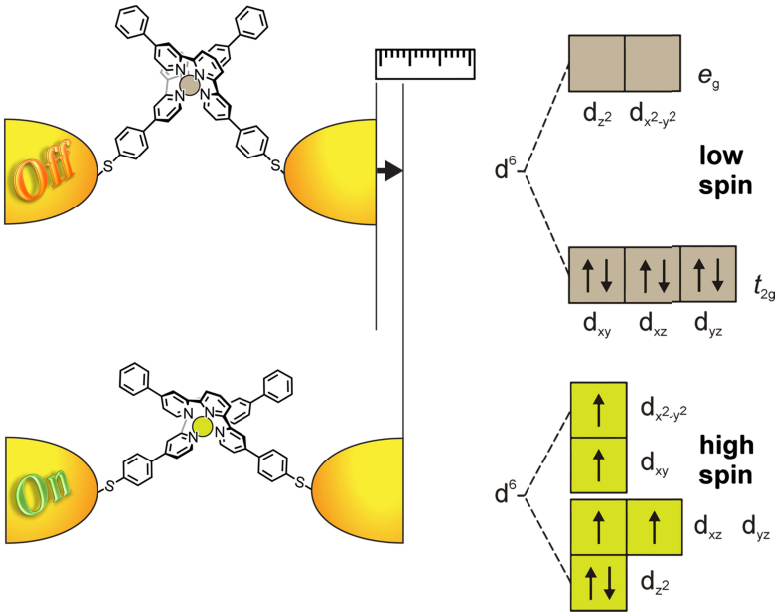

Light Switchable Iron-Terpyridine-Azobenzene Macrocycles

Three different metalloazobenzenophanes bearing optically addressable azo moieties incorporated into their molecular backbones and including potentially spin-switching iron(II) core ions have been synthesized in 9 to 15 steps, respectively. Although detailed optical and NMR-spectroscopic studies revealed the successful $(E) \rightarrow (Z)$ photoisomerization of the incorporated azo moieties, the actually envisaged switching of a coordination sphere dependent spin state of the incorporated hexa-coordinated iron(II) core ions was not observed for the investigated target structures so far. Nevertheless in the range of the project several paramagnetic iron(II) bis(terpyridine) high spin complexes have been assembled, underlining the general idea of the envisaged switching concept.

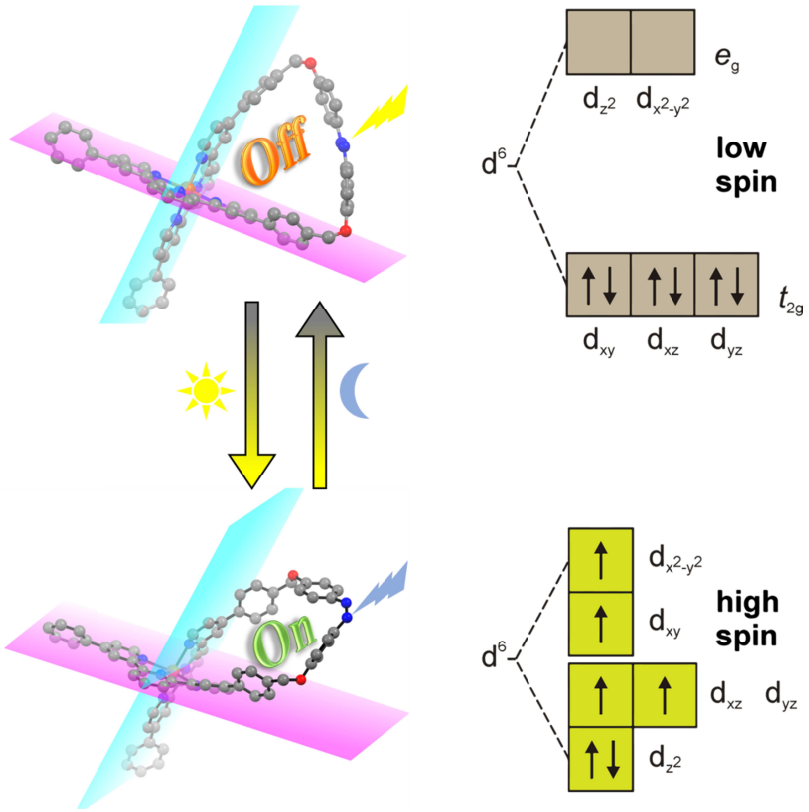

Table of Contents

List of Abbreviations

AcCl	Acetyl chloride
AFM	Atomic force microscopy
aq.	aqueous
BJ	Break junction
Boc	*tert*-butyloxycarbonyl
$(Bpin)_2$	bis(pinacolato)diboron
bpy	2,2′-bipyridine
BPDN-DT	Bipyridiyl-dinitro dithiol
BPDT	Bipyridyl dithiol
br	broad
Brine	Saturated aqueous NaCl solution
calcd.	calculated
CBPQT	Cyclobis-(paraquat-*p*-phenylene)
CMOS	Complementary metal-oxide-semiconductor
COSY	Correlated spectroscopy
C_q	Quaternary carbon
C_t	Tertiary carbon
d	doublet
dba	dibenzylideneacetone
DCM	dichloromethane
DEPT	Distorsionless enhancement by polarization transfer
DMF	Dimethylformamide
DMSO	dimethylsulfoxide
DNA	Deoxyribonucleic acid
DNP	1,5-Dioxynapthalene
dppb	1,4-Bis(diphenylphosphino)butane

dppf	1,1′-Bis(diphenylphosphino)ferrocene
dppp	1,3-Bis(diphenylphosphino)propane
DSSC	Dye-sensitized solar cell
EA	Elemental analysis
EDG	Electron-donating group
EI	Electron impact
Eq.	equivalents
ESI	Electron spray ionization
Et	ethyl
Et_2O	diethylether
EtOAc	Ethyl acetate
EtOH	ethanol
EWG	Electron-withdrawing group
FAB	Fast atom bombardment
FCC	Flash column chromatography
fcc	Face-centered cubic
FMO	Frontier molecular orbital
FWHM	Full width at half-maximum
GCMS	Gas chromatography - mass spectrometry
hcp	Hexagonal close packed
hept	heptet
HMBC	Heteronuclear multiple bond correlation
HMQC	Heteronuclear multiple quantum correlation
HOMO	Highest occupied molecular orbital
HOPG	Highly oriented pyrolytic graphite
HPLC	High-performance liquid chromatography
HR-ESI-MS	High-resolution electron spray ionization mass spectrometry
HS	High-spin

HSQC	Heteronuclear single quantum coherence
IPCE	Incident photon-to-current conversion efficiency
^{i}Pr	*iso*propyl
ITO	Indium tin oxide
LC	Ligand-centered
LD-LISC	Ligand-Driven-Light-Induced Spin Change
LEC	Light-emitting electrochemical cell
LIESST	Light-induced excited spin state trapping
LS	Low-spin
LUMO	Lowest occupied molecular orbital
m	multiplet
m/z	Mass per charge
MC	Metal-centered
MCBJ	Mechanically controllable break junction
Me	methyl
MeCN	Acetonitrile
MeOH	Methanol
MLCT	Metal-to-ligand charge transfer
MO	Molecular orbital
MS	Mass spectrometry
MTJ	Molecular transport junction
NBS	*N*-bromosuccinimide
n-BuLi	*n*-Butyllithium
NDC	Negative differential conductance
NLO	Non-linear optical
NMR	Nuclear magnetic resonance
OLED	Organic light-emitting diode
OPE	Oligophenyleneethynylene

OPV	Oligophenylenevinylene
ORTEP	Oak Ridge Thermal Ellipsoid Plot
OTf	Trifluoromethanesulfonate (triflate)
PG	Protecting group
Ph	phenyl
Phen	1,10-Phenanthroline
PLED	Polymeric light-emitting diode
Ppm	Parts per million
PSS	Photostationary state
q	quartet
QPC	Quantum point contact
r.t.	Room temperature
s	singlet
SAM	Self-assembled monolayer
SCO	Spin crossover
SEM	Scanning electron microscopy
SPM	Scanning probe microscopy
STM	Scanning tunneling microscopy
t	triplet
TBAF	Tetrabutylammonium fluoride
TBME	*tertiary* butyl methyl ether
^{t}Bu	*tertiary* butyl
TEM	Transmission electron microscopy
TFA	Trifluoroacetic acid
Tf_2O	trifluoromethanesulfonic anhydride
THF	tetrahydrofuran
TIPS	Tri*iso*propylsilyl
TLC	Thin layer chromatography

T_M	Melting point
TMS	Trimethylsilyl
ToF	Time of flight
tpy	2,2′:6′,2′′-terpyridine
TTF	Tetrathiafulvalene
UHV	Ultra high vacuum
UV/vis	Ultraviolet/visible spectroscopy
X-Phos	2-Dicyclohexylphosphino-2′,4′,6′-triisopropylbiphenyl
X-ray	X-ray spectroscopy

1 Introduction

The theoretical basis for this doctoral thesis is described in the following introductory chapter consisting of four subchapters: (1) Molecular Electronics, (2) Terpyridines, (3) Aryl-Aryl-Bond Formations – Pd(0)-Catalyzed Cross-Couplings, and (4) From Simple Azobenzenes to Switchable Metalloazobenzenophanes. These topics are directly related to the key objectives of this thesis to investigate (i) the development of a reproducible and high-yielding synthetic route to obtain the tailor-made suitably 4,4′′-disubstituted terpyridine structures required for the envisaged electronic functionalities of the target compounds of this work, (ii) the synthesis, electron transport and switching features of heteroleptic, electrical field-dependent, single molecular spin switching Fe(II)-bis(terpyridine) complexes, (iii) the synthesis and switching ability of a mechanically addressable single molecular spin switch based on homoleptic Fe(II)-bis(terpyridine) complexes, (iv) the syntheses and spin-crossover phenomena of homoleptic, dipolar Fe(II)-bis(terpyridine) complexes, and (v) the synthesis and optical and spin-switching properties of photoswitchable Fe(II)-based metalloazobenzenophanes upon external stimulation by UV light.

The interdisciplinarity of the scientific area covered in this thesis can be attributed to several fields of modern science. From the point-of-view of a chemist special focus was laid on the development of modular and efficient syntheses of the novel compounds described throughout this thesis, which was and still remains one of the biggest challenges for a synthetic chemist. Not only a high yield and excellent reproducibility are the key goals during the development of a new synthetic route, but nonetheless sustainability shows a high influence on the synthetic direction a modern organic chemist chooses. Therefore highest attention is set to the choice of readily available, environmentally passable starting materials and the realization of optimized atom economy and resource efficiency as well as on yield and reproducibility. Only the fulfilment of all of these criteria marks a novel methodology as truly successful and outstanding.

As a second superordinate scientific discipline this work can be attributed to materials science or more specifically molecular engineering. This area can be best characterized as an interdisciplinary research field in which molecular design, synthesis, and the manipulation of molecular assemblies or even single molecules are utilized for the creation of advanced functions. Generally the technical and scientific progress of mankind is based on two

principles. The first principle herein, can be named as the invention of new machines or techniques giving access to novel functionalities. The second principle can be seen in the optimization of existing technology in terms of production costs, life time, functional efficiency and size reduction. For example innovative developments within the field of electronic device fabrication permitted the miniaturization of millimeter transistors into micrometer-sized integrated circuits within the last half of the former century. It was this striving for advancement and perfection which exemplarily allowed the development of smaller, faster and much more advanced computer systems or other electronic devices of our daily life throughout the last fifty years.

1.1 Molecular Electronics

The aim of this introductory chapter is to explain the present limitations in the field of electronics and, consequently, to propose strategies for future improvements by the direction towards molecular electronics. For this purpose an overview of how properties of organic molecules can be studied with the help of nanometrological or break junction techniques is given. Furthermore, the molecules' immobilization onto metal surfaces and charge transport in molecules is explained, highlighting the most important characteristics of the Coulomb blockade and the Kondo effect phenomena, before selected examples of existing single molecular switches are discussed. Finally, a short introduction into spin crossover and *spintronics* is given before the current limitations in the field of molecular electronics are discussed.

Driven by the society's strive for technological advance, the ultimate goal of nanotechnology is to assemble and mimic key electronic components of all kinds, such as wires,[1,2] switches,[3] rectifiers,[4] transistors,[5,6] and complete memory devices[7,8] at the nanoscale. The so-called Moore's law describes the fact that computing power approximately doubles every two years going which was first described by Moore in 1965.[9] Currently this ongoing miniaturization trend of integrated circuits is still fulfilled following the top-down approach relying almost exclusively on silicon-based devices. These technologies are however facing some inherent limitations in the near future which will result in a dead end in the near future: for example limitations of the micropatterning techniques used for circuitry production on silicon wafers or the disappearance of the band structure for silicon layers with a thickness of only several atoms has to be named.[10] Another limitation is the so-called 14 nm resolution limit of silicon wafers due to quantum tunneling effects.[11] To circumvent this impending dead end for the ongoing miniaturization of integrated circuits[12] a change of the present manufacturing strategies seems inevitable. Possible alternatives could be the utilization of other metal-based materials like e.g. Ge, SiGe or GaAs,[13] or finally a total break in philosophy going along with the replacement of the current lithographic top-down approach by the fabrication of ordered nanoscale structures using the bottom-up approach based on the implementation of organic materials. It was Richard Feynman who, during his famous talk at *Caltec* back in 1959, was the first one to introduce the idea of the bottom-up approach by his famous statement: "There's plenty of room at the bottom."[14] This bottom-up

approach allows obtaining a molecular-based device consisting of single molecules or a well-defined assembly of single molecules featuring the desired electronic properties (Figure 1).

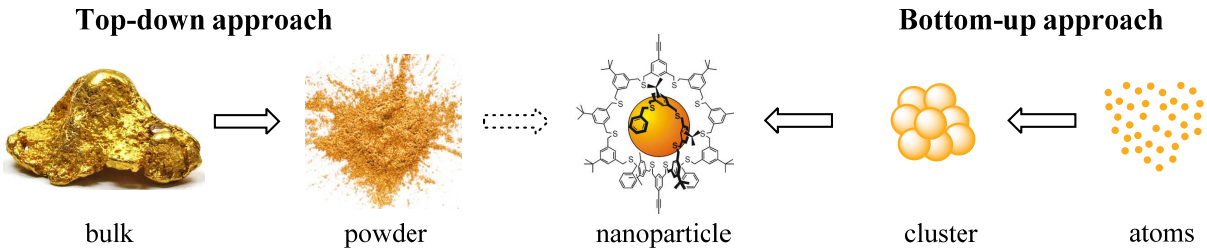

Figure 1: Comparative illustration of the top-down approach starting from bulk gold versus the bottom-up approach starting from gold atoms.

Though these ideas were visionary in 1959, some modern integrated circuits, for example, complementary metal-oxide-semiconductors (CMOS), are nowadays based on this very approach. With a size in the nanometer regime, π-conjugated molecules, with highly delocalized electrons and very small gaps between the highest occupied molecular orbital (HOMO) and the lowest unoccupied molecular orbital (LUMO) are especially attractive as components of molecular wires. Nevertheless the overall fabrication of molecular scale devices still faces ambitious challenges until the dream of equipping computers with truly "molecular" circuits actually comes into reach. Namely, it will be necessary to fully understand the electronic properties of single molecules, before one can actually tackle the design of a "multi-molecular" system. Over the last decades, a lot of knowledge has been added to the field, going along with the development of novel, revolutionary microscopy and nanometrological techniques enabling measurements on single molecules in solution as well as in solid state.[15–19] These revolutionary physical techniques, together with suitable anchoring groups for the first time render the researchers the possibility to actually address one of the smallest thinkable building blocks, namely, functional molecules, and to incorporate these into molecular junction setups (Figure 2).

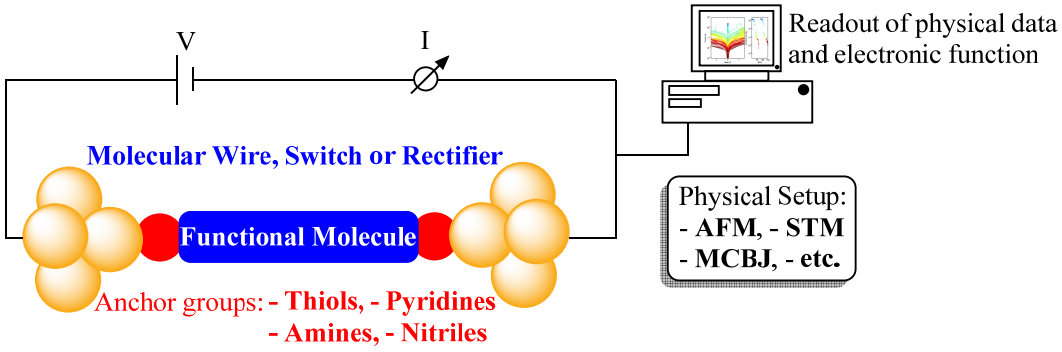

Figure 2: Schematic illustration of the exemplary setup of a molecular junction.

This interplay of innovations now allows researchers a systematic investigation of the structure-property correlation and the possibility to tune the specific electronic function of a tailor-made functional molecule, such as conduction, switching and rectification.

1.1.1 Contacting the Molecule

To introduce the field of molecular electronics, it is inevitable to first discuss the physical techniques which enable the integration of single molecules or even atoms into a circuit. Two main techniques, namely, scanning probe microscopy (SPM), and herein, especially scanning tunneling microscopy (STM) (Chapter 1.1.1.1), and break junction techniques, and herein, especially mechanically controllable break junctions (MCBJs) (Chapter 1.1.1.2), have proven to be extremely valuable in this field and are therefore discussed in the following two chapters.

1.1.1.1 Scanning Probe Techniques

The cornerstone of the SPM techniques was the development of the STM by Binnig and Rohrer[20] in 1981, which allowed researchers to study the surface structure on an atomic level for the first time. This discovery opened up new areas of engineering and science at the atomic and molecular levels and was consequentially awarded the Nobel Prize in Physics in 1986.[21,22] The common feature of all SPM techniques is the scanning of a surface with a probe while certain interactions between the surface and the probe are monitored. Specifically these interactions are:

(1) tunneling current between a metallic tip and a conducting substrate which are positioned in very close proximity to each other without being in actual physical contact (STM measurements),
(2) van der Waals forces between the tip of a cantilever and the substrate's surface (atomic force microscopy (AFM) measurements.

The latter interactions can be either long-range attractive forces (non-contact mode) or short-range repulsive forces (contact-mode). Other common features of both techniques are the requirements of:

(1) a highly accurate control over the positioning of the probe's tip with respect to the substrate's surface (in a range of less than 0.1 Å) by moving either the tip or the surface,
(2) a very sharp probe tip, ideally terminated by a single atom at the point closest to the substrate's surface.

To achieve the former requirement, a very good vibrational isolation of the microscope as well as highly sensitive piezoelectric positioning devices are required. For the latter one, a variety of different techniques have been developed, including etching, heating, and sputtering (e.g., for the metal tip of an STM-setup).[23]

For regular STM measurements, the corresponding substrate (an organic or inorganic molecule) must first be immobilized onto a conducting surface, which can be either a metallic surface (e.g., copper, gold, silver, or silicon), a transition metal dichalcogenide layer (e.g., MoS_2), or a graphene layer. Whereas for graphene or transition metal dichalcogenides it is sufficient to perform the measurements at ambient pressure, the use of a readily oxidizable metal probe requires the use of ultrahigh vacuum (UHV) conditions. After the deposition of the sample onto the surface, the conducting metal tip, usually consisting of W or Pt, is slowly approached to the surface. The tip subsequently scans the surface in close proximity to the substrate while a bias is applied between the tip and the surface to allow for a small exponentially distance-dependent tunneling current to arise (Figure 3a-e).

The quantum mechanical tunneling effect (the eponym of STM) is one of the two major principles of this technique. The other one is the piezoelectric effect, which allows for the very subtle heights adjustments required for the STM tip or the probed surface.[24,25] Due to their wave-like nature, the quantum mechanical tunneling permits electrons to pass through a potential barrier, which they could not surmount according to the laws of classical mechanics (particle-like nature). If the potential barrier is thin enough, the electrons are able to pass through this classically "forbidden" region and tunnel from one solid to the other (Figure 3f). The tunneling direction depends on the applied bias' direction (Figure 3d-e).

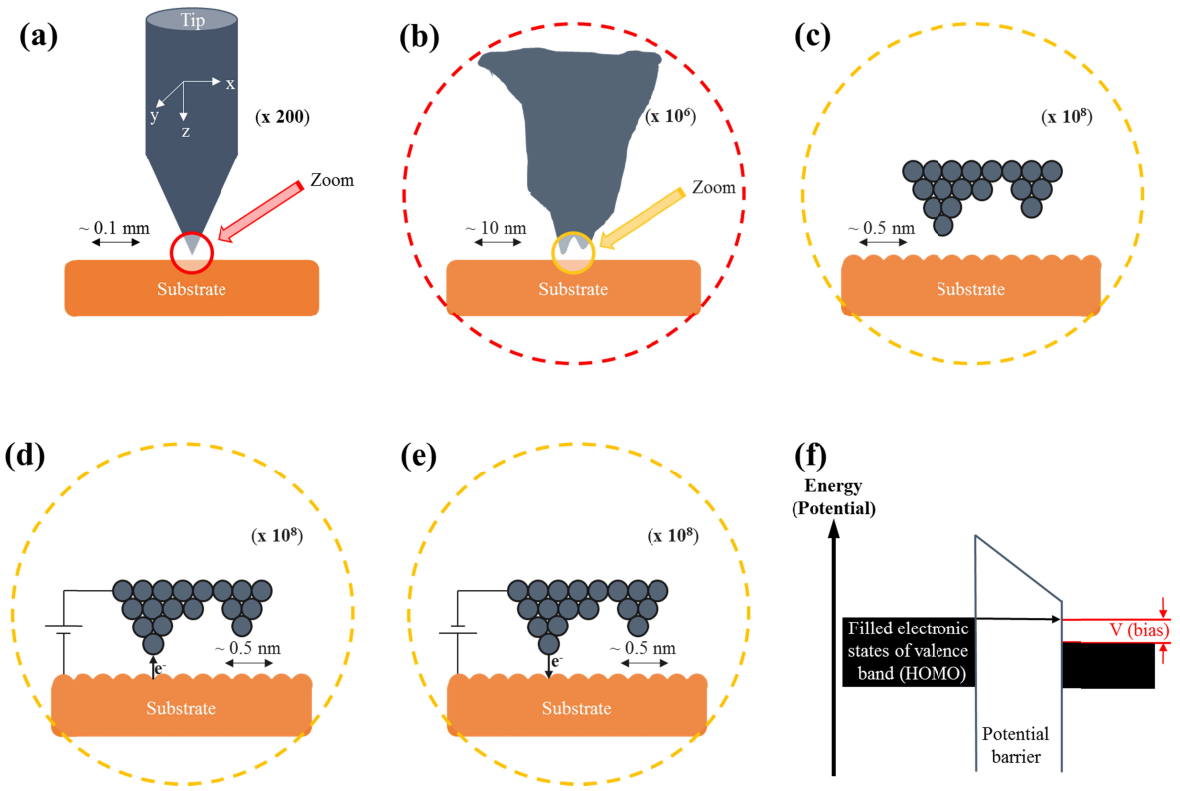

Figure 3: Schematic illustration of an STM setup: **(a)** General overview of the STM setup, **(b)** zoomed in region of the STM tip showing a variety of exposed crystal facets, **(c)** magnification down to the atomic scale showing the atomically sharp STM tip, **(d)** + **(e)** By biasing the STM tip with respect the surface a tunneling current arises whilst the bias polarity determines the electron's flow direction, **(f)** Schematic illustration of the principle of quantum mechanical tunneling.

The tunneling probability has been found to be exponentially dependent on the distance between the tip and the surface. As a consequence of the distance-dependence of the tunneling probability it is possible to perform the STM measurements using two modes (Figure 4):

(1) in constant-height mode (Figure 4a), the tunneling current is monitored as the tip moves parallel to the surface at a constant distance between the tip and the surface,

(2) in constant-current mode (Figure 4b), the distance between the tip and the surface is varied such that the tunneling current is maintained constant, with the help of a feedback loop, while the tip is moved across the substrate's surface.

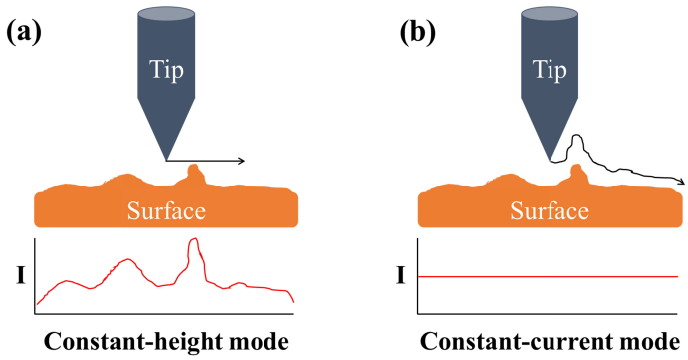

Figure 4: (a) STM operating in constant-height mode, and **(b)** STM operating in constant-current mode.

In constant-height mode, the current varies in response to the topographic or electronic surface characteristics, which requires a very smooth surface, and is a valuable tool for real-time monitoring of dynamic processes. In contrary, the constant-current mode is well suited for less smooth surfaces as the height is adjusted in order to maintain a constant current independent of the lateral tip position. In both cases a precise topographic image of the molecular surface of the substrate can be obtained.

AFM represents the second, high-resolution surface imaging SPM technique. As the advancement of the original STM developed by Binnig, the AFM was patented in 1988.[26] In the simplified AFM setup[27,28] (Figure 5a), the cantilever's tip, usually consisting of Si or Si_3N_4, has an average width of only a few nanometers (Figure 5b).

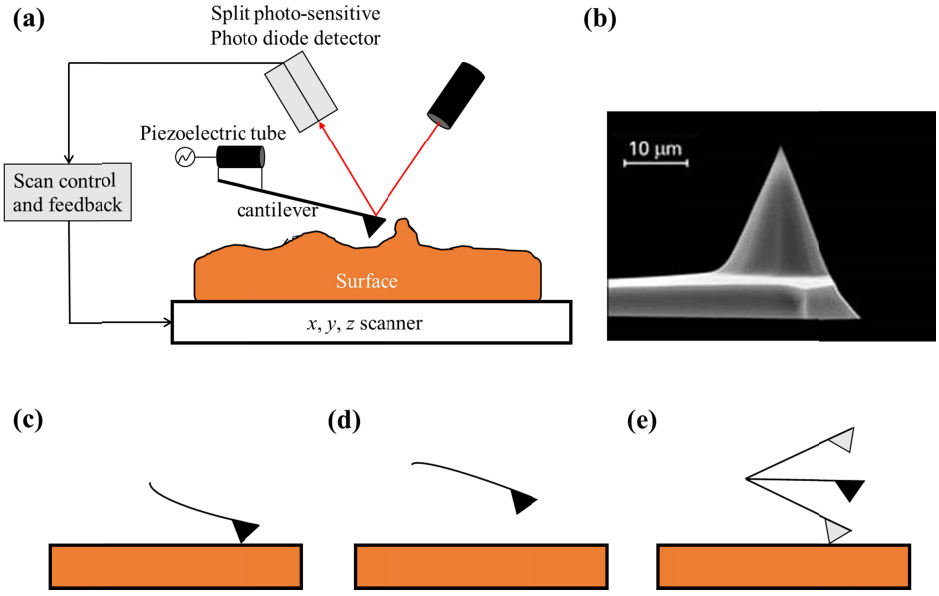

Figure 5: (a) Schematic illustration of an AFM setup, **(b)** magnification of an AFM cantilever tip, **(c)** schematic representation of a cantilever in AFM contact mode, **(d)** schematic representation of a cantilever in AFM non-contact mode, **(e)** schematic illustration of an oscillating cantilever in AFM tapping mode. Figure 5b is reprinted from the webpage indicated in the literature.[29]

In an AFM setup, the deflection of the cantilever due to interatomic forces (van der Waals forces or electrostatic interactions) between the tip and the substrate's surface is measured according to Hooke's law. For this purpose, the cantilever's back side is hit with a laser beam, which is reflected onto a split position-sensitive photodiode detector. The photodiode signals are transduced by a feedback loop to determine the cantilever's position relative to the laser as well as the angular deflection of the cantilever. There are three different imaging modes in an AFM set-up:

(1) the contact mode (Figure 5c) based on repulsive interactions between the tip and the surface,
(2) the non-contact mode (Figure 5d), based mainly on attractive interactions between the tip and the surface,
(3) the intermittent mode or tapping mode (Figure 5e) combining modes (1) and (2).

The contact mode consists of two different sub-modes, namely, the static constant-height mode, in which the cantilever scans the surface while remaining at a constant height, and the constant-force mode, in which the *z*-position of the cantilever is piezoelectrically controlled and adapted to maintain a constant force. Though the latter mode is less invasive than the former one, both contact modes usually cause strong damages to the surface, making this mode particularly useful for hard and very smooth surfaces. In the dynamic non-contact mode, the cantilever, which is oscillating due to external trigger, is scanning the surface at a short distance (5-10 nm). Interactive forces between the tip and the surface are observed due to a change in the resonance frequency of the oscillating circuit the cantilever is integrated into. Whereas the non-contact mode is usually used under UHV conditions, the tapping mode can also be used under ambient conditions. For the latter mode, a feedback loop is usually keeping the vibrational amplitude of the cantilever constant, by adapting the distance and thus the interactive forces between the cantilever tip and the surface.

1.1.1.2 Mechanically Controllable Break Junctions

The mechanically controllable break junction (MCBJ) represents another very important technique in molecular electronics, which is well suited for the investigating the properties of single molecules and the charge transfer (CT) processes through the molecules within such

molecular junctions. The development of the MCBJ is based on the seminal studies on electron tunneling phenomena within Sn-Nb break junctions (BJs) published by Moreland and Ekin,[30] to whom the discovery of BJs is attributed. The first MCBJ was reported by Muller and Ruitenbeek in the early 1990s.[31] The preparation of such MCBJ starts with the immobilization of a small metallic wire (usually a gold wire) onto a flexible substrate (usually polyimide). The metallic wire is usually fabricated either by electron beam lithography to create a constriction in the wire, or by physically cutting a notch into a macroscopic wire (Figure 6b). In this set-up (Figure 6a), which consists of a pushrod and two counter supports to bend or relax the substrate and the attached wire, it is possible to create two atomic-scale nanoelectrodes directly facing each other. This small nano-gap can be reversibly closed and re-opened by varying the pushrod's *z*-axial displacement.[32] This closing and re-opening of molecular junctions, at least at room temperature, is inevitable since the average life-time of such junctions is only a few minutes. Figure 6c presents a schematic illustration of the stepwise process of the BJ formation.

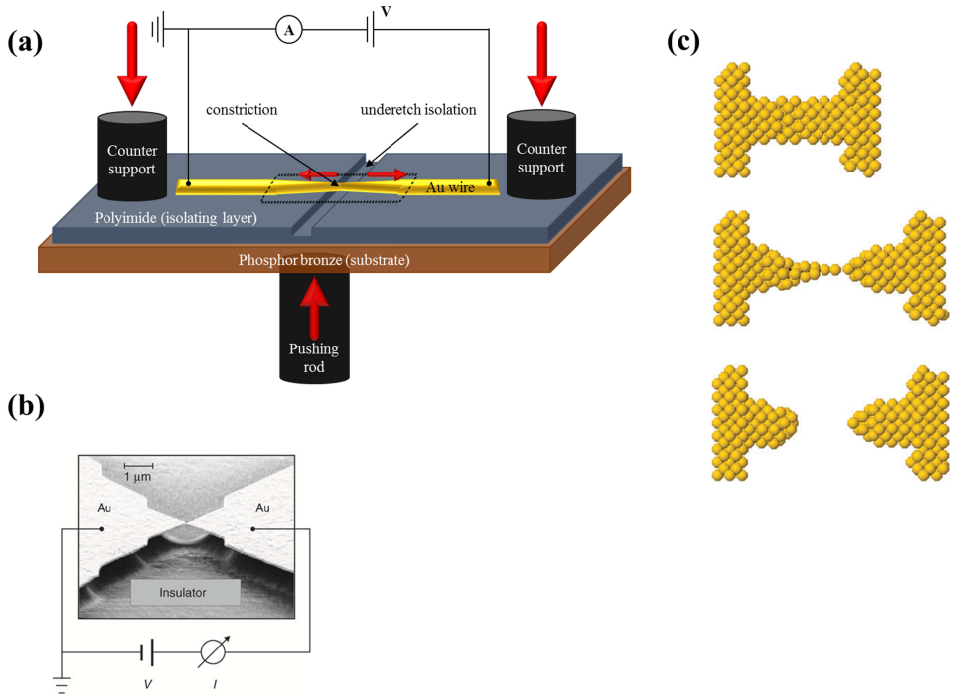

Figure 6: Schematic illustration of an MCBJ setup: **(a)** macroscopic scaled view of an entire typical MCBJ setup, **(b)** scanning electron microscope (SEM) image of an MCBJ fabricated by electron-beam lithography, and **(c)** illustration of the stepwise elongation and eventual breaking process of a gold wire at atomic scale during the formation of an MCBJ. Figure 6b is reprinted from Lörtscher *et al.*[33] and Figure 6c is reprinted with permission from Turanský *et al.*[34]

The ultimate goal of MCBJ measurements is to measure the conductivity of a single molecule. To achieve that, it has to be immobilized inside the junction such that each end is connected to one of the two opposing nanoelectrodes, thus bridging the MCBJ. The MCBJ

measurements are highly sensitive and the obtained breaking traces can differ significantly. Therefore, it is essential to perform hundreds of measurements on one single type of molecule, to allow for a statistical result. The results are usually plotted in logarithmic histograms showing the conductance G of the respective molecule as a peak or as a log$G$(z) trace (Figure 7b). Figure 7d exhibits three different (G/G_0) versus z traces in which the observed plateaus correspond to the conductance measured for the respective molecule bridging the MCBJ. By measuring the conductance of a single molecule within an MCBJ, the conductance G can no longer be described using Ohm's law (Equation 1), which is only valid on the macroscopic scale.

$$G = \frac{I}{V}$$

Equation 1: Ohm's law: G is the conductance, I is the current, and V represents the applied potential.

Instead, the electrical conductance on the level of a quantum conductor G_0 can be derived from the Landauer formula (Equation 2).[35,36]

$$G = G_0 * T$$

Equation 2: Landauer formula: G is the conductance, G_0 is the quantum of conductance, and T is the transmission.

In this context, for a single conducting gold atom the transmission $T = 1$, corresponding to the availability of a single channel for the charge transport. Thus the conductance G of a single gold atom, per definition, equals to the quantum of conductance of 1 G_0 (Equation 3).

$$G_0 = \frac{2e^2}{h} = 77.5\,\mu S$$

Equation 3: Definition of the quantum of conductance G_0, where e is the electron charge, and h represents the Planck constant.

In this context the limited conductance of a single gold atom is defined to $G = 1\ G_0$. At the beginning of the bending process, during the BJ formation (Figure 7a, **1**), the measured conductance G still exceeds G_0 ($G > G_0$) since the wire still has a thickness of several atoms. However, at the breaking point (Figure 7a, **2**), having a single atom in the "bridge", the resulting conductance G is equal to G_0 ($G = G_0$). This phenomenon has been first observed in 1988 independently by Wharam[37] and van Wees[38] and is usually referred to as quantum point contact (QPC). If the electrodes are pulled apart further (Figure 7a, **3** and **4**) the conductance G drops below G_0 ($G < G_0$) and if no molecule is captured inside the junction, an

exponential decay of the conductance can be observed (Figure 7c). In contrast, if a molecule is bridging the junction, a conductance plateau is observed as illustrated in Figure 7d.

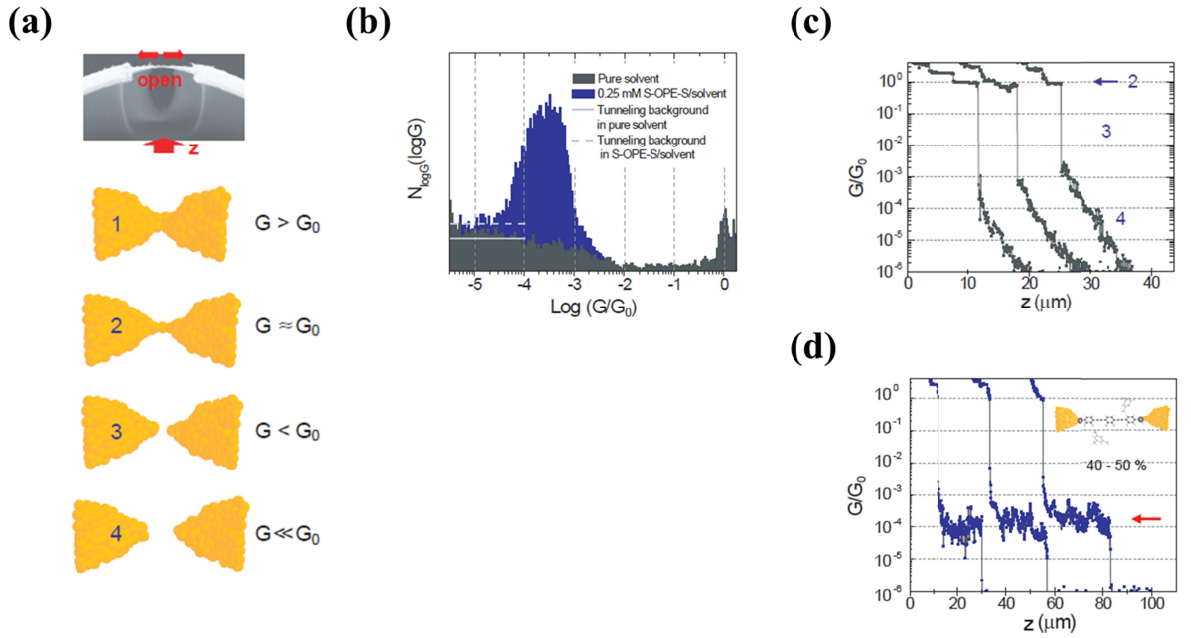

Figure 7: (a) Illustrative step-by-step overview over the different stages during the formation of an MCBJ, **(b)** a logarithmic conductance histogram contrasting tunneling background versus an MCBJ with incorporated molecule showing a clear peak at around $G = 10^{-4}\ G_0$, **(c)** three typical conduction traces of opening MCBJ junctions in pure solvent displaying the different events illustrated in figure 7a, and **(d)** three log$G(z)$ curves of occupied MCBJs exhibiting clearly visible conductance plateaus at around $G = 10^{-4}\ G_0$. All pictures are reprinted from Wu.[39]

At a certain point of elongation the BJ eventually breaks as well, resulting in a decrease of the conductance to zero. Hence, every conducting organic molecule, which can be inserted into such an MCBJ, shows a conductance smaller than G_0, but bigger than the observed tunneling current within an empty MCBJ. The advantages of MCBJ are: (1) the stability of the system towards mechanical vibrations, and (2) the formation of a "fresh" junction for each molecule and the statistical acquirement of data usually consisting of hundreds of measurements, minimizes the risk of data misinterpretation. There are, however, also certain drawbacks of the technique, namely: (1) the exact shape of the nanoelectrodes remains unknown due to the nature of the breaking process, (2) the technique is so far only suitable for laboratory scale experiments and not for larger productions, and (3) the implementation of MCBJ experiments into a three-electrode setup remains a big challenge.

1.1.2 Charge Transport in and Immobilization of Organic Molecules

Obeying the Ohm's law (Equation 1), the electrons within macroscopic molecular wires travel by diffusive transport. Hence, the conductance G is inversely proportional (Equation 4) to the length L of the conductor and directly proportional to the transverse area A of the wire.

$$G = \frac{\sigma A}{L}$$

Equation 4: Conductance G of a macroscopic molecular wire: G is the conductance, σ is the conductivity, A is the transverse area, and L represents the length of the conductor.

If the length L of the conductor becomes smaller than the elastic mean free path l, which represents the average distance "travelled" by an electron between two scattering events, then the electron transport mechanism changes from diffusive to ballistic transport (Figure 8). Herein, the electron's momentum is assumed to be constant and only limited by scattering with the sample's boundaries. For molecular wires, the Landauer formula describes this transmission process in the quantum regime and results in a maximum conductance of $G_0 = 77.5\ \mu S$.

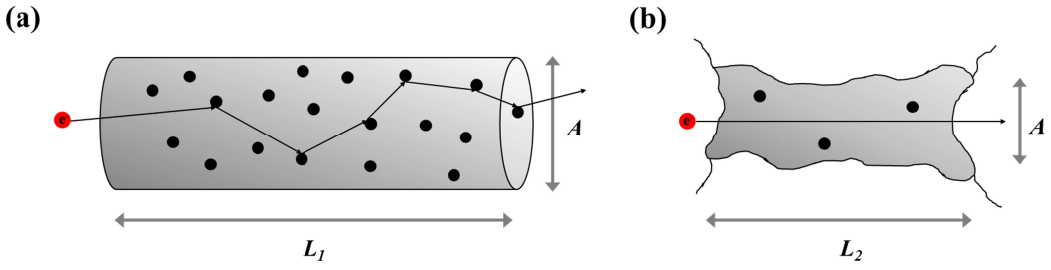

Figure 8: Illustrative comparison between: **(a)** diffusive electron transport through a macroscopic wire; and **(b)** ballistic electron transport through a molecular wire linking two nanoelectrodes. ($L_1 >> L_2$)

To be able to conduct STM and MCBJ measurements, the immobilization of organic molecules represents an essential part, which can be achieved by incorporation of suitable anchoring groups in the molecules of interest. Acting as a "molecular alligator clip", an anchoring group should exhibit a strong binding affinity to the noble-metal surface as well as a negligible charge-injection barrier.[40,41] The latter requirement represents the energy difference between the transport level (LUMO or HOMO) of the respective anchoring group and the Fermi level of the metal electrode, and is required to be as low as possible to facilitate the hole transport. According to the level alignment of the molecular frontier orbitals with the

electrode Fermi energy either hole or electron transport can take place inside the molecular junction. Furthermore, a strong coupling between the electrode and molecule is required for large overlap integrals between the frontier orbitals of the bridging molecule and the Fermi level of the metal electrodes.[42] The fulfillment of this requirement allows for an efficient electron transport from one electrode to the other in a one-step coherent process without the electron being trapped on the bridging molecule (Figure 9c). In contrast, in a low-coupling regime there is only little overlap of the molecule's wavefunctions with the electrode's electronic states (Figure 9a). Consequentially, in a two-step process electrons first have to "hop" from the electrode to the molecule, which requires energy levels to match, and then "hop" onto the opposing electrode. Without matching electron levels, or at low temperatures, the electron transport through the molecule is blocked, resulting in a phenomenon described as the Coulomb blockade (Chapter 1.1.2.1). Another case is the regime of intermediate coupling (Figure 9b). In this case, the electrons within a molecule can affect the electrons transferred from the electrode. For example, the spin-state of an unpaired electron within the molecule can be flipped by an electron trespassing from the electrode resulting in spin screening. Thus, new transport channels can be opened up resulting in zero-bias Kondo resonances (Chapter 1.1.2.2) taking place below a certain temperature (Kondo temperature T_K). Furthermore, a co-tunneling process can occur, during which one electron tunnels into the LUMO of the bridging molecule and, simultaneously, a second electron tunnels out of the molecule's HOMO onto the electrode, leaving the molecule in an excited state.

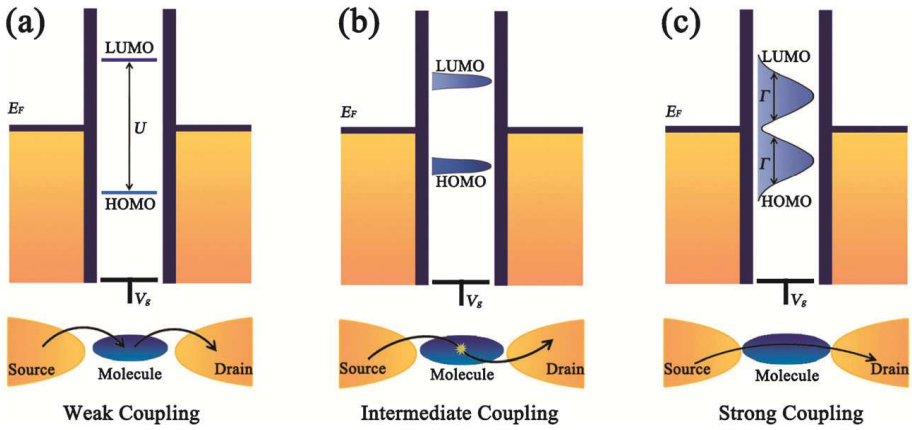

Figure 9: Schematic illustration presenting an overview of different coupling strengths between electrodes and molecules inside molecular transport junctions (MTJs) with the corresponding energy levels and charge transport processes. **(a)** Weak coupling regime exhibiting a two-step electron transport process and well-defined HOMO and LUMO on the molecule. **(b)** Intermediate coupling regime with slightly broadened HOMO and LUMO levels increasingly approaching the electrodes' Fermi energy E_F. Transferred electrons might interact with the (unpaired) electrons on the bridging molecules. **(c)** Strong coupling regime with largely broadened HOMO and LUMO levels enabling and a one-step electron transport process. Picture is reprinted with permission from Jia *et al.*[40]

So far, a broad variety of different anchoring groups, such as thiols,[43–45] pyridines,[46–49] phosphines,[50–52] amines ,[44,50,52,53] nitriles,[54,55] nitro,[55] isocyanides,[56] isothiocyanates,[57] selenium,[42,58–60] carbamates,[61] carboxylic acids,[44,62] fullerenes,[63,64] and in situ cleavable trimethylstannanes,[65] has been investigated for their use in molecular electronic devices. All of these groups exhibit the required strong binding affinities towards noble metals, such as silver, copper, and gold, together with low charge-injection barriers. Thiols herein, represent the first and still the most widely used anchoring group used in MCBJ experiments.[66] The appearance of broadened or even multiple conductance traces,[67] as well as the ease of undesired oxidative disulfide formation of the bifunctional bridging ligands, are, however, disadvantageous in the use of thiols as anchoring groups for the described experiments. It was shown that selenium would represent a more suitable anchoring moiety than thiols due to a lower density of states (0.9 eV vs. 1.2 eV) and consequently, also a lower injection barrier.[42] However, the toxicity of selenium compounds limits their applications. In contrast to the covalent sulfur-gold bindings, a non-covalent binding results in a dramatically lowered density of states (0.5 eV vs. 1.2 eV).[8] Although there are some examples of methylsulfides as anchoring groups,[50,52] generally the covalent binding mode between sulfur and gold still dominates in charge-transport experiments. In a recent study Wandlowski and co-workers investigated 4,4′-disubstituted oligophenyleneethynylene (OPE) derivatives bearing different anchoring groups, namely, thiols (-SH), pyridyls (-PY), amines ($-NH_2$) and cyanides (-CN)), with regard to their capability to bind to gold electrodes (MCBJ and STM-BJ measurements). It was found that stability and junction formation probability decreases in the following order: -PY > -SH > $-NH_2$ > -CN. The hole transport via the HOMO dominates the charge transport in -SH/$-NH_2$-bound molecular junctions due to the HOMO's proximity to the metals' Fermi level.[68–70] It is expected, however, that charge transport in -PY/-CN-bound molecular junctions dominantly takes place via the LUMO.[54,71] additionally, it was found that the conductances of -SH-, $-NH_2$-, and carboxylic acid (-COOH)- terminated molecules shows the following order: -SH > $-NH_2$ > -COOH, which was attributed to the different electronic coupling efficiencies between electrode and molecules.[44] furthermore, it was found that various other factors can have influence on the molecule's conductance, such as:

(a) the substitution pattern (*ortho*, *meta*, or *para*) of an aromatic molecule,[72]
(b) the molecule's conjugation (e.g., oligophenylenevinylene (OPV)[73] vs. OPE),[74]
(c) the length of the bridging molecule integrated into the junction,[44,73]
(d) the torsion angle (e.g., in biphenyl systems).[18,54,75]

Finally, it remains to state that the thiol anchoring group still is the most widely used and also the most suitable “alligator clip” to covalently immobilize organic molecules into molecular charge transfer junctions.

1.1.2.1 Coulomb Blockade

The concept of a Coulomb blockade describes a phenomenon, which can occur in molecular charge-transport junctions. The presence of an injected electron on the bridging molecule prevents other electrons from moving onto the molecule. Hence the current flow through the molecule within these electrode-molecule-electrode junctions is blocked, unless the source-drain voltage (two-terminal devices) or the gate voltage (three-terminal devices) is high enough.[7] This phenomenon can only be observed in the regimes of weak or intermediate coupling between the molecules’ wavefunctions and the electronic states of the electrodes (Figure 9a and b).[40] For an accurate definition of the coupling strength, which can be physically depicted as an energy barrier between the electrodes and the bridging molecule, two different parameters are of importance, namely:

(a) the coupling parameter Γ,
(b) the addition energy $U_{Add.}$

The coupling parameter Γ represents the broadening of the energy levels within the molecule, being relatively small for a case of weak electrode-molecule coupling. The addition energy U_{Add} describes the difference between the energy required to extract one electron from the HOMO of the system (U^{N-1}-U^{N}) and the energy gained by adding one electron to the LUMO of the system (U^{N}-U^{N+1}). Combination of these equations gives Equation 5:

$$U_{Add} = U^{N+1} + U^{N-1} - 2U^{N}$$

Equation 5: Description of the addition energy U_{Add} representing the difference between the energy needed for electron extraction from HOMO and the energy gained from electron insertion into the LUMO, where U^{N} represents the total energy of a system with N electrons.

As illustrated in Figure 9a and b in the weak- or in the intermediate-coupling regime we find $\Gamma << U_{Add}$, whereas in the strong-coupling regime (Figure 9c) the relation $\Gamma >> U_{Add}$ applies. Since the intermediate-coupling regime, apart from Coulomb blockade also shows several other possible features, such as Kondo resonances (Chapter 1.1.2.2), here the focus is set to the weak-coupling regime. Figure 10a illustrates the charge-transport mechanism for

classical quantum mechanical tunneling during which no free electronic states on the bridging molecule are applicable for a charge injection from the electrode. In the case of a good alignment between the involved molecular orbitals (MO) of the molecule's anchoring group (either HOMO or LUMO) and the electrode's Fermi level E_F, the charge to be injected can occupy some states of the relevant MOs due to a hybridization of the concerned orbitals leading to a good electrical coupling. In this scenario, the conductivity will be determined by the electronic coupling of the various sites of the molecular backbone of the bridging molecule. Therefore, the various sites of the molecular backbone take the role of a bottleneck concerning the charge transport through the junction. While for a good intramolecular coupling the bridging molecule would simply act as a wire, in the case of a weaker intramolecular coupling an activated hopping process (Figure 10b) of the electrodes would dominate over the transport mechanism.[76,77] There are two main possibilities to induce such a hopping mechanism, namely:

(a) the thermal activation of the activated transport,
(b) an increase in bias-voltage ideally leading to a level-alignment of E_F and the frontier molecular orbitals (FMO) of the immobilized molecule.[44]

In the case of a weak coupling of the anchoring group to the metallic electrode, with suitably accessible electronic states within the molecular backbone, the whole molecular junction can act as a capacitor (one plate represented by the molecule vs. one plate represented by the electrode) (Figure 10c). As a consequence of the inverse proportionality between the energy E_C required to charge a capacitor with a charge q and the resulting capacitance C (Equation 6), a reduction of the capacitor's size, and thus a reduction of C, results in an increased E_C.[77]

$$E_C = \frac{q^2}{2C}$$

Equation 6: Expression for the charging energy E_C of a capacitor, where q is the charge and C represents the capacitance of the capacitor

The thermal energy required to charge such an almost ultimately small capacitor, even if with only one electron, exceeds the energy available in such a system. The current flow through the bridging molecule is thus blocked due to electrostatic repulsion, which defines the phenomenon of a Coulomb blockade. To overcome this Coulomb blockade, the system needs additional energy to allow for an unhindered charge transport through the bridging molecule.

With the thermal energy being insufficient, the bias-voltage has to be elevated until the charging energy of the molecular capacitor can be overcompensated (Figure 10d).

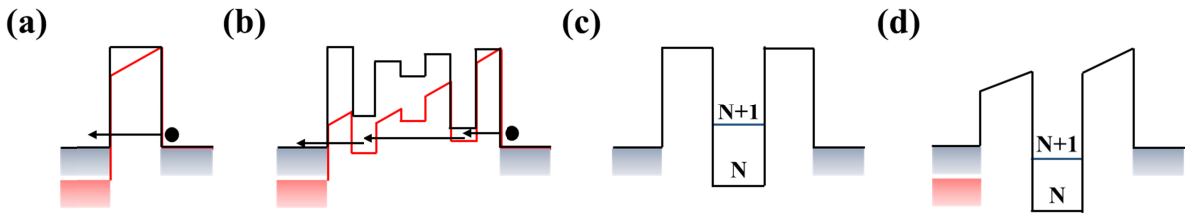

Figure 10: Schematic illustration of different charge transport mechanisms in molecular transport junctions. The blue boxes correspond to the Fermi level of the electrodes, the black lines represent the unperturbed electronic energy levels of the bridging molecule, and the red lines display the energy levels under an applied bias voltage. **(a)** Charge transport for quantum mechanical tunneling, **(b)** charge transfer during an activated hopping process through a bridging molecule with several sites, **(c)** Coulomb blockade in which electrode and molecule act as a capacitor. Upon charging the capacitor the energy level can be raised from *N* to *N+1*. **(d)** By the application of a bias voltage the charges can flow due to abatement of the energy levels.

Figure 11a and b illustrate two typical *I-V*-characteristics for a system exhibiting a Coulomb blockade (Figure 11a) versus a system featuring activated transport (Figure 11b). Whereas for the Coulomb blockade a broad low bias regime of blocked current flow can be observed, systems with an activated transport usually exhibit rather S-shaped *I-V*-curves.

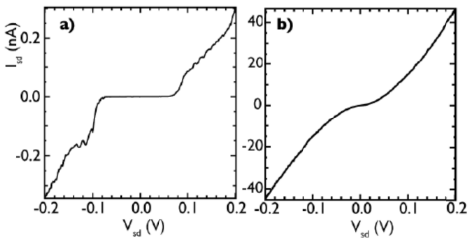

Figure 11: Typical *I-V* characteristics of polythiophene molecules measured at 4.5 K. **(a)** A system showing a Coulomb blockade, and **(b)** a system featuring activated hopping transport. Picture is reprinted from Erbe *et al*.[77]

1.1.2.2 Kondo Effect

In the context of molecular transport junctions, the Kondo effect is described as the formation of a bound state (or a spin-singlet state) between a localized unpaired electron on the bridging molecule (usually a transition-metal complex) and the conducting electrons from the electrodes (delocalized Fermi sea). The result is a highly temperature-dependent enhancement of conductance at low biases (zero-bias conductance anomaly).[16,78] As

explained in chapter 1.1.2 and illustrated in Figure 9b, such a coupling of unpaired spins can only occur in the intermediate coupling regime of transport junctions and below a certain temperature barrier, the so-called Kondo temperature (T_K). Originally, the Kondo theory explains an increasing resistivity of a metal with magnetic impurities at low temperatures.[79] As a next step in 1988, predictions were made that quantum dots could exhibit the Kondo effect leading to an increased conductance G eventually reaching the unitary limit ($G = 2e^2/h$).[80,81] Though the presence of the Kondo effect was confirmed in the following, it was only in 2000 when van der Wiel *et al.* demonstrated the achievement of a unitary-limit Kondo effect in a semiconductor quantum dot.[78] To observe Kondo resonances in organic molecules[16,82–86] within charge-transport experiments, it turned out to be of imminent importance that the molecular bridge possesses an electronic state with an overall non-zero net spin S, giving the bridging molecule or complex a magnetic moment.[76] Hence in this context, such systems are often named single-electron devices.[83,86] In 2007, Parks *et al.* succeeded in tuning the Kondo effect they observed during measurements on C_{60}-molecules investigated vian MCBJ.[87] In physical terms the Kondo effect describes an elastic co-tunneling process. Considering only the simplest case of odd-spin occupancy within the molecule represented by a single unpaired electron and a net spin of $S = ½$, the conduction mechanism involves spin-flip events, such as the ones illustrated in Figure 12.

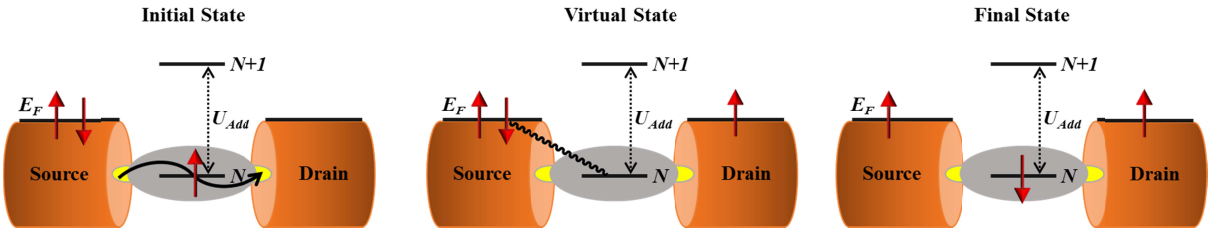

Figure 12: Schematic illustration of the spin-flip co-tunneling associated with the Kondo-effect in a molecular transport junction. A spin-up electron jumps out of the molecular backbone onto the Fermi level E_F of the drain electrode (virtual state) to be immediately replaced by a spin-down electron injected from the source electrode (final state).

A typical differential conductance spectrum (Figure 13a) illustrates the zero-bias Kondo resonance in form of a dI/dV_{SD} versus V_{SD} plot. It has been shown that for $T << T_K$, the full width at half-maximum (FWHM) of a Kondo resonance peak is in the order of $k_B T_K$, where k_B represents the Boltzmann constant. The corresponding temperature dependence of the Kondo-peak height at zero-bias is shown in Figure 13b. Below T_K, the conductance increases logarithmically with decreasing temperature, until it ultimately saturates at the value of the unitary limit of $G = 2e^2/h$.[78] Whereas for semiconductor quantum dots the typical Kondo temperatures are usually around $T_K \sim 1$ K,[88] for carbon nanotubes typical Kondo

temperatures lie around T_K ~ 1-10 K,[89,90] and for molecular devices they are usually in the range between T_K ~ 20-50 K.[16,82,83,91]

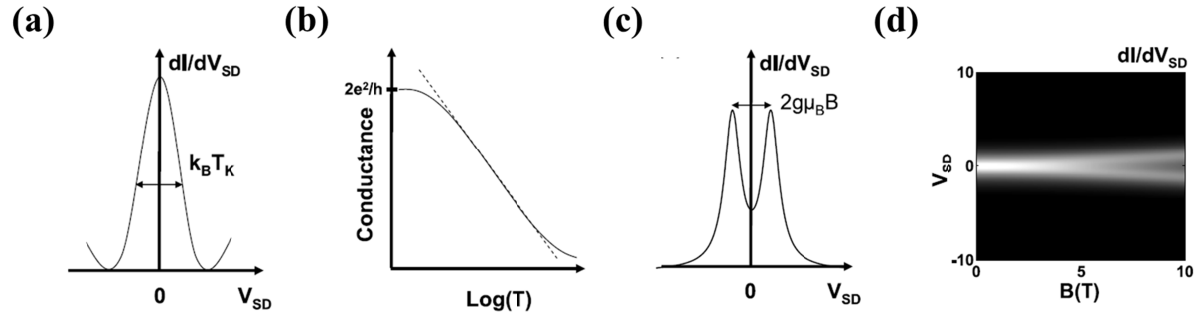

Figure 13: Typical features observed for a Kondo resonance in a molecular transport junction: **(a)** exemplary differential conductance spectrum illustrating the correlation FMHM ~ k_BT_K in the low temperature limit $T<<T_K$, **(b)** temperature dependence of the Kondo-peak height at zero-bias, **(c)** Zeeman splitting as the characteristic effect observed when a Kondo resonance is influenced by an applied magnetic field. The two observed Kondo peaks are split by twice the Zeeman energy ($2g\mu_BB$), **(d)** Illustration of the evolution of the Zeeman splitting of a Kondo resonance with the magnetic field strength B shown in plot of the differential conductance dI/dV_{SD} versus V_{SD} and B. All pictures reprinted from Osorio *et al.*[86]

If furthermore, a magnetic field is applied to the molecular transport junction, a Zeeman splitting occurs, leading to the observation of two Kondo peaks separated by twice the Zeeman energy (Figure 13c) and located symmetrically in bias. A representative dependence of the width of the Kondo resonance splitting on the strength of the applied magnetic field is illustrated in Figure 13d.

1.1.3 Single-Molecule Switches

Electronic gateways and switches are among the most important components of electronic devices. Hence, the development of molecular switches represents an essential step of making nano-circuits. The key intrinsic property of a switch is its existence in two (or even more) states, usually an ON- and an OFF-state. The reversibility of the switching process, herein, strongly depends on the ON → OFF and the respective OFF → ON interconversion barriers. Usually a switch responds to two different stimuli, one for the ON → OFF switching, and one for the OFF → ON switching process. Furthermore, a preferably high interconversion barrier between the two states can, usually, prevent an undesired back-switching (e.g., due to thermal back-conversion), which would be equivalent to a loss of the stored information. As for single molecular junctions the inspected output signal is usually represented by the

measured conductance, the two different conductance levels, corresponding to the ON- and the OFF-state, therefore, must be addressable by an external stimulus, such as temperature, pressure, light, pH, biological impulse, electricity, mechanical force, or a chemical reaction. This external stimulation needs to trigger some distinct changes[92] within the molecule bridging the junction, leading to a substantial change of the molecule's FMOs (HOMO-LUMO gap) in respect to the electrode's Fermi level E_F. There are three main types of externally triggered alterations to the molecules, namely:

(a) conformational changes (e.g., the torsion-angle-restricted rotations between neighboring phenyl subunits in poly(*p*-phenylenes) or biphenyl systems),[18,93,94]
(b) configurational and structural changes usually related to bond forming and breaking reactions (e.g., switching between an open and a closed form of dithienylethylenes upon irradiation with light),[95–99] or to photoisomerization reactions (e.g., switching between *cis*- and *trans*-state of the *N*=*N*-double bond in azobenzenes),[100–102]
(c) changes induced either by red-/ox-processes (e.g., for bipyridinium derivatives (*viologens*),[103–106] tetrathiafulvalene (TTF) derivatives,[106–108] and modifications of the (anthra)quinone/hydro(anthra)quinone pairs),[109,110] or by voltage-triggered switching with potential dynamical information storage (e.g., bistable redox-controllable molecules such as catenanes[111] and rotaxanes[112–114], or even 2D-crossbar circuits for potential logic applications).[114–116] In the latter case the oxidation states of ON- and OFF- state remain identical, although the resulting conductivities are altered nevertheless.

Conformational changes usually are very sensitive to undesired thermally activated back-switching processes. In contrast, configurational changes, mostly occurring due to the photochromic addressability of the included molecular entities,[117,118] usually show a much higher stability of initial and final states (*ON*- and *OFF*-state). In the latter case, the challenge is to make this configurational switch reversible and operational at suitable temperatures. By their implementation into nano-scale logic devices,[115] the superior stability features of electrically triggerable molecular switches entities have been demonstrated. The following subchapters give an overview of some of the most prominent examples of molecular switching motifs and the ones being most relevant to the results presented in this thesis.

1.1.3.1 Switches Undergoing Conformational Changes

This group of molecular switches undergoes geometrical alterations (conformational changes), which usually involve rotation around single bonds present in the molecular backbone of the molecular switch, and which usually occur at low energy barriers. An example of such a conformational change is an alteration of the interplanar torsion angles of benzene subunits in biphenyl derivatives (rotation around the C_{Ar}-C_{Ar} single bond). Correlation between the conductance and the torsion angle can thus be obtained in such systems. During the investigation of amino-functionalized biphenyls in molecular junctions, Venkataraman *et al*. found a linear correlation between the conductance G and the square of the cosine of the interplanar torsion angle ($\cos^2 \Theta$) of the biphenyl unit.[18] A similar effect could be observed for 4,4′-biphenyldithiols, where the conductivity was dependent on the interplanar torsion angles ($\Theta = 0°$ (*ON*), $\Theta = 90°$ (*OFF*)) and could be controlled by applying gate voltage.[93] Analogously, Lörtscher *et al*. reported a switch based on bipyridyl-dinitro-OPE dithiol (BPDN-DT, **1**) connected to two Au-electrodes (Figure 14),[119] in which a similar effect was observed.

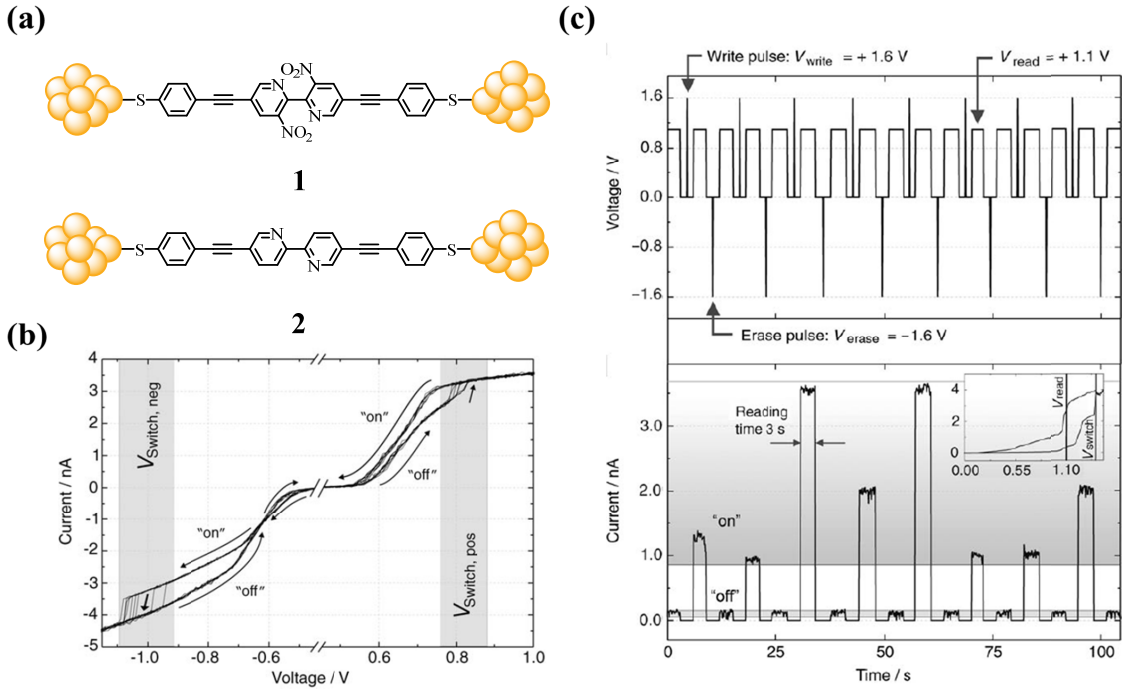

Figure 14: (a) Structures of BPDN-DT (**1**) and the reference compound BP-DT (**2**), **(b)** *I-/V*-plot illustrating repetitive switching of **1** once the bias exceeds the required thresholds, **(c)** memory operation of the BPDN-DT setup showing the write, read, and erase bias pulse pattern (top image), and the resulting switching cycles between ON- and OFF-states. Figures 14b and c reprinted with permission from Lörtscher *et al*.[119]

The conformational origin of the binary, bias-induced and hysteretic switching behavior they observed for **1** could be indirectly verified by the absence of such switching behavior in unsubstituted bipyridyl-OPE dithiol (BP-DT, **2**) (Figure 14a) due to the missing rotational restrictions in the latter one. The fact that ON- and OFF-switching only occurred above a certain threshold bias (OFF → ON), respectively, below for the opposite switching (ON → OFF) (Figure 14b) allowed a controlled memory operation of the BPDN-DT system (Figure 14c) utilizing discrete voltage pulses. However the switching performance of **1** could not be realized at room temperature, but is limited to a use at around 100 K.

The fact that the molecules in the above examples undergo conformational changes so readily is also their weak point, as the undesired thermal back-switching process can occur. This back-switching process substantially limits the temperature window in which these functional molecules can be used and hence their general applicability.

1.1.3.2 Switches Undergoing Structural or Configurational Changes

The most prominent and most widely used examples of switches undergoing structural changes are optoelectronic switches, such as those employing either *cis* ↔ *trans* photo-isomerization reactions (azobenzenes or stilbenes) or bond-breaking and –forming reactions (dithienylethenes and their derivatives). In case of dithienylethenes, the high-conducting state (*ON*-state) is attributed to the closed form **3** due to its extended conjugation, whereas the low-conducting state (*OFF*-state) arises from the open, cross-conjugated form **4** (Figure 15a). Early examples in this field exhibited problems with irreversibility of the switching process, allowing only the transition of closed (*ON*) → open (*OFF*) form to occur.[97] Failure of the reverse transformation was attributed to the quenching of the photo-excited state, most likely due to strong coupling of the open form's HOMO level with the high density of states of the Au electrodes. Introduction of two cross-conjugated *meta*-phenylene spacers between the dithienylethene core and the sulfur anchoring units (Figure 15b), though at the cost of a decreased *ON/OFF*-conductance ratio, solved the issue of switching irreversibility and allowed for a back-switching of the closed dithienylethene derivative **5** to its corresponding open form **6** by means of UV irradiation (Figure 15c).[96,98,99] furthermore, it could be shown, that also the use of single-walled carbon nanotubes allows for a reversible photochromic switching process as well.[120]

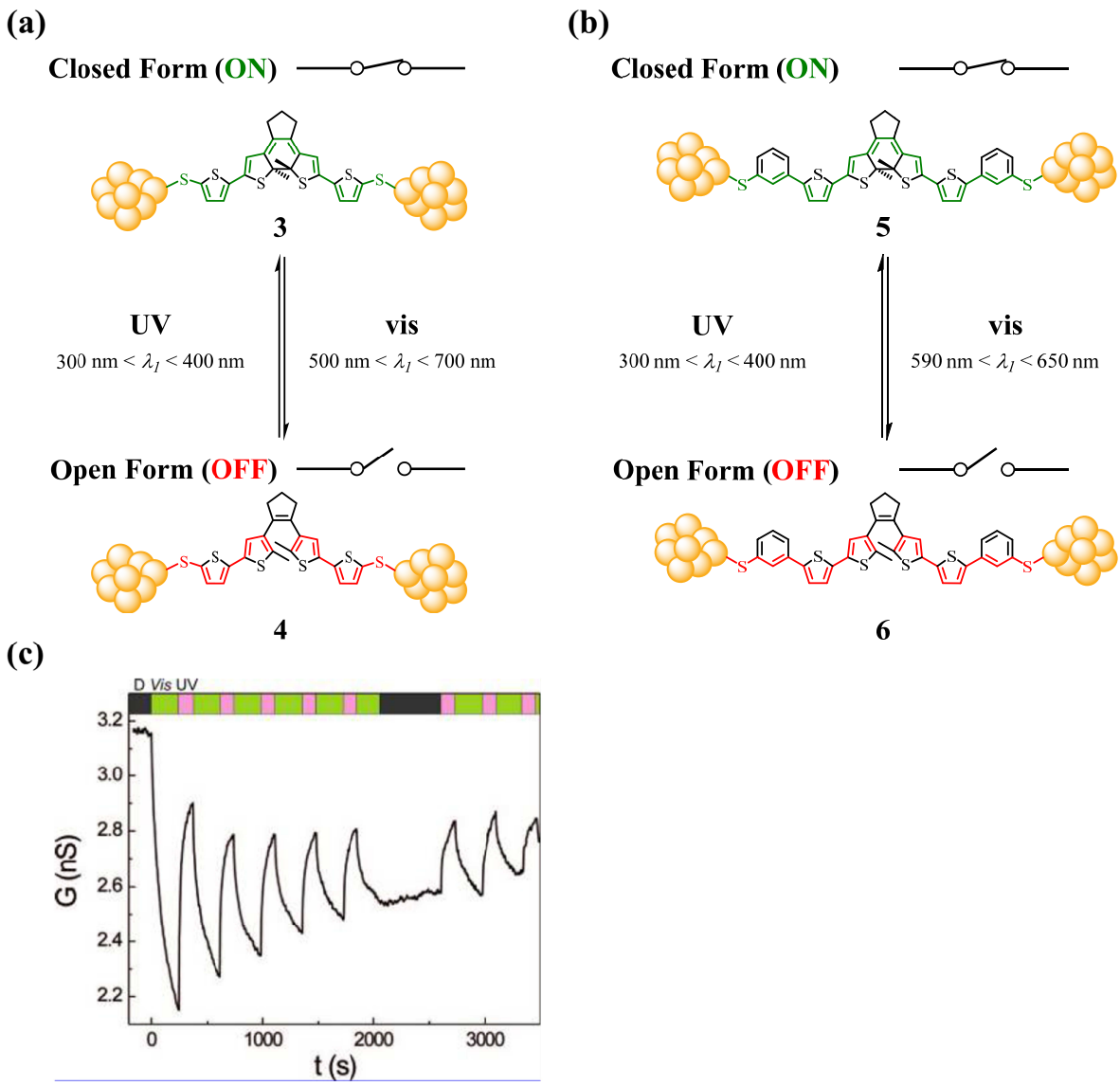

Figure 15: (a) Illustration of the switching process between the closed (**3**) and the open (**4**) form of a dithienylethene derivative exhibiting mainly one-way optoelectronic switching towards the closed form (**3**),[97] **(b)** schematic illustration of the switching process between the closed (**5**) and the open (**6**) form of an advanced generation of dithienylethene derived compounds exhibiting *meta*-phenyl spacing groups between the molecular core and the Au electrodes on both sides, **(c)** reversible switching between the closed (**5**) and the open (**6**) form was observed. Figure 15c reprinted with permission from van der Molen *et al.*[99]

The class of photoisomerizing azobenzene derivatives has been studied and is described extensively in the literature. The switching processes have been studied especially in self-assembled monolayers (SAM).[101,102,121–123] A particularly appealing example is the switching of the whole crystalline domains of the *trans*-isomer of [4′-(biphenyl-4-ylazo)-biphenyl-4-thiol] ((*E*)-**7**) to the better-conducting *cis*-isomer ((*Z*)-**7**) (Figure 16a). The experimental observation, that the *cis*-isomer is more conducting than the thermally more stable *trans*-isomer was attributed to the fact that the *cis*-isomer is significantly shorter. Taking the weak coupling between the electrode and molecule **7**

(see Chapter 1.1.2 – weak coupling regime) into account, the increase in conductivity in the case of the *cis*-isomer can be explained by the reduced resistivity of the shortened tunneling barrier. This fact is true for Au-molecule-Au-junctions when the AFM technique (Figure 16b)[101] is employed as well as for the use of the mercury-drop electrode setup (Figure 16c).[123]

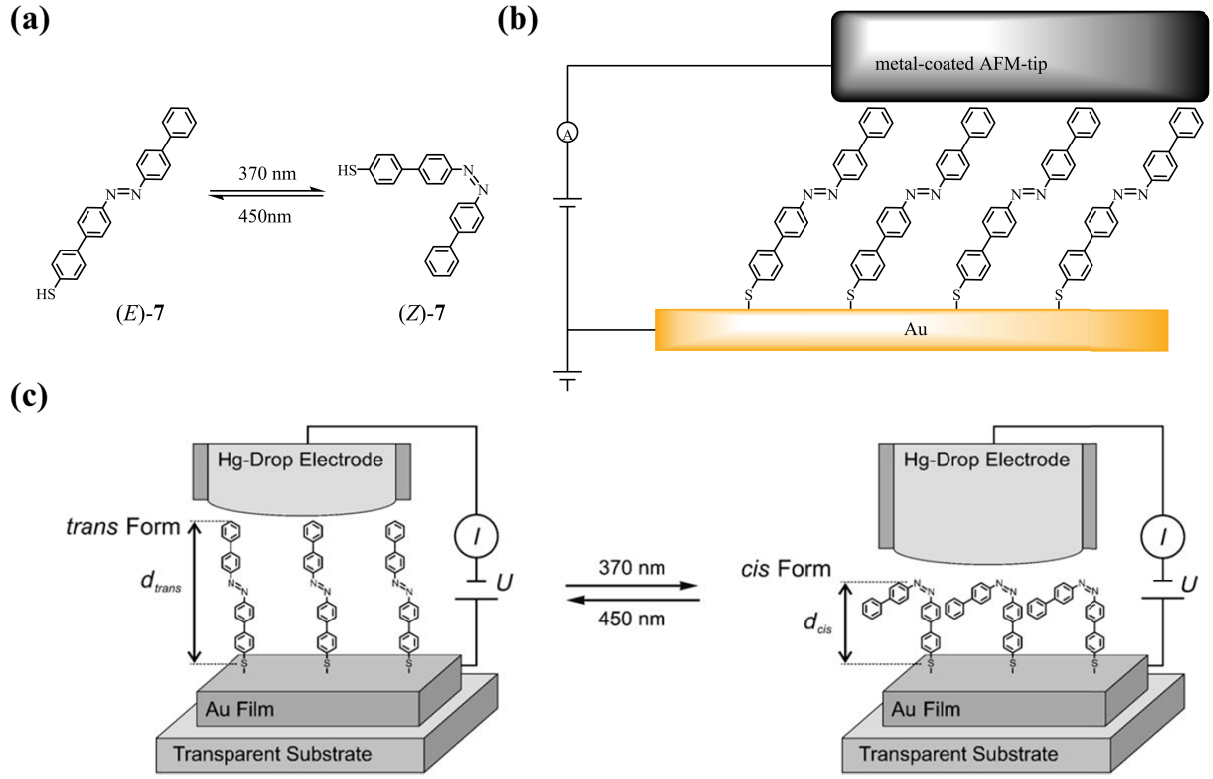

Figure 16: (a) Reversible photoisomerization between (*E*)-**7** and (*Z*)-**7**, **(b)** schematic illustration of an AFM setup to follow the switching of azobenzene derivative (*E*)-**7**,[101] **(c)** illustration of the photoswitching process between (*E*)-**7** and (*Z*)-**7** in a molecular juction setup consisting of a gold substrate and a mercury-drop electrode. Figure 16c reprinted with permission from Ferri *et al*.[123]

A very special case of conductance switching induced by structural changes, is the mechanical control of metal-molecule-metal contact configurations which Quek *et al*. recently reported utilizing Au-4,4′-bipyridine-Au single-molecule bridges.[49] They observed reversible mechanically controlled conductance switching using a sub-nanometric sinusoidal motion of the STM tip (Figure 17). Similar conductance switching was observed by Diez-Perez *et al*., during their investigation of the tilt-angle dependent, lateral π-orbital coupling of pentaphenylene molecular junctions.[124]

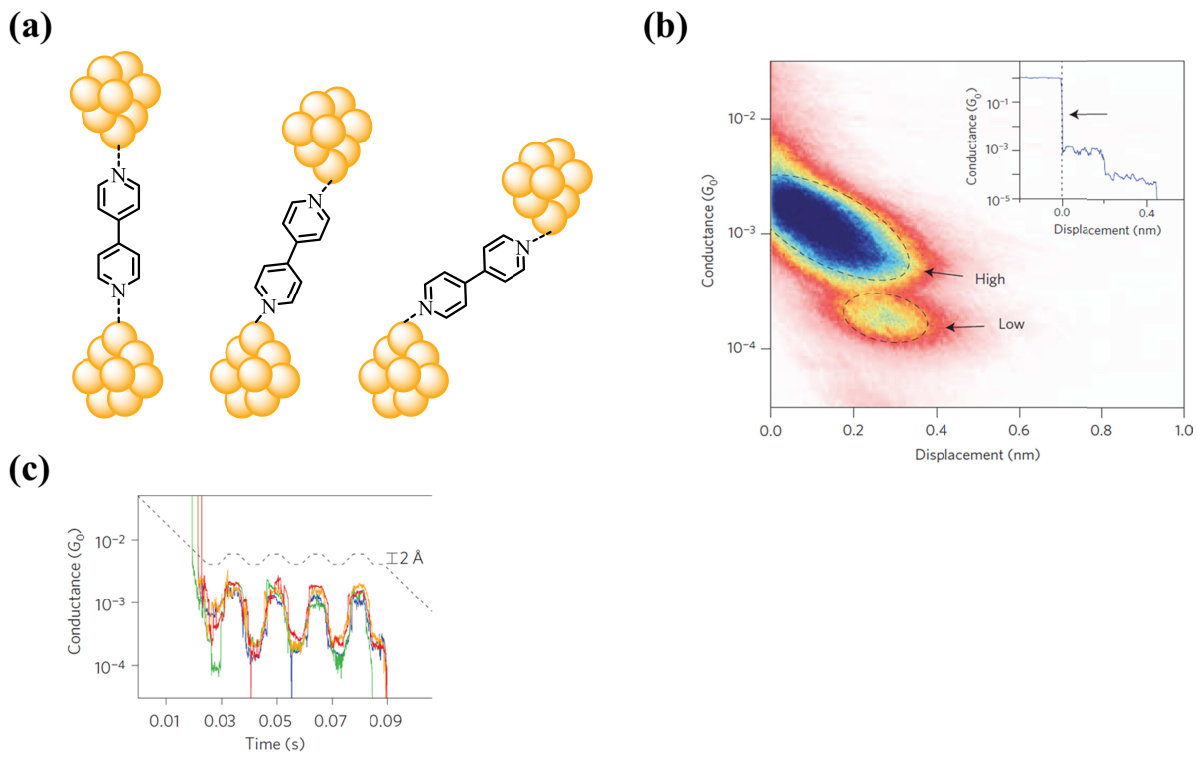

Figure 17: (a) Schematic illustration of Au-4,4′-bipyridine-Au junction showing different inter-electrode distances, **(b)** two-dimensional histogram illustrating the conductance G_0 versus the electrode's displacement, and clearly exhibiting a high- and a low-conductance region. Inset: exemplary conductance trace showing both conductance steps, **(c)** illustration of the G versus t plot during the application of a sinusoidal bias sequence. Pictures 17b and c are reprinted with permission from Quek *et al.*[49]

1.1.3.3 Switches Undergoing Electrochemical Changes (Redox Switches)

The third main class of single-molecule switches consists of several subgroups, for example, redox-switches undergoing a change of the bridging molecule's oxidations state and voltage-triggered switches in which changes in conductivity can be induced without changing the molecule's oxidation state. Since the conductance of molecular junctions is strongly dependent on the population and relative energy of the FMOs, the tuning of the electrode's electrochemical potential with respect to the molecular energy levels can result in charging of the bridging molecule if the electrochemical potential is below or above the energy levels of the LUMO or HOMO, respectively.

Common examples of a redox-based system are molecular switches operating by means of reversible reduction of the bipyridinium moiety ($bipy^{2+}$), also known as *viologen*, to its +1 or 0 charged species (Figure 18a).[103–106] Recently, Tsoi *et al.* reported quinone-based OPV

systems as efficient, reversibly switchable redox-based molecular switches (Figure 18b).[110] Furthermore, TTF derivatives have been extensively studied with regard to the switching from their neutral (*OFF*-state) species to the +2 charged (*ON*-state) species, which are more conductive (Figure 18c).[106–108]

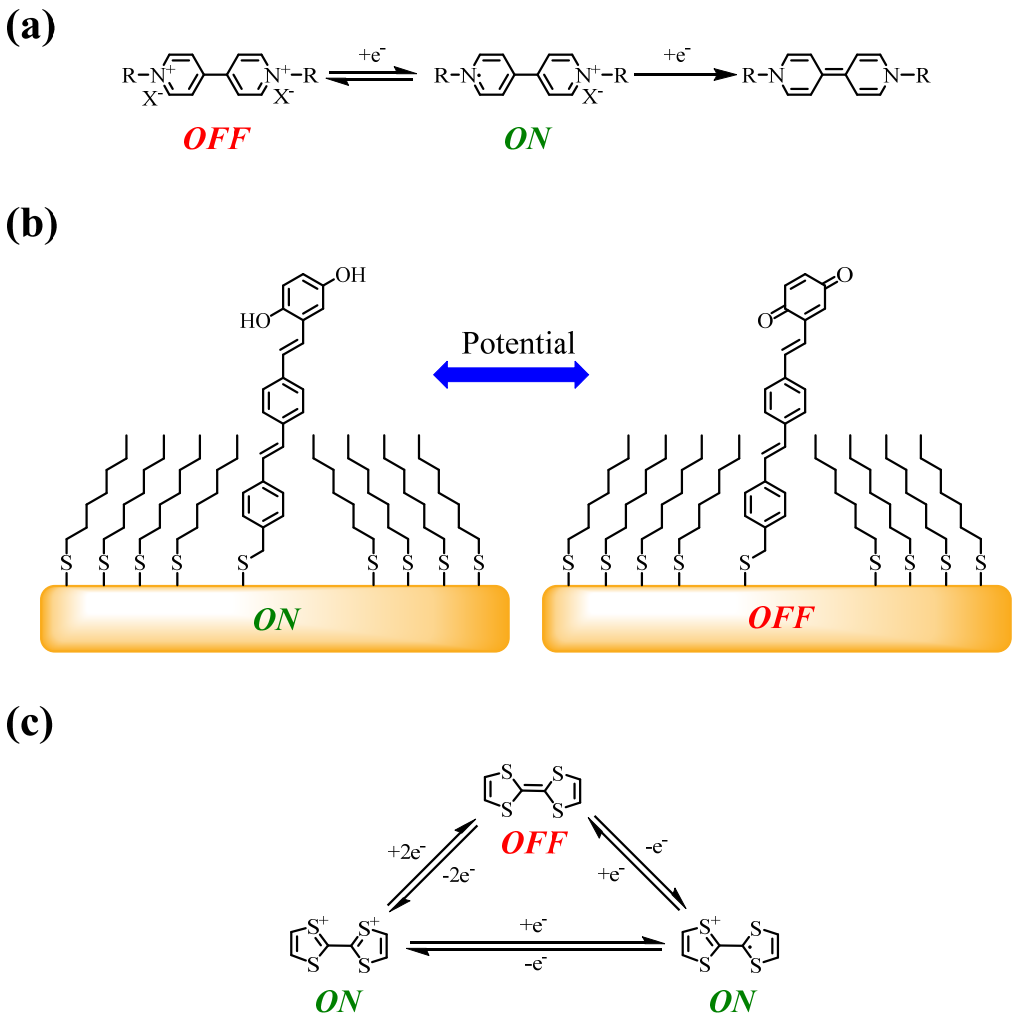

Figure 18: Illustration of some of the most common redox-based single-molecule conductance switches: **(a)** *viologen*-based molecular switch, **(b)** reversible electrochemical switching between the low-conducting quinone-OPV and the high-conducting hydroquinone-OPV, **(c)** oxidation states of TTF-based molecular switches. Figure 18b is adapted from Tsoi *et al.*[110]

Finally, a class of voltage-triggered switching devices with potential for information storage has been developed by Stoddart's and Heath's groups over the last 15 years. The switches are based on bistable redox molecules, such as catenanes[111] and rotaxanes.[112–114] The classic Stoddart-Heath [2]catenanes or [2]rotaxanes usually comprise a tetracationic cyclobis(paraquat-*p*-phenylenes) ($CBPQT^{4+}$) ring shuttling between two electron-rich stations in the dumbbell, for example, between a 1,5-dioxynapthalene (DNP) and a TTF moiety. Depending on the arrangement of the backbone one talks about catenanes (cyclic) or

rotaxanes (linear) (Figure 19a). The position of the CBPQT^{4+} ring in the switch can be controlled electrochemically. With no bias applied (ground state) the CBPQT^{4+} ring is bound to the neutral TTF unit (*OFF*-state), for which it has higher binding affinity compared to DNP. Once a sufficient voltage is applied, the TTF ring becomes positively charged. Due to electrostatic repulsion, a shuttling of the CBPQT^{4+} ring to the DNP unit (*ON*-state) occurs (Figure 19b).

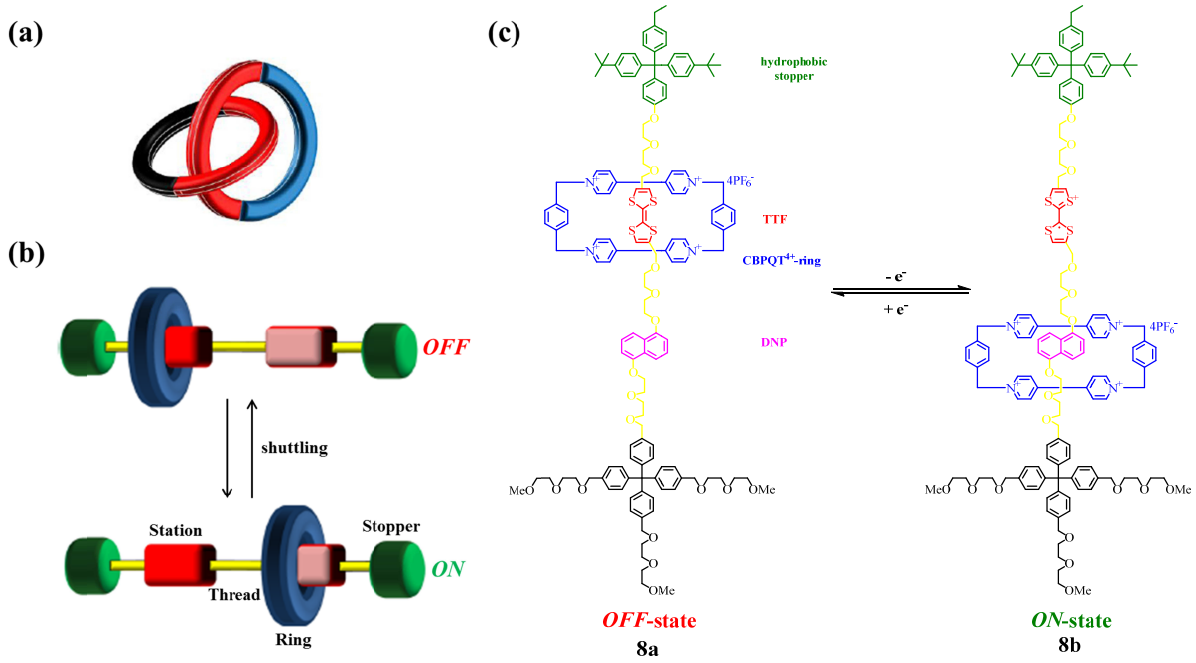

Figure 19: Schematic representations of **(a)** a [2]catenane, and **(b)** a [2]rotaxane. **(c)** Strucutre of an amphiphillic bistable [2]rotaxane that can be switched between the neutral *OFF*-state (**8a**) (left) and the oxidized metastable *ON*-state (**8b**) (right). Figures 19a and b are reprinted with permission from Konstas *et al.*[125]

The investigation of molecular switch tunnel junctions based on [2]catenanes[111] and [2]rotaxanes[114] revealed a hysteretic *I*/*V*-behavior. These loop-like characteristics potentially allow the utilization of these switches in molecular memory devices. First promising test systems including an example of two-dimensional crossbar circuits (2D crossbar random access memory)[114,116] as well as a high density logic device (10^{11} bits/cm^2)[115] have been described.

1.1.4 Spin Crossover and Spintronics

The following chapter is dedicated to a brief description of the control over electronic spin states, focusing on the impact in the field of molecular electronics. The spin crossover phenomenon (SCO) and related control mechanisms over the electronic spin state switching within suitable transition metal complexes will be elucidated. Selected examples of SCO complexes triggered thermally, light-induced or by pressure will be given before a short introduction into the field of *spintronics* (an acronym for **spin tr**ansport electr**onics**) and an outlook of potential future applications of SCO phenomena in molecular electronics will be outlined.

1.1.4.1 Spin Crossover

Linked historically as well as fundamentally to the evolution of coordination chemistry, the SCO phenomenon belongs to the field of magnetochemistry and was first described in 1931 by Cambi *et al.* in his articles on magnetic susceptibility of 3d transition-metal complexes[126,127] and polymorphism of transition-metal complex salts.[128] A classical SCO transition-metal complex exhibits a labile electronic configuration, which can be, to some extent, reversibly switched between its low-spin (LS) and its high-spin (HS) states. This switching leads to distinctive alterations in color, magnetism, and structure of the SCO compound and can be usually triggered thermally, by light, or by pressure. Although the range of the SCO compounds is not exclusively limited to the first-row transition-metal complexes, the octahedral complexes of this group exhibiting $[Ar]3d^4$-$3d^7$ electronic configurations represent the vast majority of the SCO compounds investigated to date. Generally, these compounds can adopt two different electronic ground states, namely, HS and LS state, due to the splitting of their d-orbitals into the e_g and t_{2g} subsets. The energy gap between these two subsets describes the ligand-field strength Δ (also known as crystal-field splitting energy or cubic ligand field parameter). If Δ is greater than the interelectronic repulsion energy P (also mean spin pairing energy),[129] then the electrons will occupy the lower energetic t_{2g} orbitals leading to complexes in the LS state. In the case of Δ being smaller than P, greater stability is obtained if the electrons do not pair up, but remain unpaired according to Hund's first rule, leading to metal complexes adopting the HS state (Figure 20a).

Tanabe-Sugano diagrams[130,131] are a neat way to illustrate the energy gap between the HS and LS states and the related electron distribution (Figure 20b). Herein, Δ_C represents the crossing point at which Δ and P are similar, leading to the effect that the energy difference $\Delta E^0_{HS/LS}$ between the LS and the HS state comes into the range of the thermal energy (k_BT). This, furthermore, can be illustrated by a representation of the potential wells for the HS $^1A_{1g}$ and the LS $^5T_{2g}$ states of a SCO system (Figure 20c).

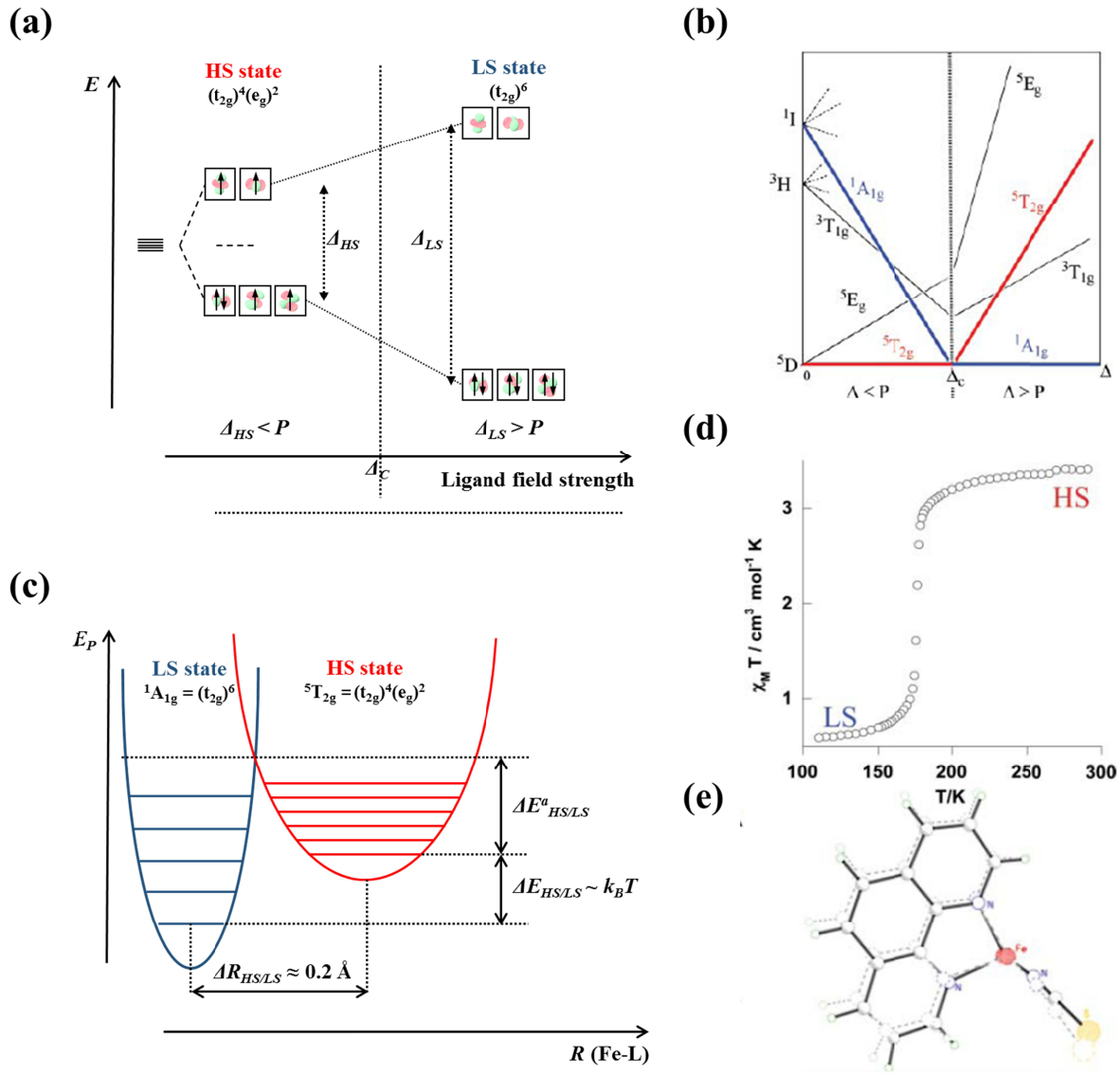

Figure 20: (a) Electron distribution for the HS and the LS states of an [Ar]3d^6 configuration and the equilibrium between both states for the case of thermal SCO, **(b)** Simplified Tanabe-Sugano diagram describing the HS and the LS states' relative dependence, **(c)** schematic representation of the potential energy wells for the HS ($^1T_{2g}$) and the LS ($^1A_{1g}$) states of an Fe(II) SCO system depicted in a plot of E_p versus $R_{(Fe\text{-}L)}$, **(d)** Depiction of the temperature-dependent magnetic behavior of [Fe(phen)$_2$(NCS)$_2$] as an exemplary SCO compound, **(e)** Overlay of the asymmetric units of the HS form (dotted line) of [Fe(phen)$_2$(NCS)$_2$] versus the LS form (line). Figures 20b,c and d are reprinted with permission from Real *et al.*[132]

Accordingly a group of complexes (usually Cr(II), Mn(II), Mn(III), Fe(II), Fe(III), Co(II), and Co(III)) can be named, which readily exhibit SCO phenomena. The interconversion of both spin states in SCO complexes can be considered as an intramolecular electron transfer between the t_{2g} and the e_g orbitals. Hence, an increase in the metal-to-ligand bond distance can be observed as a consequence of the population of the antibonding e_g subset, and, vice versa, depopulation of the e_g orbitals results in a decrease of the metal-to-ligand bond distances. Opposite effects can be observed considering an increasing population of the t_{2g} orbitals of a SCO compound, by which the electron back-donation from the occupied metal orbitals into the vacant π*-orbitals of the ligand is strengthened. Both interactions (σ- and π-factor) contribute to the overall metal-ligand bond-length change $\Delta R_{HS/LS}$,[133] which usually lies in the range of 0.1-0.2 Å for Co(II) and Fe(II).[132,134] Figure 20d and e illustrate the distinct changes in molecular size and shape as well as the coinciding changes in the magnetic properties of $[Fe(phen)_2(NCS)_2]$ observed upon thermally induced spin conversion.

The alterations of Δ upon SCO can be estimated from the relative ratio of the metal-ligand bond lengths R_{LS} and R_{HS} found in the LS and HS states, respectively. This ratio $\Delta R_{HS/LS}$ has been proven to be the dominating structural parameter to estimate the Δ_{LS}/Δ_{HS}-ratio (Equation 7).[135]

$$\frac{10Dq^{LS}}{10Dq^{HS}} = \frac{\Delta_{LS}}{\Delta_{HS}} \approx \left(\frac{R_{HS}}{R_{LS}}\right)^{n}$$

Equation 7: Correlation of the altered crystal-field splitting energies Δ in a SCO system, with n = 5-6.

From the average $\Delta R_{HS/LS}$-value of an Fe(II) SCO complex, between 0.16–0.22 Å,[136–139] an average ratio of $\Delta_{LS}/\Delta_{HS} \approx 1.75$, can be revealed.[131,132] If the potential energy E_p (Equation 8) of the SCO center (in the LS or the HS state), is plotted versus the Fe-N bond length $R_{Fe\text{-}L}$, parabolic curves, as illustrated by the potential wells within Figure 20c, are obtained. Whereas the horizontal displacement of the two parabolas corresponds to $\Delta R_{HS/LS}$, the vertical displacement indicates the relative stabilization energy $\Delta E_{HS/LS}$ between the LS state and the HS state for an isolated SCO molecule.

$$E_{p(i)} = \frac{1}{2[f_i R_i^2]}$$

Equation 8: Expression for the potential energy E_p of the SCO center: i represents either the HS or the LS state, f corresponds to the constant force of the vibrations, and R is the average metal-to-ligand bond length.

The horizontal lines within the potential wells represent the different vibrational energy levels E^{vibr}. There are more vibrational energy levels in the HS than in the LS state.[132] These levels play an important role in understanding the thermal SCO phenomenon. At low temperature the SCO compound remains in the LS state. By increasing the temperature the thermal energy is transformed into vibrational energy, leading to the population of excited vibrational levels until the crossing point Δ_C of the two adiabatic potentials is reached. At Δ_C the geometries of LS and HS state are essentially the same. According to the Franck-Condon principle, it is exactly at this point Δ_C that the thermal LS ↔ HS transformation occurs. At this point, the enthalpic energy costs to clear the gap between LS and HS state are compensated by the entropic difference between the two states, thus favoring the population of the HS state at even further elevated temperatures (Figure 20d and e).

The influence of the applied pressure can also be illustrated with the help of potential wells (Figure 21a). The main effect of the applied pressure is the destabilization of the HS state due to its larger volume if compared to the smaller LS state configuration. Therefore, externally applied pressure slightly reduces $\Delta R_{HS/LS}$, but foremost increases the zero-point energy difference $\Delta E_{HS/LS}$ by significantly increasing the HS state's potential well minimum.[140–143] Hence, the activation energy $\Delta E^{a}_{HS/LS}$, defined as the difference between the zero-vibrational HS energy level and the crossing point of both potential wells, is decreased significantly. Figure 21b and c exemplarily illustrate the observed effects upon pressure-induced spin conversion of $[Fe(phen)_2(NCS)_2]$, the first and most extensively studied SCO Fe(II) complex.[143–149] As expected, the elevation of the applied pressure at a given temperature results in an increased HS → LS conversion. This finding is also reflected by the results of the magnetic susceptibility measurements illustrated in Figure 21c,[148] which clearly show that in order to obtain an equal fraction of HS state at elevated pressures, increased temperatures are required to trigger the thermally induced LS → HS conversion (working against the pressure's driving force).

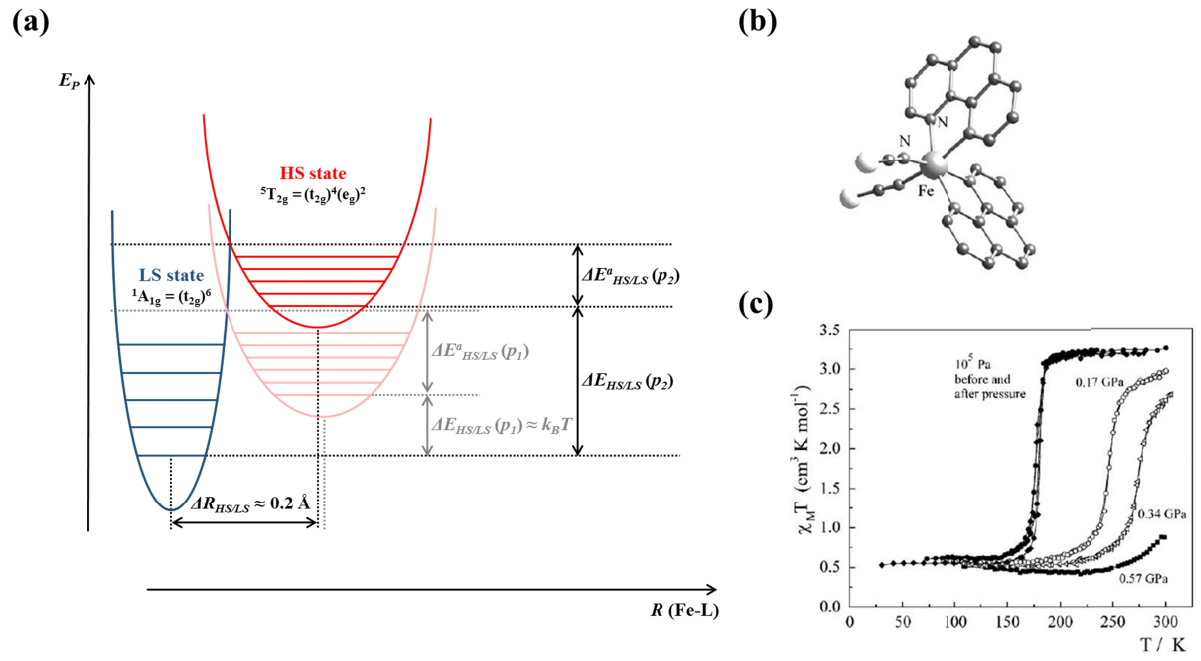

Figure 21: (a) Schematic illustration of the LS and the altered HS potential wells resulting from the application of an elevated pressure ($P_2 > P_1$) onto an Fe(II) SCO system,[142,143,149] **(b)** molecular structure of [Fe(phen)$_2$(NCS)$_2$], and **(c)** depiction of the pressure-dependent magnetic behavior of [Fe(phen)$_2$(NCS)$_2$] illustrated by the plot of magnetic susceptibility versus temperature. Figures 21b and c are reprinted with permission from Gütlich *et al.*[142]

Furthermore, the light-induced spin conversion of SCO compounds has also been studied extensively. McGarvey and Lawthers were the first ones to observe photo-induced SCO. They performed measurements in solution, however, the obtained HS states were very short-lived at that time.[150] In 1984, Decurtins *et al.* were able to observe light-induced SCO in the solid state within the complex [Fe(1-propyltetrazole)$_6$](BF$_4$)$_2$ for the first time.[151] They monitored bleaching of the originally purple LS Fe(II) complexes upon monochromatic irradiation with green laser light (λ = 514.5 nm) at relatively low temperatures (T < 50 K). This finding was attributed to the enhanced spin-allowed $^1A_1 \rightarrow {}^1T_1$ absorption stimulated by the green-light irradiation (Figure 22). Although the lifetime of a $^1T_1$ state lies in the range of nanoseconds, there is a small probability for a radiationfree relaxation of the $^1T_1$ LS state, to cascade via a twofold intersystem crossing to the $^5T_2$ HS state after passing through the intermediate $^3T_1$ spin state ($^1T_1 \rightarrow {}^3T_1 \rightarrow {}^5T_2$). Due to the forbidden $^5T_2 \rightarrow {}^1A_1$ relaxation, the $^5T_2$ HS state exhibits a very long life-time and can be trapped in the HS state at low temperatures. Hence, a photo-induced quantitative inversion of the spin-states' population can be achieved, and is usually described as light-induced excited spin state trapping (LIESST). By raising the temperature above 50 K or by irradiating the metastable HS state with red light (λ = 820 nm), a back-transformation to the LS state, the so-called reverse-LIESST, can be observed. Herein,

the molecule being present in the $^5T_2$ HS state is excited to the ^5E state, followed by two subsequent intersystem crossing processes before relaxation to the LS ground state ($^5E \rightarrow {}^3T_1 \rightarrow {}^1A_1$) occurs (Figure 22).

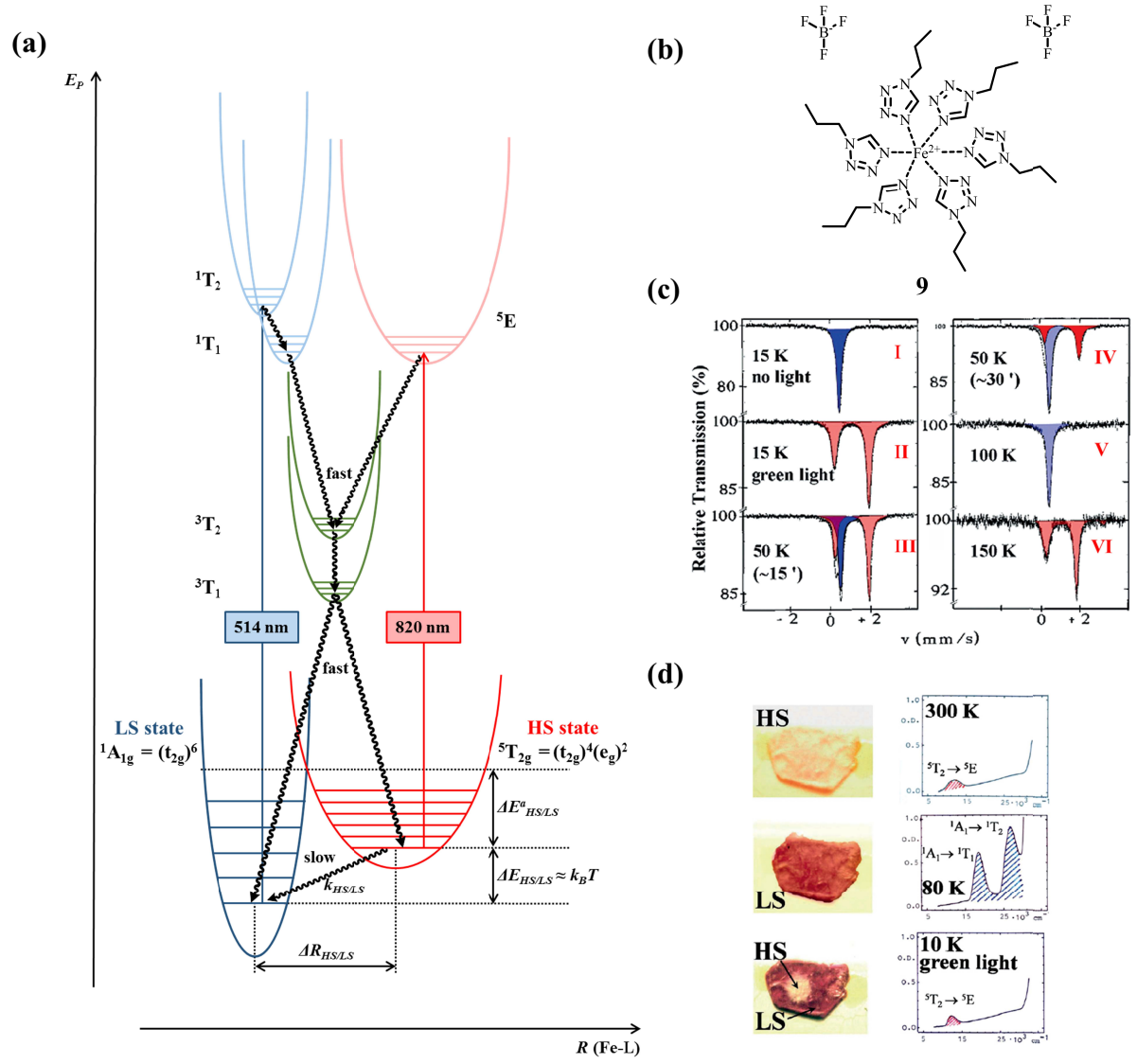

Figure 22: (a) Schematic illustration of the LIESST and the reverse-LIESST effect, **(b)** chemical structure of $[Fe(ptz)_6](BF_4)_2$ (**9**) as the first SCO compound LIESST was observed on, **(c)** ^{57}Mössbauer spectra obtained throughout the original study of LIESST phenomena in $[Fe(ptz)_6](BF_4)_2$:[151] (I) sample before bleaching of the LS state (pure LS state); (II) after 1 h of irradiation with green laser light at 514 nm (pure HS state); (III) after 15 min of warming to 50 K (46% of LS state); (IV) after 30 min of warming to 50 K (70% of LS state); (V) complete HS→LS back-conversion; (VI) after heating to 150 K ($T_C \approx 135$ K) full thermal SCO (LS → HS) is observed, **(d)** Illustration of LIESST phenomenon of $[Fe(ptz)_6](BF_4)_2$ observed on single crystals (left) and followed by optical spectroscopy (right). Figure 22c is adapted and figure 22d reprinted with permission from Gütlich *et al.*[152]

Apart from the presented systems, in which the SCO phenomena are triggered by three main classes of stimuli (temperature, pressure, and light), there are reports on several further, interesting systems in which SCO could be observed. It is this variability, which renders the

exploitation of SCO phenomena versatile potential future applications, for example, in the field of molecular electronics. An interesting effect, which can be observed in solution or in polymeric matrices, is the so-called Ligand-Driven-Light-Induced Spin Change (LD-LISC) first observed by Zarembowitch and Boillot *et al.* (Figure 23).[153–155] Conceptually, in order to induce the spin state switching and to observe the LD-LISC phenomena, complexes containing a photo-switchable functional moiety, such as an azo- or a stilbene-group, are required. Upon photo-induced modification of this functional group (e.g. *cis*↔*trans* isomerization), a change in the compound's ligand-field strength, caused by the alteration of the ligand's geometry, needs to be sufficiently big to trigger the desired SCO. This concept allows for reversible, photo-induced spin conversion between long-lived spin states at high temperatures.

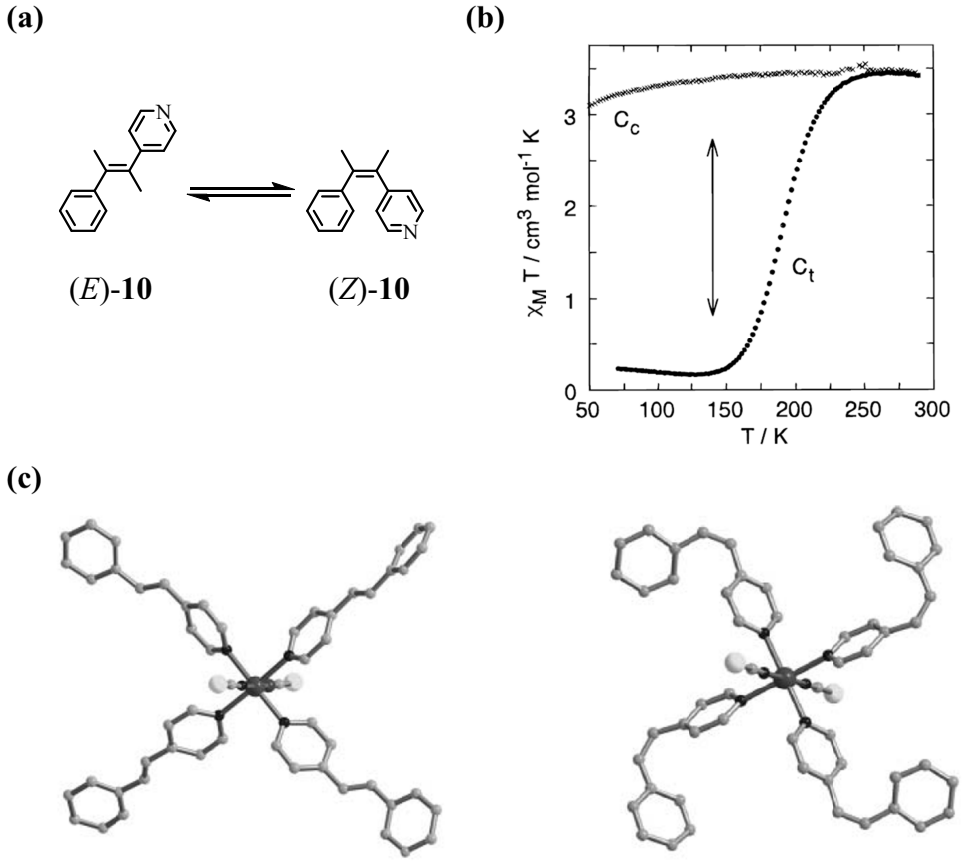

Figure 23: (a) Chemical structures of the *cis*-stpy ((*Z*)-**10**) and the *trans*-stpy ((*E*)-**10**) ligands within the $[Fe(stpy)_4(NCBPh_3)_2]$ complexes investigated by Zarembowitch and Boillot *et al.*, **(b)** depiction of the temperature-dependent magnetic behaviors of $[Fe(cis\text{-}stpy)_4(NCBPh_3)_2]$ and $[Fe(trans\text{-}stpy)_4(NCBPh_3)_2]$ illustrated by the plot of magnetic susceptibility versus temperature, **(c)** molecular structures of $[Fe(cis\text{-}stpy)_4(NCS)_2]$ and $[Fe(trans\text{-}stpy)_4(NCS)_2$ illustrating the different geometries of the two isomers. Figure 23b is reprinted with permission from Boillot *et al.*,[154] and figure 23c is reprinted with permission from Real *et al.*[132]

Another interesting approach to externally address SCO phenomena at a molecular level has recently been published by Parks *et al.*, who investigated mechanically controllable spin states of $Co(tpy\text{-}SH)_2$ complexes immobilized within MCBJ.[156] By modification of the complexes' geometry by altering the electrode's displacement within the MCBJ setup, they were able to reversibly observe different spin states, as proven by the observation of the corresponding Kondo features.

Overall, the extraordinary sensitivity of SCO systems towards relatively small structural changes makes them ideal candidates for practical applications in a multitude of different situations. In this context, two aspects of SCO are particularly appealing: (1) The potential occurrence of thermal hysteresis in the HS → LS → HS cycle, and (2) the ability of light to effect photo-induced spin alterations (LIESST and related phenomena). Hysteresis, as an effect observable for some cases of molecular bistability, offers the potential ability for SCO phenomena to be utilized in memory devices, ultimately at the level of single molecules. For a potential applicability within memory devices, the bistability, however, needs to be associated with a suitable response, which is different in an ON- and an OFF-state. To date, the response phenomena of SCO compounds, such as a change in color or magnetism, have proven to be well suited, for example, for the development of displays (color change) or pressure sensors, taking the potential changes in the behavior of SCO compounds upon applied pressure into account. In order to achieve a real application in the field of spintronics, for example, within memory devices, other stimuli and responses related to SCO need to be explored. In this case, the realization of the spin states' sensitivity towards an electrical trigger, such as applied bias or gate voltage, remains a challenge. Two promising examples have, however, been recently reported: (1) Prins *et al.* assembled a switchable molecular device contacting single nanoparticles based on SCO compounds immobilized between two nanoelectrodes[157] and observed hysteresis, which could be useful for memory applications in the future. (2) Very recently, Wagner *et al.* were able to reversibly switch between a pseudo-singlet and a pseudo-triplet state of two coupled spin centers confined within two interlinked Co^{2+} ions.[158] The assignment of the different spin states was possible based on the occurrence or absence of Kondo-like zero-bias anomalies observed within the conductance measurements performed at low temperatures. Nevertheless, the implementation of single molecules into nanoelectronic assemblies in a more controlled fashion remains the key challenge of molecular spintronics to be solved in order to allow the development of ultimately small electronic devices based on organic building blocks in the future.

1.2 Terpyridines

The purpose of this chapter is to give a brief background on 2,2′:6′,2′′-terpyridine (tpy) chemistry. A short historical overview is followed by a description of the most prominent approaches to synthesize the tpy moiety, namely, ring-assembly strategies versus cross-coupling strategies, and a section dealing with the prevailing limitations of applicable substitution patterns on the tpy unit. The second part of this chapter deals with the transition-metal complexes of tpys. Herein, the formation strategies and the most prominent applications of transition-metal tpy complexes are given.

1.2.1 History and Synthetic Approaches towards Terpyridines

The first reported synthesis of tpy (**11**),[159] involving the oxidative condensation of pyridines using $FeCl_3$ as the oxidant, dates back to 1932. It yielded very small quantities of tpy along with a multitude of other *N*-containing products, among them the predominantly obtained 2,2′-bipyridine (bpy) (**12**). Although the formation of intensively colored tpy metal complexes by the addition of Fe(II) to tpy-containing solutions was discovered soon after,[160] it took almost 60 years until the scientific community realized the true potential of tpys and their metal complexes to form supramolecular assemblies, which soon after became increasingly popular. After that an increased interest in tpy chemistry could be observed (Figure 24), following the advances in (metallo)supramolecular chemistry,[161] and selective host-guest chemistry, for which the Nobel Prize in Chemistry in 1987 was awarded to J.-M. Lehn, C.J. Pedersen, and D.J. Cram.[162–164]

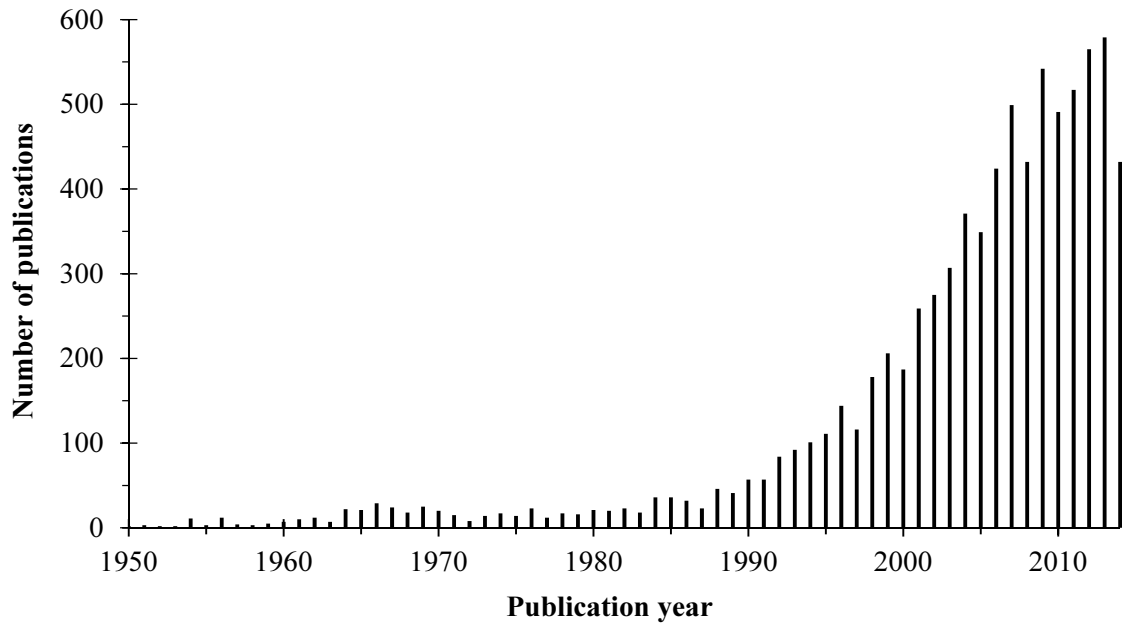

Figure 24: Histogram illustrating the referenced number of publications containing the term "terpyridine" as found by utilizing SciFinder™ (Search performed 17th September 2014).

A reason for this correlation between tpy chemistry and the advances in supramolecular chemistry lies in the fact that metal-to-ligand coordination is one of the most common tools of supramolecular chemistry. In this context, chelate complexes, especially those derived from *N*-heteroaromatic ligands, such as bpy (**12**), tpy (**11**), and 1,10-phenanthroline (phen) (**13**), play an important role (Figure 25).

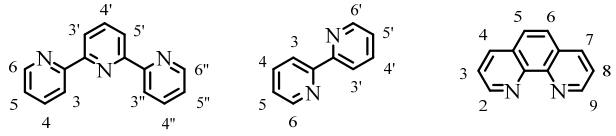

11 **12** **13**

Figure 25: Chemical structures of three very important structural motifs in supramolecular chemistry: 2,2′:6′,2′′-terpyridine (tpy) (**11**), 2,2′-bipyridine (bpy) (**12**), and 1,10-phenanthroline (phen) (**13**).

Over the last two decades, tpys gained significant interest also in fields, other than supramolecular chemistry, such as coordination chemistry and materials science.[165–172] One of the key properties making tpys so attractive for this broad variety of scientific fields is the fact, that the three nitrogen atoms contained in the tpy motif, equip tpys with the ability to act as tridentate ligands. Another key feature of tpys is their substantial coordination chemistry and binding affinity especially towards transition and rare earth metal ions. The interesting photophysical and redox properties arising from this substantial coordination chemistry give

rise to a versatility of potential applications derived from tpys today (Chapter 1.2.3). A more detailed picture of the different types of tpy motifs and their accessibility will be given hereafter, focusing only on the most prominent strategies and the ones most relevant to this work.

1.2.1.1 Ring-Assembly Methodologies

Ring-assembly strategies include the formation of one or more new aromatic rings from non-cyclic precursors. These ring-assembly strategies find broad applications during the synthesis of pyridine derivatives, and, are basically relying on the application and modification of classical Tschitschibabin-type[173] and Hantzsch-type[174] synthetic routes. Up to date, ring-assembly still represents the most prevalent method used during the synthesis of tpy-based ligands. Scheme 1 illustrates the most important ring-assembly strategies, among which the Kröhnke methodology and its modifications represent the most extensively used pathways. The method, first reported by Kröhnke in 1976,[175,176] involves the condensation of ammonia with *N*-heteropyridinium salts **14** (X^- = Br^- or I^-) and enones **15** to yield the so-called Kröhnke-type tpys **16** (Scheme 1; method I). Herein, the required *N*-heteropyridinium salts **14** can be readily accessed via an Ortoleva-King reaction,[177] whereas the enones **15** are pre-formed from 2-acetylpyridine (**19**) and a (hetero)aromatic aldehyde by performing an aldol reaction. A second method, representing an advancement of the classical Kröhnke condensation, applies a ring-closing strategy reacting 1,5-diketones **17** with appropriate *N*-sources to yield the corresponding Kröhnke-type tpys **16** (Scheme 1; method II).[178–180] A major drawback of the classical Kröhnke methodologies (I and II) is their limited modularity, because R^3 needs to be (hetero)aromatic and sensitive functional groups are not tolerated under the applied reaction conditions. Further important ring-assembly strategies include the Potts' methodology featuring an *α*-oxoketene dithioacetal (**18**) as the key intermediate during the formation of tpy derivative **20**. In this methodology a reaction of compound **18** with a previously formed potassium enolate of a derivative of 2-acetylpyridine (**19**) takes place (Scheme 1; method III).[176,181] An advancement of Potts' methodology, commonly referred to as Jameson's protocol,[182] yields **11** by performing the condensation reaction of *β*-(dimethyl-amino)vinyl 2-pyridyl ketone (**21**) with the potassium enolate of 2-acetylpyridine (**19**) followed by the subsequent ring closure of intermediate 1,5-enedione (**22**) utilizing NH_4OAc (Scheme 1; method IV), as established from the classical Kröhnke methodologies. A further

approach to make tpy derivatives is Sauer's methodology comprising an inverse-type Diels-Alder reaction of 3,5-di(pyridin-2-yl)[1,2,4]triazines (**25**), with either ethynyltri(*n*-butyl)tin or norbornadiene to obtain tpy derivatives **26** (Scheme 1; method V), or **27** (Scheme 1; method VI), respectively.[183] The key intermediate **25** can be previously synthesized via a regioselective cyclocondensation of a carboxamidrazone () with α-pyridylglyoxal (**24**).

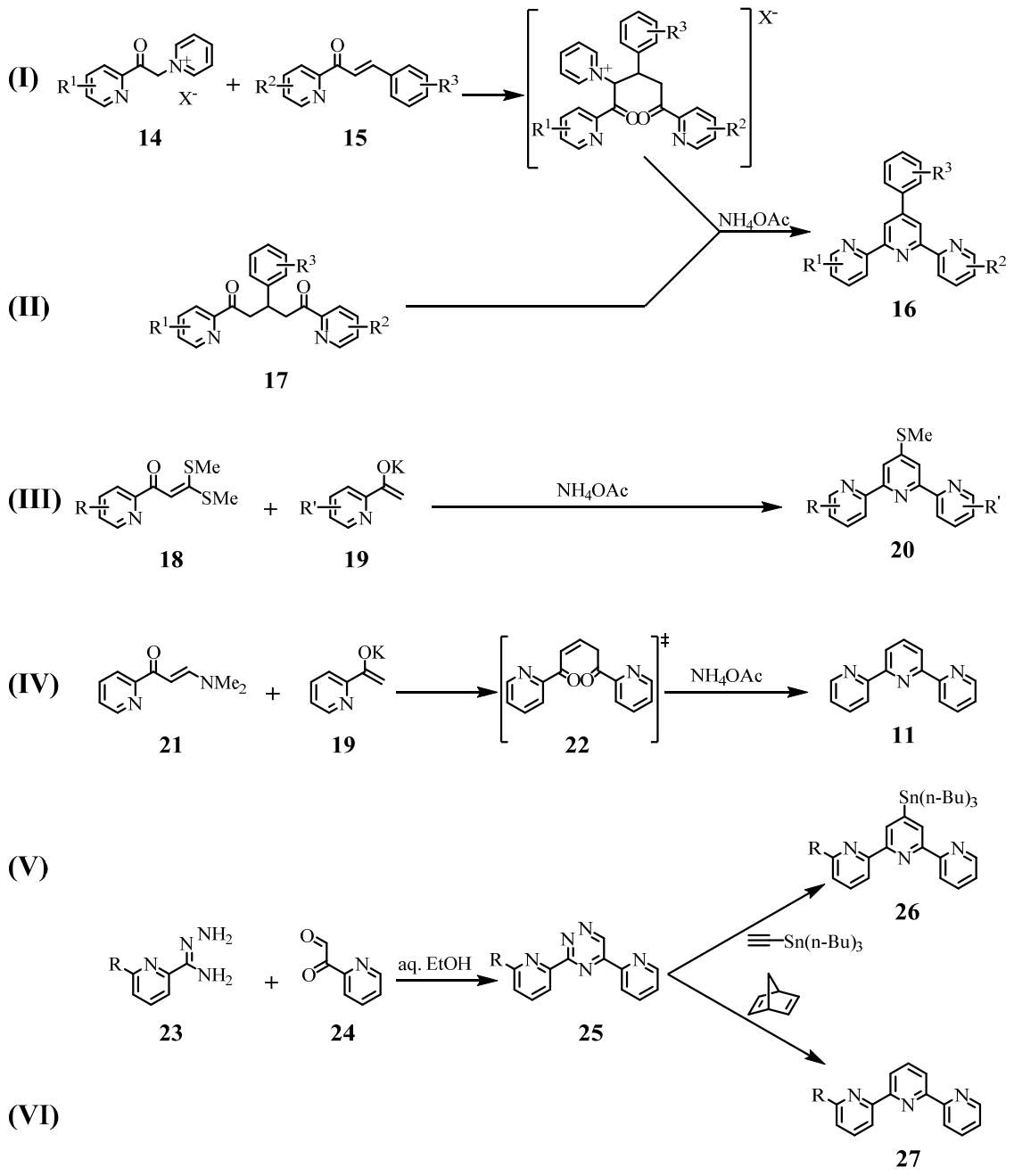

Scheme 1: Illustrative overview of the most common and general ring-assembly strategies: (I) and (II) Kröhnke condensations, (III) Potts' methodology, (IV) Jameson's protocol, (V) and (VI) Sauer's inverse-type Diels-Alder methodology.

Due to the broad application of the Kröhnke methodology, several of its modifications are discussed hereafter. Shortly after Adrian *et al.* published a high-yielding four-step route to

symmetrical tpy derivatives,[184] in 1999 Sasaki *et al.* reported an even shorter synthetic route to obtain highly substituted symmetric tpys by applying a twofold Kröhnke-type strategy, as displayed in Scheme 2.[185] herein, the transformation of 2,6-diacetylpyridine (**28**) to the corresponding bis(pyridinium) iodide salt **29** via an Ortoleva-King reaction, is followed by the reaction with an appropriate α,β-unsaturated aldehyde **30** in presence of NH_4OAc, to obtain the corresponding symmetric tpy derivative **31**.

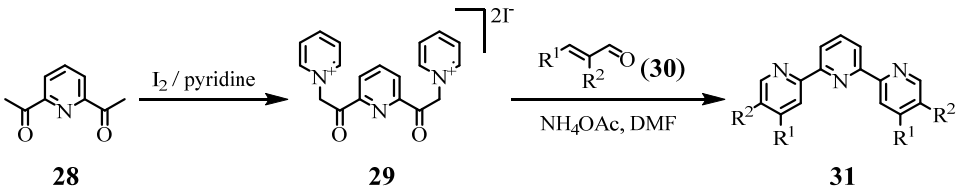

Scheme 2: Two-step variant of the Kröhnke-type condensation affording polysubstituted symmetric tpys as described by Sasaki *et al.*[185]

In 1997, Fallahpour *et al.* reported the synthesis of 4-functionalized 2,6-diacetyl-pyridines **34**, precursors for the Kröhnke methodology, starting from chelidamic acid (**32**).[186] The conversion of **32** to the corresponding 4-substituted 2,6-bis(chlorocarbonyl)pyridine **33** was followed by the treatment with Meldrum's acid prior to hydrolysis with aqueous acetic acid leading to the formation of the desired 4-functionalized 2,6-diacetylpyridines **34**. These results consequentially allowed the extension of Sasaki's procedure towards 4′-substituted tpy derivatives **35** (Scheme 3a).[187] furthermore, by applying the Tohda methodology for the formation of 3-nitropyridines,[188] it was shown that 5,5′′-dinitro-2,2′:6′2′′-terpyridine (**37**) can be obtained by the reaction of 2,6-diacetylpyridine (**28**) with electron-deficient 1-methyl-3,5-dinitro-2-pyridone (**36**) (Scheme 3b).

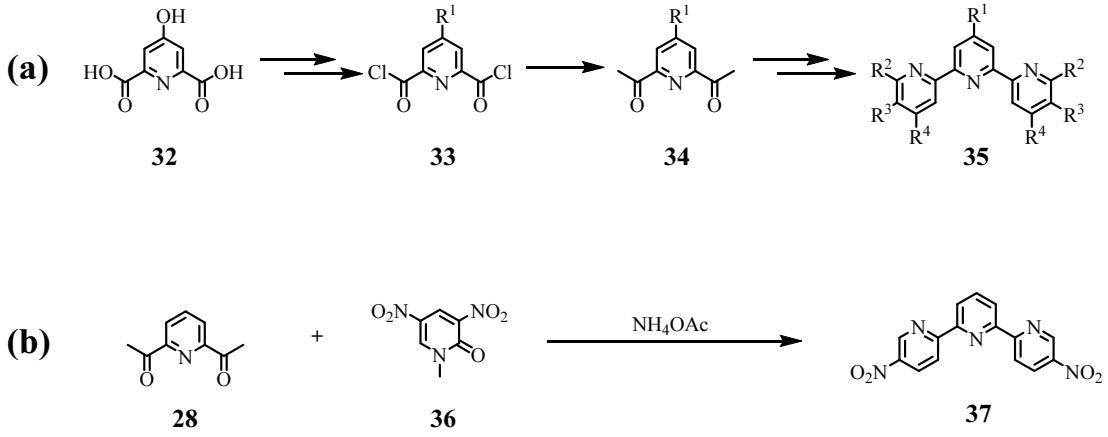

Scheme 3: (a) Illustration of the stepwise assembly of 4-functionalized 2,6-diacetylpyridines (**34**) and the subsequent transformations to the corresponding symmetric 4′-substituted poly-functionalized tpy derivatives **35**, **(b)** variant of the Kröhnke-type condensation embedding electron-deficient outer pyridine rings to afford the symmetric tpy **37**.

1.2.1.2 Cross-Coupling Methodologies

The second general approach to assemble tpys employs cross-coupling methodologies. This section focusses on palladium-catalyzed reactions, because they represent the vast majority of cross-coupling procedures. The drawback of traditional cross-coupling methods, such as the coupling of organosulfur compounds,[189] or the copper(II)-mediated coupling of lithiopyridines,[190] is, that these usually suffer from rather poor conversions and, in several cases, from low directionality. In contrast to these findings, an improved efficiency as well as readily controllable substitution patterns, mark the advantages of modern Pd(0)-catalyzed cross-coupling reactions, which consequentially in 2010 led to the awarding of the Nobel Prize in Chemistry[191–193] for the pioneering research done in this field. However, the use of cross-coupling reactions for tpy formation up to date is very limited in the literature, compared to the ring-assembly strategies discussed in the previous chapter 1.2.1.1. From the different types of Pd(0)- or occasionally Ni(0)-catalyzed cross-coupling reactions, such as the Heck-,[194–197] Kumada-,[198–200] Negishi-,[201–204] Sonogashira-,[205–207] Hiyama-,[208–210] Suzuki-Miyaura-,[211–214] and Stille cross-couplings,[215–217] the latter one has been used the most for the tpy synthesis. The advantages of this method are the multigram accessibility of the desired products, and the building blocks, as well as the possibility of a regioselective formation of tpys functionalized at the desired positions.[216] To synthesize 2,2′:6′,2′′-terpyridines by using Stille-type cross-coupling chemistry, two different approaches, utilizing the corresponding appropriate trialkylstannanes, can be employed. The first method relies on the coupling of 2,6-dihalopyridines **38**, with the appropriate 2-trialkylstannanylpyridines **39** (Scheme 4, Route A).[218–226] The second approach involves the cross-coupling of 2,6-bis(trimethylstannyl)pyridines **40**, with the corresponding 2-bromopyridines **41**, to afford the desired tpys **42** (Scheme 4, Route B).[227,228] In both cases the central and/or the outer pyridine rings can be rather modularly functionalized prior to cross-coupling, which allows for access of a broad range of usually symmetrically substituted tpy derivatives. An important drawback of Stille-type cross-couplings is the problematic purification procedure and especially the formation of highly toxic and volatile by-products during the transmetallation step and workup of the corresponding Stille cross couplings.

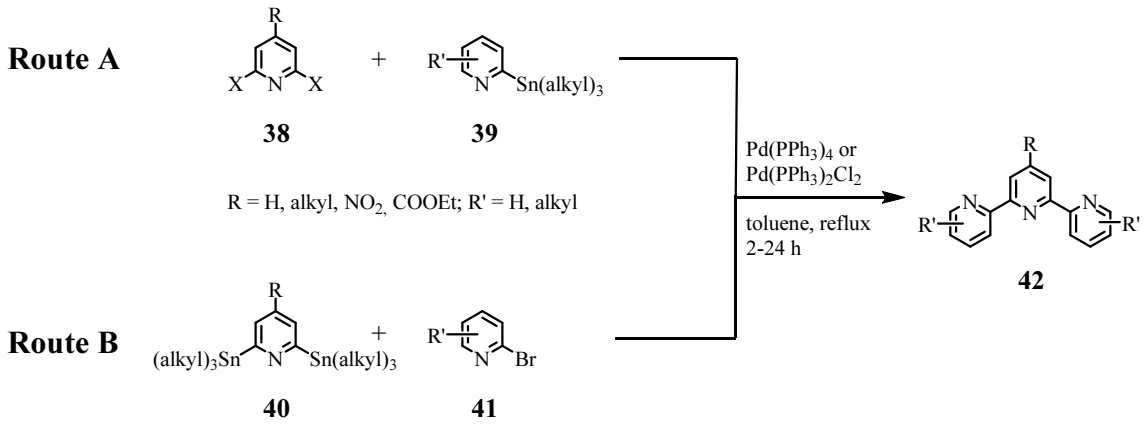

Scheme 4: Overview of the two approaches applied to synthesize substituted 2,2′:6′,2′′-terpyridines via Stille-type cross-coupling reactions.

Although other Pd-catalyzed cross-coupling procedures seem feasible for the preparation of tpys as well, only very few such examples have been reported so far. One example reported by Louërat *et al.*[229] employs a copper-mediated Hiyama cross-coupling procedure to make substituted 2,2′-bipyridines and symmetrically disubstituted tpy derivatives. Herein, they reacted 4-chloro-2-trimethylsilylpyridine (**43**) with various halopyridines **44**, to afford a variety of 4-chloro-substituted 2,2′-bipyridines **45** and even the symmetric 4,4′′-dichloro-2,2′:6′,2′′-dichloroterpyridine (**47**), if 2,6-dibromopyridine (**46**), as the corresponding halopyridine, was treated with an excess of the silylpyridine **43** (Scheme 5). Limited availability of structurally diverse starting materials, however, significantly narrows the synthetic applicability of this method for a more general approach towards tpy derivatives.

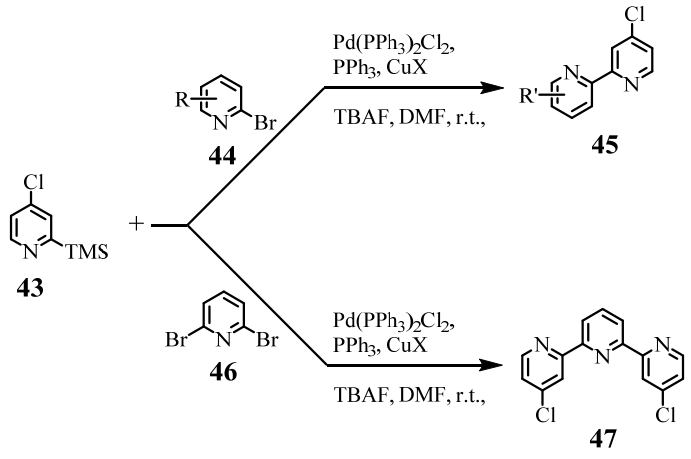

Scheme 5: Illustration of a Hiyama cross-coupling protocol describing the reaction of various substituted 2-bromopyridines with 4-chloro-2-trimethylsilylpyridine (**43**).[229]

To this day, the Negishi cross-coupling reaction has only been applied in the preparation of 2,2′-bipyridines,[230] or 2,6-di(pyridine-2-yl)benzenes,[231] but not for the preparation of tpys. The implementation of Suzuki-Miyaura cross-coupling strategies for tpy synthesis

seems particularly appealing, because of the high versatility of boronic acid / ester precursors. The lability of the required pyridin-2-yl boronic acids and their analogues (evoked by the facile proto-deboronation of these compounds), however, renders their isolation impossible. Hence, no reports on a successful tpy formation via a Suzuki-type protocol, have been reported so far.

1.2.1.3 Limitations to Applicable Substitution Patterns of Terpyridines

To this day, the variability of accessible tpy motifs underlies rather narrow restrictions. One example, is the fact that established ring-assembly strategies, particularly the classical Kröhnke methodology discussed above (Chapter 1.2.1.1), usually require an aromatic or heteroaromatic substituent at the 4′-position of the synthesized tpy moiety, as highlighted in table 1 below.

Table 1: Overview of substitution patterns at the terpyridine core and their relative appearance in the literature represented by the number of references found (search performed utilizing SciFinder™ on September 21st 2014). Herein, high numbers of references can be found for tpys including a 4′-subsituent and are marked in red, whereas frequently appearing tpys without such a 4′-substituent are marked in blue.

One substituent (asym.)	# of Ref.	Two substituents (asym.)	# of Ref.	Two substituents (sym.) at outer pyridine rings	# of Ref.	Two substituents (sym.) at outer pyridine rings + 4'-substitutent	# of Ref.	Four substituents (sym.) at outer pyridine rings	# of Ref.	Four substituents (sym.) at outer pyridine rings + 4'-substitutent	# of Ref.
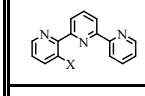	2	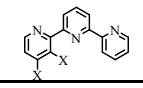	0	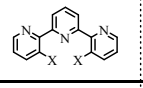	3	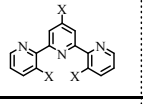	1	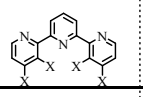	1	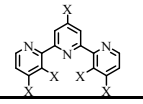	2
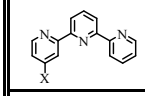	25	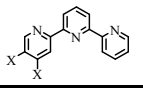	0	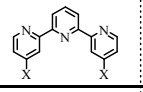	26	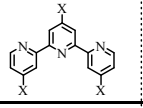	741	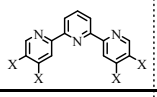	19	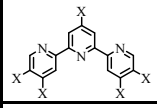	10
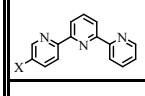	21	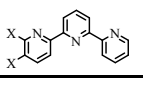	5	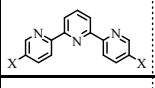	139	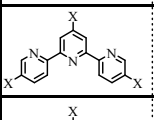	33	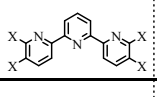	70	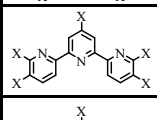	20
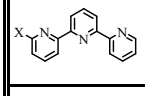	190	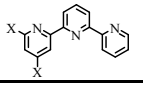	15	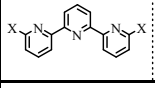	250	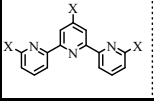	232	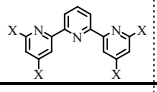	66	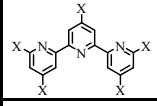	11
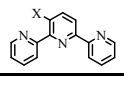	9	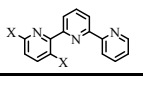	2					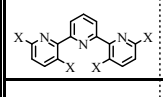	0	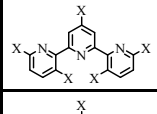	0
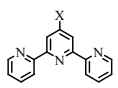	3092	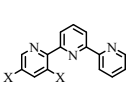	0					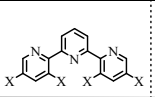	2	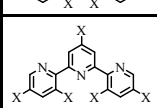	0

Furthermore, the up to date established routes allowing for the preparation of tpys with variable substituents at the outer rings rely on highly toxic organotin reagents, such as the ring-assembling Sauer methodology, or the Stille-type cross-coupling methodology discussed in the previous chapter. Table 1 gives a statistical overview of the limited accessibility of certain substitution patterns of the tpy moiety, such as at the hindered 3- and 3´´- positions of the tpy core. These limitations are in stark contrast to the very broad accessibility of a small variety of structural motives, such as especially those tpy moieties including a substituent at the 4´-position of the tpy core, namely, the classical Kröhnke tpy motif. These findings clearly disclose a variety of substitution patterns for which a decent preparation methodology is missing and might be worth exploring in the future.

1.2.2 Transition-Metal Complexes of Terpyridines

The tpy transition-metal complexes play an important role in many disciplines of modern chemistry, because of their highly versatile coordination chemistry, as well as their interesting photophysical, electrochemical, magnetic, and catalytic properties. Tpy metal complexes are thus used as central subunits in the preparation of molecular and functional devices.

1.2.2.1 Formation and Characteristics of Terpyridine Metal Complexes

The first tpy transition-metal complex was reported by Morgan and Burstall in the 1930s.[159,160] Since then, a broad variety of different tpy complexes, not only containing transition metals, but also main group metals or even lanthanide and actinide metal ions, have been reported. The reported tpy metal complexes differ from monomolecular species up to extended polynuclear macromolecules. An illustrative overview of the appearance of scientific papers or patents dealing with the various metal tpy complexes is depicted in Figure 26 below.

H																	He
Li 12	Be 0											B	C	N	O	F	Ne
Na 39	Mg 13											Al 4	Si	P	S	Cl	Ar
K 10	Ca 8	Sc 2	Ti 12	V 133	Cr 48	Mn 222	Fe 628	Co 510	Ni 249	Cu 537	Zn 342	Ga 7	Ge 5	As	Se	Br	Kr
Rb 5	Sr 2	Y 16	Zr 3	Nb 2	Mo 20	Tc 10	Ru 2370	Rh 63	Pd 108	Ag 57	Cd 101	In 16	Sn 35	Sb 4	Te	I	Xe
Cs 5	Ba 4	*	Hf 0	Ta 1	W 9	Re 50	Os 265	Ir 103	Pt 562	Au 35	Hg 30	Tl 7	Pb 27	Bi 8	Po 0	At	Rn
Fr 0	Ra 0	**															

*	La 38	Ce 17	Pr 27	Nd 54	Pm 1	Sm 34	Eu 206	Gd 52	Tb 71	Dy 39	Ho 24	Er 52	Tm 18	Yb 49	Lu 20
**	Ac 0	Th 0	Pa 0	U 19	Np 3	Pu 1	Am 2	Cm 2							

Figure 26: Periodic table of elements. For each element, the shown number represents the number of published scientific papers or patents dealing with the respective tpy metal complexes. (Search performed utilizing SciFinder™ on September 22nd 2014). Tpy metal complexes for which a surpassing amount of references has been reported are highlighted in red.

What can be seen from Figure 26 is, that tpy complexes of early transition metals can be considered as chemical obscurities, whereas tpy complexes of the late transition metals, such as metal ions with d^6 (e.g., $Fe^{(II)}$, $Ru^{(II)}$, $Co^{(III)}$ or $Os^{(II)}$), with d^8 (e.g., $Ni^{(II)}$ or $Pt^{(II)}$), or with d^{10}-configuration (e.g., $Zn^{(II)}$ or $Cu^{(I)}$), and of $Eu^{(III)}$ have been extensively studied. The by far most common coordination geometry is the (distorted) octahedral geometry, whereupon the metal core ion is usually coordinated to two tridentate ligands, forming bis(tpy) complexes with a pseudo-octahedral coordination geometry, or by one tpy ligand and additional ancillary ligands. Less common coordination geometries are for instance square-planar (e.g., $Pt^{(II)}$, $Pd^{(II)}$, or $Au^{(III)}$), or trigonal-bipyramidal (e.g., $Cu^{(II)}$) coordinative environments.[232] Because of the participation of f-orbitals rare-earth metals can have up to nine coordination sites leading to more exotic examples of metal ions binding three tpy ligands.

For the preparation of the predominantly reported bis(tpy) metal complexes, there are two different approaches, namely, either (1) a one-step procedure leading to homoleptic bis(tpy) metal complexes, which is in principle applicable to all transition metal ions forming tpy complexes (Figure 27a), or (2) a directed two-step procedure leading to heteroleptic bis(tpy) complexes (Figure 27b).

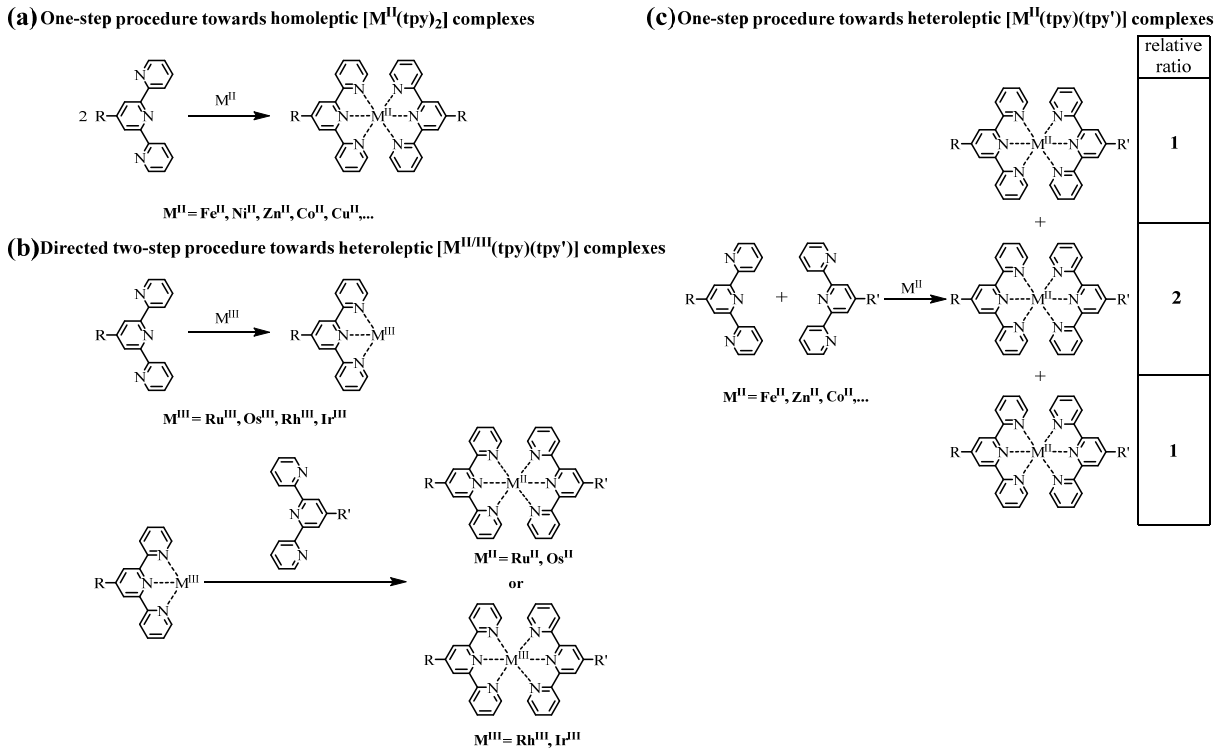

Figure 27: (a) One-step procedure towards homoleptic bis(tpy) complexes, versus **(b)** directed two-step strategy, and **(c)** altered one-step strategy towards heteroleptic bis(tpy) complexes.

Since the two-step protocol is, however, only applicable for metal ions exhibiting sufficiently high binding constants *K* to the tpy ligands (e.g., $Ni^{(II)}$,[233] $Os^{(II)}$,[234] $Ru^{(II)}$,[234,235] $Co^{(III)}$,[233] $Rh^{(III)}$,[236,237] and $Ir^{(III)}$[238]), the preparation of heteroleptic bis(tpy) metal complexes for other ions, such as the very commonly used $Fe^{(II)}$, involves the formation of kinetically labile complexes. These require a statistical synthetic approach, in one step, in order to obtain the desired heteroleptic target compounds (Figure 27c).

1.2.3 Applications of Terpyridines and Their Metal Complexes

The rich coordination chemistry of tpys as tridentate ligands together with their strong binding affinities to a broad range of different transition and rare earth metal ions forms the basis of their extraordinary electrochemical, photophysical, catalytic, and magnetic properties. These gave rise to a plethora of different applications of tpys and especially their metal complexes, such as the formation of highly versatile metallo-supramolecular architectures, biomedical applications, the introduction into a broad variety of nanostructured assemblies, and the unique optical properties and applications of the tpy metal complexes

1.2.3.1 Electrochemical and Optical Applications

One of the most popular applications of certain tpy and their metal complexes is based on the exploitation of their unique optical and electrochemical properties, in particular their high absorption coefficients. Herein, a prominent example is their high potential in the field of light-into-electricity conversion. The invention of the dye-sensitized solar cells (DSSC) in 1991 by Grätzel and O'Regan[239] marks the ultimate cornerstone of this research field. Numerous advancements have been reported over the last 20 years, such as the implementation of optimized tpy-based dyes into DSSCs, which provided cells resulting in strongly increased incident photon-to-current conversion efficiencies (IPCE), if compared to the original parent Grätzel cells.[239–242] Figure 28a depicts the exemplary setup of a classical dye-sensitized photovoltaic setup, together with the so-called black-dye (**48**),[240,243,244] as one of the most prominent Ru-tpy-based sensitizing dyes utilized within DSSCs (Figure 28b).

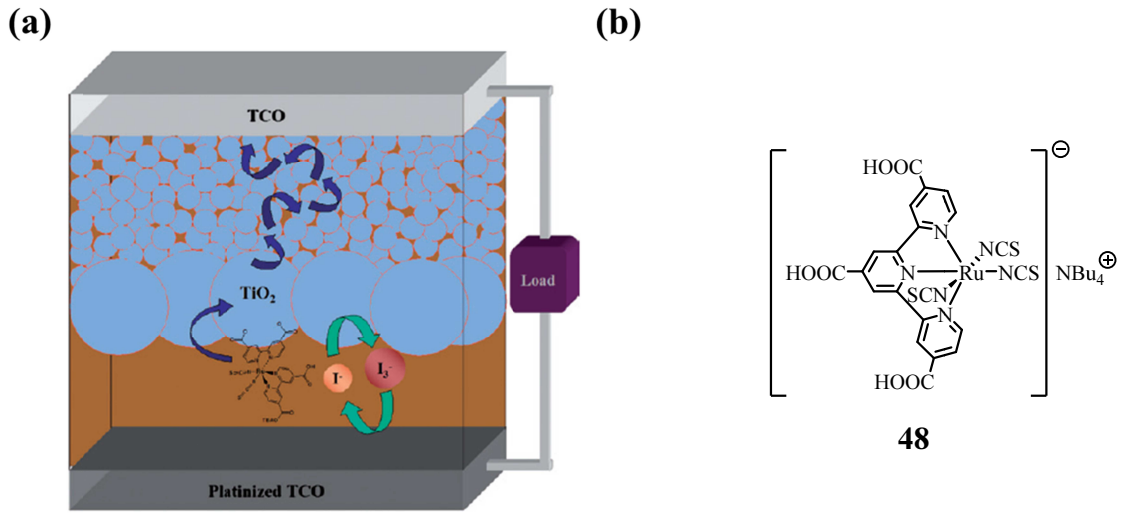

Figure 28: (a) Schematic illustration of a DSSC mainly consisting of a Ru-based light-harvesting dye bound to the TiO_2 photoanode via carboxylate groups and the I_3^-/I^--redox shuttle allowing the back–reduction of the dye after its electron injection into the TiO_2 layer. **(b)** Chemical structure of the "black dye" (**48**) as the most prominent example of a tpy-based dye utilized within DSSCs. Figure 28a reprinted with permission from Hamann *et al.*[245]

Apart from light-into-electricity conversion within DSSCs, also (electro)luminescent systems, such as organic[238,246–250] and polymeric[251–253] light-emitting diodes (OLEDs or PLEDs, respectively), light-emitting electrochemical cells (LECs),[254,255] and non-linear optical (NLO) devices[256–262] have to be named as important examples for the application of tpy-based materials in electrochemical and/or optical devices. A schematic illustration of the composition of a standard OLED system utilized in today's applications is displayed in Figure

29a. Furthermore, two interesting examples of tpy-based components used in OLEDs are depicted below. In Figure 29b a hexagonal Zn(II)-metallomacrocycle acting as a green light emitter in the OLED, and readily self-assembling due to the facile formation of the tpy-Zn(II)-tpy motif, is shown. Figure 29c illustrates two interesting trisubstituted benzene derivatives including bpy and tpy subunits within the molecule, namely, 1,3-bisbipyridyl-5-terpyridylbenzene (**49**) and 1-bipyridyl-3,5-bisterpyridylbenzene (**50**). These two structures were investigated as potential electron-transporting materials for the implementation into novel OLED devices.

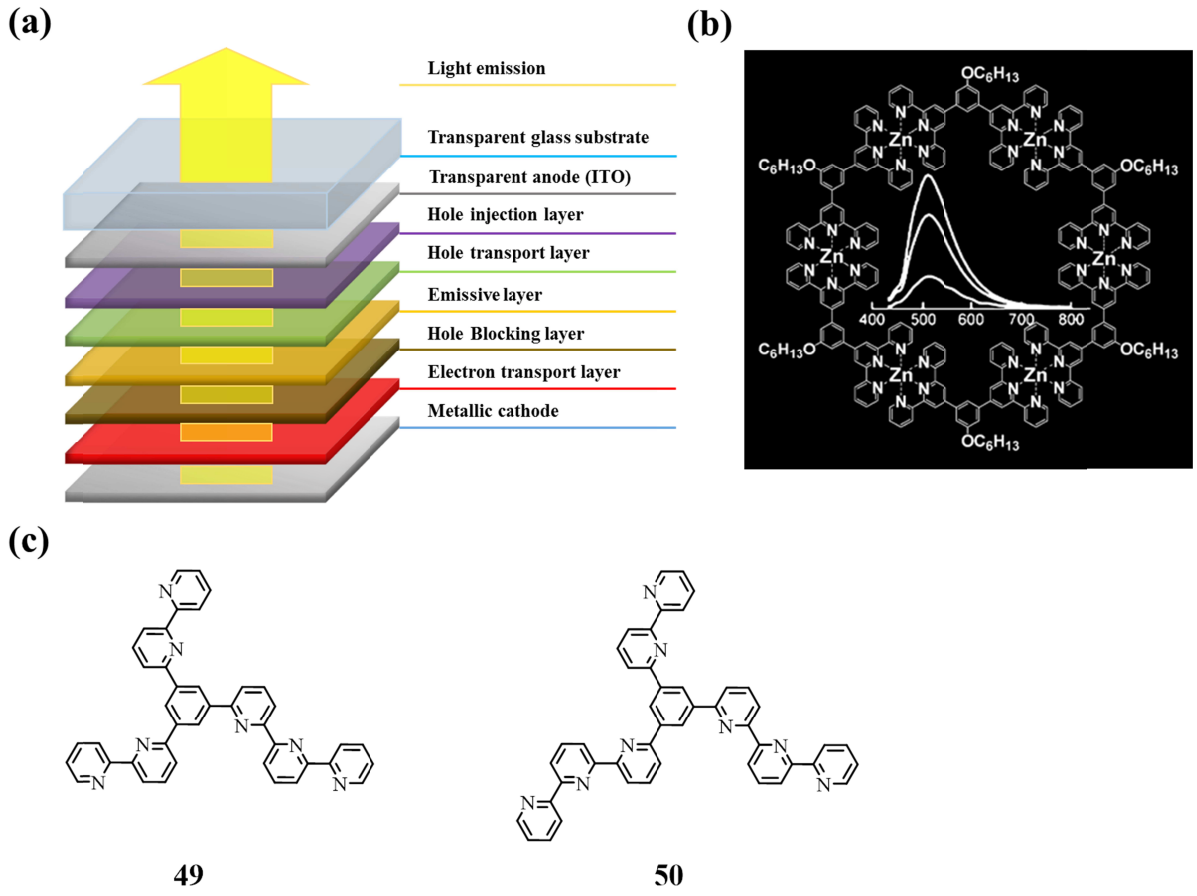

Figure 29: (a) Schematic illustration of the different components constituting a classical OLED, **(b)** depiction of a hexagonal Zn(II)-metallomacrocycle acting as a green light emitter, **(c)** Illustration of the chemical structures of two new tpy-based electron-transporting materials. Figure 29b reprinted with permission from Hwang *et al.*[247]

1.2.3.2 Metallo-Supramolecular Architectures and Polymeric Structures

Due to the facile complexation of tpy ligands with a broad variety of transition and certain rare earth metals these molecular entities tend to build up larger polytopic, dendritic or even bigger structural assemblies. The overwhelming variety of supramolecular structures based on the assembly of tpy moieties, especially 4′-substituted tpy units, has been repeatedly reviewed over the last decades. Thus from the virtual plethora of reported metallo-supramolecular architectures[234,263–266] only selected examples can be highlighted hereafter. Exemplarily the assembly of a molecular "Sierpinski hexagonal gasket", utilizing Fe- and Ru-based tpy complexes, is illustrated below (Figure 30),[267] as reported by Newkome *et al.*.

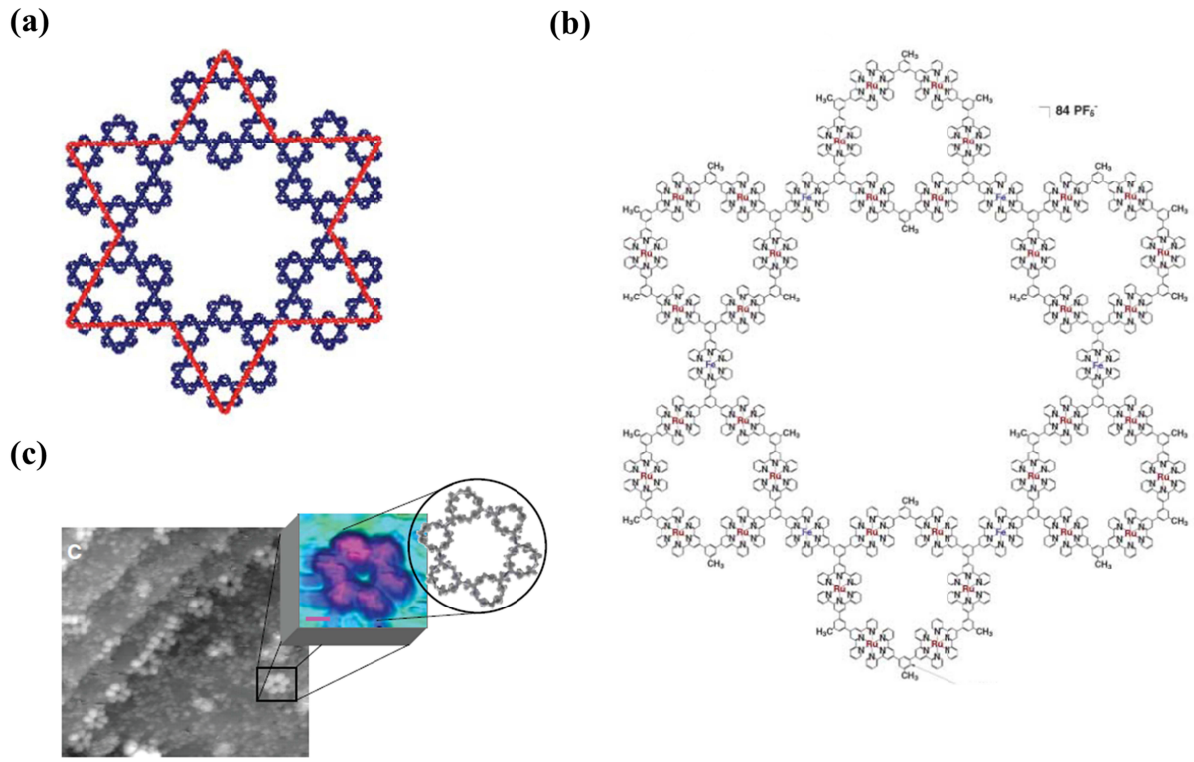

Figure 30: (a) Illustration of Sierpinski's hexagonal gasket incorporating the Star of David (red) and the Koch snowflake motifs (blue), **(b)** depiction of the chemical structure of the hexagonal gasket, **(c)** UHV-STM images revealing a linear formation of gaskets, together with a color-enhanced, enlarged extract displaying a single molecular gasket. Figure reprinted with permission from Newkome *et al.*[267]

In addition there have been reports on dendritic molecular networks based on tpy metal complexes,[268,269] as well as on molecular muscles consisting of mechanically interlocked ligands comprising tpy units,[270–273] or on functional polymers containing tpy metal complexes,[274–276] such as fully π-conjugated polymers with pendant tpy substituents showing pronounced ionochromism as well as distinct metal-dependent photoluminescence quenching

effects.[277,278] The described features for instance give rise to the potential application of these π-conjugated polymers as highly sensitive and specific fluorometric chemosensors. Furthermore, there have been reports on self-assembly processes reversibly switchable by external triggers, such as base-induced switching for certain metallo-macrocycles,[279] or redox-state dependence for helical structures.[280–282] Finally, the development of supramolecular co(polymer) architectures, derived from the facile tpy-metal connectivity, shall be named, which potentially dangles an implementation of the resulting systems towards "self-healing" materials.[283–287] Herewith manifold possibilities arising from the described properties can be envisaged, such as for instance potential switching of chemical and/or physical properties triggered by external stimuli like e.g. pH value or temperature.[233,288–290]

1.2.3.3 Biomedical Applications

Another interesting and important field, in which tpys and their metal complexes are of high potential use, is correlated to clinical applications.[291–294] Amongst these especially square-planar tpy complexes of Pd(II), Pt(II), and Au(III),[291,292,295–298] or octahedral tpy complexes of Ru(II), Ru(III), and Ir(III),[293,294,299–301] respectively, play a superordinate role. Examples of typical biomedical applications are for instance deoxyribonucleic acid (DNA) intercalation,[291,293,296,298,302] covalent or strongly coordinative binding to biomolecules,[294,295,297,299] labeling and sensory applications,[297,301,303–305] and chemo- or radiotherapy,[291,293,295,296] respectively. Hereafter, only two examples of the potential biomedical application of tpy-based materials shall be highlighted. The first example is the non-covalent DNA intercalation of square-planar $[Pt(tpy)HET]^{2+}$ (**51**) (Figure 31a), leading to neighbor exclusion binding of the intercalator to the DNA (Figure 31b+c), and hence resulting in promising cytotoxic effects dangling potential chemotherapeutical applications of the described compound.[291,292,298,302,306] The conceptual design, that platinum complexes belonging to this class, and comprising planar, aromatic ligands, may intercalate with DNA and therefore act as potential anticancer drugs, is essentially relying on the known working principle of planar dyes, such as ethidium bromide (**52**) as DNA intercalators [307]

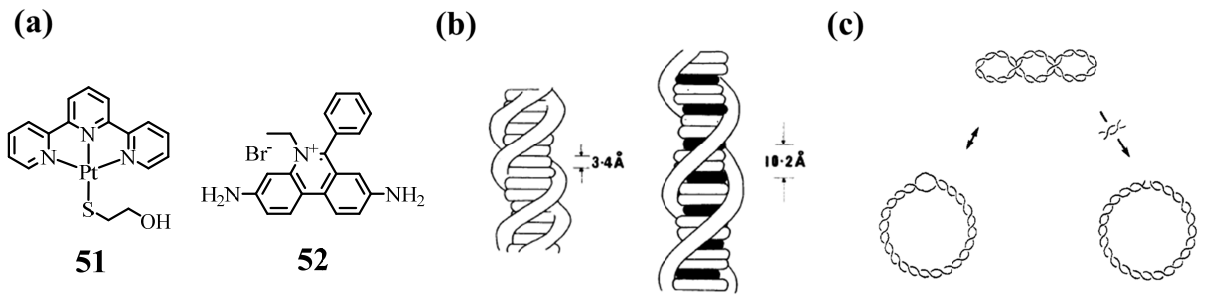

Figure 31: (a) Chemical structures of two DNA intercalators (square-planar Pt-tpy derivative **51** and the planar dye ethidium bromide (**52**)), **(b)** schematic illustration of a normal, double helical DNA strand (left) versus an intercalated system exhibiting neighbor exclusion binding an intercalator to the double-stranded DNA molecule (right), **(c)** observed unwinding of closed circular DNA upon intercalation of **51** or **52** into the superhelical or circular DNA molecules. Figures 31b and 31c are reprinted with permission from Lippard *et al.*[291] resp. Bond *et al.*[306]

The second example involves the examination of the covalent binding of [Ru(tpy)(bpy)Cl]Cl (**53**) and *mer*-[Ru(tpy)Cl_3] (**54**) to DNA molecules.[293,308] The utilization of the latter complex results in a 2% ratio of interstrand cross-links, going along with strong cytostatic activity against certain types of leukemia cells (e.g. type L1210 cells) well comparable to the activity of cis-platin or carboplatin. The structures of the biomedical active Ru-tpy agents **53** and **54** is shown in Figure 32a, whereas Figure 32b depicts the *trans*-configurational binding of **54** to two different guanine derivatives as DNA model bases illustrating the likely binding mechanism during the observed interstrand DNA cross-linking.

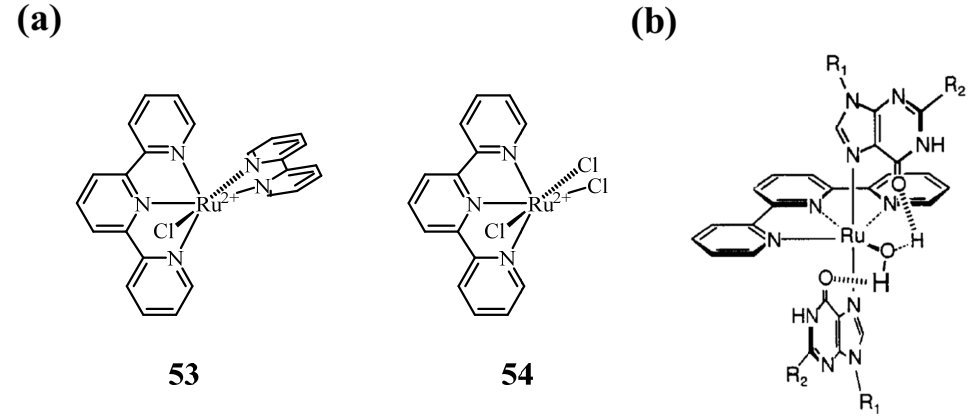

Figure 32: (a) Chemical structures of the two biomedical active Ru-tpy complexes [Ru(tpy)(bpy)Cl]Cl (**53**) and *mer*-[Ru(tpy)Cl_3] (**54**), **(b)** schematic illustration of the *trans*-configurational binding of **54** to two guanine derivatives as DNA model bases (R_1 = Me or Et; R_2 = H or NH_2). Figure 32b reprinted with permission from van Vliet *et al.*[293]

1.2.3.4 Terpyridines in Nanostructures

A last big fraction of promising applications of tpys and their metal complexes is represented by the functionalization of, and especially the tpy's self-assembly features onto nanostructures, such as silver,[309] gold,[310–312] TiO_2, CdS, polyoxometalates,[313] and carbon nanotubes,[314] or onto other more ordered surfaces, such as glass,[315] gold,[310,316–321] platinum,[322] indium tin oxide,[314] silicon,[314,315,323] glassy carbon surfaces,[324] or highly oriented pyrolytic graphite (HOPG).[322,325] Due to the versatility of the varying types of self-assembly or generally surface functionalization of tpys and their complexes in the field of nanochemistry, only selected examples can be illustrated hereafter. With regard to the methods applied within this thesis the examples discussed below are focused on the immobilization of tpy-related structures onto gold nanostructures and surfaces. A very appealing example has been reported by Tuccitto *et al.*, with their ~40 nm long, easy accessible and highly conductive molecular wires, assembled via the stepwise incorporation of metal centers (Fe^{II} / Co^{II}) and 1,4-di(2,2′:6′,2′′-terpyridine-4′-yl)benzene as the required ditopic tpy ligand onto Au surfaces functionalized with a mixed SAM containing 4′-(4-mercaptophenyl)-2,2′:6′,2′′-terpyridine as the tpy ligand and mercaptobenzene as the lateral spacer in a 1:1 ratio (Figure 33).[317,320]

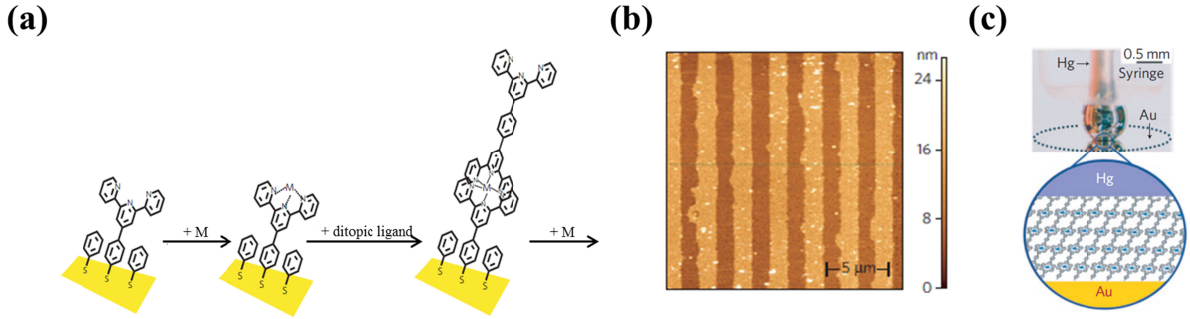

Figure 33: (a) Schematic representation of the stepwise assembly of the molecular wire onto the 4′-(4-mercaptophenyl)-2,2′:6′,2′′-terpyridine-functionalized Au surface utilizing Fe(II) or Co(II) metal ions and 1,4-di(2,2′:6′,2′′-terpyridine-4′-yl)benzene as ditopic ligand, **(b)** AFM height image illustrating the highly ordered alignment of the molecular wires onto the Au surface, **(c)** photograph and schematic illustration of the Au/molecular wire/Hg-junction used during the electrical characterization of the molecular wire's properties. Figure 33a is adapted and figures 33b+c are reprinted with permission from Tuccitto *et al.*[317]

In a second example Chan *et al.* described the self-assembly, disassembly, and partial subsequent reassembly of Au nanorods by utilizing the connectivity derived from the bis-tpy-metal complexes of Fe(II) or Cd(II), respectively (Figure 34).[311]

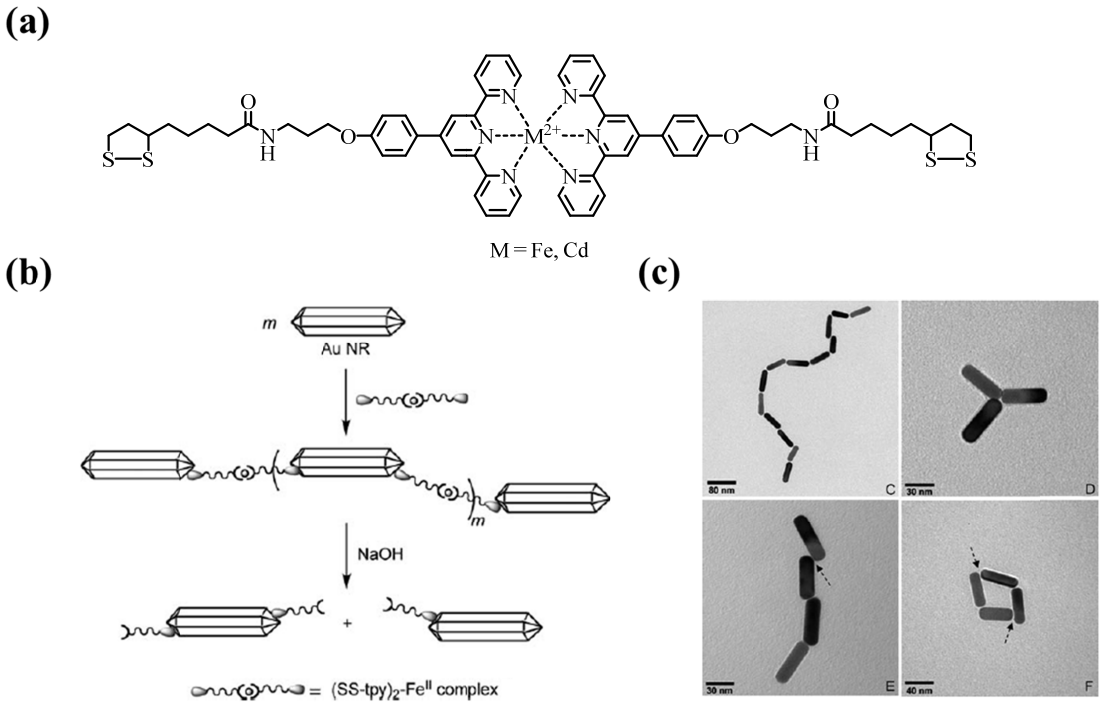

Figure 34: (a) Chemical structure of $[(SS\text{-}tpy)_2\text{-}M^{2+}]$ complexes, **(b)** schematic illustration of the idealized connection between the bis-tpy-metal complexes and the Au nanorods, depicting both, assembly and disassembly processes, **(c)** transition electron microscopy (TEM) images showing a varying connectivity between the nanorods (linear end-to-end (C), branched (D), end-to-end or end-to-wall (E), cyclic (F)). Figures 34b and c modified and reprinted with permission from Chan *et al.*[311]

What can be seen from this example is, that although extensive research has been done in the area of nanochemical utilization of tpys and their metal complexes, and despite the fact, that various highly interesting results have been obtained so far, it remains a challenge to obtain distinct nanostructural assemblies in a controlled fashion.

1.3 Aryl-Aryl Bond Formations – Pd(0)-Catalyzed Cross-Couplings

As already adumbrated in chapter 1.2.1.2 the development and ongoing subsequent improvement of Pd(0)-catalyzed cross-coupling reactions marks one of the groundbreaking, if not the utmost important discovery in the field of synthetic polyaromatic organic chemistry within the last decades.[191–193] Among all the diverse applications of these Pd(0)-catalyzed cross-coupling reactions one of the most appealing and therefore most extensively used applications is the utilization of cross-coupling reactions for the formation of aryl-aryl bonds. Over the last century a broad variety of different approaches has preceded the methods used for aryl-aryl couplings nowadays. Amongst this multitude of different synthetic pathways the probably most well-known representatives are the Ullmann coupling, the Kumada coupling, the Negishi cross-coupling, the Stille cross-coupling, and the Suzuki-Miyaura cross-coupling reaction. Whereas the original Ullmann coupling, reported in 1901,[326] relied on the use of stoichiometric amounts of copper for the reductive coupling of aromatic halides to the corresponding biaryls, and on top of that required harsh reaction conditions (T ≈ 200 °C), over the years many advancements of the classical Ullmann coupling, such as for instance those allowing the formation of unsymmetrical biaryls, were developed and repeatedly reviewed.[327–330] One of the general disadvantages of the Ullmann coupling, which is also valid for the Kumada coupling, is the limited compatibility with a broad range of functional groups. For the Kumada coupling, which was developed independently by the groups of Kumada and Corriu in the early 1970's,[198–200,331,332] and which is relying on the mostly nickel-catalyzed coupling of an aryl Grignard reagent (Ar^1MgX, X = halogen) with an aryl halide or triflate (Ar^2X, X = halogen, -OTf) in order to yield the desired biaryls (Ar^1-Ar^2), naturally the presence of aldehydes, ketones, esters, and nitro groups is precluded, due to the utilization of a Grignard reagent. In the mid 1970's, also the Negishi cross-coupling was developed,[201–204] which, instead of Grignard reagents, utilizes arylzinc derivatives (Ar^1ZnX, X = halogen), for the palladium-catalyzed coupling with an aryl halide or triflate (Ar^2X, X = halogen, -OTf), and therefore readily tolerates the previously excluded functional groups. In the late 1970's, the Stille cross-coupling reaction started to gain recognition for the synthesis of biarylic compounds.[215–217] In this novel palladium-catalyzed approach arylstannanes (Ar^1SnR_3, R = Me, Bu) are coupled with aryl halides or triflates (Ar^2X, X = halogen, -OTf). As a clear advantage, compared to the previous methodologies, the Stille reaction turned out to be highly versatile, and, due to the mild and neutral reaction conditions, tolerates the

presence of an even broader variety of substituents on both aryl coupling partners. Compared to the Kumada or the Negishi reaction, the clear disadvantage of the Stille coupling is, however, the extraordinary toxicity of the utilized organostannanes and volatile tin-containing byproducts of the Stille cross-coupling reaction. Sharing the advantages of the Stille cross-coupling reaction, such as elevated efficiency and almost general applicability towards highly diverse substitution patterns, the Suzuki-Miyaura reaction,[211–214] developed in the early 1980's, circumvents these toxicity issues related to the use of organotin derivatives, by the utilization of arylboronic acids or esters ($Ar^1B(OR)_2$, R = e.g., H, ^{i}Pr, pinacol) instead. A general overview of the last four mentioned coupling reactions (Kumada, Negishi, Stille, and Suzuki-Miyaura coupling) is given in Scheme 6. Because the Suzuki-Miyaura cross-coupling reaction is used the most it is exemplarily discussed in more detail in the following chapters.

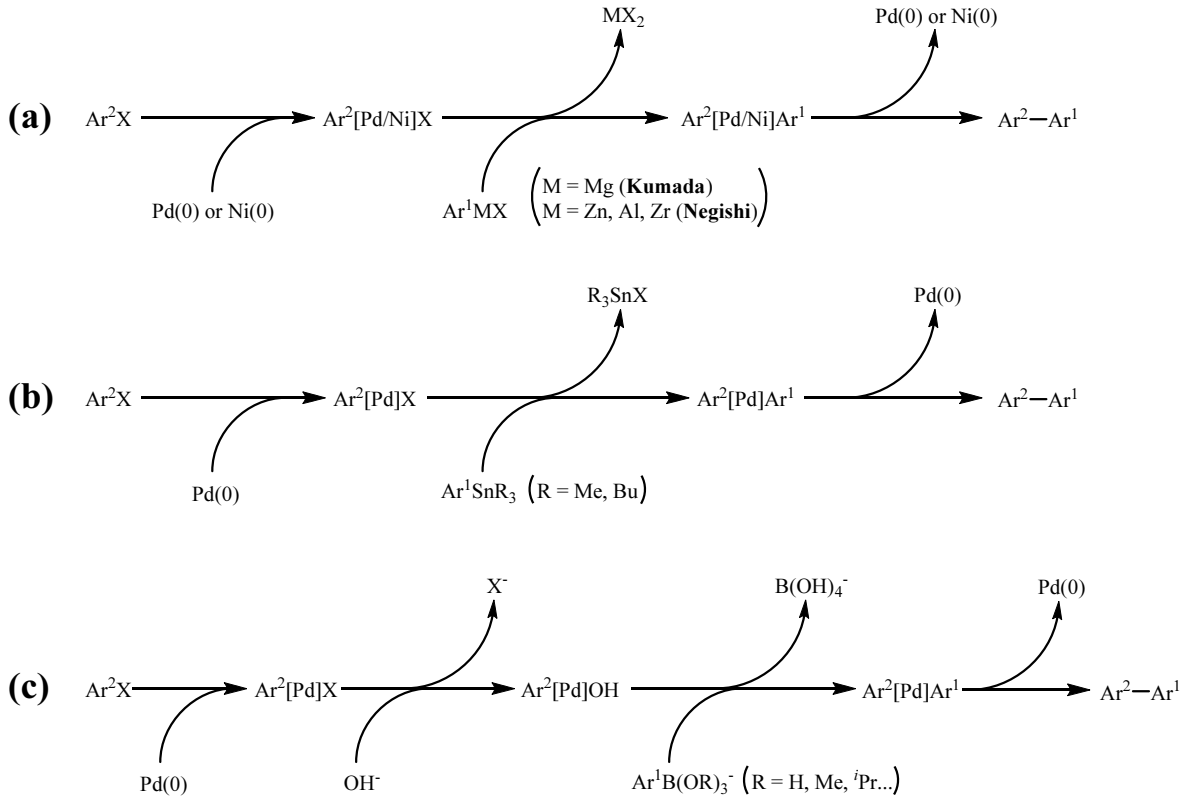

Scheme 6: Schematic illustration of the three main different approaches applicable for the formation of unsymmetrical biaryls: **(a)** Kumada respective Negishi cross-coupling pathways, **(b)** Stille cross-coupling procedure, and **(c)** Suzuki-Miyaura cross-coupling protocol.

1.3.1 The Suzuki-Miyaura Cross-Coupling

In the Suzuki-Miyaura cross-coupling reaction, just as in all the other Pd(0)-catalyzed coupling reactions, namely, Kumada-, Negishi-, Heck-, Hiyama-, Sonogashira-, and Stille-coupling alike, the catalytic cycle consists of three main consecutive steps. These are the oxidative addition, the transmetallation, and the reductive elimination. The oxidative addition, describing the addition of an organic halide (or another electrophile) (R^1-X) to a Pd(0) complex under formation of a R^1-Pd(II)-X species, and the reductive elimination, which describes the elimination of the coupling product R^1-R^2 under concerted regeneration of the Pd(0) catalyst species, are comparable for all the named cross-coupling reactions. It is the transmetallation step, however, which differentiates and thus characterizes each of the specific cross-coupling reactions. For the Suzuki-Miyaura cross-coupling, this transmetallation step involves the reaction of the R^1-Pd(II)-X species, originating from the oxidative addition, with an activated boronate species $[R^2\text{-B(OR}')_2\text{OR}]^-$, formed from $R^2\text{-B(OR}')_2$ with the aid of base (OR^-), to yield the intermediate R^1-Pd(II)-R^2 as the intermediate for the subsequent reductive elimination to afford the product. Figure 35 illustrates the simplified catalytic cycle of the Suzuki-Miyaura coupling.

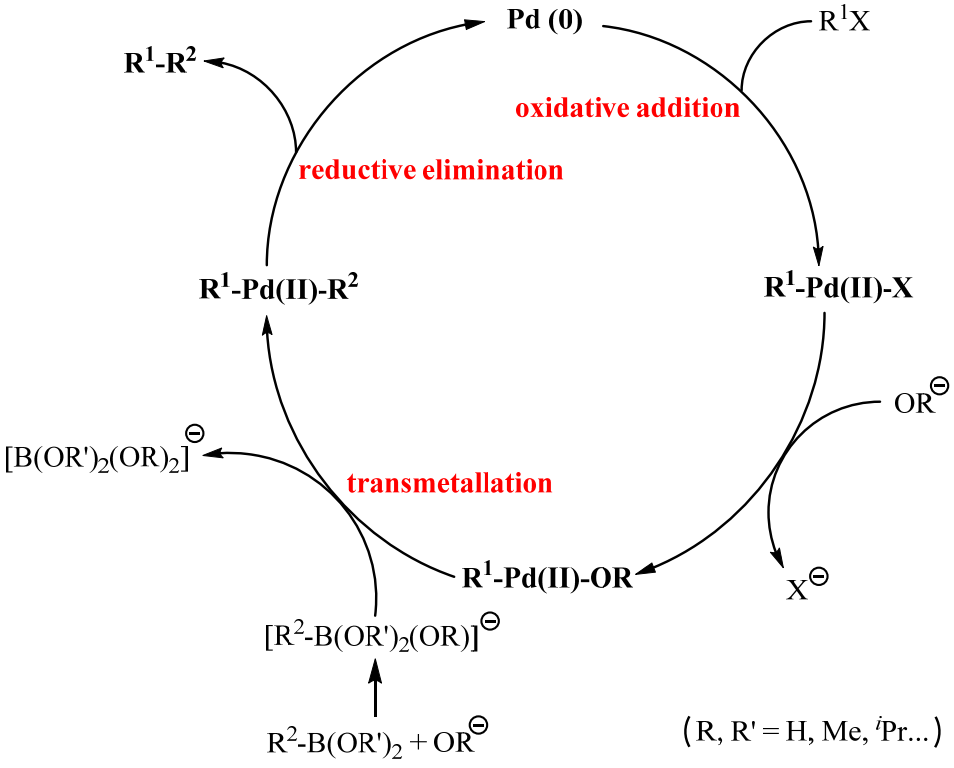

Figure 35: Schematic illustration of the catalytic cycle of a Suzuki-Miyaura cross-coupling.

As the different steps of the catalytic cycle, as well as scope and potential side-reactions of the Suzuki-Miyaura coupling have been extensively reviewed in literature,[211,333–343] only the most important facts are highlighted and summarized in the section below.

The Catalytic Cycle – The Oxidative Addition

The oxidative addition of the organohalide to the Pd(0) catalytic center often represents the rate-determining step of the Suzuki-Miyaura cross-coupling reaction. The reactivity of the corresponding haloarenes, follows the order: I > OTf ≈ Br >> Cl.[211] This order has been attributed to the relative bond strengths of the C-X bonds, and exhibits the inverted order of the bond dissociation energies of the Ph-X bonds.[344,345] Interestingly, the presence of electron-withdrawing groups (EWGs) in proximity of the halide, increases the reactivity of the halide, and allows for the utilization of less reactive aryl chlorides.[340] Generally, a broad range of different Pd-based catalysts can be utilized, whereat one usually distinguishes between two different scenarios:

(1) Either a preformed catalyst exhibiting the active, and thus less air-stable, oxidation state 0 is used right from the start (e.g., for $Pd(PPh_3)_4$), or
(2) a system of a Pd pre-catalyst, usually in the oxidation state +2, with an appropriate coordinating ligand, usually a phosphine or occasionally an amine derivative, is used, in order to reductively evolve the catalytically active form of the catalyst system in situ (e.g., for $PdCl_2(PPh_3)_2$ or for $Pd(OAc)_2/PPh_3$).

The Pd(II) catalyst is more air-stable than its Pd(0) analogues, and simplifies its handling during organic syntheses. Furthermore, the reactivity of the Pd catalysts depends on the Pd/P-ratio, as well as on the bulkiness and on the donating ability of the phosphine ligands. On top of that, Pd catalysts comprising less than four monodentate, less than two bidentate or extremely bulky phosphine ligands, respectively, turned out to be significantly more reactive during oxidative additions, because they stabilize coordinatively unsaturated Pd-species. It has been found that among these coordinatively unsaturated Pd-species, either a monophosphine Pd(0)L or a bisphosphine $Pd(0)L_2$ complex is the actual active species that takes part in the oxidative addition to organic halides.[346–348] The use of weakly coordinating ligands, such as $AsPh_3$, or of extra bulky phosphines (Table 2), such as $P(^tBu)_3$ or $P(c\text{-}C_6H_{11})_3$, can further facilitate the formation of those coordinatively unsaturated Pd-species, due to the large cone angles the named ligands exhibit at the coordinative environment of the Pd-center.

Table 2: Overview of the cone angles and coordination numbers of $M(Ph_3)_n$ (M = Pd, Pt).[212,349]

	PEt_3	PPh_3	$P(^iPr)_3$	$P(c\text{-}C_6H_{11})_3$	$P(Ph)(^tBu)_2$	$P(^tBu)_3$
Cone angle (°)	132	145	160	170	170	182
Coord. number (*n*)	3 or 4	3 or 4	2 or 3	2	2	2

Additionally, the electron-donation to the Pd(0) center has an important impact onto the efficiency of the oxidative addition process. Whereas $P(Ar)_3$-ligands are effective for the addition of aryl iodides, -bromides, or –triflates, they are insufficient for the addition of deactivated, electron-rich chloroarenes.[350] Here more bulky, highly donating ligands are required, such as $P(^tBu)_3$,[347,348] R-P(adamantyl)$_2$,[351] 2-(di-*t*-butylphosphino)biphenyl,[352,353] or Qphos,[354] which allow for a reaction even at room temperature. All the bulky ligands depicted below (Figure 36) easily donate electrons to the Pd(0) center and readily dissociate, leaving the required coordinatively unsaturated complexes.

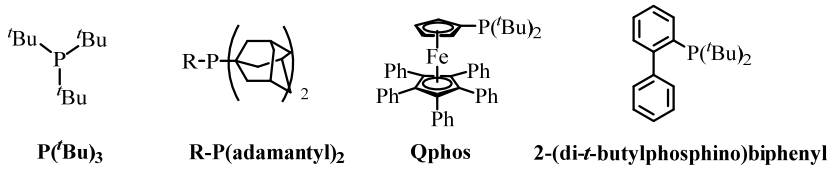

Figure 36: Depiction of bulky, highly electron-donating ligands applicable for the oxidative addition of chloroarenes during Suzuki-Miyaura cross-coupling reactions.

In contrast to the findings discussed above, it has been found, that less bulky phosphines are more suitable for slow reactions of highly functionalized substrates, as they yield stable complexes at higher temperatures, too. Figure 37 highlights several of these special tailor-made ligands, such as PCy_3,[347,348,355] (*o*-biphenyl)PCy_2,[352,353,356] $(^tBu)_2POH$,[357,358] and *N*-heterocyclic carbenes.[359–364]

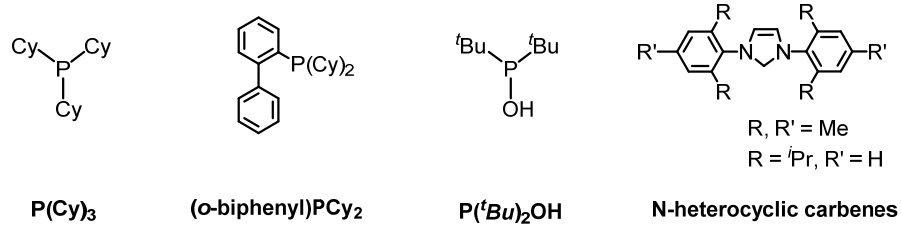

Figure 37: Depiction of several bulky ligands ideally suitable for slow reactions of functionalized substrates, due to an improved thermal stability and an undiminished high reactivity towards the oxidative addition of problematic substrates.

The Catalytic Cycle – The Transmetallation

Whereas the processes found during oxidative addition and reductive elimination are similar for most of the Pd(0)-catalyzed cross-coupling reactions and sufficiently well studied and understood, it is the transmetallation step which characterizes each individual type of cross-coupling. This transmetallation step strongly depends on the nature of the utilized organometallic reagent, as well as on the applied reaction conditions. For the Suzuki-Miyaura cross-coupling there are two widely accepted mechanisms for the transmetallation step, involving either tri- or tetravalent organoboron species. Whereas trivalent organoboron compounds **55** are usually not able to react with the R^1-Pd(II)-X (X = Cl, Br, I, OTf) species **57**, the tetravalent "ate"-complexes **56**, formed in the presence of a negatively charged base, such as $[RBBu_3]^-Li^+$,[211] $[Ph_4B]^-Na^+$,[365] $[R_3BOMe]^-Na^+$,[366,367] or $[ArB(R)(OR)_2]^-Li^+$,[368,369] readily react with **57**. The reason for the increased reactivity is attributed to the enhanced nucleophilicity of the group R^2 attached to the boron atom. This increased nucleophilicity arises from the base-induced quaternization of the organoboron species **55**, and readily allows the transfer of this organic group R^2 onto the Pd(II) center during the transition state **58** of the transmetallation. This organic group transfer leads to the liberation of **59** (R^1-Pd(II)-R^2), which will then be further transformed to the desired coupling product **60** (R^1-R^2) in the subsequent reductive elimination step (Scheme 7).

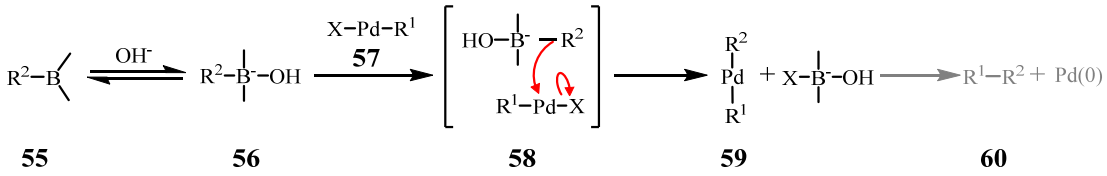

Scheme 7: First transmetallation mechanism describing the reaction of **57** (R^1-Pd(II)-X) with a tetravalent organoborate species **56**, previously formed from **55** via base-induction, and the subsequent formation of **59** (R^1-Pd(II)-R^2) as the starting point for the final reductive elimination step yielding the desired product **60** (R^1-R^2).

Additionally, it has been found that also hydroxyboronate anions $[R^2B(OH)_3]^-$ can act comparably strong alkylating or arylating, as the previously described quaternized organoboronate species. However these tetravalent anions are in equilibrium with the free boronic acid species $R^2B(OH)_2$ leading to a pH-dependent reaction efficiency of the transmetallation step, which is favored at elevated pH values above 9, in contrast to the pH-independent reactions of, for example, Ph_4BNa.[370]

The second proposed mechanism for the transmetallation step during Suzuki-Miyaura cross-couplings involves (1) a halide-base exchange, transforming the intermediate **57**

(R^1-Pd(II)-X) into **61** (R^1-Pd(II)-OR), with OR^- = OH^-,[371] OMe^-,[372] OAc^-,[373] OAr^-, or acac. The subsequent reaction of **61** with a trivalent boron derivative **55**, usually a boronic acid, (2) results in the formation of the intermediate **62**, from which **59** (R^1-Pd(II)-R^2) is readily liberated during the concerted exchange mechanism between -R^2 and -OR in the following step (Scheme 8). The driving force of this exchange reaction is the enhanced reactivity of RO-Pd complexes, which is usually attributed to the high basicity of the Pd-O species, as well as to the high oxophilicity of the boron center.

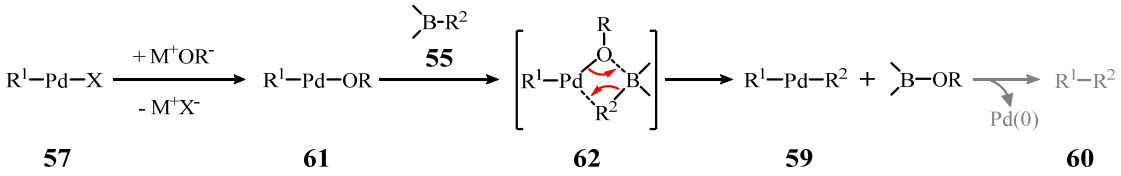

Scheme 8: Second transmetallation mechanism describing the reaction of R^1-Pd(II)-OR (**61**) with a trivalent organoboron species **55**, to **59** (R^1-Pd(II)-R^2) after passing the transition state **62** and following the precedent formation of **61** from **57** (R^1-Pd(II)-X) via a halide/base exchange.

As a consequence, in the case of the oxidative addition of organic electrophiles R^1-OR to Pd(0), which directly yield **61** (R^1-Pd(II)-OR), no base is needed to trigger the transmetallation step of the Suzuki-Miyaura cross-coupling reaction.

The Catalytic Cycle – The Reductive Elimination

The role of the reductive elimination within the catalytic cycle is the regeneration of the catalytically active Pd(0) species and the formation of the desired cross-coupling product **60** (R^1-R^2) from the precursor **59** (R^1-Pd(II)-R^2). It has been shown, that the reductive elimination of **60** only occurs from the *cis*- **59**, whereas *trans*-**59** first has to be transformed to *cis*-**59** in order for the elimination to occur.[374–379] There are two accepted mechanisms for this final reaction step of the Suzuki-Miyaura coupling, namely, the non-dissociative / non-associative mechanism (Scheme 9), or the dissociative mechanism (Scheme 10).

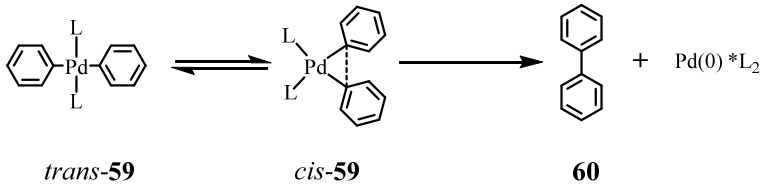

Scheme 9: Schematic illustration of the non-dissociative / non-associative pathway as proposed mechanism for the reductive elimination of **60** (R^1-R^2) from the cis-isomer of **59** (R^1-Pd(II)-R^2).

The order of the reactivity (diaryl > (alkyl)aryl > dipropyl > diethyl > dimethyl-Pd(II)·L_2), which was found for the reductive elimination step of Suzuki-Miyaura cross-couplings, suggests the participation of the π-orbitals of the aryl-groups in the *cis*-form of **59** during the R^1-R^2 bond formation.[380] It has been shown, that **60** can be directly eliminated from the tetra-coordinated *cis*-alkenyl and *cis*-aryl-Pd(II) complexes (*cis*-**59**) (non-dissociative mechanism - Scheme 9).[380,381] Since the thermolysis of (dialkyl)Pd(II)·L_2, and thus the liberation of **60** (R^1-R^2) therefrom, is inhibited by the addition of excess phosphine L, it seems feasible, that in this case the dissociation of one phosphine ligand represents the rate-determining step of the reductive elimination process and is thus inevitably required in order to allow the reductive elimination to proceed (dissociative mechanism - Scheme 10).[375–379]

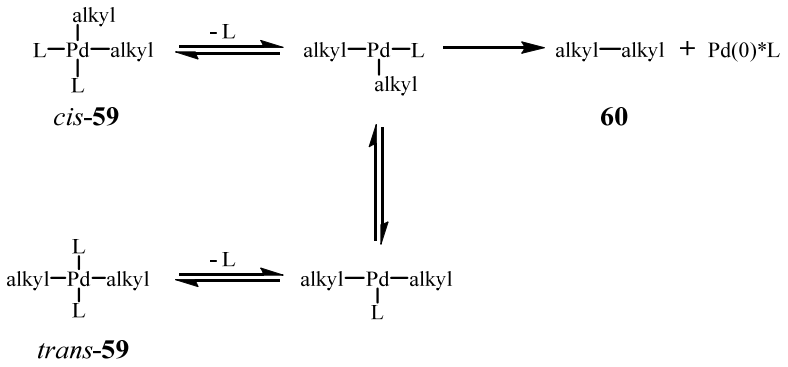

Scheme 10: Illustration of the dissociative reductive elimination mechanism of **60** (R^1-R^2) from **59** (R^1-Pd(II)-R^2), which was shown to be in particular valid for the elimination of di-alkyl compounds **60**.

Furthermore, the effect of the phosphine ligand onto the reductive elimination process can be linearly attributed to the ease of the ligand's dissociation from the Pd(II) center: dppe << PEt_3 < PEt_2Ph < $PMePh_2$ < $PEtPh_2$ < PPh_3. Therefore bisphosphine ligands exhibiting large P-M-P-angles, such as dppb, dppp, or dppf (Figure 38), are especially designed to accelerate such troublesome examples of reductive eliminations, particularly in the range of the coupling of alkylmetals (sp^3-couplings). In contrast to these findings it has been shown, that **60** is directly eliminated from the tetra-coordinated complexes of *cis*-alkenyl and *cis*-aryl-Pd(II) complexes (non-dissociative mechanism - Scheme 9).[380,381]

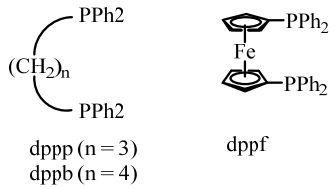

Figure 38: Overview of several tailor-made bisphosphine ligands exhibiting large P-M-P-angles

The Effect of Water and Bases in Suzuki-Miyaura Couplings

As described above cross-coupling reactions of organoboronic acids require the presence of a negatively charged base. Thus, in contrast to other cross-coupling reactions, in which not only oxygen, but also water, highly disturbs or even inhibits the reactions, for Suzuki-Miyaura cross-couplings the use of water is usually required, or at least accelerates the coupling reaction by several orders of magnitude. Usually at least two equivalents of water, as well as two equivalents of base are needed,[382] one each for the boronate formation, and another for the neutralization of the boronic acid formed during the reaction cycle. However the presence of negatively charged bases during the reaction, strongly suggests the use of water as a co-solvent. Potential drawbacks hereof, such as the saponification of esters, the racemization of optically active compounds, or aldol condensations of carbonyls, can be easily circumvented by the use of a heterogeneous phase system, such as biphasic systems of toluene and aqueous K_2CO_3, or suspensions of solid bases (K_2CO_3, $K_3PO_4 \cdot n\ H_2O$) in DMF, dioxane, or toluene.[383] Although anhydrous inorganic bases can mediate the cross-coupling as suspensions in organic solvents, the use of water significantly accelerates the reaction. Concerning the choice of the appropriate base during a Suzuki-Miyaura cross-coupling several factors have to be taken into account. As remarked above the transmetallation either involves a nucleophilic displacement of **57** (R^1-Pd-X) with $[R^2B(OH)_3]M$, yielding R^1-Pd-R^2 and MX, or Alternatively, a precedent direct displacement of **57** with a base MOH, thus yielding MX and R^1-Pd-OH. K_2CO_3 and Na_2CO_3 represent the most widely used bases. However they are not suitable for sterically highly hindered reactants, which require much stronger bases. The order of reactivity for commonly used bases has been found as follows: $TlOH > Ba(OH)_2$, $Tl_2CO_3 > NaOH > Cs_2CO_3$, $K_3PO_4 > Na_2CO_3 > NaHCO_3$.[384,385] The portrayed acceleration effects of the corresponding bases can be attributed to two major factors. The first one is represented by the basic strength ($OH^- > M_2PO_4^- > MCO_3^- > HCO_3^-$), since the concentration of $[R^2B(OH)_3]M$, which exists in equilibrium with the free boronic acid, strongly increases with the strength of the applied base. The second important factor is the affinity of the bases' counter cations for halide ions, which strongly accelerates the coupling reaction with increasing stability constant ($Ag^+ > Tl^+ >> Ba^{2+} > Cs^+ > K^+$).[212,386] furthermore, the counter cations may affect the reaction rate according to the solubility of $[R^2B(OH)_3]M$ in organic solvents (e.g. $[ArBF_3]NBu_4 >> [ArBF_3]K$).[387] Finally, it has been found, that for highly base-sensitive reactants, such as esters, very mild bases like fluoride salts (e.g. CsF, Bu_4NF, or Bu_4NHF_2) represent the appropriate base of choice in order to allow a successful Suzuki-Miyaura cross-coupling.[388]

Side Reactions of Suzuki-Miyaura Couplings

One of the most common side reactions observed in Suzuki-Miyaura cross-couplings is the participation of phosphine-bound aryls in the coupling reaction. Although phosphine ligands of the PAr_3-type are widely used in this context, depending on the other reactants, there can be massive interferences due to aryl-aryl-exchanges between Pd- and P-bound aryls.[389–391] Especially the use of electron-rich haloarenes as substrates increases the observed amounts of side-products. In contrast to this the use of electron-deficient substrates, or of haloarenes exhibiting steric hindrance due to the presence of an ortho-substituent, respectively, has been proven to mostly help to avoid the described side reactions. The same effects have been observed for the presence of electron-donating groups (EDGs) or EWGs within the phosphine ligands. All in all the amount of aryl-aryl interchange strongly depends on the electronic and steric effects of the haloarenes, as well as those of the phosphine ligands. A reason for the observed dependencies is the fact, that the interchange between **63** [Ar´Pd(PAr_3)$_2$X] and **65** [ArPd(PAr_3)(P(Ar´)Ar$_2$)X] proceeds via the formation of a phosphonium salt **64**, which can be retarded by steric hindrance, or by the utilization of electron-poor aryls, respectively, whereas the use of electron-rich aryls stabilizes the P^+-intermediate **64** and thus accelerates the unwanted exchange reactions (Scheme 11). [392–396]

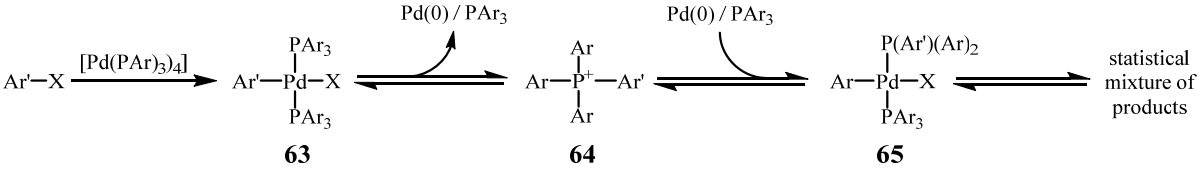

Scheme 11: Schematic illustration of the mechanism of the aryl-aryl interchange between **63** [Ar´Pd(PAr_3)$_2$X] and **65** [ArPd(PAr_3)(P(Ar´)Ar$_2$)X] via the tetravalent **64** (P^+(Ar)$_3$(Ar´)) representing one of the most common side reactions during Suzuki-Miyaura cross-couplings.

Taking the previous explanations into account in principle sterically bulky and low-donating phosphines should be the preferable ligands of Pd-catalysts during Suzuki-Miyaura couplings. However usually electron-donating, but bulky ligands are preferred, due to the enhanced oxidative addition of organic halides to coordinatively unsaturated, but electron-rich Pd(0)-complexes. Therefore altogether some of the ligands displayed in Figure 39 have been found to be extraordinarily successful in eliminating the participation of phosphine-bound aryls, without shutting down the oxidative addition as the fundament of the whole catalytic cycle.

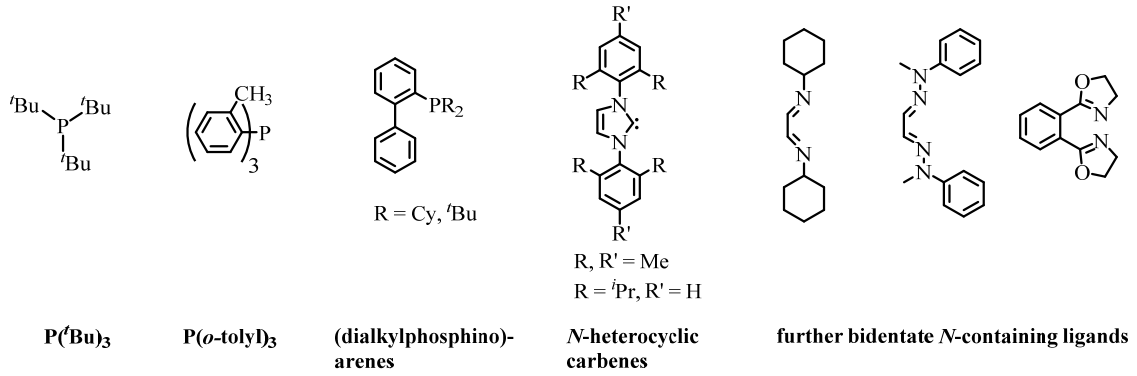

Figure 39: Depiction of tailor-made sterically bulky, but electron-donating phosphine ligands designed for the minimization of aryl-aryl interchange side reactions without negatively affecting the oxidative addition of the Suzuki-Miyaura cross-coupling reaction at the same time.

Since aryl-aryl interchange, if observed, takes place before the transmetallation step, a slow transmetallation amplifies the amount of interchange. Usually electron-rich haloarenes slow down the transmetallation, although the use of strong bases usually accelerates the transmetallation step sufficiently, to circumvent the undesired side reaction. Furthermore, the choice of halide strongly affects the rate of transmetallation reaction to **57** (X = Cl > Br > I), and thus can help to minimize aryl-aryl interchange.[397] Another common side-reaction is the oxygen-induced homocoupling of arylboronic acids. This side-reaction can be almost completely avoided, if the coupling reaction is carried out under inert atmosphere. However even traces of oxygen, especially in the presence of an aqueous base, can lead to rather large amounts of homocoupled side-product. Furthermore, cross-coupling reactions can often result in the dehalogenation of the used organic halide (R-X → R-H), especially if alcohols are used as solvents. In most cases the hydride formation herein, arises from the β-hydride eliminations of **66** (Ar-Pd-OCH_2R) yielding **67** (Ar-Pd-H) and an aldehyde.[372,398] From intermediate **67** the dehalogenated side-product **68** (Ar-H) is readily reductively eliminated (Scheme 12).

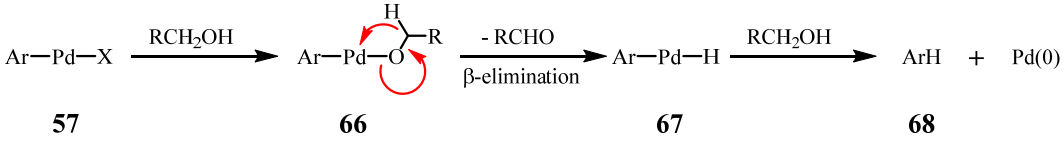

Scheme 12: Depiction of the dehalogenation of **57** (Ar-Pd-X) caused by β-hydride elimination of **66** (Ar-Pd-OCH_2R) resulting in the formation of dehalogenated product **68** (ArH).

The last very important side reaction in Suzuki-Miyaura cross-coupling reactions is the hydrolytic B-C bond-cleavage (protodeboronation). The rate of hydrolytic B-C bond-cleavage can be accelerated 10-100-fold due to *ortho*-substituents within the boronic acid, but it is much stronger accelerated (up to $>10^6$-fold) by the presence of adjacent heteroatoms within the boronic acid.[399–403] Whereas 2-thiopheneboronic acids, in spite of serious amounts of

hydrolytic B-C bond-cleavage, can, occasionally, still be used for biaryl coupling, this is not at all the case for 2-pyridiyl boronic acids, due to their very fast protodeboronation reactions. The few examples of successful Suzuki-Miyaura cross-couplings, or at least on the preparation of the 2-pyridyl organoboronic precursors, which have been reported, are those involving the preparation "ate"-complexes,[404–415] which are often in-situ reacted on via the according cross-coupling to an appropriate arylhalide (Scheme 13). A rather general method allowing this type of coupling sequence has been reported by Billingsley *et al.* The method involves the preparation of substituted 2-pyridiylborates **70** from the corresponding 2-bromopyridine precursors **69** followed by the Suzuki-Miyaura cross-coupling reaction of **70** with a substituted aryl halide yielding the pyridine-derived coupling product **71**. However until now still Negishi couplings utilizing 2-pyridiylzinc reagents[416] or Stille couplings using organostannanes[417] represent convenient alternatives to the described problematic Suzuki-Miyaura coupling.

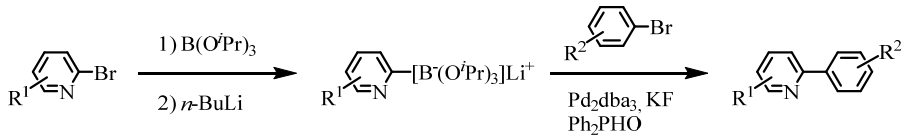

Scheme 13: Example of a method for the preparation of substituted 2-pyridylboronates **70** from the corresponding 2-bromopyridine precursors **69** followed by the subsequent Suzuki-Miyaura reaction of **70** with appropriate aryl halides yielding the pyridine-derived coupling products **71**.

1.3.2 Limitations of Suzuki-Miyaura Cross-Coupling Reactions

Although the Suzuki-Miyaura cross-coupling reaction turned into one of the most versatile and most broadly applied synthetic procedures of modern chemistry there are certain distinct drawbacks or limitations, respectively, which are briefly summed up hereafter. First of all until now for the preparation of the boronic acids or esters, as the required nucleophiles characterizing the transmetallation step of the Suzuki-Miyaura coupling, in most cases rather harsh conditions are needed, such as the use of organometallic reagents like *n*-BuLi, in order to allow a selective halogen-boron exchange. Therefore the variation of substituents at the transmetallating boron agent is limited to compounds being able to cope with the described preparation conditions. Furthermore, the requirement of usually inorganic bases for the transmetallating step can be problematic for base-labile substituents of boronic acid and

organohalide, alike. Last but not least some of the side reactions described above limit the use of Suzuki-Miyaura cross-coupling reactions. Whereas aryl-aryl interchange and homocoupling reactions can usually be circumvented rather well by optimizing the utilized catalytic system this is only true to a certain extent for hydrolytic B-C bond-cleavages. Especially for heterocyclic boron compounds, such as 2-thiophenes, 2-furanes, and in particular for 2-pyridines, the methods reported so far are extremely rare and usually limited to a very narrow flexibility concerning the applicable substituents within the organoboron compound. Therefore especially the latter problem, together with the striving for a softer preparation approach towards regular organoboron derivatives, represent two of the main focusses of modern research interests in the field of Suzuki-Miyaura cross-coupling reactions.

1.4 From Simple Azobenzenes to Switchable Metalloazobenzenophanes

After a brief introduction about azobenzenes and metallocycles, it is the aim of this chapter, to draw a connection between both of the named fields, by explaining elementary concepts of the implementation of azobenzenes, as photo-sensitive functional units, into shape-switchable macrocycles. Hereafter, selected examples, derived from the ability of these shape-switchable macrocycles to adjust the size of their cavity based on external stimuli, are given, which highlight potential applications of the named compounds within the fields of host-guest chemistry,[418–425] supramolecular self-assembly,[418,422–424,426–428] and functionalized molecular machines and devices.[429–435] Finally, with regard to one of the main experimental focusses of this thesis, selected examples of metal-containing azobenzene derivatives will be summarized.[423,426,429,431,433,434,436]

1.4.1 Azobenzenes –Overview of History, Synthesis, Properties, and Photoisomerization Mechanisms

The History of Azobenzenes

The first successful synthesis of (*E)*-azobenzene, also referred to as (*E*)-**72**, via the reaction of nitrobenzene in an ethanolic KOH solution, was described by Mitscherlich in 1834.[437] Here the term *azo* originates from the French word azote, meaning *nitrogen.* Although the IUPAC defines azobenzenes as *diphenyldiazenes*[438] the term *azo* still is widely used until today. Approximately one century after Mitscherlich's discovery, Hartley was the first to elucidate the photochemically inducible isomerization process leading to the conversion of (*E)*-azobenzene ((*E*)-**72**) to (*Z*)-azobenzene ((*Z*)-**72**) in the range of his investigations of the influence of light-exposure onto the configuration of N=N double bonds.[439] In 1939 Robertson confirmed the structures of both azobenzene isomers by means of X-ray crystallography.[440] The discovery of the *cis*-isomer of azobenzene was the starting point of the extensive research and investigations, which have been performed on the named system throughout the following decades and which are lasting until the present time.

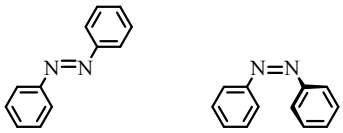

(*E*)-**72** (*Z*)-**72**

Figure 40: Depiction of the two isomers, (*E*)-**72** and (*Z*)-**72**, of azobenzene.

Just like in the first decades after its discovery also nowadays the most prominent application of azobenzenes surely still is their use as industrial dyes (azobenzene dyes constitute approximately 60% of the world production of industrial dyes).[441,442] Derived hereof azobenzene dyes are widely employed in all kinds of fields, such as paints, textile dyeing, paper printing, food-coloring, or as acid-base indicators. Furthermore, azobenzene derivatives represent one of the best and most broadly used organic molecular switches known up to date.

Synthetic Approaches to Azobenzenes

Due to the ubiquitous potential applications of azobenzenes there are numerous approaches to assemble this class of substrates. However, due to limited space only the most frequently used synthetic pathways are highlighted listed hereafter, and illustrated with selected examples in Scheme 14.[443,444] The methods are:

(a) The Electrophilic aromatic substitution reaction of diazonium salts **74**, previously prepared via diazotation of the corresponding anilines **73**, with appropriate activated aromatic compounds **75** yielding the desired azobenzene derivatives **76** (Azo coupling reaction).[444–447]

(b) The condensation reaction between aromatic nitroso derivatives **78**, usually accessible via the corresponding hydroxylamine precursors **77**, and appropriate anilines **79** yielding the desired azobenzenes **80** (Mills reaction).[122,448–450]

(c) The formation of 4-hydroxy substituted azobenzenes **82** from appropriate azoxybenzenes **81** under acidic conditions (Wallach reaction),[451–454] whereat azoxybenzenes are accessible either reductively from nitrobenzene derivatives, or oxidatively from appropriate anilines.

(d) The reductive azo coupling of aromatic nitro derivatives **83** utilizing appropriate reducing agents, such as e.g. $LiAlH_4$,[455–457] $NaBH_4$,[458] Zn/NaOH,[428,459] or KOH,[460] in order to yield the corresponding azobenzene derivatives **84**.

(e) The oxidative azo coupling of anilines **85** utilizing appropriate oxidizing agents, such as $NaBO_3 \cdot 4H_2O$ in H_3CCOOH,[461] $Pb(OAc)_2$ and NEt_3,[462] KO^{t}Bu and O_2 in ^{t}BuOH/DMSO,[435] MnO_2,[435] NaOCl,[448] or silver salts like Ag_2O[463] or Ag_2CO_3/Celite,[464] in order to obtain the desired azobenzene derivatives **86** / **87**.

(f) The dehydrogenation of *N,N´*-diarylhydrazines **88** to desired azobenzenes **89** using appropriate oxidants, such as $Pb(OAc)_4$,[465] $CuCl_2$, [466] or MnO_2.[467]

(g) the metal-catalyzed Hartwig-Buchwald type cross-coupling of *N*-Boc protected arylhydrazines **91**, prepared from aryl halides **90**, with a second appropriate aryl halides **92** yielding the *N*-Boc diarylhydrazine intermediates **93**, which are subsequently converted to the desired azobenzene **94** by oxidative deprotection using either NBS/pyridine,[468] or a Cu(I) source.[469]

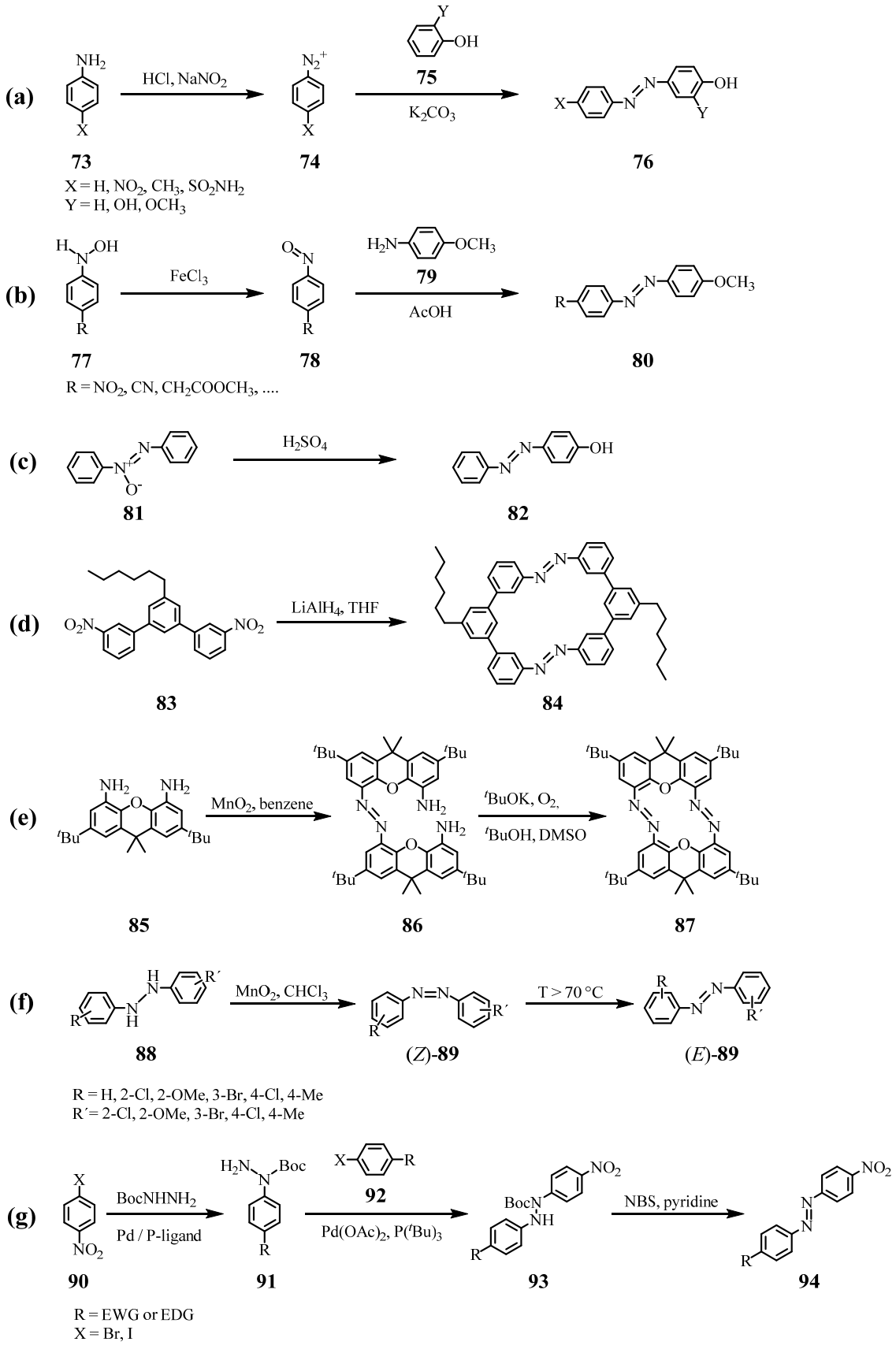

Scheme 14: Overview of the most frequently applied synthetic pathways to afford azobenzenes. Sources of the illustrated examples: **(a)** Haghbeen *et al.*,[445] **(b)** Davey *et al.*,[450] **(c)** Buncel,[453] **(d)** Müri *et al.*,[456] **(e)** Norikane *et al.*,[435] **(f)** Hyatt *et al.*,[467] **(g)** Lim *et al.*.[468]

The Properties and Photoisomerization Mechanisms of Azobenzenes

The enormous potential of azobenzene derivatives, in particular as industrial dyes, arises from their bright orange, red, or yellow colors, which can be attributed to their extended delocalized π-system. Apart from the application as dyes, these pronounced photochromic properties, based on the facile and reversible *trans* ↔ *cis* isomerization of azobenzenes in the presence of UV or visible light, represent the main focus of the research interests in the field of azobenzenes throughout recent years.[470–472]

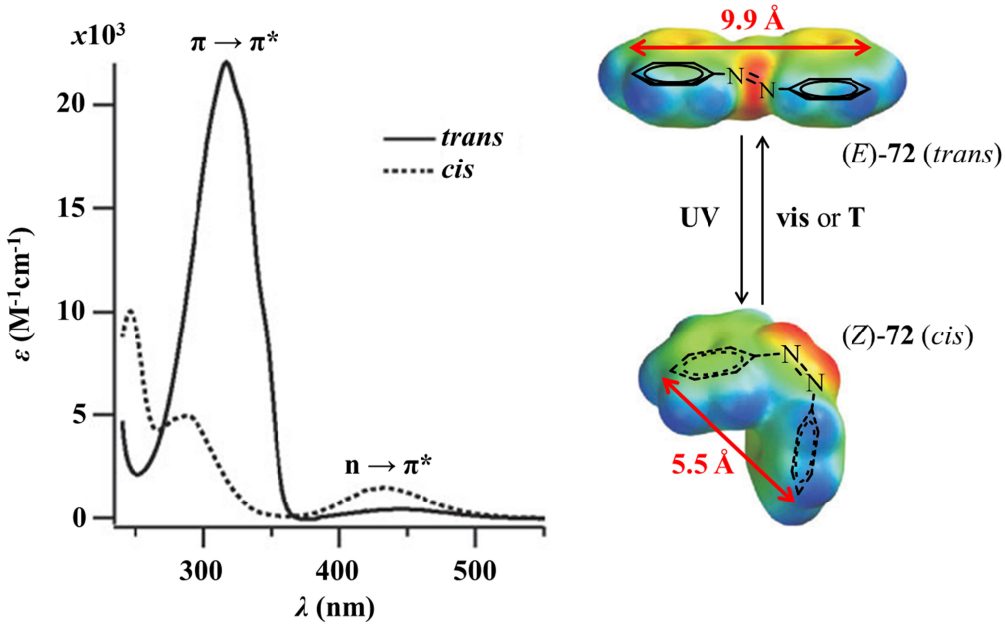

Figure 41: Absorption spectra of (*E*)-azobenzene (full line) and (*Z*)-azobenzene (dashed line) together with an illustration of the geometric alterations which are triggered by the reversible photoisomerization of both isomers ((*E*)-**72** ↔ (*Z*)-**72**). Figure 41 has been adapted with permission based on the publication of Beharry *et al.*[473]

Figure 41 illustrates the distinct changes observable in the absorption spectra of azobenzenes upon photoinduced *trans* → *cis* isomerization. Apart from these changes of the optical properties of the azobenzene derivative the *trans* → *cis* isomerization coincides with significant changes to further physical properties, such as the molecular geometry, changing from a planar molecule with a distance of 9.9 Å between the *para* carbon atoms to a non-planar molecule with an extension of 5.5 Å, or the molecule's dipole moment increasing from 0.5 D to 3.1 D upon *trans* → *cis* photoisomerization.[474]The illustration of the absorption spectra of (*E*)-**72** and (*Z*)-**72** in Figure 41 exhibits two distinct absorption bands for each of the two isomers, namely, a stronger $\pi \rightarrow \pi^*$ transition band and a much weaker $n \rightarrow \pi^*$ transition band. Herein, the intensity and wavelength of the two bands differs significantly

between the two isomers, which also describes the most important characteristic of the photoisomerization process of azobenzenes and therefore the basis for the manifold applications of azobenzene derivatives. In general the π → π* transition band of (*E*)-isomers of azobenzenes is always more intense, than the corresponding band for the (*Z*)-isomer. On the contrary the n → π* transition band is more intense for the (*Z*)-isomer than for the (*E*)-isomer, for which this transition is usually almost undetectable. The π → π* transition band is generally attributed to the azo unit and usually can be found in the near UV region (314 nm for (*E*)-**72**, and 280 nm for (*Z*)-**72**). The fact that the intensity of this π → π* transition band is much stronger for the (*E*)-isomers, than for the (*Z*)-isomers, arises from the angular geometry of the latter one (Figure 41). The opposite case can be found for the relative intensities of the absorption bands caused by the n → π* transition. These n → π* transition bands are also attributed to the azo moiety, but they usually appear in the visible region (400 nm for (*E*)-**72**, and 430 nm for (*Z*)-**72**). The different intensities found for the n → π* transition bands, to a major extent, can be deduced from the fact, that this n → π* transition originates from the lone pair of the nitrogen atoms and thus is symmetry-forbidden for the (*E*)-isomers, but symmetry-allowed for the (*Z*)-isomers. As for C=C double bonds it has been found that the (*E*)-isomers of azobenzenes, with very rare exceptions, represent the thermodynamically stable forms, e.g. (*E*)-**72** is 12 kcal·mol^{-1} more stable than (*Z*)-**72**.[475,476] furthermore, the activation energy to the photoexcited (*Z*)-state has been found to be 23 kcal·mol^{-1} in solution,[475,477] or even 31 kcal·mol^{-1} in the solid.[475,478] Hence the *trans*-isomer (*E*)-**72** represents the predominant form at room temperature in the dark. Hereby, the (*E* → *Z*) photoisomerization of *trans*-azobenzenes can be achieved upon their irradiation with UV light of the according π → π* transition band's wavelength (~ 320-350 nm), whereas the reverse isomerization process (*Z* → *E*) can be achieved either by irradiation of the *cis*-isomer with visible light of the according n → π* transition band's wavelength (~ 400-450 nm), or via thermal relaxation of the *cis*-isomer in the dark. Due to the close proximity of the two corresponding π → π* transition bands of (*E*)-**72** (314 nm) and (*Z*)-**72** (280 nm) an uttermost enrichment of 85% of the *cis*-isomer (*Z*)-**72**, also described as the photostationary state (PSS), can be obtained. For the broad majority of azobenzenes the two photochemical conversions, (*E*) → (*Z*) and (*Z*) → (*E*), respectively, occur on a picosecond timescale, whereas the thermal (*Z*) → (*E*) relaxation can be on the timescale of milliseconds to days, or even not applicable at all. It was found, that the size of the energy gap between the π → π* and the n → π* transition bands, as one of the most important properties characterizing an azobenzene derivative, strongly depends on the substituents in the 4- and 4′-positions of the azo moiety. Therefore

one generally distinguishes between three different types of azo motifs[479,480] according to this gap size (Figure 42):

(1) Azobenzene type (Ph-N=N-Ph, **72**): Exhibits a very intense $\pi \rightarrow \pi^*$ band in the UV region and a weaker $n \rightarrow \pi^*$ band in the visible region, leading to the overall yellow color. Compounds of this type generally resemble plain azobenzene (**72**).

(2) 4-Aminobenzene type (*o*- or *p*-(X)-C_6H_4-N=N-Ar, **95**): Here the $\pi \rightarrow \pi^*$ and the $n \rightarrow \pi^*$ bands are very close to each other or even collapse leading to a shoulder within the UV/vis region. Thus this type of azobenzene derivatives, in which the substituent X corresponds to an EDG in the *ortho*- or the *para*-position, usually exhibits a bright orange color, resulting from the red-shift of the transition band.

(3) Pseudo-stilbene type (*p*-(X)-C_6H_4-N=N-C_6H_4-*p*-(Y), **96**): These push-/pull systems, in which X represents an EDG, whereas Y corresponds to an EWG, usually exhibit a bright red color due to the distinct red shift of the $\pi \rightarrow \pi^*$ transition bands. The latter ones even switch positions with the $n \rightarrow \pi^*$ transition bands, leading to an inversion of the transition order of type 1 azobenzenes.

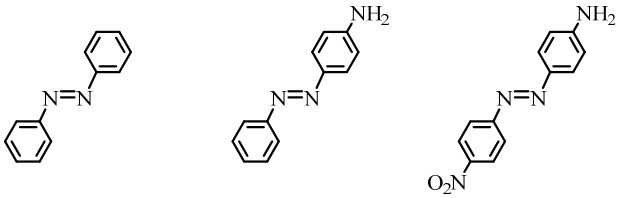

(*E*)-**72** (*E*)-**95** (*E*)-**96**

Figure 42: Representative examples of the three main different types of azobenzene derivatives, namely, azobenzene type **72**, 4-aminobenzene type **95**, and pseudo-stilbene type **96**.

Although the photoinduced isomerization of azobenzenes has been studied extensively over the last decades the mechanism of the photoisomerization process has still not been fully revealed and is until now subject of debate in the chemical community.[452–454] Various studies have been reported on the effects of substituents on the aromatic subunits of the azobenzene core,[481–483] as well as on other parameters potentially influencing the photoisomerization process, such as the steric hindrance of the structure,[482,484] solvent polarity and viscosity,[481,482,485,486] or temperature.[485,487] Therefrom four different mechanisms have been proposed for the photoisomerization of azobenzenes, namely, the inversion, the rotation, the concerted inversion, and the inversion-assisted rotation mechanism, amongst which the first two mechanisms represent the most extensively studied examples (Figure 43).[479,482,488–493]

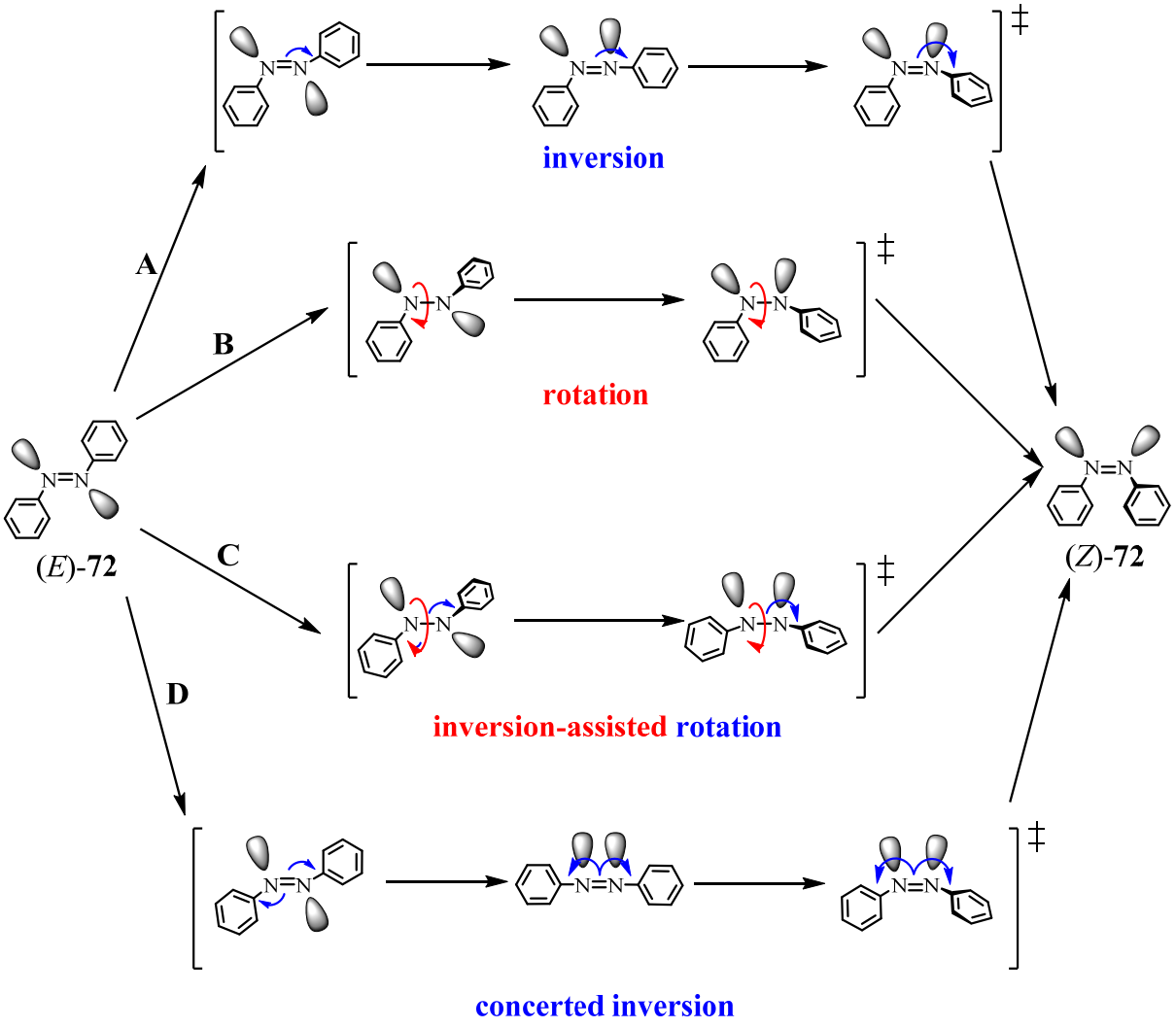

Figure 43: Schematic illustration of the four most commonly proposed mechanisms for the *trans* → *cis* photoisomerization of (*E*)-**72** to (*Z*)-**72**): **(A)** inversion mechanism, **(B)** rotation mechanism, **(C)** inversion-assisted rotation mechanism, and **(D)** concerted inversion mechanism.

For instance it could be shown, that the efficiency of the (*E*) → (*Z*) photoisomerization of azobenzene is not influenced by the temperature, whereas the isomerization quantum yield of the (*Z*) → (*E*) back-isomerization shows a significant reduction upon lowering temperatures and at 110 °C eventually stops completely.[482] furthermore, Rau and Lüddecke[490] and Tamaoki *et al.*[457] were able to show, that the thermal (*Z*) → (*E*) isomerization has to proceed via an inversion mechanism, since the strained azobenzenophanes they investigated cannot undergo a rotational isomerization process. The key issue of debate for the mechanisms illustrated above is usually linked to the role of the free valence electron pair, which is present at each of the bridging nitrogen atoms. In the range of an inverting photoisomerization mechanism (Figure 43 – Pathway A) the participation of either one of the nonbonding nitrogen's lone pairs leads to a n → π* transition ($S_0 \rightarrow S_1$), which causes the N=N-C angle at

the corresponding nitrogen atom to increases from 120° to 180°, whereas the dihedral angle remains constantly at 0°. Hence the transition state involves one sp-hybridized azo-nitrogen atom. In contrast to this the rotational isomerization mechanism (Figure 43 – Pathway B) involves a $\pi \rightarrow \pi^*$ transition ($S_0 \rightarrow S_2$) leading to the rupture of the N=N π-bond thus enabling a free rotation about the N-N bond. Although the C-N-N-C dihedral angle changes upon the rotational (*E*) → (*Z*) photoisomerization, the N-N-C angle remains ~120°.[492] The third photoisomerization mechanism, the inversion-assisted rotation (Figure 43 – Pathway C), consists of a massive change to the C-N=N-C dihedral angle coinciding with much smaller alterations to the C-N=N angle. The last proposed photoisomerization mechanism, namely, the concerted inversion (Figure 43 – Pathway D) is characterized by the fact, that both N=N-C angles increase from 120° to 180°, leading to a linear transition state, due to two concerted $n \rightarrow \pi^*$ transitions of both the nonbonding nitrogen lone pairs.[494] Whereas the first three isomerization pathways exhibit polar transition states, the concerted inversion mechanism shows no net dipole moment during its transition.

To summarize, some of the most distinct changes in chemical and physical properties arising from the photoisomerization processes between (*E*)-azobenzenes and (*Z*)-azobenzenes are listed hereafter, by exemplary discussing the corresponding details of (*E*)-**72** and (*Z*)-**72**:

(I) (*E*)-**72** represents the thermodynamically stable form, exhibiting an energetic advantage of ~12 kcal·mol^{-1} compared to the *Z*-isomer (*Z*)-**72**.[475,476]

(II) The distance between the two *para*-carbon atoms (4- and 4′-position of the two aromatic rings) changes from 9.9Å for (*E*)-**72** to 5.5Å for (*Z*)-**72** (Figure 41).[474]

(III) In order to minimize the steric interactions the structure of **72** changes from a linear, planar geometry for (*E*)-**72** to an angular, non-planar geometry for (*Z*)-**72**, in which one of the phenyl units is twisted out of the plane (Figure 41).

(IV) The dipole moment increases from 0.5 D for (*E*)-**72** to 3.1 D for (*Z*)-**72**.[474]

(V) The length of the C-N bond is slightly elongated in the (*Z*)-isomer (1.45 Å), if compared to the (*E*)- isomer (1.41 Å).[440]

(VI) Upon (*E*)→(*Z*) photoisomerization of **72** a distinct upfield shift of the ^{1}H-NMR signals corresponding to the aromatic AB system can be monitored, which arises due to the altered anisotropic effect of the π-electron cloud for the twisted structure of (*Z*)-**72** in contrast to the planar structure of (*E*)-**72**.

1.4.2 Photoswitchable Macrocycles Containing Azobenzenes

First of all, besides a multitude of potential uses of azobenzene derivatives there are certain limitations, which have to be circumvented, such as in particular the necessity of a better control of the photoisomerization processes present in azobenzenes. Herewith, the main issues, which need to be overcome, in order to gain an improved control of these photoisomerization processes are, firstly the limited conversions usually found during the isomerizations resulting in a PSS and secondly the limited stability of the (*Z*)-isomers, which readily undergo thermal $Z \rightarrow E$ isomerization, even at room temperature in the dark. Although this thermal $Z \rightarrow E$ back isomerization is usually much slower than the $E \rightarrow Z$ photo-isomerization it is fast enough to hinder a variety of interesting applications of azobenzenes, such as optical storage devices, for which a prolonged stability of both states is inevitable. To overcome these drawbacks and allow an effective utilization of azobenzenes of varying functionalities (e.g. as photostable azo dyes or as photochromic switches in macromolecular assemblies), several pathways can be followed, such as:

(a) The destabilization of the (*Z*)-isomer, required to guarantee the photostability of azobenzenes used as dyes, can be readily achieved by the introduction of hydroxyl substituents *ortho*-positioned to the azo subunit, or via the introduction of the azo motif into a push-/pull system.[495]

(b) The stabilization of the (*Z*)-isomer, required to allow efficient and controllable photochromic switching applications of azobenzenes, can be achieved either by the introduction of fluorine substituents in *ortho*-positions to the azo motif,[495] or, as much more commonly applied, by the introduction of the azo moieties into azobenzenophanes, thus generating sufficient macrocyclic strain in order to encompass the desired results.[435,496–498]

Furthermore, the class of photochromic switches based on the implementation of azobenzenes into macrocyclic structures can be further diversified taking the introduction of several azo moieties into the cyclic structure into account. Herein, by rather simple extension of the synthetic concept, a switching system bearing more than the usual two states can be accessed which potentially gives rise to novel interesting functions. However, although the synthesis of azobenzenes has been known for 180 years, the accessibility of macrocyclic azobenzene containing structures up to date still represents a rather challenging task, on which

the following two subchapters will focus by means of selected examples illustrating the applicable approaches.

1.4.2.1 Azobenzenophanes

In the synthesis of azobenzenophanes the cyclization reaction, representing the ultimate step of the macrocyclic assembly route, most often also presents itself as the most challenging step of the whole synthetic sequence. The problematic part of this final step is the fact that, against the entropic direction, the intramolecular cyclization reaction has to be preferential against the intermolecular coupling reaction leading to potential polymerization. This target can in many cases either be achieved by the utilization of high-dilution conditions, by using the template effect, or by harking back to highly reactive intermediates, which on the other hand can lead to novel problems themselves. Following the high-dilution principle, which is also named Ruggli-Ziegler dilution principle,[499] the maximum concentration of the reagents has to be in the range between 1 to 50 mM. A modification of this high-dilution principle, which does not necessarily rely on such huge amounts of solvents, is the pseudo-high-dilution principle, involving the slow addition of one or several reactants over hours or even days. However a strictly inert atmosphere can be hard to accomplish for the latter approach giving rise to potential new problems arising from these contaminations. The template effect describes specific interactions of reactants with intermediary assemblies in the range of the macrostructure's formation process, giving rise to mostly very good size control of the macrocyclic structures. Leigh's knots,[500–503] Stoddart's supramolecular structures,[504–507] and Anderson's nanorings[508–513] are just a few examples in which template effects have been exploited for macrocycle formation. Additionally, the question, if the designed macrocycle bears other heteroatoms apart from the envisaged azo motif, usually also plays a significant role for the decision which bond should be formed last during the formation of the azobenzenophane. Usually, if the bridging unit contains further heteroatoms, either a substitution,[490,496,514–516] or a condensation reaction,[422] present the method of choice for the macrocyclization reaction. For the substitution pathway especially Williamson-type reactions, with sulfides, pyridines, or amines acting as the nucleophile, are the common approach, usually using benzyl bromides as the according electrophiles. If the macrocyclic structure however lacks any further heteroatoms in the bridging unit also the formation of the azo unit in the final step represents a common approach.[435,456] In 1982 Rau and Lüddecke reported

the first azobenzenophane, which they prepared via the intermolecular dimerization reaction of Na_2S with 4,4′-di(bromomethyl)azobenzene (**97**) resulting in the formation of azobenzenophane **98** (Scheme 15a).[490,514] During their stability studies Rau *et al.* could show, that the photoisomerization of (*E*,*E*)-**98** into (*Z*,*Z*)-**98** proceeds via the intermediary mixed isomer (*E*,*Z*)-**98**, which represents the least stable form of the three. The finding of the unusual high half-life time of 5 days for (*Z*,*Z*)-**98** upon thermal back-isomerization incited the group to develop a system with even longer half-life time of the corresponding (*Z*,*Z*)-isomer. Finally the synthesis of the sterically more hindered azobenzenophane **100** from the appropriate benzylbromide precursor **99** resulted in a system showing an improved half-life time of 400 days for the (*Z*,*Z*)-**100** (Scheme 15b).[496] herein, the all-*cis* isomer (*Z*,*Z*)-**100** is thermodynamically stabilized in a bistable system, due to the fact, that the macrocyclic strain in the (*E*,*Z*)-**100** isomer is so high, that a thermal back isomerization (*Z*,*Z*)-**100** → (*E*,*Z*)-**100** → (*E*,*E*)-**100** is effectively suppressed. The possibility to exploit the promising features of the system within an optical storage device is however anticipated by two major drawbacks, namely, the instability of both isomers at 313 nm and the long irradiation time, which is necessary for the initiative photoisomerization process.

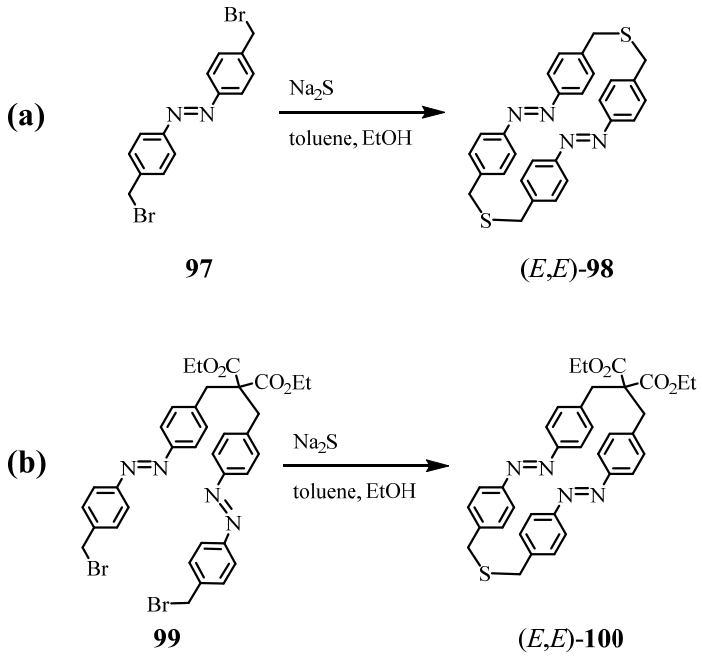

Scheme 15: Synthesis of two azobenzenophanes (*E*,*E*)-**98** and (*E*,*E*)-**100** via substitution reactions utilizing Na_2S as the nucleophile: **(a)** first generation azobenzenophane **98** exhibiting a half-life time of 5 days for the (*Z*,*Z*)-isomer as reported by Rau and coworkers,[490,514] **(b)** improved second generation azobenzenophane **100** exhibiting a half-life time of 400 days for the (*Z*,*Z*)-isomer, as reported by Röttger and Rau.[496]

Following the direction of introducing more strain into the macromolecular structures in order to obtain optimized isomerization features Tamaoki *et al.* were able to successfully synthesize *meta*-[517–519] and *para*-bridged[457,520,521] azobenzenophanes utilizing methyl or ethyl linkers, respectively. Furthermore, Tauer *et al.* were able to assemble *ortho*-bridged azobenzene macrocycles.[522] All the given examples, due to the lack of further heteroatoms in the molecular backbone, involved the formation of the azo subunits in the ultimate cyclization step utilizing reductive azobenzene formation from the corresponding nitro-derivatives by using $LiAlH_4$ as the reducing agent (Scheme 16). Furthermore, Müri *et al.* were able to synthesize larger, but fully conjugated and therefore more rigid bisterphenyl-azobenzenophanes similar to the macrocycle **84** (Scheme 14d), by applying similar reductive macrocyclodimerization conditions in the last step.

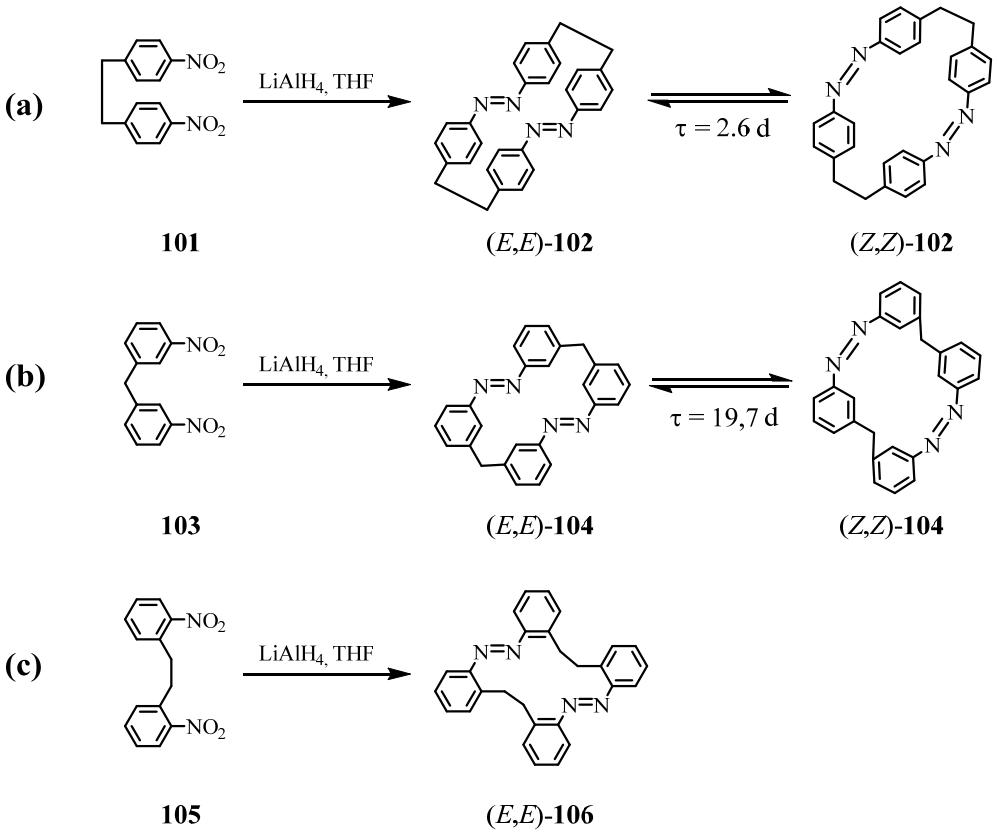

Scheme 16: Synthesis of the azobenzenophanes **102**, **104**, and **106** via reductive macrocyclo-dimerization of the corresponding nitro precursors **101**, **103**, and **105**. Thermal isomerization studies in the dark revealed a half-life time τ of 2.6 d for the *para*-ethyl-bridged azobenzenophane (*Z*,*Z*)-**102**,[457] whereas for the *meta*-methyl-bridged macrocycle **102** a thermal half-life time of the (*Z*,*Z*)-**104** isomer of τ = 19.7 d could be found.[518]

Surprisingly, the isomerization studies of Tamaoki *et al.* revealed that the *para*-ethyl-bridged azobenzenophane (*Z*,*Z*)-**102** only exhibits a thermal half-life time of τ = 2.6 d in the dark, which is approximately the same as for plain azobenzene (*Z*,*Z*)-**72**.[457] However further

thermal isomerization studies revealed an improved thermal half-life time of τ = 19.7 d for this *meta*-methyl-bridged azobenzenophane (*Z*,*Z*)-**104**.[518] Along this pathway Tamaoki and coworkers studied the isomerization characteristics of the highly strained oligoaryl system [0.0](3,3´)-azobenzenophane (**107**),[497] which has been first described by Kang *et al.,*[469] two years before (Figure 44a).

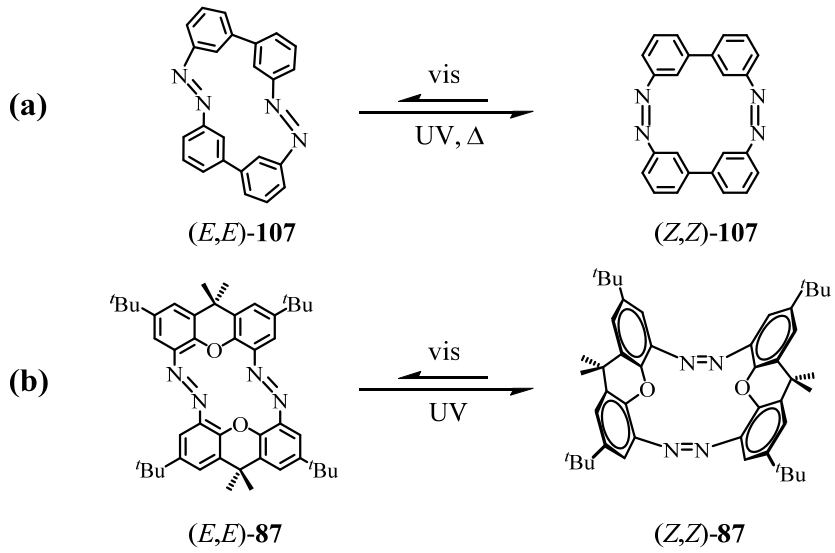

Figure 44: Two examples of azobenzenophanes exhibiting extraordinarily stable (*Z*,*Z*)-isomers with very high half-life times: **(a)** [0.0](3,3´)-azobenzenophane (**107**) with the thermally preferred isomer (*Z*,*Z*)-**107** and a half-life time of τ = 20 d,[497] **(b)** molecular hinge **87** exhibiting a half-life time of τ = 6.7 years.[435]

With an observed half-life time of τ = 20 d, (*Z*,*Z*)-**107** represents the first example of an azobenzenophane, in which the all-*cis* isomer (*Z*,*Z*)-**107** is the thermally most stable form compared to the thermodynamically less favored all-*trans* isomer (*E*,*E*)-**107**. Although the thermal stability of (*E*,*E*)-**107** is still comparable to that one of (*Z*,*Z*)-**107**, the overall system, just like the azobenzenophanes **100** and **104**, shows bistable characteristics, due to the highly-distorted, and thus energetically strongly disfavored, (*E*,*Z*)-isomers. Finally, among the oligoaryl systems, the xanthene-based hinge-like azobenzenophane **87**, synthesized via an oxidative macrocyclization reported by Norikane *et al.* (Scheme 14),[435,498] exhibits an even further improved stability of the all-*cis* isomer (*Z*,*Z*)-**87** with a thermal half-life time of τ = 6.7 years. As for azobenzenophane **107** also macrocycle **87** shows only a rather small extent of the corresponding (*E*,*E*)-isomer upon intense irradiation with visible light of the appropriate wavelengths (Figure 44b).

1.4.3.2 Metal-containing Azobenzene Macrocycles

With regard to one of the main projects of this thesis in this chapter a few examples of metal-containing azobenzene macrocycles, which have been reported until now, will be highlighted. An interesting example of this group is the symmetric azocrown ligand **108**, which exists in an open *trans*-form, but upon (*E*) → (*Z*) photoisomerization changes its shape in a butterfly-like manner allowing the specific ion recognition of monocationic alkali metal ions ($Na^+ < K^+ < Rb^+ < Cs^+$) (Figure 45), which are trapped in between the two crown ether motifs of (*Z*)-**108**.[425] The fact, that during thermal or photoinduced (*Z*) → (*E*) back-isomerization the metal ions are released again, coinciding with the disassembly of the metal-containing macrocycle, exhibits prospective applications of the described system as a potential selective photo-sensitive transport system

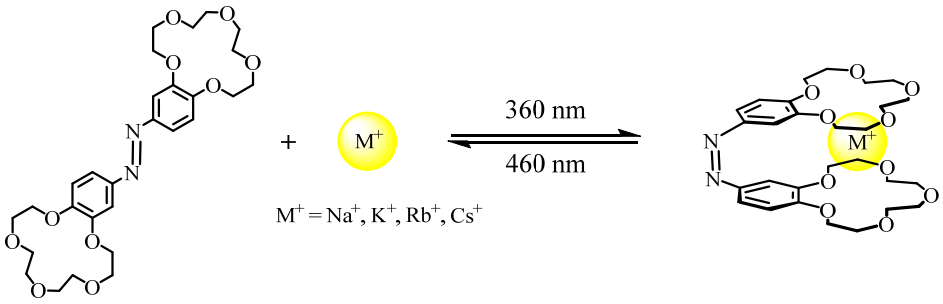

(*E*)-**108** (*Z*)-**108**

Figure 45: Illustration of the specific alkali metal ion recognition by azobenzene (*Z*)-**108**. Whereas (*E*)-**108** is not able to complex the alkali metal ions, the *Z*-isomer (*Z*)-**108** can do so. Upon UV-irradiation the (*E*) → (*Z*) photoisomerization occurs, which coincides with a sandwich-like coordination of the alkali metal ion, in particular Rb^+ and Cs^+, forming a metal-containing azobenzene macrocycle that is stable until the ion release due to (*Z*) → (*E*) back-isomerization.

Further interesting systems of metal-containing azobenzenophanes open up the field of molecular machines. For example Aida *et al.* reported a system of chiral light-driven molecular scissors **109** bearing an azobenzene motif as the key integral part of described the molecular motion (Figure 46).[523,524] Their molecular switch herein, consists of a central 1,1′,3,3′-tetrasubstituted ferrocene unit bearing two phenyl units acting as the scissor blades, whereas two phenylethylene groups act as the handles, which are linked by the photo-sensitive azobenzene moiety. Upon UV-light induced (*E*) → (*Z*) photoisomerization of the azobenzene unit (λ = 350 nm) the phenyl units (equivalent to the scissor blades) open up to an angle of more than 58° in the (*Z*)-isomer, whereas upon exposure to visible light (λ > 400 nm) the "blades" close again to an angle of around 9° in the reformed (*E*)-isomer.

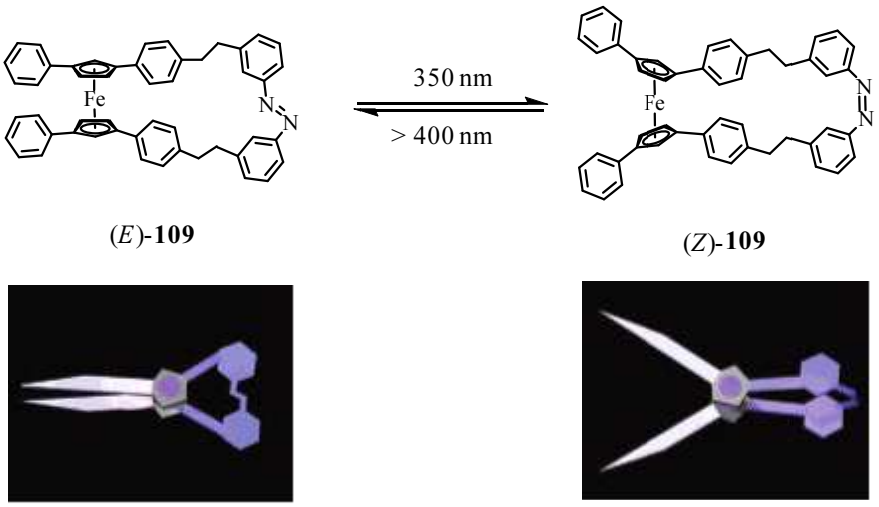

Figure 46: Illustration of chiral photo-sensitive molecular scissors based on the metal-containing azobenzenophane **109**, which can be reversibly switched between the closed form (*E*)-**109** and the opened form (*Z*)-**109**. Lower part of figure 46 adapted with permission from Muraoka *et al*.[523]

By expanding the above system via the addition of two terminal porphyrin-Zn units to the phenyl units (the former scissor blades), which are non-covalently associated with a bis-isoquinoline molecule as host, the same group was able to report the "molecular pedals" as an even more sophisticated example of a molecular machine in 2006 (Figure 47).[433,434]

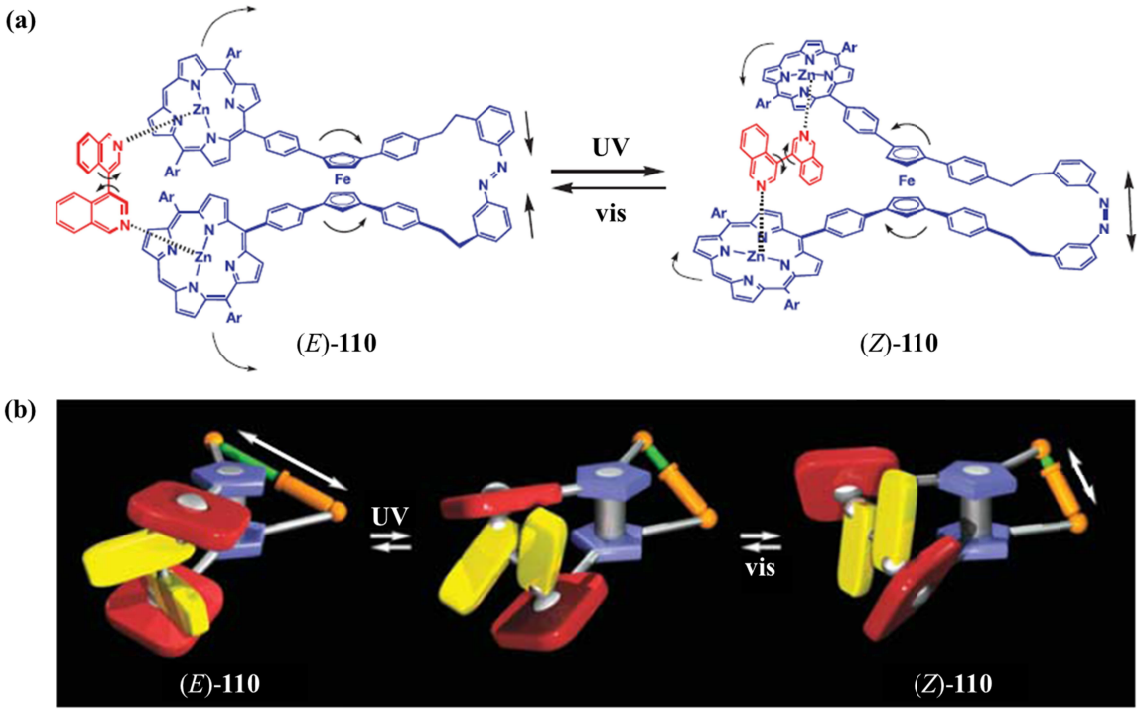

Figure 47: Illustration of the "molecular pedals" **110**. Figure adapted with permission from Muraoka et al.[433]

In the described molecular pedals the (*E*) → (*Z*) photoisomerization of the azobenzene moiety (Figure 47b – orange/green parts) triggers a cascade of subsequent molecular motions of all the other interconnected units within the macrocycle **110**, namely, the attached ferrocene unit (Figure 47b – blue parts), the zinc porphyrins (Figure 47b – red parts), and finally the bis-isoquinoline "pedals" as the rotating guest molecule (Figure 47b – yellow parts). Finally, in 2008 Gin *et al.* reported a nice example of the applicability of metalloazobenzenophanes in supramolecular chemistry.[525] Their liquid crystalline monomeric macrocycles **111** (Figure 48a), consisting of a two azobenzene ligands interlinked by two $Pt^{(II)}(PEt_3)_2$ units as bridging linkers, were shown to self-assemble into a thermotropic columnar hexagonal liquid crystalline phase (Figure 48b). Furthermore, they found, that upon (*E*,*E*) → (*Z*,*Z*) photoisomerization the interior diameter of the macrocycles, and thus also of the whole supramolecular assembly, increases from 4 Å in the (*E*,*E*)-form to over 11 Å in the (*Z*,*Z*)-form (Figure 48c). This triggers the hope for a potential application of the described system as a nanopore that can reversibly adjust its shape according to an external stimulus and can hereby, selectively allow or exhibit the passage of medium-sized molecules.

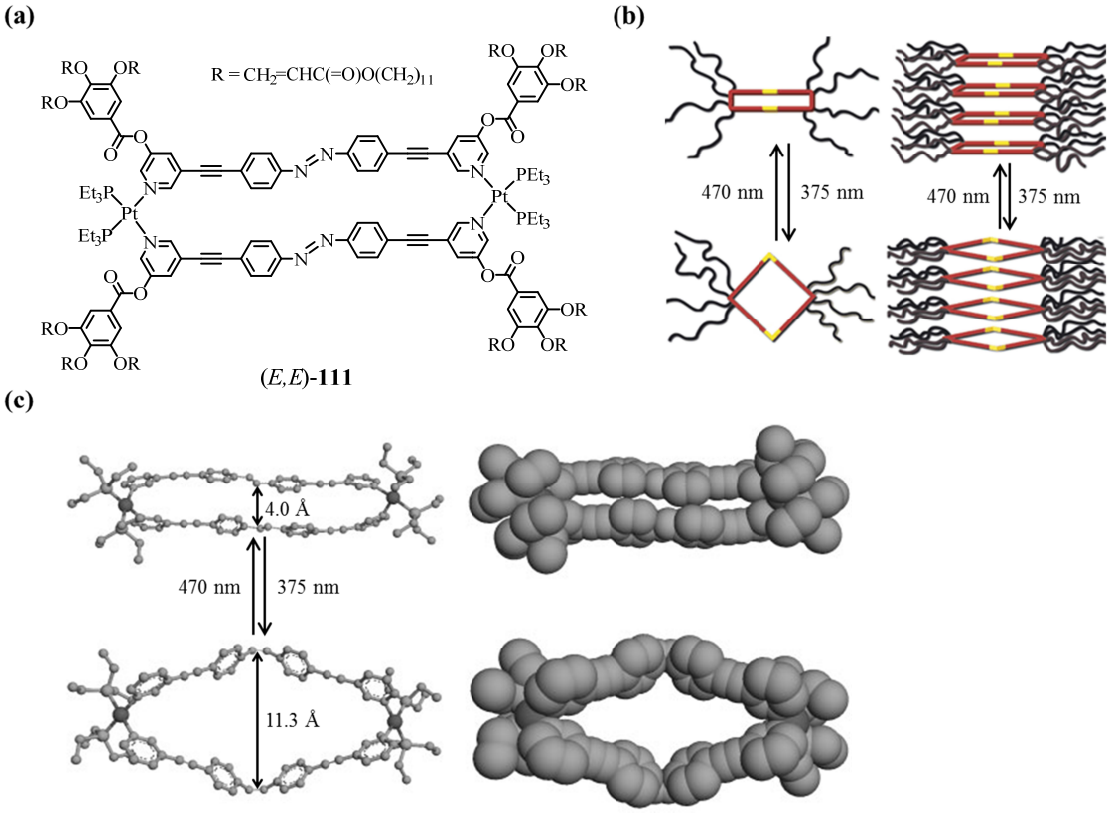

Figure 48: (a) Chemical structure of the metalloazobenzenophane (*E*)-**111**, **(b)** schematic illustration of the macrocycle's self-assembly into hexagonal columns, **(c)** Depiction of the crystal structures showing the increase of the internal pore diameter upon its (*E*,*E*) → (*Z*,*Z*) photoisomerization. Figures 48b+c adapted with permission from Pecinovsky *et al.*[525]

2 Aim of the Work

In the trendsetting field of molecular electronics quite a number of molecular devices, such as molecular wires,[1,2] switches,[3] rectifiers,[4] transistors[5,6] and complete memory devices[7,8], have been reported over the last decades. The integration as well as the advancements of such devices represent an inevitable challenge on the road towards ongoing miniaturization in future nanotechnology. In this context, especially molecular switches, as one of the above mentioned key functionalities, have attracted a lot of interest and some impressing progress has been reported in this area throughout recent years.[526] However one of the key tasks that remains to be solved, is the integration of the named functionalities at a single molecular level in order to approach the goal of ultimate miniaturization of electronic devices. This holds also true for the kinds of molecular switches reported so far, which are rarely at a single molecular level, and most often only addressable by external stimuli like light or temperature. However, the future utilization of the named external stimuli and hence the implementation of the resulting switching systems within the prospective generation of computers or electronic devices seems rather unlikely. Thus, in order to really approach an actual implementation of single molecular switches into the electronic devices of the future, the tackling of these issues appears to be inevitable. This also gave rise to the projects outlined and investigated throughout this doctoral thesis, which can be commonly ascribed to the superordinate goal of the development of externally stimulizable single molecular spin switching systems.

In detail, the work and results described throughout this doctoral thesis address three different projects. Overall topics, hereby, forming the general fundament of all the described projects are:

(a) the molecular structures of all three independent main projects include either homoleptic or heteroleptic Fe(II)-bis(terpyridine) motifs as the crucial integral parts of their core units, and

(b) the common ultimate goal of all projects is a reversible single molecular spin switching behavior (low spin $\leftrightarrow$ high spin) or generally the presence of spin crossover (SCO) phenomena based on a geometrical distortion of the $Fe^{(II)}$ core ion's coordinative environment, which should be addressable via external stimuli.

The externally induced spin switching processes, herein, are to be stimulated and studied:

(1) via the variation of the externally applied electric fields within mechanically controllable break junction (MCBJ) setups,

(2) by investigating the bias-dependency of surface-absorbed target complexes using scanning tunneling microscopy (STM) techniques,

(3) by varying the mechanical stress imposed on the investigated target structures within MCBJs,

(4) via ^{1}H-NMR spectroscopic monitoring of the effects arising from photoinduced switching of the macrocyclic target structures.

The objectives of the projects presented within this doctoral thesis therefore are:

Objective of 1st Project: The investigation of voltage-triggerable single molecular spin switching phenomena of a variety of heteroleptic Fe(II)-bis(terpyridine) complexes, containing a neutral ligand destined for the immobilization of the complex within an MCBJ setup and a second, dipolar ligand designated to effectuate the desired bias-sensitivity of the system (Figure 49). The specific targets of this project thus involve: (a) the development of an appealing, modular synthetic approach to obtain a terpyridine core moiety with the suitable 4,4′′-disubstitution pattern, which is required for the intended electronic functionalities of all the target compounds presented throughout this work, (b) the design and synthesis of the three different classes of extended terpyridine ligands needed for the envisaged target compounds, namely, (i) neutral ligands bearing a suitable anchoring group allowing the molecule's immobilization onto the Au-electrodes within the MCBJ, (ii) dipolar ligands evoking the desired bias-sensitivity of the target structures in an alterable externally applied electric field, and (iii) unsubstituted neutral ligands showing sufficient structural similarity to the dipolar ligands to serve as appropriate test systems in the corresponding complexes, (c) the development of a suitable assembly and purification strategy of the heteroleptic target complexes, and (d) the physical investigation of potential spin-switching behavior at the single molecular level by means of measuring the corresponding conductance traces and *I*/*V*-characteristics upon altered applied electric fields in an MCBJ setup.

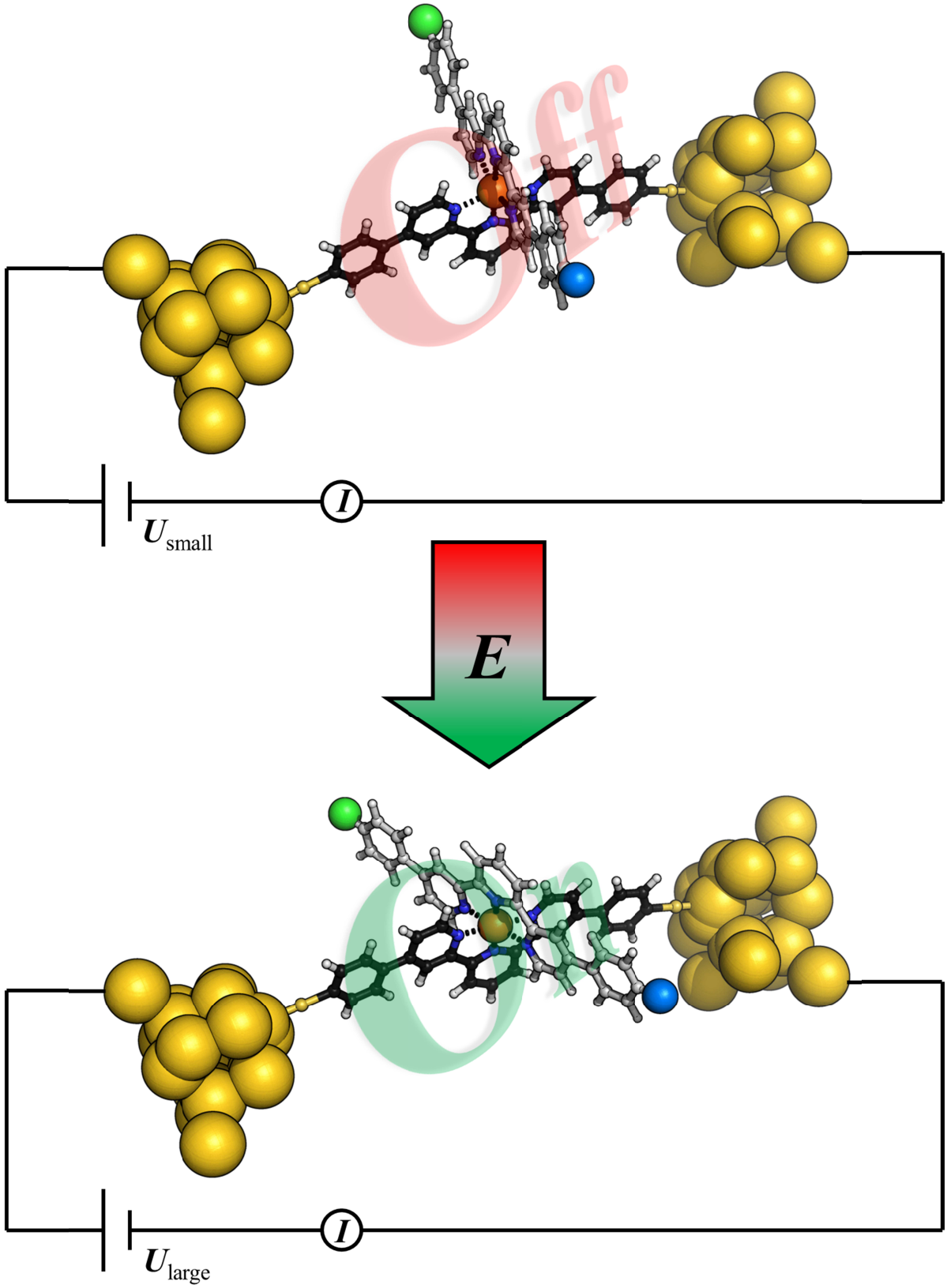

Figure 49: Concept picture of the first objective illustrating the integration of a potentially spin-switching heteroleptic Fe(II)-bis(terpyridine) complex into an MCBJ and the effect of alternating externally applied electric fields onto the structures geometry, and hence onto the core ion's spin state.

Objective of 2nd Project: To investigate bias-dependent SCO phenomena of surface-absorbed homoleptic, dipolar Fe(II)-bis(terpyridine) complexes, which were previously immobilized onto Au(111)-surfaces via electrospray ionization, by using scanning tunneling microscopy (STM) (Figure 50). The specific targets of this project therefore involve: (a) the design and synthesis of appropriate dipolar terpyridine ligands suitable for the envisaged functionality, (b) the assembly of the desired homoleptic, dipolar Fe(II)-bis(terpyridine) complexes, (c) the investigation of Au(111) surfaces functionalized with the described homoleptic, dipolar Fe(II)-bis(terpyridine) complexes via electrospray ionization, by utilizing an STM setup for the purpose of surface characterization, and (d) the effect of bias impulses of varying strength on the observed results during the STM measurements.

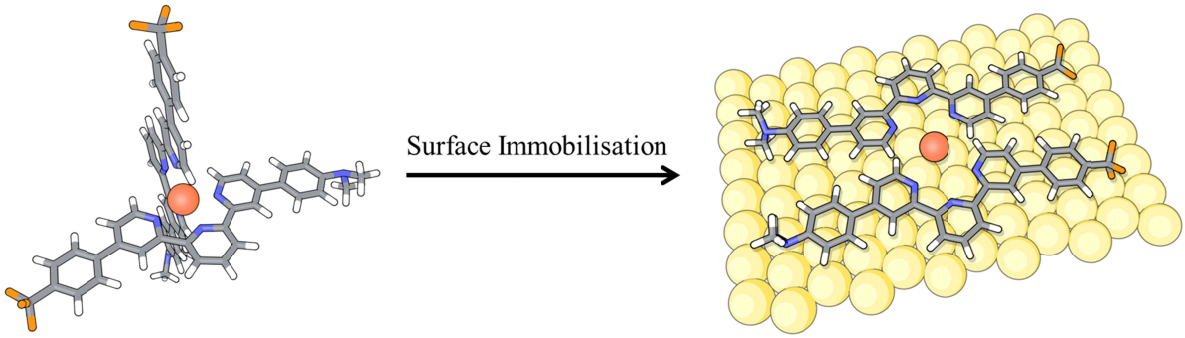

Figure 50: Concept picture of the second objective illustrating the investigation of bias-dependent SCO phenomena induced by the surface-absorption, and the coinciding distortion of the formerly octahedral complex geometry, of a homoleptic, dipolar Fe(II)-bis(terpyridine) complex, using the STM technique .

Objective of 3rd Project: To investigate mechanically induced single molecular spin switching phenomena arising from the geometrical distortion of a homoleptic Fe(II)-bis(terpyridine) complex integrated into an MCBJ setup (Figure 51). The specific targets of this project therefore involve: (a) the design of a tailor-made terpyridine ligand only allowing an unique single-sided attachment of the ligand to an electrode's surface, hence being suitable for the envisaged functionality, (b) the development of an efficient synthesis of this required ligand, (c) the assembly of the desired homoleptic Fe(II)-bis(terpyridine) complex, (d) the assembly of the analogue Ru(II)-bis(terpyridine) complex as an appropriate reference compound, and (e) the physical investigation of potential spin-switching behavior at the single molecular level by means of measuring the corresponding conductance traces and *I*/*V*-characteristics upon altered mechanical stress imposed onto the investigated target structures within MCBJs.

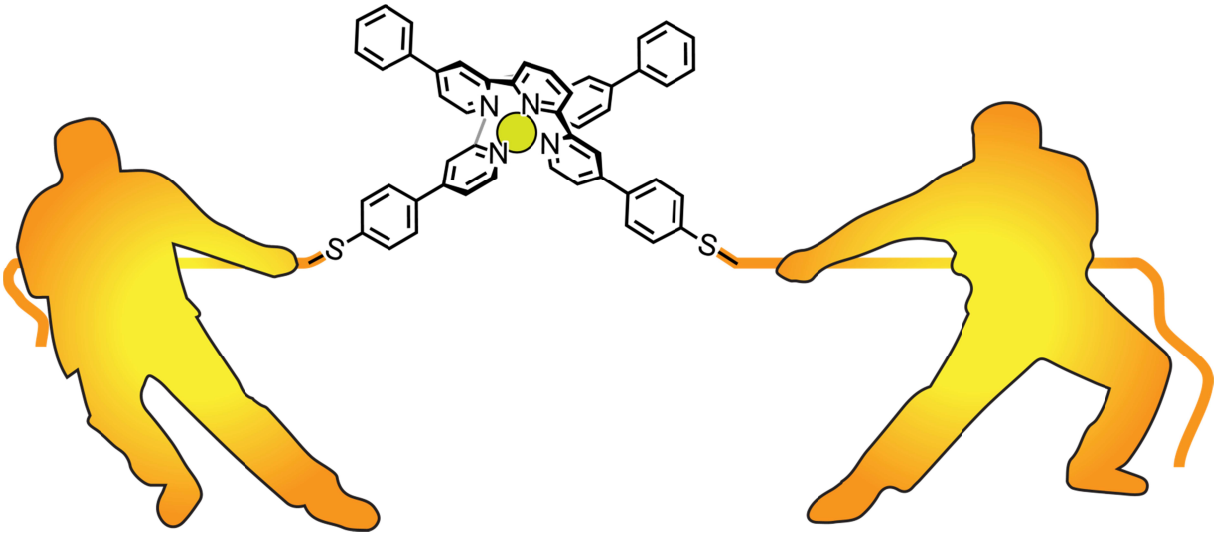

Figure 51: Concept picture of the third objective illustrating the integration of a potentially spin-switching homoleptic Fe(II)-bis(terpyridine) complex into an MCB**J** and the effect of alterable mechanical stress imposed onto the investigated target structures.

Objective of 4th Project: To investigate photosensitive metalloazobenzenophanes acting as molecular photo- and potentially spin-switching macrocyclic entities (Figure 52). The specific targets of this project thus involve: (a) the molecular design of photoswitchable metalloazobenzenophanes, (b) the development of an efficient synthesis of the required bis(terpyridine) azobenzene ligand, (c) development of a procedure for the selective intra-molecular macrocyclization leading to the assembly of the desired metalloazobenzenophanes, (d) the investigation of the optical properties of these metalloazobenzenophanes, and (e) the investigation of photoinduced $E \rightarrow Z$ and $Z \rightarrow E$ as well as thermal $Z \rightarrow E$ isomerization processes within the desired metalloazobenzenophanes by the use of ^{1}H-NMR spectroscopy.

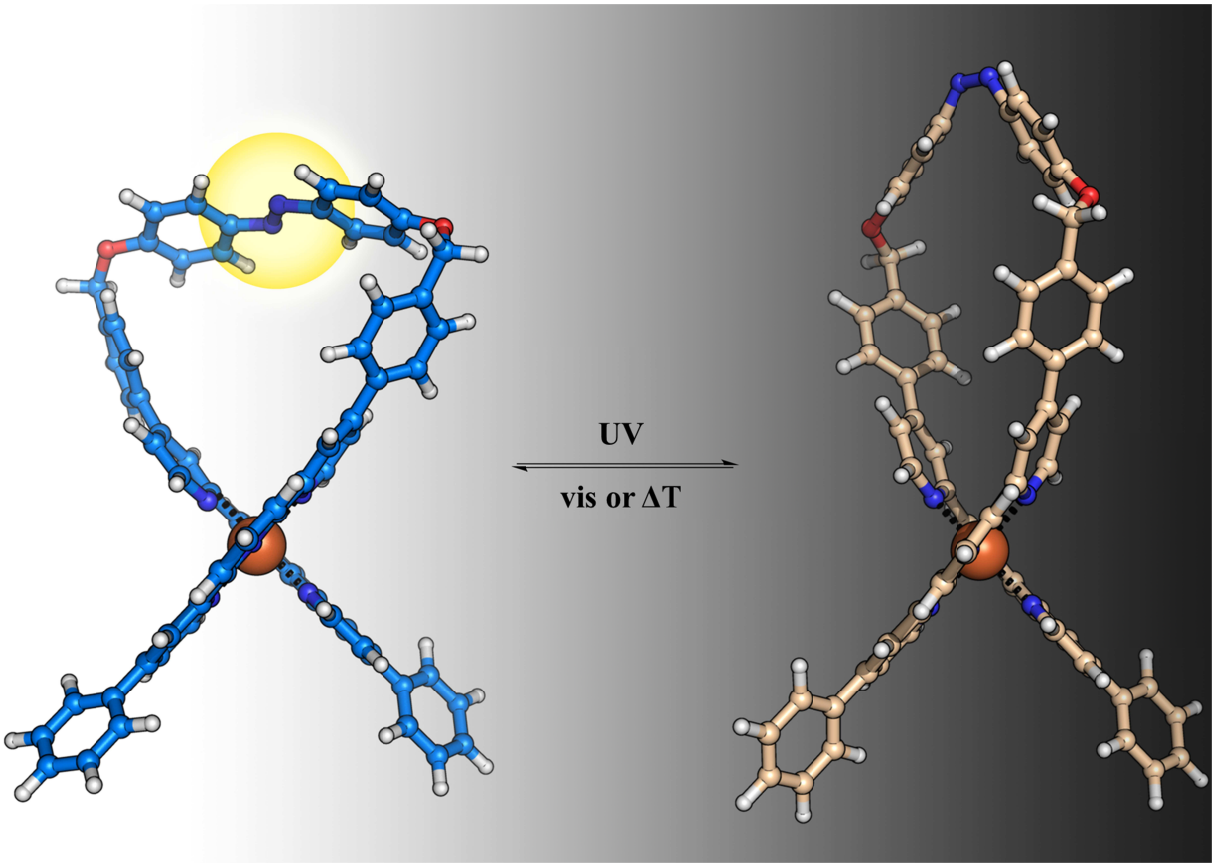

Figure 52: Concept picture of the fourth objective illustrating the reversible photoisomerization of an Fe(II)-bis(terpyridino)azobenzenophane acting as a molecular photo- and potentially spin-switching macrocycle.

3 Voltage-Triggered Single Molecular Spin Switches

The present chapter encompasses two main projects and objectives of this doctoral work:

(1) The design, synthesis and physical investigation of a variety of voltage-triggerable single molecular spin switching systems that are immobilized and consequently studied using mechanically controllable break junction (MCBJ) techniques.
(2) The design, synthesis and physical investigation of bias-dependent spin crossover (SCO) phenomena of appropriate dipolar, homoleptic target structures, which are immobilized onto Au(111)-surfaces, by means of scanning tunneling microscopy (STM).

Hereby, the molecular design, the switching concept (Chapter 3.1), the chosen synthetic approaches (Chapters 3.2 and 3.3), and the physical results (Chapter 3.4) arising from the first project, namely, the investigation of bias-sensitive single molecular spin switching systems, are presented in this chapter. The results arising from the MCBJ measurements are discussed in Chapter 3.4.3. In the second project, bias-dependent SCO phenomena of appropriate surface-absorbed dipolar complexes (Chapters 3.2.2 and 3.3.3.2), are studied. The main from the second to the first project is the use of STM as the physical investigation method of choice for the slightly different corresponding target structures of the second project. The results obtained from these measurements are comprehensively discussed within chapter 3.4.4.

The reason to present both projects within one contiguous chapter arises from the circumstance that both switching concepts rely on the application of the same external trigger, namely, the applied electric field. Although the way in which the target structures are to be exposed to these electric fields differs significantly due to the intrinsic differences of the physical techniques the measurements rely on (MCBJ vs. STM), both projects commonly aim at the investigation of the influence of electric field's strength and direction onto the investigated systems. Taking these commonalities into account it seems feasible to interlink the two projects throughout the following section.

3.1 Switching Concept and Molecular Design

3.1.1 Design of Voltage-Triggered Single Molecular Spin Switches

In order to permit the actual development a voltage-triggered single molecular spin switch the utmost significant building block required is a molecular subunit exhibiting an externally addressable spin state. Excluding organic radical chemistry, this gives rise to a very limited number of transition metals that actually feature such an externally addressable spin state, namely, iron, cobalt, and nickel. The metal ions of all three named elements likewise exhibit the capability to exist either in a high spin (HS) or in a low spin (LS) state. Due to several motives the choice fell onto complexes based on hexa-coordinate Fe(II) ions as the core subunit of the envisaged target structures. Fe(II) ions were herein, considered preferable mainly due to their usually easier synthetic access, if compared e.g. to tetra-coordinate Ni(II) complexes, as well as due to their typically facilitated analytical characterization via nuclear magnetic resonance (NMR) techniques, if compared to Co(II) complexes, arising from the fact that Fe(II) complexes in the LS ground state are diamagnetic, whereas Co(II) complexes in a LS state already exhibit paramagnetic behavior.

Most established systems comprising Fe(II) ions as the SCO system, which have also been repeatedly reported in literature, are Fe(II)-bis(terpyridine) complexes, as a typical example of an Fe(II) species exhibiting six coordination sites arranged into an octahedral coordination environment. Within such a system the accommodation of the six 3d electrons of the Fe(II) ions into five spin degenerate levels allows the system to be found in the two different desired spin states, namely, the LS and the HS state. Hereby, in the LS state, the crystal field interaction is strong enough, to pair up all the electrons giving a ground state with zero net spin (S = 0). A reduction of the crystal field strength, for example, can be induced by changing the type of ligands, or by increasing the metal-ligand distance. As a result the HS state can become energetically more favorable compared to the LS state, resulting in the envisaged LS → HS spin switching process. In the HS state the degenerate levels now are filled according to Hund's rule, thus leading to a maximization of the total net spin (S = 2). In order to allow for the integration of the desired target structures into the appropriate physical setups, in this case into an MCBJ setup, and to furthermore, ensure the addressability of the core ion's spin state by the externally applied electric field, the choice fell onto the

heteroleptic variants of Fe(II)-bis(terpyridine) complexes containing two individual ligands to fulfil the described individual functions within the target structures. Adapting the idea of a molecular cruciform, as previously reported by Grunder *et al.*,[527,528] our molecular design envisaged the utilization of a symmetric, thiol-terminated terpyridine (tpy), ensuring a proper immobilization of the desired target structures onto the gold electrodes within the MCBJ setup as the first ligand. A second, asymmetric tpy ligand was proposed to bear an inherent dipole moment. This dipolar feature arises from the presence of an intrinsic push/pull system, such as a combination of an EWG (e.g., CF_3), and an EDG (e.g., $N(CH_3)_2$) in the asymmetric ligand's structure, in order to render possible the addressability of the overall target structures by the applied electric fields (Figure 53).

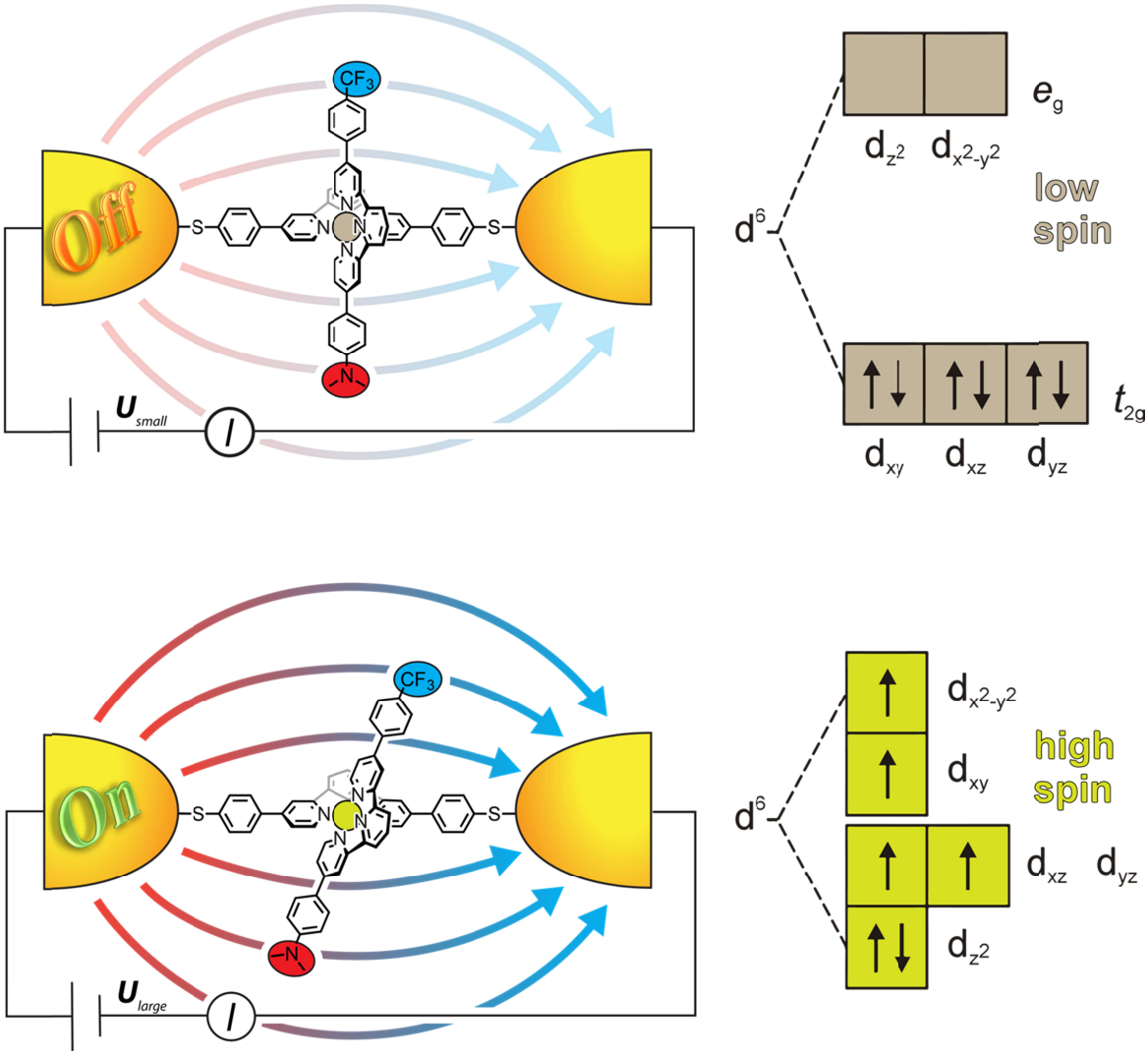

Figure 53: Schematic illustration of the postulated switching concept for the envisaged heteroleptic Fe(II)-bis(terpyridine) complexes. The two states, namely, the *OFF*-state (LS), and the *ON*-state (HS) illustrate the effect of an increasing electric field on the target structures. Herein, the geometrical distortions of the originally octahedral target structures (*OFF*-state, LS), induced by an increasing and adjustable, applied electric field, eventually results in a switching of the core ion's spin state (LS → HS) upon sufficient externally applied stimuli.

Summarizing, the addressability of the dipolar target structures **112-118** towards an alteration of the applied electric fields, as the basis for the envisaged LS → HS spin switching process, therefore conceptually originates from a cascade of different effects (for theoretical details on SCO, see chapter 1.1.4.1, particularly Figure 20), namely:

(1) The alignment of the dipolar push/pull ligand coincides with a spatial distortion of the former octahedral coordination environment of the Fe(II) LS complex.
(2) Going along with this geometrical distortion, the Fe-N bonds in the immobilized target structures are elongated, to compensate for the increasing steric repulsion between the two outer pyridine rings of the tpy ligands, respectively.
(3) This elongation of the Fe-N bonds results in an overall weakening of the ligand field (LF) strength Δ of the Fe(II)-bis(terpyridine) structural motif, which is equivalent to a reduced crystal field splitting between the lower energetic t_{2g} orbitals and the higher energetic e_g orbitals.
(4) As long as the LF splitting energy Δ is still bigger than the mean spin pairing energy P the system remains in the LS state with all electrons being paired up. This behavior changes as soon as P is no longer overcompensated by Δ. As a result the electrons will also occupy the e_g orbitals, resulting in the formation of the HS species, following Hund's rule.

Furthermore, the variation of the dipolar strengths of the push/pull ligands in the Fe(II)-based target structures should help to gain additional insights about the sources of the physical observations made. Hereby it should be sorted out, which physical observations are truly related to the desired bias-dependant spin switching phenomena, and which observations arise from some non-specifiable side effects linked to instrumental details of the applied experimental setup. The latter effects were thus hoped, to be excludible to the biggest possible extent. To allow for this required versatility of the envisaged, potentially spin-switching, heteroleptic dipolar target structures, in addition to the requirement of further reference compounds acting as conceptual, non-addressable blanks, the utilized synthetic route was required to fulfil an utmost degree of modularity. The motivation to ensure this modularity is the facilitation of the assembly of a broad variety of different dipolar, as well as non-dipolar target structures from the very same simple core building block. Figure 54, displayed hereafter, is intended to give a brief overview of the most important dipolar, heteroleptic Fe(II)-bis(tpy) complexes **112**–**118**, representing the potentially spin-switching target structures.

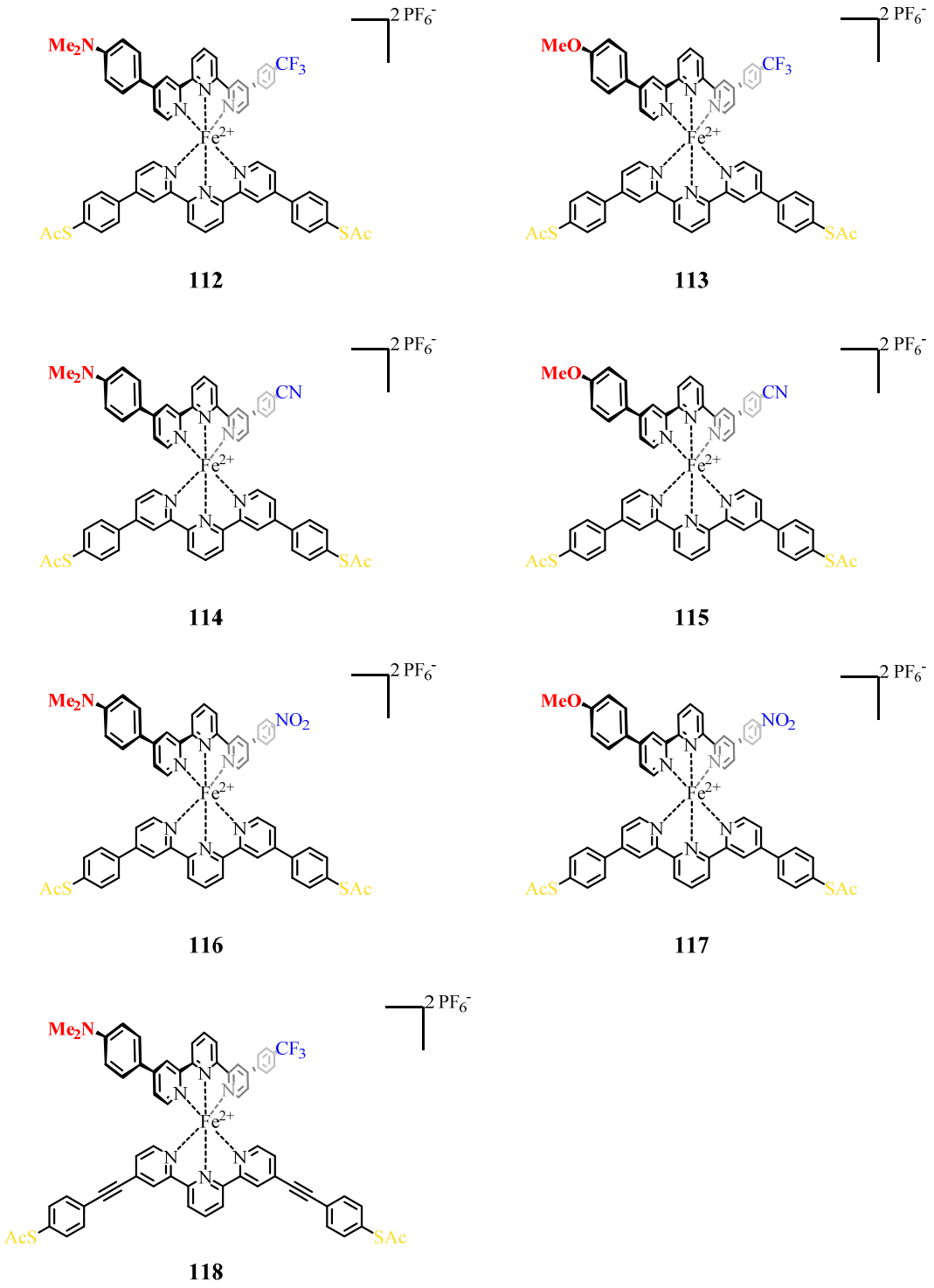

Figure 54: Envisaged heteroleptic Fe(II)-bis(tpy) target complexes **112**–**118** exhibiting an electrically addressable, dipolar tpy ligand to permit the spin switching of the Fe(II) core ion upon the alignment of the push-pull ligands' intrinsic dipole moments into the externally applied electric fields within the MCBJ setup.

Concerning the molecular design of the target structures of the above-mentioned second project, namely, the investigation of potentially bias-dependent SCO phenomena of appropriate surface-immobilized dipolar, homoleptic Fe(II)-based target complexes, it was hoped to access these from the same modular key building block, like the previously

illustrated heteroleptic target structures. Conceptually the envisaged homoleptic target complexes **119** and **120** (Figure 55) were supposed to contain two identical dipolar tpy ligands, which, after the deposition of the target complexes onto appropriate conducting Au(111) or partially insulating Cu_2N/Cu(100) surfaces, should be aligned to an electric field applied axially parallel to the surface.

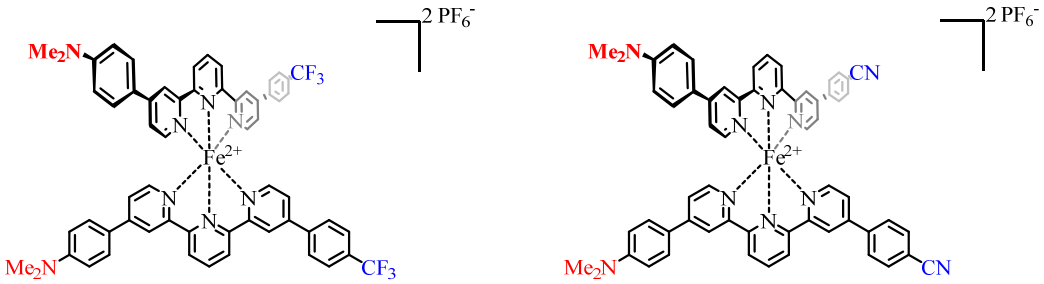

119 **120**

Figure 55: Envisaged homoleptic, dipolar Fe(II)-bis(tpy) target complexes **119** and **120** exhibiting two identical electrically addressable push/pull ligands, in order to permit the spin switching of the Fe(II) core ions by the alignment of the ligands' intrinsic dipoles into externally applied electric fields during the STM measurements on the surface-immobilized complexes.

Furthermore, we hoped that during the successive STM experiments, which were planned for the surface-attached homoleptic complexes' characterization, we would be able to demonstrate the envisaged spin switching to the HS state, by giving direct evidence for the existence of this HS state via a potentially observable Kondo effect.

3.1.2 Design of Suitable Reference Compounds

In addition to the desired potentially spin switching Fe(II)-bis(tpy) target complexes **112-118**, also a number of suitable test and reference compounds was envisaged, in order to verify the hypothesis of the named bias-sensitive target structures. Generally, two subgroups of reference compounds have been designed. The first group contains a series of Fe(II)-bis(tpy) complexes **121**–**126** (Figure 56), which should be not addressable by the utilized trigger, namely, the alteration of the applied electric fields within the MCBJ setup. Additionally, the complexes should also be inert towards the envisaged geometrical alterations of the Fe(II) core ion's coordination environment as the source of the desired spin switching.

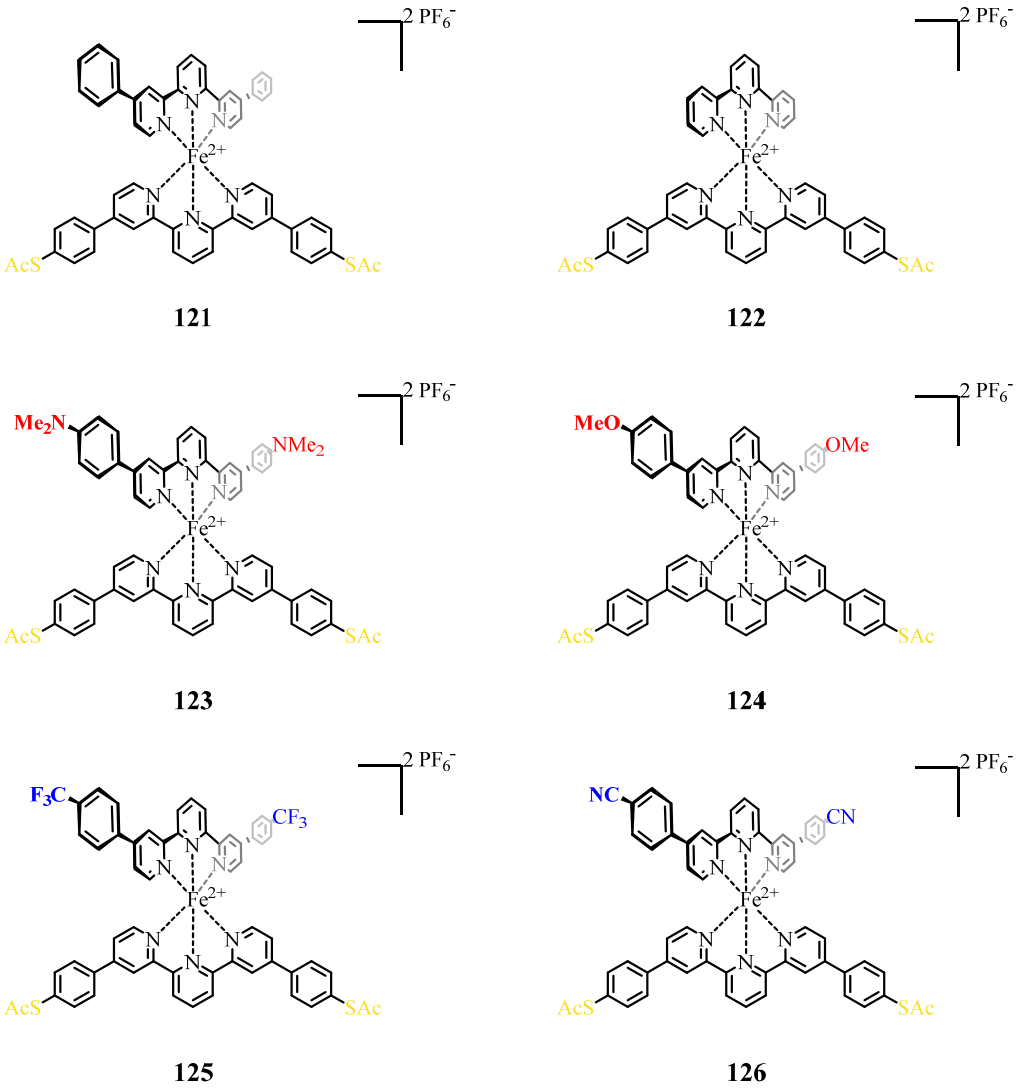

Figure 56: Envisaged heteroleptic Fe(II)-bis(tpy) reference complexes **121**–**126** acting as conceptual blanks, which are not addressable by the utilized external trigger.

According to the aspired synthesis of a highly versatile and easily modifiable core building block, as described in the previous chapter, the resulting modularity of the applicable synthetic pathways was meant to enable a facile access of this group of non-addressable reference compounds **121**–**126**, acting as conceptual blanks.

Another reference compound, appearing to be inevitable for discussing the results in the subsequent chapters, is represented by heteroleptic Ru(II)-bis(tpy) complex **127** (Figure 57). In contrast to the previous group of test compounds, this complex contains a dipolar tpy ligand, just like the Fe(II)-based envisaged SCO complexes. In contrast to those, however, the Ru(II) complex **127** should not be able to exhibit SCO at all.

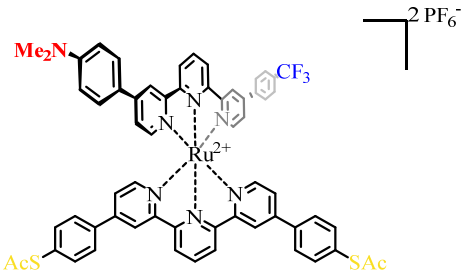

127

Figure 57: Molecular design of the envisaged heteroleptic Ru(II)-bis(tpy) complex **127** as a test system, which is addressable by the applied external stimulus, but incapable of SCO.

In summary, the two envisaged types of targeted reference complexes are supposed to deliver well-founded arguments, that observations made for the dipolar Fe(II) complexes **112**–**118** actually arise from a spin-switching process. Side effects, which should, hereby, be excluded to the greatest possible extent. These side effects include nanoscopic deviations in the nano electrode's shape, coordinative surface interactions of some of the heteroatomic end groups of the dipolar ligands, or even potential van der Waals interactions of unsubstituted phenyl end groups.

3.2 Synthetic Strategy

This chapter starts with the discussion of a general retrosynthetic analysis of the desired heteroleptic, dipolar Fe(II)-based target structures **112**–**118**. Subsequently, a discussion of the general retrosynthetic approach towards homoleptic, dipolar Fe(II)-based target structures **119** and **120** will be given, prior to the illustration of the general synthetic strategies towards the envisaged reference complexes **121**–**127**. Since all three classes of complexes should be accessible from the same modularly applicable tpy core building block **47**, in the first chapter the retrosynthetic accessibility of this key building block will be discussed separately.

3.2.1 Retrosynthesis of Heteroleptic Fe(II)-bis(tpy) Complexes

Retrosynthetically, from the class of the desired heteroleptic, dipolar Fe(II)-based target structures **112**–**118**, the complexes **112**–**117** should be accessible via an identical

retrosynthetic approach (Scheme 17), whereas complex **118** requires a slightly adapted synthetic strategy (Scheme 19).

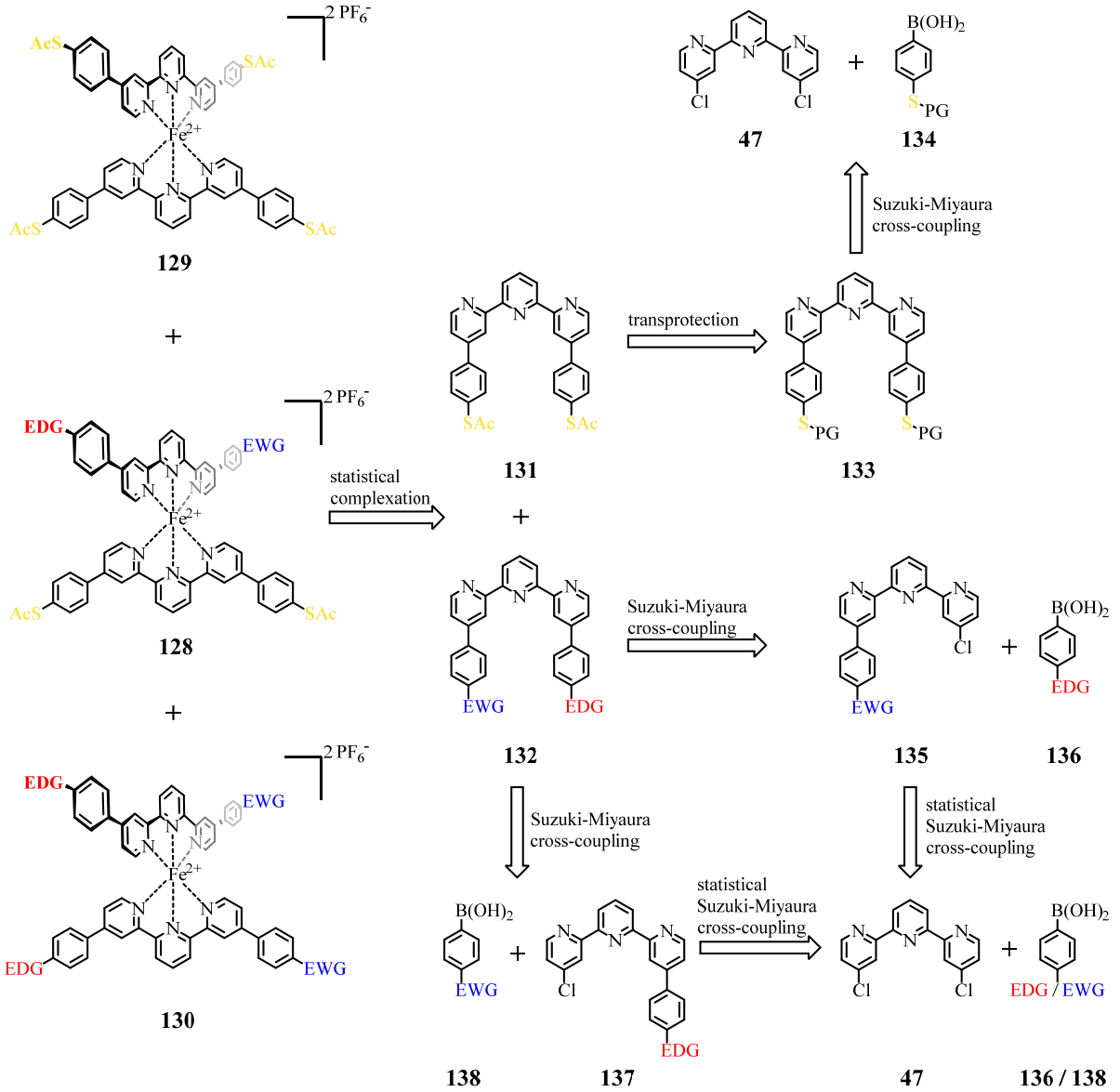

Scheme 17: Retrosynthetic analysis of the heteroleptic, dipolar Fe(II)-bis(tpy) target complexes **112 - 117**, which are represented by complex **128** for clarity reasons.

Following the retrosynthetic strategy illustrated in scheme 17 heteroleptic Fe(II)-bis(tpy) complexes **128** can be obtained in a statistical complexation reaction of a 1:1 mixture of the symmetric tpy ligand **131** and an asymmetric tpy ligand **132** bearing an intrinsic dipole moment, due to its incorporated push/pull system. According to the envisaged reaction conditions, a statistical mixture of the heteroleptic target structure **128** and the two homoleptic side products **129** and **130** has to be expected in a ratio of 1:2:1 for complexes **129:128:130**. The symmetric tpy ligand **131** can be obtained via a transprotection of the sulfur protective groups (PGs) in compound **133**, which itself should be accessible from the appropriate 4,4´´-

disubstituted tpy core building block **47** and the boronic acid **134** via a twofold Suzuki-Miyaura cross-coupling reaction. The asymmetric tpy ligand **132** can be obtained via two different routes. The first route involves a Suzuki-Miyaura cross-coupling of the asymmetric tpy derivative **135**, which is substituted with a terminal EWG, and the EDG-substituted boronic acid **136**. Alternatively, the asymmetric tpy ligand **132** can be obtained by the Suzuki coupling of the asymmetric tpy derivative **137**, which is substituted with a terminal EDG, and the corresponding EWG-substituted boronic acid **138**. Both tpy derivatives **135** and **137**, alike, can be obtained via the previous statistical Suzuki-Miyaura cross coupling reactions of 4,4′′-dichloro-2,2′:6′,2′′-terpyridine (**47**), and the appropriate boronic acid **136** or **138**, respectively. Retrosynthetically, the utmost important 4,4′′-disubstituted tpy core moiety **47** bearing two substitutable chlorine atoms in the 4- and 4′′-positions can be obtained via a variety of synthetic pathways. These pathways include, for example, ring-assembly strategies (see chapter 1.2.1.1), such as (a) the Aldol-type Kröhnke condensation reaction, or (b) the Sauer methodology as an inverse-type Diels-Alder reaction. Further possible pathways include cross-coupling reactions (see chapter 1.2.1.2), such as (c) the Stille-type coupling of the appropriate organostannylpyridine and halopyridine precursors, respectively, or (d) the Suzuki-Miyaura-type cross-coupling of the according halopyridine and organoboron pyridine precursors. With regard to the focus of this work Scheme 18 illustrates only the most feasible examples of cross-coupling pathways, namely, the two Stille-type coupling routes (red and orange routes), and the two corresponding Suzuki-Miyaura-type coupling routes (green and blue routes). By applying Suzuki-Miyaura conditions, the 4,4′′-disubstituted tpy **47** can be obtained via the twofold coupling reaction of 2,6-dihalopyridine **139** with lithium boronate **140**, which itself should be accessible from 2-bromo-4-chloropyridine (**141**) (green route). Alternatively, **47** can be obtained by the coupling of **141** with the 2,6-bis-lithium boronate salt **142**, which should be accessible via the twofold borylation of dihalopyridine **139** (blue route). If, in contrast to this, Stille-type coupling methodologies are envisaged, there are in principle two analogue pathways with the difference, that 4-chloro-2-trimethyltin pyridine **143** (orange route) and 2,6-bis-trimethyltin-pyridine derivative **144** (red route) substitute the roles of the corresponding lithium boronate salts **140** and **142**, respectively, in the Suzuki-Miyaura-type approaches.

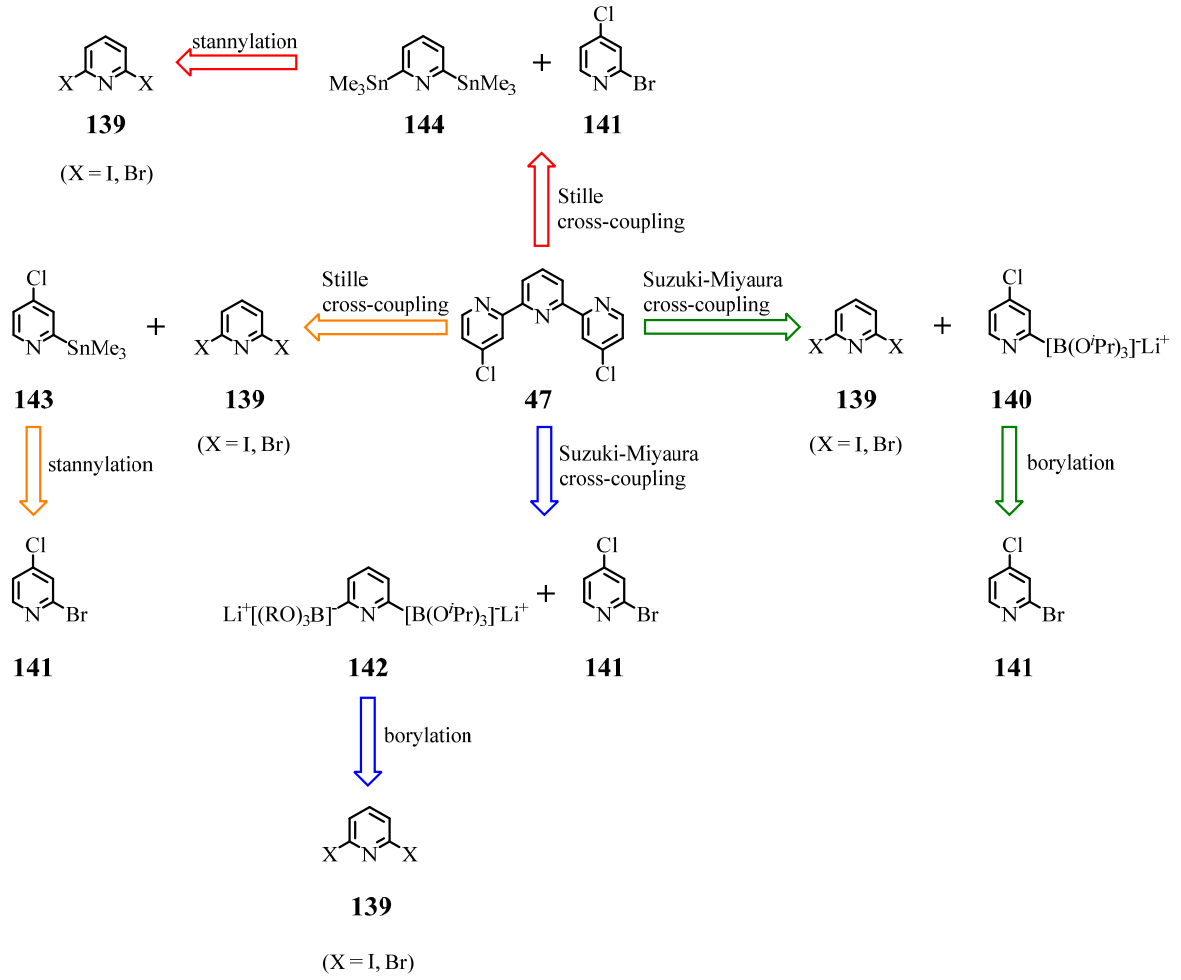

Scheme 18: Depiction of selected retrosynthetic pathways towards the 4,4′′-disubstituted tpy core building block **47** taking only Stille- and Suzuki-Miyaura-type cross-coupling methodologies into account.

The retrosynthetic analysis of target complex **118**, resembles the one illustrated for the heteroleptic target complexes of type **128**, apart from an elongation of the symmetric, thiol-terminated tpy ligand **145** by two interposed acetylene groups. Retrosynthetically, the target complex **118**, can be obtained with its homoleptic side products **145** and **119** and is afforded after a statistical complexation reaction of a 1:1 mixture of the symmetric tpy ligand **146** and the asymmetric tpy ligand **147** with an Fe(II) source. Since this asymmetric tpy derivative **147** represents an example of the tpy ligands of the type **132**, its retrosynthetic accessibility is not further illustrated in the following Scheme 19, which is focused on the synthetic strategy towards the elongated symmetric tpy ligand **146**. This is obtained from compound **148** in a two-step deprotection / reprotection sequence. Di-acetylene tpy derivative **148** should be accessible via a Sonogashira cross-coupling reaction from the 4,4′′-disubstituted tpy core subunit **47** and the free acetylene building block **149**, which can be previously obtained in a

three-step sequence, namely, a radical addition, followed by a Sonogashira cross-coupling and the subsequent deprotection of the acetylene, from 4-bromothiophenol (**150**).

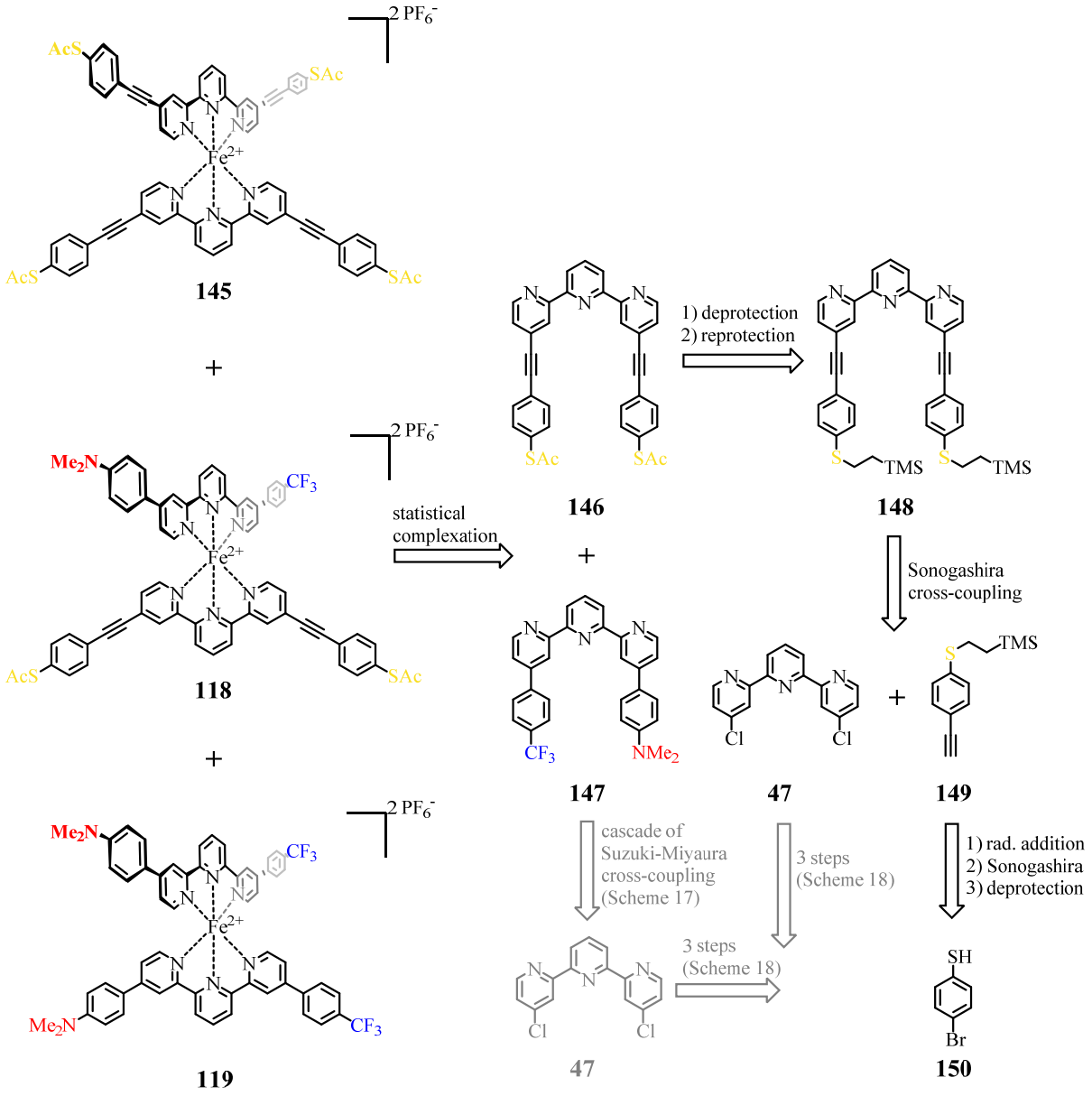

Scheme 19: Retrosynthetic analysis of the elongated heteroleptic, dipolar Fe(II)-bis(tpy) target complexes **118**.

3.2.2 Retrosynthesis of Homoleptic Fe(II)-bis(tpy) Complexes

In this section the retrosynthetic analyses will be split according to the two different subclasses of homoleptic Fe(II)-based bis(terpyridine) complexes, namely, dipolar, homoleptic Fe(II)-based tpy complexes of the type **130** (Scheme 20), containing two identical

asymmetric push/pull tpy ligands **132**, and non-dipolar, homoleptic Fe(II)-based tpy complexes structures of the type **151** (Scheme 21), which contain two identical symmetric tpy ligands **152**.

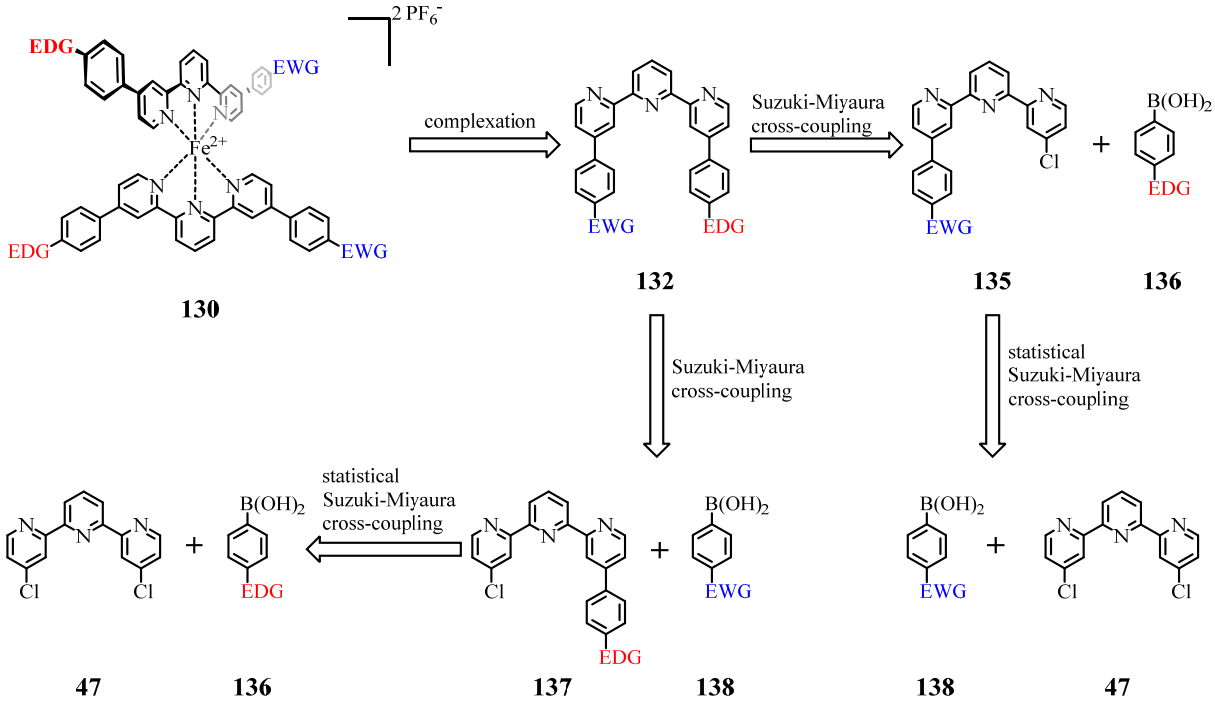

Scheme 20: Retrosynthetic analysis of dipolar, homoleptic Fe(II)-based tpy complexes of the type **130**, formed from two identical asymmetric tpy ligands **132** containing a push/pull system.

The class of dipolar, homoleptic Fe(II)-based tpy complexes of the type **130** can be accessed via the complexation reaction of two identical molecules of the corresponding asymmetric tpy ligand **132**. The retrosynthetic analysis of **132** is identical with the one displayed within scheme 17 and is therefore discussed in the previous chapter 3.2.1. The retrosynthetic analysis of the class of non-dipolar, homoleptic Fe(II)-based tpy complexes of the type **151** proceeds via the complexation reaction of two equivalents of the corresponding symmetric tpy ligand **152**. This class of symmetric tpy ligands **152** can be directly obtained via a twofold Suzuki-Miyaura cross-coupling reaction of 4,4´´-dichloroterpyridine (**47**) with the corresponding boronic acids **153**.

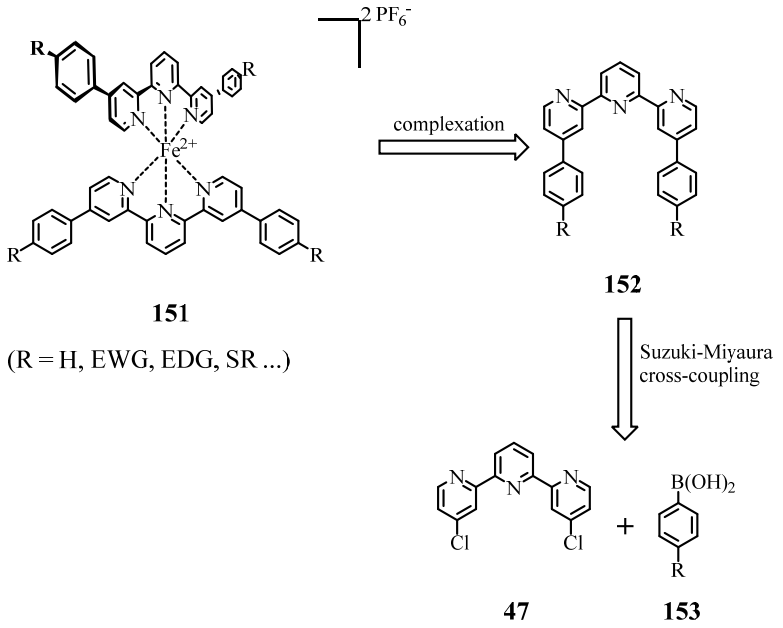

Scheme 21: Retrosynthetic analysis of non-dipolar, homoleptic Fe(II)-based tpy complexes of the type **151**, accessible from two identical symmetric tpy ligands **152**.

3.2.3 Retrosynthetic Analyses of Suitable Reference Compounds

This last retrosynthetic subchapter describes the approaches towards the heteroleptic, non-dipolar Fe(II)-based tpy complexes **121** – **126** and the heteroleptic, dipolar Ru(II)-based tpy complex **127** as the envisaged reference and test compounds of the present project. Among the first group of non-dipolar, and hence electrically non-addressable, Fe(II)-based complexes, three subgroups can be distinguished, namely, the ones containing no polar substituents (**121** and **122**), the ones containing EDGs (**123** and **124**), and the ones containing EWGs (**125** and **126**). A general retrosynthetic analysis towards all named target structures symbolized by the superordinate heteroleptic Fe(II) tpy complex **154** is shown in Scheme 22. Heteroleptic Fe(II) tpy complexes of the type **154**, in a mixture with the corresponding homoleptic side products **129** and **151**, are obtained via the Fe(II) assisted statistical complexation of the appropriate symmetric thiol-terminated tpy **131** and the non-dipolar, symmetric tpys of the type **153**. Since the retrosynthetical analyses of tpy ligands **131** and **152** have been discussed in the previous chapter 3.2.1 and in Scheme 21 the details will be skipped at this place.

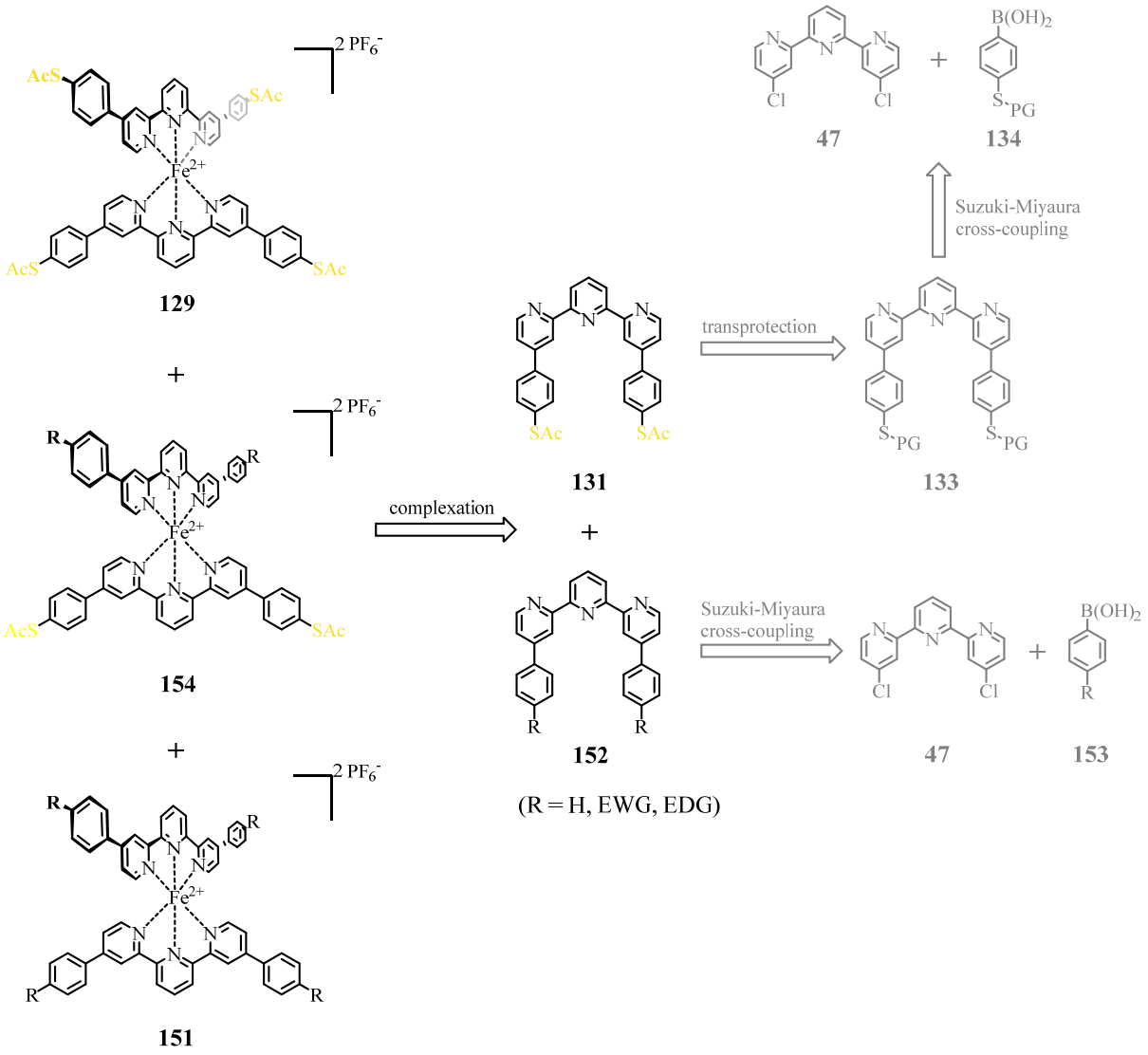

Scheme 22: Retrosynthetic analysis of heteroleptic, non-dipolar Fe(II)-bis(tpy) target complexes **121** – **126**, which are represented by complex **154**.

Finally, the retrosynthetic analysis of the heteroleptic, dipolar Ru(II)-based tpy complex **127**, representing an example of an electrically addressable, but not spin-switching complex, is displayed in Scheme 23. Herein, Ru(II)-based target complex **127** is obtained either by a statistical complexation of symmetric tpy **131** and asymmetric, dipolar tpy **132**, or it can be Alternatively, accessed by a step-by-step complexation procedure introducing one ligand at first, and then the second ligand. Since the retrosynthetic accessibility of tpys **131** and **132** has been illustrated (Scheme 17) and discussed in a previous chapter 3.2.1, the details are faded in the following overview.

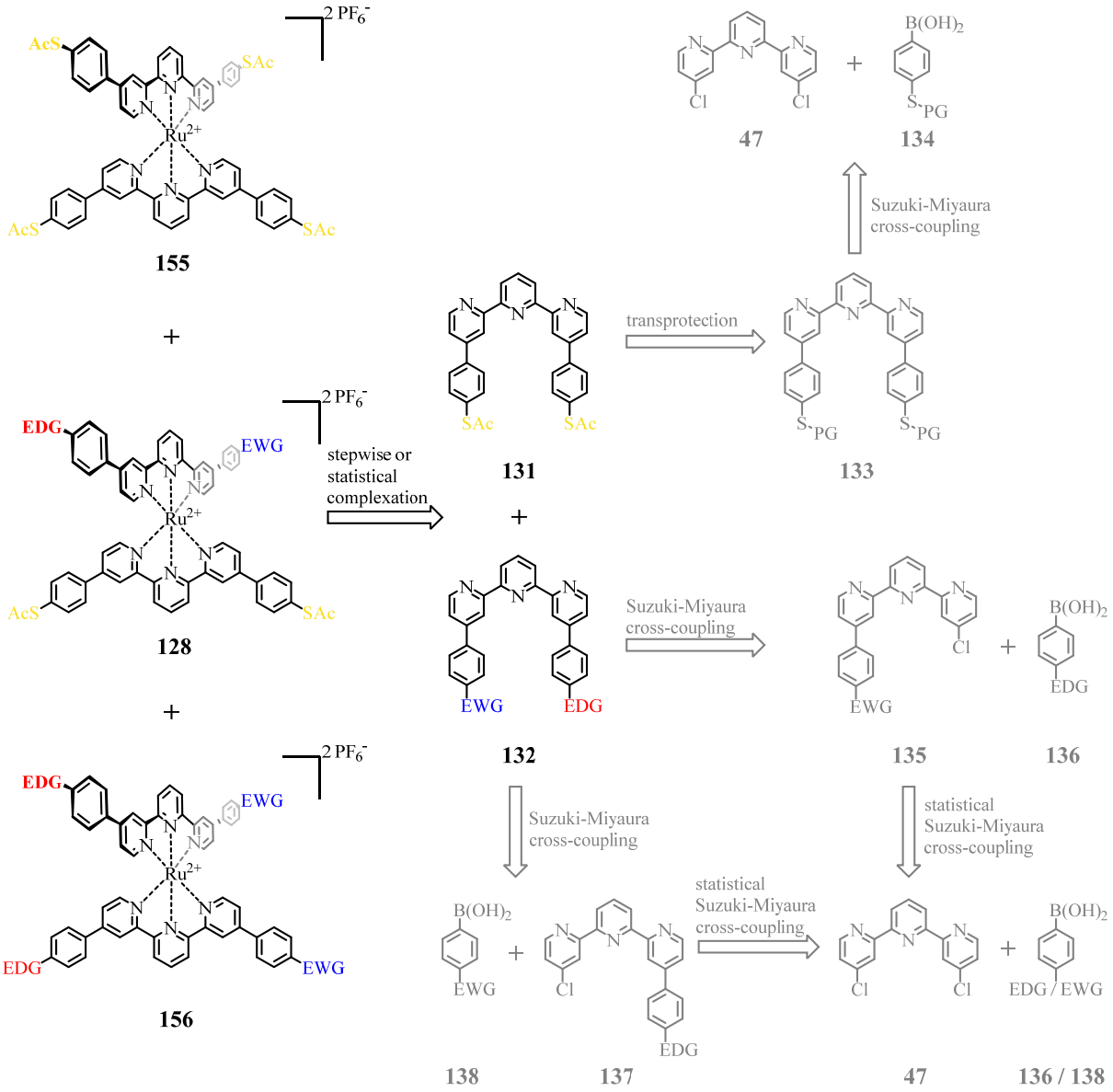

Scheme 23: General retrosynthetic pathway towards the heteroleptic, dipolar Ru(II)-bis(tpy) target complexes of the type **127**.

3.3 Synthesis

Hereafter, the synthesis of the broad variety of different target structures associated with the development of electrical field dependent single molecular spin switching molecules is described. Since the synthetic pathways during this whole work have been designed such, that they are likewise based on the same highly versatile and modularly applicable core building block **47**, the approach and synthesis of this subunit is prefixed to the detailed description of all different classes of target complexes within this project.

3.3.1 Synthesis of Terpyridine Core Subunit

Based on the variety of synthetic approaches discussed in chapter 3.2.1 and illustrated in Scheme 18, the synthesis of 4,4′′-dichloro-2,2′:6′2′′-terpyridine (**47**) was envisaged by a cross-coupling methodology. The reasons are multifaceted, and one of the main factors is the requirement of the specific described 4,4′′-disubstitution pattern in order to ensure the current transport through the Fe(II) core during the physical investigations of the assembled final target complexes. Such a substitution pattern is only very rarely reported and more or less excludes Kröhnke condensations, as the most established ring-assembly pathway towards tpy synthesis, due to the almost ubiquitous presence of extra substituents in the 4′-position of the later tpy moiety. Therefore, amongst the few reported examples of such a 4,4′′-disubstitution pattern at a tpy motif, practically all of them rely on highly toxic organotin chemistry, such as the preparation of 4,4′′-distannylated tpys, obtained via an inverse-type Diels-Alder reaction, also referred to as Sauer methodology,[529] which can be followed by a tin-halogen exchange, or the Stille-type cross-coupling formations of appropriately substituted tpy derivatives.[224] additionally, the desired building block 4,4′′-dichloro-2,2′:6′,2′′-terpyridine (**47**) was very recently assembled using a Hiyama cross-coupling protocol,[229] which from a synthetic strategy point of view however is somehow limited in versatility due to poor availability of structurally diverse starting materials. Therefore, the development of an unprecedented, Suzuki-Miyaura-type assembly strategy of the desired tpy core functionality was in the focus of research. This method should give a way broader access to a variety of different structural motifs at the tpy core, compared to the previously reported examples and meanwhile the utilization of toxic organotin derivatives can be avoided. Although it is well-known that heteroaryl boronic acids and esters bearing a C-B-bond, which is located adjacently to the heteroatom, are highly prone to proto-deboronation reactions,[399–403] inspired by the work of Billingsley and Buchwald,[407] the utilization of lithium tri*iso*propyl pyridine 2-ylborates was envisaged, to achieve the first-time preparation of a tpy moiety via a Suzuki-Miyaura cross-coupling procedure. The treatment of various commercially available 2-bromopyridine derivatives with a variety of different borylation reagents, such as $B(O\text{-}TMS)_3$, $B(OMe)_3$ and bis(pinacolato)diboron ($(Bpin)_2$), however, did not even provide traces of the desired reagents for the cross-coupling reaction. The starting material was consumed in all attempts and accordingly it was hypothesized that, if the different pyridine boronic acid derivatives were formed, they probably decomposed during the course of the reaction, work-up, or isolation

procedures. Indeed, it was found that treatment of the 2-bromo-4-substituted pyridine precursors **141** and **157**–**160** with a slight excess of *n*-BuLi in mixture of toluene and THF at -78 °C promoted the bromine-lithium exchange, and subsequent quenching with $B(O^iPr)_3$ and warming up to room temperature, provided the corresponding lithium tri*iso*propyl pyridine 2-ylborates **140** and **162**–**165** in good to excellent yields (Scheme 24). All five lithium salts described hereafter, exhibit high longterm stabilities under ambient conditions and are available in multigram quantities.

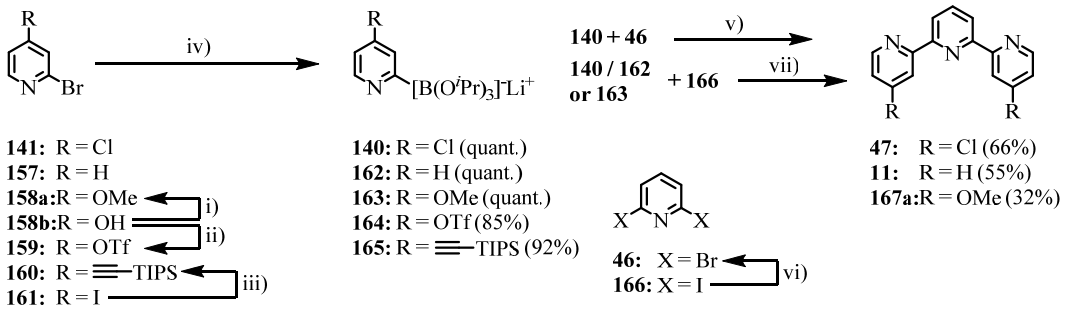

Scheme 24: Synthesis of the 4,4′′-disubstituted tpy core building blocks **11**, **47**, and **167a** via a twofold Suzuki-Miyaura cross-coupling procedure utilizing the appropriate lithium tri*iso*propyl pyridine 2-ylborate reagents **140**, **162**, and **163** as the decisive precursors allowing this coupling reaction. Reagents and conditions: **i)** NaH, MeI, DMF, 0 °C to r.t., 3d, 24%; **ii)** $(CF_3SO_2)_2O$, pyridine, 0 °C to r.t., 24h, 71%; **iii)** TIPS-acetylene, $Pd(PPh_3)_2Cl_2$, CuI, NEt_3, 0 °C to r.t., 24h, 80%; **iv)** *n*-BuLi, toluene/THF (4:1), $B(O^iPr)_3$, –78 °C to r.t., 22h; **v)** Pd_2dba_3, Ph_2PHO, KF, 1,4-dioxane, 75 °C, 60h, 50%; **vi)** NaI, HI, reflux, 7h, 76%; **vii)** Pd_2dba_3, Ph_2PHO, KF, 1,4-dioxane, 75°-85 °C, 68h.

The subsequent synthesis of the desired 4,4′′-disubstituted tpy derivatives was primarily attempted by the reaction of the 4-chloro-substituted derivative **140** and 2,6-dibromo-pyridine (**46**) to yield the desired 4,4′′-dichloro-2,2′:6′,2′′-terpyridine (**47**). For this purpose a dry Schlenk tube was charged with 1 equivalent (eq.) of **46** and 3 eq. of **140** together with the catalytic system (4 mol% Pd_2dba_3, 24 mol% Ph_2PHO) and 6 eq. potassium fluoride (KF) as base. Under an deoxygenated atmosphere the reaction mixture was dissolved in dry and degassed 1,4-dioxane. The sealed reaction vessel was subsequently heated to 75 °C for 60 h. After cooling to room temperature (r.t.) ethyl acetate (EtOAc) was added and the product **47** was isolated via filtration and subsequent flash column chromatography (FCC). Probably due to both, the air and moisture sensitivity of the catalyst/ligand complex and the limited reactivity of the bromine leaving groups of **46**, the reaction protocol faced scaling and reproducibility problems. Within several similar entries the isolated yield of **47** was found to vary between 10 and 50%. In order to maintain the successful catalytic system, the bromine atoms of **46** were substituted by iodine atoms, because these are known to be more reactive as leaving groups in Pd catalyzed cross-coupling reactions.[211] The transhalogenation of 2,6-

dibromopyridine (**46**) was achieved by refluxing the dibromide derivative with sodium iodide in concentrated hydroiodic acid and the pure 2,6-diiodopyridine (**166**) was isolated by recrystallization in a high yield of 76%.[530–532] The exchange of 2,6-dibromopyridine (**46**) for 2,6-diiodopyridine (**166**) in the reaction mixture described above, improved both, reproducibility and the isolated yield of the Suzuki cross-coupling reaction. By using otherwise identical reaction conditions, tpy **47** was isolated in 66% yield after FCC. These improved reaction conditions were further applied for the assembly of two additional terpyridine derivatives in order to substantiate the general applicability of the described synthetic approach. The unfunctionalized terpyridine **11** was isolated in 55% yield after applying the reaction conditions to the lithium boronate salt **162** and 2,6-diiodopyridine (**166**). The application of identical reaction conditions to the methoxy lithium boronate salt **163** provided 4,4′′-dimethoxyterpyridine **167a** in a moderate yield of 32% together with 4-methoxybipyridine **167b** as a major side product in an isolated yield of 36%. As this side product was mainly observed with the electron donating methoxy substituent, our working hypothesis is that the reaction intermediate formed after the first coupling reaction, 2-iodo-4-methoxybipyridine is prone to deiodination.

3.3.2 Modular Synthesis of Terpyridine Ligand Periphery

With 4,4′′-dichloro-2,2′:6′,2′′-terpyridine (**47**) as a highly versatile building block in hands the modular synthesis of symmetric as well as asymmetric extended tpy ligands could be approached. However, the poor reactivity of the chlorine substituents as the peripheral leaving groups within palladium-catalyzed cross-coupling reactions, although being advantageous during the assembly of the tpy core unit **47**, as the large difference in reactivity between the bromine and chlorine substituent provided regioselectivity, represents a synthetic challenge. Fortunately, the catalytic system developed by Guram *et al*.[533] consisting of $PdCl_2[P^tBu_2(p\text{-}NMe_2\text{-}Ph)]_2$ as catalyst and K_2CO_3 as base readily allowed to substitute the chlorine atoms of **47**.

3.3.2.1 Symmetric Terpyridine Ligands

The utmost important symmetric tpy ligand needed for the immobilization of the final heteroleptic target complexes described throughout this project is tpy ligand **131** bearing two acetyl-protected thiols at the ends. The acetyl PG herein, represents a particularly appealing thiol PG, since it prevents the formation of disulfides and is readily cleaved under very mild conditions.[534,535] However, the base lability of thiophenolacetylates prevents the presence of the named functionality during Suzuki–Miyaura cross-couplings and hence the acetyl protected tpy derivative **131** could not be obtained directly from **47**, but had to be obtained via a transprotection of an appropriately protected precursor **133**. Thus, in first attempts **47** was treated with 4-(methylthio)phenylboronic acid. An oxygen-free Schlenk tube was charged with 1 eq. of **47** and 3-7 eq. of the boronic acid together with 5 mol% of the catalyst ($PdCl_2[P^tBu_2(p\text{-}NMe_2\text{-}Ph)]_2$) and 4 eq. of K_2CO_3 as base. In a nitrogen protection atmosphere the reaction mixture was dissolved in a degassed mixture of toluene and water (5:1). The sealed reaction vessel was heated to reflux for 24 hours. After cooling to r.t. and aqueous workup the desired disubstituted product **168a** was isolated by FCC in only 16% together with 37% of the monosubstituted 4-chloro-4´´-(*p*-(methylthio)phenyl) tpy **168b**. The ratio between di- and mono- substituted products **168a** / **168b** suggests further deactivation of the second chlorine leaving group upon substitution with an electron donating group. Additionally, both methylmercapto functionalized terpyridines **168a** and **168b** displayed very limited solubility features, which might also have handicapped their reactivity. Furthermore, rather harsh reaction conditions are required to remove the methyl protection group of a methylmercapto group. To address both, the solubility issues, as well as the harsh deprotection conditions, the methyl group was replaced by an ethyl-(trimethylsilyl) group (ethyl-TMS) in a second attempt. Fortunately this rather small structural alteration turned out to have a large impact on the yield obtained. When 1 eq. **47** and a sixfold excess (2 eq.) of 2,4,6-tris(4-(2-(trimethylsilyl)ethyl)-thiophenyl)-1,3,5,2,4,6-trioxatriborinane (**170**) were dissolved in a degassed toluene/water mixture (5:1) together with 10 mol% of the Pd catalyst and 6 eq. K_2CO_3, the 4,4´´-disubstituted product **171** was isolated in a yield of 99% after aqueous work-up and FCC. The borylation agent **170** was previously prepared in two steps starting from 4-bromothiophenol (**150**) via the ethyl-TMS protected thiol intermediate **169** with a highly improved overall yield of 79% generally following literature protocols.[528,536,537] The desired acetyl protected terpyridine derivative **131** was now obtained by transprotection of **171**. First attempts using silver tetrafluoroborate in dichloromethane (DCM) in the

presence of an excess of acetyl chloride (AcCl) as mild transprotection conditions failed, and mainly the ethyl-TMS protected starting material **171** was recovered by FCC. Transprotection was finally accomplished by treating **171** with 10 eq. tetrabutylammonium fluoride (TBAF) in degassed tetrahydrofuran (THF) at r.t. and subsequent cooling to -10 °C followed by the addition of 200 eq. AcCl. Rigorous exclusion of oxygen is crucial in order to avoid polymer formation of the intermediary formed deprotected bifunctional thiophenolic tpys by impending disulfide formation. Careful aqueous work-up considering the base lability of the acetyl group followed by FCC provided the acetyl protected ligand **131** in 96% as an ivory solid. An overview of the transformations of **47** into the 4,4´´-disubstituted terpyridine ligands **168a**, **171**, and **131** is given in Scheme 25 below.

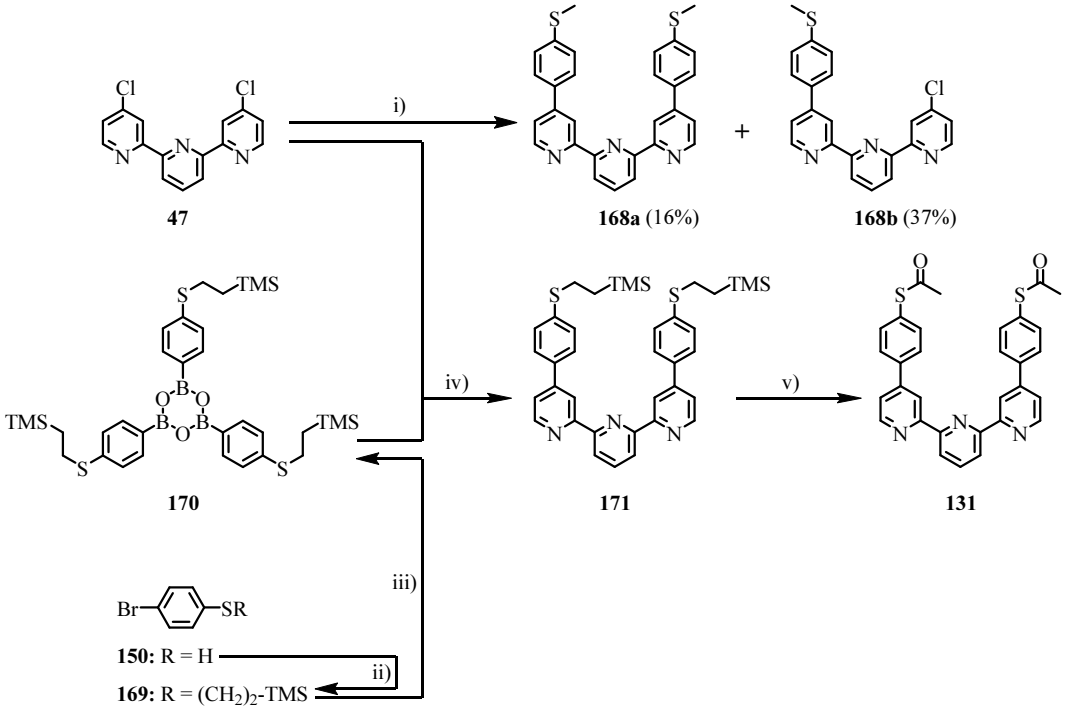

Scheme 25: Synthesis of the symmetric anchoring ligand *S,S′*-([2,2':6',2''-terpyridine]-4,4''-diylbis(4,1-phenylene)) diethanethioate (**131**) via a twofold Suzuki-Miyaura cross-coupling of the core tpy building block **47** with the appropriate borylation agents. Reagents and conditions: **i) 47** (1 eq.), 4-(methylthio)phenylboronic acid (2.5 eq.), $PdCl_2[P^tBu_2(p\text{-}NMe_2\text{-}Ph)]_2$, K_2CO_3, toluene/H_2O (10:1), reflux, 14h; **ii)** vinyltrimethylsilane, $(^tBuO)_2$, 100 °C, 5.5h, 98%; **iii)** *n*-BuLi, THF, $B(O^iPr)_3$, –78 °C to r.t., 66h, 81%; **iv) 47** (1 eq.), **170** (2 eq.), K_2CO_3, $PdCl_2[P^tBu_2(p\text{-}NMe_2\text{-}Ph)]_2$, toluene/$H_2O$ (5:1), reflux, 24h, 99%; **v) 171** (1 eq.), TBAF (10 eq.), THF, AcCl (200 eq.), r.t. to -10 °C, 3.5h, 96%.

Apart from tpy ligand **131** a variety of further symmetric tpy ligands was prepared, in order to be able to assemble the desired reference compounds **121** – **126**, representing heteroleptic, but electrically non-addressable Fe(II)-bis(tpy) complexes, due to the absence of the intrinsic dipole moment. The synthetic preparations of these extended symmetric tpy ligands are depicted in Scheme 26.

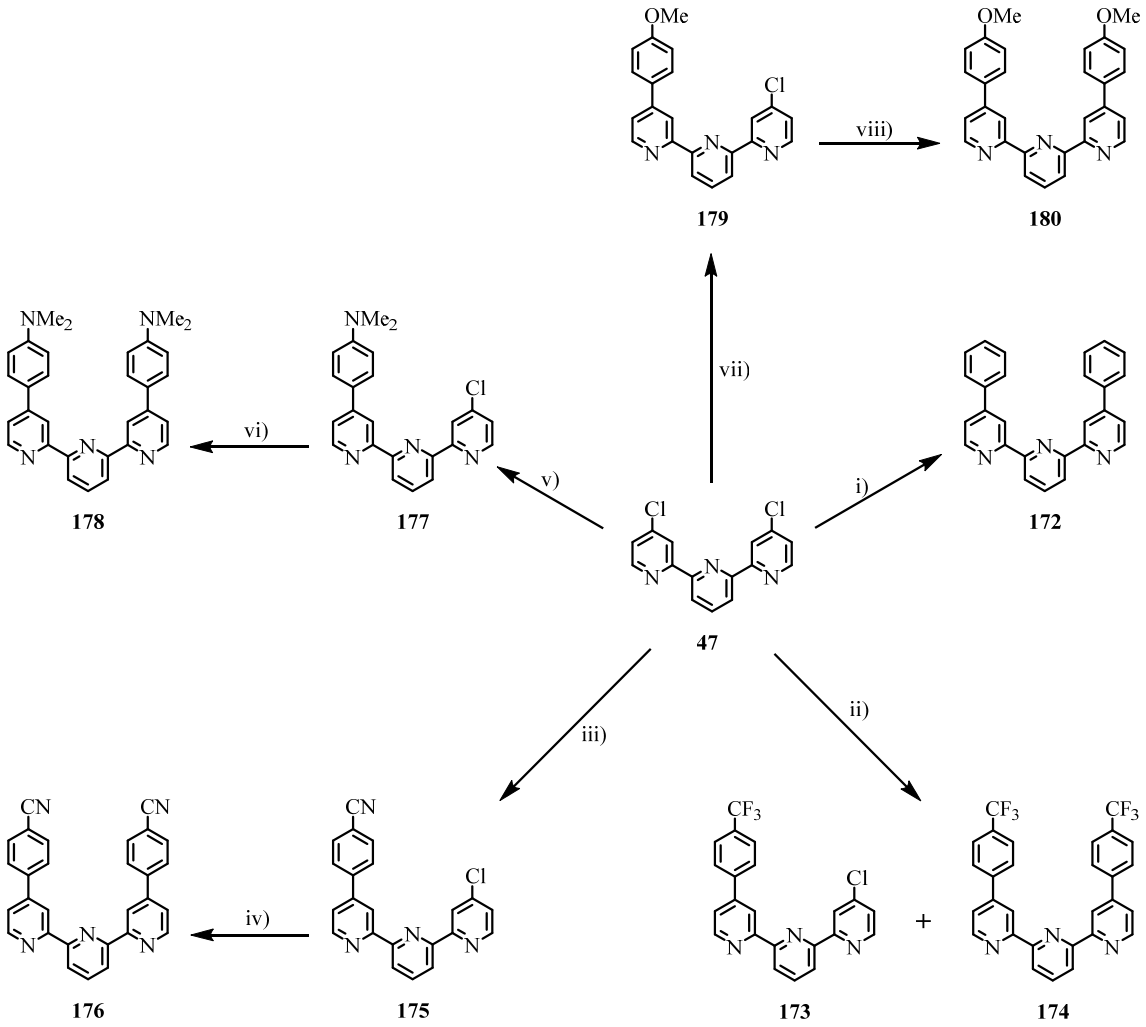

Scheme 26: Synthesis of the symmetric, peripherally extended 4,4′′-disubstituted tpy ligands **172**, **174**, **176**, **178**, and **180**, which were in equal measure assembled from the same key tpy core building block **47** in either one or two steps, respectively. Reagents and conditions: **i) 47** (1 eq.), phenylboronic acid (10 eq.), $PdCl_2[P^tBu_2(p\text{-}NMe_2\text{-}Ph)]_2$, K_2CO_3, toluene/H_2O (4:1), reflux, 24h, quant.; **ii) 47** (1 eq.), 4-(trifluoromethyl)phenylboronic acid (0.75 eq.), $PdCl_2[P^tBu_2(p\text{-}NMe_2\text{-}Ph)]_2$, K_2CO_3, toluene/H_2O (6:1), reflux, 24h, 10% (+ 44% of **173** and 44% of **47**); **iii) 47** (1 eq.), 4-(cyano)phenylboronic acid (0.75 eq.), $PdCl_2[P^tBu_2(p\text{-}NMe_2\text{-}Ph)]_2$, K_2CO_3, toluene/H_2O (6:1), reflux, 24h, 26% (+ 74% of **47**); **iv) 175** (1 eq.), 4-(cyano)-phenylboronic acid (10 eq.), $PdCl_2[P^tBu_2(p\text{-}NMe_2\text{-}Ph)]_2$, K_2CO_3, toluene/H_2O (6:1), reflux, 24h, 47%; **v) 47** (1 eq.), 4-(dimethylamino)phenylboronic acid (5.5 eq.), $PdCl_2[P^tBu_2(p\text{-}NMe_2\text{-}Ph)]_2$, K_2CO_3, toluene/H_2O (6:1), reflux, 24h, 58% (+ 40% of **47**); **vi) 177** (1 eq.), 4-(dimethyl-amino)phenylboronic acid (20 eq.), $PdCl_2[P^tBu_2(p\text{-}NMe_2\text{-}Ph)]_2$, K_2CO_3, toluene/H_2O (6:1), reflux, 24h, 98%; **vii) 47** (1 eq.), 4-(methoxy)phenylboronic acid (2 eq.), $PdCl_2[P^tBu_2(p\text{-}NMe_2\text{-}Ph)]_2$, K_2CO_3, toluene/H_2O (6:1), reflux, 24h, 42% (+43% of **47**); **viii) 179** (1 eq.), 4-(methoxy)-phenylboronic acid (10 eq.), $PdCl_2[P^tBu_2(p\text{-}NMe_2\text{-}Ph)]_2$, K_2CO_3, toluene/H_2O (5:1), reflux, 24h, 99%.

Among the illustrated symmetric tpy ligands there is a ligand terminated with two plain phenyl units, namely, 4,4′′-diphenyl-2,2′:6′,2′′-terpyridine (**172**), ligands functionalized with two terminal EWGs, namely, 4,4"-bis(4-(trifluoromethyl)phenyl)-2,2':6',2"-terpyridine (**174**) and 4,4'-([2,2':6',2"-terpyridine]-4,4"-diyl)dibenzonitrile (**176**), and ligands that are terminated with two terminal EDGs, namely, 4,4'-([2,2':6',2"-terpyridine]-4,4"-diyl)bis(*N,N*-dimethyl-

aniline) (**178**) and 4,4"-bis(4-methoxyphenyl)-2,2':6',2"-terpyridine (**180**). As for the preparation of compounds **168a** and **171** the formation of the five described ligands was performed via one, respective, two subsequent Suzuki-Miyaura cross-coupling reactions of the tpy core building block **47** with the appropriate boronic acids, using varying amounts of the catalyst ($PdCl_2[P^tBu_2(p\text{-}NMe_2\text{-}Ph)]_2$) and of the base K_2CO_3, which were altogether suspended, in a mixture of toluene and water in order to yield the desired products. It has been found, that the yields of the desired symmetrically 4,4´´-disubstituted tpy ligands are usually significantly higher, if a two-step procedure of the ligand's assembly is utilized. Furthermore, the 4-monosubstituted-4´´-chloro-tpys were also required as inevitable intermediates for the preparation of the asymmetric tpy ligands described in the following chapter 3.3.2.2. In that fashion 4,4´´-diphenyl-2,2´:6´,2´´-terpyridine (**172**) was obtained in one step from **47** and phenylboronic acid in quantitative yield. In contrast to this the one step reaction of **47** and 4-(trifluoromethyl)phenylboronic acid yielded the desired disubstituted tpy **174** in only 10% yield together with 44% of the monosubstituted 4-chloro-4"-(4-(trifluoromethyl)phenyl)-2,2':6',2"-terpyridine (**173**) and 44% of the reisolated starting material **47**. Therefore from this point ongoing the two-step procedures were preferred. In that fashion the monosubstituted 4-(4"-chloro-[2,2':6',2"-terpyridin]-4-yl)benzonitrile (**175**) was obtained in 26% yield by the reaction of **47** with 4-(cyano)phenylboronic acid, together with the remaining 74% yield being reisolated as unreacted **47**. The repeated conversion of **175** with an excess of 4-(cyano)phenylboronic acid lead to the isolation of the desired disubstituted product **176** in 47% yield. Whereas the described tpy derivatives were usually purified and isolated by means of FCC, in this case the highly insoluble product **176** readily precipitated from the organic phase after extraction. Therefore it seems that the rather poor yield of **176** to a certain extent arises from the limited solubility of the desired disubstituted product. In a similar fashion the reaction of **47** with 4-(dimethylamino)phenylboronic acid yielded monosubstituted 4-(4"-chloro-[2,2':6',2"-terpyridin]-4-yl)-*N,N*-dimethylaniline (**177**) in a yield of 58% with reisolation of 40% of **47**. The subsequent repeated reaction of **177** with 4-(dimethylamino)-phenylboronic acid yielded the desired disubstituted product **178** in 98%. Thus in this case the overall yield of 57% over two steps is significantly better, than the 12% overall yield achieved for 4,4'-([2,2':6',2"-terpyridine]-4,4"-diyl)dibenzonitrile (**176**), which once again underlines the solubility issues reported for this case. Finally the reaction of **47** with 4-(methoxy)-phenylboronic acid resulted in a 43% yield of 4-chloro-4"-(4-methoxyphenyl)-2,2':6',2"-terpyridine **179** together with 43% of the reisolated starting material **47**. The subsequent conversion of **179** to the desired 4,4"-bis(4-methoxyphenyl)-2,2':6',2"-terpyridine (**180**)

worked quantitatively upon repeated treatment of **179** with the corresponding boronic acid. With an overall yield of 42% for the two-step preparation of **180** also in this case the reported yield is much better than for the insoluble compound **176**. The last missing symmetric tpy ligand, which is needed for this project is the altered anchoring ligand **146**, which has been elongated by two acetylene bridges within the molecular backbone compared to the usually applied tpy ligand **131**. Although the synthetic pathway towards **146** shows significant similarities to the preparation of **131**, the key step in this case is represented by a twofold Sonogashira cross-coupling of the tpy core building block **47** with the previously synthesized acetylene building block **149** instead of a Suzuki-Miyaura coupling (Scheme 27).

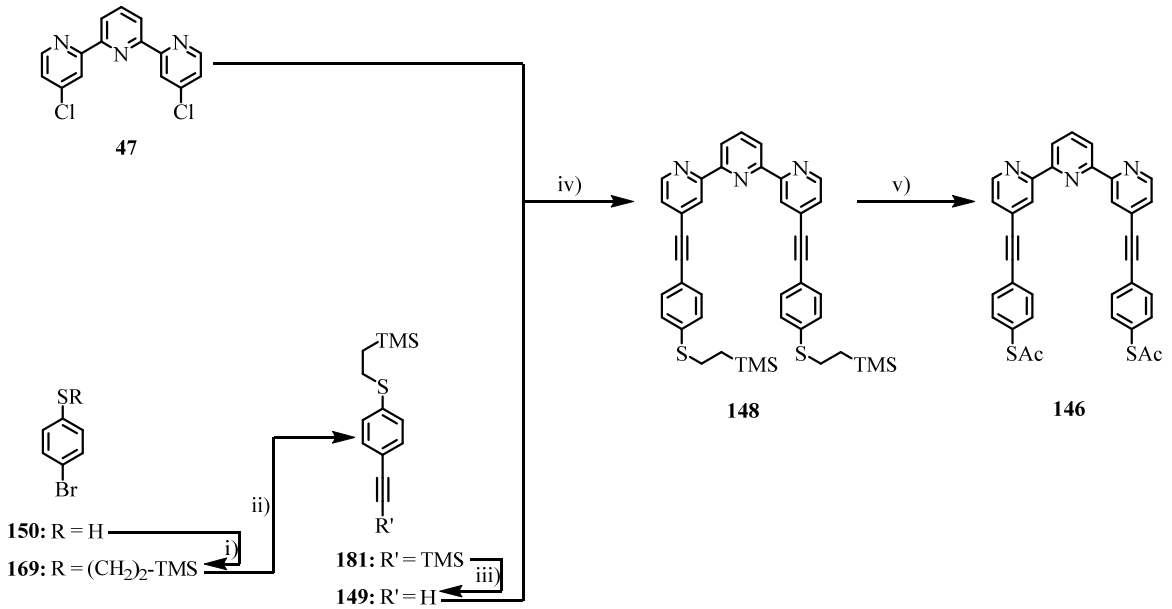

Scheme 27: Synthesis of the elongated symmetric anchoring ligand *S,S'*-(([2,2':6',2''-terpyridine]-4,4''-diylbis(ethyne-2,1-diyl))bis(4,1-phenylene)) diethanethioate (**147**) via a twofold Sonogashira cross-coupling of the core tpy building block **47** with the appropriate acetylene **150**. Reagents and conditions: **i)** vinyltrimethylsilane, (^{t}BuO)$_2$, 100 °C, 5.5h, 98%; **ii)** TMS-acetylene, Pd(PPh$_3$)$_2$Cl$_2$, CuI, HNEt$_2$, 60 °C, 18h; **iii)** K$_2$CO$_3$, MeOH, THF, r.t., 1h, 55% (over 2 steps + 37% of **169**); **iv) 47** (1 eq.), **150** (3 eq.), Cs$_2$CO$_3$, Pd(MeCN)$_2$Cl$_2$, X-Phos, propionitrile, 90 °C, 3.5h, 93%; **v) 149** (1 eq.), TBAF (10 eq.), THF, AcCl (200 eq.), r.t. to -10 °C, 3.5h, 95%.

Herein, the acetylene building block **149** can be prepared in three steps from 4-bromothio-phenol (**150**). At first **150** is reacted with vinyltrimethylsilane in a radical addition reaction to yield the ethyl-TMS protected intermediate **169** in a yield of 98%. In the subsequent step the Sonogashira reaction of **169** with TMS-acetylene yielded the intermediary TMS-protected acetylene compound **181**, which was directly deprotected to obtain the free acetylene (2-((4-ethynylphenyl)thio)ethyl)trimethylsilane (**149**) in an overall yield of 54% over the three steps.[537] The now following key step was the twofold Sonogashira cross-

coupling reaction of the tpy core building block **47** and the free acetylene compound **149**, which was performed in the presence of $Pd(MeCN)_2Cl_2$ and X-Phos as the catalyst system, Cs_2CO_3 as the base and propionitrile as the solvent, thus being an example of a rather rare Cu(I)-free Sonogashira coupling reactions,[538] which gave the desired ethyl-TMS protected dithiol tpy derivative **148** in a yield of 93%. The final transprotection was accomplished by treating **148** with 10 eq. TBAF in degassed THF at r.t. and subsequent cooling to -10 °C followed by the addition of 200 eq. AcCl. Under rigorous exclusion of oxygen, to avoid polymerization of intermediary formed deprotected bifunctional thiophenolic tpys, and careful aqueous work-up considering the base lability of the acetyl group the acetyl protected ligand **146** could be obtained in an excellent yield of 95% after FCC.

3.3.2.2 Asymmetric Terpyridine Ligands

In the present section the synthesis of a broad variety of different 4,4′′-disubstituted asymmetric tpy ligands is discussed. These represent inevitable integral parts of the desired heteroleptic, dipolar target complexes **112** – **118** (chapter 3.3.3.3) and **127** (chapter 3.3.3.5), as well as of the homoleptic, dipolar target complexes **119** + **120** and related complexes discussed in chapter 3.3.3.2. In accordance to the synthesis of the symmetric peripherally extended 4,4′′-disubstituted tpy ligands discussed in the previous chapter also these asymmetric analogues are basically assembled by the utilization of a Suzuki-Miyaura cross-coupling reactions. However, in contrast to the symmetric tpys, the synthesis of the asymmetric tpys inevitably requires a two-step procedure with a statistical introduction of the first 4-substituted phenyl substituent in a first coupling step. In principle for these kinds of statistical reactions product mixture ratios of 1:2:1, representing the ratios of starting material **47** to the desired monofunctionalized tpys and the unwanted disubstituted tpys, has to be expected. However, it was found, that by optimizing the amounts of boronic acids applied within the statistical couplings the obtained product ratios could be favorably altered into the direction of the desired products.

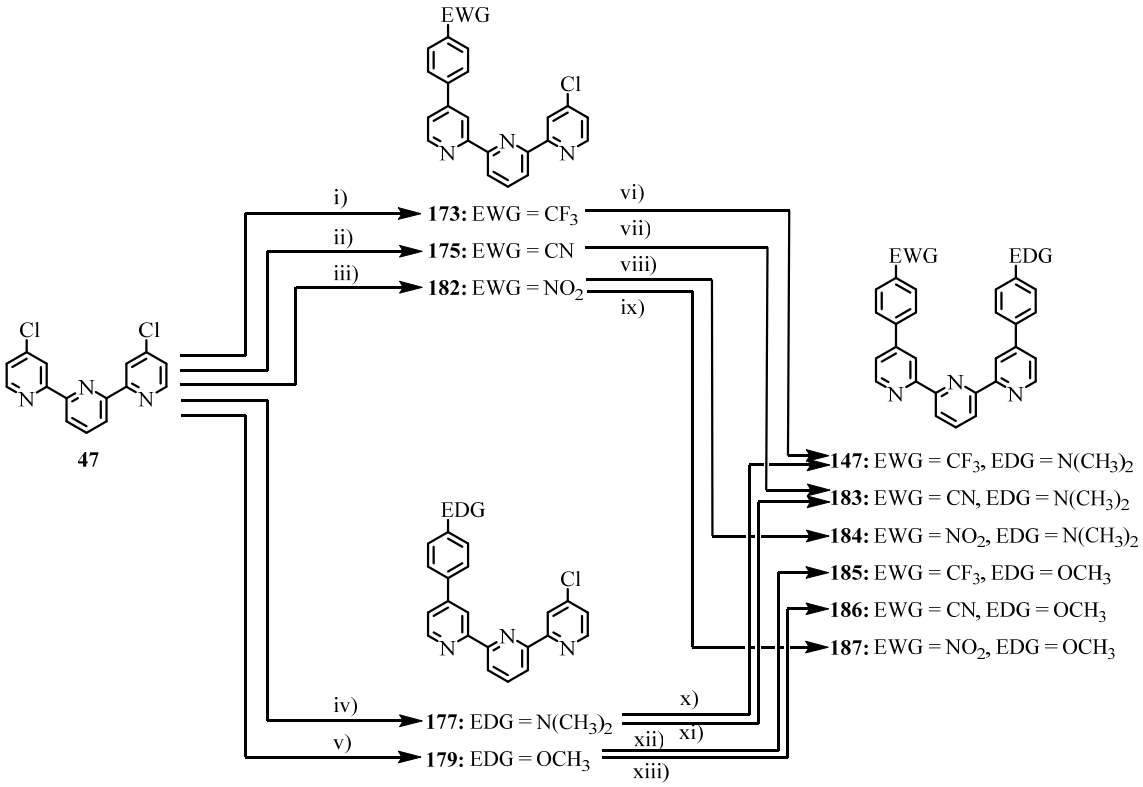

Scheme 28: Synthesis of the asymmetric, peripherally extended 4,4´´-disubstituted tpy ligands **147**, and **183 - 187**, which were in equal measure assembled from the same key tpy core building block **47** in two steps, involving a statistical Suzuki-Miyaura coupling at first place. Reagents and conditions: **i) 47** (1 eq.), 4-(trifluoromethyl)phenylboronic acid (0.75 eq.), $PdCl_2[P^tBu_2(p\text{-}NMe_2\text{-}Ph)]_2$, K_2CO_3, toluene/H_2O (6:1), reflux, 24h, 44% (+ 10% of **174** and 44% of **47**); **ii) 47** (1 eq.), 4-(cyano)phenylboronic acid (0.75 eq.), $PdCl_2[P^tBu_2(p\text{-}NMe_2\text{-}Ph)]_2$, K_2CO_3, toluene/H_2O (6:1), reflux, 24h, 26% (+ 74% of **47**); **iii) 47** (1 eq.), 4-(nitro)phenylboronic acid (1 eq.), $PdCl_2[P^tBu_2(p\text{-}NMe_2\text{-}Ph)]_2$, K_2CO_3, toluene/H_2O (5:1), reflux, 24h, 41%; **iv) 47** (1 eq.), 4-(dimethylamino)phenylboronic acid (5.5 eq.), $PdCl_2[P^tBu_2(p\text{-}NMe_2\text{-}Ph)]_2$, K_2CO_3, toluene/H_2O (6:1), reflux, 24h, 58% (+ 40% of **47**); **v) 47** (1 eq.), 4-(methoxy)phenylboronic acid (2 eq.), $PdCl_2[P^tBu_2(p\text{-}NMe_2\text{-}Ph)]_2$, K_2CO_3, toluene/H_2O (6:1), reflux, 24h, 42% (+ 43% of **47**); **vi) 173** (1 eq.), 4-(dimethylamino)phenylboronic acid (10 eq.), $PdCl_2[P^tBu_2(p\text{-}NMe_2\text{-}Ph)]_2$, K_2CO_3, toluene/H_2O (5:1), reflux, 24h, quant.; **vii) 175** (1 eq.), 4-(dimethylamino)phenylboronic acid (10 eq.), $PdCl_2[P^tBu_2(p\text{-}NMe_2\text{-}Ph)]_2$, K_2CO_3, toluene/H_2O (5:1), reflux, 24h, 92%; **viii) 182** (1 eq.), 4-(dimethylamino)phenylboronic acid (10 eq.), $PdCl_2[P^tBu_2(p\text{-}NMe_2\text{-}Ph)]_2$, K_2CO_3, toluene/H_2O (5:1), reflux, 24h, 87%; **ix) 182** (1 eq.), 4-(methoxy)phenylboronic acid (10 eq.), $PdCl_2[P^tBu_2(p\text{-}NMe_2\text{-}Ph)]_2$, K_2CO_3, toluene/H_2O (5:1), reflux, 24h, quant.; **x) 177** (1 eq.), 4-(trifluoromethyl)phenylboronic acid (3 eq.), $PdCl_2[P^tBu_2(p\text{-}NMe_2\text{-}Ph)]_2$, K_2CO_3, toluene/H_2O (5:1), reflux, 24h, quant.; **xi) 177** (1 eq.), 4-(cyano)phenylboronic acid (9.5 eq.), $PdCl_2[P^tBu_2(p\text{-}NMe_2\text{-}Ph)]_2$, K_2CO_3, toluene/H_2O (6:1), reflux, 24h, 94% (+ 6% of **177**); **xii) 179** (1 eq.), 4-(trifluoromethyl)phenylboronic acid (10 eq.), $PdCl_2[P^tBu_2(p\text{-}NMe_2\text{-}Ph)]_2$, K_2CO_3, toluene/H_2O (5:1), reflux, 24h, quant.; **xiii) 179** (1 eq.), 4-(cyano)phenylboronic acid (13 eq.), $PdCl_2[P^tBu_2(p\text{-}NMe_2\text{-}Ph)]_2$, K_2CO_3, toluene/H_2O (5:1), reflux, 24h, 80% (+ 20% of **179**).

The described use of substoichiometric amounts of boronic acids in most cases lead to the major formation of the desired monofunctionalized tpy derivatives under simultaneous reisolation of unreacted starting material, which, as for the previously discussed couplings, was the highly modularly applicable key synthon **47**. The requirement of the use of

substoichiometric amounts of borylation agents was observed to hold especially true, in the cases when the 4-EWG-substituted phenylboronic acids were introduced at first place, as it is illustrated in the recapitulatory overview of the synthesis of the desired asymmetric, push/pull tpy target ligands **147**, and **183** – **187** shown in Scheme 28 above. In detail as for the previously described mono- or disubstituted tpy derivatives the formation of the six different push/pull tpy ligands illustrated above was performed via two subsequent Suzuki-Miyaura cross-coupling reactions of the tpy core building block **47** with the appropriate boronic acids, using varying amounts of the catalyst ($PdCl_2[P^tBu_2(p\text{-}NMe_2\text{-}Ph)]_2$) and of K_2CO_3 as the base, dissolved or suspended, in a mixture of toluene and water. In that way 4-chloro-4"-(4-(trifluoromethyl)phenyl)-2,2':6',2"-terpyridine (**173**) was prepared from **47** and 4-(trifluoromethyl)phenylboronic acid (0.75 eq.) in a yield of 44% (with 44% of **47**, and 10% of **174**). From **173** and 4-(dimethylamino)phenylboronic acid the first desired asymmetric tpy ligand *N,N*-dimethyl-4-(4"-(4-(trifluoromethyl)phenyl)-[2,2':6',2"-terpyridin]-4-yl)aniline (**147**) was obtained in quantitative yield. The reaction of **47** and 4-(cyano)phenylboronic acid (0.75 eq.) resulted in the formation of 4-(4"-chloro-[2,2':6',2"-terpyridin]-4-yl)benzonitrile (**175**) in 26% yield (with 74% of **47**). The reaction of **175** with 4-(dimethylamino)phenylboronic acid resulted in the formation of asymmetric tpy **183** in a yield of 92%. When **47** was treated with 4-(nitro)phenylboronic acid (1 eq.) the monosubstituted tpy **182** was obtained in a yield of 41%. From here on the treatment of **182** with 4-(dimethylamino)phenylboronic acid resulted in the formation of the push/pull tpy ligand **184** in 87% yield, whereas the conversion of **182** with 4-(methoxy)phenylboronic acid yielded asymmetric tpy **187** in quantitative yield. The formation of the EDG-monosubstituted tpy ligand **177** could be realized by the reaction of **47** with 4-(dimethylamino)phenylboronic acid (5.5 eq.) resulting in a yield of 58% (with 40% of **47**). From here on the treatment of **177** with 4-(trifluoromethyl)phenylboronic acid resulted in the quantitative formation of the asymmetric tpy ligand **147**, whereas the conversion of **177** with 4-(cyano)phenylboronic acid yielded the push/pull ligand **183** in a yield of 94% (with 6% of **177**). Finally the monosubstituted tpy ligand **179** was obtained from the conversion of **47** with 4-(methoxy)phenylboronic acid (2 eq.) in a yield of 42% (with 43% of **47**). Also this monofunctionalized tpy could be further modularly functionalized. In that way the reaction of **179** with 4-(trifluoromethyl)phenylboronic acid resulted in the quantitative formation of the disubstituted asymmetric tpy ligand **185**, whereas the conversion of **179** with 4-(cyano)-phenylboronic acid yielded the push/pull ligand **186** in 80% yield (with 20% of reisolated **179**). Summarizing, it is quite remarkable that the introduction of the second functionality to the 4-monosubstituted-4´´-chloro-tpys works almost quantitatively in the majority of the

described examples. Furthermore, the fact, that the synthesis of the dipolar push/pull ligands **147** and **183** turned out to be independent of the step sequence of introduce functionalities and therefore emphatically underlines the modularity of the herein, presented synthetic pathways for the assemble of diversely functionalized tpy motifs.

In addition to the full characterization with standard analytical techniques several of the herein, discussed asymmetric tpy ligands, namely, **147**, **177**, and **183** could be successfully crystallized for x-ray single crystal analysis. The resulting crystal structures, together with most of those obtained from various symmetric tpy ligands, namely, **47**, **131**, **168a**, **171**, **172** and **178** are comparatively discussed in detailed form in chapter 3.4.1.1.

3.3.3 Complexation of Terpyridine Ligands

The final task of the here described projects was the assembly of the actual transition metal bis(tpy) target complexes from the corresponding tpy ligands. Generally the final complexation step can either consist of a one- or a two-step procedure depending on which transition metal is to be incorporated into the complex center, and whether a homoleptic, or a heteroleptic complex is the target molecule of the complexation reaction. Hereafter, five different types of transition metal bis(tpy) complexes are distinguished, which are of relevance throughout the physical discussions following the present chapter. Herein, **Type A** represents homoleptic Fe(II) complexes of symmetric tpy ligands, which are valuable reference compounds to evaluate the optical and structural properties of the actual heteroleptic target complexes which, without exception, at least contain one (**112 - 118**) or even two (**121 - 126**) symmetric tpy ligands within their structures. **Type B** describes the homoleptic Fe(II) complexes of asymmetric tpy ligands. These are of relevance, since they represent the target complexes of the second core project (**119** and **120**), namely, the STM-based investigation of bias-dependent SCO phenomena of surface-absorbed homoleptic, dipolar Fe(II)-bis(tpy) complexes, which are immobilized onto Au(111)-surfaces via electrospray ionization (chapter 3.4.4). Furthermore, the other examples belonging to this type are once again of relevance for the optical and structural evaluation of results obtained the heteroleptic, dipolar target complexes **112 – 118**. These main target structures are the objects of contemplation in the **Type C** complexes, which discusses exclusively the synthesis of these heteroleptic Fe(II)-based dipolar target structures **112 – 118**. In contrast to this **Type D**

complexes represent the group of reference target structures **121** – **126**, which were designed to not only evaluate optical and structural findings for the designed single molecular spin-switching complexes **112** – **118**, but to also act as comparative reference structures within the envisaged MCBJ measurements. Finally **Type E** is solely represented by the heteroleptic Ru(II)-based dipolar target structures **127**, which should further help to underline the physical findings for the Fe(II)-based target structures.

3.3.3.1 Homoleptic $[Fe^{2+}(tpy_{sym})_2](PF_6^-)_2$-Complexes (Type A)

In this section the synthesis of all homoleptic $[Fe^{2+}(tpy_{sym})_2]$-complexes of the **Type A** is described, which include the complexes of the tpy core moieties **11**, **47**, and **167a** as well as the homoleptic complexes of the peripherally extended symmetrically 4,4´´-disubstituted tpy ligands **131**, **146**, **168a**, **171**, **172**, **174**, **176**, and **180**. Among the named chelating compounds most of the ligands were transformed to the homoleptic Fe(II) complexes following a one-step procedure, as depicted in Scheme 29. Following this procedure the corresponding tpy ligands were dissolved in mixtures of organic solvents, such as ethanol (EtOH), MeOH, or DCM. To the dissolved ligand 0.5 eq. iron(II)chloride were added, whereupon the reaction mixture immediately turned deeply purple. An excess of water was added, before after 30min to 1h the organic solvents were diminished at reduced pressure. Now the PF_6^--salts of the Fe(II)-bis(tpy) complexes were precipitated by the addition of an excess of NH_4PF_6 as a saturated aqueous solution. The dark purple colored precipitates were collected by filtration and washed excessively with water. After the precipitates were dissolved in acetonitrile (MeCN), dried over magnesium sulfate and filtered, the evaporation of the solvents provided the PF_6^--salts of the Fe(II)-bis(tpy) complexes **129**, and **188** – **194** as dark purple powders in usually quantitative yields.

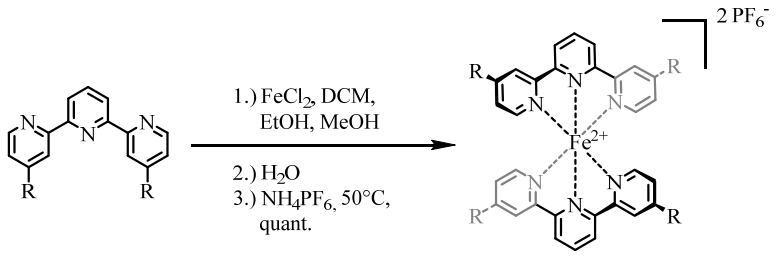

11: R = H
47: R = Cl
167a: R = OCH_3
168a: R = $p(C_6H_4)SCH_3$
171: R = $p(C_6H_4)S(CH_2)_2Si(CH_3)_3$
131: R = $p(C_6H_4)SCOCH_3$
172: R = $p(C_6H_5)$
174: R = $p(C_6H_4)CF_3$

188: R = H
189: R = Cl
190: R = OCH_3
191: R = $p(C_6H_4)SCH_3$
192: R = $p(C_6H_4)S(CH_2)_2Si(CH_3)_3$
129: R = $p(C_6H_4)SCOCH_3$
193: R = $p(C_6H_5)$
194: R = $p(C_6H_4)CF_3$

Scheme 29: General overview of the one-step procedure for the assembly of the homoleptic, symmetric Fe(II)-bis(tpy) complexes **129**, and **188** – **194**.

In contrast to the named homoleptic, symmetric Fe(II) tpy complexes **129**, and **188** – **194**, formed in a one-pot reaction, three further examples of $[Fe^{2+}(tpy_{sym})_2]$-complexes have been obtained as side-products during the synthesis of heteroleptic Fe(II) complexes (Scheme 30).

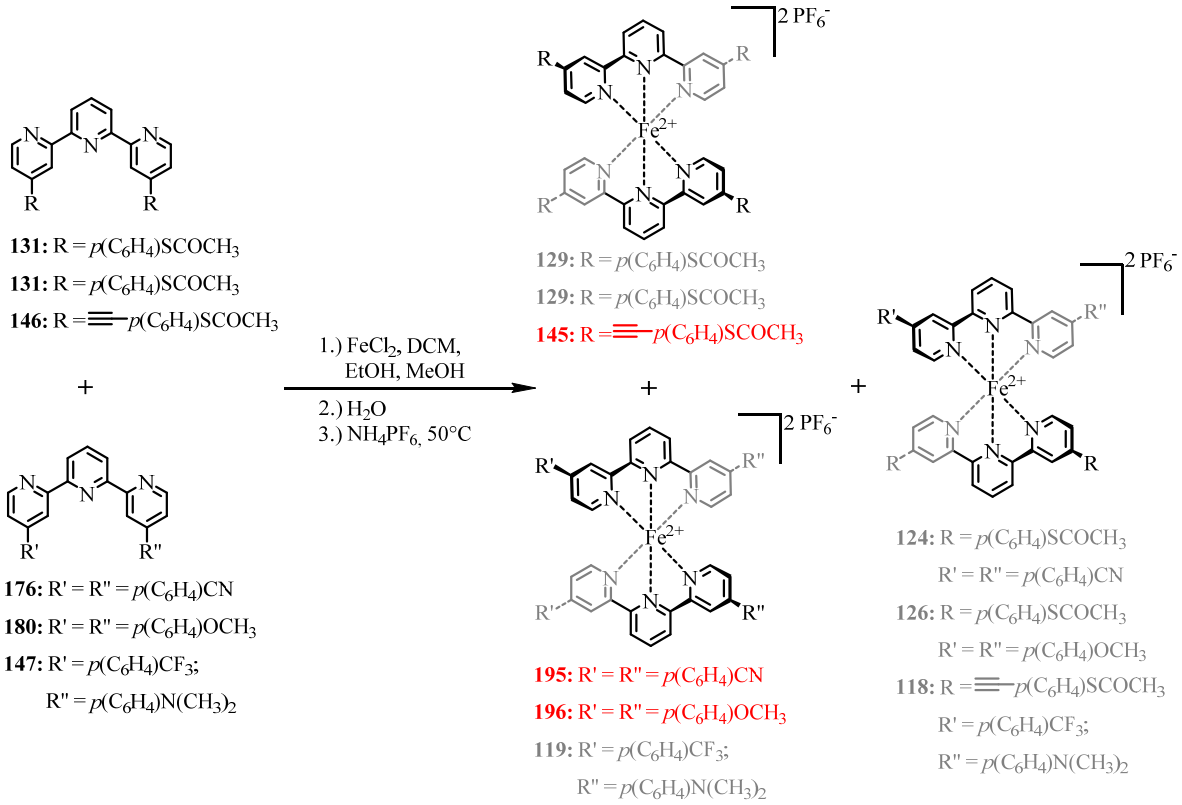

Scheme 30: Assembly of the homoleptic, symmetric Fe(II)-bis(tpy) complexes **145**, **195**, and **196** by statistical complexation of two different tpy ligands with $FeCl_2$ and subsequent isolation of the desired homoleptic complexes (highlighted in red) by means of preparative HPLC.

In principle the assembly of the heteroleptic target complexes, and hence also the formation of the desired homoleptic complexes **145**, **195**, and **196** as the incurring side-products, works analogue to the previously described one-step synthetic procedure. The difference is that in these statistical complexation reactions a 1:1 mixture of two different tpy ligands is applied to the reaction, together with an equimolar amount of $FeCl_2$. The mixture which is acquired by these complexation reactions always describes a 1:2:1 mixture of $[Fe^{2+}(tpy_{sym(I)})_2]$ to $[Fe^{2+}(tpy_{sym(I)})(tpy_{sym(II)})]$ to $[Fe^{2+}(tpy_{sym(II)})_2]$. A full overview of the formation of all the assembled heteroleptic target structures can be found in the according chapters 3.3.3.3 - 3.3.3.5, whereas Scheme 30 only displays those reactions that yield the missing desired homoleptic, symmetric Fe(II) tpy complexes **145**, **195**, or **196**, respectively, as side products. The challenging part about the isolation of **145**, **195**, and **196** from their statistical product mixtures was the task to separate these complexes from the other two Fe(II)-bis(tpy) complexes in the mixture. After repeated trials to achieve any separation via normal or reversed phase FCC, it was found, that the most convenient way to purify these mixtures of complexes was by preparative high pressure liquid chromatography (HPLC). Herein, the statistical mixtures of the three accordant Fe(II) complexes were separated via individually designed gradients of water/MeCN solvent mixtures. One representative example of such a separation trace in form of the resulting chromatogram is depicted in Figure 58 below for the isolation of complex **145**.

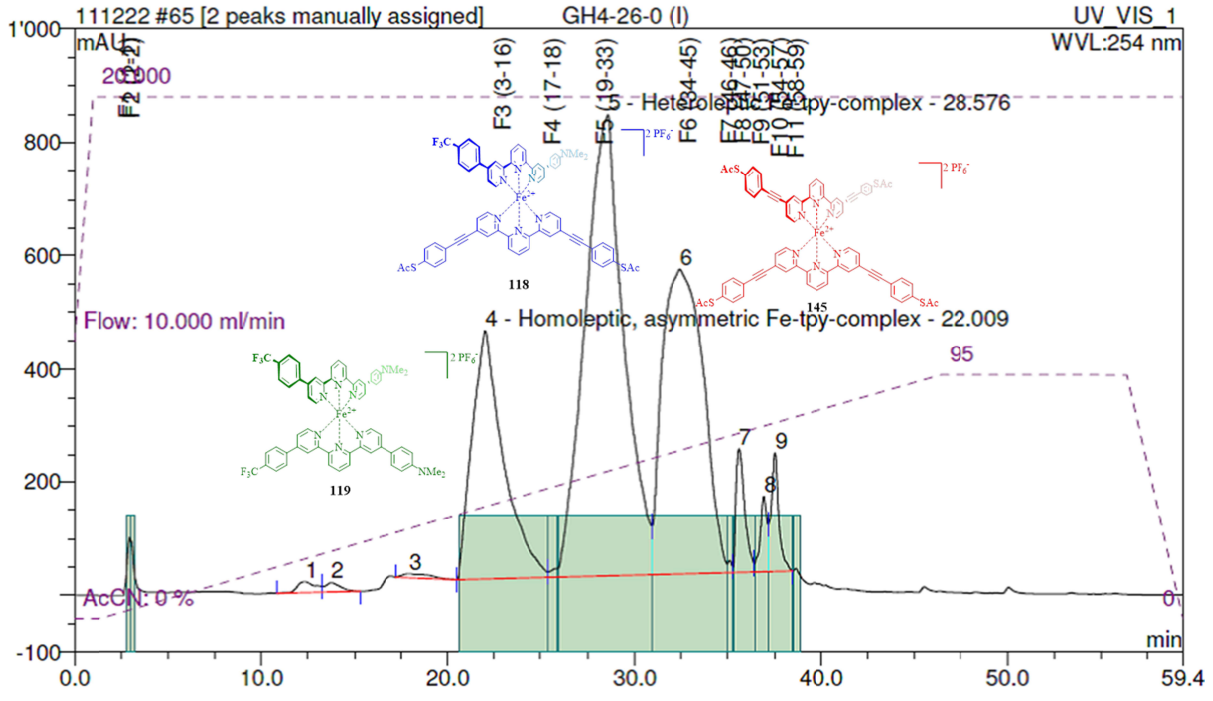

Figure 58: Depiction of the preparative HPLC chromatogram for the isolation of **145** (red) from a mixture with the complexes **119** (green) and **118** (blue).

In addition to the full characterization with standard analytical techniques several of the herein, discussed homoleptic Fe(II)-bis(tpy) complexes, namely, **189**, **191**, and **193** could be successfully crystallized to the requirements x-ray single crystal analysis. The resulting crystal structures, together with those obtained from the according symmetric tpy ligands, namely, **47**, and **168a** are comparatively discussed in detailed form in chapter 3.4.1.2. In the named chapter also the influence of these structural alterations, derived from the described crystallographic data, will be discussed in the context of alterations observed within other characteristic analytical data, such as distinct changes within the observed NMR spectra of the Fe(II) complexes in comparison to their accordant free ligands.

3.3.3.2 Homoleptic $[Fe^{2+}(tpy_{asym})_2](PF_6^-)_2$-Complexes (Type B)

In this section the synthesis of all homoleptic $[Fe^{2+}(tpy_{asym})_2]$-complexes of the **Type B** is described, which include the target complexes of the second core project, namely, complexes **119** and **120**, which were to be used for the STM-based investigation of bias-dependent SCO phenomena of surface-absorbed homoleptic, dipolar Fe(II)-bis(tpy) complexes (chapter 3.4.4), as well as the related dipolar complexes of the further peripherally extended asymmetrically 4,4´´-disubstituted tpy ligands **147**, **173**, **177**, **183**, **185**, **186**, and **187**. Among the named chelating compounds most of the ligands were transformed to the homoleptic dipolar Fe(II) complexes following the one-step procedure (Scheme 31) as described in the previous chapter.

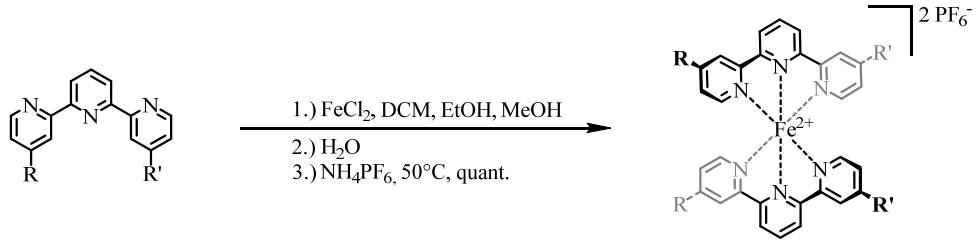

177: R = Cl; R' = *p*(C_6H_4)N(CH_3)$_2$
173: R = Cl; R' = *p*(C_6H_4)CF_3
147: R = *p*(C_6H_4)CF_3; R' = *p*(C_6H_4)N(CH_3)$_2$
183: R = *p*(C_6H_4)CN; R' = *p*(C_6H_4)N(CH_3)$_2$

197: R = Cl; R' = *p*(C_6H_4)N(CH_3)$_2$
198: R = Cl; R' = *p*(C_6H_4)CF_3
119: R = *p*(C_6H_4)CF_3; R' = *p*(C_6H_4)N(CH_3)$_2$
120: R = *p*(C_6H_4)CN; R' = *p*(C_6H_4)N(CH_3)$_2$

Scheme 31: Overview of the homoleptic, asymmetric Fe(II)-bis(tpy) complexes **119**, **120**, **197**, and **198** that could be formed via a direct one-step complexation of the corresponding ligands.

However also for this group several of the desired homoleptic, dipolar Fe(II)-bis(tpy) complexes, namely, **199 - 201** were isolated from the mixtures resulting from the statistical complexation reactions of the accordant asymmetric tpy ligand and the symmetric thiol-terminated anchoring ligand **131** in the presence of equimolar amounts of $FeCl_2$. As for the symmetric homoleptic complexes **145**, **195**, and **196** also the statistical product mixtures containing the desired dipolar complexes **199 - 201** were purified by preparative HPLC.

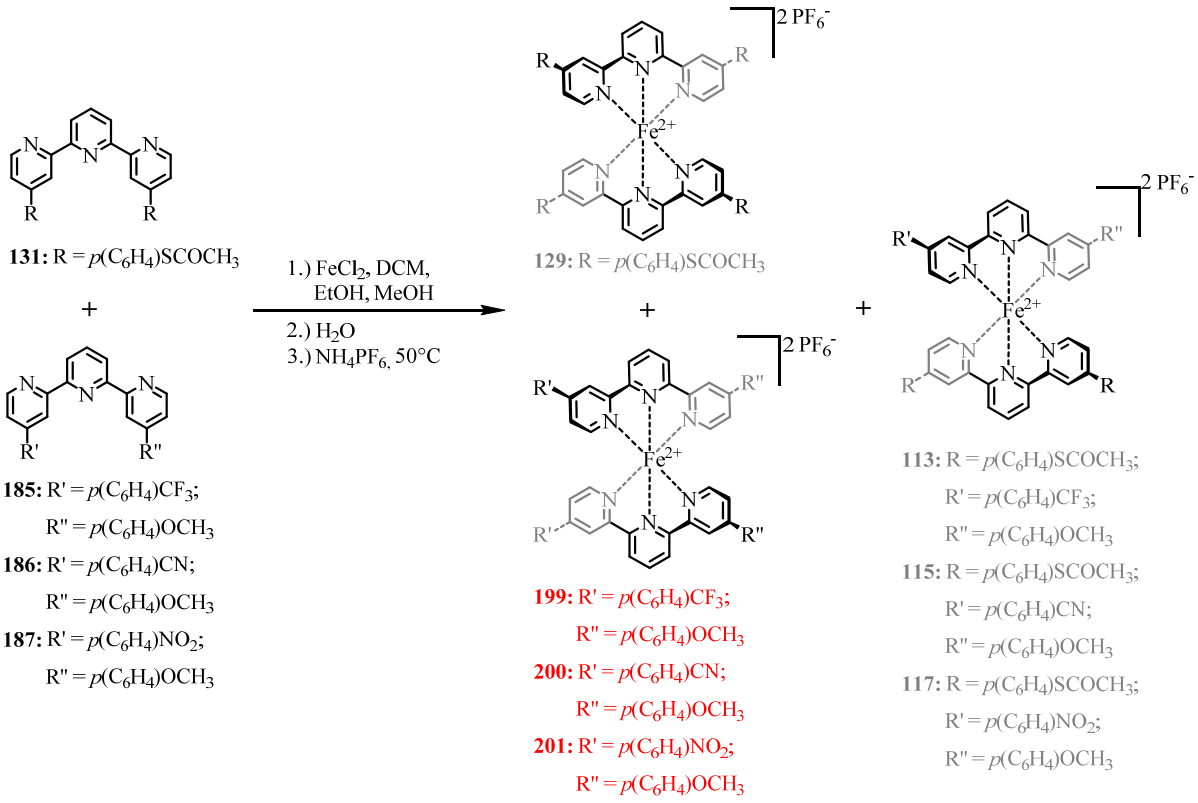

Scheme 32: Assembly of the homoleptic, asymmetric Fe(II)-bis(tpy) complexes **199** – **201** by statistical complexation of two different tpy ligands with $FeCl_2$ and subsequent isolation of the desired homoleptic complexes (highlighted in red) by means of preparative HPLC.

3.3.3.3 Heteroleptic $[Fe^{2+}(tpy_{sym})(tpy_{asym})](PF_6^-)_2$-Complexes (Type C)

In this chapter the assembly and isolation of the heteroleptic Fe(II)-based dipolar target structures **112** – **118**, representing the envisaged electric field dependent single molecular spin switches, are described. In contrast to the previously discussed homoleptic Fe(II) complexes the target structures discussed herein, inevitably require the statistical formation of the accordant $[Fe^{2+}(tpy_{sym})_2]$ to $[Fe^{2+}(tpy_{sym})(tpy_{asym})]$ to $[Fe^{2+}(tpy_{asym})_2]$ mixtures obtained in the

expectable 1:2:1 ratio of the three named compounds. The reason hereof lies in the fact, that there is no known procedure to prepare Fe(II)-complexes, which are coordinated to only one tpy ligand, since this would result in a coordinationally unsaturated Fe(II) core ion. This in principle differentiates the formation pathway towards heteroleptic Fe(II) complexes from those applicable for other transition metal species, such as Ru(III) or Ir(III), which allow a step-by-step introduction of the desired tpy ligands. Therefore, as described in the previous chapters, in each case the accordant tpy ligands, namely, one symmetric thiol-terminated tpy ligand for the complexes' later immobilization onto the gold electrodes, and an asymmetric, dipolar tpy ligand to trigger the bias-sensitivity of the overall target complexes, are reacted with an equimolar amount of $FeCl_2$. After the transformation to the PF_6^--salts of the product mixtures containing the desired heteroleptic target complexes, these are separated from the homoleptic side-products via preparative HPLC. An overview showing the complexation reactions yielding the target structures **112** – **117** is illustrated in Scheme 33.

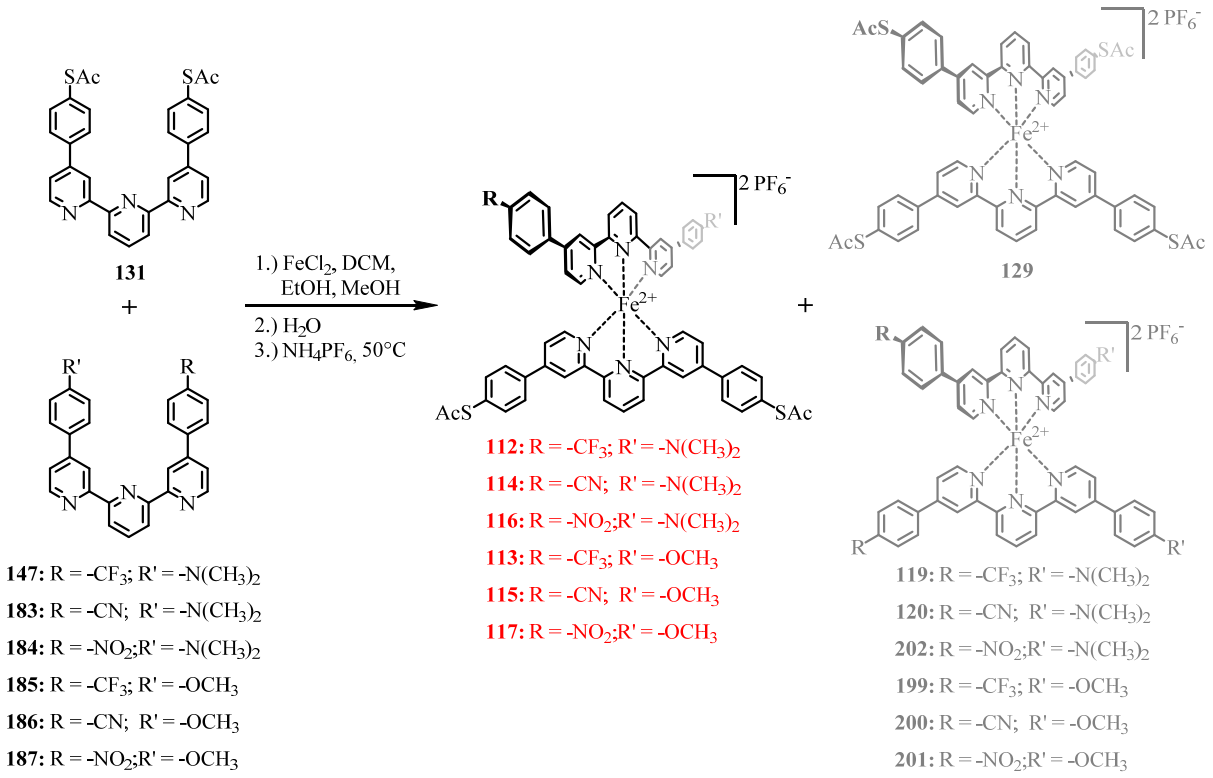

Scheme 33: Assembly of the heteroleptic, dipolar Fe(II)-bis(tpy) complexes **112** – **117** by statistical complexation of two different tpy ligands with $FeCl_2$ and subsequent isolation of the desired heteroleptic complexes (highlighted in red) by means of preparative HPLC.

However, hereafter, exemplarily the outcome of the separation of target compound **112** shall be elucidated in more detail. The expectable 1:2:1 ratio of (a) the homoleptic, symmetric Fe(II) tpy complex **129** to (b) the desired heteroleptic Fe(II) target compound **112** and to (c) the homoleptic, asymmetric Fe(II) tpy complex **119** could be underlined

via the analysis of the crude product mixture of all three complexes using analytical HPLC with electrospray ionization (ESI) mass spectrometry (MS). Figure 59 displays the HPLC-ESI-MS spectrum of the mixture prior to purification via preparative HPLC and clearly exhibits the named **129:112:119**-ratio of 1:2:1.

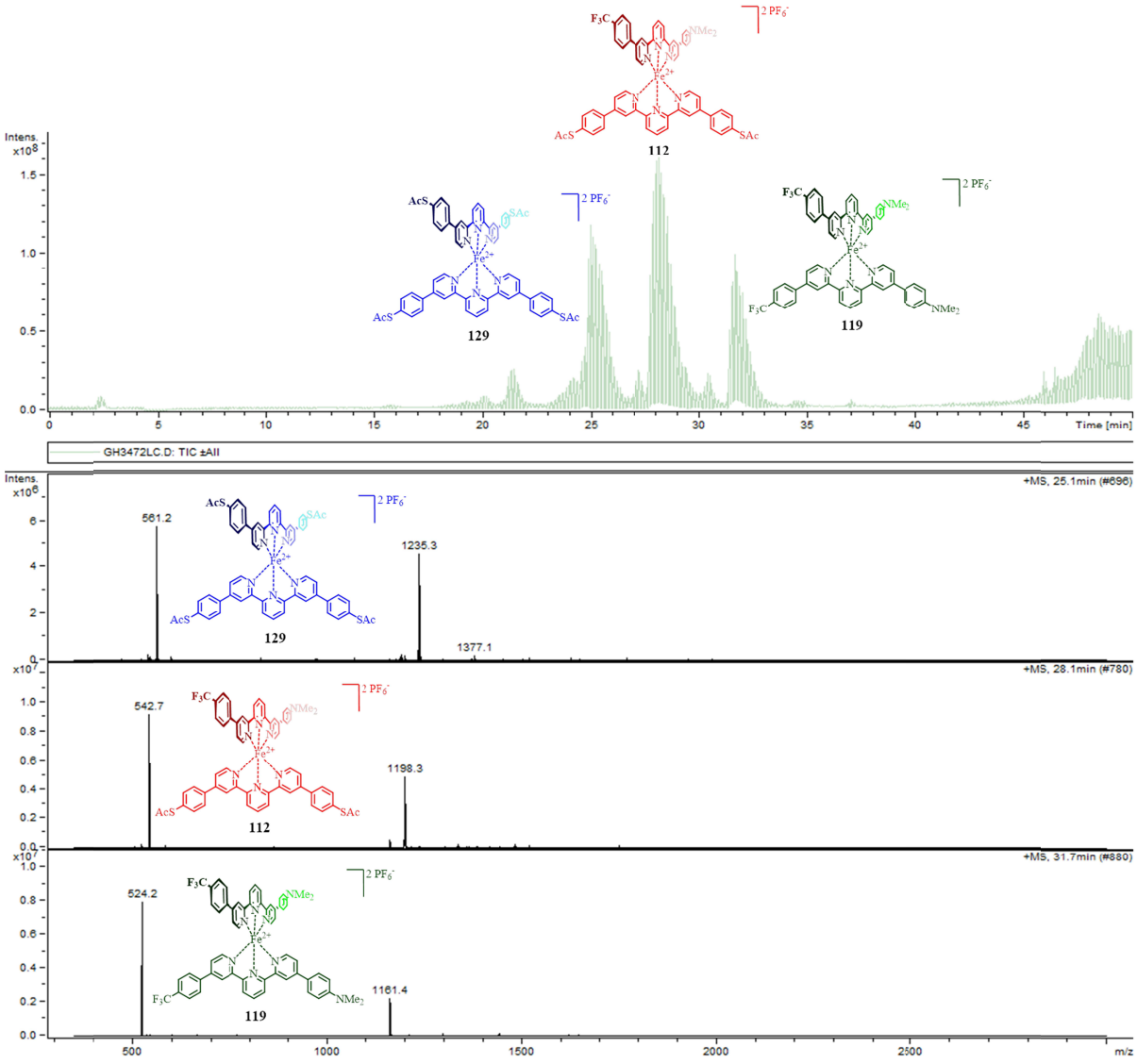

Figure 59: HPLC-ESI-MS analysis of the crude mixture of the desired heteroleptic target structure **112** with the two accordant homoleptic side-products **119** and **129** nicely illustrating the expectable **129:112:119** ratio of 1:2:1.

After separation of the three individual complexes via preparative HPLC (Figure 60) the resulting ESI-MS spectra clearly show the high purity of the desired compounds which is representatively shown by the according ESI-MS and ESI-MS/MS spectra of the purified heteroleptic target complex **112** in Figure 61.

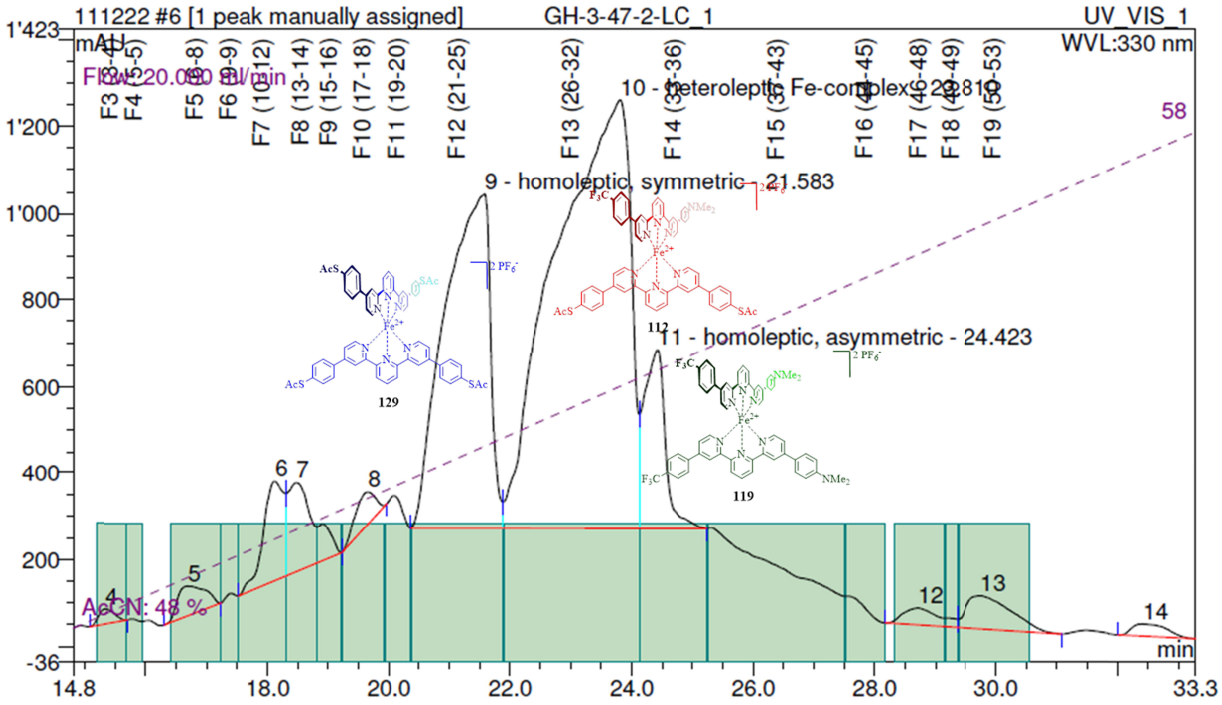

Figure 60: Depiction of the preparative HPLC chromatogram for the isolation of **112** (red) from a mixture with the complexes **119** (green) and **129** (blue).

As for all the statistical complexation reactions described in this work, the resulting heteroleptic products could be isolated in a very pure fashion. Therefore all slightly impure mixed fractions still containing the desired products were reunited and could be purified by repeated preparative HPLC runs. Apart from quantitative conversion of the ligands and the $FeCl_2$ to the accordant product complex mixtures, for the example shown below, namely, compound **112**, the amount of pure isolated product **112** was around 8% in the first run and could therefore be successively increased by repeated purification cycles.

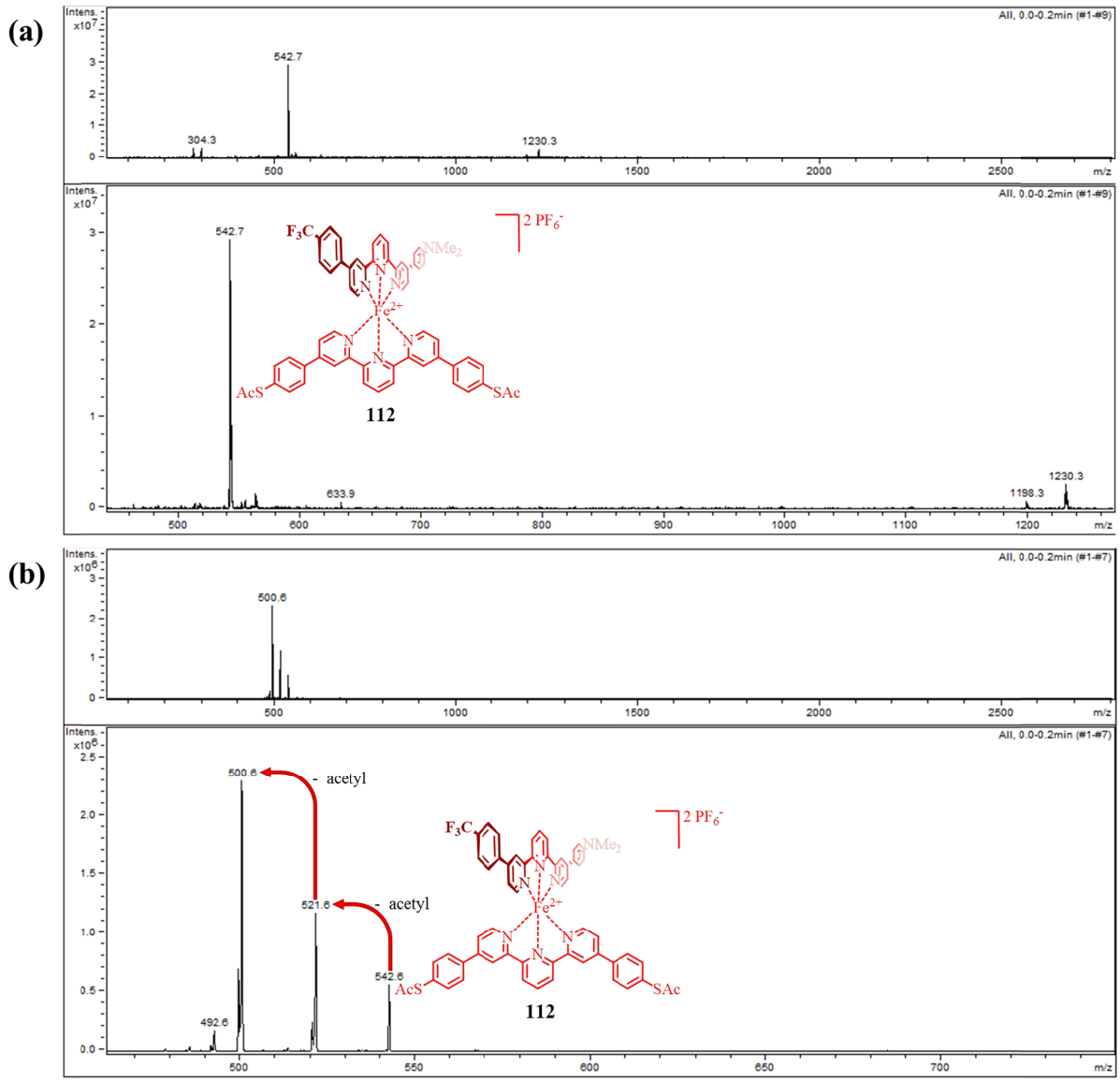

Figure 61: HPLC-ESI-MS analysis of the isolated desired heteroleptic target structure **112** after the purification via preparative HPLC. (a) ESI-MS spectrum exhibiting the pure isolated heteroleptic complex **112**. **(b)** ESI-MS/MS spectrum depicting the stepwise fragmentation of the desired target structure **112**, namely, the elimination of the two incorporated acetyl-PGs, giving therefore further proof for the structural identity of the investigated structure.

The synthesis of the remaining heteroleptic Fe(II)-based target structure **118** was done analogously and is depicted in Scheme 34 below. In this case the chromatographic separation of the heteroleptic target complex from its homoleptic side-products gave an appealing separation which has already been illustrated within Figure 58 in the previous section.

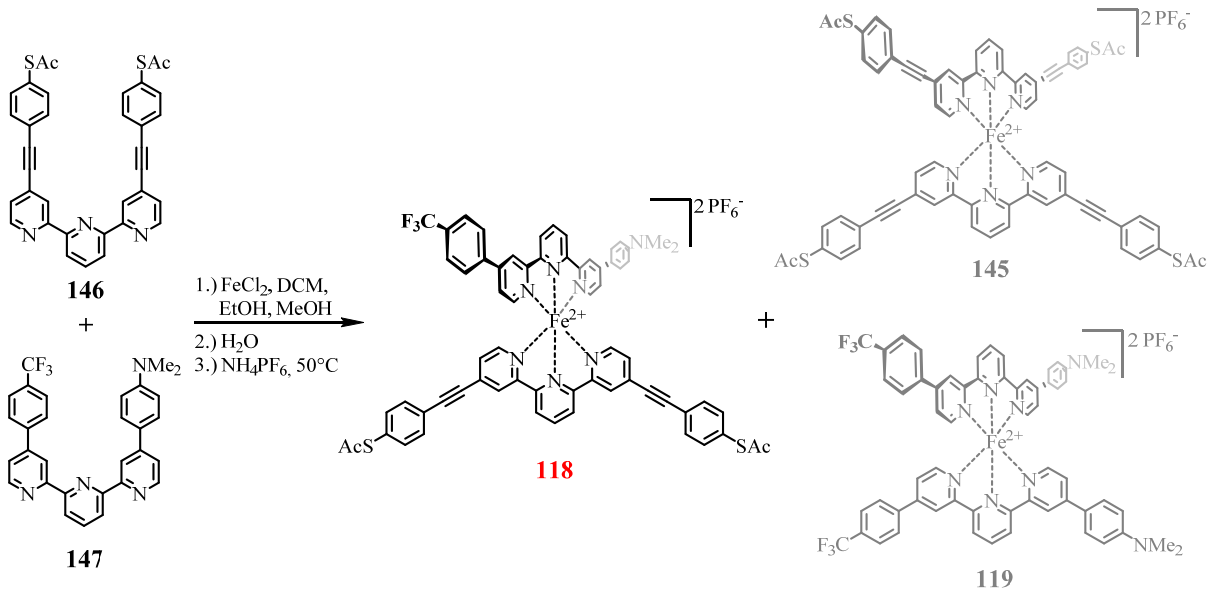

Scheme 34: Assembly of the elongated heteroleptic, dipolar Fe(II)-bis(tpy) complexes **118** via the $FeCl_2$-induced statistical complexation of the dipolar push/pull tpy ligand **147** and the altered anchoring tpy ligand **146**, which has been elongated by two acetylene functions in the molecular backbone, compared to the all-aryl substituent **131**.

3.3.3.4 Heteroleptic $[Fe^{2+}(tpy_{sym})(tpy_{sym}')](PF_6^-)_2$-Complexes (Type D)

In this chapter the assembly and isolation of the heteroleptic Fe(II)-based non-dipolar target structures **121** – **126**, representing the envisaged reference structures for the previously described single molecular spin switching target compounds **112** - **118**, is described. As for these dipolar heteroleptic Fe(II) complexes, also the assembly of the non-dipolar heteroleptic Fe(II) target complexes discussed herein, inevitably requires the statistical formation of the accordant $[Fe^{2+}(tpy_{sym1})_2]$ to $[Fe^{2+}(tpy_{sym1})(tpy_{sym2})]$ to $[Fe^{2+}(tpy_{sym2})_2]$ mixtures obtained in the expectable 1:2:1 ratio of the three named compounds (Scheme 35). Therefore, as for the dipolar heteroleptic target structures discussed in the previous chapter, also here the separation of the obtained product mixtures had to be performed via preparative HPLC, in order to purely yield the desired complexes **121** – **126**.

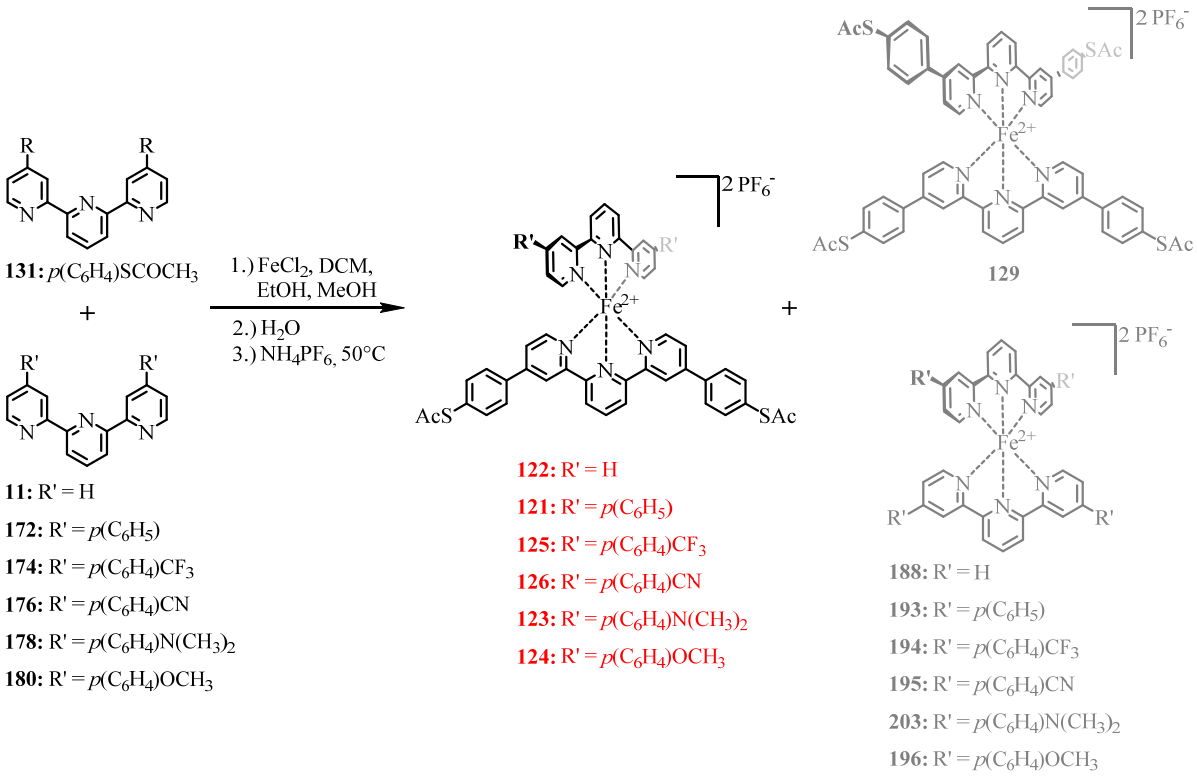

Scheme 35: Assembly of the heteroleptic, non-dipolar Fe(II)-bis(tpy) complexes **121** – **126** by statistical complexation of two different tpy ligands with $FeCl_2$ and subsequent isolation of the desired heteroleptic complexes (highlighted in red) by means of preparative HPLC.

3.3.3.5 Heteroleptic $[Ru^{2+}(tpy_{sym})(tpy_{asym})](PF_6^-)_2$-Complex 127 (Type E)

The last important reference compound within this project, whose synthesis needed to be developed was the corresponding heteroleptic, dipolar Ru(II)-based-bis(tpy) analogue **127** of the previously described heteroleptic Fe(II)-based dipolar target structures **112** – **118**. The reason for the utmost importance of complex **127** lies in the fact, that although it should be addressable by the applied electric field alterations, just like the corresponding Fe(II) complex **112**, it has to be expected, that no molecular spin switching can occur. Therefore, due to the fact that both complexes **112** and **127** alike contain the identical tpy ligands, **127** is designed to give an indirect, but inevitable proof, that potential conductance alterations observed for Fe(II) complex **112**, but not for Ru(II) complex **127**, are arising from SCO phenomena, which are impossible for the Ru(II)-center. In principle two pathways have been followed for the preparation of complex **127**, which are shown below. The difference between both approaches lies in the fact, that the first literature-inspired pathway[539–542] (Scheme 36a) relies on a step-by-step introduction of the tpy ligands to the Ru(III) source, and proceeds via the intermediate

mono-tpy Ru(III) complex **204**, whereas the second pathway (Scheme 36b) follows a statistical one-step reaction of $RuCl_3 \cdot x\ H_2O$ with both the tpy ligands **131** and **147**.

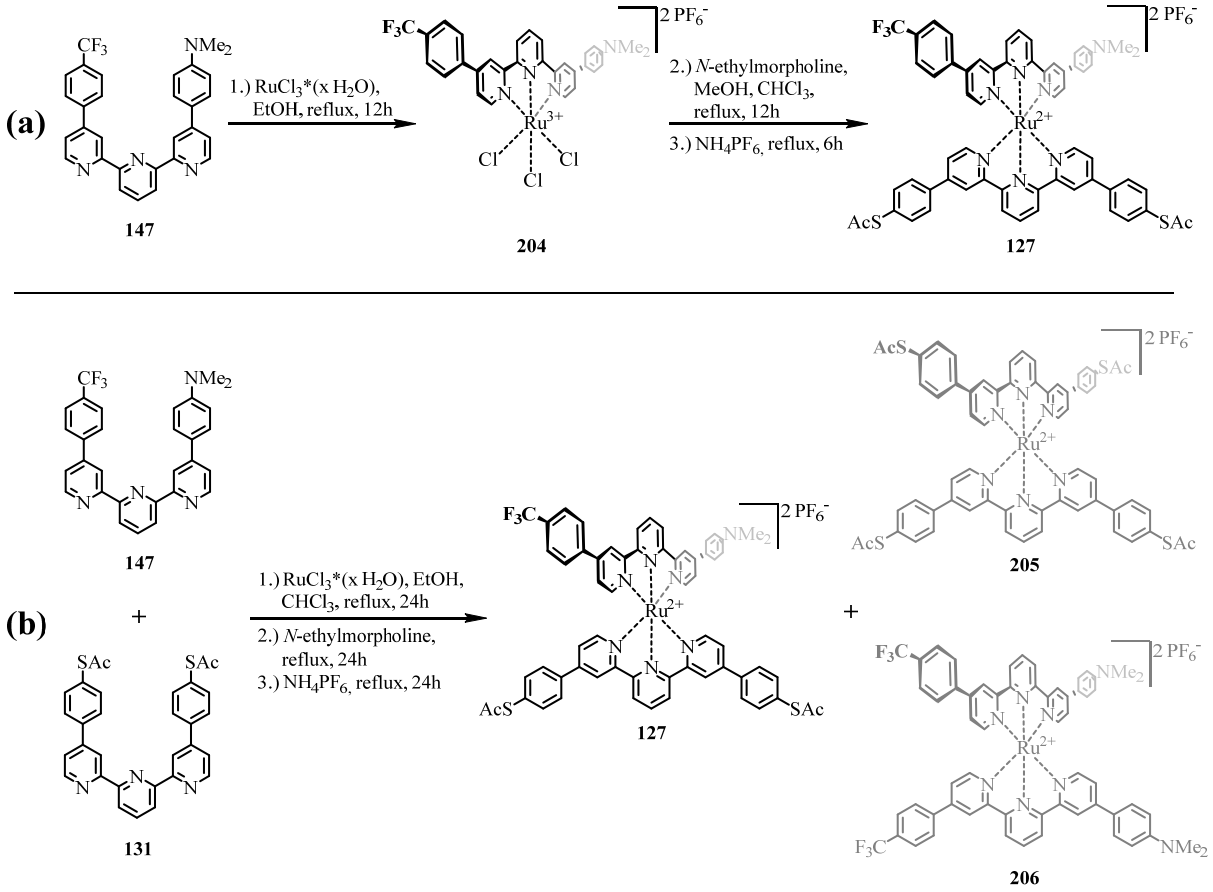

Scheme 36: Overview of the two synthetic approaches towards the heteroleptic, dipolar Ru(II)-based bis(tpy) complex **127**. **(a)** Illustration of the two-step synthetic pathway via the intermediary Ru(III)-mono-tpy complex **204**. **(b)** Depiction of the statistical one-step approach reacting $RuCl_3 \cdot xH_2O$ with an equimolar amount of the two tpy ligands **131** and **147**, respectively, yielding a statistical mixture of the heteroleptic Ru(II)-bis(tpy) complex **127** together with half the amount of each of the homoleptic side products **205** and **206**.

During the step-by-step assembly pathway $RuCl_3 \cdot x\ H_2O$ was first heated with the dipolar push/pull tpy ligand **147** in EtOH for 12h to yield the Ru(III) mono-tpy complex **204** as the crude product, which was used for the second step without further purification. In this step the intermediary complex **204** was mixed with the symmetric tpy anchoring ligand **131** and dissolved in a mixture of EtOH and $CHCl_3$, before *N*-ethylmorpholine as the reductant was added. Upon addition of NH_4PF_6 to the reaction mixture, the target complex **127** could be isolated in form of its PF_6^--salt. In contrast to this approach the one-pot synthesis of heteroleptic, dipolar Ru(II)-bis(tpy) complex **127** was done analogously to the preparation of the accordant Fe(II) analogues. The difference to these just lies in an extra intermediate step, namely, the addition of *N*-ethylmorpholine, after the mixing of the Ru(III) source and both tpy

ligands in the initial reaction mixture. After precipitation of the products via the addition of NH_4PF_6 the resulting deep red crude product was purified by means of preparative HPLC.

3.4 Physical Characterization

Following the discussion of the synthetic access towards the described target compounds hereafter, the corresponding physical results are highlighted, whereat the discussion of crystallographic structures and optical properties is followed by a detailed description of the performed physical measurements vian MCBJ and STM experiments.

3.4.1 Solid-State Investigations

All novel tpy ligands as well as the accordant Fe(II) bis(tpy) complexes have been fully characterized by ^{1}H- and ^{13}C-NMR spectroscopy, by mass spectrometry and by elemental analysis or high resolution mass spectra (HRMS), respectively. Probably due to the co-crystallization of solvent molecules into the molecular structures, no correct elemental analyses for the Fe(II) tpy complexes could be obtained and thus, these compounds were analyzed by HRMS. In addition the chemical identity of some compounds was corroborated by x-ray analysis as suitable single crystals were obtained for the terpyridine ligands **47**, **131**, **147**, **168a**, **171**, **177**, **178**, and **183**, as well as for the Fe(II)-bis(tpy) complexes **189**, **191**, and **193**. Single crystals were herein, obtained either by slow evaporation of the solvent or by diffusion techniques and details of the single crystal growth procedure are given in the experimental part for each case individually. Furthermore, after showing the named crystal structures in the following two passages also the exemplary influence of the complexation of the tpy ligands onto their distinct ^{1}H-NMR signal's shifts will be discussed on the examples of tpy core ligand **47** and its corresponding Fe(II) complex **189**, as well as on an extended example, namely, the ligand **168a** and the Fe(II) complex **191**, which could all four be successfully crystallized according to the requirements of x-ray crystal analysis.

3.4.1.1 Terpyridine Ligands

The solid state structures of the symmetric tpy ligands **47**, **131**, **168a**, **171**, and **178** and the asymmetric tpy ligands **147**, **177**, and **183** are displayed in Figure 62, 63 and 64. In all cases the three pyridine rings are almost arranged in a plane with the nitrogen atoms on opposite sites (all-*anti* conformation) enabling the formation of intramolecular hydrogen bonds between neighboring pyridine rings. Neither particular bond lengths nor angles between bonds differ considerably from already reported solid state structures comprising comparable structural motives and thus, the solid state structures served mainly in order to underline the ligands' identities and give argumentative foundation for findings from other analytical techniques, such as NMR measurements, or optical properties.

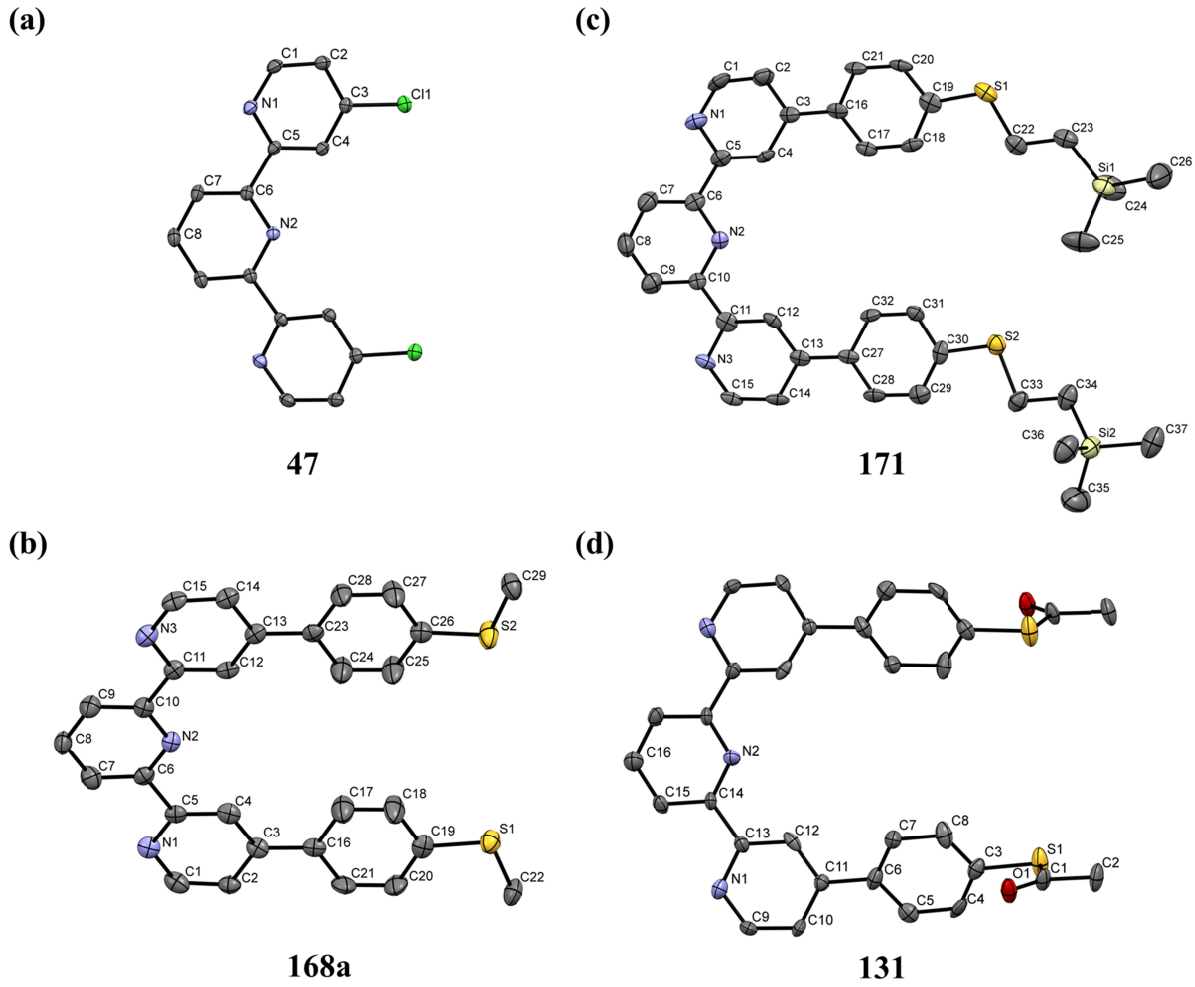

Figure 62: ORTEP plots of the solid state structures of the symmetric tpy ligands **47**, **131**, **168a** and **171** with the ellipsoids plotted at 50% probability level. The hydrogen atoms were omitted for clarity reasons.

Figure 62 displays the core tpy moiety **47** as a reference structure together with the three symmetric tpy structures **131**, **168a**, and **171** all bearing two protected thiols at the two termini of the extended tpy molecules. The crystallographic details of the four illustrated structures are comparatively listed in Table 11 in the corresponding crystallographic appendix chapter 9.2.

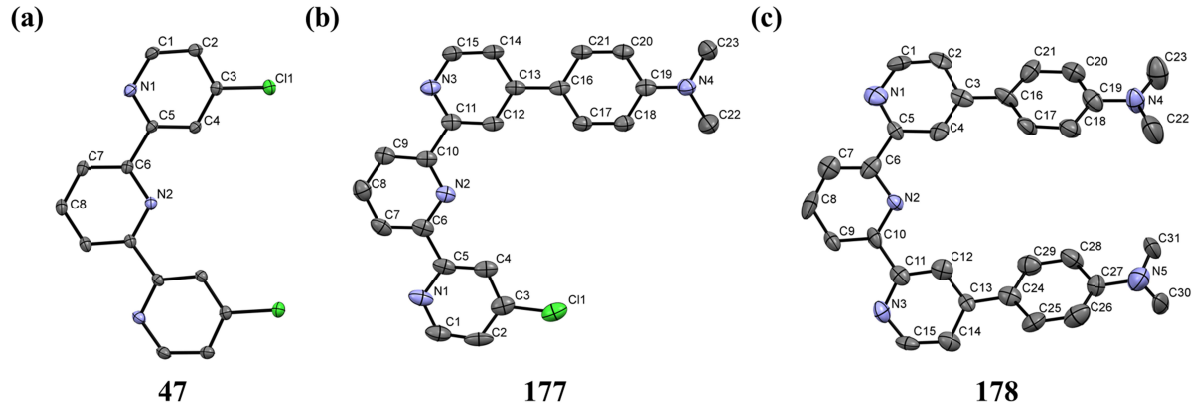

Figure 63: ORTEP plots of the solid state structures of the tpy ligands **47**, **177**, and **178** with the ellipsoids plotted at 50% probability level. The hydrogen atoms were omitted for clarity reasons. The comparative illustration of the tpy core motif **47** versus the monosubstituted tpy derivative **177** and the symmetrically disubstituted tpy derivative **178** represents the structural parallels of the extended tpys in relation to the unsubstituted core subunits.

Figure 63 illustrates the structural parallels of the unsubstituted tpy core motif **47** to the monosubstituted tpy derivative **177** and to the symmetrically disubstituted tpy derivative **178**. These give a decent explanation for the comparability of the NMR- and UV/vis-spectroscopic similarities, which have been monitored between the different novel tpy derivatives reported within this work. The crystallographic details of the three illustrated structures are comparatively listed in **Table 12** in the corresponding crystallographic appendix chapter 9.2. Furthermore, two of the final dipolar, asymmetric tpy ligands bearing an intrinsic push/pull system, namely, the tpy derivatives **147** and **183**, could be successfully crystallized and are illustrated in Figure 64. Also for these two tpy ligand structures, whose crystallographic details are comparatively listed in Table 13 in the corresponding crystallographic appendix chapter 9.2, a comparable similarity at the tpy core can be found as for the symmetric tpy ligands' structures illustrated above. Although the peripheral phenyl units are slightly tilted out-of-plane for all the shown examples of extended tpy structures, namely, the tpys **131**, **147**, **168a**, **171**, **177**, **178** and **183**, the most important structural details, the all-*anti* conformation of the heteroaromatic pyridine nitrogen atoms, can be found for all the tpy ligands as for the tpy core moiety **47** alike.

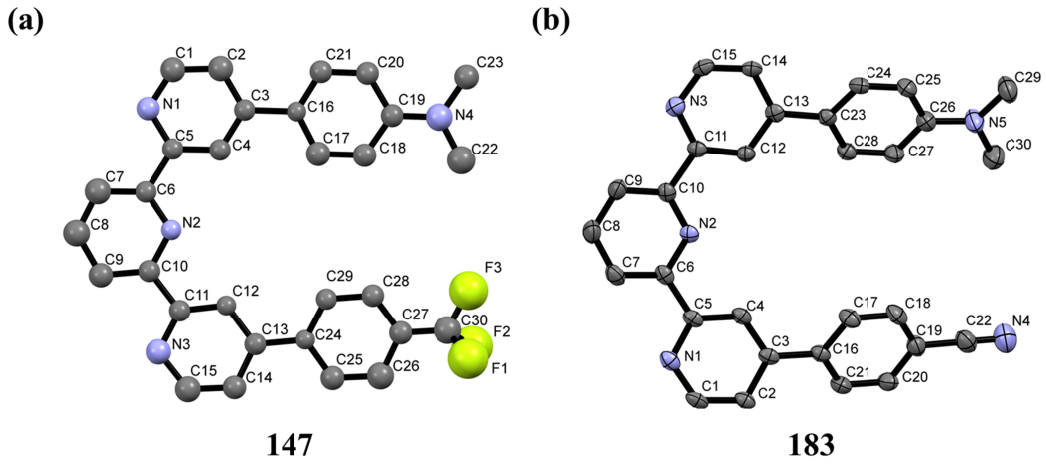

Figure 64: ORTEP plots of the solid state structures of the asymmetric, dipolar push/pull tpy ligands **147**, and **183** with the ellipsoids plotted at 50% probability level. The hydrogen atoms were omitted for clarity reasons.

3.4.1.2 Metal Complexes

In this chapter the main characteristics of the solid state structures of the three symmetric, homoleptic Fe(II)-bis(tpy) complexes **189**, **191**, and **193** are highlighted. The crystallographic details of the three named structures are comparatively listed in Table 14 in the corresponding crystallographic appendix chapter 9.2. Within Figure 65, the ORTEP plots of the dicationic Fe(II)-bis(tpy) complexes are displayed on the left side, whereas on the right side of the figure the relative spatial arrangements of both tpy ligands are highlighted by displaying the planes defined by the atoms of each terpyridine subunit. With interplanar angles of 89.82° for **189**, and 88.70° for **191**, and 89.52° for **193** all three ligand systems provide an almost perfect octahedral ligand sphere around the Fe(II) core ions resulting in the expected low-spin Fe(II)-bis(tpy) complexes. The observed bond lengths and atom positions of the tpy subunits and the central metal ion of the complexes are within small deviations comparable to common $[M(tpy)_2]$ motifs.[167] As expected the complex structure is hardly affected by substituents in the remote 4- and 4´´-positions of the tpy subunit. Therefore also the geometries of the remaining target M(II)-bis(tpy) complexes, of which no suitable single crystals could be obtained, such as the heteroleptic target structures **112**–**118** and **121**–**127**, as well as the homoleptic target compounds **119** and **120**, can be expected to be in the same diamagnetic, octahedral LS state as the examples **189**, **191**, and **193** discussed herein.

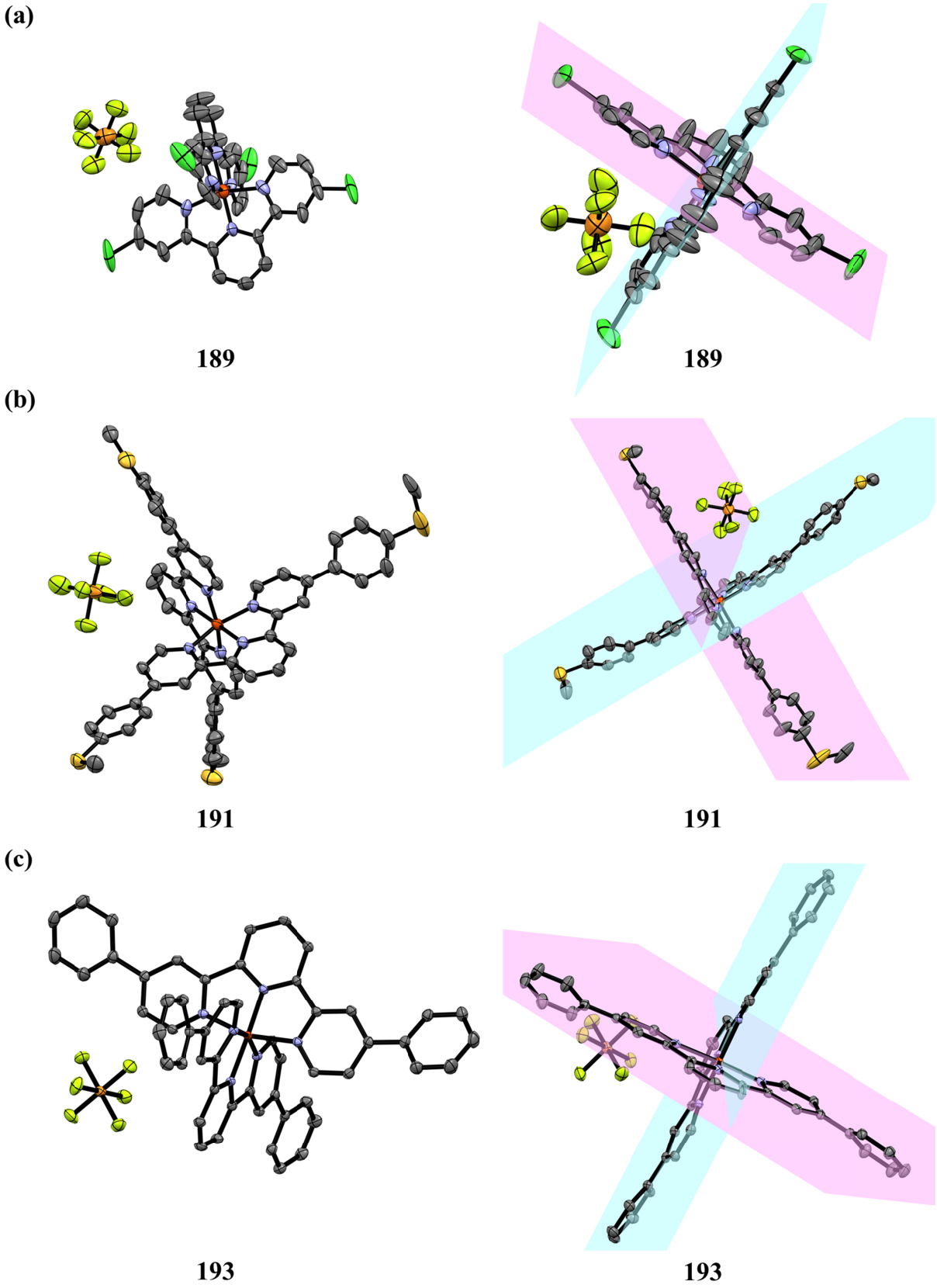

Figure 65: Left side: ORTEP plots of the crystal structures of the Fe(II)-bis(tpy) complexes (**a) 189**, **(b) 191**, and **(c) 193** (in all cases the ellipsoids are plotted at 50% probability level and H-atoms, solvent molecules and additional molecules or counter ions in the asymmetric unit are omitted for clarity). Right side: Geometric illustration of the virtual planes comprising the complexes' tpy ligands.

The complexation of the tpy ligands with iron had a major influence on the chemical environment of the coordinating nitrogen atoms due to a structural change from an all-*anti* conformation in the free ligands (Figure 62, 63 and 64) to an all-*syn* conformation in the Fe(II)-bis(tpy) complexes (Figure 65). Naturally, this structural transformation is also reflected in pronounced shifts of the tpys' ^{1}H-NMR signals. Exemplarily, the ^{1}H-NMR spectra of the free tpy ligands **47** and **168a** together with those of the corresponding Fe(II)-bis(tpy) complexes **189** and **191** are displayed in Figure 66a-d, respectively. Colored dots are Hereby, utilized to guide the eye through the assignment of the ^{1}H-signals. Considerable shifts were observed for most signals of the tpy subunits. Of those shifts, with values of 1.18 ppm and 1.26 ppm, respectively, the most dramatic changes were observed for the H-atoms in the 6- and 6′′-positions of the tpy subunit. These very distinct up-field shifts of the named 6- and 6′′-protons from the free ligands towards the Fe(II)-bis(tpy) species can be explained by the protons' location right above the anisotropic cone of the central pyridine ring of the second tpy ligand within the complex. The chemical shifts of the remaining H-atoms remain either rather unaffected upon complexation, like in the case of the protonic signals in 5- and 5′′-positions of the two outer pyridine moieties or for the AB system of the *para*-methyl-sulfanyl-phenyl substituents of **191**, or they face varyingly strong down-field shifts. Those shifts are either moderately pronounced, as for the protons in 3- and 3′′-position with 0.34 ppm, or more severe for the signals of the protons in 3′- and 5′-position (0.89 ppm and 1.02 ppm, respectively) or the signals of the central 4'-position (0.97 ppm and 1.02 ppm, respectively).

Analogue observations have been seen for the other Fe(II)-bis(tpy) complexes reported in this chapter. The chemical shifts found for the ^{1}H-NMR signals of the Fe(II) complexes throughout corroborate the low-spin states of the complexed Fe(II) ions going along with the octahedral geometries exemplarily observed for the Fe(II)-bis(tpy) complexes **189**, **191**, and **193**.

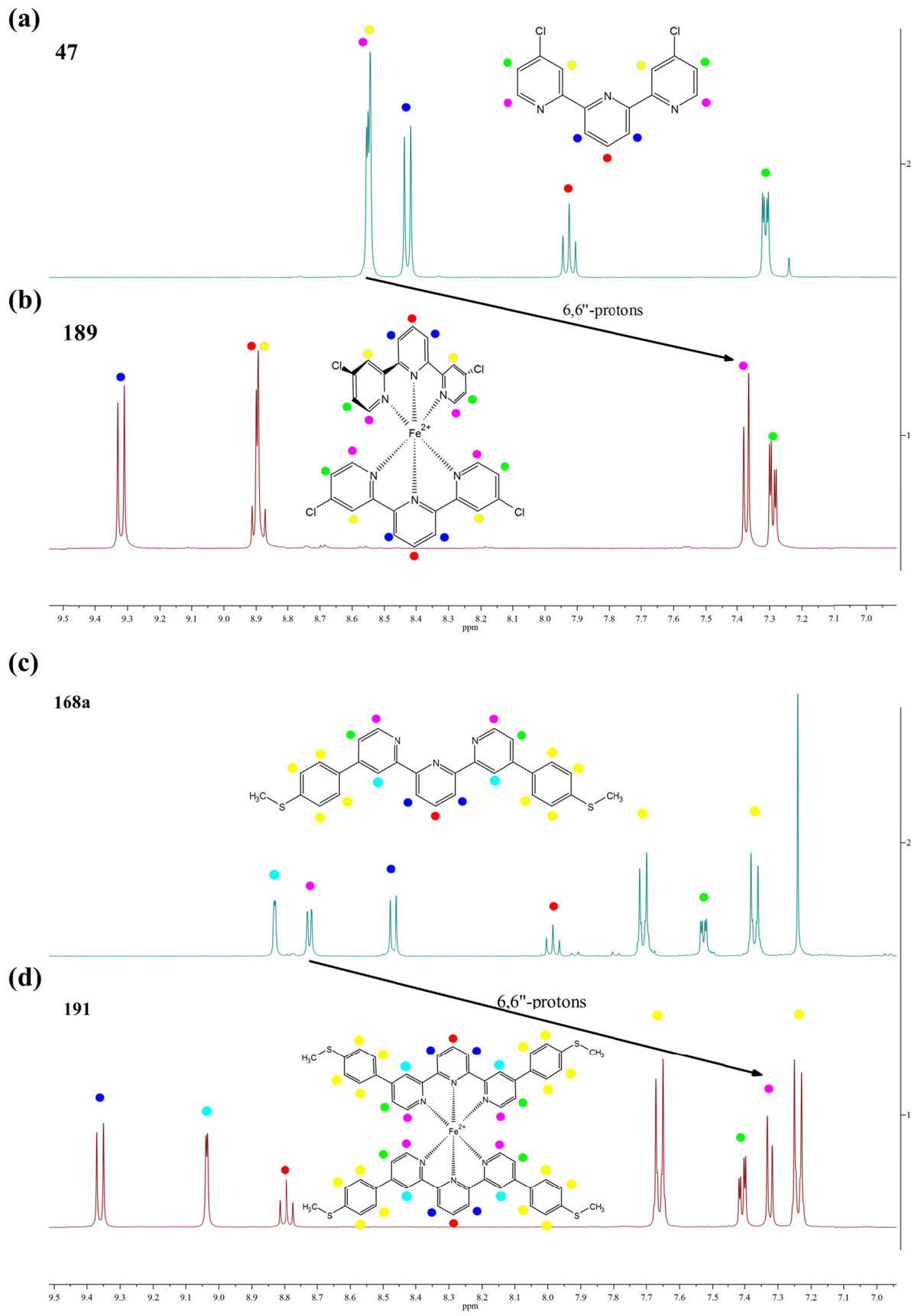

Figure 66: Visualization of the chemical shift of the ligands' H-atoms upon complexation for **(a) 47** to **(b) 189** and for **(c) 168a** to **(d) 191**. The H-atom positions are indicated by colored dots.

3.4.2 Optical Investigation of Terpyridine Complexes

The UV-spectra of the all homoleptic and heteroleptic Fe(II)- and Ru(II)-bis(tpy) complexes described throughout the present chapter were recorded at several concentrations (0.001 mM, 0.005 mM, 0.01 mM, 0.025 mM, and 0.05 mM, respectively) in acetonitrile at room temperature and their averaged absorbances, following Beer's Law (Equation 9), were converted into the corresponding extinction coefficients ε, which are plotted against the respective wavelengths λ (Figures 67-70 and Tables 3-6).

$$A=\varepsilon \cdot c \cdot d$$

Equation 9: Beer's Law relating the absorbance A with the extinction coefficient ε, the concentration c and the path length d of the light in the UV/vis cuvette.

Characteristic bands can be unambiguously identified within all the complexes' optical spectra. In particular the metal-to-ligand charge-transfer (MLCT) bands found in the region between 550 to 575 nm are typical for all Fe(II)-bis(tpy) complexes, alike. Those MLCT-transitions arise from the charge transfer of a primarily metal-localized electron from the respective 3dπ-orbital into the lowest unoccupied molecular orbital (LUMO) of the tpy ligands (π* ← 3dπ–transition). Table 3 and Figure 67 compare the λ_{max}-values of the LC-, the MC-, and the MLCT-bands of the homoleptic, non-dipolar Fe(II)-bis(tpy) complexes **188**-**196**, **129**, and **145** (**Type A**) with the parent $[Fe(tpy)_2]^{2+}$ complex **188.**[543]

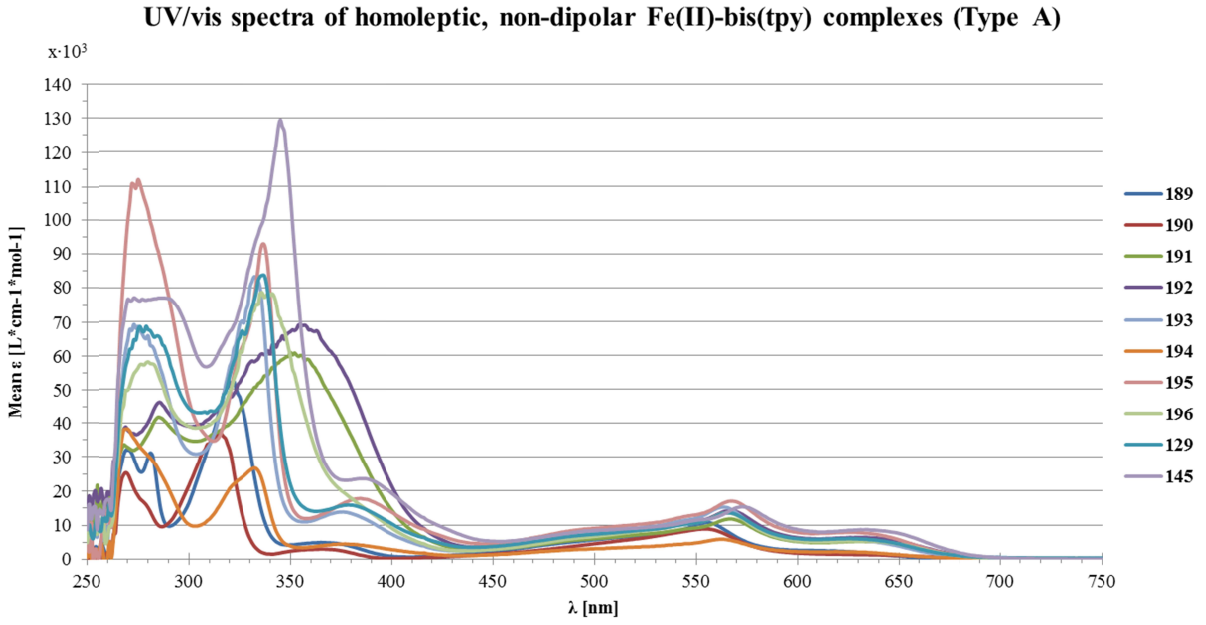

Figure 67: UV-VIS absorption spectra of homoleptic, non-dipolar Fe(II)-bis(tpy) complexes **189** – **196**, **129**, and **145** (**Type A**).

Table 3: Characteristic bands in the UV/vis spectra of the homoleptic, non-dipolar Fe(II)-bis(tpy) complexes **188** – **196**, **129**, and **145** (**Type A**).

Complex	λ_{max} (LC/MC) [nm]	ε [L*cm^{-1}*mol^{-1}]	λ_{max}(MLCT) [nm]	ε [L*cm^{-1}*mol^{-1}]
188[544]	318	38 000	552	11 900
189	270	32 115	555	10 690
	281	31 265		
	322	52 320		
	365	4 860		
190	269	25 442	555	8 820
	315	37 468		
	365	2 924		
191	268	33 685	567	11 775
	285	41 835	631	5 165
	350	60 830		
192	269	38 945	567	14 245
	284	46 155	631	6 340
	354	69 000		
193	273	69 165	563	15 240
	332	83 255	623	5 560
	376	13 835		
194	270	38 353	562	5 760
	332	26 813	619	2 153
	377	4 427		
195	275	111 867	567	17 000
	336	92 800	625	7 813
	384	17 773		
196	280	58 080	565	13 575
	336	78 560	630	5 340
129	276	68 550	566	13 540
	336	83 685	626	5 965
	379	15 880		
145	274	76 740	572	15 347
	345	129 560	633	8 573
	386	23 653		

In more detail the $\lambda_{max.}$-values of the Fe(II) complexes **189** and **190** display with 555 nm (ε = 10690 or 8820 L*cm^{-1}*mol^{-1}, respectively) only a small bathochromic shift in relation to the parent complex **188**. Interestingly both, the chlorine substituents of **189** with a *Hammet* σ parameter of +0.5 and the methoxy substituents of **190** with a *Hammet* σ parameter of -0.5 result in a similar reduction of the energy of the MLCT-band compared to the parent complex **188** ($\lambda_{max.}$ = 552 nm, ε = 11900 L*cm^{-1}*mol^{-1}). In analogy to the substituents in 4′-positions of Ru(II) tpy complexes,[541] it seems that the electron accepting chlorine substituents in **189** reduce the MLCT-band by stabilizing the ligand-based LUMO π*-orbital stronger than the iron-centered HOMO π-orbital, while the electron donating methoxy substituents in **190**

reduce the HOMO-LUMO gap by a stronger destabilization of the metal-centered HOMO in comparison to the ligand-centered LUMO. For the other homoleptic, non-dipolar Fe(II)-bis(tpy) complexes with $\lambda_{max.}$-values of 562 nm for **194** (ε = 5760 L*cm^{-1}*mol^{-1}), 563 nm for **193** (ε = 15240 L*cm^{-1}*mol^{-1}), 565 nm for **196** (ε = 13575 L*cm^{-1}*mol^{-1}), 566 nm for **129** (ε = 13540 L*cm^{-1}*mol^{-1}), 567 nm for **191**, **192**, and **195** (ε = 11775, 14245 and 17000 L*cm^{-1}*mol^{-1}, respectively), and 572 nm for **145** (ε = 15347 L*cm^{-1}*mol^{-1}) more pronounced bathochromic shifts of the MLCT-bands were observed. According to previous reports in literature the reduction of the energy gap can be attributed in this case to the stabilizing effect of the additional *para*-phenyl substituents.[545] In detail the enlarged conjugated π-system stabilizes the ligand-based LUMO π*-orbital, making **129**, **145**, and **191 - 196** better π-acceptors than the parent $[Fe(tpy)_2]^{2+}$ complex **188**. Going along with this argumentation it does not surprise that complex **145**, exhibiting an even further π-extended ligand system with its additional two acetylene bridges included within each of the two identical tpy ligands, shows the strongest bathochromic shift of the relevant MLCT-band. Furthermore, in the higher energetic spectral region several absorbance maxima can be found between 268 – 386 nm which are summarized in Table 3. The weaker bands between 365 and 386 nm most likely can be attributed to metal-centered electronic transitions whereas the more intense bands in the higher energetic region between 268 and 354 nm presumably arise from ligand-centered transitions (either π* ← π or π* ← n).[545] In the case of the thioether-functionalized complexes **191** and **192**, as well as for complex **196**, bearing methoxy-terminated tpy ligands, the expected MC-bands seem to be overlapped by the very intense LC-bands, whereas in all the remaining UV/vis spectra of the complexes **129**, **145**, **189**, **190**, **193** – **195** the LC- and the MC-bands can be discretely resolved.

In analogy to the homoleptic, non-dipolar Fe(II)-bis(tpy) complexes **129**, **145**, and **188 - 196** described above, Table 4 compares the λ_{max}-values of the LC-, the MC-, and the MLCT-bands of the homoleptic, dipolar Fe(II)-bis(tpy) complexes **119**, **120**, and **197 - 201** (**Type B**) with the parent $[Fe(tpy)_2]^{2+}$ complex **188**,[543] of which the optical spectra are displayed in Figure 68.

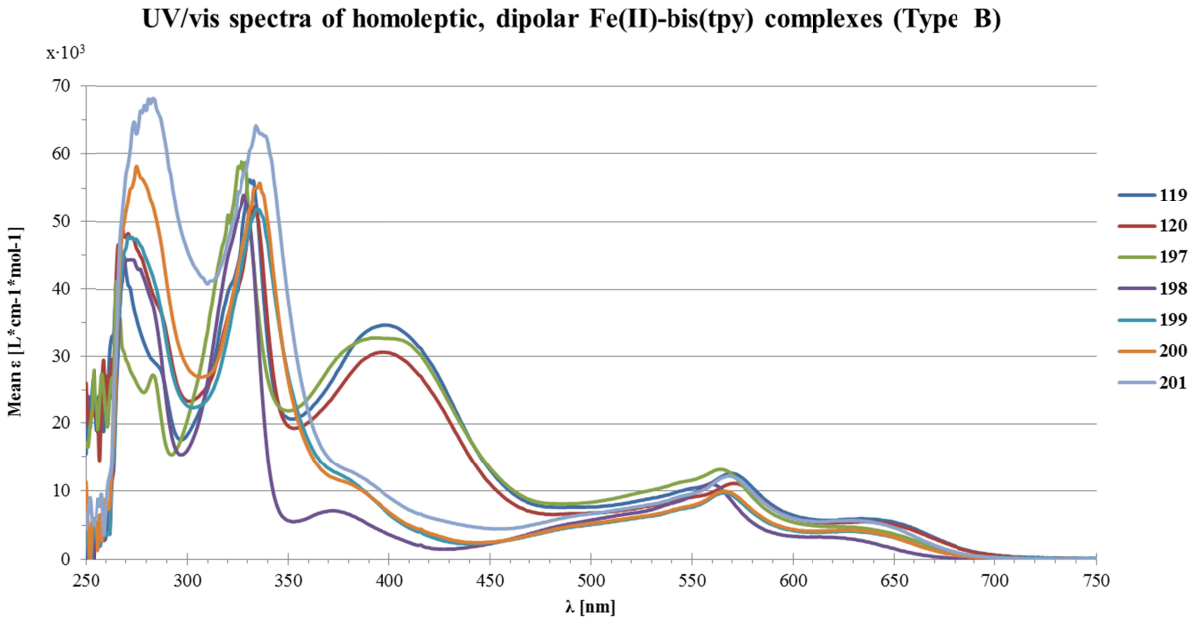

Figure 68: UV-VIS absorption spectra of homoleptic, dipolar Fe(II)-bis(tpy) complexes **119**, **120**, and **197** – **201** (**Type B**).

Table 4: Characteristic bands in the UV/vis spectra of the homoleptic, dipolar Fe(II)-bis(tpy) complexes **119**, **120**, and **197** – **201** (**Type B**).

Complex	λ_{max} (LC/MC) [nm]	ε [L*cm^{-1}*mol^{-1}]	λ_{max}(MLCT) [nm]	ε [L*cm^{-1}*mol^{-1}]
188[544]	318	38 000	552	11 900
119	269	44 790	569	12 670
	331	56 190	635	5 960
	397	34 630		
120	268	48 985	571	11 150
	333	52 165	634	5 505
	397	30 635		
197	265	41 067	564	13 240
	283	27 247		
	327	58 807		
	393	32 720		
198	272	44 415	560	11 080
	328	53 885	614	3 285
	372	7 115		
199	271	47 740	566	9 745
	335	51 845	627	4 110
200	275	58 125	566	10 010
	336	55 680	625	4 285
201	283	68 245	568	12 235
	334	64 195	629	5 695

In accordance with the observed stabilization of the ligand-based LUMO π*-orbital for enlarged conjugated π-systems, as discussed for the homoleptic, non-dipolar Fe(II)-bis(tpy)

complexes **129**, **145**, and **191** – **196** (**Type A**), also the homoleptic, dipolar Fe(II)-bis(tpy) complexes **119**, **120**, and **197** - **201** (**Type B**) show similar effects. Therefore it fits well to this argumentation, that the Fe(II) complexes of the smaller monosubstituted tpy ligands, namely, the complexes **197** and **198**, exhibit a smaller bathochromic shift of the relevant MLCT-bands, with $\lambda_{max.}$ = 564 nm (ε = 13240 L*cm^{-1}*mol^{-1}) for **197** and $\lambda_{max.}$ = 560 nm (ε = 11080 L*cm^{-1}*mol^{-1}) for **198**, in relation to the parent $[Fe(tpy)_2]^{2+}$ complex **188**,[543] than the Fe(II)-bis(tpy) complexes of the asymmetrically disubstituted push/pull tpy ligands, namely, **119**, **120**, and **199** – **201**. With $\lambda_{max.}$-values of 566 nm for the complexes **199** and **200** (ε = 9745 and 10010 L*cm^{-1}*mol^{-1}, respectively), 568 nm for **201** (ε = 12235 L*cm^{-1}*mol^{-1}), 569 nm for **119** (ε = 12670 L*cm^{-1}*mol^{-1}), and 571 nm for **120** (ε = 11150 L*cm^{-1}*mol^{-1}), these complexes of the bigger disubstituted π-extended tpy ligand show a significantly more pronounced shift in comparison to the $\lambda_{max.}$ of 552 nm for the parent $[Fe(tpy)_2]^{2+}$ complex **188**.[543] For the homoleptic, dipolar Fe(II)-bis(tpy) complexes the absorbances in the higher energetic spectral regions, attributed to the LC- and MC-transitions, lie in a similar range as for the homoleptic, non-dipolar Fe(II)-bis(tpy) complexes, described above. However the three complexes containing tpy ligands with an incorporated NMe_2-group, namely, the monosubstituted tpy ligand **197** and the two disubstituted complexes **119** and **120**, seem to represent slight exceptions, since these exhibit strong absorbance bands at a $\lambda_{max.}$ of 393 nm for **197** (ε = 32720 L*cm^{-1}*mol^{-1}), and a $\lambda_{max.}$ of 397 nm for **119** and **120** (ε = 34630 and 30635 L*cm^{-1}*mol^{-1}, respectively). As for the homoleptic, non-dipolar complexes, including thioether- or methoxy-terminated substituents (**191**, **192** and **196**) also for the herein, described homoleptic, dipolar Fe(II)-bis(tpy) complexes, with the exception of complex **198**, the expected MC-bands seem to be overlapped by the very intense LC-bands.

Additionally, the λ_{max}-values of the LC-, the MC-, and the MLCT-bands of the heteroleptic, dipolar Fe(II)-bis(tpy) target complexes **112** - **118** (**Type C**) and the ones of the heteroleptic, dipolar Ru(II)-bis(tpy) target complex **127** (**Type E**) are compared with the parent $[Fe(tpy)_2]^{2+}$ complex **188**,[543] and the $[Ru(tpy)_2]^{2+}$ complex **207**,[546,547] within Table 5 of which the optical spectra are displayed in Figure 69.

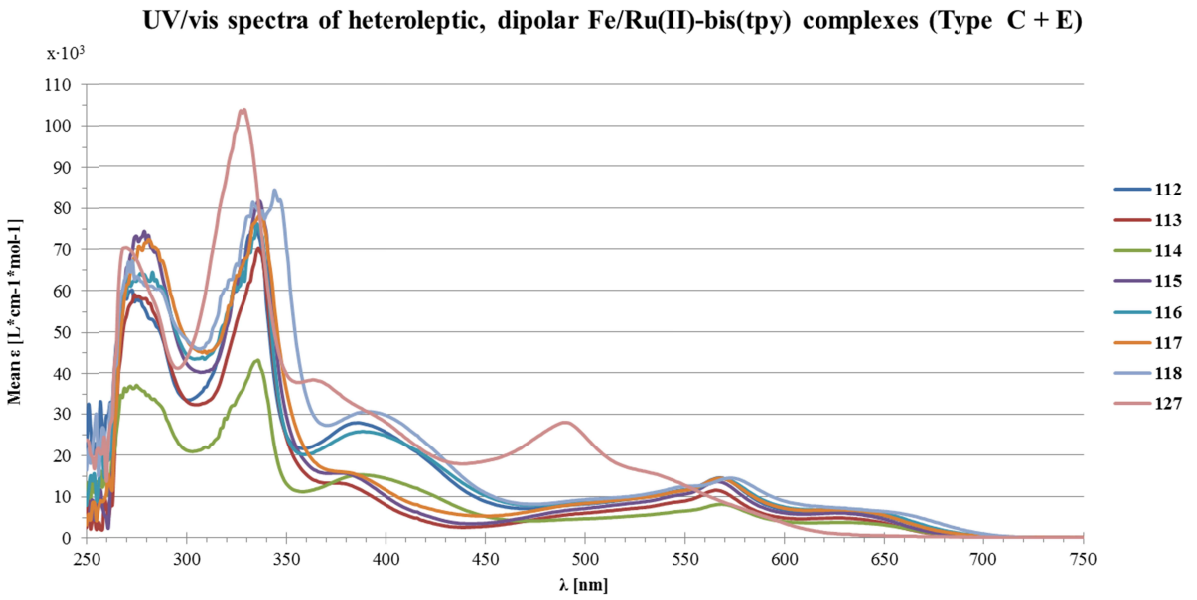

Figure 69: UV-VIS absorption spectra of heteroleptic, dipolar Fe(II)-bis(tpy) complexes **112 - 118** (**Type C**), and heteroleptic, dipolar Ru(II)-bis(tpy) complex **127** (**Type E**).

Table 5: Characteristic bands in the UV/vis spectra of the heteroleptic, dipolar Fe(II)-bis(tpy) complexes **112 - 118** (**Type C**), and heteroleptic, dipolar Ru(II)-bis(tpy) complex **127** (**Type E**).

Complex	λ_{max} (LC/MC) [nm]	ε [L*cm^{-1}*mol^{-1}]	λ_{max}(MLCT) [nm]	ε [L*cm^{-1}*mol^{-1}]
188[544]	318	38 000	552	11 900
112	273	60 010	568	14 515
	335	75 830	628	3 740
	386	27 940		
113	274	58 960	566	11 525
	336	70 255	627	4 845
114	275	36 972	568	8 142
	336	43 004	629	3 740
	387	15 262		
115	281	73 400	566	13 615
	336	81 770	626	6 030
116	283	64 465	569	14 290
	335	76 100	625	6 910
	389	25 825		
117	281	72 330	566	14 410
	338	78 415	626	6 790
118	271	67 035	573	14 470
	344	84 165		
	391	30 595		
207[546]	270	43 652	475	16 596
	308	70 795		
127	270	70 413	490	27 993
	329	103 893		
	363	38 313		

In accordance with the observed stabilization of the ligand-based LUMO π*-orbital for enlarged conjugated π-systems, as discussed for the homoleptic, non-dipolar Fe(II)-bis(tpy) complexes **129**, **145**, and **191** – **196** (**Type A**) and for the homoleptic, dipolar Fe(II)-bis(tpy) complexes **119**, **120**, and **197** - **201** (**Type B**), also the heteroleptic, dipolar Fe(II)-bis(tpy) target complexes **112** - **118** (**Type C**) show very similar effects. With $\lambda_{max.}$-values of 566 nm for the complexes **113**, **115**, and **117** (ε = 11525, 13615 and 14410 L*cm^{-1}*mol^{-1}, respectively), 568 nm for **112**, and **114** (ε = 14515 and 8142 L*cm^{-1}*mol^{-1}, respectively), 569 nm for **116** (ε = 14290 L*cm^{-1}*mol^{-1}), and 573 nm for **118** (ε = 14470 L*cm^{-1}*mol^{-1}), the complexes of these π-extended tpy ligands show very pronounced bathochromic shifts in relation to the $\lambda_{max.}$ of 552 nm for the MLCT-band of the parent $[Fe(tpy)_2]^{2+}$ complex **188**.[543] It therefore fits well, that complex **118** shows the strongest bathochromic shift of the relevant MLCT-band, which can be ascribed to the incorporation of one even further π-extended tpy ligand, bearing two additional acetylene bridges, into the complex compared to the other examples of these **Type C** complexes. For all these heteroleptic, dipolar Fe(II)-bis(tpy) complexes (**Type C**) the absorbances in the higher energetic spectral regions, attributed to the LC- and MC-transitions, lie in a comparable range as for the previously described homoleptic, dipolar Fe(II)-bis(tpy) complexes (**Type B**). However, once again the four complexes containing tpy ligands with an incorporated NMe_2-group, namely, the complexes **112**, **114**, **116**, and **118**, represent special cases, since all of these exhibit bathochromic shifted strong absorbance bands at a $\lambda_{max.}$ of 386 nm for **112** (ε = 27940 L*cm^{-1}*mol^{-1}), a $\lambda_{max.}$ of 387 nm for **114** (ε = 15262 L*cm^{-1}*mol^{-1}), a $\lambda_{max.}$ of 389 nm for **116** (ε = 25825 L*cm^{-1}*mol^{-1}), and a $\lambda_{max.}$ of 391 nm for **118** (ε = 30595 L*cm^{-1}*mol^{-1}). Furthermore, the fact, that in these heteroleptic, dipolar complexes **112**, **114**, **116**, and **118** only one NMe_2-group is included, whereas the respective homoleptic, dipolar complexes **119**, **120**, and **197** contain two such substituents, agrees with the more pronounced shifts observed for the latter group. The remaining heteroleptic, dipolar Ru(II)-bis(tpy) target complex **127** (**Type E**) shows similar effects, as the Fe(II)-bis(tpy) analogues. However, as expectable for Ru(II)-bis(tpy) complexes the MLCT-band is located at a much higher energetic region of the visible light's range leading to an overall red color instead of the outward purple appearance of the Fe(II)-bis(tpy) complexes. Nevertheless in relation to the parent $[Ru(tpy)_2]^{2+}$ complex **207**,[546,547] a pronounced analogue bathochromic shift of the MLCT-band, from a $\lambda_{max.}$ of 475 nm for the parent $[Ru(tpy)_2]^{2+}$ complex **207**,[546] to a $\lambda_{max.}$ of 490 nm for the target complex **127**, can be observed, as it has been found for the Fe(II) complexes discussed above.

The λ_{max}-values of the LC-, the MC-, and the MLCT-bands of the heteroleptic, non-dipolar Fe(II)-bis(tpy) target complexes **121** - **126** (**Type D**) are compared with the parent $[Fe(tpy)_2]^{2+}$ complex **188**,[543] within Table 6 of which the optical spectra are displayed in Figure 70.

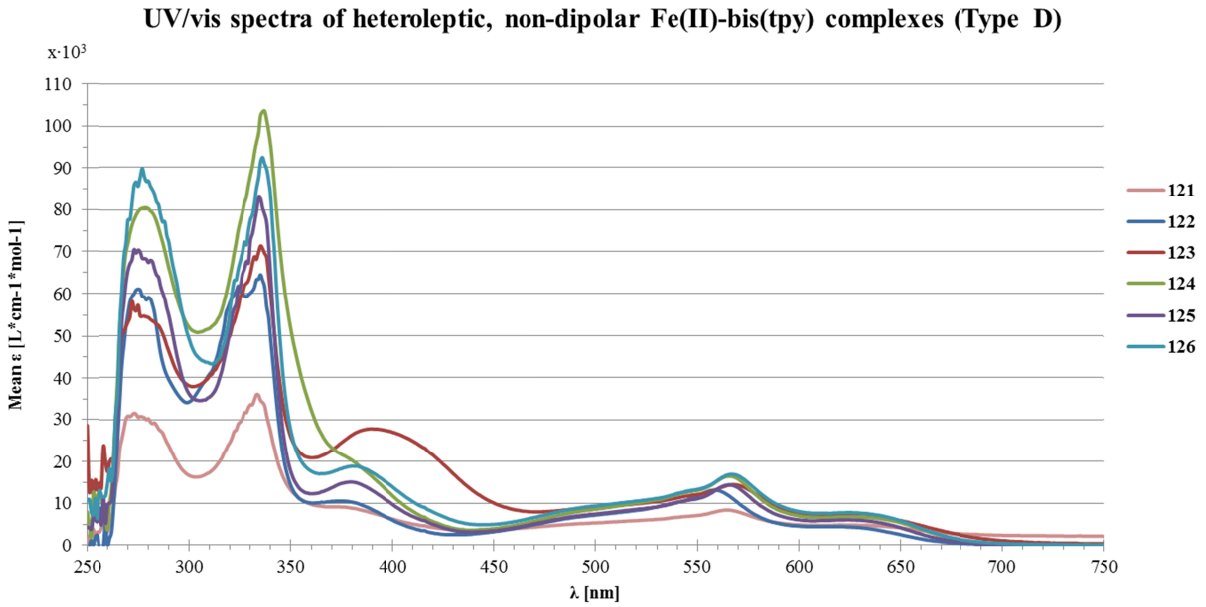

Figure 70: UV-VIS absorption spectra of heteroleptic, non-dipolar Fe(II)-bis(tpy) complexes **121** - **126** (**Type D**).

Table 6: Characteristic bands in the UV/vis spectra of the heteroleptic, non-dipolar Fe(II)-bis(tpy) complexes **121** - **126** (**Type D**).

Complex	λ_{max} (LC/MC) [nm]	ε [L*cm^{-1}*mol^{-1}]	λ_{max}(MLCT) [nm]	ε [L*cm^{-1}*mol^{-1}]
188[544]	318	38 000	552	11 900
121	273	31 538	564	8 392
	333	35 956	621	4 832
122	274	60 810	558	13 170
	335	64 490		
	374	10 550		
123	272	58 125	567	14 470
	335	71 385	625	7 095
	389	27 810		
124	278	80 533	566	16 493
	337	103 633	626	6 767
125	273	70 520	566	14 400
	334	82 980	625	6 070
	379	15 105		
126	277	89 755	564	16 690
	336	92 405	625	7 780
	382	18 910		

In accordance with the observed stabilization of the ligand-based LUMO π*-orbital for enlarged conjugated π-systems, as discussed for the previously described complexes of the **Types A – C**, and **E** also the heteroleptic, non-dipolar Fe(II)-bis(tpy) target complexes **121 - 126** (**Type D**) show comparable effects. In this context it was observed, that the complex **122**, which bears only one π-extended tpy ligand, exhibits a significantly smaller bathochromic shift of the MLCT-band, with a $\lambda_{max.}$ = 558 nm (ε = 13170 L*cm^{-1}*mol^{-1}) in relation to the observed $\lambda_{max.}$ = 552 nm of the parent $[Fe(tpy)_2]^{2+}$ complex **188**,[543] than the other complexes of **Type D**, namely, **121**, and **123 – 126**. For these five complexes the MLCT-bands can once again be found severely bathochromically shifted between a $\lambda_{max.}$ of 564 nm for **121** (ε = 8392 L*cm^{-1}*mol^{-1}) and for **126** (ε = 16690 L*cm^{-1}*mol^{-1}), a $\lambda_{max.}$ of 566 nm for **124** (ε = 16493 L*cm^{-1}*mol^{-1}) and for **125** (ε = 14400 L*cm^{-1}*mol^{-1}), and a $\lambda_{max.}$ of 567 nm for **123** (ε = 14470 L*cm^{-1}*mol^{-1}). For all heteroleptic, non-dipolar Fe(II)-bis(tpy) complexes (**Type D**) the absorbances in the higher energetic spectral regions, attributed to the LC- and MC-transitions, lie in the expectable range related to the previously described heteroleptic, dipolar Fe(II)-bis(tpy) complexes (**Type C**). However, once more the only complex containing a tpy ligand with two incorporated NMe_2-groups, namely, complex **123**, represents an exception, due to the extraordinarily strong, bathochromic shift of the absorbance band at a $\lambda_{max.}$ of 389 nm (ε = 27810 L*cm^{-1}*mol^{-1}). The further absorbance bands in this higher energetic region of the UV/vis spectra of the investigated **Type D** complexes do not show any exceptional features, which is why the corresponding details are only listed in Table 6 above.

3.4.3 Mechanically Controllable Break-Junction Experiments

The present chapter describes the physical investigations performed for the first main project, namely, the development of bias-sensitive, single molecular spin switching systems, that are to be immobilized and studied using mechanically controllable break junction (MCBJ) techniques. All the MCBJ experiments described hereafter, have been performed by Riccardo Frisenda in the group of Prof. Dr. Herre van der Zant at the TU Delft in the Netherlands. Due to the nature and core of this thesis the main focus hereafter, will however be laid on the results so far obtained from the MCBJ measurements and possible interpretations of the observed effects. First of all the most important features of the utilized MCBJ setup are highlighted (Figure 71a). Additionally, the postulated interactions of our

envisaged electrical-field dependant single molecular spin switching target systems (**Type C**) within the MCBJ are illustrated (Figure 71b).

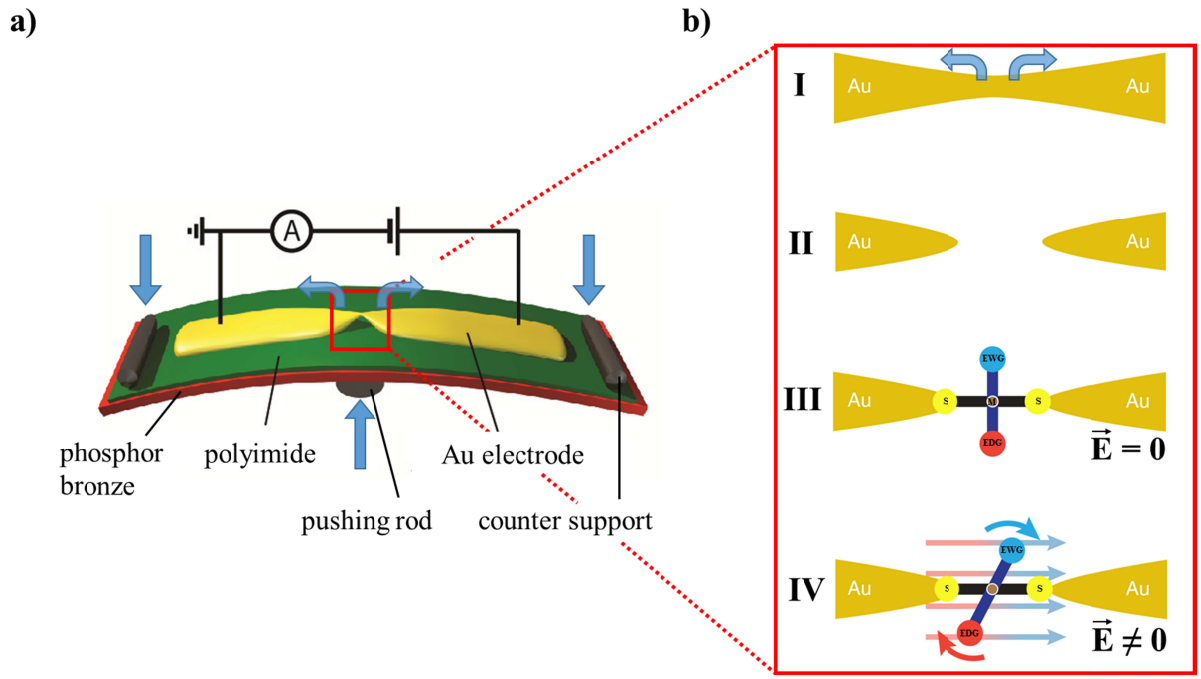

Figure 71: (a) Schematic illustration of the physical setup of an MCBJ. **(b)** Schematic step-by-step illustration of the processes occurring during breaking and junction formation in an MCBJ setup: **(I)** stretching of the gold wire with the help of a piezoelectrically controlled pushing rod and two opposing counter supports (see Figure 71a), **(II)** rupture of the gold wire resulting in the formation of two gold nano-electrodes facing each other. **(III)** Immobilization of the envisaged heteroleptic, dipolar target structures (**Type C**) into the MCBJ without externally applied electrical fields. **(IV)** Alteration of the immobilized structure's geometry by variation of the applied electrical fields resulting in an alignment of the dipolar tpy ligand into this externally applied electrical field and ideally coinciding with SCO at the single molecular level.

In detail for the exemplary execution of such an MCBJ measurement the MCBJ sample is immersed into a 0.5mM solution of the according target complex in MeCN for 5 h to allow for the self-assembly of the molecules onto the gold wire. Experiments are performed in vacuum (10^{-7} mbar) and at liquid Helium temperature (~4 K). By bending the substrate, the gold wire stretches, until it eventually breaks, leaving two broken extremities facing each other, which act as nano-scale electrodes, as schematically shown in Figure 71b – steps I+II. During the rupture process a molecule can potentially bridge the nano-electrodes allowing the measurements of transport through the junction, as depicted in Figure 71b – steps III+IV.

However, before some exemplary results from the multitude of obtained *I-V* curves and conductance traces are shown and discussed, several points, which are of utmost importance for a scientifically reliable and trustworthy interpretation of the results from single molecule measurements vian MCBJ, shall be addressed. First of all, although the integration of single,

switchable molecules into such nanojunctions seems very appealing with regard to the present degree of miniaturization, especially in comparison to macroscopically miniaturized switching devices fabricated via regular top-down approaches, there is the problem of the utilization of nanoelectrodes, which, of course, is inevitable for single molecular measurements. In the present case, especially the rupture of the Au wire (Figure 71b – steps I) can raise distinct reproducibility issues concerning the electrode's atomic tip shape. Especially in single molecular conductance measurements, such as e.g. MCBJ, these effects can have an enormous impact on the observed experimental outcome. Hence the interplay of a sufficiently huge number of experiments, giving a large enough statistical basis, in addition to the investigation of a sufficiently broad variety of studied systems, is required, to be able to distinguish between effects observed as a consequence of the designed experiment, and observations that arise from artifacts caused by the described minor deviations in the electrodes' surface. The fact that, in order to obtain reliable results, each individual measurement has to be performed within a freshly formed break junction, further documents the necessity of a broad statistical basis. The named requirements *a fortiori* hold true for the herein, described experiments, in particular since in single molecular contacting experiments also the anchoring geometry of the investigated molecules to the nanoelectrodes' surface can be strongly affected by minor differences of the electrodes, even on an atomic scale. Therefore, apart from the execution of a sufficiently huge number of experiments, with the aim to obtain a broad statistical basis for the performed experiments, several tailor-made target structures were planned to be investigated, in order to comply with the demand of adequate test systems and to thus rule out, which observations can be truly related to the desired bias-dependant spin switching phenomena and which might potentially arise from some non-specifiable side effect, which should thus be excludible to the biggest possible extent. In detail these test systems, on the one hand, encompass the complexes **121** – **126** (**Type D**), which in relation to the applied trigger, namely, the alteration of the applied electric field, can be considered as non-addressable systems, and should therefore not show any bias-induced bistability. On the other hand the Ru-based target complex **127** (**Type E**), represents an electrically addressable structure, which however cannot react with a SCO phenomenon to the external stimulus, as it is envisaged for the Fe-based dipolar target structures **112 - 118** (**Type C**), and which therefore should, if at all, only react in a strongly alleviated form to the externally applied electrical impulse. Furthermore, the variation of the dipolar strengths within the group of the dipolar Fe(II)-based target structures**112** – **118** (**Type C**) should help to gain additional insights concerning the question, which observations can be

truly related to the desired bias-dependant spin switching phenomena and which might potentially arise from some non-specifiable side effect, which thus should be excludible to the biggest possible extent.

To exemplarily cover all the named types of target structures, namely, **Types C**, **D**, and **E**, Figure 72 and 73 display *I-V* curves of selected representatives of all groups. In detail the highlighted complexes include the dipolar, heteroleptic Fe(II)-bis(tpy) target complexes **112** and **114** (exhibiting strong dipole moments) (Figure 72a+b), as well as complex **113** (weak dipole moment) (Figure 72c), and complex **118** (strong dipole moment, but anchoring ligand elongated by two acetylene bridges) (Figure 72d) as representatives of **Type C** complexes. Furthermore, as an example of **Type D** complexes, which can be considered as non-sensitive to the strength of the applied electric field, complex **121** is discussed in more details (Figure 72e), and finally the investigations of the dipolar, heteroleptic Ru(II)-bis(tpy) target complex **127** (**Type E**), which is unable to undergo any SCO at all, are shown as well (Figure 72f). In general the exemplary *I-V* curves displayed in Figure 72 exhibit three different types of bistability features, which were observed for the investigated complexes during the herein, presented experiments. For all the shown *I-V* curves the forward (blue) and the backward (red) voltage bias sweeps are Hereby, shown in different colors with the measurement starting from zero bias on the forward (blue) branch. The left column of *I-V* curves shown in Figure 72 displays examples exhibiting hysteretic behavior observed on the different target complexes, respectively. Herein, each of the investigated systems exhibits a low and a high current configuration, of which the latter one, according to literature,[548] can be attributed to the HS state of the SCO system. The middle column of *I-V* curves in Figure 72 displays examples exhibiting pronounce negative differential conductances (NDCs) observed for the different target complexes, respectively. In these traces, upon increasing the bias voltage towards more negative values, the current drops to lower values in a more gradual way than for the sudden drop observed in the hysteretic switching and it is reproducibly observed in both sweep directions (blue and red in Figure 72 – middle column). These NDC *I-V* traces are less frequent and can be interpreted as the adaption of a less conducting state in the bias window of the NDC dip. A closer inspection of the *I-V* curves herein, indicates the presence of two-level fluctuations in the transition regions. Finally the right column of illustrated *I-V* curves in Figure 72 displays examples exhibiting more abrupt step-like switches.

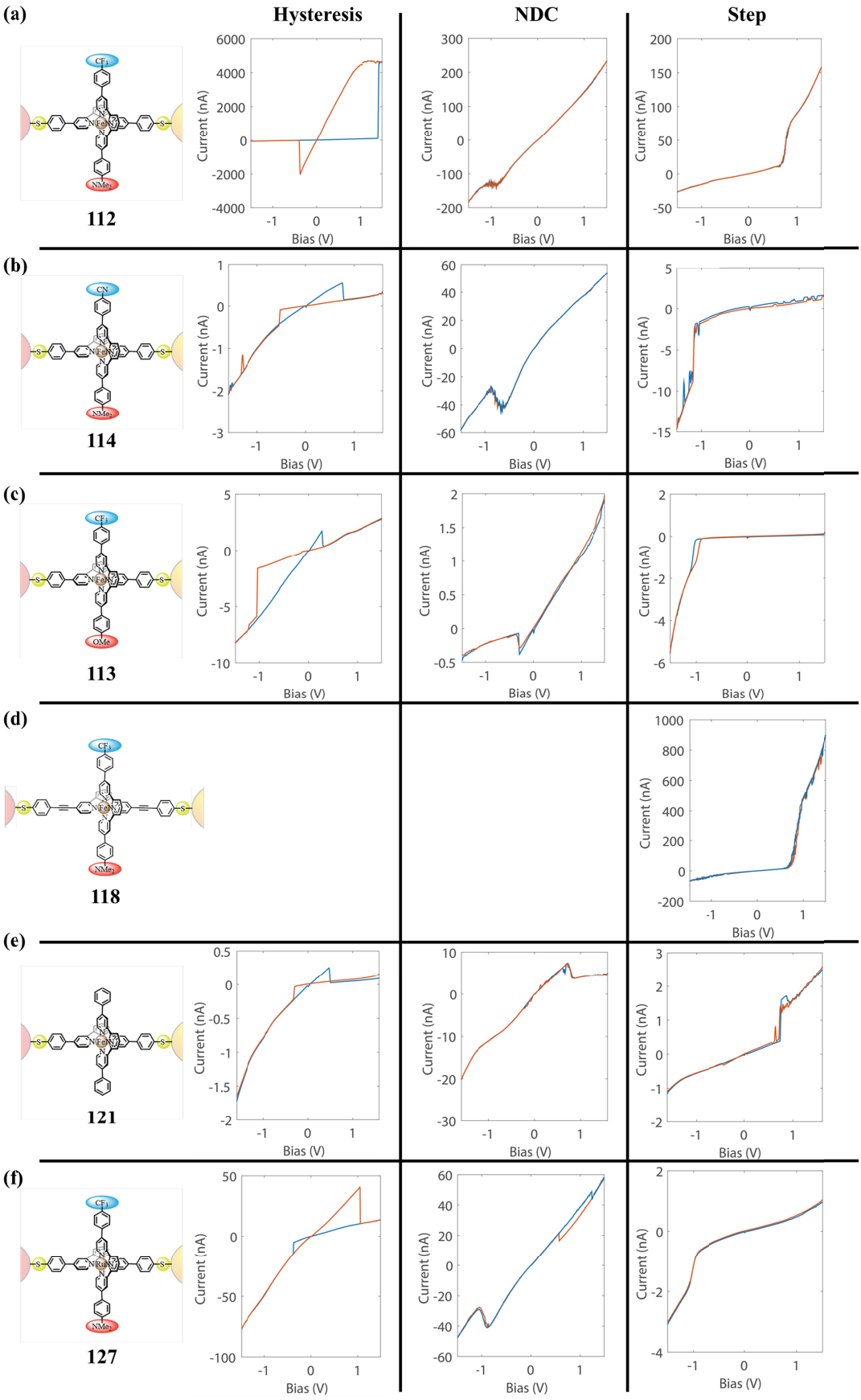

Figure 72: Overview of typical exemplary current-voltage characteristics measured on target complexes **112** – **114**, **118**, **121**, and **127**. For each of the investigated target structures the *I-V* curves display examples of hysteretic behavior (left column), NDCs (middle column), or step-

like behavior (right column). Fe(II)-based target complexes displayed in figures 72a-e: **(a)** + **(b)** complexes **112** and **114** (**Type C**), exhibiting a strong intrinsic dipole moment, **(c)** complex **113** (**Type C**), exhibiting a weakened intrinsic dipole moment, **(d)** complex **118** (**Type C**), exhibiting a strong intrinsic dipole moment and a twofold elongated anchoring ligand, and **(e)** complex **121** (**Type D**), exhibiting no intrinsic dipole moment at all. Additionally, **(f)** displays the Ru(II)-based reference complex **127** (**Type E**), exhibiting a strong intrinsic dipole moment without being applicable to any SCO phenomena.

Due to the vast amounts of different examples of *I-V* curves for different types of observed effects, namely, NDC and steps with or without hysteresis, hereafter, only one example shall be elucidated in detail representatively for all the other ones. For this purpose, first of all, a closer look is taken exclusively onto junctions containing target complex **114**, and herein, only the cases exhibiting hysteretic switching behavior are contemplated. Hereafter, the analysis of the exemplary distance dependence of the current-voltage characteristics for increasing electrode's separations of junctions containing target complex **114** (Figure 73), will be followed by detailed explanations for the accordant *I-V* curves' shape of complex **114** exhibiting hysteretic behavior together with appropriate simulations further underlining the obtained results (Figure 74). Finally, hereafter, a broad statistical overview of the overall outcome of the MCBJ measurements will be given for all complexes in order to comparatively discuss the obtained results versus the expectable outcome (Figure 75).

One of the most appealing features of the MCBJ experiment is that the electrode spacing can be slightly altered without losing the bridging molecule. In detail, upon an increased electrode's displacement, the bistability is typically preserved and in most cases shifts to higher bias voltages. Thus, since the electric field E inside the junction correlates linearly with the applied voltage U divided by the electrode spacing d (Equation 10), it was expected that the threshold voltage required to trigger the SCO in the immobilized complex should increase linearly, when the electrodes are displaced further away from each other.

$$E = \frac{U}{d}$$

Equation 10: Expression correlating the dependence of applied electric fields E, bias voltage U, and the interelectrode's spacing d.

After all, the inspection of the conductance jumps found for the bistable junctions of complex **114** displaying hysteretic *I-V* curves, was recorded as a function of the electrode's displacement and indeed, the voltage required for triggering the jump, was found to increase linearly in both bias directions (red and blue line in Figure 73b) with a very similar rate of about 1 V/Å. Furthermore, as the values of the switching voltages have been collected for all bistable *I-V* curves, the results are illustrated in form of a histogram displaying the applied

biases at which switching was observed summed up over all junctions (Figure 73c) in question. Herein, two maxima, one at negative and one at positive bias, are clearly observed representing a typical switching voltage for junctions of **114** between 0.25 and 1.5 V.

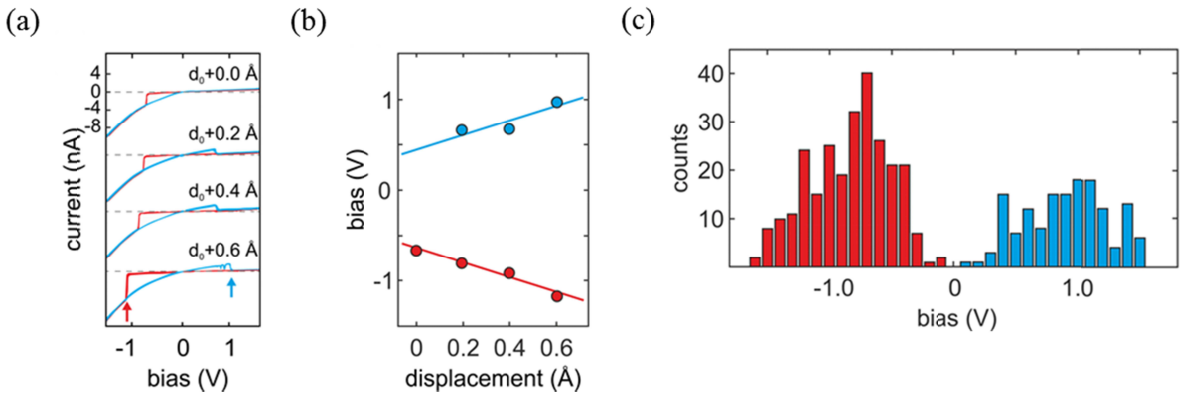

Figure 73: Inspection of bistable junctions formed by the Fe(II)-bis(tpy) target complex **114**. **(a)** Current-voltage characteristics for increasing electrode separation showing a hysteretic switching behavior. The curves are offset in the vertical direction for clarity. The red and blue arrows indicate the switching points for the electrode spacing d_0 + 0.6 Å. **(b)** Switching bias as a function of electrodes separation for the *I-V* curves, whereas the straight red and blue lines are guides for the eyes displaying the linear relationship. **(c)** Histogram of the switching voltage for all *I-V* curves of **114** displaying bistability features.

In the following an explanation for the hysteretic behavior of the *I-V* characteristic of target complex **114** shown in Figure 72b will be given. The named *I-V* curve of **114** exhibits a hysteretic behavior, whereat the current switches to a lower value at a positive bias of $V = 0.7$ V and switches back to high values at a negative bias of $V = -0.5$ V. Herein, it is worth noticing that the full bias sweep starts and ends with the system in the high current configuration, which, as mentioned before, according to literature can be attributed to the HS state of the SCO system.[548]

In order to gain more insight into the observed bistability features of the discussed *I-V* curves (*experimental:* Figure 72b; *simulated:* Figure 74a) our collaborators in Delft suggested a model reproducing the current-voltage characteristics on a qualitative level. Herein, the position of the dipolar tpy ligand arm of the molecule is modeled by a triple well potential, shown in Figure 74b. Among these the central well corresponds to the system in the LS state while the two side wells both describe the HS state. The angle of the dipolar push/pull arm with respect to the anchoring backbone tpy ligand in this connection determines in which well the molecule resides. In analogy to the low and high conductance states observed in the experimental *I-V* curves (Figure 72b), we assign two different conductance values to the LS and HS state, hereby, being consistent with earlier scanning probe experiments on Fe-based SCO compounds. The actual simulation of the hysteretic *I-V* curves was performed by

analyzing the status of the system as a function of the electric field, using a Monte Carlo method in the Metropolis approximation. Further computational details shall not be discussed at this place, as they exceed the scope of this work. However, the exemplary outcome of the accordant simulations for the hysteretic bistable switching behavior observed for target compound **114** is illustrated in Figure 74, and nicely correlates the simulated *I-V* curve (Figure 74a), with the simulated potential landscape of complex **114** (Figure 74b), and the according molecular geometries of the target complex within the break junction, as well as to the corresponding spin states (Figure 74c). In the present case the system was initialized in the left well (HS state) at zero E-field. By increasing the electric field into the positive direction, the system jumps into the central well (LS). Furthermore, only the application of a sufficiently strong negative electric field allows the system to jump back to the left well (HS). In the following no additional switching events happen when decreasing the electric field back to zero. Therefore the outcome of the illustrated simulations shows a rather ideal match with the observed experimental findings and thus further corroborates our postulated switching mechanism.

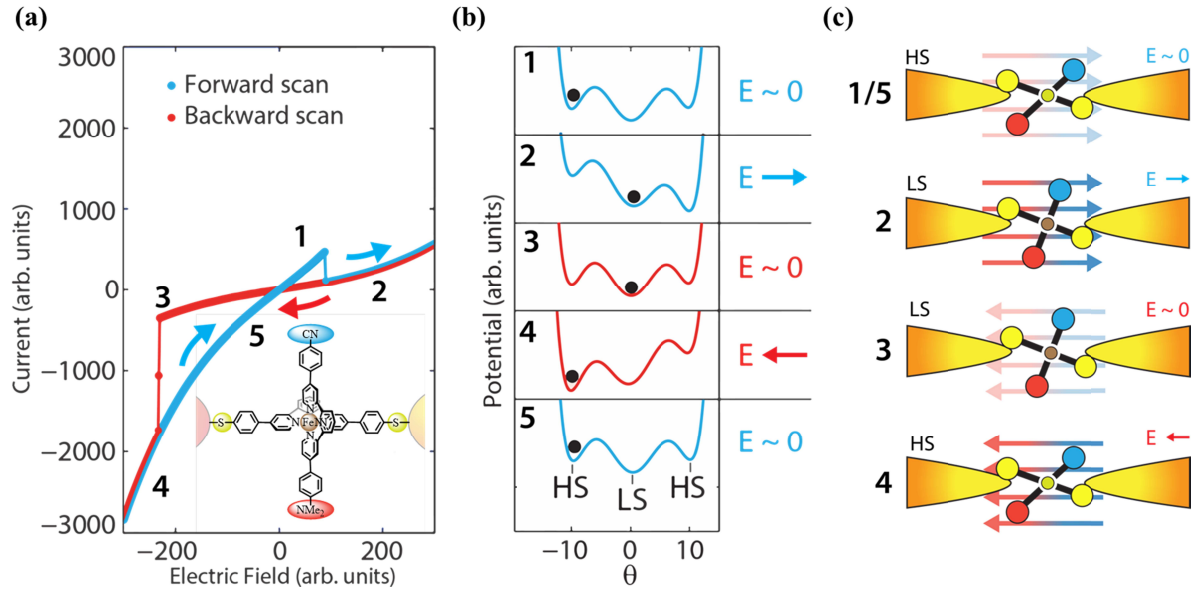

Figure 74: Model calculations and simulated *I-V* curve for the exemplary explanation of the hysteretic switching behavior found for the heteroleptic Fe(II)-bis(tpy) target complex **114** in comparison to the experimental *I-V* characteristic of the described system illustrated in Figure 72b (left side). **(a)** The illustrated *I-V* curve has been simulated using Monte Carlo-Metropolis dynamics, mimicking the current-voltage characteristics shown in Figure 72b. **(b)** Correlation of the different stages (1 – 5) observed in the simulated as well as in the experimentally measured *I-V* curves to the potential landscape of an exemplary SCO complex bearing an accordant dipole arm at varying applied electric field strengths. **(c)** Actual correlation of the five stages to the according molecular geometries of the target complex **114** within the MCBJ, as well as to the corresponding spin states.

In order to finally evaluate the consistency of the obtained and discussed results, we performed extended statistical analyses for the observed findings for all the six measured

target compounds, namely, the four heteroleptic Fe(II)-based target structures **112** – **114**, and **118** as potential SCO complexes, the non-dipolar and thus electrically non-addressable heteroleptic Fe(II)-bis(tpy) complex **121**, and the electrically addressable heteroleptic, dipolar Ru(II)-bis(tpy) complex **127**, which however cannot undergo SCO (Figure 75). In each series for each of the named complexes, the electrodes were first pushed together to form metallic wires, after which they were pulled apart while measuring the resulting *I-V* diagrams. We can divide the measurements into three categories:

(1) series without a trapped molecule, in which the low-bias conductance either decays monotonically and exponentially when increasing the distance between the electrodes or in which it falls directly below the noise level of the setup,

(2) series with a trapped molecule, but no clear indication of bistability, exhibiting plateau-like features in the conductance versus displacement trace, and

(3) series with a molecule trapped inside the junction and bistable *I-V* features.

With each complex **112**, **113**, **118**, **121**, and **127**, as well as for the metal-free reference molecule **OPE3** large enough numbers (269 - 758) of junctions were formed to analyze their voltage dependent behavior statistically. First staying with the exemplary discussion of the strong dipolar, heteroleptic Fe(II)-bis(tpy) target complex **114**, from 293 junctions formed, 224 (76%) displayed an exponential decay of the current with increased electrode spacing as the typical behavior of a pair of gold electrode without a bridging molecule (first category). The remaining 69 (24%) junctions displayed current plateaus more than two orders of magnitude beyond G_0 indicative for the incorporation of a bridging molecule. From these junctions 41 (59% of the junctions comprising a molecule) belong to the second category, in which no bistability features could be observed in the accordant *I-V* curves, whereas 28 (41%) of the molecule-bridged junctions actually display voltage dependent bistability features (third category). The considerable variety of observed *I-V* characteristics (Figure 72), was to some extent surprising, but reflects the limited control over the arrangement of the electrode-molecule-electrode junctions. However, due to the extended series of control experiments performed we were anyways able to extract reliable scientific findings from the obtained results. First of all the investigation of the molecular junctions containing the organic rigid rod-type **OPE3** molecule, exhibiting comparable dimensions and the same terminal anchor groups as our target metal structures, gave corroborative results. In detail from 856 rupture experiments with **OPE3** a fraction of 65 (7%) junctions contained an immobilized molecule.

However, not any of these 65 junctions displayed any bistability features, thus heavily supporting the hypothesis that the bistability features observed for our target complexes actually emerges from the immobilized metal complexes. As foreshadowed above in order to further substantiate the voltage triggered origin of the rearrangement of the dipolar ligands we investigated a large number of junctions with the heteroleptic Fe(II)-based bis(tpy) complexes **112** - **114**, **118**, and **121** exhibiting various strengths of the incorporated push/pull systems. While **121** has no dipole moment in the second tpy ligand, **113** exhibits a clearly weaker dipole moment than **112** and **114**. If our hypothesized mechanism really applies these differences should be reflected in the statistics of the junctions' *I-V* characteristics. Finally, the MCBJ studies were complemented by the heteroleptic, dipolar Ru(II)-based complex **127** comprising an identical intrinsic dipole moment as **112**. As **127** cannot exhibit SCO phenomena, it should be a further valuable model compound to identify bistability features rather arising from the molecules shape and/or interactions with the electrodes, than from a voltage triggered SCO in the central metal ion. An overview of the overall results of these extended statistical investigations is given in Figure 75, below

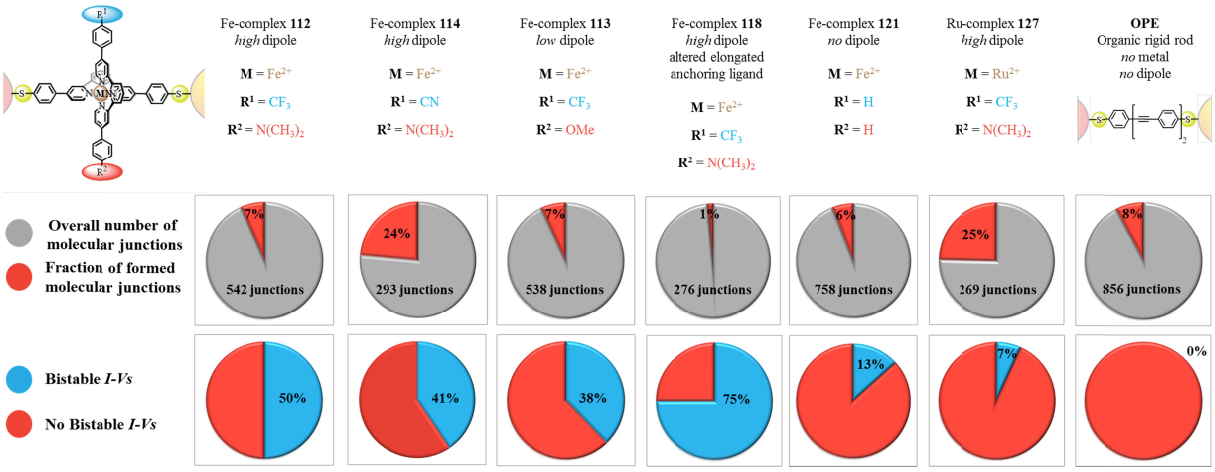

Figure 75: Illustration of the statistical analysis of the MCBJ experiments with the heteroleptic metal bis(tpy) target complexes **112** – **114**, **118**, **121**, and **127**, complemented by a rigid rod-type OPE molecule as an appropriate metal-free reference compound. The upper row of pie charts depicts in red the molecular junction formation probability of the corresponding complexes, whose chemical structures, or characteristic substituents, are highlighted above. On the other hand the lower row of pie charts displays in blue the fractions of the molecule-containing junctions, which actually display bistability features in their *I-V* curves.

The upper row of pie charts in Figure 75 herein, displays the fractions of junctions comprising an immobilized molecule for each investigated compound. Although the ratios vary from 6% to 25% we were not able to correlate these numbers to particular structural parameters of the analyzed molecules. The fact, that these experimental data are not suited to draw conclusions between the obtained ratios and the molecule's structure can be clearly

underlined by the big difference in formed molecular junctions between the target complexes **112** and **127**, which differ solely in their central metal ion (Fe^{2+} vs. Ru^{2+}, respectively). Furthermore, the heteroleptic, dipolar Fe(II)-bis(tpy) complex **118**, containing an elongated molecular backbone ligand even only exhibits a junction formation probability of 1%, which after all however might be deduced to the much longer molecular structure. The second row of pie charts in Figure 75 illustrates the fraction of molecular junctions containing immobilized molecules that actually exhibit bistability features. Herein, a clear trend can be seen that the relative amount of junctions exhibiting bistability is increasing with the strength of the dipole moment and the presence of central Fe^{2+} ion. While not a single junction displaying bistability was found for the organic OPE rod, however, also the Ru(II)-based complex **127**, without a SCO compatible central ion, and the Fe(II)-based complex **121**, lacking a perpendicular dipole moment, formed some bistable junctions. Even though the fractions are significantly smaller, the fact that such junctions are observed at all, suggests that there are other mechanisms, beyond the envisaged and herein, investigated voltage triggered ligand distortion with concomitant SCO, which might result in bistable junctions as well. While in the case of the non-dipolar Fe(II) complex **121** the tpy ligand perpendicular to the junction might align in the electric field due to its polarizability, the bistabilities occasionally observed for the Ru(II)-based complex **127** cannot be related to a SCO phenomenon of the central ion. In contrast to this rather surprising finding, in the series of the Fe(II)-based complexes, the fractions of bistable junctions among the ones actually containing immobilized complexes, display the expected increase of the SCO phenomena with increasing dipole moments in the order **121** (13%) < **113** (38%) < **114** (41%) < **112** (50%) = **118** (75%) , and thus supports the hypothesized switching mechanism. Considering the structural similarity of **112** and **127**, which differ solely in their central ion, the hypothesized voltage triggered ligand rearrangement with concomitant distortion of the coordination sphere is probably not the only mechanism contributing to the 50% of bistable junctions obtained for complex **112**, although it represents the by far most important factor. The only extraordinary finding concerning the relative amount of junctions exhibiting bistability features was observed for the target complex **118**, which contains the elongated molecular backbone extended by two acetylene moieties within the anchoring tpy ligand. Among its four molecule-containing junctions three (75%) showed bistability features, although the dipolar subunit of complex **118** is identical with the one of complex **112**, which only exhibits 50% of bistable junctions. Furthermore, all examples of bistable junctions of the elongated target complex **118** (Figure 72d) without exception exhibit a switching from low conductance values

at low bias to high conductance values at high bias. Possible explanations for this finding can be, that the influence of the electrodes, and thus also the potential side-effects, are less strong, thus allowing an eased and more reproducible electric-field driven LS→HS transition. Apart from this the findings fit into the general picture of the other investigated complexes, that low conductance values correspond to the LS state and high conductance values can be correlated to the HS state. However, a broader statistical basis seems to be inevitable in order to reliable draw any conclusions form the promising results for the MCBJ experiments of complex **118**. For this purpose also the issue of the severely reduced junction formation probability of the elongated structure **118**, being only around 1%, needs to be tackled in the future.

3.4.4 STM Investigations

The present chapter describes the physical investigations, by means of STM experiments, that were performed for the second project, namely, the investigation of bias-dependent SCO phenomena of surface-absorbed homoleptic, dipolar Fe(II)-bis(tpy) complexes (**Type B**), which were previously immobilized onto appropriate surfaces, such as Au(111), via ESI. The STM experiments described hereafter, have been performed by Thomas Knaak in the group of Prof. Dr. Richard Berndt at the University of Kiel in Germany. After briefly introducing the most important features of the utilized STM setup the results obtained for the investigation of the homoleptic, dipolar Fe(II)-bis(tpy) complex **119** are discussed in detail. Hereby, it shall be revealed, whether the real outcome of the application of bias impulses of varying strengths onto the investigated homoleptic, dipolar target structure's geometry and hence also onto its core ion's spin state resembles the postulated result for the investigation of the named dipolar target structure (Figure 76).

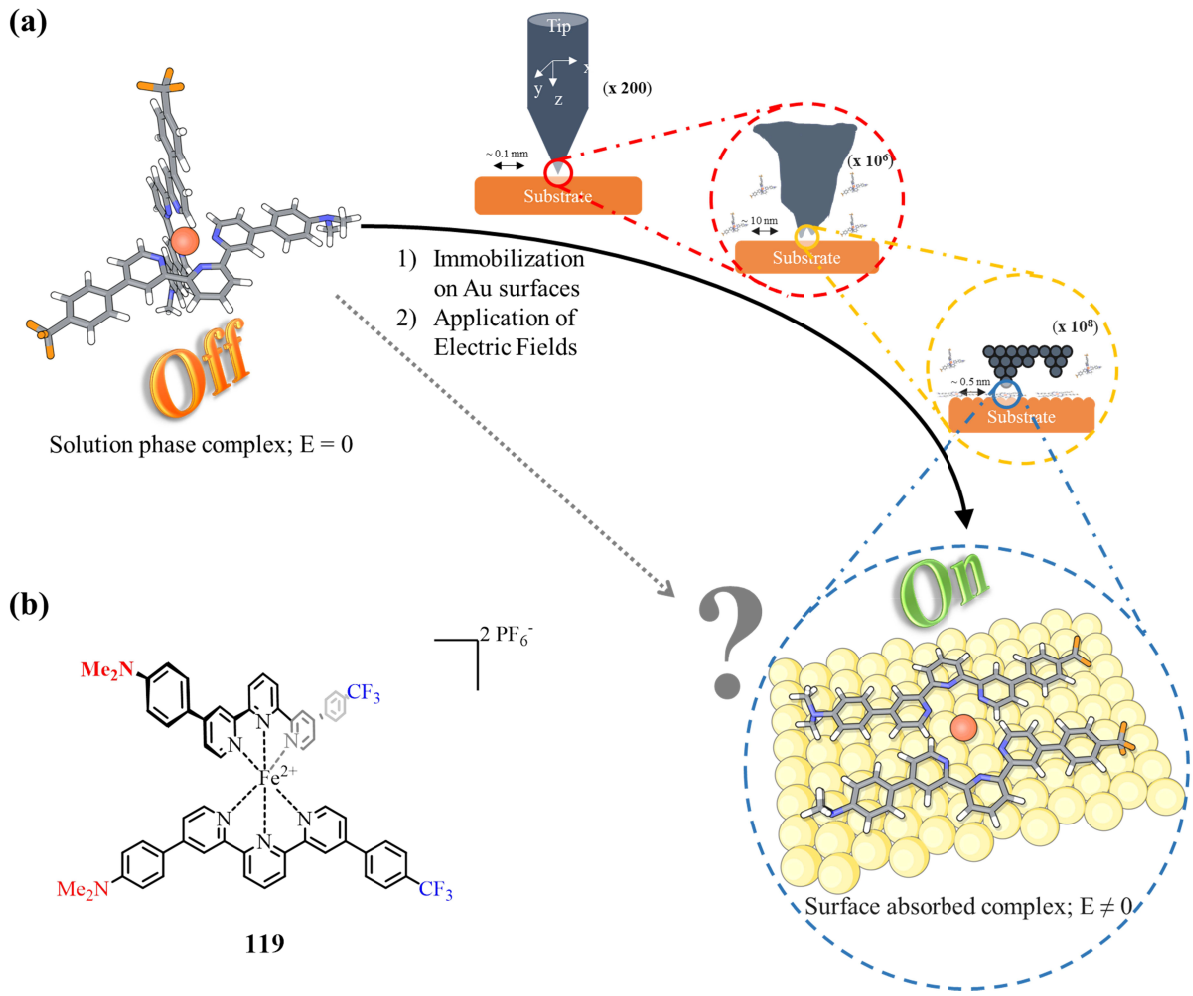

Figure 76: (a) Schematic step-by-step illustration of the envisaged outcome of the surface immobilization of the homoleptic, dipolar Fe(II)-bis(tpy) target complex **119** onto an Au(111) surface and the postulated effect of the application of bias impulses of varying strengths in the range of the performed STM experiments onto the molecular geometry and hence onto the core ion's spin state of target complex **119**. **(b)** Chemical structure of the electrically addressable target complex **119**.

In detail the STM experiments were performed at liquid Helium temperature (~4 K) under UHV conditions. For the immobilization of the target complex **119** onto the metal surface the compound was dissolved in MeCN prior to its deposition onto the Au(111) surface via an ESI setup[549] allowing the spray deposition of appropriate substances onto STM surfaces. The number of molecules actually applied to the Au(111) surface was herein, controlled by means of a mass-selected ion flow, whereat the chemical integrity of the molecules hitting the surface was previously confirmed via an interposed MS device.

To give an first overview of the deposited structures, Figure 77 displays a constant current STM image after a deposition lasting for 45min, using an impact energy of 2.5±1 eV with an ion current of ~50 pA. The Au(111) surface exhibits a reconstruction of alternating face-centered cubic (fcc) and hexagonal close packed (hcp) regions separated by

discommensuration lines with a vertical displacement of ~0.2 Å. A periodic bending of these lines by ±120° creates a zig-zag pattern, which in literature is referred to as herringbone reconstruction.[550,551] The observed adsorbates are distributed on both regions of the Au(111) surface, hereby, mainly being aggregated into small clusters.

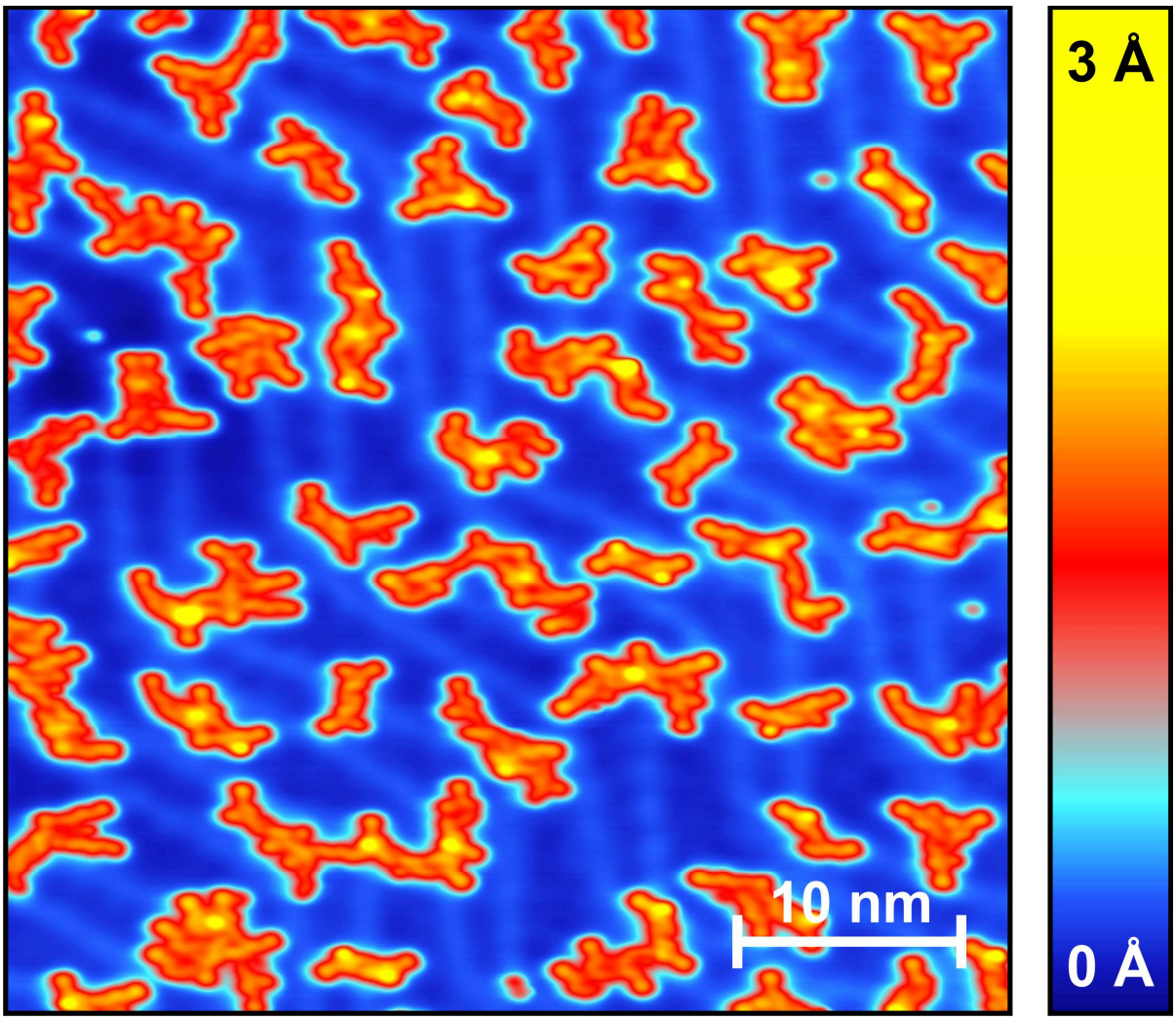

Figure 77: Typical constant current STM image (50 mV, 50 pA) of the homoleptic, dipolar Fe(II)-bis(tpy) target complex **119** deposited on an Au(111) surface. The submonolayer coverage was prepared by UHV electrospray deposition. Although most of the molecules are broken into the according tpy ligands, also intact complexes can be found.

The observed adsorbates can be classified into three general species, namely, either a single isolated tpy ligand (**red**), a tpy ligand with an attached Fe(II) ion (**cyan**), or the actual homoleptic, dipolar Fe(II)-based target complex **119** containing two identical ligands attached to the central Fe(II) ion (**black**) (Figure 78).

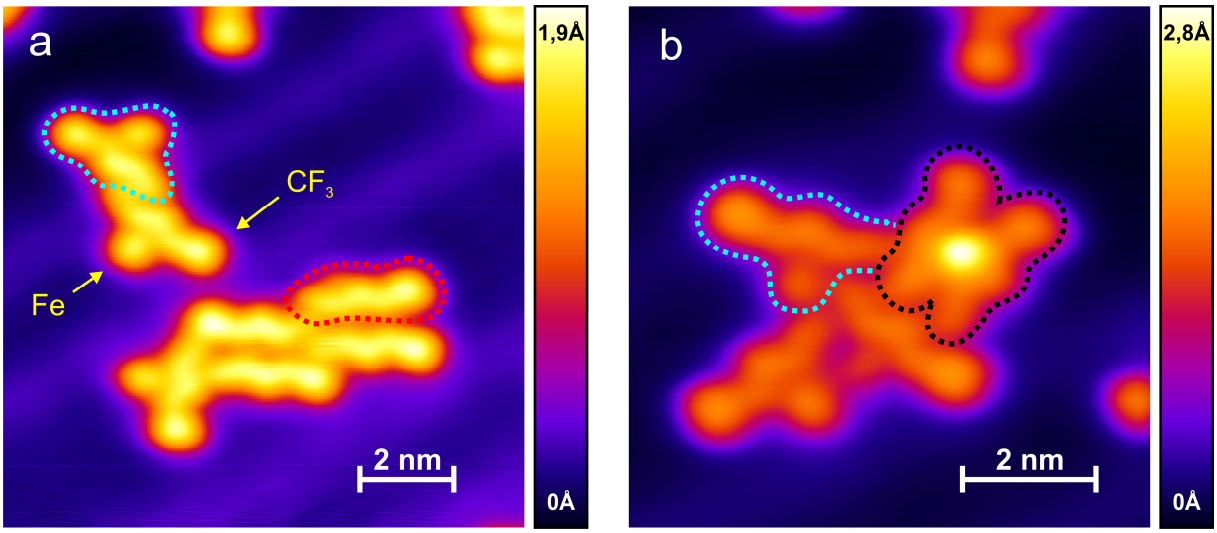

Figure 78: Constant current STM images (-100 mV, 100 pA) of **(a)** tpy ligands with (**cyan**) and without a coordinated Fe(II) ion (**red**) and **(b)** a complete homoleptic, dipolar Fe(II)-bis(tpy) complex (**black**) and three single tpy ligands with coordinated to an Fe(II) ion (**cyan**).

The tpy ligands, no matter in which species they are contemplated, exhibit a length of ~3 nm and a height of ~1.5 Å. In addition, the tpy ligands throughout show an asymmetric shape with a protrusion on one end of the ligand, which can be attributed to the respective CF_3-group, being located exclusively at one end of the tpy ligand. Furthermore, in contrast to its coordinated analogues, the free tpy ligand can be found in three different conformations (Figure 79e – types 3-5), due to the rotation around the bonds between neighboring aryl rings.

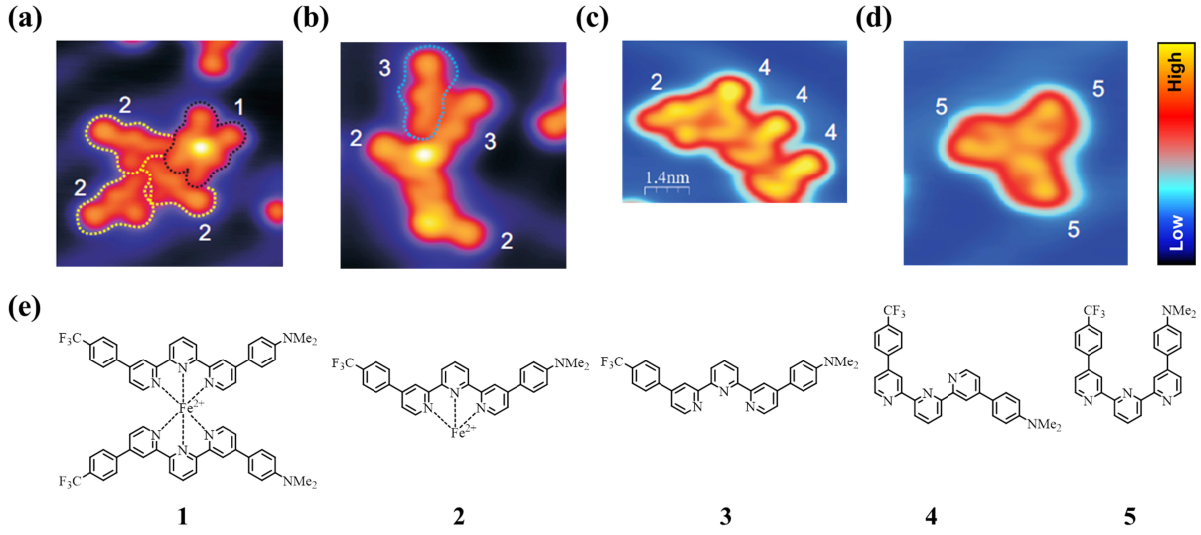

Figure 79: Illustration of the three applicable conformations observed for surface-immobilized free tpy ligand **147** in comparison to the corresponding Fe(II)-mono- and the Fe(II)-bis(tpy) motifs. **(a) – (d)** Constant current STM images displaying the five different types of fragments observed. **(e)** Chemical structural representations of the five different fragments observed.

Among all the surface-absorbed species less than 1% actually represents the shape of the intact homoleptic, dipolar Fe(II)-based target complex **119**. Within the observed structures both ligands are absorbed parallel onto the surface, herein, being coordinated to the same Fe(II) ion. In contrast to the regular octahedral geometry Fe(II)-bis(tpy) complexes usually exhibit, which is coinciding with their LS state, the structures found during the present STM investigations feature an interplanar angle of the two incorporated tpy ligands of 0° being equivalent to a completely planar complex' geometry. The reason for this finding is deduced to the known affinity of the heteroaromatic π-electrons to metal substrates. The apparent height of the Fe(II) ion of such an intact complex **119** within the corresponding constant current STM image (Figure 80) is up to 1 Å higher than the according height of an Fe(II) ion attached to only one tpy unit. Furthermore, the structure displayed below exhibits a significant asymmetry, which can be attributed to the fact that the more electron-rich CF_3-groups are found on the same side of the complex, namely, on the left in the picture shown in Figure 80.

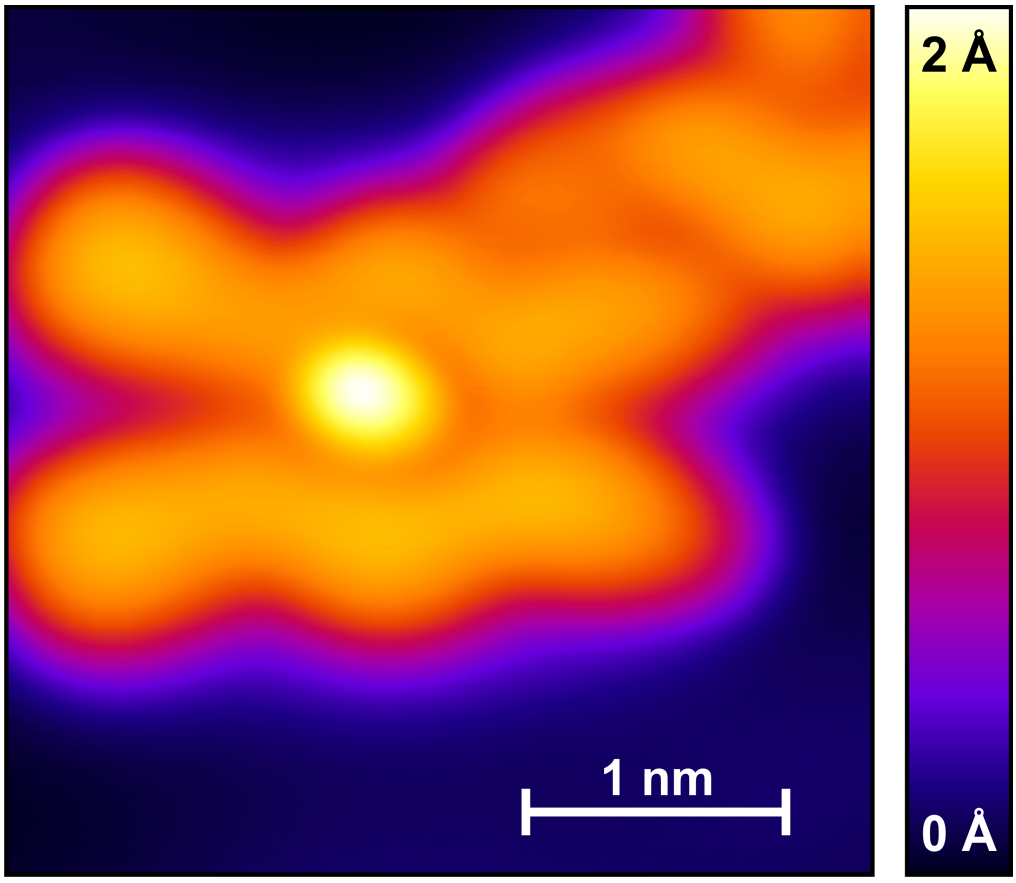

Figure 80: Constant current STM image (10 mV, 15 pA) of an intact surface-deposited Fe(II)-bis(tpy) complex **119** on an Au(111) surface, exhibiting a completely planar geometry instead of the regular octahedral environment of the Fe(II) core ion. The ligands exhibit a strong asymmetry probably arising from the fact that the more electron-rich CF_3-groups within each of the tpy units, can be found on the same side of the complex, namely, on the left in the present picture shown above.

To further evaluate the structural and magnetic properties of the surface-immobilized, planar dipolar Fe(II)-based target complexes **119**, these were subdued to spectroscopic measurements, such as the recording of spectra displaying the differential conductance d*I*/d*V* as a function of the sample voltage. Since the d*I*/d*V* signal behaves proportional to the density of states of the investigated sample, it is possible to draw conclusions about the relative positions of the HOMO and the LUMO. Hereby, the application of negative potentials gives information about the occupied states, whereas by the application of positive voltages conclusions can be drawn about the unoccupied states of the investigated molecules. In order to obtain information about the core ion's spin state and a potential Kondo signature a small bias ramp was applied, with small voltages (-100 mV - +100 mV) instead of the usually ramped bigger voltage ranges (e.g. from -1 V - +1 V). In this fashion a higher resolution can be obtained around the level of the Fermi energy E_F. The Hereby, obtained spectra of the central Fe(II) ion revealed a narrow antiresonance at the Fermi level (Figure 81). The observed feature showed consistency with the typical Fano line shape,[552] due to the Kondo effect and hence indicates the presence of unpaired electrons.

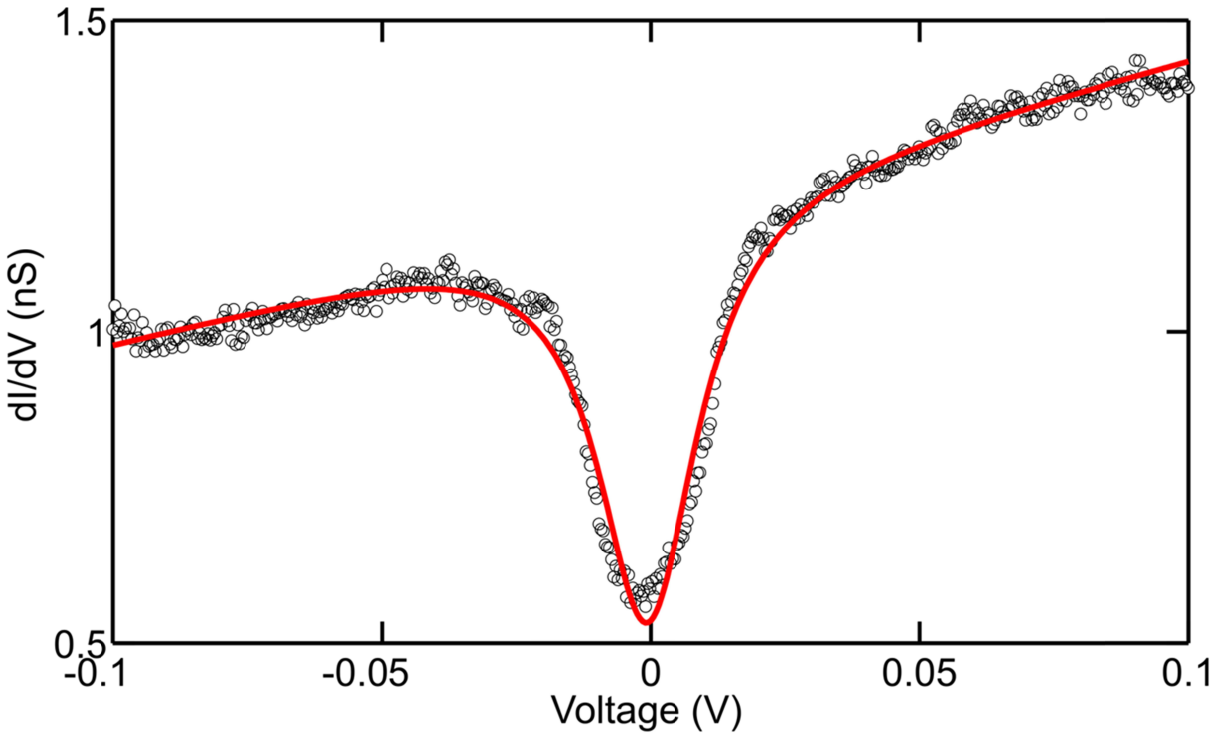

Figure 81: Spectra of the differential conductance (d*I*/d*V*) recorded above an Fe(II) ion of an intact homoleptic, dipolar Fe(II)-bis(tpy) complex **119**. The black dots represent the experimental data, whereas the solid red line indicates a Fano line shape fit to the obtained data corresponding to the observation of a distinct Kondo resonance. The displayed Fano fit yields a Kondo temperature of $T_K \sim 131$ K and an asymmetry of $q \sim 0.01$. For the mono-tpy Fe(II) species no such Kondo resonance features could be found.

The Fano fit (red line) shown in Figure 81 above, yields a Kondo temperature $T_K \sim 131$ K and an asymmetry of $q \sim 0.01$. Correspondingly, the HS state of other SCO molecules has been previously addressed using Kondo resonances.[553]Furthermore, the fact that the resonance is not observed for the Fe(II) ions of the mono-tpy complexes (Figure 79 – Type 2), further underlines the obtained results and substantiates the hypothesis, that the planar, surface-deposited Fe(II)-bis(tpy) complexes **119** are present in their HS state, in contrast to their octahedral, LS configuration in solution.

3.5 Conclusion and Outlook

First of all, the assembly routes of the target compounds of both herein, described projects are based on the very same modularly applicable key building block **47**. Throughout the present projects a completely novel synthetic approach was followed in order to allow the assembly of the required 4,4´´-disubstitution pattern at the tpy core moiety. The herein, described high-yielding synthesis, for the first time, utilizes a Suzuki-Miyaura cross-coupling protocol for the assembly of the tpy core and was furthermore, shown to be readily adaptable to other substituents in the 4,4´´-positions of the tpy unit.[415] The further functionalization of the described tpy core synthon **47** readily allowed the synthesis of the various desired target structures of the herein, described first two main projects of the present thesis.

In the range of the first project a new single molecule switching concept relying on the coordination sphere dependent spin state of hexa-coordinate Fe(II)-bis(tpy) complexes is presented. While one tpy ligand fixes the molecule inside the junction and guarantees electronic transport through the central metal ion, due to the tailor-made 4,4´´-disubstitution pattern at the tpy core, the second tpy ligand exhibits electron-donating and electron-withdrawing substituents resulting in an intrinsic dipole moment due to an overall asymmetric electron distribution. This leads to an interaction of the named push/pull ligand with the applied electric field inside the MCBJ. This electrostatic alignment of the dipolar ligand along the applied electric field results in a distortion of the complexes' originally octahedral coordination sphere. As a consequence an alteration of the relative energy of the complexes' frontier orbitals and hence of their electron populations can be observed, commonly known as SCO. Several heteroleptic Fe(II)-based target complexes as well as a Ru(II)-based reference complex have been synthesized to investigate the envisaged phenomenon gradually and in

more details. Extensive single molecule transport studies utilizing the MCBJ technique in UHV at liquid helium temperature revealed, after comprehensive statistical analyses, that the voltage dependent bistability correlates with the extent of the intrinsic dipole moments exhibited by the accordant Fe(II)-bis(tpy) complexes. Furthermore, the simulative inspection of individual junctions strongly supports the envisaged and postulated switching mechanism. On top of that, upon the variation of the electrode's spacing, constant and reproducible switching thresholds, together with the expected electric-field dependence of the investigated switching events, could be revealed.

Additionally, very promising and reproducible preliminary results have been obtained from the MCBJ experiments on the dipolar Fe(II)-based complex **118**, containing an extended molecular backbone as anchoring unit. Since the experiments for all investigated bistable junctions of complex **118** without exception reveal a switching from low conductance values (LS state) at low bias to high conductance values (HS state) at high bias, it seems very promising to further follow the route of using elongated anchoring tpy units for the herein, described systems. Therefore, by establishing a broader statistical basis for the named preliminary results of complex **118**, as well as by the investigation of accordant reference compounds, e.g. via the variation of the complexes' intrinsic dipole moments or the incorporated central metal ion, highly promising results can be expected from the present systems in the future. Nevertheless, the severely reduced junction formation probability of the elongated structure **118**, which is only around 1%, represents a significant drawback arising from the incorporation of the acetylene bridges, which needs to be further evaluated and overcome in the future.

Finally, in the range of the second project the coordination sphere dependent spin state switching of hexa-coordinate Fe(II)-bis(tpy) complexes was investigated. For this purpose the homoleptic, dipolar Fe(II)-bis(tpy) complex **119** was deposited onto an Au(111) surface via electron-spraying. The somehow surprising and successful results revealed, that those complexes remaining intact are immobilized to the Au(111) surface in a completely planar fashion. Consequentially, for these surface-deposited Fe(II)-bis(tpy) complexes distinct Kondo resonances were observed, which can be perfectly matched with the corresponding HS state of the Fe(II) core ion in these planarized systems. However, since the investigated complexes reside in the planar configuration right from the start upon their surface deposition, an actual switching process from the octahedral, LS form to the planar HS form of the complexes could not be achieved so far. Nevertheless, there are plenty of possible approaches

to tackle this problem. For example experiments trying to deposit complex **119** on a Cu_2N/Cu(100) surface, in order to decouple the deposited complexes from the metal surface via a small insulating layer, are under investigation at the moment. Also the implementation of an insulating interlayer, such as NaCl on an Au(111) surface represents an Feasible approach to circumvent the described issues. Furthermore, an alteration of the ligand system in the fashion of introducing geometrical limitations to the tpy ligand in order to prevent a complete planarization of the complex upon surface immobilization seems to be a thinkable alternative. In the end it will be decisive to find a suitable molecule as well as the appropriate deposition conditions in order to allow a successful immobilization of the according complex to the surface in its octahedral LS form, before exposing it to the external voltage trigger leading to the distortion of the coordination sphere up to the HS state's geometry.

4 Mechanically-Triggered Single Molecular Spin Switches

The present chapter covers the third main project and objective of this doctoral work:

(1) Design, synthesis and physical investigation of a mechanically triggerable single molecular spin switching system that is to be immobilized and studied using the mechanically controllable break junction (MCBJ) technique.

Hereby, the molecular design and switching concept (Chapter 4.1), the chosen synthetic approaches (Chapters 4.2 and 4.3), and the physical characterizations (Chapter 4.4) arising from the project, represent the core of the present chapter and are treated in a step-by-step fashion. Finally a comparative conclusion will be drawn, which relates the physical results obtained for the present project to the results obtained for the previous projects, namely, the investigation of electrical-field driven single molecular spin switching systems, presented in chapter 3.

4.1 Switching Concept and Molecular Design

Following the relevant constraints discussed for the previous project (Chapter 3.1) first of all a molecular subunit exhibiting an externally addressable spin state represents the utmost important requirement to actually allow the development a mechanically addressable single molecular spin switch. As for the voltage-driven single molecular spin switches discussed above (Chapter 3), from the limited number of transition metals (Fe, Co, and Ni) that actually feature such an externally addressable spin state, either high-spin (HS) or low-spin (LS), the choice fell onto complexes based on hexa-coordinate Fe(II) ions as the core subunit of the envisaged target structures. As stated before the main factors that turned the balance towards Fe(II) complexes as the envisaged target structures are their facilitated synthetic accessibility, if compared e.g. to tetra-coordinate Ni(II) complexes, as well as their simplified analytical characterization via nuclear magnetic resonance (NMR) techniques, if compared to Co(II) complexes, which exhibit paramagnetic behavior already in the LS state.

Going along with the previous project, Fe(II)-bis(terpyridine) complexes, comprising Fe(II) ions as the spin crossover (SCO) system, were envisaged. Herein, the six coordination

sites of the Fe(II) species are arranged in an octahedral fashion around the metal core ion. Hence the accommodation of the six present 3d electrons of the Fe(II) ions into the five spin degenerate levels allows the system to be found in the two different desired spin states, namely, the LS and the HS state. Whereas in the LS state the crystal field interaction is strong enough to pair up all the electrons resulting in a zero net spin (S = 0), a reduction of the crystal field interaction, e.g. by increasing the metal-ligand distance, can result therein, that the HS state, exhibiting a maximized total net spin of (S = 2), can become energetically more favorable resulting in the envisaged LS → HS spin switching phenomenon. In order to, first of all, allow the integration of the desired target structures into the appropriate physical setups, in this case into an MCBJ setup, and to furthermore, ensure the external mechanical addressability of the core ion's spin state, the choice fell onto homoleptic Fe(II)-bis(terpyridine) complexes, which contain two identical terpyridine (tpy) ligands in order to fulfil the envisaged function. Taking the molecular design of the voltage-driven single molecular spin switches into account, in which the immobilization of the respective target structures onto the gold surfaces within the MCBJ setup is enabled via the use of thiol-terminated tpy ligands (**131** and **146**), the same type of anchoring group was envisaged for the present project. However, in order to maintain a mechanical addressability of the desired target structure, each individual tpy ligand was destined to bear only a single anchoring group. This lead to the target complex' **208** molecular structure displayed in Figure 82.

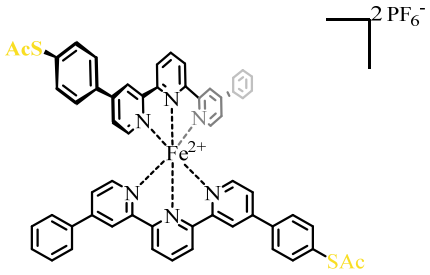

208

Figure 82: Chemical structure of the envisaged, mechanically addressable homoleptic Fe(II)-bis(tpy) target complex **208** permitting the spin switching of the Fe(II) core ion upon the geometrical distortion of the core ion's coordinative environment.

Consequently, the coordination environment of the envisaged mechanically triggerable single molecular spin switch was postulated to be externally alterable, therefore resulting in the desired addressability of the Fe(II) core ion's spin state (Figure 83). This addressability of the metal ion's spin state should be brought about upon a gradual variation of the distance between the two nanoelectrodes of the MCBJ to which the target complex is attached.

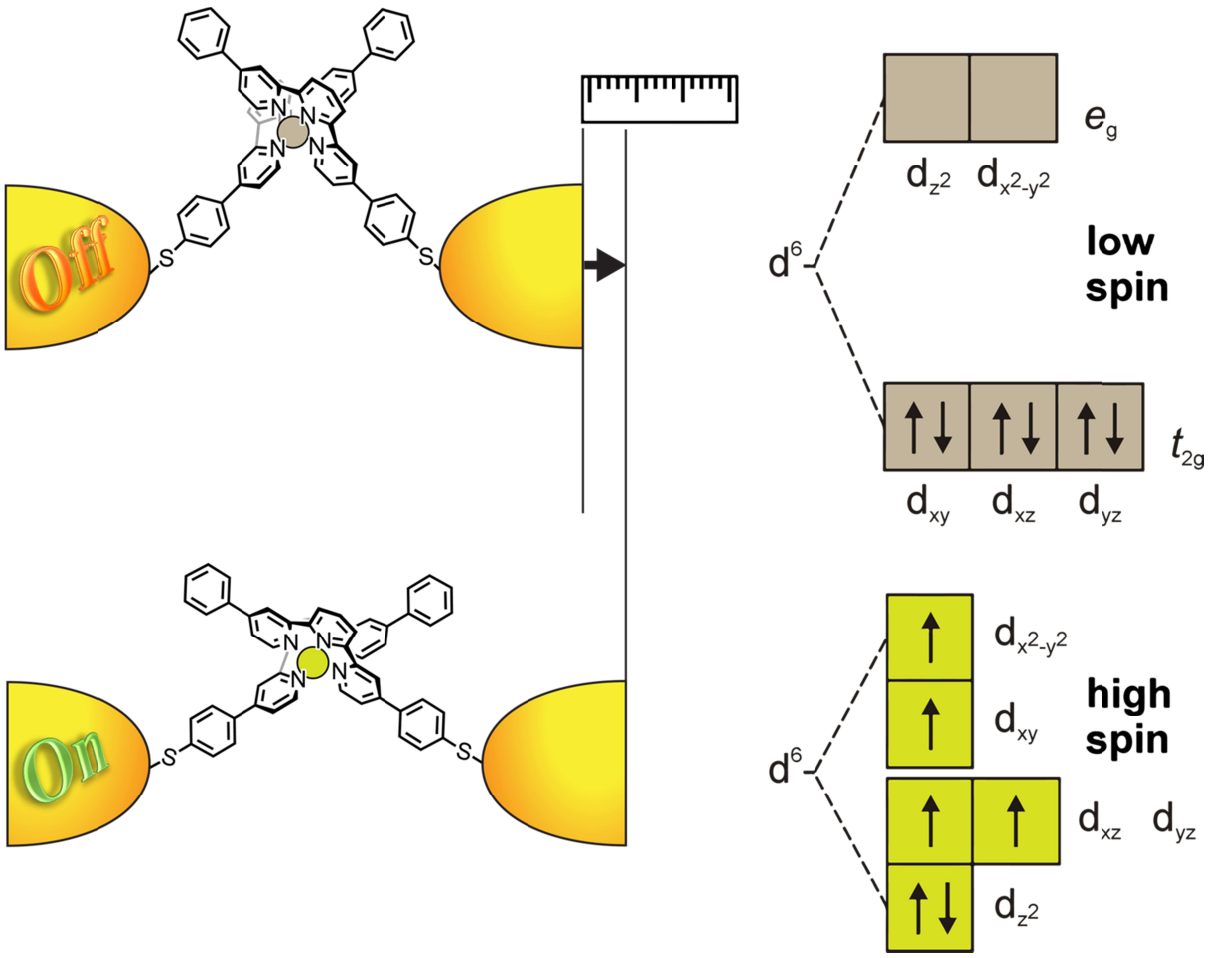

Figure 83: Schematic illustration of the postulated switching concept for the envisaged homoleptic Fe(II)-bis(tpy) complex **208**. The two states, namely, the *OFF*-state (LS), and the *ON*-state (HS) illustrate the desired effect of a mechanical elongation of the immobilized target structure **208** upon an increase of the inter-electrode distance within the MCBJ. The invoked geometrical distortion of the originally octahedral coordinated target structure (*OFF*-state, LS), should eventually result in a switching of the core ion's spin state (LS → HS) upon sufficient externally applied mechanical stimulus.

Summarizing, the addressability of the target complex **208** towards an externally applied mechanical stimulus, as the basis for the envisaged LS → HS spin switching process, conceptually originates from a cascade of different effects (for theoretical details on SCO, see chapter 1.1.4.1, particularly Figure 20), namely:

(1) The alteration of the inter-electrode distance, when a target molecule is immobilized into the MCBJ setup results in a spatial distortion of the former octahedral coordination environment of the Fe(II) LS complex **208**.

(2) Going along with this geometrical distortion, the Fe-N bonds in the immobilized target structures are elongated, to compensate for the increasing steric repulsion between the two outer pyridine rings of the tpy ligands, respectively.

(3) This elongation of the Fe-N bonds leads to a weakening of the ligand field (LF) strength Δ, which is equivalent to a reduced crystal field splitting between the lower energetic t_{2g} orbitals and the higher energetic e_g orbitals.

(4) As long as the LF splitting energy Δ is bigger than the mean spin pairing energy P the system remains in the LS state with all electrons being paired up. However, as soon as P is no longer overcompensated by Δ, according to Hund's rule, the electrons will also populate the e_g orbitals resulting in the formation of the HS species.

Finally, a suitable reference compound had to be designed, in order to allow a decent line of argument concerning the results discussed in subsequent chapters. Hence, the homoleptic Ru(II)-bis(tpy) complex **209** (Figure 84) was envisaged, which bears an identical ligand environment as the analogue Fe(II)-based complex **208**. In contrast to this, however, the Ru(II) complex **209** should not be able to exhibit any SCO at all, due to the nature of the core ion itself.

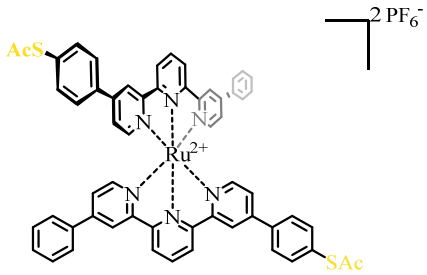

209

Figure 84: Molecular design of the envisaged homoleptic Ru(II)-bis(tpy) complex **209**, as a reference compound, which should not be able to undergo any SCO at all, due to the core ion's nature, although it bears the identical ligand environment, as the desired mechanically addressable homoleptic Fe(II)-bis(tpy) target complex **208**.

4.2 Synthetic Strategy

Within this chapter the synthetic strategy towards the assembly of the envisaged mechanically triggerable, single molecular spin switching, homoleptic Fe(II)-bis(tpy) target complex **208**, and its analogue Ru(II)-based reference complex **209**, is discussed (Scheme 37).

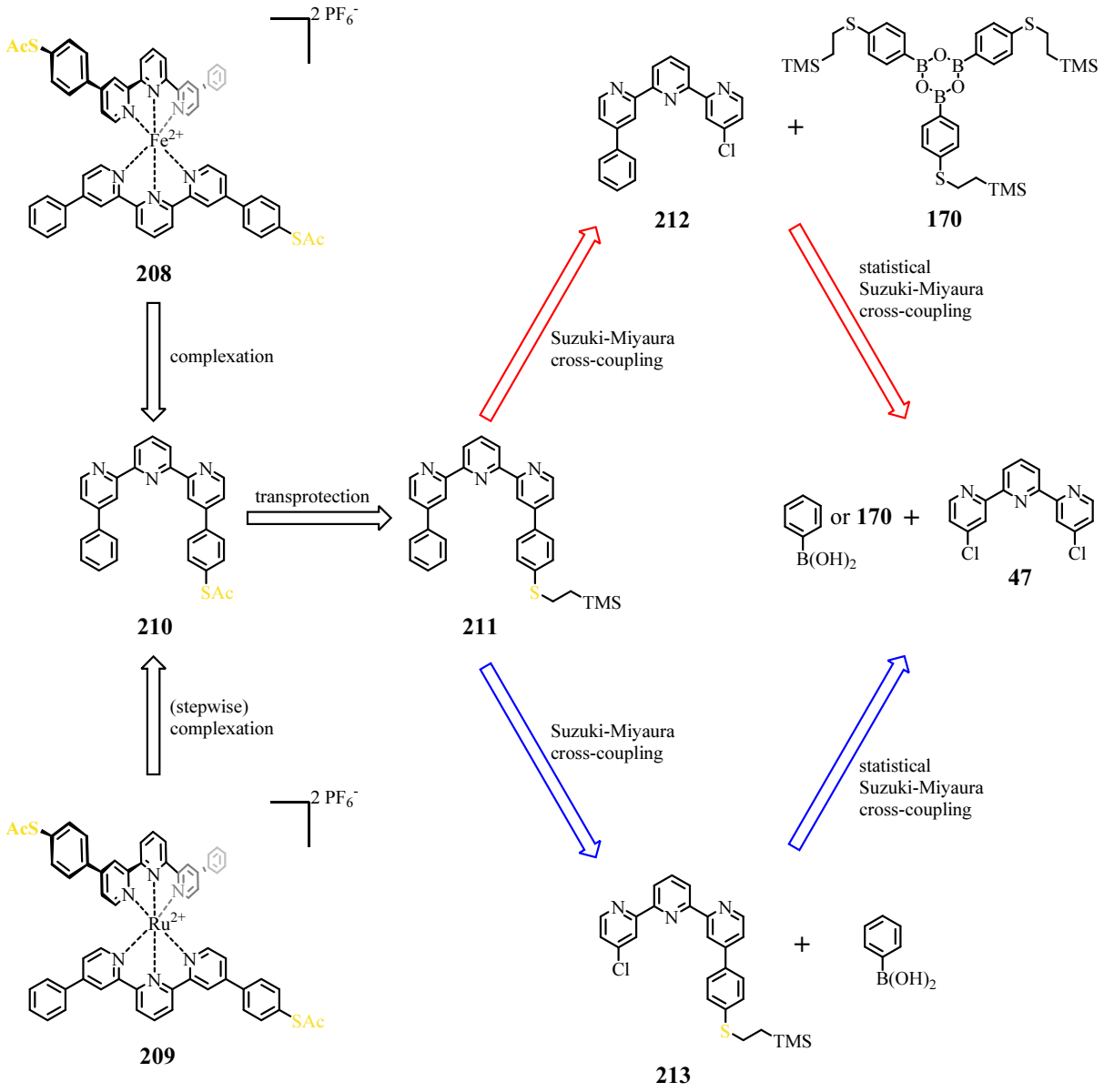

Scheme 37: Retrosynthetic analysis of the homoleptic, mechanically triggerable, single molecular spin switching Fe(II)-bis(tpy) target complex **208**, and its analogue Ru(II)-based reference complex **209**. The two alternative reaction pathways are highlighted in color code (red and blue reaction pathway).

Retrosynthetically, the homoleptic Fe(II)-bis(tpy) target complex **208** and the homoleptic Ru(II)-bis(tpy) reference complex **209** are accessible via the corresponding complexation reactions from the very same, one-sided thioacetyl-terminated asymmetric tpy ligand **210**.

These complexations should proceed in one step for the assembly of the Fe(II) complex **208** or Alternatively, in one or two steps, respectively, for the assembly of the Ru(II) complex **209**. Tpy ligand **210** can be obtained via the transprotection of the ethyl-TMS protected thiolated tpy derivative **211**. This asymmetrically, disubstituted tpy ligand **211** can be accessed by following two different routes (red and blue pathway) involving differently ordered sequences of Suzuki-Miyaura cross-coupling reactions. Following the red reaction pathway, the asymmetric key tpy ligand **211** is obtained via Suzuki coupling of the monofunctionalized tpy derivative **212** and the borylation agent **170**, whereas on the blue reaction pathway **211** is obtained via the Suzuki coupling reaction of the monofunctionalized tpy derivative **213** and phenylboronic acid. Accordingly the two tpy derivatives **212** and **213** are accessible via the precedent Suzuki-Miyaura cross-coupling reactions of the core tpy building block **47** with the corresponding borylation agents **170** or phenylboronic acid, respectively. Since the synthetic strategy for the assembly of the modularly applicable core tpy subunit **47** has been described in detailed form in the corresponding chapter 3.2.1 of the previous project, its accessibility is taken for granted in the given context.

4.3 Synthesis

Hereafter, the synthesis of the different target structures associated with the development of a mechanically addressable single molecular spin switching system is described. Since the synthetic pathways during this whole doctoral work have been designed such, that they are likewise based on the same highly versatile and modularly applicable core building block **47**, whose synthesis has been described earlier in chapter 3.3.1, all the synthetic procedures discussed within this chapter, focus on the later part of the synthetic routes starting from the named key subunit **47**.

4.3.1 Assembly of One-Sided Anchoring Terpyridine Ligand 210

In the present section the synthesis of the peripherally extended 4,4´´-disubstituted asymmetric tpy ligand **210** is described. Hereby, the red reaction pathway (Scheme 37) was followed, starting with a Suzuki-Miyaura cross coupling reaction of the tpy key building

block **47** with phenylboronic acid. In contrast to the one-step formation of symmetrically 4,4´´-disubstituted tpy derivatives, the synthesis of asymmetric tpys inevitably requires a two-step procedure including a statistical introduction of the first 4-substituted phenyl substituent in the precedent coupling step (Scheme 38).

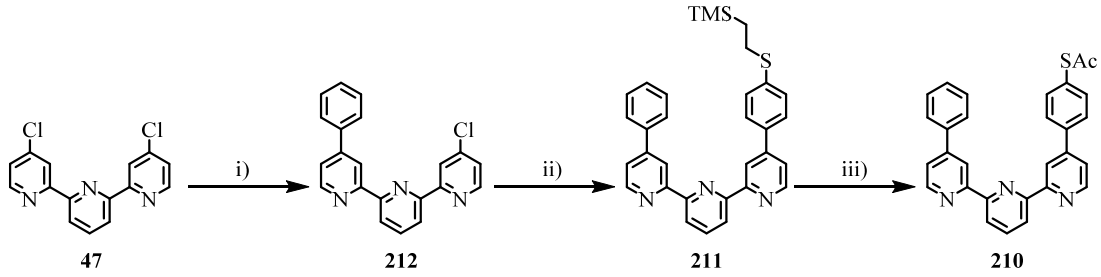

Scheme 38: Synthesis of the asymmetric, peripherally extended 4,4´´-disubstituted tpy **210** in three steps starting from the key tpy core building block **47**, involving a statistical Suzuki-Miyaura coupling at first place. Reagents and conditions: **i) 47** (1 eq.), phenylboronic acid (0.8 eq.), $PdCl_2[P^tBu_2(p\text{-}NMe_2\text{-}Ph)]_2$, K_2CO_3, toluene/H_2O (5:1), 110 °C, 36h, 44% (+ 18% of **172** and 38% of **47**); **ii) 212** (1 eq.), 2,4,6-Tris(4-(2-(trimethylsilyl)ethyl)thiophenyl)-1,3,5,2,4,6-trioxatri-borinane (**170**) (2 eq.), $PdCl_2[P^tBu_2(p\text{-}NMe_2\text{-}Ph)]_2$, K_2CO_3, toluene/H_2O (5:1), reflux, 72h, quant.; **iii) 211** (1 eq.), TBAF (12.5 eq.), THF, AcCl (250 eq.), r.t. to -10 °C, 4.5h, 90%.

In detail, as described earlier, for these kinds of statistical reactions usually product mixture ratios of 1:2:1, representing the ratios of starting material **47** to the desired monofunctionalized tpys and the unwanted disubstituted tpys, have to be expected. However, for the present synthesis of monofunctionalized tpy derivative **212** from the tpy core motif **47**, and phenylboronic acid, it was found, that by the use of substoichiometric amounts of the borylation agent the obtained product ratio could be favorably altered. In that way the described cross-coupling reaction yielded 44% of the desired 4´-monofunctionalized tpy **212**, together with 18% of the 4,4´´-disubstituted tpy side product **172**, in addition to 38% of reisolated starting material **47**, by applying otherwise comparable reaction parameters as described in the previous chapters, using ($PdCl_2[P^tBu_2(p\text{-}NMe_2\text{-}Ph)]_2$) as the catalyst and K_2CO_3 as the base in a solvent mixture of toluene and water. From the subsequent Suzuki-Miyaura cross-coupling reaction of the 4´-monofunctionalized tpy **212** with an excess of the borylation agent **170** in a degassed toluene/water mixture (5:1) together with ($PdCl_2[P^tBu_2(p\text{-}NMe_2\text{-}Ph)]_2$) as the catalyst and K_2CO_3 as the base, the desired asymmetric 4,4´´-disubstituted product **211** was isolated quantitatively after aqueous work-up and FCC. As described above the borylation agent **170** was previously prepared in two steps starting from 4-bromothiophenol (**150**) via the ethyl-TMS protected thiol intermediate **169**. The desired acetyl protected tpy derivative **210** was now obtained by transprotection of **211**. This

transprotection was accomplished by treating **211** with 12.5 eq. TBAF in degassed THF at r.t. and subsequent cooling to -10 °C followed by the addition of an excess of acetyl chloride. As for the synthesis of the symmetric tpy anchoring ligand **131** the rigorous exclusion of oxygen turned out to be of utmost importance in order to avoid the impending disulfide formation of the intermediary formed deprotected thiophenolic tpy. Careful aqueous work-up considering the base lability of the acetyl group followed by FCC provided the poorly soluble acetyl protected ligand **210** in a very good yield of 90%.

4.3.2 Complexation of One-Sided Anchoring Terpyridine Ligand

Hereafter, the assembly of the desired homoleptic Fe(II)-bis(tpy) complex **208** as the envisaged mechanically addressable, single molecular spin switching system is described. In addition the assembly of the analogue Ru(II)-based complex **209** as the corresponding suitable reference compound is discussed.

4.3.2.1 Assembly of Homoleptic, Asymmetric Fe(II)-bis(tpy) Complex 208

Following the procedures described in chapter 3.3.3 the homoleptic Fe(II)-bis(tpy) complex **208** was prepared via the one-step complexation of $FeCl_2$ (1 eq.) and the accordant tpy ligand **210** (2 eq.) in mixture of MeOH, DCM, and water (**Scheme 39**). After anion exchange from Cl^- to PF_6^- using NH_4PF_6 (50 eq.), followed by excessive washing with water, drying and filtration the desired product **208** was quantitatively isolated as a dark purple solid.

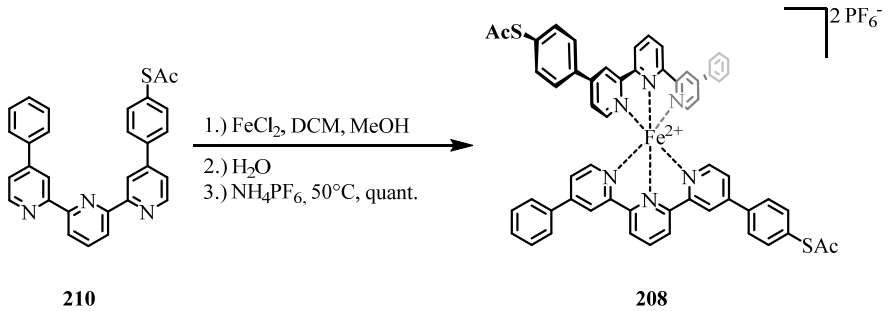

210 **208**

Scheme 39: Assembly of the desired homoleptic, asymmetric Fe(II)-bis(tpy) complex **208**.

4.3.2.2 Assembly of Homoleptic, Asymmetric Ru(II)-bis(tpy) Complex 209

The desired homoleptic Ru(II)-bis(tpy) complex **209** was prepared by following a literature-inspired[539–542] adaptation of the previously described single-step complexation method utilized for Fe(II)-bis(tpy) complex **208**. However, also in this procedure the intermediately formed mono-tpy-Ru(III)Cl_3-complex **214** was not isolated but directly converted into the desired target compound **209** in the following step in a modified one-pot strategy (Scheme 40).

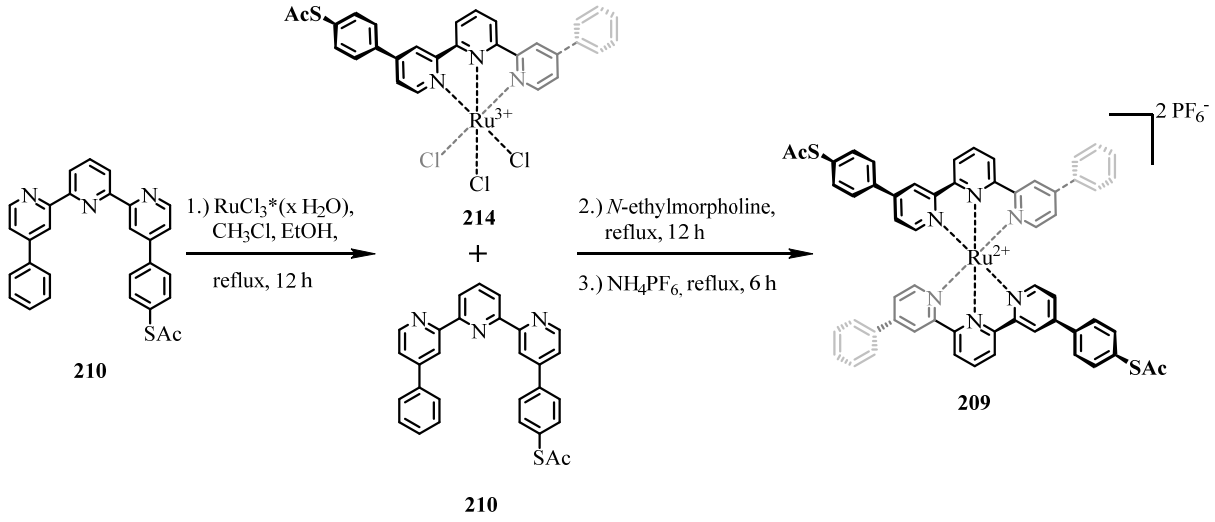

Scheme 40: Assembly of the desired homoleptic, asymmetric Ru(II)-bis(tpy) reference complex **209** in a one-pot procedure proceeding via the intermediary formed mono-tpy-Ru(III)Cl_3 complex **214**.

In detail $RuCl_3$ (1 eq.) and the asymmetric tpy ligand **210** (2 eq.) were refluxed in a mixture of EtOH and $CHCl_3$ to form the intermediate mono-tpy-Ru(III)Cl_3-complex **214**. By the addition of *N*-ethylmorpholine (50 eq.) as the reductant, the intermediate **214** was directly reduced to the corresponding Ru(II) species in situ, thus facilitating the addition of the second equivalent of **210** to the mono-tpy complex intermediate. Subsequent anion exchange from Cl^- to PF_6^- using NH_4PF_6 (50 eq.), followed by excessive washing with water, drying and filtration yielded the crude product of **209**, which still contained unreduced Ru(III) species and unreacted ligand **210**. Therefore the desired homoleptic Ru(II)-bis(tpy) reference complex **209** was obtained by purification of the crude mixture via preparative reversed-phase HPLC yielding the product **209** as a deep red solid in a yield of 18%.

4.4 Physical Characterization

Following the discussion of the synthetic access of the desired homoleptic, asymmetric Fe(II)-bis(tpy) target complex **208**, representing the envisaged mechanically addressable single molecular spin switch, as well as of the Ru(II) based reference complex **209 hereafter**, the corresponding physical results are highlighted, whereat the discussion of the optical properties is followed by a detailed description of the performed MCBJ experiments.

4.4.1 Optical Investigations

As for the optical spectra discussed in chapter 3.4.2 the UV/vis spectra of the homoleptic Fe(II)-based target complex **208** and of the Ru(II)-based reference compound **209** were recorded at several concentrations (0.001 mM, 0.005 mM, 0.01 mM, 0.025 mM, and 0.05 mM, respectively) in acetonitrile at room temperature (r.t.) and their averaged absorbances were converted into the corresponding extinction coefficients ε which are plotted against the respective wavelengths λ (Figure 85 and Table 7).

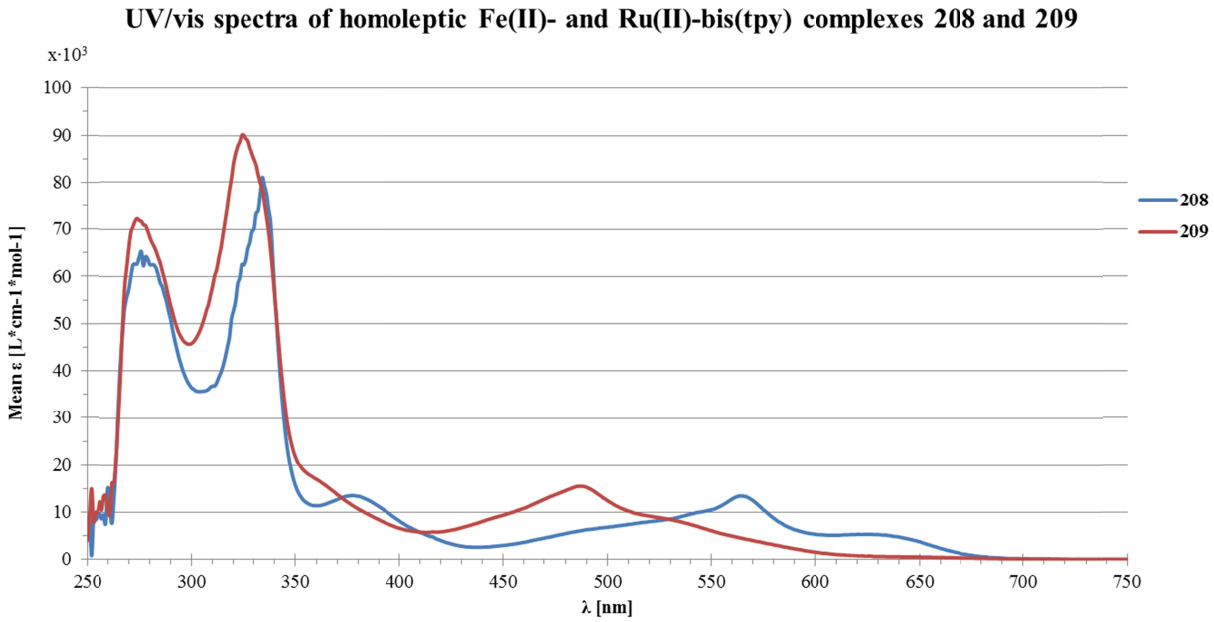

Figure 85: Comparative illustration of the UV/vis absorption spectra of the homoleptic Fe(II)-bis(tpy) target complex **208** and of the corresponding Ru(II)-bis(tpy) reference complex **209**.

Table 7: Characteristic bands in the UV/vis spectra of the homoleptic, dipolar Fe(II)-bis(tpy) target complex **208** and of the corresponding Ru(II)-bis(tpy) reference complex **209**.

Complex	λ_{max} (LC/MC) [nm]	ε [L*cm^{-1}*mol^{-1}]	λ_{max}(MLCT) [nm]	ε [L*cm^{-1}*mol^{-1}]
188[544]	318	38 000	552	11 900
208	276	65 390	565	13 500
	334	80 930	626	5 365
	377	13 605		
207[546]	270	43 652	475	16 596
	308	70 795		
209	274	72 350	487	15 550
	325	90 100		

Analogously to the findings discussed previously (confer Chapter 3.4.2) rather distinct bathochromic shifts of the MLCT-bands could be observed in the optical spectra of the target complexes **208** and **209**. According to the earlier described postulations these can be deduced from the stabilization of the ligand-based LUMO π*-orbitals for the described enlarged conjugated π-system of the tpy ligand **210** incorporated into the complexes **208** and **209**, if compared to the much smaller tpy ligand **11** that is incorporated within the accordant parent complexes $[Fe(tpy)_2]^{2+}$ **188**,[543] and $[Ru(tpy)_2]^{2+}$ **207**.[546,547] Accordingly for the Fe(II)-based complex **208** a $\lambda_{max.}$-value of 565 nm (ε = 13500 L*cm^{-1}*mol^{-1}) was found, in comparison to the $\lambda_{max.}$ of 552 nm for the MLCT-band of parent $[Fe(tpy)_2]^{2+}$ complex **188**,[543] whereas for Ru(II)-based complex **209** a $\lambda_{max.}$-value of 487 nm (ε = 15500 L*cm^{-1}*mol^{-1}) was found, in comparison to the $\lambda_{max.}$ of 475 nm for the MLCT-band of parent $[Ru(tpy)_2]^{2+}$ complex **207**.[546] furthermore, in the higher energetic spectral region several absorbance maxima can be found between 270 – 377 nm which are summarized in Table 7. Herein, the stronger, higher energetic bands at $\lambda_{max.}$-values of 276 nm and 334 nm (ε = 65390 and 80930 L*cm^{-1}*mol^{-1}, respectively) for the Fe(II)-based complex **208**, and at $\lambda_{max.}$-values of 270 nm and 308 nm (ε = 43652 and 70795 L*cm^{-1}*mol^{-1}, respectively) for the Ru(II)-based complex **209**, presumably arise from ligand-centered transitions (either π* ← π or π* ← n).[545] In addition to this the UV/vis spectrum of the Fe-complex **208** exhibits an additional weaker absorption band at a $\lambda_{max.}$-value of 377 nm (13605 L*cm^{-1}*mol^{-1}) which can be attributed to a metal-centered electronic transition. In the UV/vis spectrum of the Ru-complex **209** the corresponding MC-band can only be surmised in form of a shoulder at around 360 nm.

4.4.2 Break-Junction Experiments

As for the experimental details discussed in chapter 3.4.3 all the MCBJ measurements described hereafter, have been performed by Riccardo Frisenda in the group of Prof. Dr. Herre van der Zant at the TU Delft in the Netherlands. Due to the nature and core of this thesis the main focus hereafter, will however be laid on the results so far obtained from the MCBJ measurements and possible interpretations of the observed effects. First of all the most important features of the utilized MCBJ setup (Figure 86a) together with the postulated interactions of our envisaged mechanically addressable single molecular spin switching target complex **208** within the MCBJ are illustrated (Figure 86b).

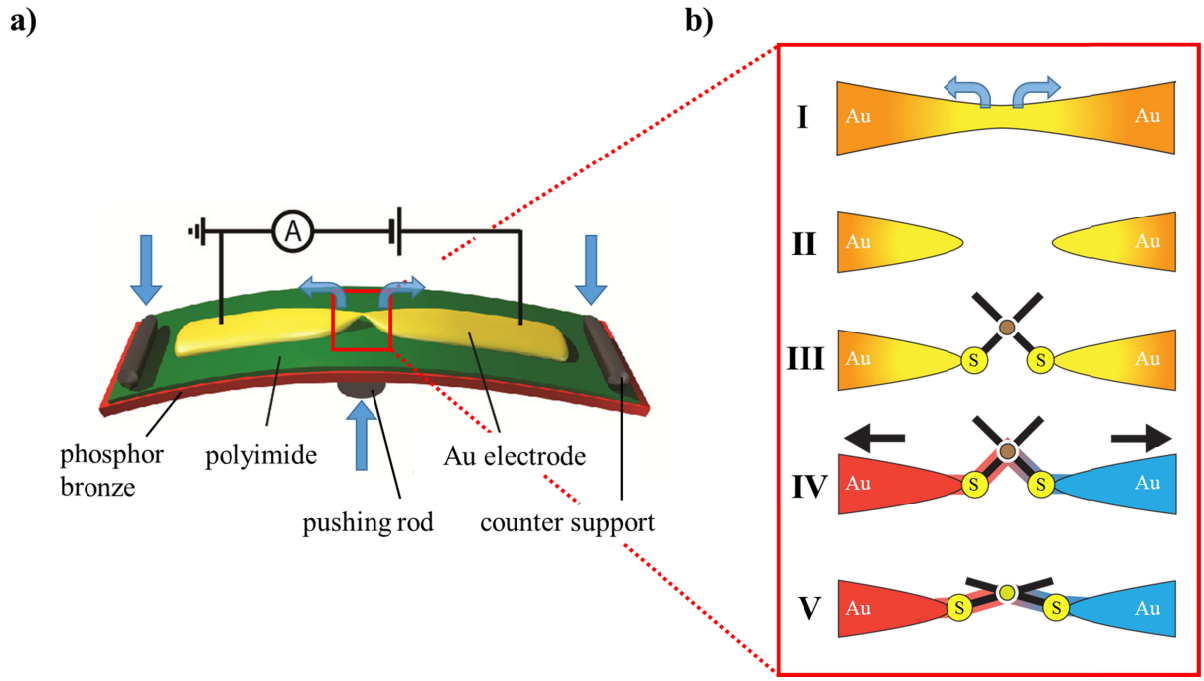

Figure 86: (a) Schematic illustration of the physical setup of an MCBJ. **(b)** Schematic step-by-step illustration of the processes occurring during breaking and junction formation in the present MCBJ setup: **(I)** stretching of the gold wire with the help of a piezoelectrically controlled pushing rod and two opposing counter supports (see Figure 86a**)**, **(II)** rupture of the gold wire resulting in the formation of two gold nano-electrodes facing each other. **(III)** Immobilization of the envisaged homoleptic, mechanically addressable target structure **208** into the MCBJ without externally applied mechanical tension. **(IV)** Alteration of the immobilized structure's geometry by pulling apart the opposing Au nanoelectrodes. **(V)** Further stretching of the target structure ideally coinciding with a SCO phenomenon at the single molecular level upon sufficient distortion of the Fe(II) ion's coordination sphere.

As for the MCBJ measurements on the heteroleptic, dipolar, electric-field dependent single molecular spin switches discussed in chapter 3.4.3 also for the present experiments the sample preparation is rather similar. After immersing the MCBJ sample into an 0.5 mM

solution of the according target complex in MeCN for 5 hours to the actual measurements are performed in UHV (10^{-7} mbar) and at liquid Helium temperature (~4 K). By bending the substrate, the gold wire stretches, until it eventually breaks, leaving two broken extremities facing each other, acting as nano-scale electrodes, as schematically illustrated in Figure 86b - stages I+II. During the rupture process a molecule can potentially bridge the nano-electrodes allowing distance-dependant conductance measurements through the break junction, as depicted in Figure 86b – steps III - V.

The details of the most important intrinsic problems of the MCBJ technique, namely, the utilization of nanoelectrodes resulting in reproducibility issues, due to the variable atomic tip shape of the electrodes as well as due to the different potential anchoring geometries of the investigated molecules upon the nanoelectrodes' surface, have already been addressed earlier within chapter 3.4.3. Consequentially, as for the measurements described within chapter 3.4.3, also the herein, discussed investigations of the envisaged mechanically addressable, single molecular spin switching Fe(II)-bis(tpy) complex **208** and the corresponding Ru(II)-based reference compound **209**, lacking the potential capability of exhibiting SCO phenomena, require a broad statistical basis to rule out the named potential side effects arising from the experimental frame conditions.

For both described target compounds **208** and **209** a sufficiently big number of conductance versus electrode's displacement traces (~500 traces each) has been collected. As displayed in Figure 87. Herein, amongst the 530 MCBJ measurements on Fe(II)-based target structure **208** in 60 traces (11%) a molecule was successfully introduced into the actual MCBJ. Among these formed junctions 33 (55%) exhibited plateau-like respective decreasing conductance values upon increasing electrode's displacements which represent the expectable result for such measurements. However in 27 (45%) of the investigated form a certain point the observed traces exhibit varyingly strong increases in the conductance upon a further increase of the corresponding electrode's displacement. In the case of the Ru(II)-based reference compound **209** the investigation of 483 attempted MCBJ measurements yielded 112 (23%) successful junction formations, of which 96 (86%) exhibited the regular decreasing respective plateau-like conductance values upon increasing the electrode's displacements, whereas only 16 (14%) of the investigated junctions showed an increase of the conductance, which was significantly less pronounced than for the corresponding Fe(II)-based analogue.

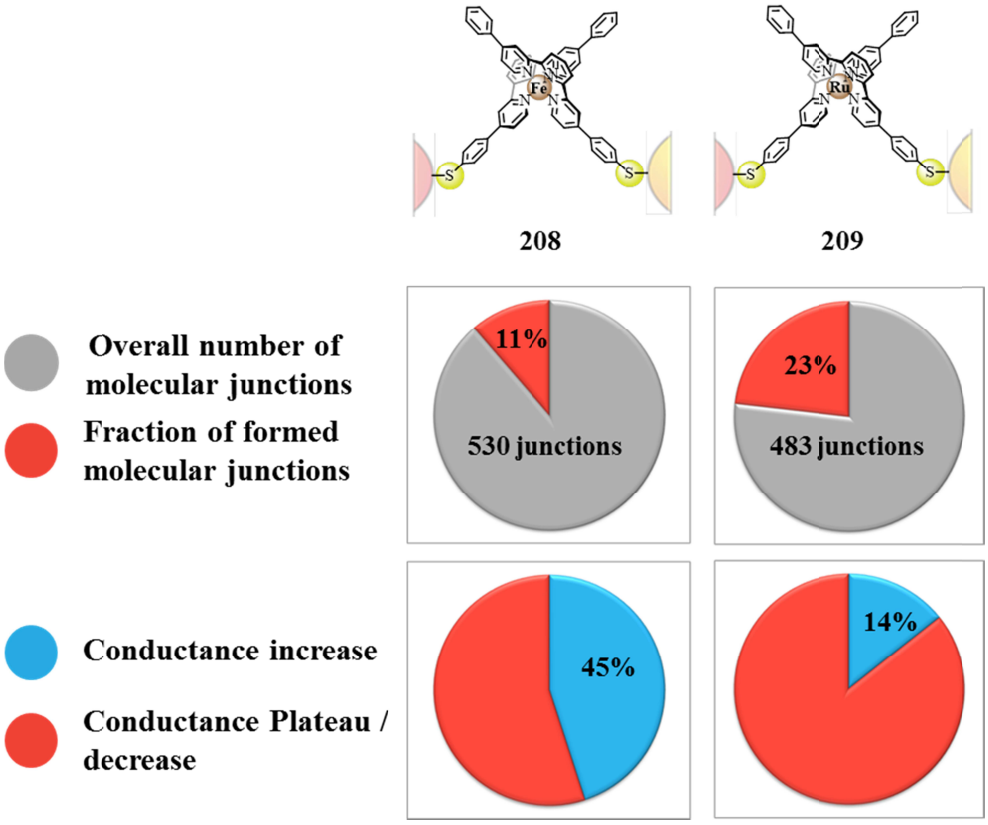

Figure 87: Illustration of the statistical analysis of the MCBJ experiments with the homoleptic metal bis(tpy) target complexes **208** and **209**. The upper row of pie charts depicts in red the molecular junction formation probability of the corresponding complexes, whose chemical structures, are highlighted above. On the other hand the lower row of pie charts displays in blue the fractions of the molecule-containing junctions, which actually display an increase in the observed conductance upon stretching the corresponding break junctions.

Hereafter, some of these representative examples for the obtained conductance versus electrode's displacement traces, exhibiting varyingly pronounced increases in the observed conductances, are displayed (Figure 88). As it can be clearly seen from the shown examples the traces look rather different for the Fe(II)-based complex **208** if compared to the results obtained for the Ru(II)-based complex **209**. If an increase of the conductance is observed upon stretching the corresponding junction, it is usually in the range of a factor of 10^2 G_0 for the examples of **208**, whereas for the Ru(II)-based analogue the respective conductance increases, if observed at all, are more than one order of magnitude smaller. Furthermore, the observed minor conductance increases for complex **209** to a high extent show unsteady behavior, whereas the conductance increases observed for the Fe(II)-based analogue **208** usually exhibit a highly ordered and monotonous devolution.

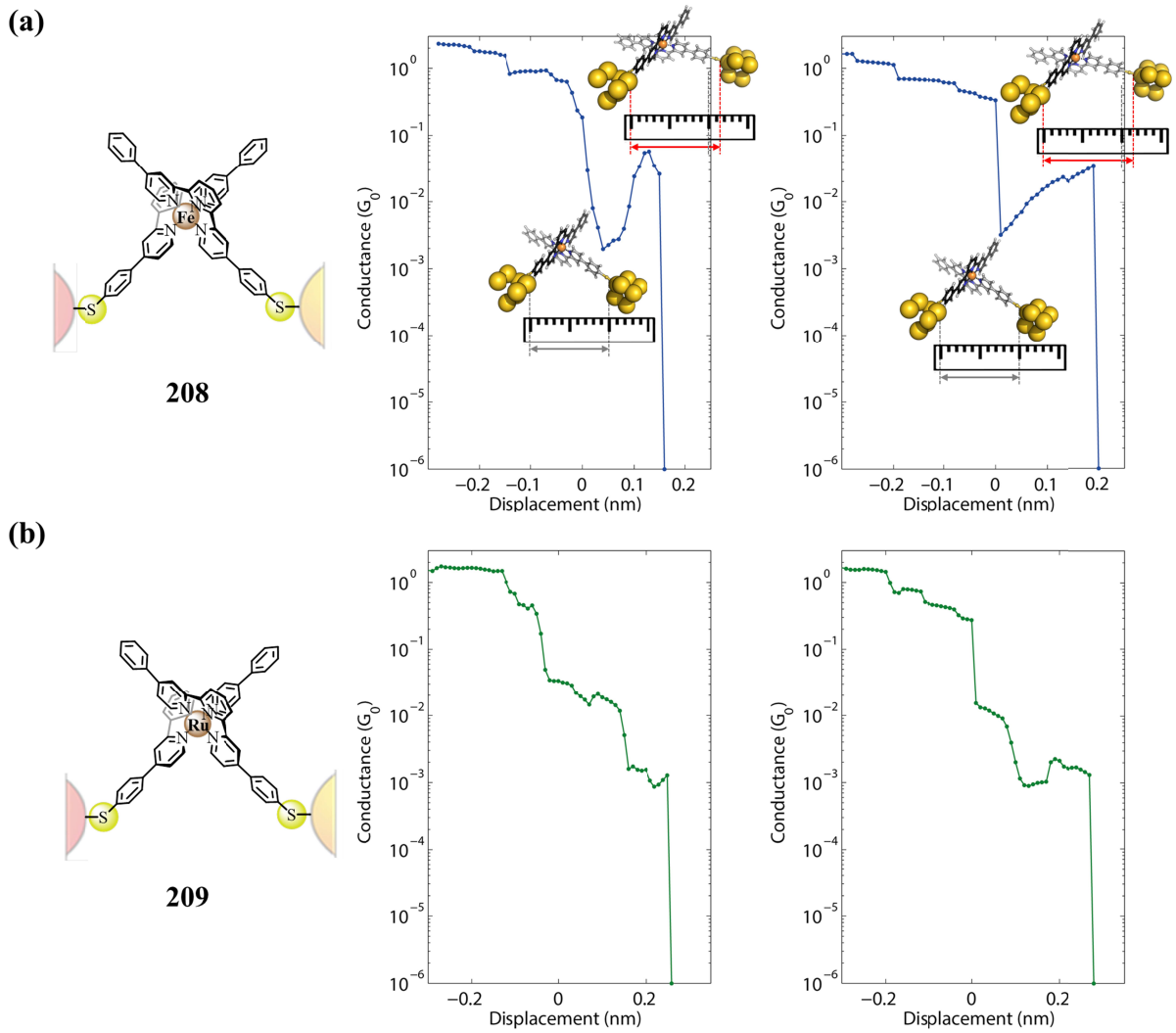

Figure 88: Exemplary overview of typical conductance-displacement characteristics measured on target complexes **208** and **209** and exhibiting varyingly strong conductance increases. **(a)** The displayed traces for the homoleptic Fe(II)-based target structure **208** after a certain point exhibit a rather strong increase in the conductance G_0 upon stretching the junction, in contrast to the commonly observed monotonous conductance decay known for regular MCBJ measurements. **(b)** In contrast to the traces observed for the Fe(II)-based complex **208** the traces recorded for the Ru(II)-based analogue rarely show any increase of conductance upon junction stretching. In the few cases such an increase has been observed its dimensions appeared to be significantly smaller than for the Fe(II)-based systems and much less continuous.

A closer inspection of the relative increases of the observed conductances during these unusual MCBJ experiments is shown below. Herein, Figure 89a displays the histograms of the magnitude of conductance increase, by relating the conductance after the increase G_{final} to the conductance prior to the increase G_{start}. The same data is displayed in form of a semi-logarithmic plot within Figure 89b, which readily illustrates the differences between the Fe(II) complex **208** (shown in red) and the Ru(II) complex **209** (shown in green) concerning the obtained orders of magnitude of the observed conductance increases.

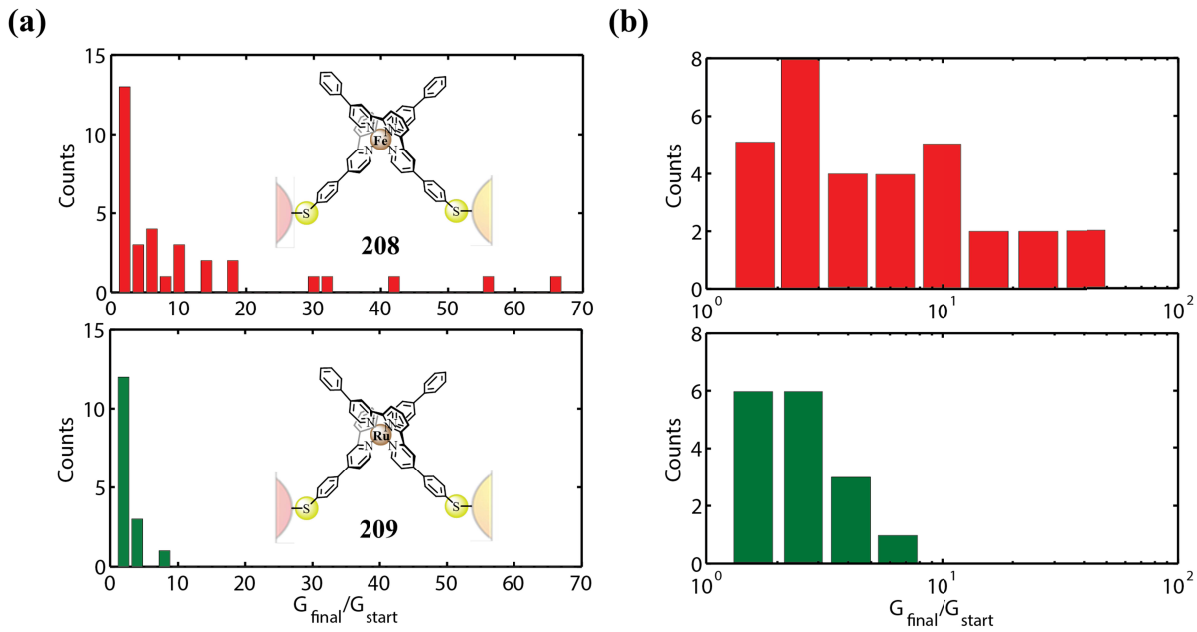

Figure 89: Statistical evaluation of the ratios between the final (G_{final}) and the starting (G_{start}) conductances for traces showing an increase in conductance while stretching the junction. **(a)** Histograms displaying the magnitude of the observed conductance increase, where the potentially spin switching Fe(II) complex **208** is displayed in red and the Ru(II)-based reference compound is shown in green. **(b)** Semi-logarithmic histogram plot illustrating the named G_{final}/G_{start}–ratios found for complexes **208** and **209**.

As it can be seen from Figure 89a+b above, in contrast to the drastic conductance increases observed for the Fe(II)-based complex **208** the according increases found for the Ru(II)-based complex **209** are rather small in comparison. As the two compounds are identical apart from their core ion this allows the conclusion, that the stronger conductance increases ($\geq 10^1\ G_0$) can be related to the metal's nature. This finding strongly suggests a that the observed dramatic conductance increases observed for the Fe(II) complex **208** can be deduced to the desired and postulated mechanically induced SCO of the Fe(II) core ion. As the minor conductance increases, although occurring much more often for the Fe(II)-based complex **208**, can be observed for both complexes **208** and **209** alike, the source of these less pronounced increases in conductance most probably can be derived from some ligand induced effects or from geometrical differences in the nano-electrodes atomic shape.

4.5 Conclusion

The herein, reported assembly routes of the target complexes **208** and **209** rely on the very same modularly applicable key building block **47** as the ones described in the previous

chapter 3.5. In this fashion the named target structures could be assembled in very satisfying overall yields taking the statistical nature of the intermediate Suzuki-Miyaura cross-coupling reactions into account.

In the range of this third main project of the present thesis a rarely reported switching concept addressing the coordination sphere dependent spin state of the hexa-coordinated homoleptic Fe(II)-bis(tpy) complex **208** is presented. Due to the molecular design, utilizing the single-sided thiol-terminated tpy ligand **210**, the according homoleptic Fe(II)-based target complex **208** could be incorporated into the molecular junction of an MCBJ setup and be investigated on a single molecular level in a fashion guaranteeing electronic transport through the central metal ion. Upon increasing the relative electrode's displacement, the incorporated target complex is simultaneously stretched, leading to a distortion of the complex' originally octahedral coordination sphere. As a consequence of this mechanical distortion of the complex' geometry, an alteration of the relative energy of the complex' frontier orbitals and hence of its electron population can be observed, commonly referred to as SCO. The additional investigation of the Ru(II)-based reference complex **209**, itself being unable to undergo any SCO, under the same conditions, allows it to draw substantive conclusions from the observed results. Extensive single molecule transport studies on both named target complexes **208** and **209** revealed, after comprehensive statistical analyses, that the conductance-displacement characteristics of the Fe(II)-based target compound **208** show a clear distance-dependent bistability, exhibiting G_{final}/G_{start}–ratios of up to 10^2 G_0. The analogue measurements of the Ru(II)-based reference complex **209** revealed a significantly smaller number of drastically less pronounced conductance increases. Whereas these minor conductance alterations exhibited by both metal's complexes can supposedly be derived from some ligand induced effects or from geometrical differences in the nano-electrodes atomic shape, the much more pronounced conductance augmentations ($\geq 10^1$ G_0) observed exclusively for the Fe(II)-based complex **208** indicate a clear correlation of the findings to the core metal ion's nature. Therefore the observed effects, with the utmost probability, can be attributed to the postulated and desired mechanically addressable SCO phenomenon from the LS state at small electrode's displacements coinciding with low conductance values towards the HS state at increased relative electrode's displacements accordingly going along with high conductance values.

5 Light Switchable Iron-Terpyridine-Azobenzene Macrocycles

The present chapter covers the fourth project and objective of this thesis:

(1) Design and synthesis of photosensitive metalloazobenzenophanes acting as molecular photo- and potentially spin-switching macrocyclic systems, which are to be investigated physically by appropriate UV/vis- and NMR spectroscopic means.

Hereby, the molecular design and switching concept (Chapter 5.1), the chosen synthetic approaches (Chapters 5.2 and 5.3), and the physical characterizations (Chapter 5.3.3) arising from the project, represent the core of the present chapter and are treated in a step-by-step fashion. Finally a comparative conclusion will be drawn, which relates the physical results obtained for the present project to the results obtained for the previous projects, namely, the investigation of electrical-field driven single molecular spin switching systems, presented in chapter 3, as well as the investigation of mechanically triggerable single molecular spin switching systems, presented in chapter 4.

5.1 Switching Concept and Molecular Design

Following the relevant constraints discussed in previous projects (Chapters 3.1 and 4.1) first of all a molecular subunit exhibiting an externally addressable spin state represents one of the utmost important requirements to actually allow the development of an optically addressable molecular spin switching metallocyclophane. As for the voltage-driven single molecular spin switches (Chapter 3) and the mechanically addressable single molecular spin switches (Chapter 4) discussed above, from the limited number of transition metals, namely, Fe, Co, and Ni that actually feature such an externally addressable spin state, the choice fell onto complexes based on hexa-coordinate Fe(II) ions as the core subunit of the envisaged target structures. As stated before the main factors that turned the balance towards Fe(II) complexes as the envisaged target structures are their facilitated synthetic accessibility, if compared e.g. to tetra-coordinate Ni(II) complexes, as well as their simplified analytical characterization via nuclear magnetic resonance (NMR) techniques, if compared to Co(II) complexes, which exhibit paramagnetic behavior already in the LS state. Furthermore, in

order to conform to the second main requirement of the herein, described project, namely, the optically addressability of the envisaged metallocyclophane, a photosensitive functional group needed to be implemented into the molecular backbone of the according target structure. Among these, the most prominent examples are represented by stilbenes and azobenzenes, respectively. Both functional groups can be optically switched between the *trans*- and the *cis*-isomer or the *E*- and the *Z*-form, respectively. Additionally, a thermal $Z \rightarrow E$ isomerization can be induced. Since however the optical absorption bands of the stilbenes moieties are expected to overlap with the ligand- and metal-centered absorption bands in the corresponding UV/vis spectrum of the envisaged Fe(II)-bis(tpy) backbone of the target structures the choice fell onto the implementation of azobenzene motifs into our target structure. Following the previous projects, Fe(II)-bis(tpy) complexes, comprising Fe(II) ions as the SCO system, were envisaged. Within these hexa-coordinate complexes the accommodation of the six present 3d electrons of the Fe(II) core ions into the five spin degenerate levels allows the system to be found in the two different desired spin states, namely, the LS and the HS state. Whereas in the LS state the crystal field interaction is strong enough to pair up all the electrons resulting in a zero net spin (S = 0), a reduction of the crystal field interaction, e.g. by increasing the metal-ligand distance, should result in the fact, that the HS state, exhibiting a maximized total net spin of (S = 2), becomes energetically favorable resulting in the envisaged LS → HS spin switching phenomenon. As this desired SCO phenomenon of the target structure is meant to be induced by the *trans* ↔ *cis* isomerization of the according azobenzene moiety included into the molecular backbone of the envisaged iron(II)-bis(terpyridino)azobenzenocyclophanes, the accordant hexacoordinate Fe(II) core should be sensitive enough to appropriately react to the subtle changes such a *trans* ↔ *cis* isomerization induces to the coordination sphere of the named metal core. Therefore the envisaged switching concept, illustrated below in Figure 91, resembles the so-called ligand-driven-light-induced spin change (LD-LISC) first observed by Zarembowitch and Boillot *et al.* (Figure 23).[153–155] In contrast to the previously described bias-sensitive (Chapter 3) and the mechanically addressable single molecular spin switches (Chapter 4), the envisaged iron(II)-bis(tpy)azobenzenocyclophanes **215** - **217** (Figure 90) discussed within the present chapter, are not meant to be immobilized onto Au surfaces in order to investigate possible SCO processes vian MCBJ or STM measurements. They should rather be examined by appropriate analytical methods, such as UV/vis- and NMR-spectroscopy. Both methods alike, should readily allow the investigation, of the envisaged *E* ↔ *Z* isomerization processes as well as the detection of a potentially coinciding LS ↔ HS spin switching phenomenon.

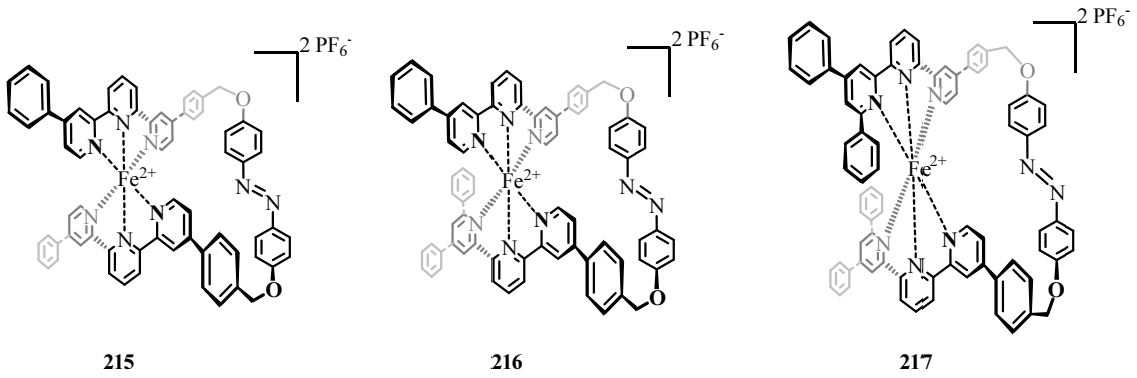

Figure 90: Chemical structure of the envisaged optically addressable iron(II)-bis(terpyridino)-azobenzenocyclophanes **215**, **216**, and **217** potentially permitting the desired spin switching of the Fe(II) core ion upon the geometrical distortion of the core ion's coordinative environment.

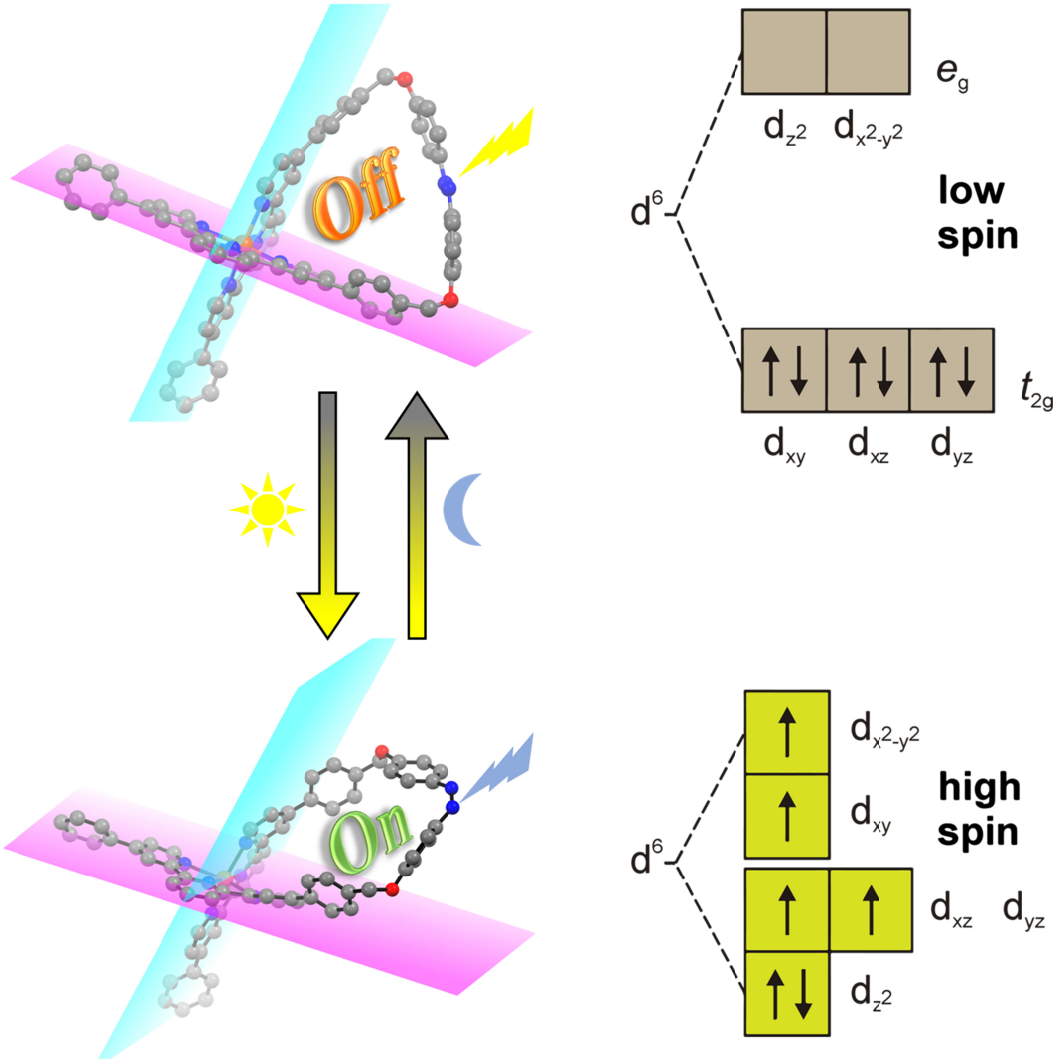

Figure 91: Schematic illustration of the postulated switching concept for the envisaged iron(II)-bis(terpyridino)azobenzenocyclophane **215**. The two states, namely, the *OFF*-state (LS), and the *ON*-state (HS) illustrate the desired effects of photo-induced *E* ↔ *Z*-isomerizations onto the target structures geometry. The invoked distortion of the originally octahedral coordinated target structure (*OFF*-state, LS), should eventually result in the switching of the core ion's spin state (LS ↔ HS) upon the appropriate externally applied optical stimuli.

To sum up, the overall optical addressability of the envisaged iron(II)-bis(terpyridino)-azobenzenocyclophanes **215**, **216**, and **217**, as the basis for the desired LS → HS spin switching process, conceptually originates from a cascade of different effects (for theoretical details on SCO, see chapter 1.1.4.1, particularly Figure 20), namely:

(1) The $E \leftrightarrow Z$ photoisomerization of the azobenzene moiety incorporated into the molecular backbone of the macrocycles should result in the spatial distortion of the formerly octahedral coordination environment of the three postulated Fe(II)-based LS metallocyclophanes **215 - 217**.

(2) Going along with this geometrical distortion, the Fe-N bonds in the target macrocycles are elongated, in order to compensate for the increasing steric repulsion between the two outer pyridine rings of the tpy ligands, respectively.

(3) This elongation of the Fe-N bonds leads to a weakening of the ligand field (LF) strength Δ, which is equivalent to a reduced crystal field splitting between the lower energetic t_{2g} orbitals and the higher energetic e_g orbitals.

(4) As long as the LF splitting energy Δ is still bigger than the mean spin pairing energy P the system remains in the LS state with all electrons being paired up. However, as soon as P is no longer overcompensated by Δ, according to Hund's rule, the electrons will also populate the e_g orbitals resulting in the formation of the HS species.

5.2 Synthetic Strategy

Within this chapter the synthetic strategies towards the assembly of the envisaged optically addressable molecular spin switching iron(II)-bis(tpy)azobenzenocyclophanes **215**, **216**, and **217** are discussed (Scheme 41 - 43).

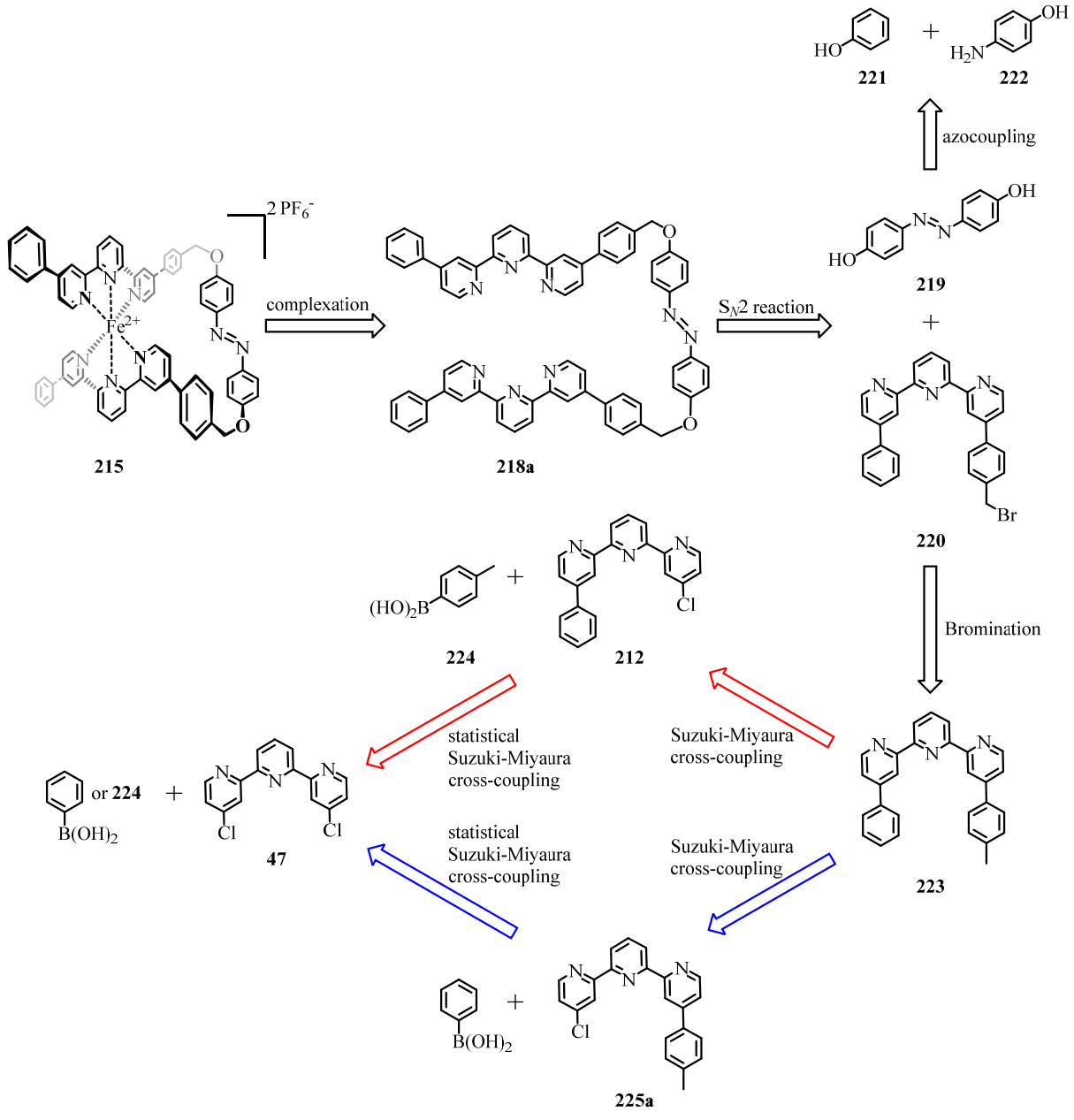

Scheme 41: Retrosynthetic analysis of the optically addressable iron(II)-bis(tpy)azobenzeno-cyclophane **215**. The two alternative reaction pathways are highlighted in color code (red and blue reaction pathway).

Retrosynthetically, the symmetric metalloazobenzenophane **215** is accessible via the complexation of the symmetric hexadentate bis-tpy azobenzene precursor **218a**. The named ligand **218a** is obtained via a twofold S_N2 reaction of (*E*)-4,4'-(diazene-1,2-diyl)diphenol (**219**) and the asymmetric benzylbromo-tpy derivative **220**. Whereas 4,4´-dihydroxyazobenzene **219** should be accessible via the azocoupling of phenol (**221**) and 4-hydroxyaniline (**222**) the asymmetric benzylbromo derivative **220** can be obtained via radical side-chain bromination of the according tpy precursor **223**. This asymmetrically, disubstituted tpy ligand **223** can be accessed by following two different routes (red and blue pathway) involving differently ordered sequences of Suzuki-Miyaura cross-coupling reactions. Following the red reaction pathway, the asymmetric key tpy ligand **223** is obtained via the Suzuki coupling of the monofunctionalized tpy derivative **212** and *p*-tolylboronic acid (**224**), whereas on the blue reaction pathway **223** is obtained via the Suzuki coupling reaction of the monofunctionalized tpy derivative **225a** and phenylboronic acid. Accordingly the two tpy derivatives **212** and **225a** are accessible via the precedent Suzuki-Miyaura cross-coupling reactions of the core tpy building block **47** with the corresponding borylation agents **224** or phenylboronic acid, respectively. Since the synthetic strategy towards the modularly applicable core tpy subunit **47** has been described in detailed form in chapter 3.2.1, its accessibility is taken for granted in the given context.

In contrast to the synthetic strategy described in Scheme 41, the retrosynthetic analyses of the asymmetric metalloazobenzenophane **216** as well as the one for the symmetric metalloazobenzenophane **217** rely on a significantly different approach, including a statistical key step close to the end as well as a differing formation strategy for the altered tpy core unit **230**. As displayed in Scheme 42 the target macrocycles **215 – 217** are obtained via the complexation reactions of $FeCl_2$ with the corresponding hexadentate bis-tpy azobenzene precursors **218a**, **226**, and **227a**, respectively. Whereas the synthetic strategy for the exclusive assembly of the symmetric bis-tpy azobenzene precursor **218a** is described above (Scheme 41), the asymmetric bis-tpy azobenzene precursor **226** is obtained via a statistical, asymmetric twofold S_N2 reaction of the azobenzene derivative (*E*)-4,4'-(diazene-1,2-diyl)diphenol (**219**) together with the asymmetric benzylbromo-tpy ligands **220** and **228**. During this reaction, apart from the named asymmetric bis-tpy azobenzene precursor **226** also the two symmetric bis-tpy azobenzene precursors **218a** and **227a** can be accessed in an expectable statistical ratio of 1:2:1 for the ligands **218a : 226 : 227a**.

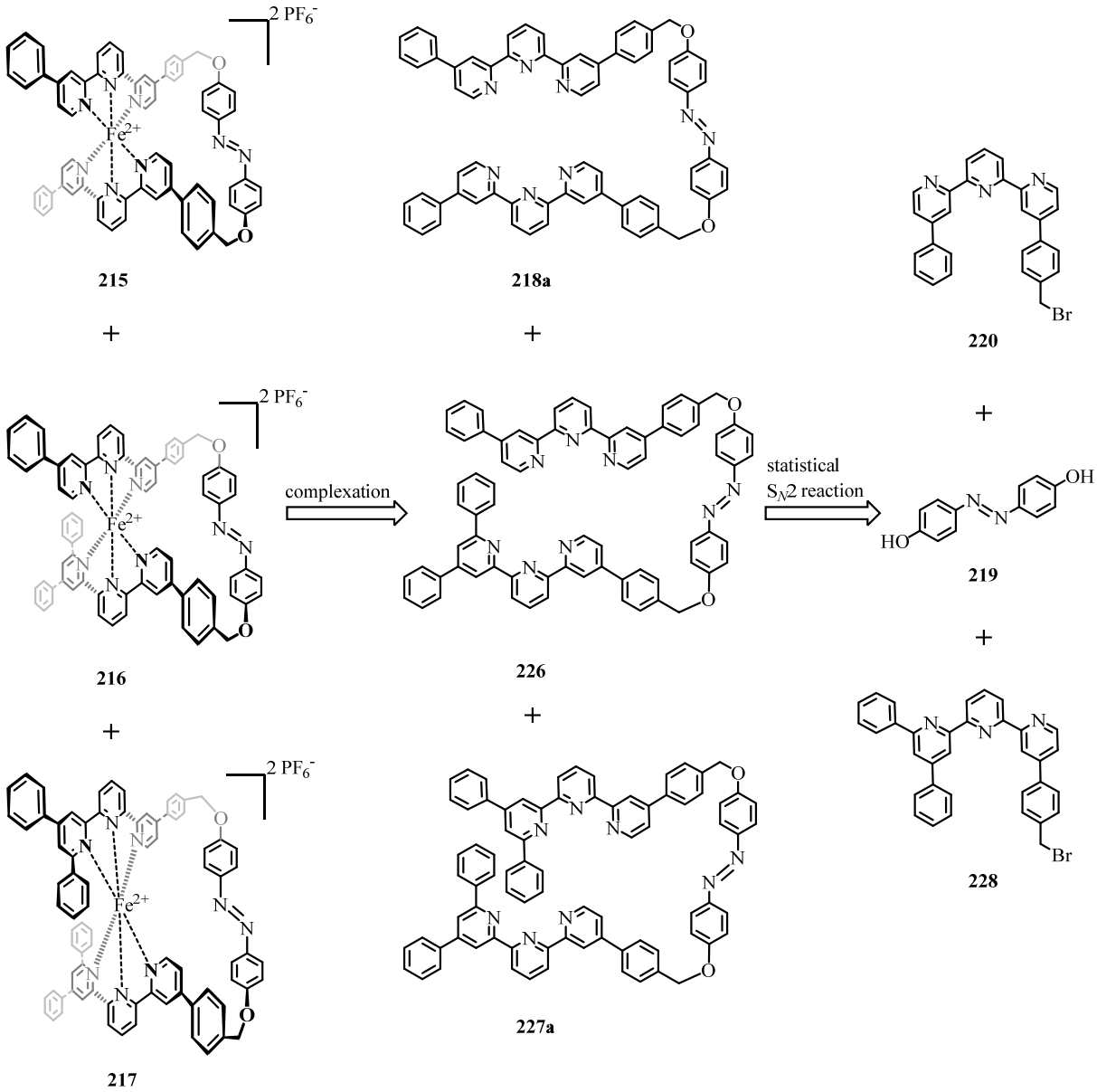

Scheme 42: Retrosynthetic analysis of the final reaction steps during the assembly of the optically addressable iron(II)-bis(tpy)azobenzenocyclophanes **215 - 217**.

Whereas the synthetic strategy for the assembly of the asymmetric benzylbromo-tpy derivative **220** as well as for 4,4´-dihydroxyazobenzene **219** is displayed above (Scheme 41), the retrosynthetic analysis for the assembly of the second asymmetric benzylbromo-tpy building block **228** is illustrated in Scheme 43 below. Analogously to compound **220** also the asymmetric benzylbromo derivative **228** can be obtained via radical side-chain bromination of its according tpy precursor **229**. The asymmetric key tpy ligand **229** is accessible via the Suzuki-Miyaura cross-coupling reaction of the monofunctionalized tpy derivative **230** and *p*-tolylboronic acid (**224**). **230** itself can be assembled in a Suzuki coupling of 6'-iodo-4,6-diphenyl-2,2'-bipyridine (**231**), which can be previously obtained via the trans-halogenation of the accordant brominated bpy precursor **232**, and the borylation agent **140**, whose formation

has been described in previous parts of this thesis (Chapter 3.2.1). Finally the brominated bpy precursor **232** is accessible via the Kröhnke condensation of ammonium acetate, the pyridinium salt 1-(2-oxo-2-phenylethyl)pyridin-1-ium bromide (**233**), and the α,β-unsaturated carbonyl compound (*E*)-1-(6-bromopyridin-2-yl)-3-phenylprop-2-en-1-one (**234**), which itself can be assembled via the according aldol condensation of benzaldehyde (**235**) and 2-acetyl-6-bromopyridine (**236**).

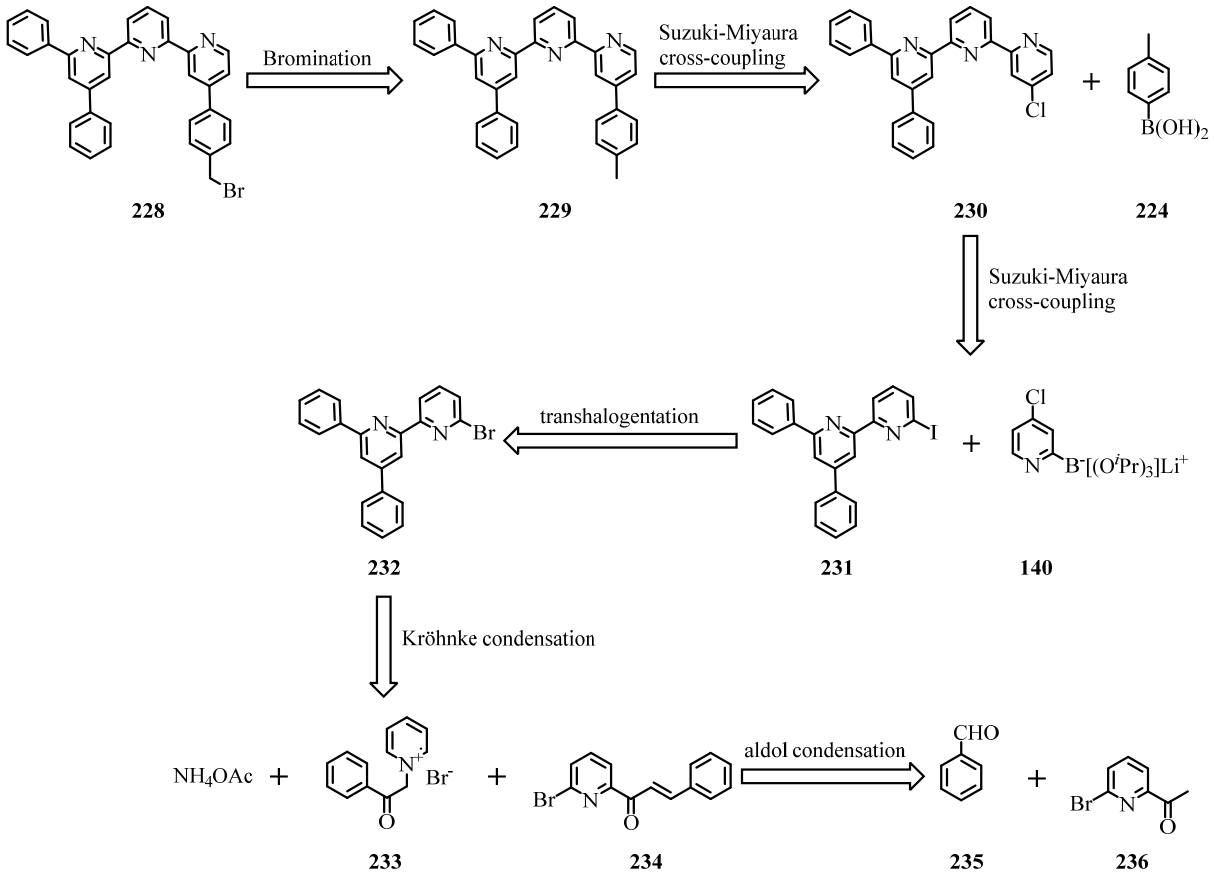

Scheme 43: Depiction of the synthetic strategy towards the assembly of the asymmetric key intermediate 4''-(4-(bromomethyl)phenyl)-4,6-diphenyl-2,2':6',2''-terpyridine (**228**).

5.3 Synthesis

Hereafter, the synthetic procedures related to the assembly of the optically addressable, potentially molecular spin switching iron(II)-bis(tpy)azobenzenocyclophanes **215**, **216**, and **217** are discussed, whereat the synthetic details for the preparation of the inter-mediates **47**, **140**, and **212** were described earlier and hence are omitted due to limited space.

5.3.1 Symmetric Iron(II)-bis(terpyridino)azobenzenocyclophane

In the present section the synthesis of the symmetric metalloazobenzenophane **215** via the symmetric, hexadentate bis-tpy azobenzene precursor **218a** is described (Scheme 44), whereat both proposed reaction pathways described in Scheme 41 above were considered and followed, alike.

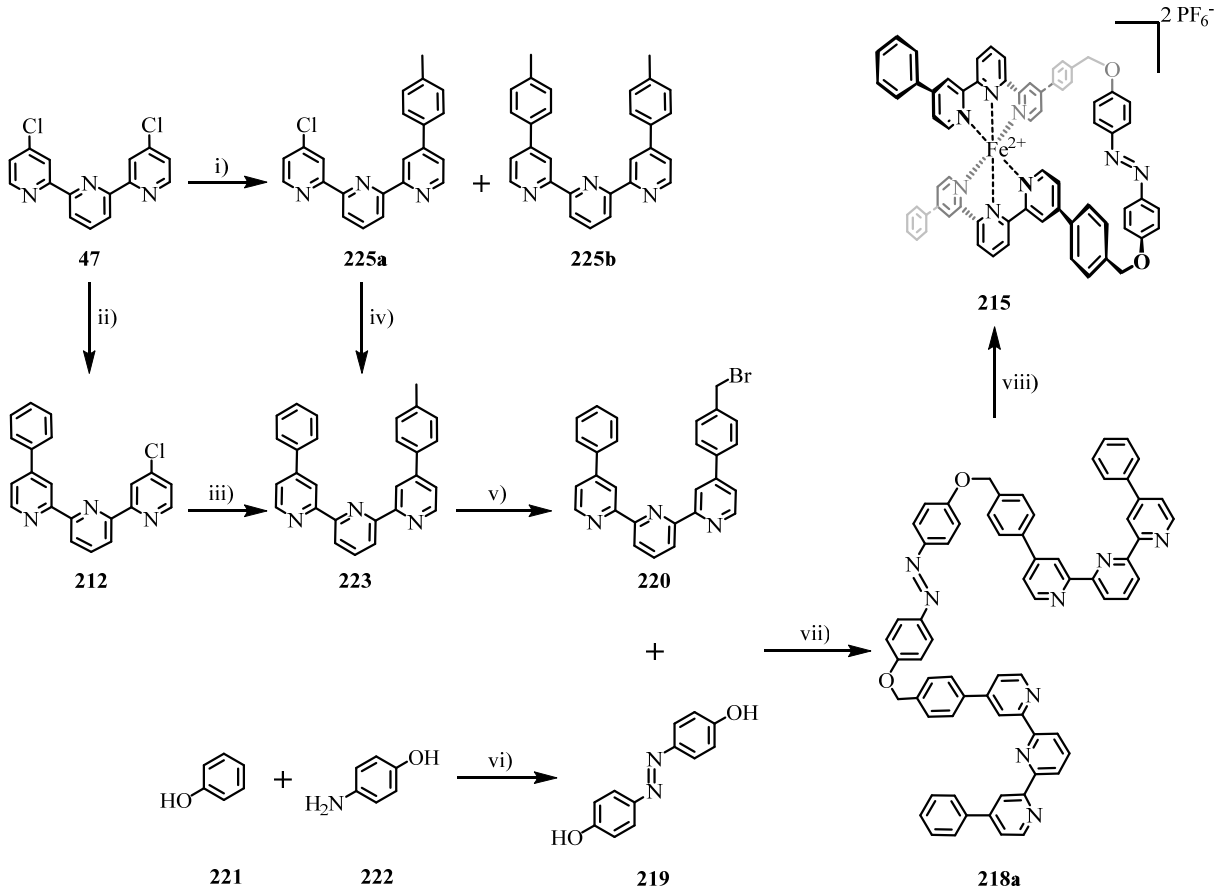

Scheme 44: Overview of the synthetic assembly of the optically addressable iron(II)-bis-(terpyridino)azobenzenocyclophane **215** via the concluding complexation of the symmetric hexadentate bis-tpy azobenzene precursor **218a**. Reagents and conditions: **i) 47** (1 eq.), **224** (0.8 eq.), $PdCl_2[P^tBu_2(p\text{-}NMe_2\text{-}Ph)]_2$, K_2CO_3, toluene/H_2O (5:1), reflux, 22h, 41% (+ 21% of **225b**); **ii) 47** (1 eq.), phenylboronic acid (0.8 eq.), $PdCl_2[P^tBu_2(p\text{-}NMe_2\text{-}Ph)]_2$, K_2CO_3, toluene/H_2O (5:1), 110 °C, 36h, 44% (+ 18% of **172** and 38% of **47**); **iii) 212** (1 eq.), **224** (10 eq.), $PdCl_2[P^tBu_2(p\text{-}NMe_2\text{-}Ph)]_2$, K_2CO_3, toluene/H_2O (5:1), reflux, 24h, quant.; **iv) 225a** (1 eq.), phenylboronic acid (10 eq.), $PdCl_2[P^tBu_2(p\text{-}NMe_2\text{-}Ph)]_2$, K_2CO_3, toluene/H_2O (5:1), reflux, 24h, quant.; **v) 223** (1 eq.), *N*-bromosuccinimide (NBS) (1.2 eq.), $(PhCOO)_2$ (0.25 eq.), CCl_4, 75 °C, 5h, 84% (16% of reisolated **223**); **vi) 221** (1 eq.), **222** (1 eq.), $NaNO_2$ (1 eq.), KOH (2 eq.), HCl, MeOH, 0 °C, 2h, 10%; **vii) 219** (1 eq.), **220** (2.2 eq.), K_2CO_3 (2.6 eq.), acetone, reflux, 20h; **viii) 218a** (1 eq.), $FeCl_2$ (1 eq.), NH_4PF_6 (50 eq.), MeOH, THF, H_2O, r.t., 4h, 62%.

The key intermediate 4-Phenyl-4´´-(*p*-tolyl)-2,2´:6´,2´´-terpyridine (**223**) has been assembled via two different approaches (Scheme 41 – red and blue pathway) each involving a cascade of two subsequent Suzuki-Miyaura cross-coupling reactions, starting from the tpy key building block **47**. As described earlier throughout this work, the synthesis of asymmetric tpys inevitably requires this two-step procedure including the statistical intro-duction of the first 4-substituted phenyl substituent in the precedent coupling step, in contrast to the possible one-step formation of symmetrically 4,4´´-disubstituted tpy derivatives. As described in chapter 4.3.1 the synthesis of monofunctionalized tpy derivative **212** from the tpy core motif **47**, and phenylboronic acid was performed using substoichiometric amounts of the borylation agent to favorably alter the expectable 1:2:1 product ratio. In that way the described cross-coupling reaction yielded 44% of the desired 4´-monofunctionalized tpy **212**, together with 18% of the 4,4´´-disubstituted tpy side product **172**, in addition to 38% of reisolated starting material **47**, by applying otherwise comparable reaction parameters as described in the previous chapters, using ($PdCl_2[P^tBu_2(p\text{-}NMe_2\text{-}Ph)]_2$) as the catalyst and K_2CO_3 as the base in a solvent mixture of toluene and water. Further following the red pathway the subsequent Suzuki-Miyaura cross-coupling of the 4´-monofunctionalized tpy **212** with an excess of *p*-tolylboronic acid (**224**) in a degassed toluene/water mixture (5:1) with ($PdCl_2[P^tBu_2(p\text{-}NMe_2\text{-}Ph)]_2$) as the catalyst and K_2CO_3 as the base quantitatively yielded the desired asymmetric 4,4´´-disubstituted tpy derivative **223**. Alternatively, following the blue reaction pathway, the precedent Suzuki coupling of the tpy core building block **47** with substoichiometric amounts of *p*-tolylboronic acid (**224**) afforded 41% of the desired 4´-monofunctionalized tpy **225a** together with 21% of the undesired 4,4´´-disubstituted tpy side product **225b**. The according subsequent second Suzuki coupling of **225a** with an excess of phenylboronic acid quantitatively yielded the desired asymmetric 4,4´´-disubstituted tpy derivative **223**. The subsequent literature-inspired radical side chain bromination[554,555] of tpy **223** using NBS and dibenzoylperoxide in tetrachloromethane (CCl_4) yielded the desired asymmetric benzyl-bromo tpy derivative **220** in 84% yield under simultaneous reisolation of the remaining 16% of the starting material **223**. The following twofold S_N2 reaction required the prevenient preparation of 4,4´-dihydroxyazobenzene **219**. The azo-diol **219** was obtained via a classical two-step azocoupling procedure consisting of a prior diazotation of 4-hydroxy-aniline (**222**) with aqueous $NaNO_2$ at 0 °C followed by the coupling of the intermediate diazonium species with the precooled phenolate solution (0 °C) prepared from phenol (**221**).) and KOH. After extensive purification involving FCC and repeated recrystallization the obtained 4,4´-dihydroxyazobenzene **219** was obtained in 10% yield. The subsequent twofold S_N2 reaction of

219 with 4-Phenyl-4´´-(4-(bromomethyl)phenyl)-2,2´:6´,2´´-terpyridine (**220**), in adaptation of a protocol reported in literature,[556] was performed by using heat dried K_2CO_3 as the base under inert atmosphere in dry acetone. The excessive insolubility of the obtained product prevented any NMR-analytical characterization or a possible purification of the crude product via FCC. However, by means of HR-ESI-MS, the two components contained in the crude mixture could be identified as the desired twofold substituted symmetric, hexadentate bis-tpy azobenzene precursor **218a** and the mono-reacted single-tpy azobenzene precursor **218b** as the expectable side-product. The fraction of the latter one could be reduced to a minimum by excessive washing of the crude mixture with THF. The final complexation of the symmetric, hexadentate bis-tpy azobenzene precursor **218a** with $FeCl_2$ was performed in a 1:1 mixture of MeOH and THF under high dilution conditions (40 µM), during which the Fe(II) source was added dropwise to the solution / suspension of the bis-tpy azobenzene precursor **218a** as methanolic solution. After anion exchange utilizing an excess of NH_4PF_6, removal of the organic solvents and subsequent washing of the obtained purple precipitate with excessive amounts of water the crude product was further purified by means of preparative reversed-phase HPLC finally yielding the desired pure, monomeric symmetric metalloazobenzenophane **215** in a yield of 62%. The detailed discussion of the NMR-spectroscopic *E* ↔ *Z*-photoisomerization studies together with the according NMR-spectra of the pure (*E*)- and (*Z*)-isomers can be found in the according chapter 5.4.2. However a HR-ESI-MS spectrum proofing the identity and purity of the obtained monomeric target macrocycle **215** is displayed in Figure 92 below.

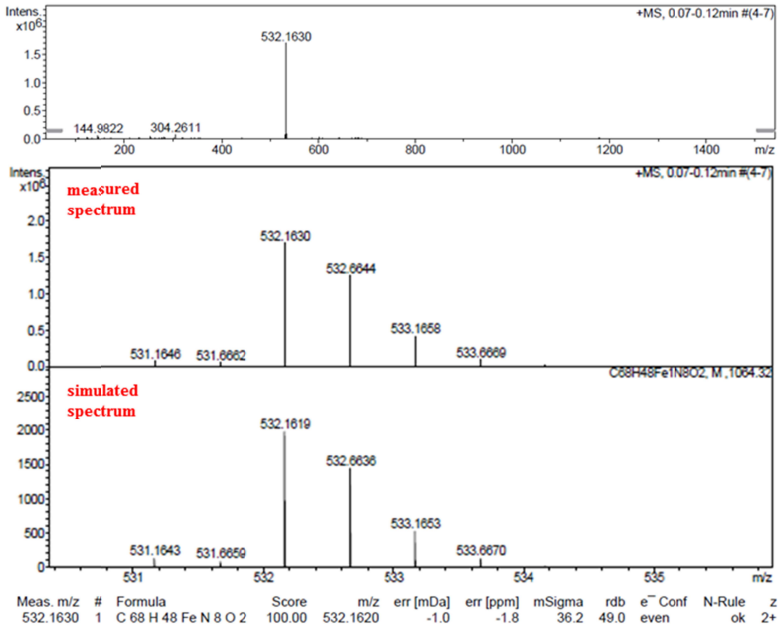

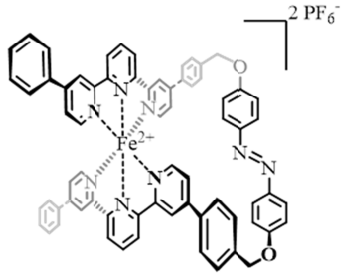

215

Chemical Formula: $C_{68}H_{48}FeN_8O_2^{2+}$
Exact Mass: 1064,3239

Figure 92: HR-ESI-MS spectrum proofing identity and purity of metalloazobenzenophane **215**.

5.3.2 Asymmetric Iron(II)-bis(terpyridino)azobenzenocyclophane

In the present section the synthetic efforts towards the asymmetric metalloazobenzenophane **216** as well as towards the symmetric metalloazobenzenophane **217** via the hexadentate bis-tpy azobenzene precursors **226** and **227a**, respectively are described (Scheme 45 + 46). The impetus to prepare the named macrocycles arises from the increased steric hindrance around the Fe(II) core ions of the named metalloazobenzenophanes **216** and **217**. As reported in literature[557] this additional steric bulk, induced by the implementation of one (**216**) or even two (**217**) phenyl units in the 6-positions of the corresponding tpy fragments, significantly alters the coordination sphere of the Fe(II) core ions and should therefore facilitate the induction of a HS state at the named Fe(II) species.

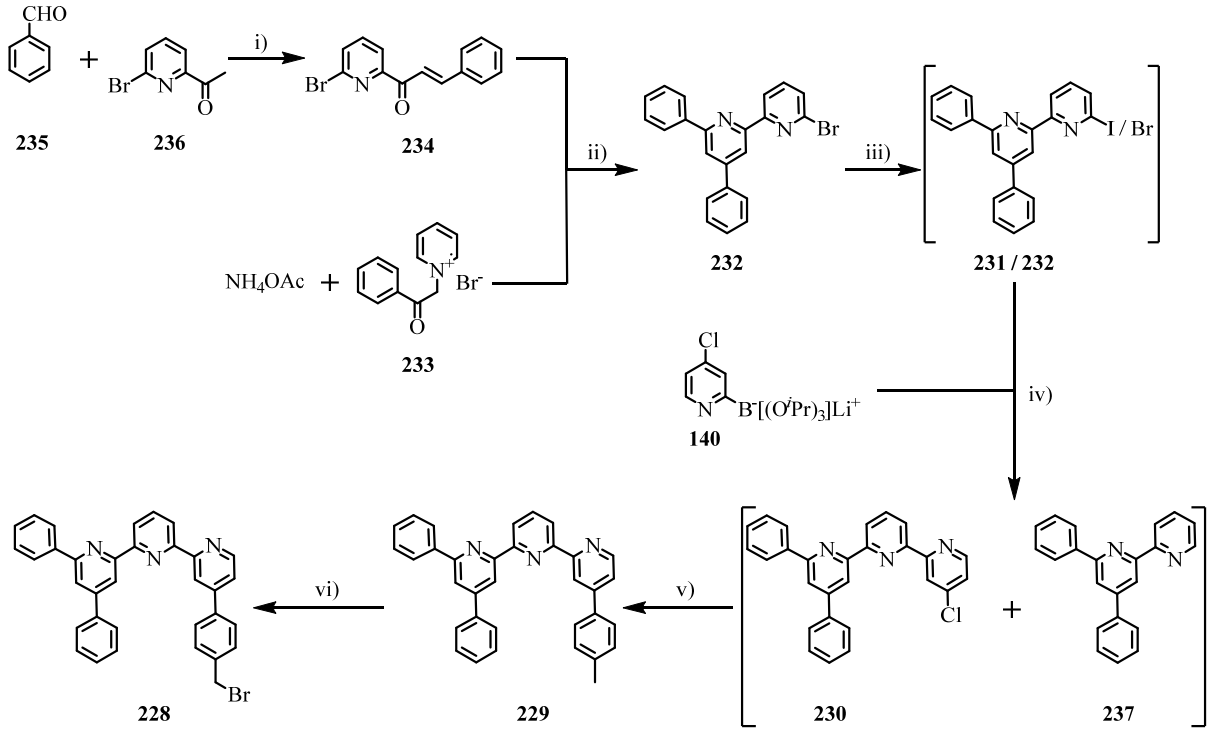

Scheme 45: Depiction of the synthesis of the asymmetric benzyl-bromo tpy key intermediate 4''-(4-(bromomethyl)phenyl)-4,6-diphenyl-2,2':6',2''-terpyridine (**228**). Reagents and conditions: **i) 235** (1 eq.), **236** (1 eq.), NaOH (1.1 eq.), MeOH, r.t., 3h, 90%; **ii) 233** (1 eq.), **234** (1 eq.), NH_4OAc (30 eq.), MeOH, reflux, 24h, 55%; **iii) 232** (1 eq.), NaI (1.4 eq.), HI (12 eq.), reflux, 7h, **231** and **232** isolated as inseparable 1:2-ratio (GCMS); **iv) 231** (1 eq.), **232** (2 eq.), **140** (10 eq.), KF (20 eq.), Pd_2dba_3 (0.18 eq.), Ph_2PHO (1.08 eq.), 1,4-dioxane, 100 °C, 72h, **230** and **237** isolated as mixture; **v) 230**, **237**, **224**, $PdCl_2[P^tBu_2(p\text{-}NMe_2\text{-}Ph)]_2$, K_2CO_3, toluene/H_2O (5:1), 125 °C, 24h; **vi) 229** (1 eq.), NBS (1.2 eq.), $(PhCOO)_2$ (0.25 eq.), CCl_4, 75 °C, 5h, 82% (17% of reisolated **229**).

As mentioned above the target structures **226** and **227a** include additional sterically demanding phenyl units in the 6-positions of the corresponding tpy fragments of the

respective molecular backbones. This however implicates that the corresponding asymmetric tpy key building blocks **230**, **229**, and **228** are no longer derived and thus cannot be assembled from the previously described modularly deployed tpy core subunit **47**. In this case the assembly of the corresponding tpy core building block rather relies on well-established ring-assembly strategies, namely, on the Kröhnke methodology (for details see chapter 1.2.1.1). In detail, in a first step benzaldehyde (**235**) and 2-acetyl-6-bromopyridine (**236**) are converted to the according α,β-unsaturated carbonyl compound (*E*)-1-(6-bromopyridin-2-yl)-3-phenylprop-2-en-1-one (**234**) in an aldol-type condensation reaction affording **234** in a good yield of 90%. Subsequently, inspired by a procedure previously reported in literature,[558,559] compound **234** was converted to the bpy building block 6'-bromo-4,6-diphenyl-2,2'-bipyridine (**232**), which was obtained in 55% yield, via the Kröhnke condensation reaction utilizing NH_4OAc and the required pyridinium salt 1-(2-oxo-2-phenylethyl)pyridin-1-ium bromide (**233**) as the further reactants. Prior to the required completion of the tpy motif by the coupling reaction of the bpy subunit with an appropriately 4-substituted borylation agent, a transhalogenation of the bromo-bpy compound **232** to the iodo-bpy analogue **231** was attempted by refluxing the reactant **232** with NaI in HI for several hours. However no full conversion to the iodo compound **231** could be achieved, and furthermore, the mixture of **231** and **232** turned out to be inseparable by means of FCC and repeated recrystallization. Therefore a mixture of **231** and **232**, in an approximate ratio of 1:2 according to GCMS analysis, was used for the subsequent coupling step. In this Suzuki-Miyaura cross-coupling reaction the mixture of **231** and **232** was reacted with tri*iso*propyl-2-(4-chloropyridyl) borate **140**, using KF as the base, Pd_2dba_3 as the catalyst, and diphenylphosphine oxide as ligand. In the range of this reaction the desired asymmetric tpy derivative **230** was obtained in a mixture with the bpy compound **237** arising from the dehalogenation of the according starting materials (most likely of the less reactive bromo-bpy compound **232**). Also this mixture of the desired tpy intermediate **230** and the undesired side product **237** turned out to be very challenging to purify, and was therefore used as obtained for the subsequent Suzuki-Miyaura cross-coupling reaction, since a facilitated separation upon further extension of the tpy ligand **230** towards **229** was expected. This is due to the fact, that the impurity **237** is inert to any further functionalization under Suzuki-Miyaura coupling conditions. The actual Suzuki coupling reaction of the mixture of the tpy building block **230** and the inert bpy derivative **237** with *p*-tolylboronic acid (**224**) finally yielded the desired, purifiable 4,6-diphenyl-4''-(*p*-tolyl)-2,2':6',2''-terpyridine (**229**), which could be further converted to the asymmetric, benzyl-bromo tpy key intermediate **228**, via the subsequent radical side-chain bromination of **229**. The bromination reaction of tpy **229**

using NBS and dibenzoylperoxide in tetrachloromethane (CCl_4) yielded the desired asymmetric benzyl-bromo tpy derivative **228** in 82% yield under simultaneous reisolation of 17% of the starting material **229**. In order to enable the assembly of the desired metalloazo-benzenophanes **216** and **217** (Scheme 46), the hexadentate bis-tpy azobenzene precursors **226** and **227a** needed to be synthesized at first. This, at least for the preparation of the asymmetric bis(tpy) derivative **226**, inevitably requires a statistical reaction, which should in principle yield the symmetric bis(tpy) derivatives **218a** and **227a** at the same time.

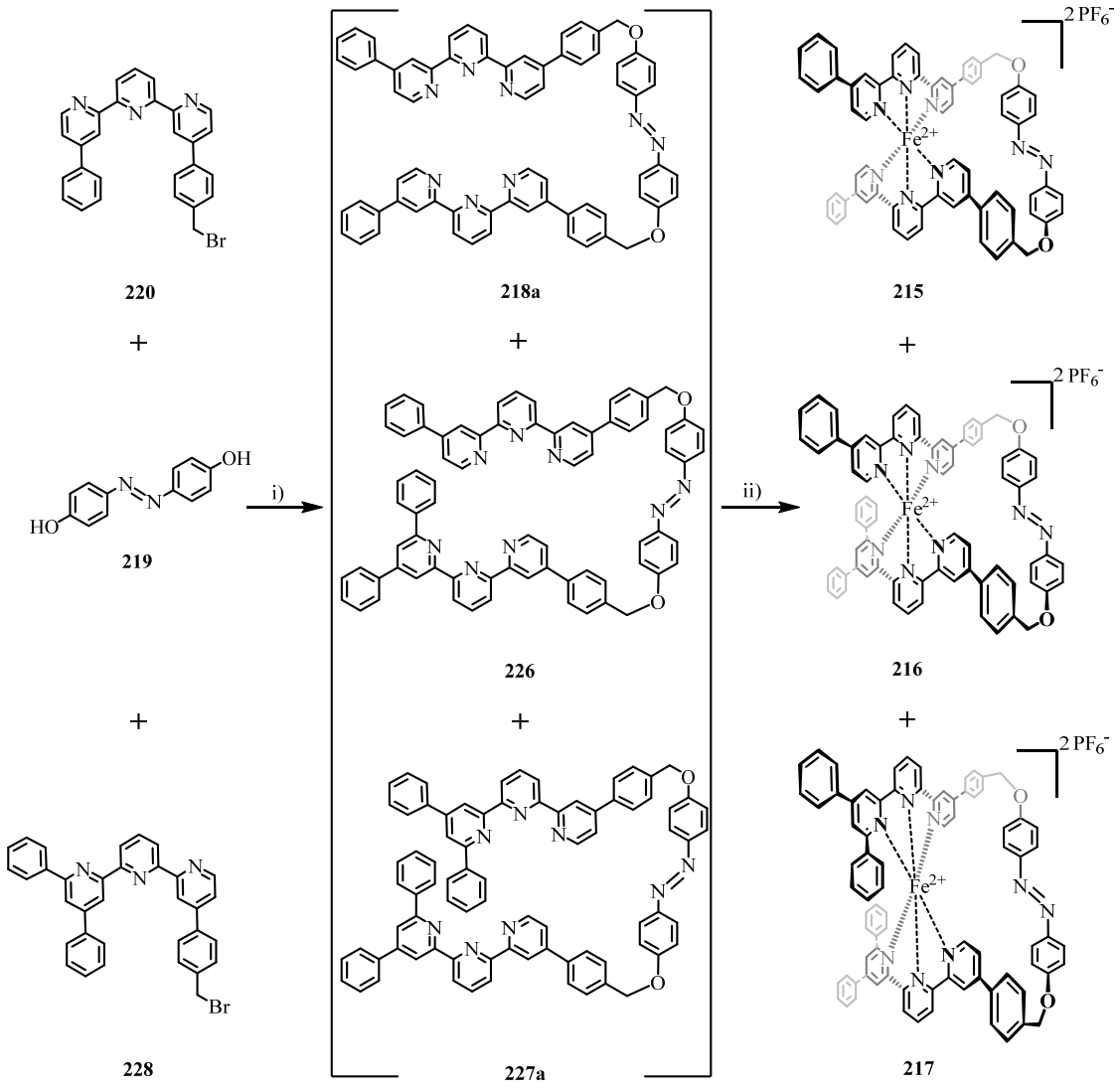

Scheme 46: Depiction of the synthesis of the iron(II)-bis-(terpyridino)azobenzenocyclophanes **215 – 217**. Reagents and conditions: **i) 219** (1 eq.), **220** (1 eq.), **228** (1 eq.), K_2CO_3 (2.6 eq.), acetone, reflux, 24h; **ii) 218a / 226 / 227a** (1 eq.), $FeCl_2$ (1 eq.), NH_4PF_6 (50 eq.), MeOH, THF, H_2O, r.t., 24h.

In detail, the named statistical twofold S_N2 reaction of the azo compound **219** with the two benzyl-bromo tpy precursors **220** and **228**, in adaptation of a literature procedure,[556] was once more performed by using heat dried K_2CO_3 as the base under inert atmosphere in dry

acetone. As described for the exclusive synthesis of the symmetric, hexadentate bis-tpy azobenzene ligand **218a** in the previous chapter 5.3.1, also for the present reaction the obtained crude product was highly insoluble, thus preventing any NMR-analytical characterization or a possible purification of the crude product via FCC. As expectable, also the mono-reacted single-tpy azobenzene side-products **218b** and **227b** were formed, but their fraction, according to ESI-MS analysis, could be successfully reduced to a minimum by excessive washing of the crude mixture with THF. Therefore the resulting "semi-crude" product, still containing the statistical mixture of the three hexadentate bis-tpy azobenzene ligands **218a**, **226**, and **227a**, whose identity could be successfully proven via HR-ESI-MS analytics, was used as obtained for the final complexation step. According to the procedure used for the formation of the monomeric symmetric metalloazobenzenophane **215** also in this case, for the synthesis of the desired metalloazobenzenophanes **215**, **216**, and **217**, equimolar amounts of $FeCl_2$ and the mixture of the three hexadentate bis-tpy azobenzene ligands **218a**, **226**, and **227a** were reacted in a 1:1 mixture of MeOH and THF under high dilution conditions (40 μM), during which the Fe(II) source was added dropwise to the solution / suspension of the ligands **218a**, **226**, and **227a** as methanolic solution. After anion exchange utilizing an excess of NH_4PF_6, removal of the organic solvents and subsequent washing of the obtained purple precipitate with excessive amounts of water the crude product mixture was further purified by means of preparative reversed-phase HPLC. Unfortunately, the results of the HPLC separation turned out to be rather surprising. Whereas, according to ESI-MS analysis, prior to the preparative reversed-phase HPLC purification, the crude mixture clearly contained the expectable mixture of **215**, **216**, and **217** (Figure 93a) in their monomeric forms (always including a single Fe(II) center, respectively), the according HR-ESI-MS only proved the presence of the two macrocycles **216**, and **217** (Figure 93b). The analysis of the products isolated after the preparative HPLC run exhibited even more deviant results. Whereas the symmetric metalloazobenzenophane **215** could be isolated in its expected monomeric form (Figure 94), the desired asymmetric metalloazobenzenophane **216** was isolated in its dimeric form **238** (containing two Fe(II) centers) as it could be proven by the corresponding HR-ESI-MS spectra illustrated in Figure 95, which clearly exhibit the accordant tetracationic peak at $m/z = 570.1787$ and peak of the tricationic trifluoroacetic acid (TFA) adduct at $m/z = 797.9003$. Furthermore, the third expected macrocycle **217** could not be isolated at all. The repeated investigation of the isolated dimeric metalloazobenzenophane **238** via HR-ESI-MS revealed that the dimeric macrocycle **238** forms an isomerization equilibrium with the monomeric metalloazobenzeno-phane **216**. This made a clean NMR-spectroscopic

characterization as well as further optical switching experiments very difficult, which will be addressed in the according chapter 5.3.3.

(a)

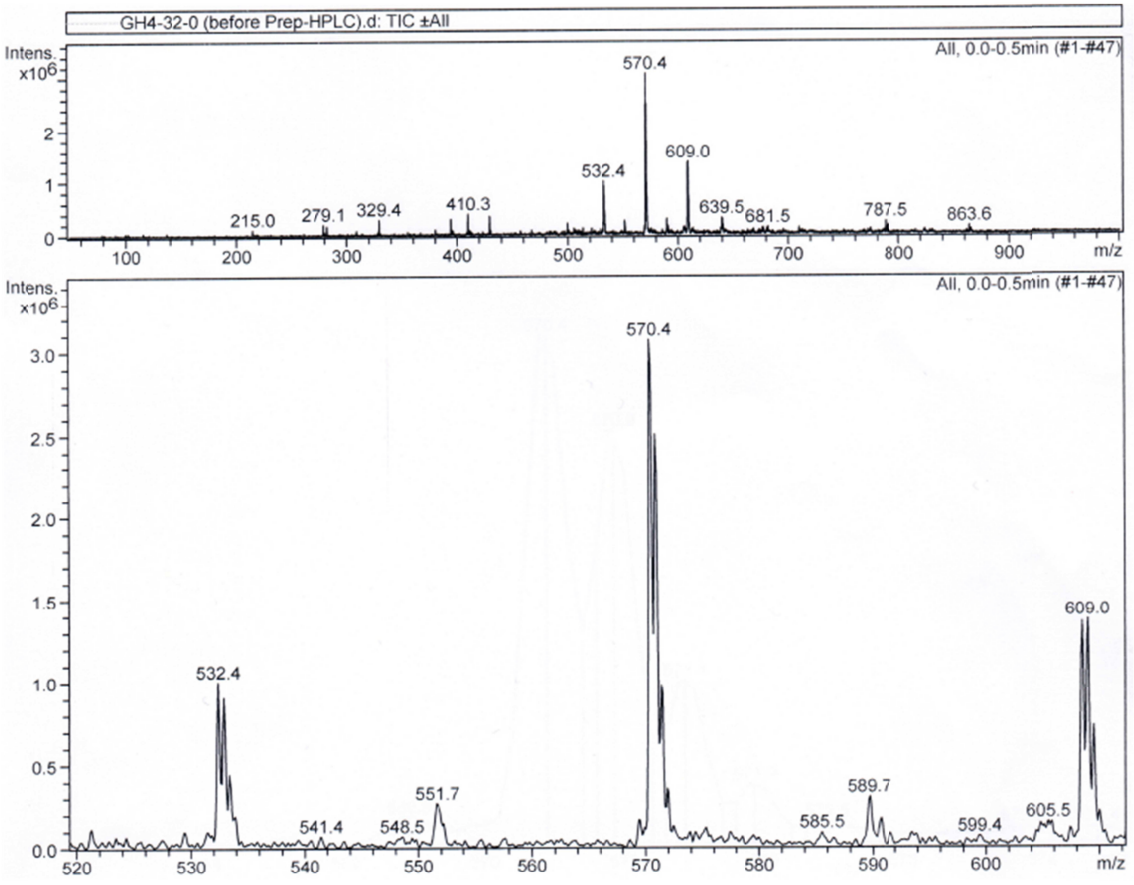

(b)

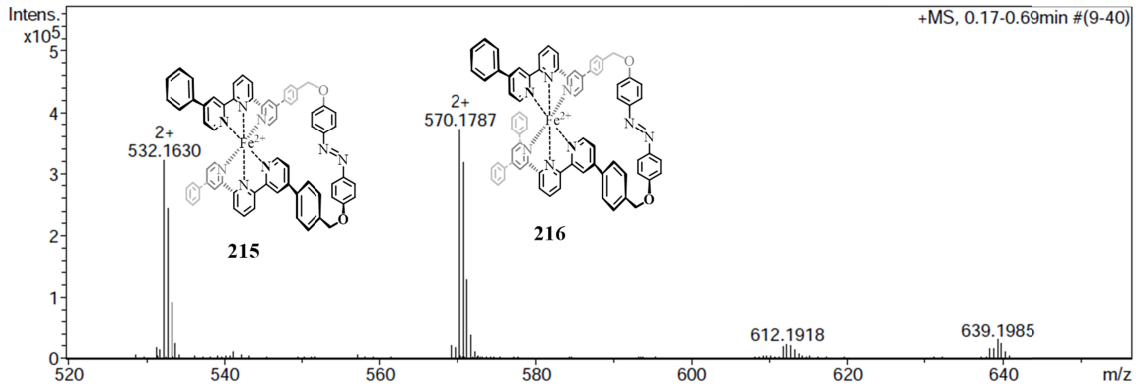

Meas. m/z	#	Formula	Score	m/z	err [mDa]	err [ppm]	mSigma	rdb	e⁻ Conf	N-Rule	z
532.1630	1	C 68 H 48 Fe N 8 O 2	100.00	532.1620	-0.9	-1.8	13.1	49.0	even	ok	2+
570.1787	1	C 74 H 52 Fe N 8 O 2	100.00	570.1777	-1.0	-1.8	7.6	53.0	even	ok	

Figure 93: (a) ESI-MS spectrum exhibiting the expected mixture of the three metalloazobenzenophanes **215**, **216**, and **217** after the complexation of the according three hexadentate bis-tpy azobenzene ligands **218a**, **226**, and **227a**. **(b)** HR-ESI-MS of the crude product only proving the presence of the two macrocycles **215**, and **216**.

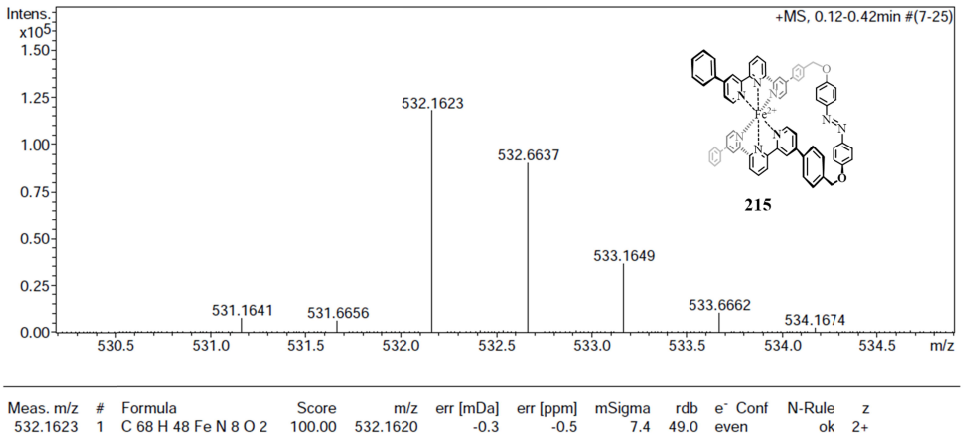

Meas. m/z	#	Formula	Score	m/z	err [mDa]	err [ppm]	mSigma	rdb	e⁻ Conf	N-Rule	z
532.1623	1	C 68 H 48 Fe N 8 O 2	100.00	532.1620	-0.3	-0.5	7.4	49.0	even	ok	2+

Figure 94: HR-ESI-MS of the purified monomeric metalloazobenzenophane **215** isolated after the preparative HPLC purification of the mixture of the macrocycles **215**, **216**, and **217**.

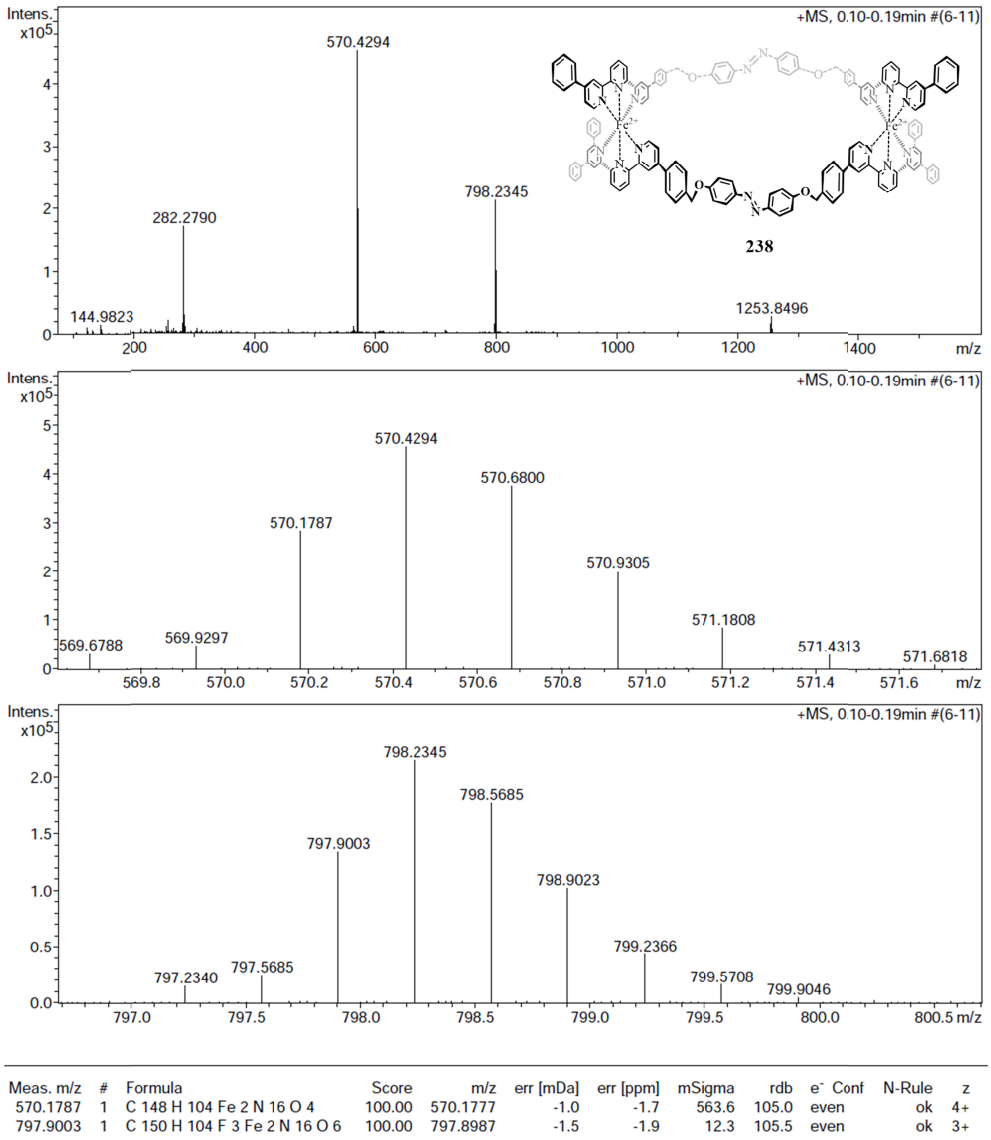

Meas. m/z	#	Formula	Score	m/z	err [mDa]	err [ppm]	mSigma	rdb	e⁻ Conf	N-Rule	z
570.1787	1	C 148 H 104 Fe 2 N 16 O 4	100.00	570.1777	-1.0	-1.7	563.6	105.0	even	ok	4+
797.9003	1	C 150 H 104 F 3 Fe 2 N 16 O 6	100.00	797.8987	-1.5	-1.9	12.3	105.5	even	ok	3+

Figure 95: HR-ESI-MS of the purified dimeric metalloazobenzenophane **238** unexpectedly isolated after the preparative HPLC purification of the mixture of the macrocycles **215**, **216**, and **217**, as clearly proven by the tetracationic peak at *m/z* = 570.1787 and peak of the tricationic TFA-adduct at *m/z* = 797.9003.

The described findings prompted us to attempt another approach for the possible formation of the desired asymmetric metalloazobenzenophane **216** as displayed in Scheme 47, below. In the displayed approach, instead of performing the complexation of the hexadentate bis-tpy azobenzene ligand **226** as the method of choice for the final ring-closing step, the final cyclisation was envisaged to comprise the twofold S_N2 reaction of the previously synthesized heteroleptic Fe(II)-bis(tpy) complex **240** with the accordant 4,4′-dihydroxyazobenzene **219**.

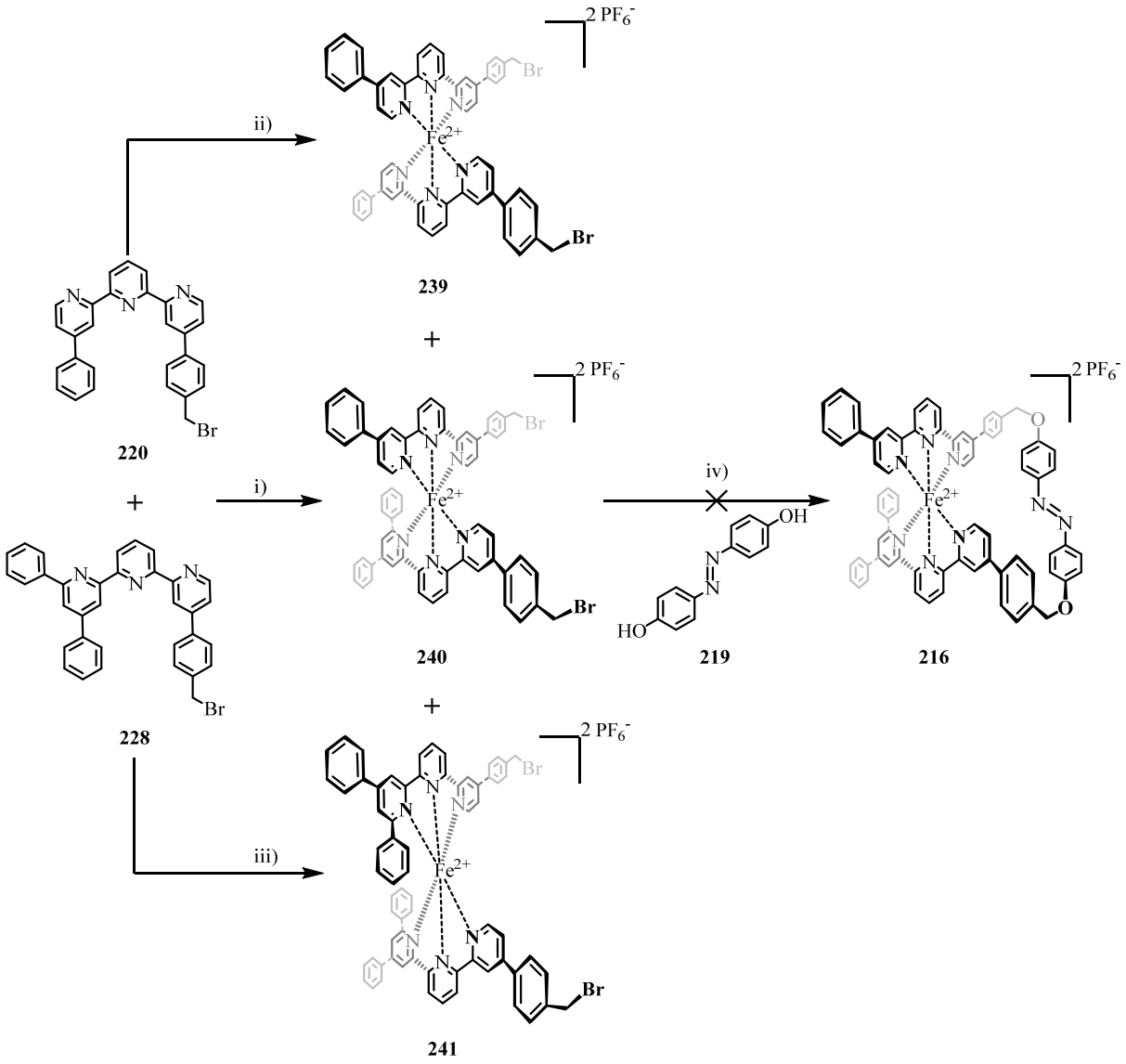

Scheme 47: Overview of alternative synthetic approaches followed for the attempted synthesis of the desired asymmetric iron(II)-bis-(terpyridino)azobenzenocyclophane **216**. Reagents and conditions: **i) 220** (1 eq.), **228** (1 eq), $FeCl_2$ (1 eq.), NH_4PF_6 (50 eq.), MeOH, DCM, H_2O, r.t., 5h; **ii) 220** (2 eq.), $FeCl_2$ (1 eq.), NH_4PF_6 (50 eq.), MeOH, DCM, H_2O, r.t., 5h, quant.; **iii) 228** (2 eq.), $FeCl_2$ (1 eq.), NH_4PF_6 (50 eq.), MeOH, DCM, H_2O, r.t., 5h, quant.; **iv) 219** (1 eq.), **240** (1 eq.), K_2CO_3 (2.6 eq.), acetone, reflux, 24h.

According to the procedures reported for the preparation of heteroleptic Fe(II)-bis(tpy) complexes in previous sections of this work (Chapters 3.3.3.3 and 3.3.3.4) also in this case the two corresponding tpy ligands **220** and **228** were reacted with an equimolar amount of $FeCl_2$ as the Fe(II) source in a solvent mixture of MeOH, DCM, and water to yield the statistical 1:2:1-mixture of the three expectable Fe(II)-bis(tpy) complexes **239**, **240**, and **241**. After purification via preparative reversed-phase HPLC using a solvent gradient ranging from H_2O / MeCN (50:50) up to H_2O / MeCN (25:75) at a flow rate of 20 mL/min the desired pure heteroleptic product **240** was obtained as a dark purple solid in a yield of 20%. Furthermore, the two homoleptic Fe(II)-bis(tpy) complexes **239** and **241** have additionally, been synthesized separately to quantitatively obtain each individual complex from the respective homoleptic complexation reaction. Unfortunately the finally envisaged ring-closing reaction utilizing the twofold S_N2 reaction of the heteroleptic Fe(II)-bis(tpy) complex **240** with 4,4´-dihydroxy-azobenzene **219** did afford neither the desired ring-closed asymmetric metalloazobenzeno-phane **216**, nor the previously observed dimeric macrocycle **238**. This appears especially invidious with regard to the NMR-spectroscopic observations which have been made on the complexes **239**, **240**, and **241**. Although the results are discussed in a more detailed form in chapter 5.4.2, the major findings are, that the Fe(II)-complexes **239** and **240** exhibit the regular diamagnetic NMR-spectra, which can be related to the presence of a LS state at the respective Fe(II) cores, whereas for the Fe(II)-complex **241**, surprisingly, a strongly paramagnetic NMR-spectrum, corresponding to the presence of a HS-state at the Fe(II) core ion, has been found. This finding, that the heteroleptic complex **240**, containing one sterically more hindered tpy ligand **228** still resides in the LS state, whereas the complex **241**, comprising two of those hindered tpy ligands **228**, resides in the HS state, proposes, that the Fe(II) core in complex **240**, with its given coordination sphere, is most likely at the edge of a SCO between a LS and the HS state. This would fit quite well to the envisaged optical triggering of the Fe(II) ion's spin state switching in the final metalloazobenzenophane **216** and thus underlines the appropriate direction of the present investigations. In order to validate the correctness of the described observations the similar, slightly modified homoleptic Fe(II)-bis(tpy) complex **242** was synthesized, which comprises two equivalents of the tpy ligand **229** (Scheme 48). As it was expected also **242** exhibited paramagnetic behavior documenting the presence of an Fe(II) core ion in its HS state.

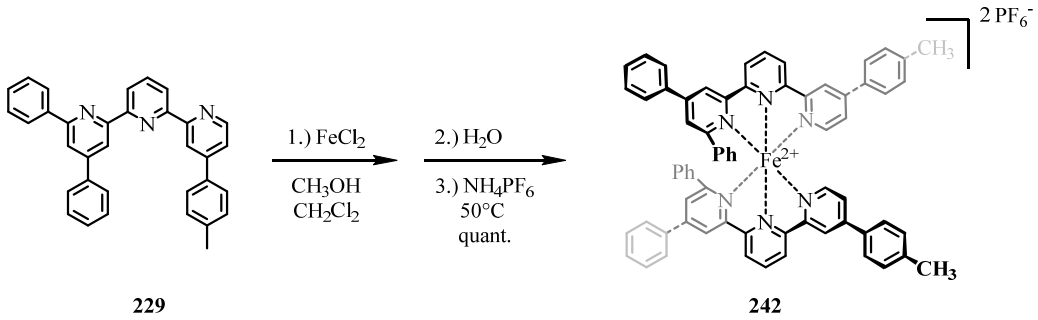

229 242

Scheme 48: Synthesis of the paramagnetic Fe(II)-based HS reference complex **242**.

5.3.3 Miscellaneous Synthetic Pathways

In this chapter a brief overview is given about miscellaneous synthetic pathways followed during the attempted assembly of several metalloazobenzenophanes. At first Scheme 49 displays two alternative routes attempted towards the assembly of macrocycle **215**.

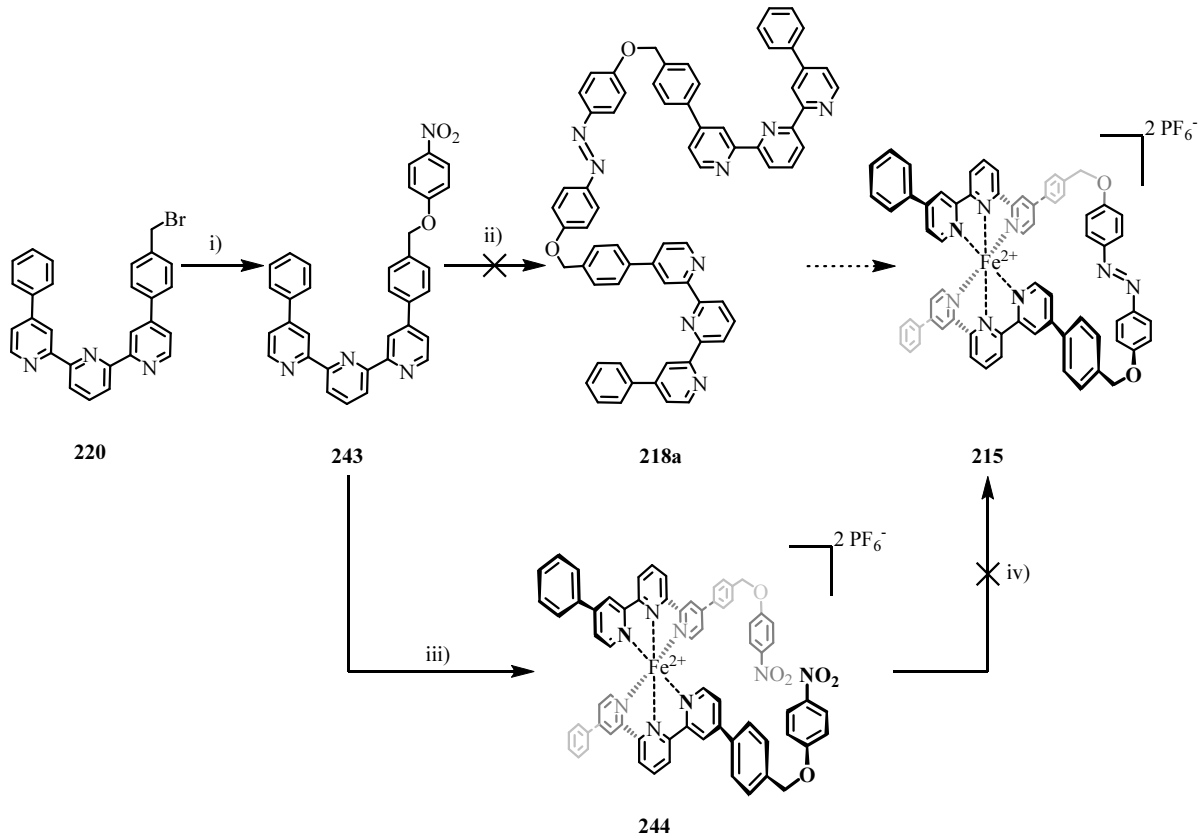

220 243 218a 215 244

Scheme 49: Alternative, unsuccessful synthetic route towards the metalloazobenzenophane **215**. Reagents and conditions: **i) 220** (1 eq.), 4-nitrophenol (1 eq.), K_2CO_3 (2.6 eq.), acetone, reflux, 24h, 98%; **ii) 223**, $LiAlH_4$, THF, r.t., 5h; **iii) 243** (2 eq.), $FeCl_2$ (1 eq.), NH_4PF_6, MeOH, DCM, H_2O, 50 °C, 4h, quant.; **iv) 244**, $LiAlH_4$, THF, r.t., 5h.

Based on the bromo-benzyl precursor **220**, whose synthesis was described in the previous chapter, the assembly of **215** was envisaged via the intermediary building block 4-(4-((4-nitrophenoxy)methyl)phenyl)-4''-phenyl-2,2':6',2''-terpyridine (**243**), which was successfully obtained via the S_N2 reaction of benzyl bromide **220** with 4-nitrophenol, yielding the desired intermediate **243** in 98% yield. However the attempted reductive azocoupling of two equivalents of **243**, which was meant to afford the hexadentate bis-tpy azobenzene precursor **218a** failed, thus preventing any further proceeding towards the desired target structure **215**. The second pathway, followed the strategy to perform the complexation in the second-last step. Therefore the tpy intermediate **243** was successfully transformed to the homo-leptic Fe(II)-bis(tpy) complex **244** in quantitative yield following the previously reported strategy. Since the Fe(II) complex **244** comprises two nitro-groups, a reductive azocoupling as the reaction of choice for the final macrocyclization step appeared feasible. However, also in this case the envisaged macrocyclization strategy, utilizing $LiAlH_4$ as the reducing agent, failed, which gave rise to the investigation of other routes, such as the finally successful one described in chapter 5.3.1.

The second alternative, but also unsuccessful synthetic route (Scheme 50), aimed at the synthesis of the symmetric metalloazobenzenophane **250**, which is shortened by the two ether-linkages in its molecular backbone, if compared to the macrocycle **215**. In detail, in a first reaction step 1-bromo-4-(4-nitrobenzyl)benzene (**246**) was prepared from 4-bromobenzyl bromide (**245**) and 4-nitrophenylboronic acid following a literature-inspired Suzuki-Miyaura cross-coupling procedure,[555,560] to yield the desired intermediate **246** in yield of 32%. In adaptation of a literature protocol[561] the subsequent Miyaura borylation reaction of bromide **246** utilizing bis(pinacolato)diboron ($(Bpin)_2$) resulted in the quantitative formation of the desired borylation agent **247**. In the following step, the according Suzuki-Miyaura coupling reaction of the borylation agent **247** with the previously described monofunctionalized tpy building block **212**, utilizing the established reaction conditions, namely, using K_2CO_3 as the base and $PdCl_2\{P^tBu_2(p\text{-}NMe_2\text{-}Ph)\}_2$ as the catalyst in a mixture of toluene and water, resulted in the formation of the envisaged tpy key building block **248** in a very good yield of 91%. The same compound **248** was also synthesized on another route, by the Suzuki coupling of benzyl-bromo tpy precursor **220** with 4-nitrophenyl-boronic acid using the same catalytic system as described above. However on this route the desired intermediate **248** could only be afforded in a comparatively low yield of 28%. The next step on the synthetic pathway to the envisaged symmetric metalloazo-benzenophane **250** was the formation of the hexadentate bis-tpy azobenzene precursor **249**, which was repeatedly tried using reductive azocoupling

conditions, in order to convert two equivalents of the nitro compound **248** into the desired intermediate **249**. However all attempts to successfully assemble compound **249** failed, which prevented a progress to the final macrocycle **250**.

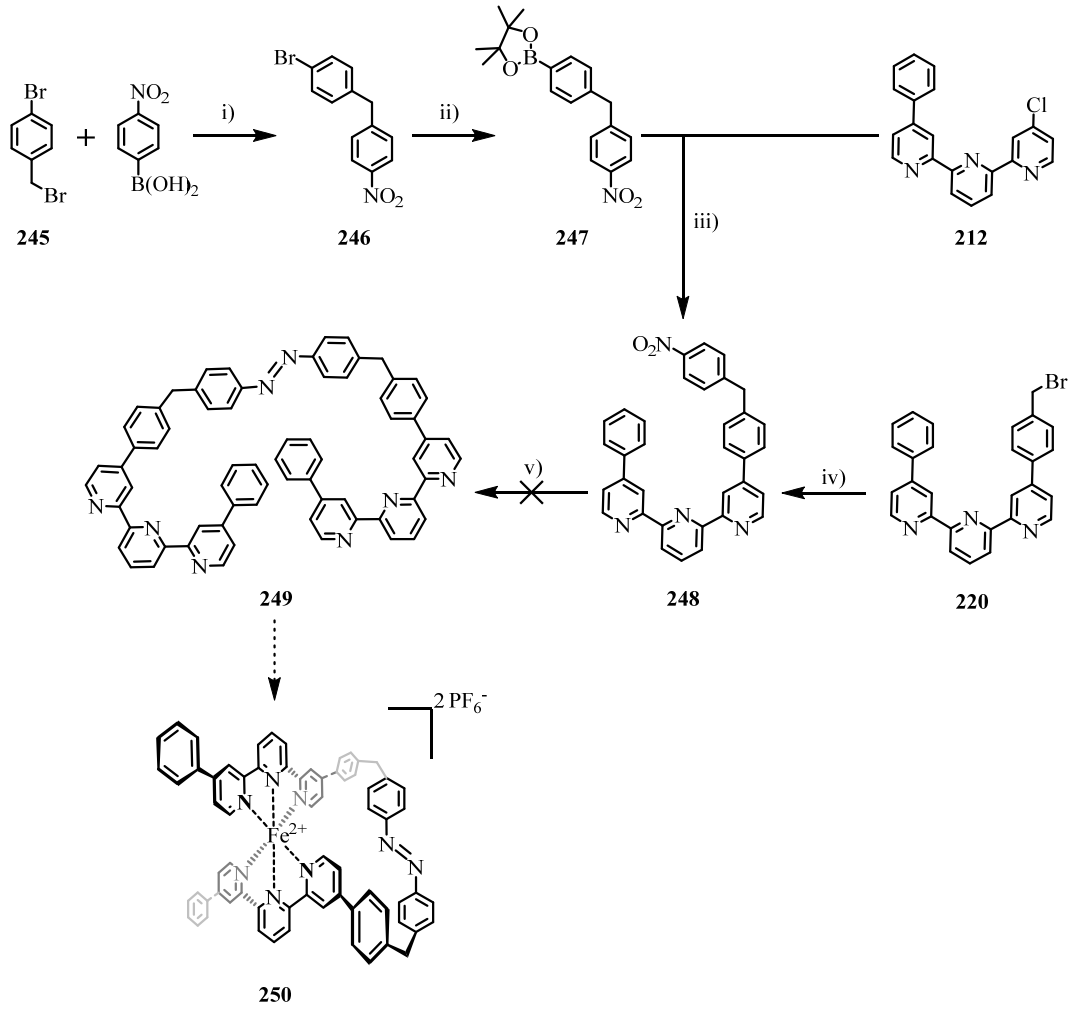

Scheme 50: Envisaged, but unsuccessful synthetic route towards metalloazobenzenophane **250**. Reagents and conditions: **i) 245** (1 eq.), 4-nitrophenylboronic acid (1 eq.), Na_2CO_3, $Pd(PPh_3)_4$, toluene, EtOH, H_2O, 80 °C, 16h, 32%; **ii) 246** (1 eq.), bis(pinacolato)diboron ($(Bpin)_2$) (1.1 eq.), KOAc, $Pd(dppf)Cl_2$, dimethylformamide (DMF), 100 °C, 2h, quant.; **iii) 212** (1 eq.), **247** (5 eq.), $PdCl_2[P^tBu_2(p\text{-}NMe_2\text{-}Ph)]_2$, K_2CO_3, toluene/H_2O (5:1), 125 °C, 24h, 91%; **iv) 220** (1 eq.), 4-nitrophenylboronic acid (10 eq.), $PdCl_2[P^tBu_2(p\text{-}NMe_2\text{-}Ph)]_2$, K_2CO_3, toluene/H_2O (5:1), 125 °C, 24h, 28%; **v) 248**, $LiAlH_4$, THF, r.t., 5h.

5.4 Physical Characterization

Following the discussion of the synthetic access of the macrocycle **215**, representing one of the desired optically addressable, potentially spin-switching metalloazobenzenophanes, as well as after the description of the assembly of several other Fe(II)-based complexes, hereafter, the corresponding physical results are highlighted, whereat the discussion of the optical properties is followed by a detailed description of the performed NMR-spectroscopic investigations.

5.4.1 Optical Investigation of Terpyridine Complexes

As for the optical spectra discussed in the chapters 3.4.2 and 4.4.1 the UV/vis spectra of the metalloazobenzenophane **215**, as well as of the Fe(II)-based bis(tpy) complexes **240 - 242**, and **244** were recorded at varying concentrations (0.001 mM, 0,0025 mM, 0.005 mM, 0.01 mM, 0.025 mM, and 0.05 mM, respectively) in acetonitrile at room temperature (r.t.) and their averaged absorbances were converted into the corresponding extinction coefficients ε which are plotted against the respective wavelengths λ. Figure 96 and Table 8 display the corresponding data for the four Fe(II)-based bis(tpy) complex **240 – 242**, and **244**.

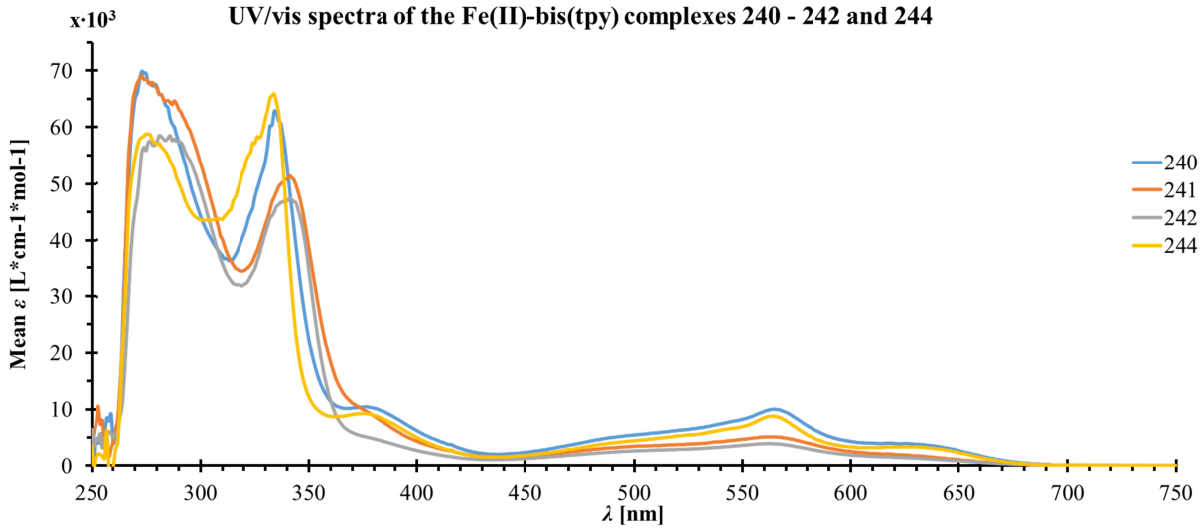

Figure 96: Comparative illustration of the UV/vis absorption spectra of the Fe(II)-bis(tpy) complexes **240 – 242**, and **244**.

Table 8: Characteristic bands in the UV/vis spectra of the Fe(II)-bis(tpy) complexes **240 – 242**, and **244**.

Complex	λ_{max} (LC/MC) [nm]	ε [L*cm^{-1}*mol^{-1}]	λ_{max}(MLCT) [nm]	ε [L*cm^{-1}*mol^{-1}]
188[544]	318	38 000	552	11 900
240	275	69 550	564	9 990
	334	62 840		
	376	10 440		
241	273	69 155	563	5 115
	341	51 325		
242	286	58 490	563	3 920
	341	47 340		
244	275	58 775	564	8 790
	334	65 845		
	375	9 245		

Analogously to the findings discussed previously (Chapters 3.4.2 and 4.4.1) rather distinct bathochromic shifts of the MLCT-bands were observed in the optical spectra of the Fe(II)-based complexes **240 – 242**, and **244** compared to parent complex $[Fe(tpy)_2]^{2+}$ **188**,[543] which, in accordance to the earlier described findings and postulations, can be deduced from the stabilization of the ligand-based LUMO π*-orbitals for the described enlarged conjugated π-systems of the accordant incorporated tpy ligands. It can be summarized, that the overall shifts of the LC-, the MC-, and the MLCT-bands lie in a very comparable range for all four discussed complexes, if related to the parent complex **188**. However it is worth noticing, that the intensities of the MLCT-bands, and thus the corresponding extinction coefficients ε resulting thereof, differ significantly from the diamagnetic, LS complexes **240** and **244**, to the paramagnetic, HS complexes **241** and **242**, being much more pronounced for the LS complexes, than for the two HS species. In contrast to this the corresponding extinction coefficients ε of the LC-bands are comparably strong for all four complexes. These findings underline the fact, that especially the Fe-N bond lengths, and hence the whole Fe-N bond character, represent the most strongly affected factor upon the transition of the coordinative environment of an Fe(II) LS-complex (**240** or **244**) towards the environment of an Fe(II) HS-complex (**241** or **242**).

If compared to the UV/vis spectra obtained for the open Fe(II)-based bis(tpy) complexes discussed above, the corresponding optical spectrum acquired for the symmetric metalloazo-benzenophane **215** (Figure 97) differs significantly from the former ones. An overview of the wavelengths λ of the most prominent absorption bands in the UV/vis-spectrum of **215**, together with their corresponding extinction coefficients ε is displayed in Table 9.

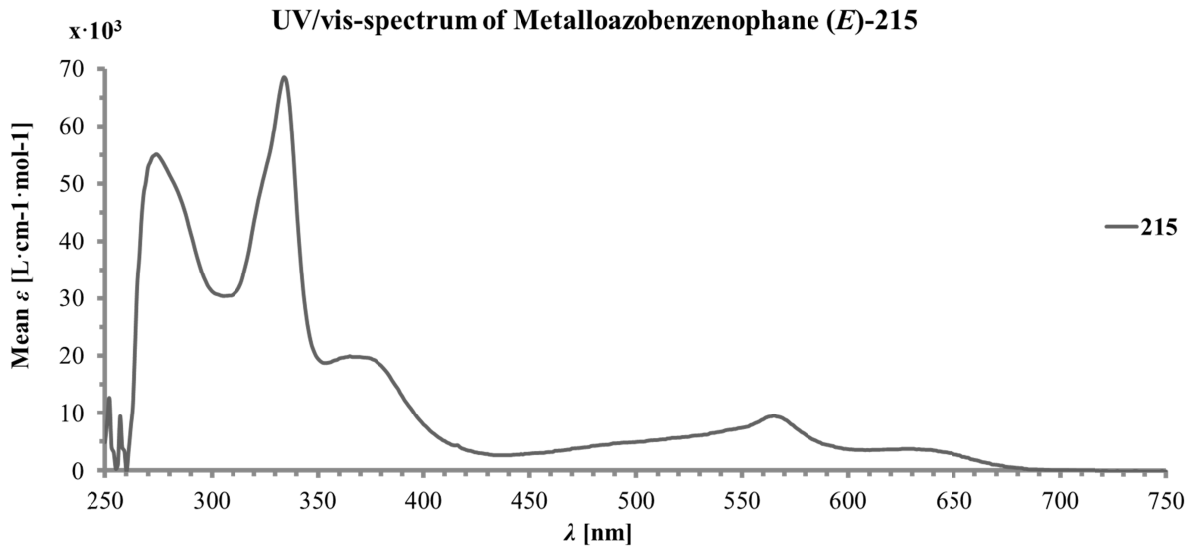

Figure 97: Depiction of the UV/vis absorption spectrum of metalloazobenzenophane **215.**

Table 9: Characteristic bands in the UV/vis spectrum of metalloazobenzenophane **215**.

λ_{max} [nm]	ε [L*cm^{-1}*mol^{-1}]	Type of absorption band
274	55 135	LC – band (either π*←π or π*←n transition)
334	68 595	LC – band (either π*←π or π*←n transition)
365	19 960	*E*→Z photoisomerization of azo moiety (π*←π transition)
565	9 530	MLCT - band (π*←3dπ–transition)

When the obtained results for the metalloazobenzenophane **215** are related to the most comparable open Fe(II)-bis(tpy) complex **244**, which solely lacks the ring-closure of the two present nitro-groups to yield the azo-motif present in the macrocycle **215**, several striking similarities can be observed. On the one hand the higher energetic bands in the UV region of the spectrum, which can be attributed to the LC bands of the complexes, arising either from a π* ← π or a π* ← n transition, are very similar for the open **244** and for the macrocyclic complex **215**. Furthermore, also the MLCT-bands arising from a π* ← 3dπ-transition are very similar for both optical spectra. The biggest difference between the UV/vis spectra of both compounds can be found in the weaker UV region, which exhibits a rather weak metal-centered (MC) electronic transition band with a $\lambda_{max.}$ = 375 nm (ε = 9245 L*cm^{-1}*mol^{-1}) for the open complex **244** in the named region, whereas for the macrocycle **215** a much more intense, and slightly higher energetic band with a $\lambda_{max.}$ = 365 nm (ε = 19960 L*cm^{-1}*mol^{-1}) can be found. The very broad shape, together with the higher intensity of the named π* ← π transition band, which is correlated to the *E* → Z photoisomerization of the azo moiety of macrocycle **215**, explains the superposition of the much less intense MC transition, being probably hidden underneath the pronounced *E* → Z photoisomerization band.

The irradiation of the thermodynamically favored *trans*-isomer (*E*)-**215** of the named metalloazobenzenophane with UV light of the appropriate wavelength, corresponding to the observed π*←π transition band, namely, at λ = 365 nm, resulted in the expected (*E*) → (*Z*) photoisomerization of (*E*)-**215** to (*Z*)-**215**. Figure 98 displays the thermal decay of (*Z*)-**215**, which is equivalent to the back isomerization of (*Z*)-**215** to (*E*)-**215**. However, since the π* ← π transition band correlated to the *E* → Z photoisomerization of the azo moiety of the macrocycle **215** and the complex' metal-centered transition band are partially superposed it is not possible to determine the relative *E* : *Z*-ratio at the photostationary state (PSS) from the present optical spectra. Thus, in order to obtain further insights about this question, extended NMR-spectroscopic isomerization studies have been performed, which are discussed in the following chapter 5.4.2. Nevertheless it can be seen, that after 90 min the *cis*-isomer (*Z*)-**215** seems to be fully converted back to the *trans*-isomer (*E*)-**215**.

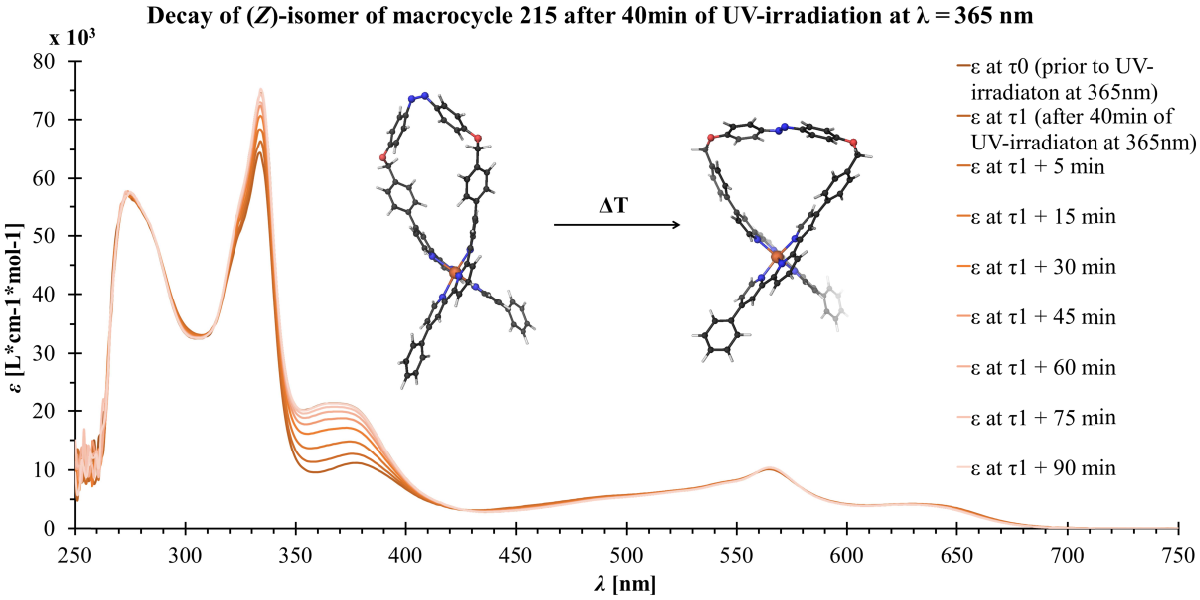

Figure 98: Depiction of the absorption spectra of metalloazobenzenophane **215** prior (τ_0) and after 40 min of UV irradiation (τ_1) at λ = 365 nm. Furthermore, the thermal decay of (*Z*)-**215** equivalent to the (*Z*) → (*E*)-back-isomerization is illustrated.

5.4.2 NMR Experiments

In this chapter predominantly the results of the NMR-spectroscopic experiments performed on metalloazobenzenophane **215** are discussed. The named macrocycle was irradiated with UV light of the appropriate wavelength ($\lambda = 365$ nm), corresponding to the absorption maximum of the accordant $\pi^* \leftarrow \pi$ transition band observed in the UV/vis spectrum of (*E*)-**215**. This UV irradiation lead to the expected (*E*) → (*Z*) photoisomerization of (*E*)-**215** to (*Z*)-**215**. The main motivation of the present experiments now was:

(1) the elucidation of the extent, to which the (*E*) → (*Z*) photoisomerization of the metalloazobenzenophane **215** occurs, and
(2) the investigation of the thermal (*Z*) → (*E*) back-isomerization of **215** revealing the stability and the temperature dependant isomerization behavior of the (*Z*)-isomer.

All the present switching experiments on metalloazobenzenophane **215** were performed using a monochromator to select the appropriate wavelengths of the irradiated light. Herewith the according NMR sample could be measured immediately after the UV irradiation, by directly linking the monochromator to the probe head of the NMR spectrometer with the help of an optical fiber and irradiating the sample within the spectrometer. A schematic illustration of the measurements' experimental setup is illustrated in Figure 99 below.

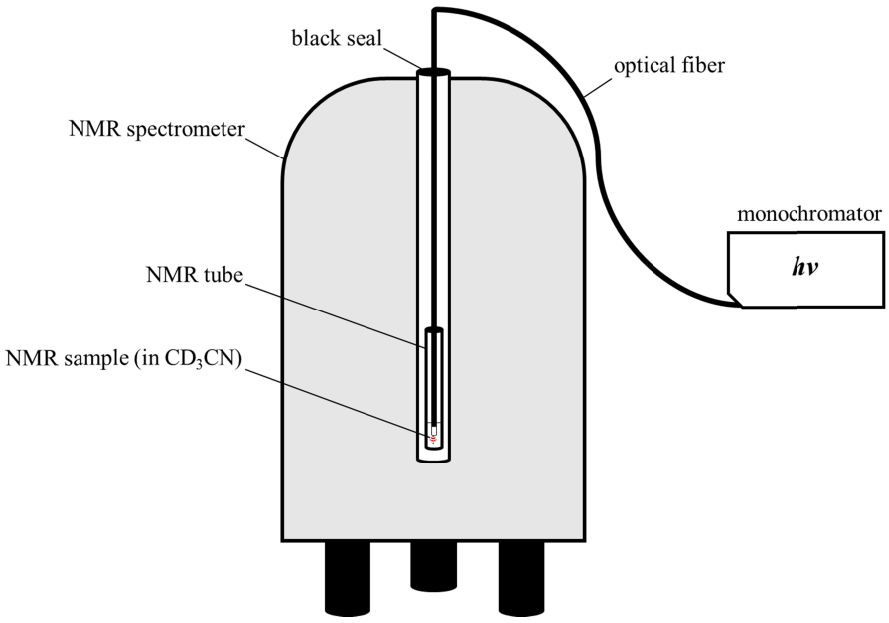

Figure 99: Schematic illustration of the experimental setup for the investigation of the photoinduced (*E*) → (*Z*) isomerization process of the metalloazobenzenophane **215** by implementation of the light source into the NMR-spectrometer.

Before the temperature-dependence of the thermal back-isomerization of the (*Z*)-isomer of metalloazobenzenophane **215** is described, at first the ^{1}H-NMR spectra of the pure (*E*)-isomer of **215** and the one obtained for the PSS of the (*E*) → (*Z*) photoisomerization after 30 min of irradiation at λ = 365 nm is displayed (Figure 100). The according 2D-NMR spectra, such as ^{1}H,^{1}H-COSY, ^{1}H,^{13}C-HMQC, ^{1}H,^{13}C-HSQC and ^{1}H,^{13}C-HMBC spectra, which were used for the unambiguous assignment of the listed ^{1}H-NMR-signals of **215** are displayed in the according chapter 9.1.1 of the appendix.

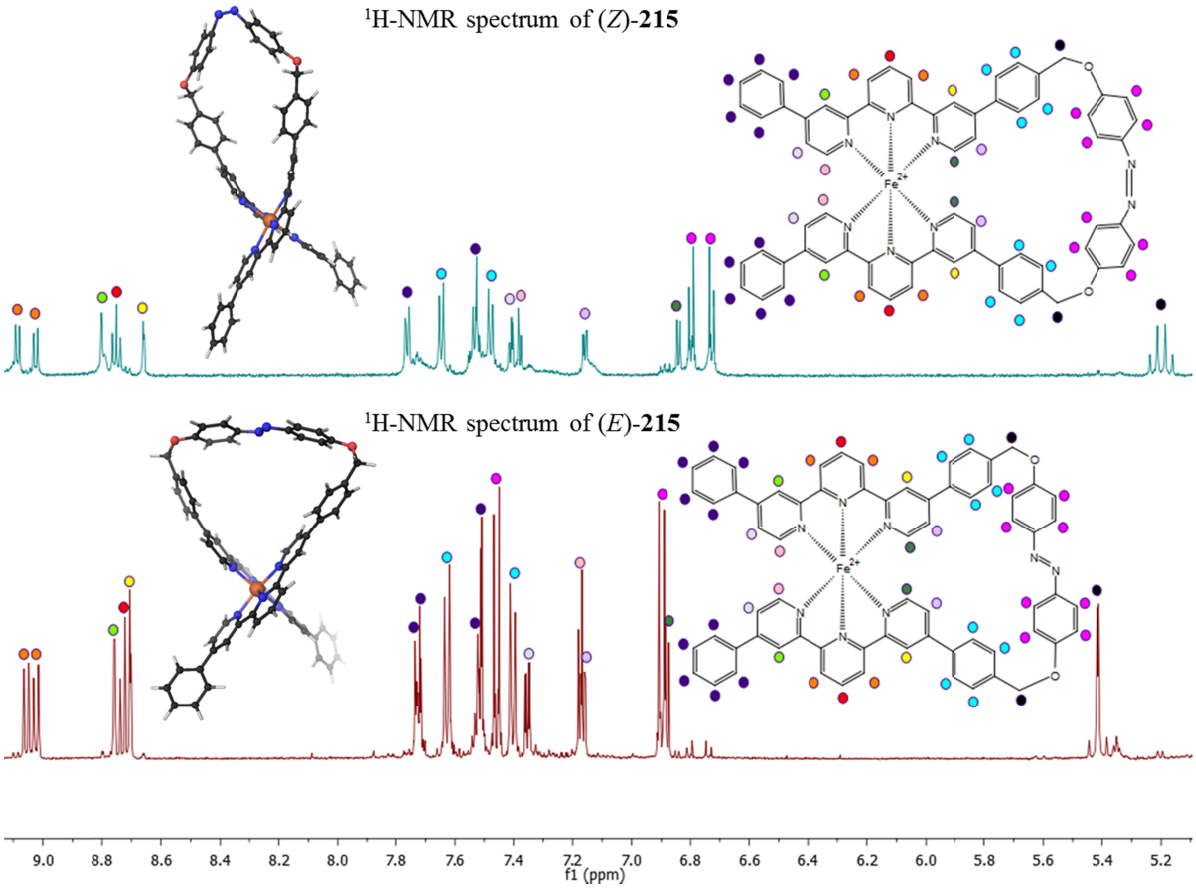

Figure 100: Depiction of the fully assigned NMR-spectra of (*E*)-**215** prior to the UV irradiation at λ = 365 nm (lower spectrum), and of (*Z*)-**215** immediately after the 30 min of UV irradiation (upper spectrum)

It was found, that the PSS state, which is reached by the UV irradiation of (*E*)-**215** at the accordant $\pi^* \leftarrow \pi$ transition band corresponding to the azo moiety, yielded the pure *cis*-isomer (*Z*)-**215**, as displayed above (Figure 100 - upper spectrum), permitting an unambiguous assignment of the NMR spectra of both isomers via the appropriate 2D-NMR spectra. After the efficiency of the (*E*) → (*Z*) photoisomerization of metalloazobenzenophane **215** has been elucidated, the temperature-dependence of the thermal (*Z*)-**215** → (*E*)-**215** back-isomerization (Figure 101) was investigated next.

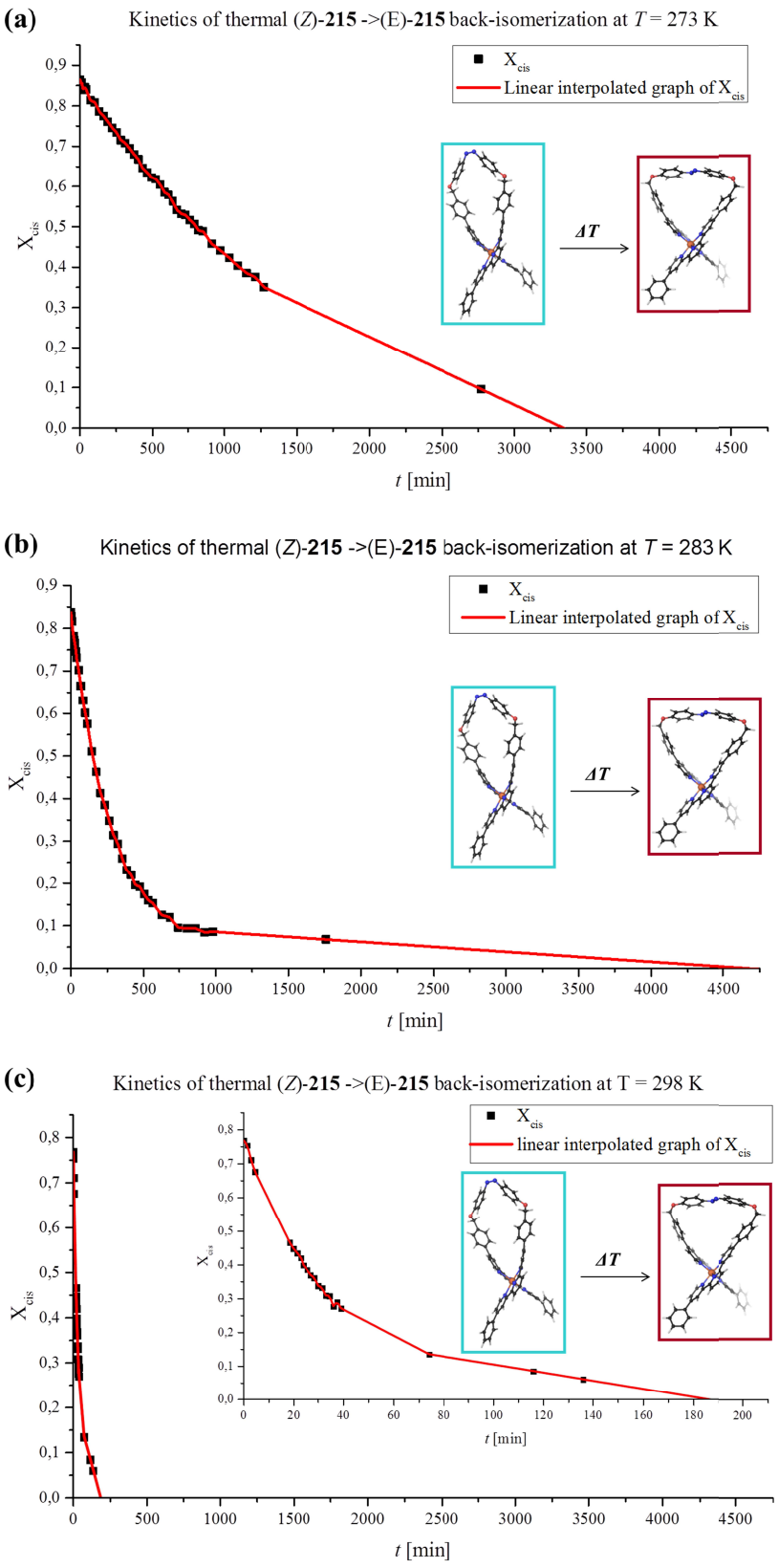

Figure 101: Depiction of the thermal (*Z*)-**215** →(*E*)-**215** back-isomerization at three different temperatures: **(a)** $T = 273$ K, **(b)** $T = 283$ K, **(c)** $T = 298$ K. The decay of (*Z*)**-215** was probed by recording a sufficiently big number of data points (30 - 60) (indicated with black squares) at each temperature, which were obtained from ^{1}H-NMR spectroscopy, and applying a linear interpolation on the graph (red line) using Origin®. All ^{1}H-NMR spectra were recorded in CD_3CN.

From the plots of the decreasing molar fractions of (*Z*)-**215** versus time (X_{cis}/t - plot), which are illustrated in Figure 101 above, a clear tendency can be seen. Whereas at $T = 273$ K the half-life time of (*Z*)-**215** is approximately $\tau_{1/2} \approx 1030$ min, at $T = 283$ K the half-life time of (*Z*)-**215** is decreased to $\tau_{1/2} \approx 213$ min, and at $T = 298$ K the half-life time of (*Z*)-**215** is reduced further to a value of $\tau_{1/2} \approx 29.5$ min. Following the overall tendency it becomes visible that for every 10 °C difference in temperature the half-life time $\tau_{1/2}$ of the (*Z*)-**215** isomer is reduced by a factor of around five. This linear temperature-dependence of the thermal (*Z*)-**215** → (*E*)-**215** back-isomerization rate strongly resembles an Arrhenius-like behavior, which however requires further statistical validation and the verification of the hypothesis at other temperatures, to be further underlined.

After all, from the present NMR spectroscopic investigations of **215**, several interesting findings can be reported:

(1) By UV light irradiation at $\lambda = 365$ nm an unexpected full (*E*)-**215** → (*Z*)-**215** photoisomerization can be observed.
(2) Both isomers, (*E*)-**215** and (*Z*)-**215**, alike, exhibit fully diamagnetic ^{1}H-NMR spectra leading to the conclusion, that the Fe(II) cores of both isomers are present in their diamagnetic LS state.
(3) The reaction rate of thermal (*Z*)-**215** → (*E*)-**215** back-isomerization shows a clear temperature-dependence, strongly resembling the linear dependencies found for an Arrhenius-like behavior.

In addition to the NMR-spectroscopic investigations of metalloazobenzenophane **215** in the range of the synthetic pathways towards the monomeric metalloazobenzenophanes **216**, and **217** or towards the dimeric macrocycle **238**, respectively, two homoleptic Fe(II)-bis(tpy) complexes, exhibiting paramagnetic behavior during the NMR spectroscopic characterization, have been revealed. Of the named paramagnetic complexes **241**, and **242** only the ^{1}H-NMR spectrum of the latter one shall be displayed hereafter, (Figure 102). The ^{1}H-NMR signals exhibited in the ^{1}H-NMR spectrum of the prior complex **241** are listed in a comparative overview to the values obtained for complex **242** within Table 10, below. All the values observed for ^{1}H-NMR signals of the two discussed paramagnetic complexes **241** and **242**, strongly resemble those previously described in literature for comparable Fe(II)-bis(tpy) HS complexes.[557] The only two ^{1}H-NMR signals, which are recognizably different between both

complexes **241** and **242** are those corresponding to the CH_3-groups of **242** and the ones arising from the CH_2Br-groups within complex **241** (Table 10- marked in red).

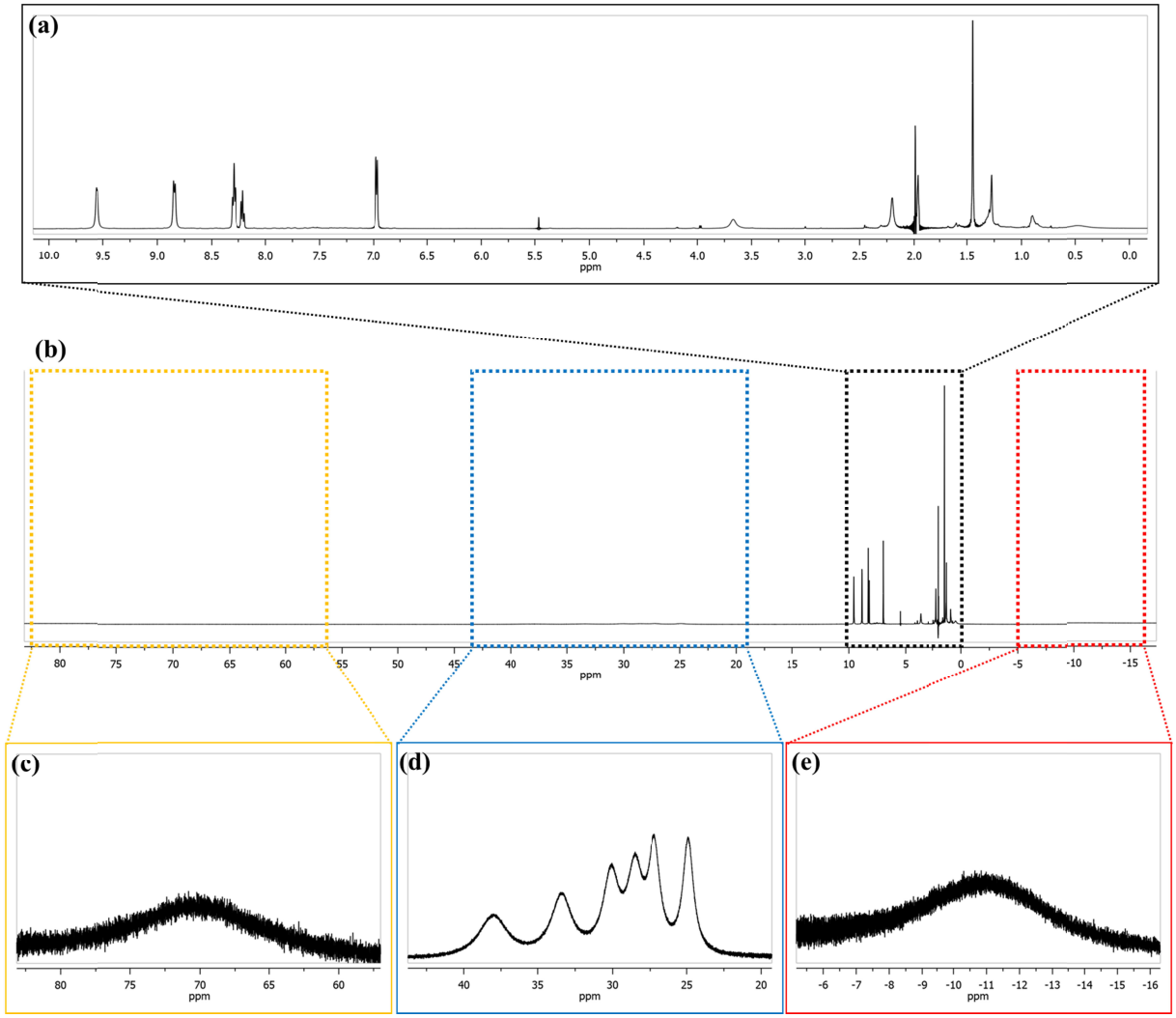

Figure 102: Paramagnetic ^{1}H-NMR spectrum of Fe(II)-bis(tpy) complex **242**. **(b)** Depiction of the total ^{1}H-NMR spectrum from -17 ppm up to +83 ppm recorded in CD_3CN. **(a)** Extract of the ^{1}H-NMR spectrum from 0 to +10 ppm. **(c)** Extract of the highest downfield region of the ^{1}H-NMR spectrum from 57 to 83 ppm. **(d)** Extract of the downfield region of the ^{1}H-NMR spectrum from 20 to 43 ppm. **(e)** Extract of the upfield region of the ^{1}H-NMR spectrum from -16 to -5 ppm.

Table 10: ^{1}H-NMR spectroscopic chemical shift data (500 MHz, 298 K) for the CD_3CN solutions of the paramagnetic Fe(II)-bis(tpy) complexes **241** and **242**.

Complex	Chemical shift δ_H of according ^{1}H-NMR signals [ppm]
241	74, 39.2, 34.1, 30.9, 29.0, 27.2, 25.1, 9.57, 8.90, 8.30, 8.18, 7.09, 4.12, 3.52, 0.29, -12.0
242	70, 38.0, 33.4, 30.0, 28.5, 27.2, 24.9, 9.53 8.82, 8.27, 8.19, 6.94, 3.64, 1.42, 0.45, -10.9

5.5 Conclusion and Outlook

Whereas the herein, reported assembly route of the targeted azobenzenophane **215** relies on the same modularly applicable key building block **47** as the ones described in the previous chapters 3.5 and 4.5, the target structures **216** and **238**, respectively, were assembled following a different route utilizing a Kröhnke-type strategy for the formation of the tpy core unit. Taking the statistical nature of the intermediate Suzuki-Miyaura cross-coupling reactions into account, both final compounds **215** and **216** could by assembled in high yields.

In the range of this fourth and last main project of the present thesis a switching concept addressing the coordination sphere dependent spin state of a hexa-coordinated Fe(II) ion incorporated into a metalloazobenzenophane was aimed for. However, this goal could only be partially fulfilled. Although the target structures **215** and **216**, each containing a hexa-coordinate Fe(II) ion incorporated into a macrocyclic structure bearing a photo-sensitive azo moiety in the molecular backbone, were successfully assembled, the envisaged SCO phenomena could not be observed. Interestingly, the metalloazobenzenophane **215**, which was extensively studied via UV/vis- and NMR spectroscopic techniques, revealed a complete (*E*) → (*Z*) photoisomerization of **215**, which however did not result in a sufficient alteration of the coordination sphere of the Fe(II) core ion to evoke a SCO of the diamagnetic LS complex to the desired paramagnetic HS form. This fact was proven without doubt, since both, the (*E*)- and the (*Z*)-isomer of the symmetric metalloazobenzenophane **215** alike, exhibit clearly diamagnetic ^{1}H-NMR spectra. The second target compound, the asymmetric azobenzenophane **216** was found to be in equilibrium with its dimeric form **238** containing two Fe(II) cores instead of the one Fe(II) core present in **216**.

Furthermore, the two paramagnetic homoleptic Fe(II)-bis(tpy) complexes **241** and **242** have been synthesized. These clearly show, that the overall structural concept of the designed complexes is relatively close to the one, which should be required to form a system exhibiting both optical addressability as well as potential SCO properties. To allow a successful realization of the envisaged switching concept in the future very subtle changes to the envisaged molecular structures might already be enough to trigger a sufficiently strong deformation of the Fe(II) core ion's coordinative environment.

6 Summary and Outlook

This present PhD thesis was purposive to the design and development of an innovative synthetic approach towards the terpyridine (tpy) motif. Tpys represent one of the most prominent and most versatile classes of chelating ligands with manifold applications in the fields of metalorganic and coordination chemistry, supramolecular chemistry, polymer science, optoelectronics, and nanotechnology. Furthermore, this work aimed at the development of novel functional materials, mainly targeted for an application in the fields of material science and molecular electronics. The main focus of this work was the design and synthesis of suitable tailor-made target compounds to allow the comprehensive investigation and application of a variety of different stimuli, likewise, aiming at a novel single molecular switching concept, which relies on the coordination sphere dependent spin state switching of hexa-coordinate Fe(II)-bis(tpy) complexes, commonly referred to as spin crossover. Herein, it was demonstrated, that by the specifically tailor-made design of the corresponding target compounds, these can be addressable by very different external impulses, such as an alteration of the applied electrical fields, the mechanical distortion of the target structures, or the optical addressability of functional subgroups within the molecular backbone of the target compounds. All these external stimuli were shown to result in the very same output of a geometrical distortion of the coordination sphere of the central Fe(II) core ion as the basis of the envisaged and observed spin crossover phenomena. Without any doubt it was inevitable to conscientiously investigate the fundamental aspects of the single molecular spin switching entities, representing the core of the present thesis. Only by the interplay of tailor-made molecular design, chemical synthesis, and preliminary physical-chemical investigations, marking the main focus of the present thesis from the chemist's point of view, together with specialists' expertise in the range of sophisticated physical experiments, allowed a profound understanding of the observed phenomena described herein.

In the first main project of this thesis the objective was to investigate the voltage-driven single molecular spin switching phenomena of a variety of heteroleptic Fe(II)-bis(tpy) complexes, containing a neutral ligand destined for the immobilization of the complex within a mechanically controllable break junction (MCBJ) setup and a second, dipolar tpy ligand designated to effectuate the desired bias-sensitivity of the system due to an intrinsic dipole moment arising from the incorporation of an electron-withdrawing (EWG) and an electron-

donating (EDG) end group into this push/pull ligand. To guarantee electronic transport through the central Fe(II) ion, the utilized tpy ligands, representing integral building blocks of the overall target structures, were required to exhibit a rarely reported tailor-made 4,4´´-disubstitution pattern at the tpy core moiety. Hence the first task, as the common basis for all further projects discussed hereafter, was the assembly of this 4,4´´-disubstituted tpy core subunit, in order to allow a modular approach towards all further target compounds, requiring molecular conductance measurements through a central Fe(II) core ion. In this context, for the first time, a Suzuki-Miyaura cross-coupling approach could be utilized to assemble the desired, highly modularly applicable tpy key building block **47** (Scheme 51) as the starting material for most of the further synthetic pathways described throughout this work.

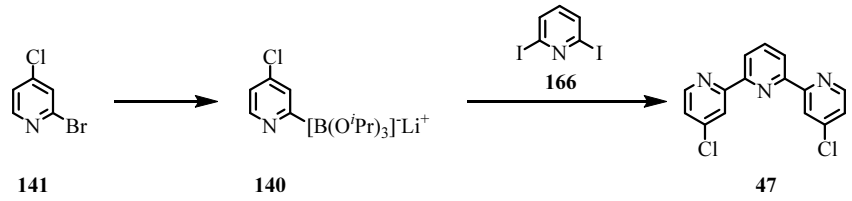

Scheme 51: Synthetic assembly of the modularly applicable 4,4´´-disubstituted tpy core unit **47**.

Based on the named key synthon **47** a plethora of symmetric (Figure 103a and b) and asymmetric (Figure 104) 4,4´´disubstituted tpy ligands has been synthesized utilizing individually optimized Suzuki-Miyaura cross-couplings.

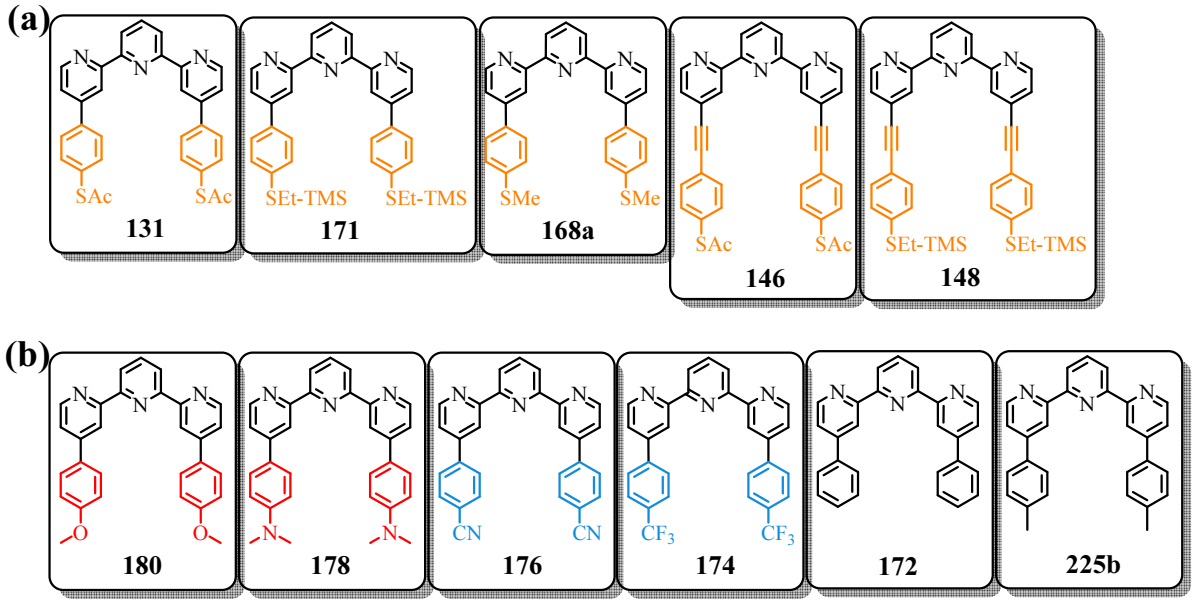

Figure 103: Overall overview of the isolated extended symmetrically 4,4´´-disubstituted tpy ligands. **(a)** Thiol-terminated anchoring tpy ligands **131**, **146**, **148**, **168a**, and **171** aimed for the complexes immobilization inside the MCBJ setup. **(b)** Non-dipolar tpy ligands **172**, **174**, **176**, **178**, **180**, and **225b** designed for the assembly of suitable reference complexes non-addressable by the applied trigger.

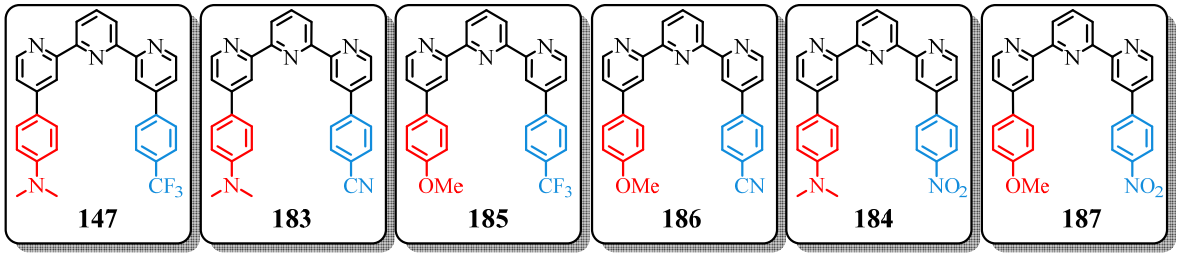

Figure 104: Overview of the extended asymmetrically 4,4′′-disubstituted tpy ligands **147**, and **183–187** bearing an intrinsic dipole moment due to the stepwise incorporation of an EWG and an EDG into the molecular structure during their respective assemblies.

The displayed tpy ligands formed the basis for the multitude of different target structures ranging from heteroleptic, dipolar Fe(II)-bis(tpy) complexes (**Type C**) as potentially spin-switching structures (Figure 105) addressable by applied electric fields, over heteroleptic non-dipolar and hence electrically non-addressable reference compounds (**Type D**) (Figure 106) up to the heteroleptic, dipolar Ru(II)-based target complex **127** (**Type E**) (Figure 107), which, although being addressable by an alteration of the applied electric fields, is incapable of undergoing any spin crossover due to the core ion's nature.

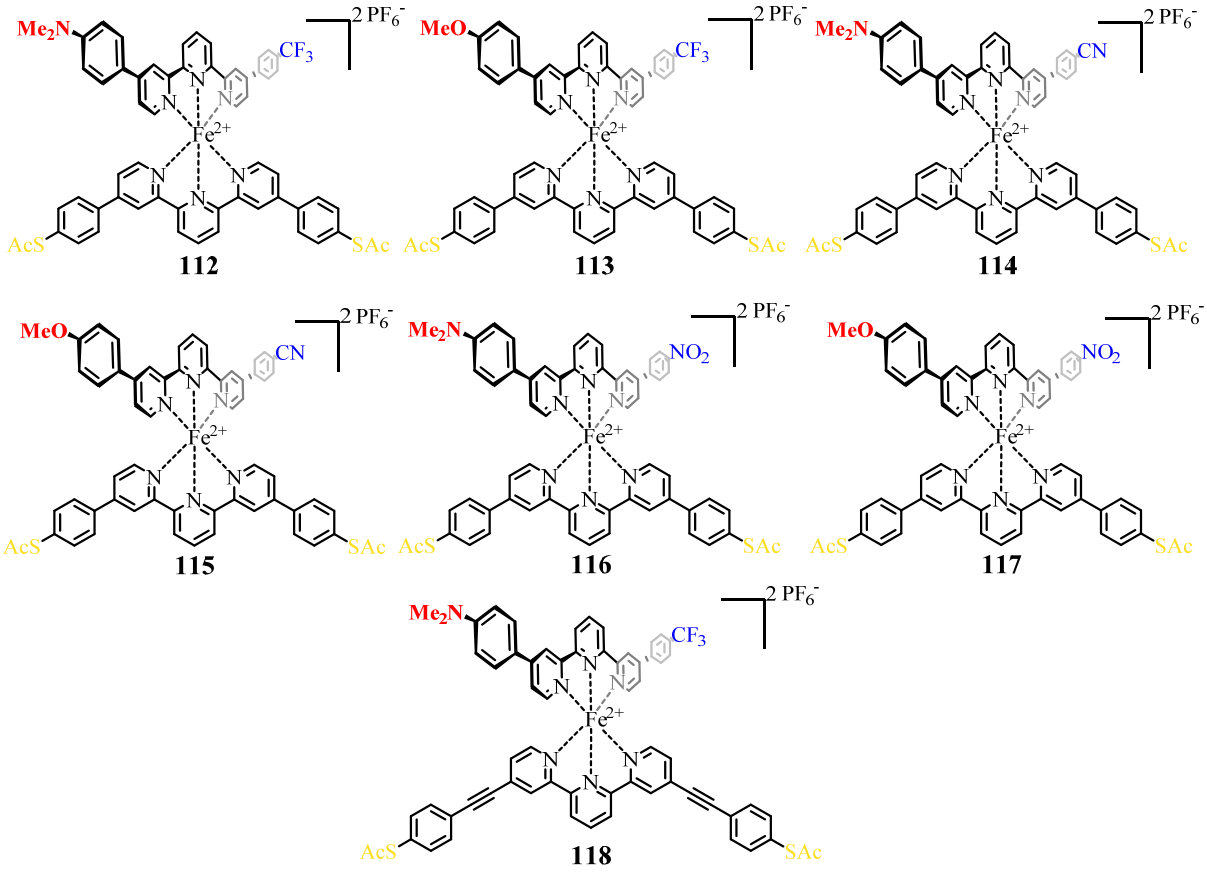

Figure 105: Recapitulatory depiction of the different synthesized bias-sensitive, dipolar heteroleptic Fe(II)-bis(tpy) target structures **112–118** of **Type C**.

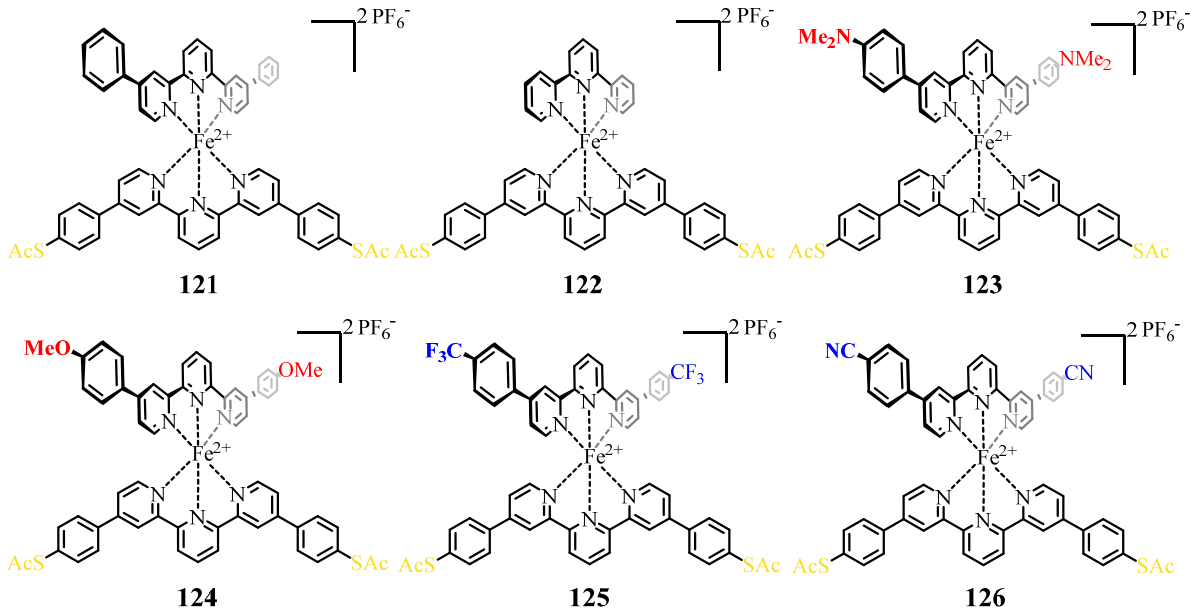

Figure 106: Overview of the non-dipolar and thus electrically non-addressable reference compounds **121**–**126** of **Type D**.

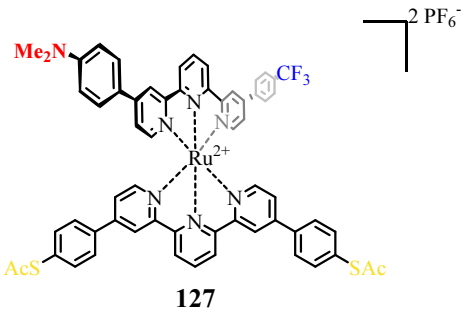

Figure 107: Illustration of the successfully synthesized electrically addressable, dipolar heteroleptic Ru(II)-bis(tpy) target complex **127** (**Type C**) representing an externally addressable complex being unable to undergo any SCO due to the nature of the metal core ion.

In the range of this first project, dealing exclusively with the electrical-field dependent alteration of the coordination sphere dependent spin state of the named hexa-coordinate Fe(II)-bis(tpy) complexes, single molecule transport studies utilizing the MCBJ technique in UHV at liquid helium temperature have been performed in collaboration with Riccardo Frisenda in the group of Prof. Herre van der Zant at the TU Delft. In this context, after comprehensive statistical analyses, it was found, that the voltage-dependent bistability correlates with the extent of the intrinsic dipole moments exhibited by the accordant Fe(II)-bis(tpy) complexes **112–114** (**Type C**) and **121** (**Type D**), which have been physically examined up to date. Furthermore, the simulative inspection of individual junctions strongly supports the envisaged and postulated switching mechanism. On top of that, upon the variation of the electrode's spacing, constant and reproducible switching thresholds, together with the expected electric-field dependence of the investigated switching events, could be

revealed. Furthermore, very promising preliminary results were obtained from the MCBJ experiments on the dipolar Fe(II)-based complex **118** (**Type C**), containing an extended molecular backbone, elongated by two acetylene-bridges, as anchoring ligand. Since the conductance experiments for all bistable junctions of complex **118** that have been investigated until now, reveal a switching from low conductance values (LS state) at low bias to high conductance values (HS state) at high bias, it seems very promising to further follow the route of implementing elongated anchoring tpy units into the previously described systems investigated so far. However, the reduced junction formation probability of the elongated structure **118**, which is only around 1%, seems to be a significant drawback arising from the incorporation of the acetylene bridges, which needs to be further evaluated in the future. Additionally, it will be interesting to see, whether the results of the momentarily ongoing MCBJ measurements of the remaining target structures that have already been synthesized, but not physically examined, up to now, namely, the potentially spin-switching, dipolar **Type C** complexes **115–117**, as well as the non-dipolar, non-addressable **Type D** reference complexes **122–126**, follow the general trends, observed so far. Herein, especially the remaining **Type D** reference compounds should help to exclude potential side effects arising from surface interactions of the included non-anchoring, but highly polar, terminal functional groups, such as –CN, -CF_3, -NO_2, -OMe, and –NMe_2 substituents. By the exclusive incorporation of the twofold acetylene-extended molecular backbone into the anchoring ligand, this issue should be sorted out effectively.

In the second project, representing a conceptual modification of the first project, the homoleptic, dipolar Fe(II)-bis(tpy) complexes **119**, **120**, and **199-201** (**Type B**) have been designed, to investigate potential bias-induced SCO phenomena, after the complexes' deposition onto highly ordered Au(111) surfaces, by means of STM. The physical results, obtained for the measurement of target complex **119** (Figure 108), revealed that those complexes, which actually are immobilized to the Au(111) surface, are deposited in a completely planar fashion.

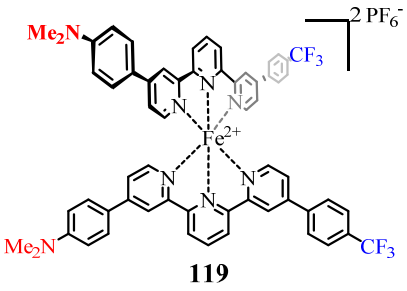

Figure 108: Illustration of the homoleptic, dipolar Fe(II)-bis(tpy) complexes **119** utilized for the investigation of bias-induced SCO phenomena at Au(111) surfaces, by means of STM.

Consequentially, for these surface-deposited complexes distinct Kondo resonances were observed, which can be matched with the corresponding HS state of the Fe(II) core ion in these planarized systems. However, since the investigated complexes reside in a planar configuration right away upon their surface deposition, an actual switching process from the octahedral, LS form to the planar HS form of the complexes could not be achieved. Nevertheless, there are plenty of possible approaches to tackle this problem. First of all, the remaining Fe(II)-bis(tpy) complexes **120**, and **199–201** (Figure 109), which have already been synthesized, will be investigated.

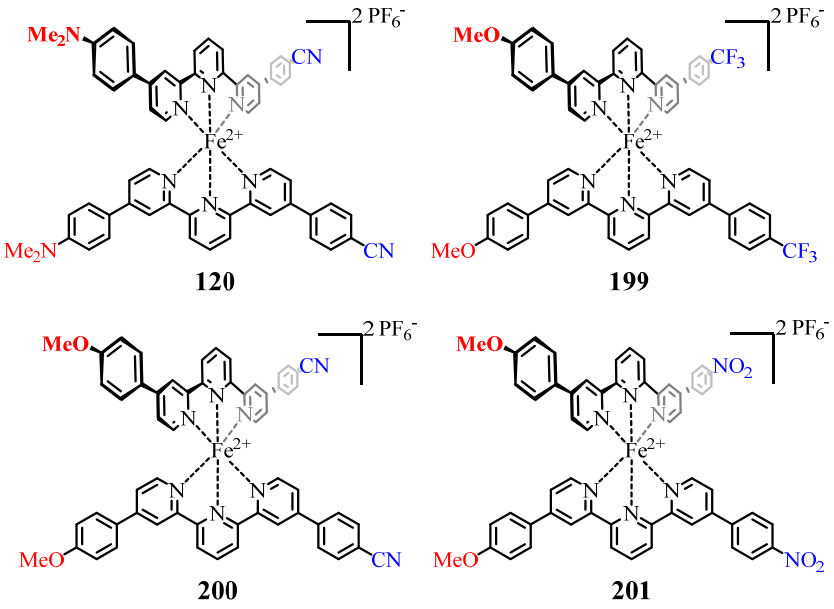

Figure 109: Overview of the assembled dipolar, electrically addressable target compounds **120**, and **199-201** (**Type B**), whose physical investigation is momentarily ongoing.

Furthermore, experiments trying to deposit complex **119** and the other remaining complexes on a $Cu_2N/Cu(100)$ surface, in order to decouple the deposited complexes from the metal surface via a small insulating layer, are under investigation at the moment. Also the implementation of an insulating interlayer, such as NaCl on an Au(111) surface represents a feasible approach, to circumvent the described issues. Should these changes to the physical

investigation setup show no effect, also an alteration of the incorporated ligand system, imposing geometrical limitations to the tpy ligand, seems to be a possible alternative, to prevent a complete planarization of the complex upon surface immobilization. After all, it will be decisive to find a suitable molecule, as well as the appropriate deposition conditions, to permit a successful immobilization of the according complex to the surface in its octahedral LS form, prior to its exposure to the external voltage trigger. This approach hopefully leads to the required distortion of the core metal ion's coordination sphere up to the HS state's geometry.

The third main project of this work synthetically relies on the same tpy core building block **47**, as the two previously highlighted projects. Conceptually, the objective of this part was, to mechanically induce a geometrical distortion of the coordination sphere of the central Fe(II) core ion of hexa-coordinated, homoleptic Fe(II)-bis(tpy) complex **208** (Figure 110a), as the basis of an envisaged SCO trigger. Consequentially, as a suitable reference compound, the analogue Ru(II)-based complex **209** (Figure 110b) was assembled.

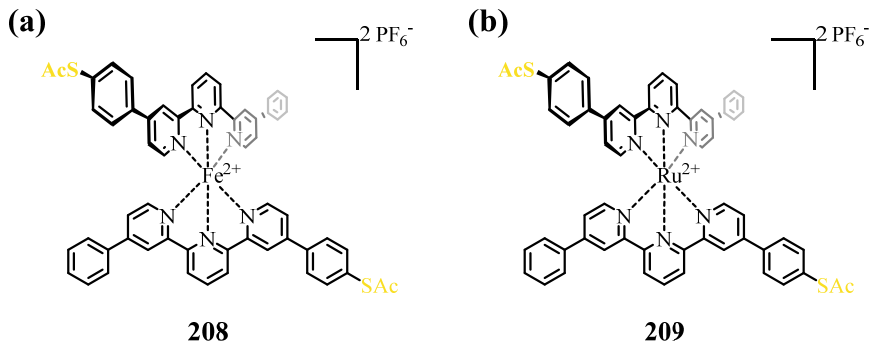

Figure 110: Overview of the mechanically addressable, single molecular spin switching homoleptic Fe(II)-bis(tpy) complex **208** and the Ru(II)-based analogue **209** as a reference compound being unable to undergo any SCO itself.

Due to the molecular design, utilizing the single-sided thiol-terminated tpy ligand **210**, the target complex **208** could be incorporated into the molecular junction of an MCBJ setup, and was investigated on a single molecular level in a fashion guaranteeing electronic transport through the central metal ion. Conceptually, upon the increase of the relative electrode's displacement of a junction comprising the Fe(II)-based complex **208**, the originally octahedral coordination sphere of the incorporated complex is distorted as well. This, consequentially, leads to an alteration of the relative energy of the complex' frontier orbitals and, hence, of its electron population resulting in the desired SCO. The investigation of the Ru(II)-based reference complex **209**, itself being unable to undergo any SCO, was envisaged to complement the results obtained for complex **208**. Extensive single molecule transport studies

on both named target complexes, **208** and **209**, revealed, after comprehensive statistical analyses, that the conductance-displacement characteristics of the Fe(II)-based target compound **208** show a clear distance-dependent bistability, exhibiting G_{final}/G_{start}–ratios of up to 10^2 G_0. In contrast, the analogue measurements of the Ru(II)-based complex **209** revealed a significantly smaller number of drastically less pronounced conductance increases. These minor conductance alterations, exhibited by both metal's complexes, can supposedly be derived from some ligand induced effects, or from geometrical differences in the electrodes atomic shape, whereas the much more pronounced conductance augmentations ($\geq 10^1$ G_0), observed exclusively for the Fe(II)-based complex **208**, indicate a clear correlation of the findings to the core metal ion's nature. Summarizing, the observed effects, with the utmost probability, can be attributed to the postulated and desired mechanically addressable SCO phenomenon, switching from the LS state at small electrode displacements coinciding with low conductances, towards the HS state at increased relative electrode displacements consistently going along with high conductance values.

Finally, the fourth and last main project of this thesis aimed at the optical addressability of the coordination sphere dependent spin state of a hexa-coordinated Fe(II) ion, being incorporated into appropriate metalloazobenzenophanes (Figure 111). Synthetically, the assembly route for the first targeted macrocycle **215** relies on the same key building block **47**, as applied within the other projects described above. In contrast to this, the metalloazobenzenophanes **216** and **238**, respectively, were assembled using a different synthetic approach, following a Kröhnke-type strategy for the formation of the tpy core unit.

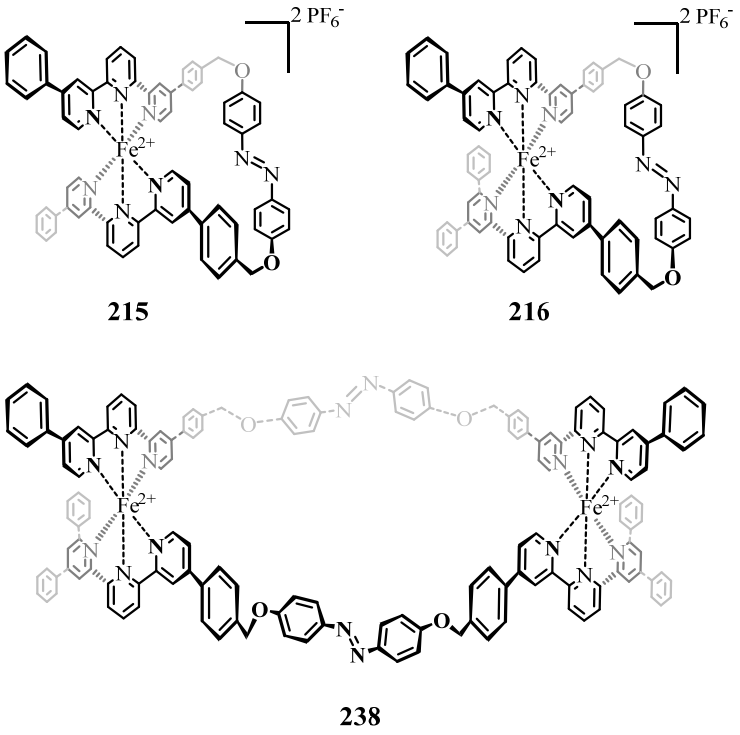

Figure 111: Overview of the assembled monomeric metalloazobenzenophanes **215**, **216**, and the dimeric **238**, as envisaged optically addressable single molecular spin switches.

Taking the statistical nature of the intermediate Suzuki-Miyaura cross-coupling reactions into account, both final compounds **215** and **216** could be assembled in high yields in 9 and 15 steps, respectively. Unfortunately, the overall objective of the projects could, however, only be partially fulfilled. Although detailed optical and NMR-spectroscopic studies, performed in particular on macrocycle **215**, revealed a successful and even complete (*E*) → (*Z*) photoisomerization of the incorporated azo moiety, the actually envisaged switching of the coordination sphere dependent spin state of the incorporated Fe(II) core ions was not observed for the investigated target structures so far. Therefore, it has to be assumed, that the (*E*) → (*Z*) photoisomerization of **215**, did not result in a sufficient alteration of the coordination sphere of the Fe(II) core ion, to evoke the SCO of the diamagnetic LS complex to the desired paramagnetic HS form. Furthermore, the monomeric, asymmetric metalloazo-

benzenophane **216** was found to be in equilibrium with its dimeric form **238**, containing two Fe(II) cores instead of only one Fe(II) core being present in **216**. Nevertheless, the structural similarity of the described metalloazobenzenophanes to the two paramagnetic, homoleptic Fe(II)-bis(tpy) complexes **241** and **242** (Figure 112), which have further been synthesized throughout this project, substantiates the general idea of the envisaged switching concept.

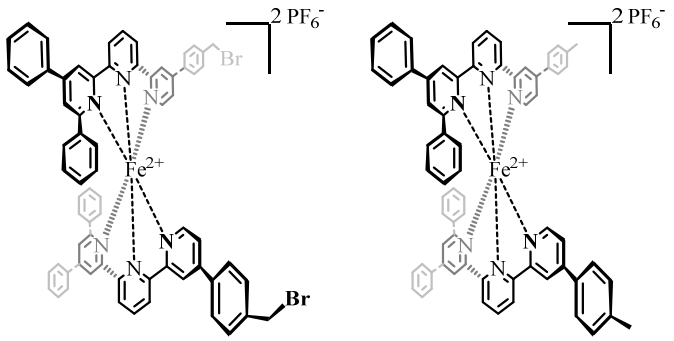

241 **242**

Figure 112: Depiction of the paramagnetic, homoleptic Fe(II)-bis(tpy) complexes **241** and **242**.

Therefore, to allow a successful realization of the envisaged switching concept in the future, very subtle changes to the utilized molecular structures might already be enough, to trigger a sufficiently strong deformation of the Fe(II) core ion's coordinative environment upon external stimulation, while at the same time leaving the system in the LS state under non-stimulated circumstances.

Scheme 52, displayed below, exemplarily illustrates the synthetic approaches towards the altered metalloazobenzenophanes **252** and **254**, which has already been initiated, but requires further advancements to eventually yield the desired target structures.

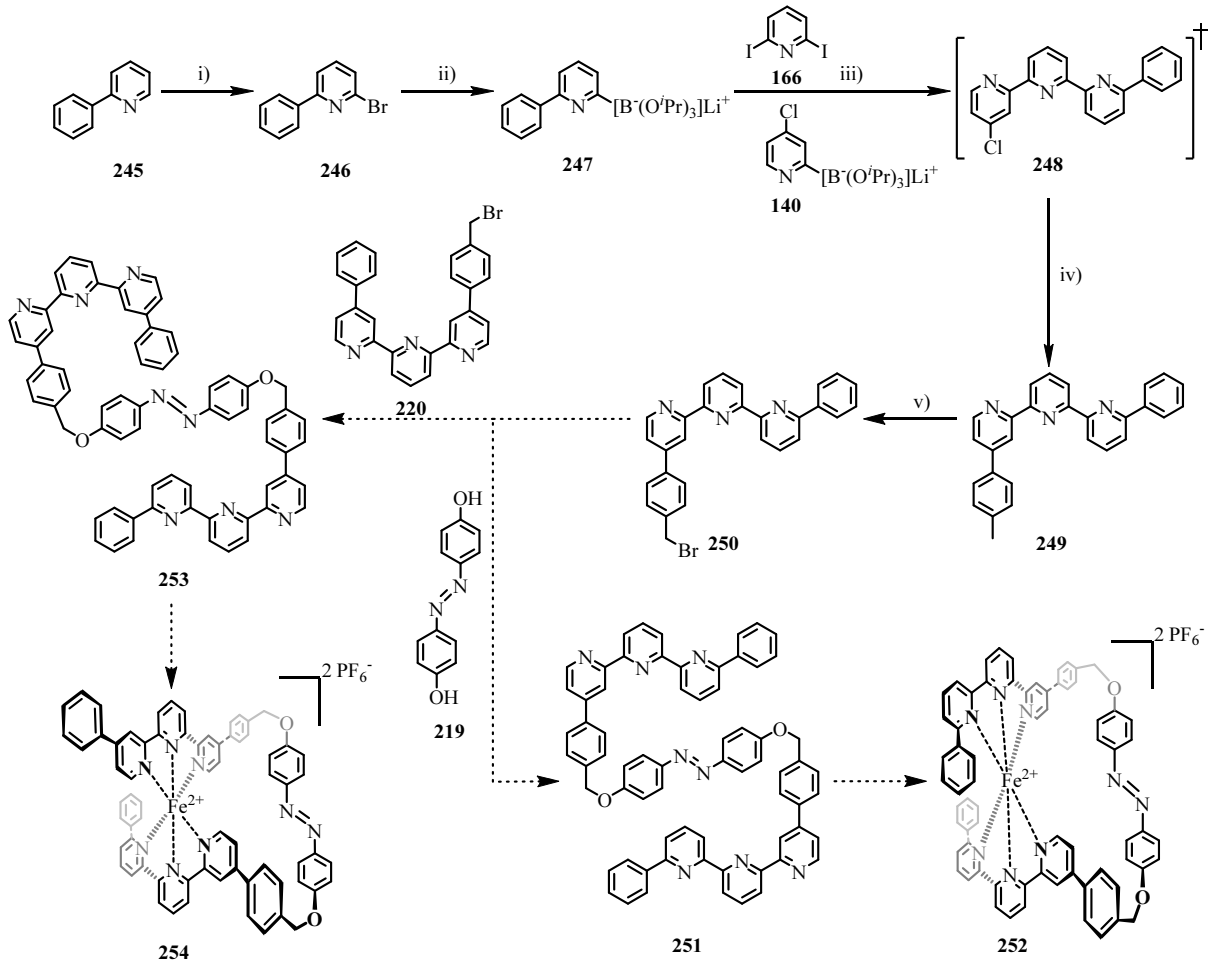

Scheme 52: Illustration of the proposed, already initiated, synthesis of the altered metalloazobenzenophanes **252** and **254**. Reagents and conditions: **i) 245** (1 eq.), CBr_4, *n*-BuLi, *N,N*-dimethylethanolamine, *n*-hexane, 0 °C → -78 °C → r.t., 16h, 75%; **ii) 246** (1 eq.), *n*-BuLi, $B(O^iPr)_3$, toluene/THF (4:1) *n*-hexane, -78 °C → r.t., 24h, 88%; **iii) 166** (1 eq.), **247** (2 eq.), **140** (2 eq.), KF, Pd_2dba_3, Ph_2PHO, 1,4-dioxane, 85 °C, 48h; **iv) 248** (1 eq.), **224** (10 eq.), $PdCl_2[P^tBu_2(p\text{-}NMe_2\text{-}Ph)]_2$, K_2CO_3, toluene/H_2O (5:1), reflux, 24h, quant.; **v) 249** (1 eq.), NBS (1.2 eq.), $(PhCOO)_2$, CCl_4, 75 °C, 7.5h, 78% (22% of reisolated **249**).

All in all, diverse synthetic strategies for the assembly of variably utilizable functional molecules have been developed and described throughout this thesis. The exposure of these tailor-made functional molecules to the suitable external triggers, going along with their investigation by appropriate physical techniques, gave a variety of highly interesting and unprecedented results in the field of single molecular switches. It will be very interesting to follow the further advancements within this area of coordination sphere dependent spin switching entities and to see, whether one of the concepts can be applied on a bigger scale in the future.

7 Experimental Part

7.1 General Remarks

All compounds, if commercially available, were purchased as reagent grade and used as received from *Fluka AG* (Buchs, Switzerland), *Acros AG* (Basel, Switzerland), *Merck* (Darmstadt, Germany), *ABCR* (Karlsruhe, Germany), *Alfa Aesar* (Karlsruhe, Germany), *Sigma-Aldrich* (Buchs, Switzerland), *Indofine* (Hillsborough, NJ, USA), *Combi-Blocks* (San Diego, CA, USA), *Apollo Scientific* (Manchester, United Kingdom), *Synchem OHG* (Felsberg, Germany), *Strem* (Kehl, Germany), *Activate Scientific* (Prien, Germany), *VWR* (Dietikon, Switzerland), *fluorochem* (Hadfield, United Kingdom), without further purification if nothing else is explicitly remarked. Dry solvents were purchased from *Sigma-Aldrich*, stored over 4 Å molecular sieves, and handled under inert atmosphere. For this purpose *Nitrogen 5.0* from *PanGas AG* (Damarsellen, Switzerland) was used. All oxygen-sensitive reactions were performed under inert atmosphere utilizing regular Schlenk-techniques in oven-dried glassware. For this purpose only dry solvents were used which were additionally, previously degassed with argon or nitrogen for at least 15 minutes. For regular normal phase column chromatography (CC) *silica gel 60* (40-63 µm) from *Fluka* or *SilicaFlash® P60* (40-63 µm) from *Silicycle* was used. Thin Layer Chromatography (TLC) was carried out using *Silica gel 60 F_{254}* glass plates with a thickness of 0.25 mm purchased from *Merck*. For peak detection a UV lamp with 254 nm or 366 nm, respectively was used.

Nuclear Magnetic Resonance (NMR)

All ^{1}H-Nuclear- (^{1}H-NMR), ^{13}C-Nuclear- (^{13}C-NMR and DEPT-135), ^{19}F-Nuclear- (^{19}F-NMR), ^{31}P-Nuclear- (^{31}P-NMR) and ^{11}B-Nuclear- (^{11}B-NMR) magnetic resonance spectra were recorded either on a *Bruker BZH 250 MHz NMR* with a QNP probehead at 250 and 63 MHz, respectively, on an *Oxford 400 MHz NMR* equipped with an *Avance III 400 spectrometer* and with a BBFO^{+} probehead operating at 400, 376, 162, 128 and 101 MHz, respectively, on a *Bruker 500 MHz Ultra Shield Avance III spectrometer* with a BBO probehead with z-gradients at 500 and 126 MHz, respectively, on a *Bruker 600 MHz Ultra Shield Avance III spectrometer* with a *BBFO+* probehead at 600 and 151 MHz, respectively

or on a *Bruker 600 MHz Avance III HD NMR spectrometer* equipped with a 5 mm $^{1}H/^{19}F–^{13}C/^{15}N–^{2}D$ QCI cryoprobe head with *z*-axis pulsed field gradients operating at 600 and 151 MHz, respectively. All two-dimensional NMR experiments required to elucidate unclear of ^{1}H- and ^{13}C-signals like $^{1}H,^{1}H$-COSY, $^{1}H,^{13}C$-HMQC, $^{1}H,^{13}C$-HMBC and $^{1}H,^{1}H$-NOESY were recorded either on a *Bruker 500 MHz Ultra Shield Avance III spectrometer* equipped with a BBO probehead with z-gradients at 500 and 126 MHz, respectively, on a *Bruker 600 MHz Ultra Shield Avance III spectrometer* with a BBFO+ probehead at 600 and 151 MHz, respectively or on a *Bruker 600 MHz Avance III HD NMR spectrometer* equipped with a 5 mm $^{1}H/^{19}F–^{13}C/^{15}N–^{2}D$ QCI cryoprobe head with *z*-axis pulsed field gradients operating at 600 and 151 MHz, respectively. Chemical shifts (δ) are reported in parts per million (ppm) relative to tetramethylsilane or residual solvent peak for ^{1}H-NMR and ^{13}C-NMR or uncorrected for ^{11}B-NMR, ^{19}F-NMR or ^{31}P-NMR and the coupling constants (*J*) are given in Hertz (± 0.1 Hz). The order of coupling constants is specified by a superscript number (^{n}J). Deuterated NMR solvents were obtained from *Cambridge Isotope Laboratories, Inc. (Andover, MA, USA)*. All spectra were recorded at 298 K if not stated otherwise. The multiplicities are written as: s = singlet, d = doublet, t = triplet, q = quartet, hept = heptet, m = multiplet and br = broad.

Mass Spectrometry (MS)

All Mass spectra (MS) were recorded either on a *Bruker Esquire 3000 plus* or a *Bruker amazon™ X* for Electron Spray Ionization (ESI), a *Finnigan MAT 95Q* for Electron Impact (EI) or a *Finnigan MAT 8400* for Fast Atom Bombardment (FAB) measurements. MS spectra were measured in *m/z* (%). For GC/MS analysis a *Shimadzu GCMS-QP2010 SE* gas chromatograph with a *ZB-5HT inferno* column (30 m *x* 0.25 mm *x* 0.25 mm) at 1 mL/min He-flow rate (split = 20:1) with a *Shimadzu* mass detector (EI 70eV) was used. All high resolution mass spectra (HRMS) were measured as HR-ESI-ToF-MS on a *maXis™ 4G* instrument from *Bruker*.

Elemental Analysis (EA)

Elemental analyses were performed either on a *Perkin-Elmer Analysator 240* or on a *Vario Micro Cube* by *Elementar* and values are given in mass percent (calculated vs. measured abundance).

Ultraviolet – Visible Absorption Spectroscopy (UV/VIS)

The absorption spectra were recorded at room temperature with a *Shimadzu UV 1800* diode array detector spectrophotometer using optical 114-QS *Hellma* cuvettes with 10 mm light path. If not stated otherwise the measurements were performed under ambient conditions. Measurements are given with the corresponding solvents and the resulting wavelengths of maxima (λ_{max}) in nm (relative extinction coefficients in %)

Monochromator

The switching experiments on metalloazobenzenophane **215** were performed using a Polychrome V device from TILL Photonics GmbH with a 150 W xenon high-stability lamp (output power > 10 mW at 470 nm) and a half-power bandwidth of 14 nm. For the switching experiments, NMR samples were irradiated with the monochromator via an optical fiber (length 6 m) directly in a 5 mm ^{1}H/^{19}F–^{13}C/^{15}N–^{2}D QCI cryoprobe head with *z*-axis pulsed field gradients The insulation of the optical fiber (UV/Vis quartz–quartz fiber) was removed at the rear part of the fiber. This part was dipped into the solution (NMR solvent and sample) to a depth of about 4 mm and finally the NMR tube was sealed with Parafilm®. The measurements were performed at varying temperatures.

Melting Points (T_M)

Melting points were measured in °C using a *Stuart SMP3* apparatus and are given uncorrected.

High-Performance Liquid Chromatography (HPLC) techniques

Analytical reversed phase HPLC-ESI-MS measurements were performed either on an *Agilent 1100* HPLC-MS system (series 1100) using a *Reprosil 100 C18, 3 µm* column (125 mm *x* 3 mm) from *Morvay Analytik GmbH* or on a *Shimadzu LC-20AD* using a *Reprospher 100 C18-Aqua, 5 µm* column (125 mm *x* 2 mm) from *Maisch GmbH*. Furthermore, on a Shimadzu LC-20AT semi-preparative normal phase HPLC measurements using a *Reprospher 100 SI, 5 µm* column (250 mm *x* 16 mm) or semi-preparative reversed phase HPLC measurements using a *Reprosil 100 C18, 5 µm* column (250 mm *x* 16 mm) column from

Maisch GmbH were performed. Finally preparative reversed phase HPLC separations were performed on a *Varian PrepStar* HPLC using a *Phenomenex Gemini NX-C18 10 µm* column (250 mm *x* 1.2 mm) with solvent gradients specified in detail for the corresponding separation issues at a flow rate of 20 mL/min.

7.2 Synthetic Procedures

7.2.1 Externally Triggerable Single-Molecular Spin Switches

2-Bromo-4-methoxypyridine (158a)

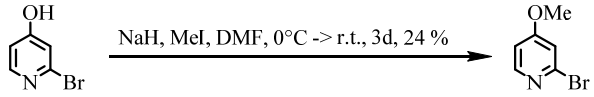

158a **158b**

158a was prepared in adaptation of a related protocol.[562] 2-Bromo-4-hydroxy-pyridine (**158b**) (1.74 g, 10.0 mmol, 1.00 equivalents (eq.)) and NaH (60% dispersion in mineral oil, 560 mg, 14.0 mmol, 1.40 eq.) were dissolved in DMF (20 mL) and stirred for 30 min. The black solution was cooled to 0 °C and MeI (2.87 g, 1.26 mL, 20.0 mmol, 2.00 eq.) was added dropwise. Due to high viscosity the mixture was warmed to ambient temperature and additional DMF (20 mL) was added. Now the reaction mixture was stirred for 3 days and afterwards was quenched by the addition of water and extracted with TBME (5 *x* 150 mL). The combined organic layers were washed with brine, dried over $MgSO_4$, and subsequently concentrated under reduced pressure. The crude product was purified by FCC on silica using EtOAc / *n*-hexane (1:1) as an eluent. Upon evaporation of the solvent the product **158a** was obtained as a yellow oil in a yield of 24% (433 mg, 2.35 mmol).

Analytical data of 158a:

^{1}H-NMR (400 MHz, $CDCl_3$, ppm, 25 °C): δ_H = 8.07 (d, $^3J_{H,H}$ = 5.8 Hz, 1H, *H6*), 6.91 (d, $^4J_{H,H}$ = 2.3 Hz, 1H, *H3*), 6.70 (dd, $^3J_{H,H}$ = 5.8 Hz, $^4J_{H,H}$ = 2.3 Hz, 1H, *H5*), 3.76 (s, 3H, *–OCH$_3$*).

^{13}C-NMR (101 MHz, $CDCl_3$, ppm, 25 °C): δ_C = 166.87 (C_q, 1C), 150.63 (C_t, 1C), 142.95 (C_q, 1C), 113.31 (C_t, 1C), 110.22 (C_t, 1C), 55.67 ($C_{methoxy}$, 1C).

MS (EI$^+$, 70 eV): *m/z* [ion, intensity (%)] = 187.0 (M^+, 45), 108.0 (M^+-Br, 100), 93.0 (M^+-Br-CH_3, 17).

HRMS (ESI-ToF): *m/z* calcd. for $[C_6H_6BrNO+H]^+$: 187.9706; found: 187.9707.

2-Bromo-4-(trifluoromethylsulfonate)pyridine (159)

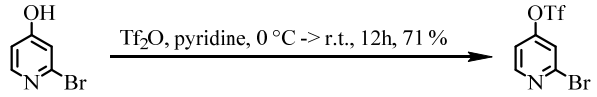

158b **159**

159 was prepared in adaptation of a related literature protocol.[563] 2-Bromo-4-hydroxy-pyridine (**158b**) (1.31 g, 7.50 mmol, 1.00 eq.) was dissolved in dry pyridine and cooled to 0 °C before trifluoromethanesulfonic anhydride (2.12 g, 1.24 mL, 7.50 mmol, 1.00 eq.) was added under inert atmosphere. Now the reaction was allowed to warm up to room temperature and stirred overnight. The reaction mixture was quenched by the addition of water (25 mL) and subsequently extracted with EtOAc (2 *x* 100 mL). Afterwards the combined organic layers were washed with 1N HCl (3 *x* 35 mL) and brine (50 mL) before being dried over $MgSO_4$, and subsequently concentrated under reduced pressure. The crude product was purified by filtration over a plug of silica using hexane to elute the product triflate **159** which was obtained in a yield of 71% (1.63 g, 5.34 mmol).

Analytical data of 159:

^{1}H-NMR (400 MHz, $CDCl_3$, ppm, 25 °C): δ_H = 8.44 (d, $^{3}J_{H,H}$ = 5.6 Hz, 1H, *H6*), 7.41 (d, $^{4}J_{H,H}$ = 2.2 Hz, 1H, *H3*), 7.20 (dd, $^{3}J_{H,H}$ = 5.6 Hz, $^{4}J_{H,H}$ = 2.2 Hz, 1H, *H5*).
^{13}C-NMR (101 MHz, $CDCl_3$, ppm, 25 °C): δ_C = 156.48 (C_q, 1C), 152.36 (C_t, 1C), 143.45 (C_q, 1C), 120.84 (C_t, 1C), 118.65 (q, $^{1}J_{C,F}$ = 320.9 Hz, C_q, 1C), 115.69 (C_t, 1C).
^{19}F-NMR (376 MHz, $CDCl_3$, ppm, 25 °C): δ_F = -73,05 (3F)
MS (EI$^+$, 70 eV): *m/z* [ion, intensity (%)] = 306.9 (M^+, 87), 226.0 (M^+-Br, 19), 162.1 (M^+-Br-SO_2, 100), 69.0 (CF_3, 48).

2-bromo-4-((tri*iso*propylsilyl)ethynyl)pyridine (160)

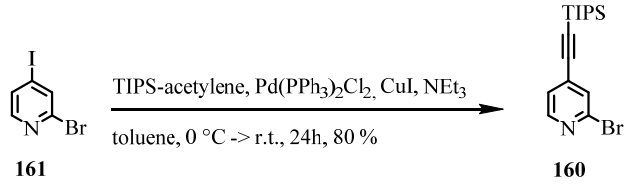

161 **160**

160 was prepared according to a protocol previously reported in literature.[564] 2-Bromo-4-iodopyridine (**161**) (1.47 g, 5.04 mmol, 1.00 eq.), CuI (99.0 mg, 0.52 mmol, 0.10 eq.) and the catalyst $Pd(PPh_3)_2Cl_2$ (183 mg, 0.26 mmol, 0.05 eq.) were dissolved in a mixture of toluene (20 mL) and triethylamine (40 mL) and vigorously degassed with nitrogen before being cooled to 0 °C. Now TIPS-acetylene was added at 0 °C slowly leading to a color change of the solution from yellow to green-yellow. The reaction was allowed to warm to room temperature overnight. The now orange reaction mixture was quenched by the addition of water and DCM to dissolve the precipitate formed during the reaction. The organic layers were washed subsequently with saturated NH_4Cl-solution, cold 1N HCl and with 10% $NaHCO_3$-solution before the organic fractions were reunited, dried over $MgSO_4$, filtered and subsequently concentrated under reduced pressure. The crude product was purified by FCC on silica using cyclohexane / DCM (1:1) as an eluent. Upon evaporation of the solvent product **160** was obtained as a colorless liquid in a yield of 80% (1.33 g, 3.93 mmol).

Analytical data of 160:

^{1}H-NMR (400 MHz, $CDCl_3$, ppm, 25 °C): δ_H = 8.27 (d, $^3J_{H,H}$ = 5.1 Hz, 1H, *H6*), 7.48 (s, 1H, *H3*), 7.23 (dd, $^3J_{H,H}$ = 5.1 Hz, $^4J_{H,H}$ = 1.3 Hz, 1H, *H5*), 1.09 (s, 21H, TIPS).
^{13}C-NMR (101 MHz, $CDCl_3$, ppm, 25 °C): δ_C = 149.96 (C_t, 1C), 142.30 (C_q, 1C), 134.09 (C_q, 1C), 130.20 (C_t, 1C), 125.03 (C_t, 1C), 102.56 ($C_{acetylene}$, 1C), 99.03 ($C_{acetylene}$, 1C), 18.70 ($C_{isopropyl}$, 3C), 11.27 (C_{methyl}, 6C).
MS (EI$^+$, 70 eV): *m/z* [ion, intensity (%)] = 339.1 (M^+, 4), 296.0 (M^+-C_3H_7, 100), 268.0 (M^+- C_5H_{11}, 34), 254.0 (M^+-C_6H_{13}, 24), 240.0 (M^+- C_7H_{15}, 64), 226.0 (M^+- C_9H_{19}, 64).
ESI-MS (MeOH, *positive* ion mode): *m/z* [ion, intensity (%)] = 340.1 ($M+H^+$, 100), 362.1 ($M+Na^+$, 50).
HRMS (ESI-ToF): *m/z* calcd. for $[C_{16}H_{24}BrNSi+H]^+$: 338.0934 ; found: 338.0935.

Representative Procedure A (Synthesis of 4-Substituted Lithium Tri*iso*propyl 2-Pyridylborates):

The 4-substituted lithium tri*iso*propyl 2-pyridylborates (**140**, **162** - **165**) were prepared transferring a procedure described in literature.[407] An oven-dried round bottom flask was charged with the adequate 2,4-disubstituted pyridine derivative and placed under argon atmosphere. The reactant (1.0 eq.) was dissolved in a 4:1 solvent mixture of toluene and THF and tri*iso*propyl-borate (1.1 eq.) was added to the reaction mixture. Now the reaction mixture was cooled to -78 °C before *n*-BuLi (1.6M in hexanes, 1.1 eq.) was added dropwise via a syringe pump. After the addition was completed the reaction mixture was kept for an additional 30 min at -78 °C and was then left in the cooling bath and allowed to slowly warm up to room temperature overnight (22 h). The crude mixture was now concentrated under reduced pressure followed by rigorous drying under high vacuum at 110 °C for 10 h to give the corresponding products in very good to quantitative yields.

Lithium tri*iso*propyl 2-pyridyl borate (162)

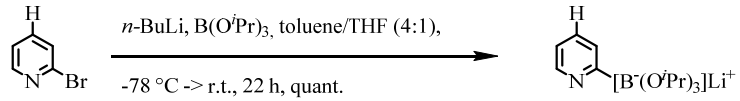

157 **162**

162 was prepared according to representative procedure A. Therefore 2-Bromo-pyridine (**157**) (3.32 g, 2.01 mL, 21.0 mmol, 1.00 eq.), tri*iso*propyl borate (4.34 g, 5.34 mL, 23.1 mmol, 1.10 eq.), *n*-BuLi (1.6M in hexanes, 14.4 mL, 23.1 mmol, 1.10 eq.), THF (15 mL) and toluene (60 mL) were used to give the desired product as an ivory solid in quantitative yield (5.74 g, 21.0 mmol).

Analytical data of 162:

T_M: >300 °C.

^{1}H-NMR (400 MHz, CD_3OD, ppm, 25 °C): δ_H = 8.39 (m, 1H, *H6*), 7.57 (d, 2H, *H3 / H4*), 7.09 (m, 1H, *H5*), 3.93 (hept, $^3J_{H,H}$ = 6.2 Hz, 3H, *–CH(CH$_3$)$_2$*), 1.15 (d, $^3J_{H,H}$ = 6.2 Hz, 18H, *-CH(CH$_3$)$_2$*).

^{13}C-NMR (101 MHz, CD_3OD, ppm, 25 °C): δ_C = 149.64 (C_t, 1C), 144.87 (C_q, 1C), 128.64 (C_t, 1C), 122.16 (C_t, 1C), 64.87 ($C_{isopropyl}$, 3C), 25.43 (C_{methyl}, 6C).

Note: The carbon-atom bound to the boron atom cannot be seen in the ^{13}C-NMR spectrum.

^{11}B-NMR (128 MHz, CD_3OD, ppm, 25 °C): δ_B = 2.96 (s, 1B).

Lithium tri*iso*propyl 2-(4-chloropyridyl) borate (140)

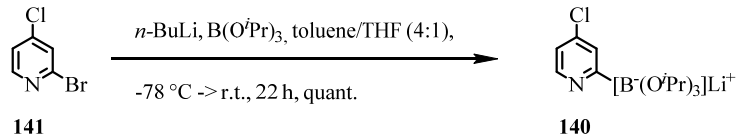

141 **140**

Compound **140** was prepared according to representative procedure A. 2-bromo-4-chloro-pyridine (**141**) (4.75 g, 24.7 mmol, 1.00 eq.), tri*iso*propylborate (5.20 g, 6.39 mL, 27.1 mmol, 1.10 eq.), *n*-BuLi (1.6M in hexanes, 16.9 mL, 27.1 mmol, 1.10 eq.), THF (25 mL) and toluene (100 mL) were used to give the desired off-white product as a powder in quantitative yield (7.59 g, 24.7 mmol).

Analytical data of 140:

T_M: >300 °C.

^{1}H-NMR (400 MHz, CD_3OD, ppm, 25 °C): δ_H = 8.32 (dd, $^3J_{H,H}$ = 5.5 Hz, *H6*), 7.56 (d, $^4J_{H,H}$ = 2.1 Hz, 1H, *H3*), 7.15 (dd, $^3J_{H,H}$ = 5.5 Hz, $^4J_{H,H}$ = 2.3 Hz, 1H, *H5*), 3.93 (hept, $^3J_{H,H}$ = 6.2 Hz, 3H, *–C**H**(CH$_3$)$_2$*), 1.15 (d, $^3J_{H,H}$ = 6.2 Hz, 18H, *–CH(C**H**$_3$)$_2$*).

^{13}C-NMR (101 MHz, CD_3OD, ppm, 25 °C): δ_C = 149.67 (C_t, 1C), 144.85 (C_q, 1C), 128.61 (C_t, 1C), 122.15 (C_t, 1C), 64.87 ($C_{isopropyl}$, 3C), 25.44 (C_{methyl}, 18C).

Note: The carbon-atom bound to the boron atom cannot be seen in the ^{13}C-NMR spectrum.

^{11}B-NMR (128 MHz, CD_3OD, ppm, 25 °C): δ_B = 2.98 (s, 1B).

Lithium tri*iso*propyl 2-(4-methoxypyridyl) borate (163).

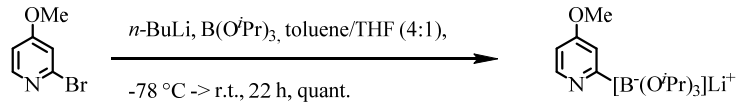

158a **163**

163 was prepared according to representative procedure A. Toluene (32 mL), THF (8 mL), 2-bromo-4-methoxypyridine (**158a**) (873 mg, 4.55 mmol, 1.00 eq.), tri*iso*propyl borate (960 mg, 1.18 mL, 5.00 mmol, 1.10 eq.) and *n*-BuLi (1.6M in hexanes, 3.13 mL, 5.00 mmol, 1.10 eq.) were used to quantitatively yield the desired product **163** (1.38 g, 4.54 mmol) as an orange-brown solid.

Analytical data of 163:

T_M: >300 °C.

^{1}H-NMR (500 MHz, CD_3OD, ppm, 25 °C): δ_H = 8.22 (d, $^3J_{H,H}$ = 6.0 Hz, 1H, *H6*), 7.13 (d, $^4J_{H,H}$ = 2.7 Hz, 1H, *H3*), 6.69 (dd, $^3J_{H,H}$ = 6.0 Hz, $^4J_{H,H}$ = 2.8 Hz, 1H, *H5*), 3.93 (hept, $^3J_{H,H}$ = 6.2 Hz, 3H, *–C**H**(CH$_3$)$_2$*), 3.84 (s, 3H, *–OC**H**$_3$*), 1.15 (d, $^3J_{H,H}$ = 6.2 Hz, 18H, *–CH(C**H**$_3$)$_2$*).

^{13}C-NMR (126 MHz, CD_3OD, ppm, 25 °C): δ_C = 167.01 (C_q, 1C), 148.90 (C_t, 1C), 113.28 (C_t, 1C), 109.18 (C_t, 1C), 64.89 ($C_{isopropyl}$, 3C), 55.49 ($C_{methoxy}$, 1C), 25.42 (C_{methyl}, 18C).

Note: The carbon-atom bound to the boron atom cannot be seen in the ^{13}C-NMR spectrum.

^{11}B-NMR (128 MHz, CD_3OD, ppm, 25 °C): δ_B = 2.94 (s, 1B).

Lithium tri*iso*propyl 2-((4-trifluoromethylsulfonate)pyridyl) borate (164).

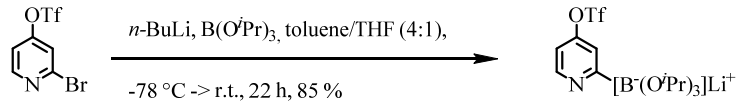

159 **164**

164 was prepared according to the representative procedure A. Toluene (14 mL), THF (3.5 mL), tri*iso*propyl borate (691 mg, 0.85 mL, 3.60 mmol, 1.10 eq.), 2-bromo-4-(trifluoromethylsulfonate)pyridine (**159**) (1.00 g, 3.27 mmol, 1.00 eq.), and *n*-BuLi (1.6M in hexanes, 2.25 mL, 3.60 mmol, 1.10 eq.) were used to yield the desired product **164** as a dark brown solid in a yield of 85% (1.17 g, 2.77 mmol).

Analytical data of 164:

^{1}H-NMR (400 MHz, CD_3OD, ppm, 25 °C): δ_H = 8.59 (dd, $^3J_{H,H}$ = 5.8 Hz, $^5J_{H,H}$ = 0.4 Hz 1H, *H6*), 7.50 (d, $^4J_{H,H}$ = 2.7 Hz, 1H, *H3*), 7.17 (dd, $^3J_{H,H}$ = 5.8 Hz, $^4J_{H,H}$ = 2.8 Hz, 1H, *H5*), 3.93 (hept, $^3J_{H,H}$ = 6.2 Hz, 3H, *–C**H**(CH$_3$)$_2$*), 1.15 (d, $^3J_{H,H}$ = 6.2 Hz, 18H, *–CH(C**H**$_3$)$_2$*).

Lithium tri*iso*propyl 2-((4-(tri*iso*propylsilyl)ethynyl)pyridyl) borate (165).

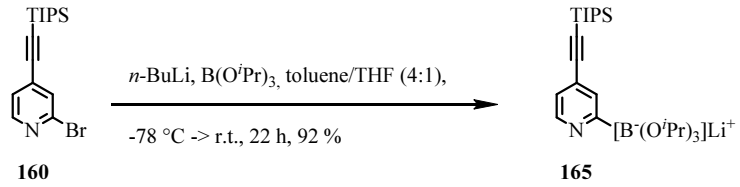

160 **165**

165 was prepared according to the representative procedure A. Toluene (4 mL), THF (1 mL), 2-bromo-4-((tri*iso*propylsilyl)ethynyl)pyridine (**160**) (338 mg, 1.00 mmol, 1.00 eq.), tri*iso*-propyl borate (207 mg, 254 µL, 1.10 mmol, 1.10 eq.) and *n*-BuLi (1.6M in hexanes, 688 µL, 1.10 mmol, 1.10 eq.) were used to yield the desired product **165** as a brown solid in a yield of 92% (1.38 g, 4.54 mmol).

Analytical data of 165:

^{1}H-NMR (400 MHz, CD_3OD, ppm, 25 °C): δ_H = 8.36 (d, $^{3}J_{H,H}$ = 5.3 Hz, 1H, *H6*), 7.59 (s, 1H, *H3*), 7.09 (dd, $^{3}J_{H,H}$ = 5.2 Hz, $^{4}J_{H,H}$ = 1.7 Hz, 1H, *H5*), 3.90 (hept, $^{3}J_{H,H}$ = 6.1 Hz, 3H, *–C**H**(CH$_3$)$_2$*), 1.15 (d, $^{3}J_{H,H}$ = 6.1 Hz, 39H, *–CH(C**H**$_3$)$_2$*).

^{13}C-NMR (101 MHz, CD_3OD, ppm, 25 °C): δ_C = 150.30 (1C), 148.01 (1C), 131.11 (1C), 123.68 (1C), 107.49 ($C_{acetylene}$, 1C), 105.19 ($C_{acetylene}$, 1C), 64.89 ($C_{C\text{-}H,\ (B(OiPr))}$, 3C), 25.41 ($C_{CH3,\ (B(OiPr))}$, 6C), 19.21 ($C_{CH,\ (TIPS)}$, 1C), 12.61 ($C_{CH3,\ (TIPS)}$, 1C).

Note: The carbon-atom bound to the boron atom cannot be seen in the ^{13}C-NMR spectrum.

2,6-Diiodopyridine (166)

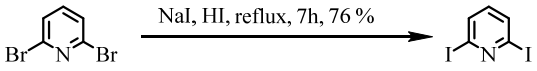

46 **166**

166 was prepared by the modification of a procedure described previously in literature.[530–532] 2,6-Dibromopyridine (**46**) (4.83 g, 19.8 mmol, 1.00 eq.) and NaI (4.00 g, 27.7 mmol, 1.40 eq.) were dissolved in HI (57 wt%, 15 mL, 199 mmol, 10.0 eq.) and refluxed for 7 h under inert atmosphere. The mixture was slowly poured onto ice cold aqueous sodium hydroxide solution (40%, 15 mL) and ice (20 g) and extracted with ether (3 *x* 15 mL). The combined extracts were successively washed with water, aqueous Na_2SO_3 and once more with water, dried over $MgSO_4$, filtered and the solvent evaporated under reduced pressure. The crude product was repetitively recrystallized from a mixture of chloroform and *n*-hexane to afford pure **166** as voluminous colorless needles in a yield of 76% (4.49 g, 13.6 mmol).

Analytical data of 166:

T_M: 180 °C; Lit.: 185 – 186 °C.

^{1}H-NMR (400 MHz, $CDCl_3$, ppm, 25 °C): δ_H = 7.67 (d, $^3J_{H,H}$ = 7.8 Hz, 2H, *H3 / H5*), 6.92 (t, $^3J_{H,H}$ = 7.7 Hz, 1H, *H4*).

^{13}C-NMR (101 MHz, $CDCl_3$, ppm, 25 °C): δ_C = 138.60 (C_t, 1C), 134.41 (C_t, 2C), 116.45 (C_q, 2C).

MS (EI$^+$, 70 eV): *m/z* [ion, intensity (%)] = 330.8 (M^+, 100), 203.9 (M^+-I, 73), 126.9 (I^+, 7), 77.0 (M^+-2I, 25).

HRMS (ESI-ToF): *m/z* calcd. for $[C_5H_3I_2N+H]^+$: 331.8428; found: 331.8424.

2,2´:6´2´´-Terpyridine (11)

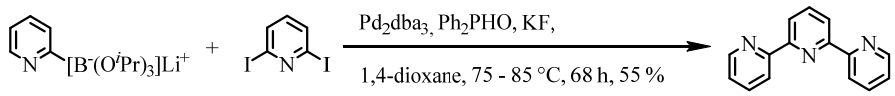

162 **166** **11**

11 was prepared in adaptation of a related protocol.[407] A Schlenk tube was charged with 2,6-diiodopyridine (**166**) (844 mg, 2.55 mmol, 1.00 eq.) and mixed with a 1.5 fold excess of the lithium tri*iso*propyl 2-pyridyl borate **162** (2.11 g, 7.71 mmol, 3.00 eq.) using KF (804 mg, 13.7 mmol, 5.37 eq.) as base, Pd_2dba_3 (83.7 mg, 90 µmol, 0.03 eq.) as the catalyst and diphenylphosphine oxide (114 mg, 550 µmol, 0.22 eq.) as the ligand. All those reagents were evacuated and the flask was put under inert atmosphere three times. Now the mixture was dissolved in 1,4-dioxane (30 mL), which was previously degassed for 30 min and the Schlenk tube was sealed pressure safe and heated up to 85 °C for 72 h. After diluting the reaction mixture with EtOAc it was filtered through a plug of silica gel to get rid of insoluble side products. Concentration of the solvent under reduced pressure yielded the crude product, which was now subjected to flash column chromatography on silica gel using EtOAc / *n*-hexane (15:85) as the eluent. Upon evaporation of the solvent under reduced pressure the desired product **11** was obtained as a white solid in a yield of 55% (325 mg, 1.39 mmol).

Analytical data of 11:

T_M: 88-90 °C; Lit.: 88 °C.

^{1}H-NMR (400 MHz, $CDCl_3$, ppm, 25 °C): δ_H = 8.74 (ddd, $^3J_{H,H}$ = 4.8 Hz, $^4J_{H,H}$ = 1.7 Hz, $^5J_{H,H}$ = 0.9 Hz, 2H, *H6 / H6´´*), 8.66 (dt, $^3J_{H,H}$ = 8.0 Hz, $^4J_{H,H}$ = 1.0 Hz, 2H, *H3 / H3´´*), 8.51 (d, $^3J_{H,H}$ = 7.8 Hz, 2H, *H3´ / H5´*), 7.99 (t, $^3J_{H,H}$ = 7.8 Hz, 1H, *H4´*), 7.34 (ddd, $^3J_{H,H}$ = 7.5 Hz, $^3J_{H,H}$ = 4.8 Hz, $^4J_{H,H}$ = 1.2 Hz, 2H, *H5 / H5´´*).

^{13}C-NMR (101 MHz, $CDCl_3$, ppm, 25 °C): δ_C = 156.22 (C_q, 2C), 155.35 (C_q, 2C), 149.13 (C_t, 2C), 137.86 (C_t, 1C), 136.80 (C_t, 2C), 123.74 (C_t, 2C), 121.13 (C_t, 2C), 120.99 (C_t, 2C).

HRMS (ESI-ToF): *m/z* calcd. for $[C_{15}H_{11}N_3+H]^+$: 234.1026; found: 234.1026.

EA: Anal. calcd. for $C_{15}H_{11}N_3$ (M_W: 233.27): C, 77.23; H, 4.75; N, 18.01. Found: C, 77.41; H, 4.85; N, 18.20.

4,4´´-Dichloro-2,2´:6´2´´-terpyridine (47)

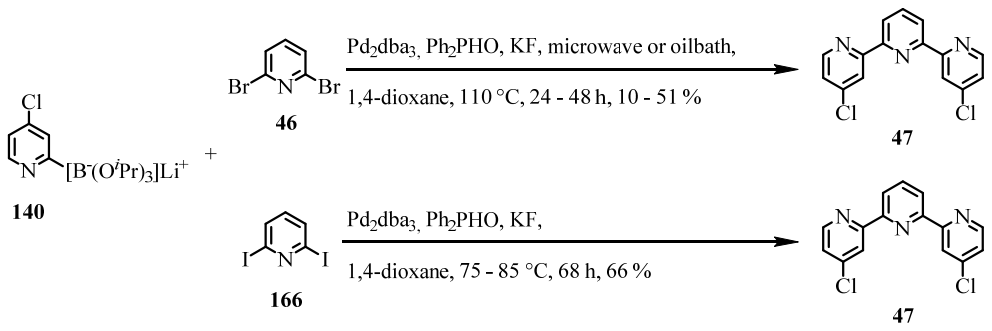

To prepare compound **47** two different assembly routes were followed in adaptation of a related protocol.[407] **Route A** describes the direct reaction of **140** with 2,6-dibromo-pyridine (**46**). In contrast **route B** describes the formation of **47** using **140** and 2,6-diiodo-pyridine (**166**) formed by previous transhalogenation from **46**.

Route A: For this procedure a microwave vessel was charged with 2,6-dibromo-pyridine (**46**) (60.4 mg, 0.25 mmol, 1.00 eq.) and mixed with a 1.5 fold excess of the lithium tri*iso*propyl-2-(4-chloropyridyl) borate **140** (231 mg, 0.75 mmol, 3.00 eq.) using KF (88.0 mg, 1.50 mmol, 6.00 eq.) as the base, Pd_2dba_3 (4.58 mg, 5.00 µmol, 0.02 eq.) as the catalyst and diphenylphosphine oxide (6.07 mg, 30.0 µmol, 0.12 eq.) as the ligand. All those reagents were evacuated and the flask was put under inert atmosphere three times. Now the mixture was dissolved in 1,4-dioxane (2 mL), which was previously degassed for 30 min and the microwave vessel was sealed pressure safe and heated up to 110 °C for 48 h in an oilbath. After diluting the reaction mixture with EtOAc it was filtered through a plug of silica gel (4 cm) to get rid of insoluble side products. Concentration of the solvent under reduced pressure yielded the crude product, which was now subjected to flash column chromatography on silica gel using a gradient of EtOAc / *n*-hexane (15:85 to 25:75) as the eluent. Upon evaporation of the solvent under reduced pressure the desired product **47** was obtained as white crystalline needles in a decent yield of 51% (38.4 mg, 127 µmol). However due to the severe scaling and reproducibility problems the reaction was facing, **route B** was developed as an alternative, using 2,6-diiodopyridine (**166**) as the transiodination product of **46**.

Route B: For this procedure a Schlenk tube was charged with 2,6-diiodo-pyridine (**166**) (331 mg, 1.00 mmol, 1.00 eq.) and mixed with a 1.5 fold excess of the lithium tri*iso*propyl-2-(4-chloropyridyl) borate **140** (971 mg, 3.00 mmol, 3.00 eq.) using KF (352 mg, 6.00 mmol, 6.00 eq.) as the base, Pd_2dba_3 (36.6 mg, 40.0 µmol, 0.04 eq.) as the

catalyst and diphenylphosphine oxide (50.0 mg, 240 µmol, 0.24 eq.) as the ligand. All those reagents were evacuated and the flask was put under inert atmosphere three times. Now the mixture was dissolved in 1,4-dioxane (8 mL), which was previously degassed for 30 min and the Schlenk tube was sealed pressure safe and heated up to 75 °C for 60 h. After diluting the reaction mixture with EtOAc it was filtered through a plug of silica gel (4 cm) to get rid of insoluble side products. Concentration of the solvent under reduced pressure yielded the crude product, which was now subjected to flash column chromatography on silica gel using a gradient of EtOAc / *n*-hexane (15:85 to 25:75) as the eluent. Upon evaporation of the solvent under reduced pressure the desired product **47** was obtained as white crystalline needles in a good yield of 66% (199 mg, 660 µmol). By applying a solvent diffusion technique using dichloromethane and hexane with an intermediate spacer layer of benzene it was possible to obtain single crystals of **47** suitable for x-ray structure determination. The crystallographic data of compound **47** are discussed in detailed form in chapter 9.2. Thus hereafter, only the remaining analytical data of target compound **47** are discussed.

Analytical data of 47:

T_M: 171-173 °C.

^{1}H-NMR (400 MHz, $CDCl_3$, ppm, 25 °C): δ_H = 8.55 (m, 4H, *H3 / H6 / H3´´ / H6´´*), 8.43 (d, $^3J_{H,H}$ = 7.8 Hz, 2H, *H3´ / H5´*), 7.92 (t, $^3J_{H,H}$ = 7.8 Hz, 1H, *H4´*), 7.31 (dd, $^3J_{H,H}$ = 5.4 Hz, $^4J_{H,H}$ = 1.9 Hz, 2H, *H5 / H5´´*).

^{13}C-NMR (101 MHz, $CDCl_3$, ppm, 25 °C): δ_C = 157.63 (C_q, 2C), 154.46 (C_q, 2C), 150.20 (C_t, 2C), 145.38 (C_q, 2C), 138.29 (C_t, 1C), 124.23 (C_t, 2C), 122.10 (C_t, 2C), 121.63 (C_t, 2C).

MS (EI$^+$, 70 eV): *m/z* [ion, intensity (%)] = 301.0 (M^+, 100), 266.0 (M^+-Cl, 33).

EA: Anal. calcd. for $C_{15}H_9Cl_2N_3$ (M_W: 302.16): C, 59.63; H, 3.00; N, 13.91. Found: C, 59.59; H, 3.04; N, 13.70.

4,4´´-Dimethoxy-2,2´:6´2´´-terpyridine (167a)

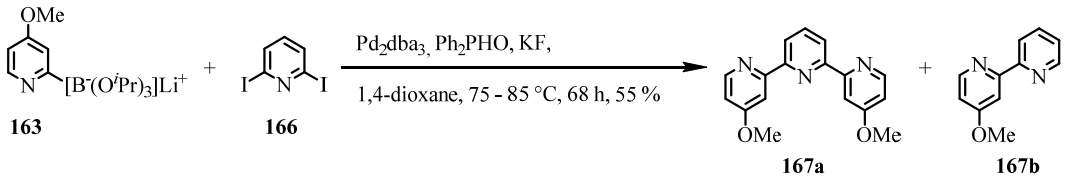

167a was prepared in a similar way to compound **47**. A Schlenk tube was charged with 2,6-diiodopyridine (**166)** (331 mg, 1.00 mmol, 1.00 eq.) and mixed with a 1.5 fold excess of lithium tri*iso*propyl 2-(4-methoxypyridyl) borate **163** (909 mg, 3.00 mmol, 3.00 eq.). KF (352 mg, 6.00 mmol, 6.00 eq.) was used as the base, Pd_2dba_3 (36.6 mg, 40.0 µmol, 0.04 eq.) as the catalyst and diphenylphosphine oxide (50.0 mg, 240 µmol, 0.24 eq.) as the ligand. All those reagents were evacuated and the flask was put under inert atmosphere three times. The mixture was dissolved in previously degassed 1,4-dioxane (16 mL) before the reaction vessel was sealed. The reaction was heated to 85 °C for 68 h. After dilution with EtOAc the reaction mixture was filtered through a plug of silica gel to get rid of insoluble side products. Concentration of residual solvent yielded the crude product which was now subjected to flash column chromatography on silica gel using a gradient from EtOAc / *n*-hexane (1:1) to pure EtOAc as the eluent. Evaporation of the solvent under reduced pressure yielded the desired terpyridine product **167a** in a yield of 32% (92.4 mg, 320 µmol) as well as the deiodinated 4-methoxybipyridine **167b** as a side product in a yield of 36% (66.5 mg, 360 µmol). By applying a solvent diffusion technique using dichloromethane and hexane with an intermediate spacer layer of benzene it was additionally, possible to obtain single crystals of **167a** suitable for x-ray structure determination. The crystallographic data of compound **167a** are discussed in detailed form in chapter 9.2. Thus hereafter, only the remaining analytical data of target compound **167a** are discussed.

Analytical data of 167a

T_M: 167-169 °C.

^{1}H-NMR (500 MHz, $CDCl_3$, ppm, 25 °C): δ_H = 8.50 (d, $^3J_{H,H}$ = 5.6 Hz, 2H, *H6 / H6´*), 8.41 (d, $^3J_{H,H}$ = 7.8 Hz, 2H, *H3´/ H5´*), 8.12 (d, $^4J_{H,H}$ = 2.5 Hz, 2H, *H3 / H3´*), 7.91 (t, $^3J_{H,H}$ = 7.8 Hz, 1H, *H4´*), 6.84 (dd, $^3J_{H,H}$ = 5.7 Hz, $^4J_{H,H}$ = 2.6 Hz, 2H, *H5 / H5´*), 3.94 (s, 6H, *–OCH_3*).

^{13}C-NMR (126 MHz, $CDCl_3$, ppm, 25 °C): δ_C = 166.79 (C_q, 2C), 158.14 (C_q, 2C), 155.24 (C_q, 2C), 150.61 (C_t, 2C), 138.04 (C_t, 1C), 121.54 (C_t, 2C), 110.10 (C_t, 2C), 107.18 (C_t, 2C), 55.40 ($C_{methoxy}$, 2C).

MS (EI$^+$, 70 eV): *m/z* [ion, intensity (%)] = 292.1 (M^+-H, 100), 278.1 (M^+-CH_3, 22), 263.1 (M^+-$2CH_3$, 44), 262.1 (M^+-OCH_3, 19), 146.6 (M^{2+}, 5).

HRMS (ESI-ToF): *m/z* calcd. for $[C_{17}H_{15}N_3O_2+H]^+$: 294.1237; found: 294.1238.

Analytical data of 167b

T_M: 65-67 °C.

^{1}H-NMR (250 MHz, $CDCl_3$, ppm, 25 °C): δ_H = 8.65 (d, $^3J_{H,H}$ = 4.0 Hz, 1H, *H6´*), 8.47 (d, $^3J_{H,H}$ = 5.7 Hz, 1H, *H6*), 8.37 (d, $^3J_{H,H}$ = 8.0 Hz, 1H, *H3´*), 7.95 (d, $^3J_{H,H}$ = 2.5 Hz, 1H, *H3*), 7.79 (app. td, $^3J_{H,H}$ = 7.8 Hz, $^4J_{H,H}$ = 1.8 Hz, 1H, *H4´*), 7.29 (ddd, $^3J_{H,H}$ = 7.4 Hz, $^3J_{H,H}$ = 4.8 Hz, $^4J_{H,H}$ = 1.0 Hz, 1H, *H5´*), 6.83 (dd, $^3J_{H,H}$ = 5.7 Hz, $^4J_{H,H}$ = 2.6 Hz, 1H, *H5*), 3.93 (s, 3H, *–OCH$_3$*).

^{13}C-NMR (126 MHz, $CDCl_3$, ppm, 25 °C): δ_C = 166.90 (C_q, 1C), 158.15 (C_q, 1C), 156.06 (C_q, 1C), 150.37 (C_t, 1C), 149.22 (C_t, 1C), 137.10 (C_t, 1C), 124.04 (C_t, 1C), 121.47 (C_t, 1C), 111.08 (C_t, 1C), 106.20 (C_t, 1C), 55.49 ($C_{methoxy}$, 1C).

MS (EI$^+$, 70 eV): *m/z* [ion, intensity (%)] = 186.1 (M^+, 85), 185.1 (M^+-H, 100), 156.1 (M^+-OCH_3 + H, 55), 155.1 (M^+-OCH_3, 22).

HRMS (ESI-ToF): *m/z* calcd. for $[C_{11}H_{10}N_2O+H]^+$: 187.0866; found: 187.0869.

Representative Procedure B (Functionalization of 4,4´´-disubstituted 2,2´:6´,2´´-terpyridines applying Suzuki-Miyaura reactions):

The described Suzuki-Miyaura cross-coupling reactions were performed by modification of a known literature procedure,[533] which was adapted according to the requirements and optimizations of each individual coupling reaction, respectively. Generally an oven-dried Schlenk tube was charged with 4,4´´-Dichloro-2,2´:6´2´´-terpyridine (**47**) or its corresponding derivative and the appropriate amount of arylboronic acid depending on the desired degree of substitution. Additionally, $PdCl_2\{P^tBu_2(p\text{-}NMe_2\text{-}Ph)\}_2$ (0.01 – 0.10 eq.) was used as the catalyst and K_2CO_3 (2 – 6 eq.) as the base. Once the reaction vessel has been charged with all the corresponding reagents the flask was repeatedly evacuated and backfilled with inert gas. Afterwards the reagents were suspended in a previously degassed solvent mixture of H_2O / toluene (usually 1:6). Once the solvents were added the Schlenk tube was sealed and heated to reflux (approx. 125 °C oilbath temp.) for usually 24h. The workup strongly varied based on the respective reagents and functional groups present and will be specified for each corresponding reaction.

4,4´´-Bis(4-(methylthio)phenyl)-2,2´:6´,2´´-terpyridine (168a)

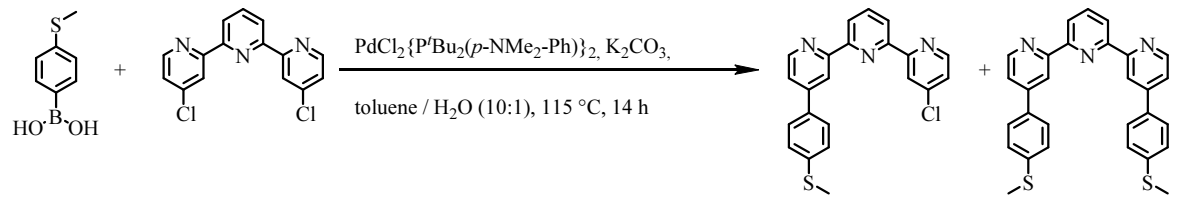

47 **168a** (37 %) **168b** (16 %)

168a was prepared applying the representative procedure B described above. 4,4´´-Dichloro-2,2´:6´2´´-terpyridine (**47**) (60.0 mg, 200 µmol, 1.00 eq.), 4-(methylthio)phenylboronic acid (84.0 mg, 500 µmol, 2.50 eq.), K_2CO_3 (112 mg, 800 µmol, 4.00 eq.) as the base and $PdCl_2\{P^tBu_2(p\text{-}NMe_2\text{-}Ph)\}_2$ (2.83 mg, 4.00 µmol, 0.02 eq.) as the catalyst were charged into a microwave vessel and suspended in degassed toluene (2.5 mL) and H_2O (250 µL). The reaction vessel was sealed and heated up to 115 °C for 14 h. The bright yellow mixture was allowed to cool to room temperature and was subsequently diluted with DCM and water. Now the reaction mixture was extracted with DCM (3 *x*) and with EtOAc (2 *x*) followed by extraction of the individual organic phases with brine (3 *x* each). The combined organic phases were dried over $MgSO_4$, filtered and residual solvent was evaporated under reduced pressure. The crude product was further purified by FCC using a gradient of EtOAc / *n*-hexane (1:3 to 1:1) to yield the desired disubstituted product 4,4´´-bis(4-(methylthio)phenyl)-2,2´:6´,2´´-terpyridine (**168a**) in a yield of 16% (15.0 mg, 30.0 µmol). By applying a solvent diffusion technique using dichloromethane and hexane with an intermediate spacer layer of benzene it was additionally, possible to obtain single crystals of **168a** suitable for x-ray structure determination. The crystallographic information of compound **168a** are discussed in detailed form in section 9.2. Thus hereafter, only the remaining analytical data of target compound **168a** are discussed. Additionally, 4-chloro-4´´-(4-(methylthio)phenyl)-2,2´:6´,2´´-terpyridine (**168a**) was isolated as the undesired monosubstituted side product in a moderate yield of 37% (29.0 mg, 70.0 µmol).

Analytical data of 168a:

$\mathbf{T_M}$: decomposition > 245 °C.

^{1}H-NMR (400 MHz, $CDCl_3$, ppm, 25 °C): δ_H = 8.83 (d, $^4J_{H,H}$ = 1.2 Hz, 2H, *H3 / H3´´*), 8.72 (dd, $^3J_{H,H}$ = 5.1 Hz, $^4J_{H,H}$ = 0.5 Hz,2H, *H6 / H6´´*), 8.47 (d, $^3J_{H,H}$ = 7.8 Hz, 2H, *H3´´ / H5´*), 7.99 (t, $^3J_{H,H}$ = 7.8 Hz, 1H, *H4´*), 7.71 (d, $^3J_{H,H}$ = 8.5 Hz, 4H, H_{phenyl}),

7.53 (dd, $^{3}J_{H,H}$ = 5.1 Hz, $^{4}J_{H,H}$ = 1.9 Hz,2H, *H5 / H5´´*), 7.37 (d, $^{3}J_{H,H}$ = 8.5 Hz, 4H, H_{phenyl}), 2.55 (s, 6H, *–SCH₃*).

^{13}C-NMR (101 MHz, $CDCl_3$, ppm, 25 °C): δ_C = 157.08 (C_q, 2C), 155.63 (C_q, 2C), 149.95 (C_t, 2C), 148.70 (C_q, 2C), 140.55 (C_q, 2C), 138.24 (C_t, 1C), 135.19 (C_q, 2C), 127.62 (C_{phenyl}, 4C), 126.88 (C_{phenyl}, 4C), 121.55 (C_t, 2C), 121.44 (C_t, 2C), 119.04 (C_t, 2C), 15.73 ($C_{thiomethyl}$, 2C). Note: Some quaternary carbon atoms cannot be unambiguously identified in the ^{13}C-NMR spectrum.

MS (EI$^+$, 70 eV): *m/z* [ion, intensity (%)] = 477.1 (M^+, 100), 462.1 (M^+-CH_3, 11), 430.2 (M^+-SCH_3, 8), 415.0 (M^+-SCH_3-CH_3, 6), 238.6 (M^{2+}, 8).

HRMS (ESI-ToF): *m/z* calcd. for $[C_{29}H_{23}N_3S_2+H]^+$: 478.1406; found: 478.1407.

Analytical data of 168b:

T_M: 133-136 °C.

^{1}H-NMR (400 MHz, $CDCl_3$, ppm, 25 °C): δ_H = 8.74 (d, $^{4}J_{H,H}$ = 1.2 Hz, 1H, *H3*), 8.71 (d, $^{3}J_{H,H}$ = 5.1 Hz, 1H, *H6*), 8.58 (m, 2H, *H3´´ / H6´´*), 8.49 (d, $^{3}J_{H,H}$ = 7.8 Hz, 1H, *H3´ or H5´*), 8.44 (d, $^{3}J_{H,H}$ = 7.8 Hz, 1H, *H3´ or H5´*), 7.96 (t, $^{3}J_{H,H}$ = 7.8 Hz, 1H, *H4´*), 7.70 (d, $^{3}J_{H,H}$ = 8.4 Hz, 2H, H_{phenyl}), 7.51 (dd, $^{3}J_{H,H}$ = 5.1 Hz, $^{4}J_{H,H}$ = 1.8 Hz, 1H, *H5*), 7.39 (d, $^{3}J_{H,H}$ = 8.4 Hz, 2H, H_{phenyl}), 7.32 (dd, $^{3}J_{H,H}$ = 5.2 Hz, $^{4}J_{H,H}$ = 2.1 Hz, 1H, *H5´´*), 2.54 (s, 3H, *–SCH₃*).

^{13}C-NMR (101 MHz, $CDCl_3$, ppm, 25 °C): δ_C = 157.96 (C_q, 1C) 156.75 (C_q, 1C), 155.85 (C_q, 1C), 154.39 (C_q, 1C), 150.22 (C_t, 1C), 149.90 (C_t, 1C), 148.96 (C_q, 1C), 145.32 (C_q, 1C), 140.56 (C_q, 1C), 138.25 (C_t, 1C), 135.14 (C_q, 1C), 127.67 (C_{phenyl}, 2C), 126.92 (C_{phenyl}, 2C), 124.13 (C_t, 1C), 122.12 (C_t, 1C), 121.72 (C_t, 1C), 121.68 (C_t, 1C), 121.67 (C_t, 1C), 118.88 (C_t, 1C), 15.70 ($C_{thiomethyl}$, 1C).

MS (EI$^+$, 70 eV): *m/z* [ion, intensity (%)] = 389.1 (M^+, 100), 374.1 (M^+-CH_3, 15), 342.1 (M^+-SCH_3, 19), 194.6 (M^{2+}, 5).

HRMS (ESI-ToF): *m/z* calcd. for $[C_{22}H_{16}ClN_3S+H]^+$: 390.0826; found: 390.0824.

2-((4-Bromophenyl)thio)ethyltrimethylsilane (169)

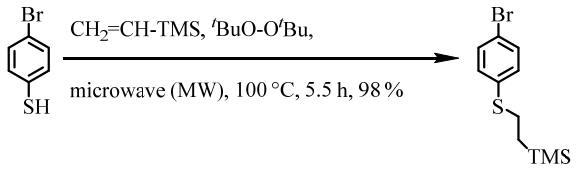

150 **169**

169 was prepared according to reported literature protocols.[536,565,537] A microwave vessel was charged with 4-bromothiophenol (**150**) (11.1 g, 58.8 mmol, 1.00 eq.), vinyltrimethylsilane (7.29 g, 10.7 mL, 70.6 mmol, 1.20 eq.) and di-*tert*-butyl peroxide (^{t}BuO)$_2$ (1.29 g, 1.61 mL, 8.82 mmol, 0.15 eq.). The reaction mixture was degassed before the vessel was closed and heated to 100 °C for 5.5 h. After cooling down to room temperature the reaction mixture was diluted with *n*-hexane and washed twice with aqueous NaOH-solution (1M). The combined aqueous phases were washed with *n*-hexane (3 *x*) and the combined organic layers were dried over $MgSO_4$, and subsequently concentrated under reduced pressure. Finally the crude product was purified by vacuum distillation (b.p.: 103 °C at $9.4 \cdot 10^{-2}$ mbar) to yield the desired product **169** as a colorless liquid in a yield of 98% (16.7 g, 57.8 mmol).

Analytical data of 169:

^{1}H-NMR (400 MHz, $CDCl_3$, ppm, 25 °C): δ_H = 7.37 (d, $^3J_{H,H}$ = 8.6 Hz, 2H, H_{phenyl}), 7.14 (d, $^3J_{H,H}$ = 8.6 Hz, 2H, H_{phenyl}), 2.91 (m, 2H, *–S–**CH$_2$**–CH$_2$–TMS*), 0.90 (m, 2H, *-S-CH$_2$-**CH$_2$**–TMS*), 0.02 (s, 9H, H_{TMS}).

^{13}C-NMR (101 MHz, $CDCl_3$, ppm, 25 °C): δ_C = 136.68 (C_q, 1C), 132.02 (C_t, 2C), 130.63 (C_t, 2C), 119.59 (C_q, 1C), 29.88 (C_{ethyl}, 1C), 16.97 (C_{ethyl}, 1C), -1.56 (C_{TMS}, 3C).

MS (EI$^+$, 70 eV): *m/z* [ion, intensity (%)] = 290.0 (M^+, 8), 73.0 (TMS^+, 100).

EA: Anal. calcd. for $C_{11}H_{17}BrSSi$ (M_W: 289.31): C, 45.67; H, 5.92; N, 0.00. Found: C, 45.70; H, 5.95; N, 0.00.

2,4,6-Tris(4-(2-(trimethylsilyl)ethyl)thiophenyl)-1,3,5,2,4,6-trioxatriborinane (170)

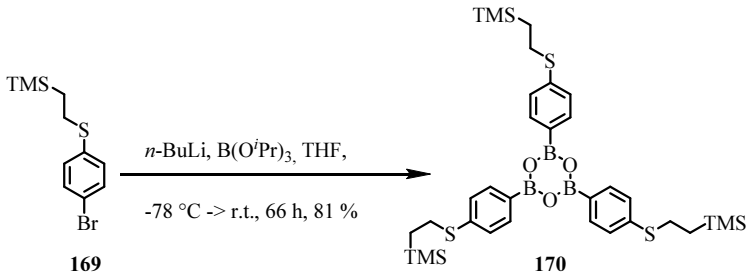

170 was prepared in adaptation of a reported literature procedure.[536,565] 2-((4-Bromophenyl)-thio)ethyltrimethylsilane (**169**) (9.55 g, 33.0 mmol, 1.00 eq.) was dissolved in THF (90 mL) and degassed for 30 min before it was cooled to –78 °C. Subsequently *n*-BuLi (2.5M in hexanes, 21.8 mL, 54.4 mmol, 1.65 eq.) was added dropwise via a syringe pump over 2 h causing the solution to turn yellow. After 30 min of further stirring at -78 °C tri*iso*propylborate (22.5 g, 27.6 mL, 116 mmol, 3.52 eq.) was added dropwise over 1 h. The reaction was allowed to slowly warm up to room temperature in the cooling bath for 66 h before it was quenched by the addition of water. The reaction mixture was concentrated to the water phase prior to extraction with Et_2O (3 *x* 100 mL). The combined organic layers were washed with water, brine and once more with water, dried over $MgSO_4$ and concentrated under reduced pressure to yield the crude product as a colorless solid. Repeated recrystallization from *n*-hexane afforded the desired pure product **170** in a good yield of 81% (6.29 g, 8.88 mmol) as a white powder

Analytical data of 170:

^{1}H-NMR (400 MHz, $CDCl_3$, ppm, 25 °C): δ_H = 8.08 (d, $^3J_{H,H}$ = 8.2 Hz, 6H, H_{phenyl}), 7.34 (d, $^3J_{H,H}$ = 8.2 Hz, 6H, H_{phenyl}), 3.04 (m, 6H, *–S–**CH₂**–CH₂–TMS*), 0.98 (m, 6H, *-S-CH₂-**CH₂**–TMS*), 0.06 (s, 27H, H_{TMS}).

^{13}C-NMR (101 MHz, $CDCl_3$, ppm, 25 °C): δ_C = 143.96 (C_q, 3C), 136.13 (C_t, 6C), 126.69 (C_t, 6C), 28.36 (C_{ethyl}, 3C), 16.85 (C_{ethyl}, 3C), 1.52 (C_{TMS}, 9C). Note: The carbon atom bound to the boron cannot be seen in the ^{13}C-NMR spectrum.

MS (EI$^+$, 70 eV): *m/z* [ion, intensity (%)] = 708.3 (M^+, 9), 101.1 (Et–TMS^+, 20), 73.1 (TMS^+, 100).

4,4´´-bis(4-((2-(trimethylsilyl)ethyl)thio)phenyl)-2,2´:6´,2´´-terpyridine (171)

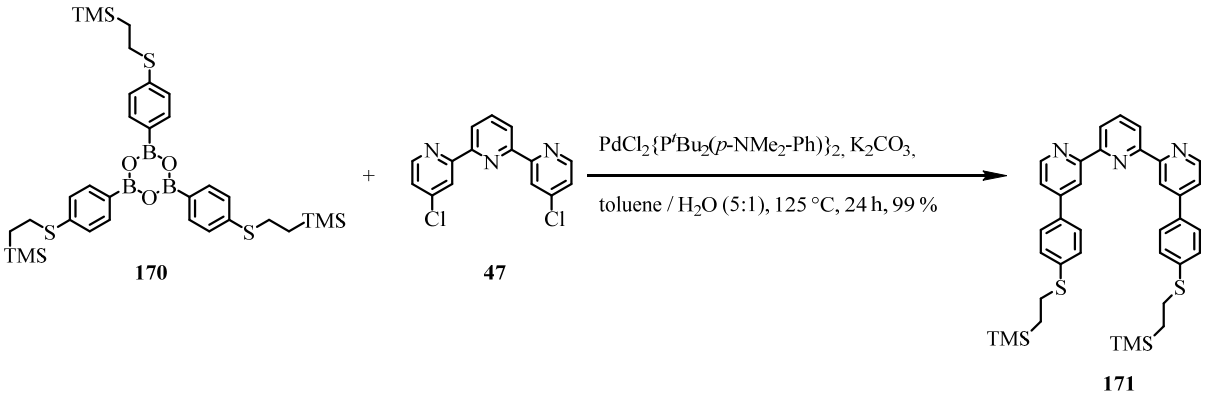

171 was prepared applying the representative procedure B described above. The starting materials 4,4´´-Dichloro-2,2´:6´2´´-terpyridine **47** (159 mg, 500 µmol, 1.00 eq.) and 2,4,6-tris(4-(2-(trimethyl-silyl)ethyl)thiophenyl)-1,3,5,2,4,6-trioxatriborinane **170** (709 mg, 1.00 mmol, 2.00 eq.) together with the base K_2CO_3 (419 mg, 3.00 mmol, 6.00 eq.) and $PdCl_2\{P^tBu_2(p\text{-}NMe_2\text{-}Ph)\}_2$ (35.4 mg, 50.0 µmol, 1.00 eq.) as the catalyst were charged into a Schlenk tube and suspended in degassed toluene (25 mL) and H_2O (5 mL). The reaction vessel was sealed and heated up to 125 °C for 24 h. The black suspension was allowed to cool to room temperature and successively diluted with DCM and water. Now the reaction mixture was extracted with DCM (3 *x*) and with EtOAc (3 *x*) followed by washing of the individual organic layers with brine (3 *x* each). The combined organic phases were dried over $MgSO_4$, filtered and concentrated under reduced pressure. Finally the crude product was further purified by FCC using EtOAc / *n*-hexane (1:3) as eluent to yield the desired disubstituted product 4,4´´-bis(4-((2-(trimethylsilyl)ethyl)thio)phenyl)-2,2´:6´,2´´-terpy-ridine **171** in a yield of 99% (320 mg, 490 µmol). By applying a solvent diffusion technique using dichloromethane and hexane with an intermediate spacer layer of benzene it was additionally, possible to obtain single crystals of **171** suitable for x-ray structure determination. The crystallographic information of compound **171** is discussed in detailed form in section 9.2. Thus hereafter, only the remaining analytical data of target compound **171** are discussed.

Analytical data of 171:

T_M: 172-173 °C.

^{1}H-NMR (400 MHz, $CDCl_3$, ppm, 25 °C): δ_H = 8.80 (d, $^4J_{H,H}$ = 1.2 Hz, 2H, *H3 / H3´´*), 8.70 (d, $^3J_{H,H}$ = 5.1 Hz, 2H, *H6´/H6´´*), 8.46 (d, $^3J_{H,H}$ = 7.8 Hz, 2H, *H3´/H5´*),

7.96 (t, $^{3}J_{H,H}$ = 7.8 Hz, 1H, *H4´*), 7.68 (d, $^{3}J_{H,H}$ = 8.4 Hz, 4H, H_{phenyl}), 7.50 (dd, $^{3}J_{H,H}$ = 5.1 Hz, $^{4}J_{H,H}$ = 1.8 Hz, 2H, *H5 / H5´´*), 7.39 (d, $^{3}J_{H,H}$ = 8.4 Hz, 4H, H_{phenyl}), 3.03 (m, 4H, *-S-**CH₂**-CH₂–TMS*), 0.98 (m, 4H, *–S–CH₂–**CH₂**–TMS*), 0.06 (s, 18H, H_{TMS}).

^{13}C-NMR (101 MHz, $CDCl_3$, ppm, 25 °C): δ_C = 157.03 (C_q, 2C), 155.66 (C_q, 2C), 149.86 (C_t, 2C), 148.60 (C_q, 2C), 139.55 (C_q, 2C), 138.07 (C_t, 1C), 135.50 (C_q, 2C), 128.73 (C_{phenyl}, 4C), 127.53 (C_{phenyl}, 4C), 121.55 (C_t, 2C), 121.38 (C_t, 2C), 118.89 (C_t, 2C), 29.19 (C_{ethyl}, 2C), 16.89 (C_{ethyl}, 2C), 1.49 (C_t, 2C).

MS (EI$^+$, 70 eV): *m/z* [ion, intensity (%)] = 649.2 (M^+, 28), 73.0 (TMS^+, 100).

EA: Anal. calcd. for $C_{37}H_{43}N_3S_2Si_2$ (M_W: 650.06): C, 68.36; H, 6.67; N, 6.46. Found: C, 68.52; H, 6.66; N, 6.43.

_S,S´_-([2,2´:6´,2´´-terpyridine]-4,4´´-diylbis(4,1-phenylene)) diethanethioate (131)

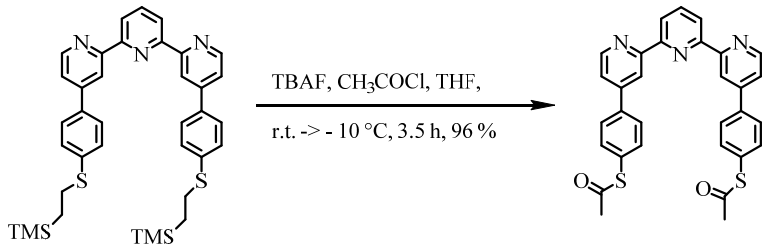

171 **131**

131 was prepared by transprotection of 4,4´´-bis(4-((2-(trimethylsilyl)ethyl)thio)phenyl)-2,2´:6´,2´´-terpyridine **171**. An oven-dried round-bottom flask was charged with terpyridine precursor **171** (650 mg, 1.00 mmol, 1.00 eq.) and put under inert atmosphere. Subsequently the terpyridine ligand was dissolved in rigorously degassed THF (120 mL) as the solvent, before TBAF (1M in THF, 10.0 mL, 10.0 mmol, 10.0 eq.) was added which caused the former colorless solution to turn orange immediately. After 1.5 h of stirring the reaction mixture was cooled down to -10 °C and previously degassed acetyl chloride (15.7 g, 14.3 mL, 200 mmol, 200 eq.) was added dropwise to the orange solution which subsequently turned colorless again followed by a bright yellow color. After further 2 h in the cooling bath the reaction was cautiously quenched by the addition of saturated $NaHCO_3$ -solution (240 mL). The reaction mixture was extracted with DCM (2 *x*) and with EtOAc (2 *x*), before the combined organic phases were dried over $MgSO_4$, filtered and concentrated under reduced pressure. Finally the resulting crude product was further purified by FCC using a gradient from EtOAc / *n*-hexane (1:1) to pure EtOAc to yield the desired disubstituted and poorly soluble product *S,S´*-([2,2´:6´,2´´-terpyridine]-4,4´´-diylbis(4,1-phenylene)) diethanethioate **131** in an excellent yield of 96% (514 mg, 964 µmol). By applying a solvent diffusion technique using dichloromethane and hexane with an intermediate spacer layer of benzene it was additionally, possible to obtain single crystals of **131** suitable for x-ray structure determination. The crystallographic information of compound **131** are discussed in detailed form in section 9.2. Thus hereafter, only the remaining analytical data of target compound **131** are discussed.

Analytical data of 131:

T_M: 241-244 °C.

^{1}H-NMR (400 MHz, $CDCl_3$, ppm, 25 °C): δ_H = 8.82 (d, $^4J_{H,H}$ = 1.2 Hz, 2H, *H3 / H3´*), 8.77 (d, $^3J_{H,H}$ = 5.1 Hz, 2H, *H6´ / H6´´*), 8.50 (d, $^3J_{H,H}$ = 7.8 Hz, 2H, *H3´ / H5´*),

8.00 (t, $^{3}J_{H,H}$ = 7.8 Hz, 1H, *H4´*), 7.80 (d, $^{3}J_{H,H}$ = 8.4 Hz, 4H, H_{phenyl}), 7.55 (app. dd, $^{3}J_{H,H}$ = 5.1 Hz, $^{4}J_{H,H}$ = 3.2 Hz, 6H, *H5 / H5´´ /* H_{phenyl}), 2.45 (s, 3H, H_{methyl}).

^{13}C-NMR (101 MHz, $CDCl_3$, ppm, 25 °C): δ_C = 193.77 ($C_{C=O}$, 2C), 156.88 (C_q, 2C), 149.76 (C_t, 2C), 148.79 (C_q, 2C), 139.69 (C_q, 2C), 138.34 (C_t, 1C), 135.29 (C_{phenyl}, 4C), 129.40 (C_q, 2C), 128.12 (C_{phenyl}, 4C), 125.23 (C_q, 2C), 121.98 (C_t, 2C), 121.90 (C_t, 2C), 119.61 (C_t, 2C), 30.55 (C_{methyl}, 2C).

MS (FAB$^+$): *m/z* [ion, intensity (%)] = 534.1 (M^+, 100), 491.1 (M^+-[(C=O)CH_3], 17), 449.1 (M^+-2[(C=O)CH_3], 17).

MS (EI$^+$, 70 eV): *m/z* [ion, intensity (%)] = 491.1 (M^+-[(C=O)CH_3], 25), 449.1 (M^+-2[(C=O)CH_3], 100).

HRMS (ESI-ToF): *m/z* calcd. for $[C_{31}H_{23}N_3O_2S_2+H]^+$: 534.1304; found: 534.1305.

4-chloro-4′′-phenyl-2,2′:6′,2′′-terpyridine (212)

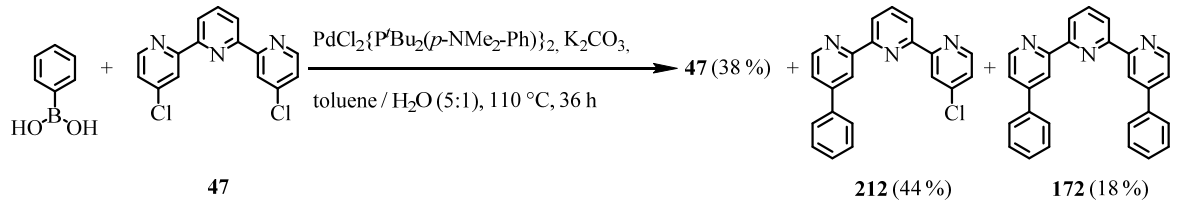

212 was prepared applying the representative procedure B described above. The starting material 4,4′′-Dichloro-2,2′:6′2′′-terpyridine (**47**) (302 mg, 1.00 mmol, 1.00 eq.), the coupling agent phenylboronic acid (101 mg, 0.80 mmol, 0.80 eq.), K_2CO_3 (349 mg, 2.50 mmol, 2.50 eq.) as the base and the catalyst $PdCl_2\{P^tBu_2(p\text{-}NMe_2\text{-}Ph)\}_2$ (35.8 mg, 50.0 µmol, 0.05 eq.) were charged into a Schlenk tube and suspended in degassed toluene (30 mL) and H_2O (6 mL). The reaction vessel was sealed and heated to 110 °C for 36 h. The reaction mixture was allowed to cool to room temperature and was subsequently diluted with DCM, water and brine. Now the reaction mixture was extracted with DCM (3 *x*) and with EtOAc (2 *x*). The combined organic layers were dried over $MgSO_4$, filtered and residual solvent was removed under reduced pressure. The crude product was purified by FCC using a solvent gradient ranging from EtOAc / *n*-hexane (3:17) to EtOAc / *n*-hexane (1:3). First of all the unreacted starting material **47** was reisolated in a yield of 38% (117 mg, 384 µmol). The desired monosubstituted target compound 4-chloro-4′′-phenyl-2,2′:6′,2′′-terpyridine **212** could be isolated in a yield of 44% (150 mg, 437 µmol).. Additionally, the disubstituted side product 4,4′′-diphenyl-2,2′:6′,2′′-terpyridine **172** was obtained in a yield of 18% (70.1 mg, 182 µmol). Another method to yield the disubstituted derivative 4,4′′-diphenyl-2,2′:6′,2′′-terpyridine (**172**) quantitatively is described below and required an alteration of the reagents′ stoichiometric ratios. Hence the analytical details of compound **172** are also discussed in the passage below.

Analytical data 212:

^{1}H-NMR (400 MHz, $CDCl_3$, ppm, 25 °C): δ_H = 8.79 (dd, $^4J_{H,H}$ = 1.7 Hz, $^5J_{H,H}$ = 0.6 Hz 1H, *H3′′*), 8.74 (dd, $^3J_{H,H}$ = 5.1 Hz, $^5J_{H,H}$ = 0.6 Hz 1H, *H6′′*), 8.60 (d, $^4J_{H,H}$ = 1.7 Hz, 1H, *H3*), 8.58 (d, $^3J_{H,H}$ = 5.2 Hz, 1H, *H6*), 8.52 (dd, $^3J_{H,H}$ = 7.8 Hz, $^4J_{H,H}$ = 1.0 Hz, 1H, *H3′* / H5′**), 8.46 (dd, $^3J_{H,H}$ = 7.8 Hz, $^4J_{H,H}$ = 1.0 Hz, 1H, *H3′* / H5′**), 7.98 (t, $^3J_{H,H}$ = 7.8 Hz, 1H, *H4′*), 7.79 (dd, $^3J_{H,H}$ = 8.3 Hz, $^4J_{H,H}$ = 1.3 Hz, 2H, H_{phenyl}), 7.59 – 7.45 (m, 4H, *H5′′* + $3H_{phenyl}$), 7.33 (dd, $^3J_{H,H}$ = 5.2 Hz, $^4J_{H,H}$ = 2.0 Hz, 1H, *H5*).

^{13}C NMR (101 MHz, $CDCl_3$, ppm, 25 °C): δ_C = 157.86 (C_q, 1C), 156.62 (C_q, 1C), 155.77 (C_q, 1C), 154.30 (C_q, 1C), 150.11 (C_t, 1C), 149.76 (C_t, 1C), 149.59 (C_q, 1C), 145.22 (C_q, 1C), 138.70 (C_q, 1C), 138.14 (C_t, 1C), 129.29 (C_{phenyl}, 2C), 129.20 (C_t, 1C), 127.35 (C_{phenyl}, 2C), 124.03 (C_t, 1C), 122.08 (C_t, 1C), 122.04 (C_t, 1C), 121.62 (C_t, 1C), 121.56 (C_t, 1C), 119.27 (C_t, 1C).

ESI-MS (MeOH, *positive* ion mode): *m/z* [ion, intensity (%)] = 344.1 ($M+H^+$, 100).

HRMS (ESI-ToF): *m/z* calcd. for $[C_{21}H_{14}ClN_3+H]^+$: 344.0949; found: 344.0955.

4,4´´-Diphenyl-2,2´:6´,2´´-terpyridine (172)

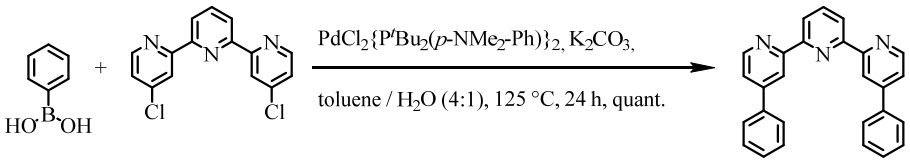

47 172

172 was prepared by modifying the representative procedure B described above. 4,4´´-Dichloro-2,2´:6´2´´-terpyridine (**47**) (90.6 mg, 0.30 mmol, 1.00 eq.), phenylboronic acid (377 mg, 3.00 mmol, 10.0 eq.), $PdCl_2\{P^tBu_2(p\text{-}NMe_2\text{-}Ph)\}_2$ (10.7 mg, 15.0 µmol, 0.05 eq.), and K_2CO_3 (105 mg, 0.75 mmol, 2.50 eq.) were charged into a Schlenk tube and suspended in previously degassed toluene (8 mL) and H_2O (2 mL). The reaction vessel was sealed and heated to 125 °C for 24 h. After cooling to room temperature the reaction mixture was diluted with DCM, brine and water prior to the extraction with DCM (3 *x*). The combined organic phases were washed with brine (2 *x*), dried over $MgSO_4$ and subsequently filtered prior to the evaporation of residual solvent under reduced pressure. The crude product was purified by FCC using a gradient of solvent mixtures ranging from EtOAc / *n*-hexane (3:17) up to EtOAc / *n*-hexane (1:3). The desired disubstituted 4,4´´-diphenyl-2,2´:6´,2´´-terpyridine **172** could be isolated as colorless needles in quantitative yield (116 mg, 301 µmol).

Analytical data 172:

^{1}H-NMR (400 MHz, $CDCl_3$, ppm, 25 °C): δ_H = 8.91 (dd, $^4J_{H,H}$ = 1.8 Hz, $^5J_{H,H}$ = 0.7 Hz 2H, *H3 / H3´´*), 8.76 (dd, $^3J_{H,H}$ = 5.1 Hz, $^5J_{H,H}$ = 0.7 Hz 2H, *H6 / H6´´*), 8.51 (d, $^3J_{H,H}$ = 7.8 Hz, 2H, *H3´ / H5´*), 8.01 (t, $^3J_{H,H}$ = 7.8 Hz, 1H, *H4´*), 7.83 – 7.78 (m, 4H, H_{phenyl}), 7.58 (dd, $^3J_{H,H}$ = 5.1 Hz, $^4J_{H,H}$ = 1.9 Hz, 2H, *H5 / H5´´*), 7.56 – 7.47 (m, 6H, H_{phenyl}).
^{13}C NMR (101 MHz, $CDCl_3$, ppm, 25 °C): δ_C = 156.90 (C_q, 2C), 155.48 (C_q, 2C), 149.79 (C_t, 2C), 149.37 (C_q, 2C), 138.66 (C_q, 2C), 138.19 (C_t, 1C), 129.30 (C_{phenyl}, 4C), 127.29 (C_{phenyl}, 4C), 121.82 (C_t, 2C), 121.49 (C_t, 2C), 119.43 (C_t, 2C). In the ^{13}C-spectrum and in the DEPT-135 one signal less than expected was found most likely due to coincident signals.
MS (EI$^+$, 70 eV): *m/z* [ion, intensity (%)] = 385.2 (M^+, 100), 231.1 (M^+-2 Phenyl, 6), 192.6 (M^{2+}, 12).
ESI-MS (MeCN, *positive* ion mode): *m/z* [ion, intensity (%)] = 386.2 ($M+H^+$, 100)
HRMS (ESI-ToF): *m/z* calcd. for $[C_{27}H_{19}N_3+H]^+$: 386.1652; found: 386.1657.

4-chloro-4´´-(4-(trifluoromethyl)phenyl)-2,2´:6´,2´´-terpyridine (173)

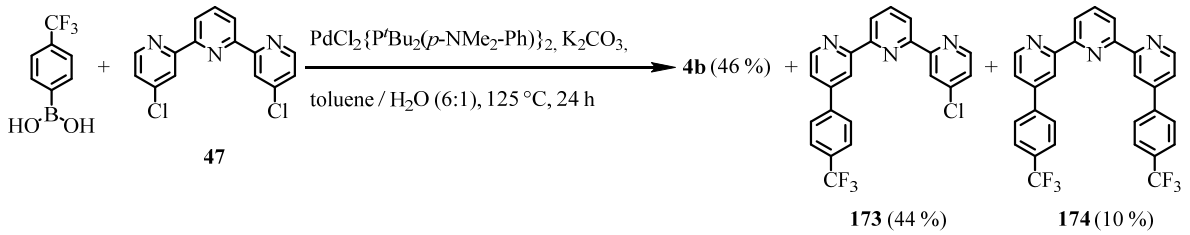

173 was prepared applying the representative procedure B described above. The reagents 4,4´´-Dichloro-2,2´:6´2´´-terpyridine **47** (90.6 mg, 300 µmol, 1.00 eq.) and 4-(trifluoromethyl)phenylboronic acid (42.7 mg, 225 µmol, 0.75 eq.), the catalyst $PdCl_2\{P^tBu_2(p\text{-}NMe_2\text{-}Ph)\}_2$ (6.37 mg, 9.00 µmol, 0.03 eq.) and the required base K_2CO_3 (83.8 mg, 600 µmol, 2.00 eq.) were charged into a Schlenk tube and suspended in previously degassed toluene (6 mL) and H_2O (1 mL). The reaction vessel was sealed and heated up to 125 °C for 24 h. The reaction mixture was allowed to cool down to room temperature and was subsequently diluted with DCM and water. Now the reaction mixture was extracted with DCM (2 *x*) and with EtOAc (2 *x*) followed by extraction of the combined organic phases with brine (3 *x*). The organics were dried over $MgSO_4$, filtered and residual solvent was removed under reduced pressure. The crude product was purified by FCC using a solvent mixture of EtOAc / *n*-hexane (1:3) to yield the desired monosubstituted 4-chloro-4´´-(4-(trifluoromethyl)phenyl)-2,2´:6´,2´´-terpyridine **173** in a yield of 44% (53.9 mg, 131 µmol).Additionally, the starting material **47** in a yield of 44% (41.8 mg, 138 µmol) and the disubstituted side product 4,4´´-bis(4-(trifluoromethyl)phenyl)-2,2´:6´,2´´-terpyridine **173** in 10% (29.0 mg, 70.0 µmol) yield could be isolated.

Analytical data of 4-Chloro-4´´-(4-(trifluoromethyl)phenyl)-2,2´:6´,2´´-terpyridine (173):

^{1}H-NMR (400 MHz, $CDCl_3$, ppm, 25 °C): δ_H = 8.75 (app. dd, $^3J_{H,H}$ = 5.7 Hz, $^4J_{H,H}$ = 0.8 Hz, 2H, *H3* / H6* / H3´´* / H6´´**), 8.56 (app. dd, $^3J_{H,H}$ = 5.3 Hz, $^4J_{H,H}$ = 3.7 Hz, 2H, *H3* / H6* / H3´´* / H6´´**), 8.50 (dd, $^3J_{H,H}$ = 7.8 Hz, $^4J_{H,H}$ = 1.0 Hz, 1H, *H3´* / H5´**), 8.44 (dd, $^3J_{H,H}$ = 7.8 Hz, $^4J_{H,H}$ = 1.0 Hz, 1H, *H3´* / H5´**), 7.96 (t, $^3J_{H,H}$ = 7.8 Hz, 1H, *H4´*), 7.85 (d, $^3J_{H,H}$ = 8.2 Hz, 2H, H_{phenyl}), 7.78 (d, $^3J_{H,H}$ = 8.2 Hz, 2H, H_{phenyl}), 7.51 (dd, $^3J_{H,H}$ = 5.0 Hz, $^4J_{H,H}$ = 1.9 Hz, 1H, *H5*), 7.31 (dd, $^3J_{H,H}$ = 5.2 Hz, $^4J_{H,H}$ = 2.1 Hz, 1H, *H5´´*).

^{13}C-NMR (101 MHz, $CDCl_3$, ppm, 25 °C): δ_C = 157.84 (C_q, 1C), 156.99 (C_q, 1C), 155.50 (C_q, 1C), 154.47 (C_q, 1C), 150.25 (C_t, 1C), 150.07 (C_t, 1C), 148.23 (C_q, 1C),

145.32 (C_q, 1C), 142.35 (C_q, 1C), 138.29 (C_t, 1C), 131.27 (q, $^1J_{C,F}$ = 32.5 Hz, -CF_3, 1C), 127.84 (C_{phenyl}, 2C), 126.34 (q, $^3J_{C,F}$ = 3.7 Hz, C_{phenyl}, 2C), 124.17 (C_t, 1C), 122.17 (C_t, 1C), 122.14 (C_t, 1C), 121.88 (C_t, 1C), 121.66 (C_t, 1C), 119.36 (C_t, 1C). In the ^{13}C-spectrum and in the DEPT-135 one signal less than expected was found most likely due to coincident signals.

^{19}F NMR (376 MHz, $CDCl_3$, ppm, 25 °C): δ_F = –62.60 (3F).

MS (EI$^+$, 70 eV): *m/z* [ion, intensity (%)] = 411.1 (M^+, 100), 342.2 (M^+-CF_3, 5), 205.6 (M^{2+}, 8).

ESI-MS (MeOH, *positive* ion mode): *m/z* [ion, intensity (%)] = 412.1 ($M+H^+$, 100).

HRMS (ESI-ToF): *m/z* calcd. for $[C_{22}H_{13}ClF_3N_3+H]^+$: 412.0823; found: 412.0829.

EA: Anal. calcd. for $C_{22}H_{13}ClF_3N_3$ (M_W: 411.81): C, 64.17; H, 3.18; N, 10.20. Found: C, 64.08; H, 3.40; N, 10.15.

4,4´´-Bis(4-(trifluoromethyl)phenyl)-2,2´:6´,2´´-terpyridine (174)

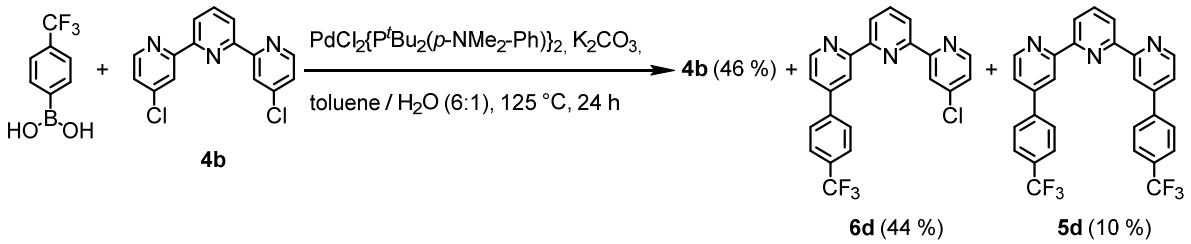

As discussed above the reaction of 4,4´´-Dichloro-2,2´:6´2´´-terpyridine (**47**) with 4-(trifluoromethyl)phenylboronic acid also yielded the undesired disubstituted compound 4,4´´-bis(4-(trifluoromethyl)phenyl)-2,2´:6´,2´´-terpyridine **174** apart from the desired 4-chloro-4´´-(4-(trifluoromethyl)phenyl)-2,2´:6´,2´´-terpyridine **173**. The analytical data of this unavoidable side product **174** are listed below.

Analytical data of 4,4´´-Bis(4-(trifluoromethyl)phenyl)-2,2´:6´,2´´-terpyridine (174):

^{1}H-NMR (400 MHz, $CDCl_3$, ppm, 25 °C): δ_H = 8.79 (m, 4H, *H3 / H6 / H3´´ / H6´´*),8.50 (d, $^{3}J_{H,H}$ = 7.8 Hz, 2H, *H3´ / H5´*), 8.00 (t, $^{3}J_{H,H}$ = 7.8 Hz, 1H, *H4´*), 7.84 (d, $^{3}J_{H,H}$ = 8.2 Hz, 2H, H_{phenyl}), 7.75 (d, $^{3}J_{H,H}$ = 8.2 Hz, 2H, H_{phenyl}), 7.54 (dd, $^{3}J_{H,H}$ = 5.0 Hz, $^{4}J_{H,H}$ = 1.9 Hz, 2H, *H5 / H5´´*).

^{13}C-NMR (101 MHz, $CDCl_3$, ppm, 25 °C): δ_C = 157.24 (C_q, 2C), 155.46 (C_q, 2C), 150.15 (C_t, 2C), 148.08 (C_q, 2C), 142.40 (C_q, 2C), 138.35 (C_t, 1C), 131.38 (q, $^{1}J_{C,F}$ = 32.9 Hz, -CF_3, 2C), 127.76 (C_{phenyl}, 4C), 126.28 (q, $^{3}J_{C,F}$ = 3.6 Hz, C_{phenyl}, 4C), 122.01 (C_t, 2C), 121.86 (C_t, 2C), 119.55 (C_t, 2C). In the ^{13}C-spectrum and in the DEPT-135 one signal less than expected was found most likely due to coincident signals.

^{19}F NMR (376 MHz, $CDCl_3$, ppm, 25 °C): δ_F = –62.72 (3F).

MS (EI$^+$, 70 eV): *m/z* [ion, intensity (%)] = 521.1 (M^+, 100), 260.5 (M^{2+}, 11).

ESI-MS (MeOH, *positive* ion mode): *m/z* [ion, intensity (%)] = 522.2 ($M+H^+$, 100).

HRMS (ESI-ToF): *m/z* calcd. for $[C_{29}H_{17}F_6N_3+H]^+$: 522.1399; found: 522.1394.

4-(4′′-Chloro-[2,2′:6′,2′′-terpyridin]-4-yl)benzonitrile (175)

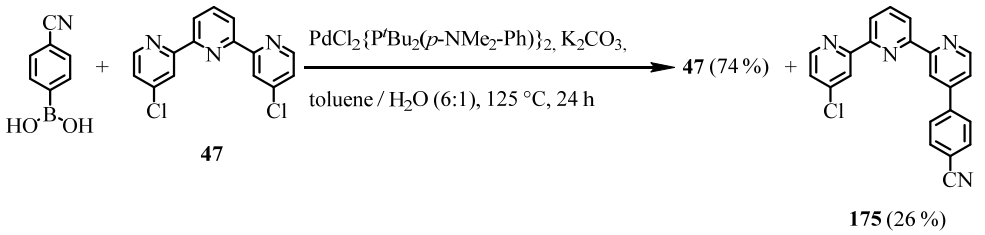

175 was prepared applying the representative procedure B described above. The starting material 4,4′′-Dichloro-2,2′:6′2′′-terpyridine (**47**) (90.6 mg, 300 µmol, 1.00 eq.), together with the coupling agent 4-(cyano)phenylboronic acid (34.1 mg, 225 µmol, 0.75 eq.), the catalyst $PdCl_2\{P^tBu_2(p\text{-}NMe_2\text{-}Ph)\}_2$ (6.37 mg, 9.00 µmol, 0.03 eq.) and the base K_2CO_3 (83.8 mg, 600 µmol, 2.00 eq.) were charged into a Schlenk tube and suspended in previously degassed toluene (6 mL) and H_2O (1 mL). The reaction vessel was sealed and heated up to 125 °C for 24 h. The yellow reaction mixture was allowed to cool to room temperature and was subsequently diluted with DCM and water. Now the reaction mixture was extracted with DCM (2 *x*) and with EtOAc (2 *x*) followed by extraction of the combined organic phases with water (1 *x*) and brine (2 *x*). The organics were dried over $MgSO_4$, filtered and residual solvent was removed under reduced pressure. The crude product was purified by FCC using a gradient of solvent mixtures ranging from EtOAc / *n*-hexane (1:3) to EtOAc / *n*-hexane (1:1). These conditions delivered exclusively the unreacted starting material **47** in a yield of 74% (66.8 mg, 221 µmol) together with the desired monosubstituted 4-(4′′-chloro-[2,2′:6′,2′′-terpyridin]-4-yl)benzonitrile **175** in a yield of 26% (28.6 mg, 77.5 µmol). A method to yield the disubstituted 4,4′-([2,2′:6′,2′′-terpyridine]-4,4′′-diyl)dibenzonitrile **176** is described below.

Analytical data 175:

^{1}H-NMR (400 MHz, $CDCl_3$, ppm, 25 °C): δ_H = 8.79 (d, $^3J_{H,H}$ = 5.0 Hz, 1H), 8.75 (s, 1H), 8.58 (d, $^3J_{H,H}$ = 5.2 Hz, 1H), 8.55 (d, $^4J_{H,H}$ = 1.4 Hz, 1H), 8.52 (d, $^3J_{H,H}$ = 7.8 Hz, 1H, *H3′* / H5′**), 8.46 (d, $^3J_{H,H}$ = 7.8 Hz, 1H, *H3′* / H5′**), 7.98 (t, $^3J_{H,H}$ = 7.8 Hz, 1H, *H4′*), 7.86 (m, 4H, H_{phenyl}), 7.52 (dd, $^3J_{H,H}$ = 5.0 Hz, $^4J_{H,H}$ = 1.3 Hz, 1H), 7.34 (dd, $^3J_{H,H}$ = 5.1 Hz, $^4J_{H,H}$ = 1.6 Hz, 1H).

^{13}C-NMR (101 MHz, $CDCl_3$, ppm, 25 °C): δ_C = 157.81 (C_q, 1C), 157.17 (C_q, 1C), 155.39 (C_q, 1C), 154.55 (C_q, 1C), 150.31 (C_t, 1C), 150.22 (C_t, 1C), 147.73 (C_q, 1C), 145.33 (C_q, 1C), 143.32 (C_q, 1C), 138.39 (C_t, 1C), 133.19 (C_{phenyl}, 2C), 128.20 (C_{phenyl}, 2C),

124.23 (C_t, 1C), 122.21 (C_t, 1C), 122.01 (C_t, 2C), 121.68 (C_t, 1C), 119.29 (C_t, 1C), 118.68 (C_t, 1C), 113.05 ($C_{q\,(CN)}$, 1C). In the ^{13}C-spectrum and in the DEPT-135 one signal less than expected was found most likely due to coincident signals.

MS (EI$^+$, 70 eV): *m/z* [ion, intensity (%)] = 368.1 (M^+, 100), 184.1 (M^{2+}, 7).

ESI-MS (MeOH, *positive* ion mode): *m/z* [ion, intensity (%)] = 369.1 ($M+H^+$, 100).

HRMS (ESI-ToF): *m/z* calcd. for $[C_{22}H_{13}ClN_4+H]^+$: 369.0902; found: 369.0905.

EA: Anal. calcd. for $C_{22}H_{13}ClN_4$ (M_W: 368.82): C, 71.64; H, 3.55; N, 15.19. Found: C, 70.95; H, 3.88; N, 14.70.

4,4′-([2,2′:6′,2′′-terpyridine]-4,4′′-diyl)dibenzonitrile (176)

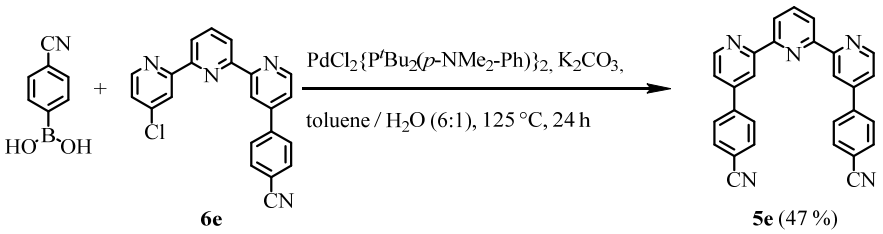

176 was prepared by modifying the representative procedure B described above. 4-(4′′-chloro-[2,2′:6′,2′′-terpyridin]-4-yl)benzonitrile **175** (73.8 mg, 200 µmol, 1.00 eq.), 4-(cyano)-phenylboronic acid (306 mg, 2.00 mmol, 10.0 eq.), the base K_2CO_3 (83.8 mg, 600 µmol, 3.00 eq.) and the catalyst $PdCl_2\{P^tBu_2(p\text{-}NMe_2\text{-}Ph)\}_2$ (14.2 mg, 20.0 µmol, 0.10 eq.) were charged into a Schlenk tube and suspended in previously degassed toluene (18 mL) and H_2O (3 mL). The reaction vessel was sealed and heated up to 125 °C for 24 h. The yellow reaction mixture was allowed to cool to room temperature and was subsequently diluted with DCM and water. Now the reaction mixture was extracted with DCM (2 *x* 250 mL) and with EtOAc (2 *x* 250mL) followed by extraction of the combined organic phases with brine (2 *x*). The organics were dried over $MgSO_4$, filtered and concentrated down to 200 mL under reduced pressure. The appearing precipitate was filtered off and dried under high vacuum. The isolated crude product turned out to be hard to re-dissolve and after NMR-analysis was characterized as the desired disubstituted target compound 4,4′-([2,2′:6′,2′′-terpyridine]-4,4′′-diyl)dibenzonitrile **176** which was purely obtained in a yield of 47% (41.2 mg, 94.6 µmol).

Analytical data 176:

^{1}H-NMR (400 MHz, $CDCl_3$, ppm, 25 °C): δ_H = 8.83 (dd, $^3J_{H,H}$ = 5.1 Hz, $^5J_{H,H}$ = 0.7 Hz, 2H, *H6 / H6′′*), 8.74 (dd, $^4J_{H,H}$ = 1.8 Hz, $^5J_{H,H}$ = 0.7 Hz, 2H, *H3 / H3′′*), 8.53 (d, $^3J_{H,H}$ = 7.8 Hz, 2H *H3′ / H5′*), 8.04 (t, $^3J_{H,H}$ = 7.8 Hz, 1H, *H4′*), 7.87 - 7.80 (m, 8H, H_{phenyl}), 7.55 (dd, $^3J_{H,H}$ = 5.1 Hz, $^4J_{H,H}$ = 1.9 Hz, 2H, *H5 / H5′′*).

^{13}C-NMR (101 MHz, $CDCl_3$, ppm, 25 °C): δ_C = 157.33 (C_q, 2C), 155.48 (C_q, 2C), 150.25 (C_t, 2C), 147.55 (C_q, 2C), 143.25 (C_q, 2C), 138.34 (C_t, 1C), 133.06 (C_{phenyl}, 4C), 128.03 (C_{phenyl}, 4C), 122.09 (C_t, 2C), 121.93 (C_t, 2C), 119.23 (C_t, 2C), 118.49 (C_q, 2C), 113.12 ($C_{q\,(CN)}$, 2C).

ESI-MS (MeCN, *positive* ion mode): *m/z* [ion, intensity (%)] = 436.2 ($M+H^+$, 100)

HRMS (ESI-ToF): *m/z* calcd. for $[C_{29}H_{17}N_5+H]^+$: 436.1557; found: 436,1553.

4-(4´´-chloro-[2,2´:6´,2´´-terpyridin]-4-yl)-*N,N*-dimethylaniline (177)

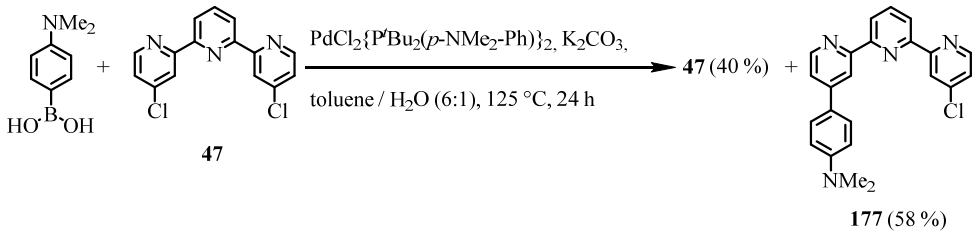

177 was prepared applying the representative procedure B described above. The starting material 4,4´´-Dichloro-2,2´:6´2´´-terpyridine (**47**) (549 mg, 1.73 mmol, 1.00 eq.), together with the coupling agent 4-(dimethylamino)phenylboronic acid (1.57 g, 9.53 mmol, 5.51 eq.), the catalyst $PdCl_2\{P^tBu_2(p\text{-}NMe_2\text{-}Ph)\}_2$ (61.1 mg, 86.2 µmol, 0.05 eq.) and the base K_2CO_3 (1.20 g, 8.62 mmol, 4.97 eq.) were charged into a Schlenk tube and suspended in previously degassed toluene (24 mL) and H_2O (4 mL). The reaction vessel was sealed and heated up to 125 °C for 24 h. The yellow reaction mixture was allowed to cool down to room temperature and was subsequently diluted with DCM and water. Now the reaction mixture was extracted with DCM (4 *x*) and with EtOAc (2 *x*) followed by extraction of the combined organic phases with water (1 *x*) and brine (2 *x*). The organics were dried over $MgSO_4$, filtered and residual solvent was removed under reduced pressure. The crude product was purified by FCC using a solvent mixture of EtOAc / *n*-hexane (1:3). These conditions delivered exclusively the unreacted starting material **47** in a yield of 40% (206 mg, 682 µmol) together with the monosubstituted 4-(4´´-chloro-[2,2´:6´,2´´-terpyridin]-4-yl)-*N,N*-dimethylaniline **177** in a yield of 58% (384 mg, 991 µmol). A method to yield the disubstituted 4,4´-([2,2´:6´,2´´-terpyridine]-4,4´´-diyl)bis(*N,N*-dimethylaniline) **178** is described below. By applying a solvent diffusion technique using dichloromethane and hexane with an intermediate spacer layer of benzene it was additionally, possible to obtain single crystals of **177** suitable for x-ray structure determination. The crystallographic information of compound **177** are discussed in detailed form in section 9.2. Thus hereafter, only the remaining analytical data of target compound **177** are discussed.

Analytical data 177:

^{1}H-NMR (400 MHz, $CDCl_3$, ppm, 25 °C): δ_H = 8.73 (d, $^4J_{H,H}$ = 1.3 Hz, 1H, *H3´´*), 8.64 (d, $^3J_{H,H}$ = 5.1 Hz, 1H, *H6´´*), 8.61 (d, $^4J_{H,H}$ = 1.9 Hz, 1H, *H3*), 8.56 (d, $^3J_{H,H}$ = 5.2 Hz, 1H, *H6*), 8.48 (d, $^3J_{H,H}$ = 7.2 Hz, 1H, *H3´* / H5´*), 8.42 (app. dd, $^3J_{H,H}$ = 7.8 Hz, $^4J_{H,H}$ = 0.6 Hz, 1H, *H3´* / H5´*), 7.95 (t, $^3J_{H,H}$ = 7.8 Hz, 1H, *H4´*), 7.71 (d, 2H, $^3J_{H,H}$ = 8.9 Hz, H_{phenyl}),

7.50 (dd, $^{3}J_{H,H}$ = 5.2 Hz, $^{4}J_{H,H}$ = 1.8 Hz, 1H, *H5´´*), 7.31 (dd, $^{3}J_{H,H}$ = 5.2 Hz, $^{4}J_{H,H}$ = 2.0 Hz, 1H, *H5*), 6.83 (d, $^{3}J_{H,H}$ = 8.9 Hz, 2H, H_{phenyl}), 3.02 (s, 6H, H_{methyl}).

^{13}C NMR (101 MHz, $CDCl_3$, ppm, 25 °C): δ_C = 158.06 (C_q, 1C), 156.41 (C_q, 1C), 156.21 (C_q, 1C), 154.25 (C_q, 1C), 151.33 (C_q, 1C), 150.14 (C_t, 1C), 149.65 (C_t, 1C), 149.36 (C_q, 1C), 145.27 (C_q, 1C), 138.11 (C_t, 1C), 128.04 (C_{phenyl}, 2C), 125.63 (C_q, 2C), 124.03 (C_t, 1C), 122.07 (C_t, 1C), 121.72 (C_t, 1C), 121.39 (C_t, 1C), 120.84 (C_t, 1C), 118.02 (C_t, 1C), 112.69 (C_{phenyl}, 2C). NMR-signals were confirmed by conventional 2D-NMR techniques. However in the ^{13}C-spectrum and in the DEPT-135 one signal less than expected was found most likely due to coincident signals.

MS (EI$^+$, 70 eV): *m/z* [ion, intensity (%)] = 386.1 (M^+, 100), 342.0 (M^+-NMe_2, 6), 193.1 (M^{2+}, 7).

ESI-MS (MeOH, *positive* ion mode): *m/z* [ion, intensity (%)] = 387.2 ($M+H^+$, 100).

HRMS (ESI-ToF): *m/z* calcd. for $[C_{23}H_{19}ClN_4+H]^+$: 387.1374; found: 387.1377.

4,4′-([2,2′:6′,2′′-terpyridine]-4,4′′-diyl)bis(*N*,*N*-dimethylaniline) (178)

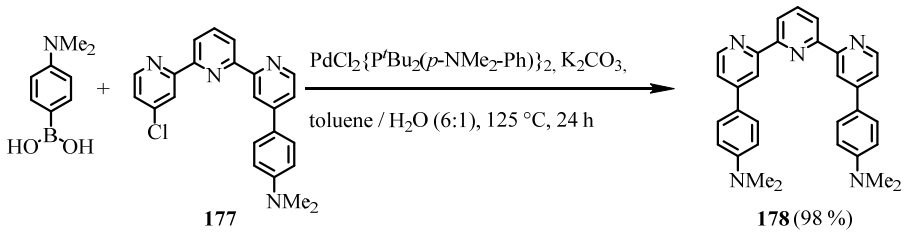

178 was prepared by modifying the representative procedure B described above. 4-(4′′-chloro-[2,2′:6′,2′′-terpyridin]-4-yl)-*N,N*-dimethylaniline **177** (54.2 mg, 140 µmol, 1.00 eq.), 4-(dimethylamino)phenylboronic acid (462 mg, 2.80 mmol, 20.0 eq.), K_2CO_3 (58.6 mg, 420 µmol, 3.00 eq.), and $PdCl_2\{P^tBu_2(p\text{-}NMe_2\text{-}Ph)\}_2$ (9.91 mg, 14.0 µmol, 0.10 eq.) were charged into a Schlenk tube and suspended in previously degassed toluene (18 mL) and H_2O (3 mL). The reaction vessel was sealed and heated to 125 °C for 24 h. The yellow reaction mixture was allowed to cool to room temperature and was subsequently diluted with DCM and water. Now the reaction mixture was extracted with DCM (5 *x* 200 mL) followed by extraction of the combined organic phases with brine (2 *x*). The organic phases were dried over $MgSO_4$, filtered and residual solvent was evaporated under reduced pressure. The crude product was purified by FCC using a solvent gradient ranging from EtOAc / *n*-hexane (1:1) to pure EtOAc. The almost insoluble isolated product turned was characterized as the desired disubstituted target compound 4,4′-([2,2′:6′,2′′-terpyridine]-4,4′′-diyl)bis(*N,N*-dimethyl-aniline) **178**, which was obtained in a yield of 98% (64.5 mg, 137 µmol).

Analytical data 178:

^{1}H-NMR (400 MHz, $CDCl_3$, ppm, 25 °C): δ_H = 8.89 (d, $^4J_{H,H}$ = 1.1 Hz, 2H, *H3 / H3′′*), 8.69 (d, $^3J_{H,H}$ = 5.2 Hz, 2H, *H6 / H6′′*), 8.49 (d, $^3J_{H,H}$ = 7.6 Hz, 2H *H3′ / H5′*), 8.00 (t, $^3J_{H,H}$ = 7.8 Hz, 1H, *H4′*), 7.78 (d, $^3J_{H,H}$ = 8.8Hz, 4H, H_{phenyl}), 7.56 (dd, $^3J_{H,H}$ = 5.1 Hz, $^4J_{H,H}$ = 1.4 Hz, 2H, *H5 / H5′′*), 6.84 (d, $^3J_{H,H}$ = 8.9Hz, 4H, H_{phenyl}), 3.05 (s, 12H, H_{methyl}).
^{13}C-NMR (101 MHz, $CDCl_3$, ppm, 25 °C): δ_C = 151.28 (C_q, 2C), 149.50 (C_q, 2C), 142.19 (C_q, 2C), 138.46 (C_q, 2C), 128.71 (C_q, 2C), 128.35 (C_t, 1C), 127.98 (C_{phenyl}, 4C), 125.65 (C_q, 2C), 121.25 (C_t, 2C), 120.46 (C_t, 2C), 118.15 (C_t, 2C), 112.65 (C_{phenyl}, 4C), 40.47 (C_{methyl}, 4C).
ESI-MS (MeCN, *positive* ion mode): *m/z* [ion, intensity (%)] = 472.3 ($M+H^{+/}$)
HRMS (ESI-ToF): *m/z* calcd. for $[C_{31}H_{29}N_5+H]^+$: 472.2496; found: 472.2489.

4-chloro-4´´-(4-methoxyphenyl)-2,2´:6´,2´´-terpyridine (179)

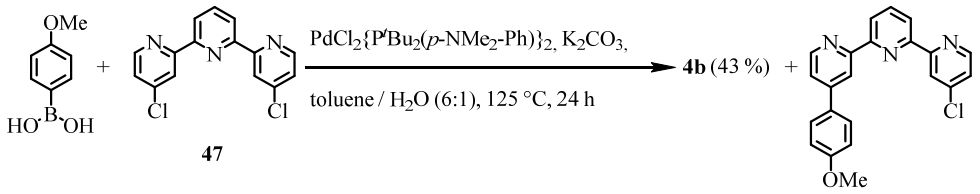

179 was prepared applying the representative procedure B described above. The starting material 4,4´´-Dichloro-2,2´:6´2´´-terpyridine (**47**) (302 mg, 1.00 mmol, 1.00 eq.), together with the coupling agent 4-(methoxy)phenylboronic acid (310 mg, 2.00 mmol, 2.00 eq.), the catalyst $PdCl_2\{P^tBu_2(p\text{-}NMe_2\text{-}Ph)\}_2$ (35.4 mg, 50.0 µmol, 0.05 eq.) and the base K_2CO_3 (349 mg, 2.50 mmol, 2.50 eq.) were charged into a Schlenk tube and suspended in previously degassed toluene (24 mL) and H_2O (4 mL). The reaction vessel was sealed and heated up to 125 °C for 24 h. The yellow reaction mixture was allowed to cool to room temperature and was subsequently diluted with DCM, water and brine. Now the reaction mixture was extracted with DCM (3 *x*) and with EtOAc (2 *x*). The combined organic layers were dried over $MgSO_4$, filtered and residual solvent was removed under reduced pressure. The crude product was purified by FCC using a gradient of solvent mixtures ranging from EtOAc / *n*-hexane (1:3) up to EtOAc / *n*-hexane (1:1). These conditions delivered exclusively the unreacted starting material **47** in a yield of 43% (130 mg, 430 µmol) together with the monosubstituted 4-chloro-4´´-(4-methoxyphenyl)-2,2´:6´,2´´-terpyridine **179** in a yield of 42% (156 mg, 417 µmol). Another method to yield the disubstituted derivative 4,4´´-bis(4-methoxyphenyl)-2,2´:6´,2´´-terpyridine **180** is described below and required an alteration of the reagents' stoichiometric ratios.

Analytical data 179:

^{1}H-NMR (400 MHz, $CDCl_3$, ppm, 25 °C): δ_H = 8.72 (dd, $^4J_{H,H}$ = 1.9 Hz, $^5J_{H,H}$ = 0.8 Hz 1H, *H3´´*), 8.68 (dd, $^3J_{H,H}$ = 5.2 Hz, $^5J_{H,H}$ = 0.8 Hz 1H, *H6´´*), 8.59 (d, $^4J_{H,H}$ = 1.8 Hz, 1H, *H3*), 8.56 (d, $^3J_{H,H}$ = 5.2 Hz, 1H, *H6*), 8.48 (dd, $^3J_{H,H}$ = 7.8 Hz, $^4J_{H,H}$ = 1.0 Hz 1H, *H3´* / H5´**), 8.43 (dd, $^3J_{H,H}$ = 7.8 Hz, $^4J_{H,H}$ = 1.0 Hz 1H, *H3´* / H5´**), 7.95 (t, $^3J_{H,H}$ = 7.8 Hz, 1H, *H4´*), 7.72 (d, 2H, $^3J_{H,H}$ = 8.8 Hz, H_{phenyl}), 7.49 (dd, $^3J_{H,H}$ = 5.1 Hz, $^4J_{H,H}$ = 1.9 Hz, 1H, *H5´´*), 7.31 (dd, $^3J_{H,H}$ = 5.2 Hz, $^4J_{H,H}$ = 2.1 Hz, 1H, *H5*), 7.05 (d, $^3J_{H,H}$ = 8.8 Hz, 2H, H_{phenyl}), 3.87 (s, 3H, $H_{methoxy}$).

^{13}C NMR (101 MHz, $CDCl_3$, ppm, 25 °C): δ_C = 160.78 (C_q, 1C), 157.98 (C_q, 1C), 156.60 (C_q, 1C), 155.96 (C_q, 1C), 154.33 (C_q, 1C), 150.19 (C_t, 1C), 149.79 (C_t, 1C), 149.11 (C_q, 1C), 145.28 (C_q, 1C), 138.19 (C_t, 1C), 130.95 (C_q, 1C), 128.56 (C_{phenyl}, 2C), 124.09 (C_t, 1C), 122.11 (C_t, 1C), 121.70 (C_t, 1C), 121.56 (C_t, 2C), 118.73 (C_t, 1C), 114.80 (C_{phenyl}, 2C), 55.62 ($C_{methoxy}$, 1C). In the ^{13}C-spectrum and in the DEPT-135 one signal less than expected was found most likely due to coincident signals.

ESI-MS (MeOH, *positive* ion mode): *m/z* [ion, intensity (%)] = 374.1 ($M+H^+$, 100).

HRMS (ESI-ToF): *m/z* calcd. for $[C_{22}H_{16}ClN_3+H]^+$: 374.1055; found: 374.1060.

4,4´´-bis(4-methoxyphenyl)-2,2´:6´,2´´-terpyridine (180)

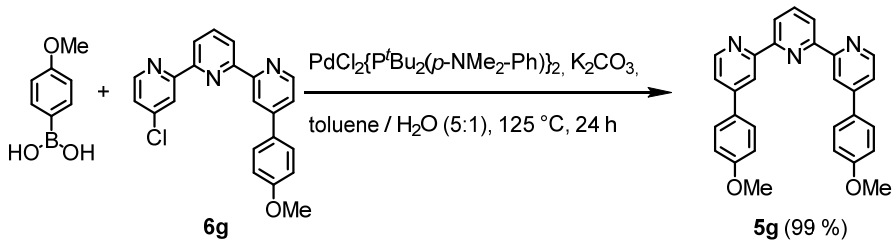

6g **5g** (99 %)

180 was prepared by modifying the representative procedure B described above. 4-chloro-4´´-(4-methoxyphenyl)-2,2´:6´,2´´-terpyridine **179** (22.8 mg, 61.0 µmol, 1.00 eq.), 4-(methoxy)-phenylboronic acid (94.6 mg, 0.61 mmol, 10.0 eq.), the base K_2CO_3 (25.5 mg, 183 µmol, 3.00 eq.) and the catalyst $PdCl_2\{P^tBu_2(p\text{-}NMe_2\text{-}Ph)\}_2$ (2.16 mg, 3.05 µmol, 0.05 eq.) were charged into a Schlenk tube and suspended in previously degassed toluene (20 mL) and H_2O (4 mL). The reaction vessel was sealed and heated up to 125 °C for 24 h. The reaction mixture was allowed to cool to room temperature and was subsequently diluted with DCM, brine and water. Now the reaction mixture was extracted with DCM (4 *x*) and EtOAc (1 *x*). The organic phases were combined, dried over $MgSO_4$, filtered and residual solvent was evaporated under reduced pressure. The crude product was purified by FCC using a gradient of solvent mixtures ranging from EtOAc / *n*-hexane (1:3) via EtOAc / *n*-hexane (1:1) up to pure EtOAc. The pure product was gained via recrystallization achieved by adding MeOH to a solution of the pre-purified product in DCM. The desired product precipitates as colorless solid which was subsequently filtered of and dried at the high vacuum to yield the desired disubstituted target compound 4,4´´-bis(4-methoxyphenyl)-2,2´:6´,2´´-terpyridine **180** in a yield of 99% (27.0 mg, 61.0 µmol).

Analytical data 180:

^{1}H-NMR (400 MHz, $CDCl_3$, ppm, 25 °C): δ_H = 8.85 (d, $^4J_{H,H}$ = 1.2 Hz, 2H, *H3 / H3´´*), 8.72 (d, $^3J_{H,H}$ = 5.1 Hz, 2H, *H6 / H6´´*), 8.49 (d, $^3J_{H,H}$ = 7.8 Hz, 2H *H3´ / H5´*), 8.00 (t, $^3J_{H,H}$ = 7.8 Hz, 1H, *H4´*), 7.77 (d, $^3J_{H,H}$ = 8.8Hz, 4H, H_{phenyl}), 7.54 (dd, $^3J_{H,H}$ = 5.1 Hz, $^4J_{H,H}$ = 1.9 Hz, 2H, *H5 / H5´´*), 7.05 (d, $^3J_{H,H}$ = 8.8Hz, 4H, H_{phenyl}), 3.90 (s, 6H, $H_{methoxy}$). Due to the very limited solubility of the product, no ^{13}C-spectrum could be obtained.

ESI-MS (MeCN, *positive* ion mode): *m/z* [ion, intensity (%)] = 468.4 ($M+Na^+$, 100)

4-Chloro-4´´-(4-(nitro)phenyl)-2,2´:6´,2´´-terpyridine (182)

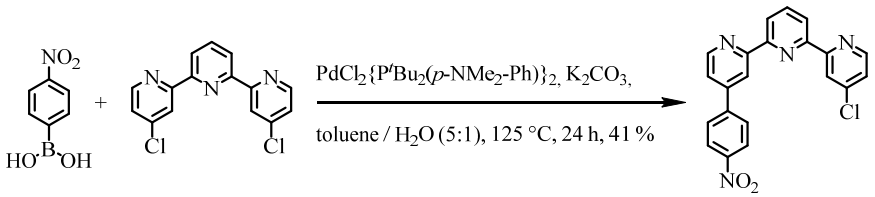

47 **182**

182 was prepared applying the representative procedure B described above. The starting materials 4,4´´-Dichloro-2,2´:6´2´´-terpyridine (**47**) (302 mg, 1.00 mol, 1.00 eq.), 4-(nitro)-phenylboronic acid (167 mg, 1.00 mmol, 1.00 eq.), the base K_2CO_3 (279 mg, 2.00 mmol, 2.00 eq.), and the catalyst $PdCl_2\{P^tBu_2(p\text{-}NMe_2\text{-}Ph)\}_2$ (35.4 mg, 50.0 µmol, 0.05 eq.) were charged into a Schlenk tube and suspended in degassed toluene (20 mL) and H_2O (4 mL). The reaction vessel was sealed and heated to 125 °C for 24 h. After cooling to room temperature the reaction mixture was diluted with DCM, brine and water. Now the reaction mixture was extracted with DCM (5 *x*) before the organic phases were reunited and pre-dried over $MgSO_4$, filtered and residual solvent was removed under reduced pressure. The crude product was purified by FCC using a gradient of solvent mixtures ranging from EtOAc / *n*-hexane (1:1) up to pure EtOAc. The desired monosubstituted product 4-Chloro-4´´-(4-(nitrophenyl)-2,2´:6´,2´´-terpyridine **182** could be isolated in a yield of 41% (160 mg, 411 µmol).

Analytical data 182:

^{1}H-NMR (400 MHz, $CDCl_3$, ppm, 25 °C): δ_H = 8.80 (d, $^3J_{H,H}$ = 5.6 Hz, 1H), 8.78 (s, 1H), 8.59 (d, $^3J_{H,H}$ = 4.8 Hz, 1H), 8.56 (s, 1H), 8.53 (d, $^3J_{H,H}$ = 7.8 Hz, 1H, *H3´* / H5´**), 8.47 (d, $^3J_{H,H}$ = 7.5 Hz, 1H, *H3´* / H5´**), 8.40 (d, $^3J_{H,H}$ = 8.1 Hz, 2H, H_{phenyl}), 7.99 (t, $^3J_{H,H}$ = 7.8 Hz, 1H, *H4´*), 7.91 (d, $^3J_{H,H}$ = 8.0 Hz, 2H, H_{phenyl}), 7.55 (d, $^3J_{H,H}$ = 3.7 Hz, $^4J_{H,H}$ = 1.3 Hz, 1H), 7.34 (dd, $^3J_{H,H}$ = 5.4 Hz, 1H).

^{13}C-NMR (101 MHz, $CDCl_3$, ppm, 25 °C): δ_C = 157.81 (C_q, 1C), 157.22 (C_q, 1C), 155.33 (C_q, 1C), 154.58 (C_q, 1C), 150.33 (C_t, 1C), 150.26 (C_t, 1C), 148.48 (C_q, 1C), 147.37 (C_q, 1C), 145.35 (C_q, 1C), 145.20 (C_q, 1C), 138.41 (C_t, 1C), 128.45 (C_{phenyl}, 2C), 124.65 (C_{phenyl}, 2C), 124.24 (C_t, 1C), 122.23 (C_t, 1C), 122.11 (C_t, 2C), 122.06 (C_t, 1C), 121.69 (C_t, 1C), 119.42 (C_t, 1C).

ESI-MS (MeOH, *positive* ion mode): *m/z* [ion, intensity (%)] = 389.1 ($M+H^+$, 100).

HRMS (ESI-ToF): *m/z* calcd. for $[C_{21}H_{13}ClN_4+H]^+$: 389.0800; found: 389.0802.

_N,N_-dimethyl-4-(4´´-(4-(trifluoromethyl)phenyl)-[2,2´:6´,2´´-terpyridin]-4-yl)aniline (147)

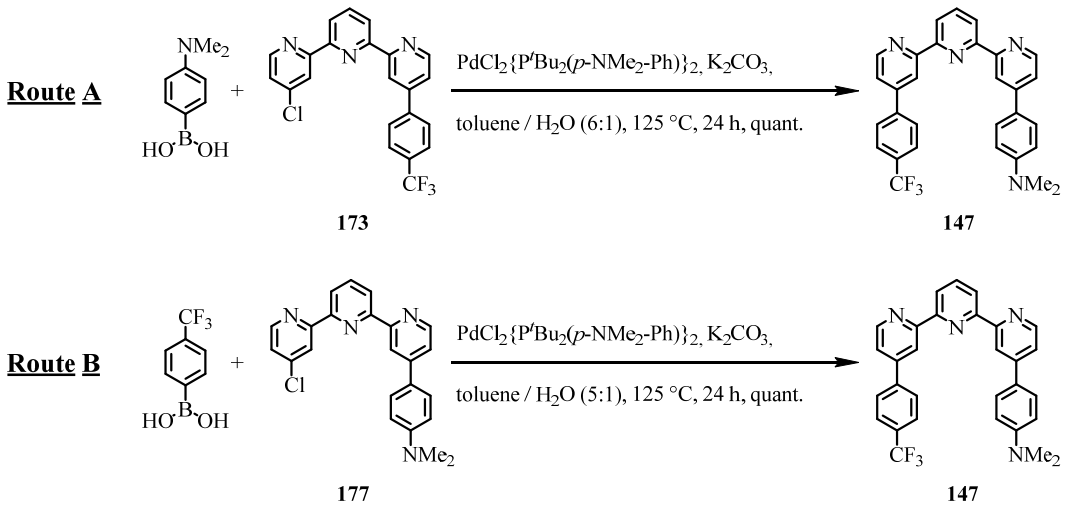

To prepare compound **147** two different routes have been established. Both procedures are applying a modification of the representative procedure B described above. In the following passage both routes will be discussed separately, whereas the common analytical results of the target compound **147** will be listed below the experimental procedures.

Route A: For this first procedure a Schlenk tube was charged with 4-chloro-4´´-(4-(trifluoromethyl)phenyl)-2,2´:6´,2´´-terpyridine (**173**) (42.8 mg, 104 µmol, 1.00 eq.), 4-(dimethylamino)phenylboronic acid (172 mg, 1.04 mmol, 10.0 eq.), K_2CO_3 (29.0 mg, 208 µmol, 2.00 eq.), and $PdCl_2\{P^tBu_2(p\text{-}NMe_2\text{-}Ph)\}_2$ (3.68 mg, 5.20 µmol, 0.05 eq.). All reagents were mixed and suspended in previously degassed toluene (5 mL) and H_2O (1 mL). The reaction vessel was sealed and heated to 125 °C for 24 h. After cooling to room temperature the reaction mixture was diluted with DCM, brine and water. Now the reaction mixture was extracted with DCM (3 *x*) and EtOAc (3*x*). The organic phases were combined, dried over $MgSO_4$, filtered and residual solvent was evaporated under reduced pressure. The crude product was purified by FCC using a solvent mixture of EtOAc / *n*-hexane (1:3) to afford the asymmetric product *N,N*-dimethyl-4-(4´´-(4-(trifluoromethyl)phenyl)-[2,2´:6´,2´´-terpyridin]-4-yl)aniline (**147**) purely and in quantitative yield (51.7 mg, 104 µmol) as a colorless solid.

Route B: For this first procedure a Schlenk tube was charged with 4-(4´´-chloro-[2,2´:6´,2´´-terpyridin]-4-yl)-*N,N*-dimethylaniline (**177**) (116 mg, 0.30 mmol, 1.00 eq.), 4-(trifluoromethyl)phenylboronic acid (171mg, 0.90 mmol, 3.00 eq.), $PdCl_2\{P^tBu_2(p\text{-}NMe_2\text{-}Ph)\}_2$ (10.6 mg, 15.0 µmol, 0.05 eq.), and K_2CO_3 (105 mg, 0.75 mmol, 2.50 eq.). All reagents were

mixed and suspended in previously degassed toluene (24 mL) and H_2O (4 mL). The reaction vessel was sealed and heated up to 125 °C for 24 h. The reaction mixture was allowed to cool down to room temperature and was subsequently diluted with DCM, brine and water. Now the reaction mixture was extracted with DCM (5 *x*) and subsequently washed with brine three more times. Now the organic phases were combined, dried over $MgSO_4$, filtered and residual solvent was evaporated under reduced pressure. The crude product was purified by FCC using a gradient of solvent mixtures ranging from EtOAc / *n*-hexane (1:3) up to EtOAc / *n*-hexane (1:1) to afford the pure product *N,N*-dimethyl-4-(4´´-(4-(trifluoromethyl)phenyl)-[2,2´:6´,2´´-terpyridin]-4-yl)aniline (**147**) in quantitative yield (150 mg, 0.30 mol) as colorless needles. By applying a solvent diffusion technique using DCM and *n*-hexane with a benzene layer as intermediate spacer single crystals of **147** suitable for x-ray structure determination could be obtained. The detailed crystallographic information of compound **147** is discussed in chapter 9.2. Thus hereafter, only the remaining analytical data of target compound **147** are listed.

Analytical data 147:

^{1}H-NMR (400 MHz, $CDCl_3$, ppm, 25 °C): δ_H = 8.94 (d, $^{4}J_{H,H}$ = 1.0 Hz, 1H, *H3* / H3´´**), 8.85 (d, $^{4}J_{H,H}$ = 1.2 Hz, 1H, *H3* / H3´´**), 8.78 (d, $^{3}J_{H,H}$ = 5.0 Hz, 1H, *H6* / H6´´**), 8.66 (d, , $^{3}J_{H,H}$ = 5.1 Hz, 1H, *H6* / H6´´**), 8.48 (dd, $^{3}J_{H,H}$ = 7.8 Hz, $^{4}J_{H,H}$ = 1.1 Hz, 2H, *H3´ / H5´*), 7.99 (t, $^{3}J_{H,H}$ = 7.8 Hz, 1H, *H4´*), 7.90 (d, $^{3}J_{H,H}$ = 8.1 Hz, 2H, $H_{phenyl(pull)}$), 7.78 (d, $^{3}J_{H,H}$ = 8.2 Hz, 2H, $H_{phenyl(pull)}$), 7.71 (d, $^{3}J_{H,H}$ = 8.8 Hz, 2H, $H_{phenyl(push)}$), 7.54 (dd, $^{3}J_{H,H}$ = 5.0 Hz, $^{4}J_{H,H}$ = 1.7 Hz, 1H, *H5* / H5´´**), 7.52 (dd, $^{3}J_{H,H}$ = 5.2 Hz, $^{4}J_{H,H}$ = 1.8 Hz, 1H, *H5* / H5´´**), 6.80 (d, $^{3}J_{H,H}$ = 8.8 Hz, 2H, $H_{phenyl(push)}$), 3.04 (s, 6H, H_{methyl}).
^{13}C-NMR (101 MHz, $CDCl_3$, ppm, 25 °C): δ_C = 157.39 (C_q, 1C), 156.56 (C_q, 1C), 155.90 (C_q, 1C), 154.96 (C_q, 1C), 151.36 (C_q, 1C), 150.07 (C_t, 1C), 149.73 (C_t, 1C), 149.06 (C_q, 1C), 147.80 (C_q, 1C), 142.47 (C_q, 1C), 142.45 (C_q, 1C), 138.22 (C_t, 1C), 131.16 (q, $^{1}J_{C,F}$ = 32.8 Hz, -CF_3, 1C), 127.94 (C_{phenyl}, 2C), 127.77 (C_{phenyl}, 2C), 126.24 (q, $^{3}J_{C,F}$ = 3.7 Hz, C_{phenyl}, 2C), 125.54 (C_q, 1C), 121.68 (C_t, 1C), 121.55 (C_t, 1C), 121.15 (C_t, 1C), 120.59 (C_t, 1C), 119.66 (C_t, 1C) , 118.14 (C_t, 1C), 112.54 (C_{phenyl}, 2C), 40.41 (C_{methyl}, 1C).
^{19}F NMR (376 MHz, $CDCl_3$, ppm, 25 °C): δ_F = –62.63 (3F).
MS (EI$^+$, 70 eV): *m/z* [ion, intensity (%)] = 496.2 (M^+, 100), 248.1 (M^{2+}, 8).
ESI-MS (MeOH, *positive* ion mode): *m/z* [ion, intensity (%)] = 497.2 ($M+H^+$, 100).
HRMS (ESI-ToF): *m/z* calcd. for $[C_{30}H_{23}F_3N_4+H]^+$: 497.1948; found: 497.1945.

4-(4′′-(4-(Dimethylamino)phenyl)-[2,2′:6′,2′′-terpyridin]-4-yl)benzonitrile (183)

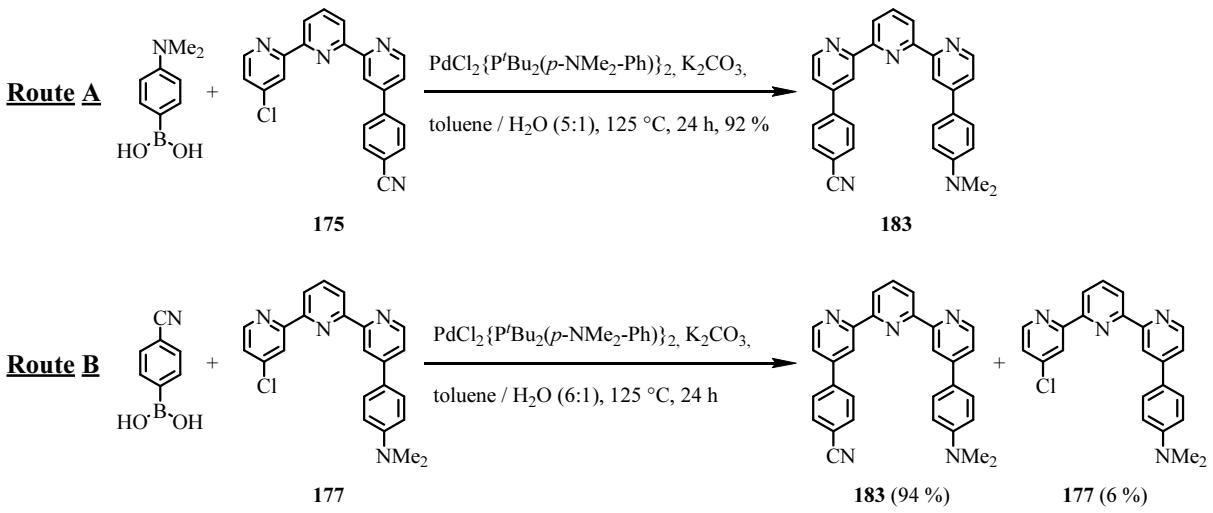

To prepare compound **183** two different routes have been followed. Both procedures are applying a modification of the representative procedure B described above. In the following passage both routes will be discussed separately, whereas the common analytical results of the target compound **183** will be listed below the experimental procedures.

Route A: For this first procedure a Schlenk tube was charged with 4-(4′′-chloro-[2,2′:6′,2′′-terpyridin]-4-yl)benzonitrile (**175**) (73.8 mg, 200 µmol, 1.00 eq.), 4-(dimethylamino)phenylboronic acid (330 mg, 2.00 mmol, 10.0 eq.), $PdCl_2\{P^tBu_2(p\text{-}NMe_2\text{-}Ph)\}_2$ (7.08 mg, 10.0 µmol, 0.05 eq.), and K_2CO_3 (55.8 mg, 400 µmol, 2.00 eq.). All reagents were mixed and suspended in previously degassed toluene (15 mL) and H_2O (3 mL). The reaction vessel was sealed and heated to 125 °C for 24 h. The reaction mixture was allowed to cool down to room temperature and was subsequently diluted with DCM and water. Now the reaction mixture was extracted with DCM (4 *x*) and EtOAc (2 *x*). The organic phases were combined after extraction with brine, dried over $MgSO_4$, filtered and residual solvent was evaporated under reduced pressure. The crude product was purified by FCC using a gradient of solvent mixtures ranging from EtOAc / *n*-hexane (1:3) up to EtOAc / *n*-hexane (1:1) to afford the asymmetric product 4-(4′′-(4-(dimethylamino)phenyl)-[2,2′:6′,2′′-terpyridin]-4-yl)benzonitrile (**183**) purely and in a yield of 92% (83.1 mg, 183 µmol) as a colorless solid.

Route B: For this second procedure a Schlenk tube was charged with 4-(4′′-chloro-[2,2′:6′,2′′-terpyridin]-4-yl)-*N,N*-dimethylaniline (**177**) (71.3 mg, 184 µmol, 1.00 eq.), 4-(cyano)phenylboronic acid (268 mg, 1.75 mmol, 9.51 eq.), K_2CO_3 (48.9 mg, 0.35 mmol,

1.90 eq.), and $PdCl_2\{P^tBu_2(p\text{-}NMe_2\text{-}Ph)\}_2$ (6.37 mg, 9.00 µmol, 0.05 eq.). All reagents were mixed and suspended in previously degassed toluene (24 mL) and H_2O (4 mL). The reaction vessel was sealed and heated to 125 °C for 24 h. The reaction mixture was allowed to cool down to room temperature and was subsequently diluted with DCM, brine and water. Now the reaction mixture was extracted with DCM (5 *x*) and subsequently washed with brine three more times Now the organic phases were combined, dried over $MgSO_4$, filtered and residual solvent was evaporated under reduced pressure. The crude product was purified by FCC using a gradient of solvent mixtures ranging from EtOAc / *n*-hexane (1:3) up to EtOAc / *n*-hexane (1:1) to afford the asymmetric product 4-(4´´-(4-(dimethylamino)phenyl)-[2,2´:6´,2´´-terpyridin]-4-yl)benzonitrile (**183**) purely and in a yield of 94% (78.0 mg, 172 µmol) in shape of colorless needles. Additionally, the starting material **177** was isolated in a yield of 6% (4.50 mg, 11.6 µmol). By applying a solvent diffusion technique using dichloromethane and hexane with an intermediate spacer layer of benzene it was possible to obtain single crystals of **183** suitable for x-ray structure determination. The crystallographic information of compound **183** is discussed in detailed form in chapter 9.2. Thus hereafter, only the remaining analytical data of target compound **183** are discussed.

Analytical data 183:

^{1}H-NMR (400 MHz, $CDCl_3$, ppm, 25 °C): δ_H = 8.92 (s, 1H, *H3* / H3´´**), 8.78 (d, $^3J_{H,H}$ = 5.1 Hz, 1H, *H6* / H6´´**), 8.72 (d, $^4J_{H,H}$ = 1.3 Hz, 1H, *H3* / H3´´**), 8.69 (d, $^3J_{H,H}$ = 5.4 Hz, 1H, *H6* / H6´´**), 8.50 (dd, $^3J_{H,H}$ = 7.7 Hz, $^4J_{H,H}$ = 1.1 Hz, 1H, *H3´* / H5´**), 8.46 (dd, $^3J_{H,H}$ = 7.8 Hz, $^4J_{H,H}$ = 0.8 Hz, 1H, *H3´* / H5´**), 7.99 (t, $^3J_{H,H}$ = 7.8 Hz, 1H, *H4´*), 7.91 (d, $^3J_{H,H}$ = 8.3 Hz, 2H, $H_{phenyl(pull)}$), 7.79 (d, $^3J_{H,H}$ = 8.5 Hz, 2H, $H_{phenyl(pull)}$), 7.69 (d, $^3J_{H,H}$ = 8.9 Hz, 2H, $H_{phenyl(push)}$), 7.54 (dd, $^3J_{H,H}$ = 5.3 Hz, $^4J_{H,H}$ = 1.7 Hz, 1H, *H5* / H5´´**), 7.52 (dd, $^3J_{H,H}$ = 5.1 Hz, $^4J_{H,H}$ = 1.9 Hz, 1H, *H5* / H5´´**), 6.78 (d, $^3J_{H,H}$ = 8.9 Hz, 2H, $H_{phenyl(push)}$), 3.05 (s, 6H, H_{methyl}). **^{13}C-NMR** (101 MHz, $CDCl_3$, ppm, 25 °C): δ_C = 158.20 (C_q, 1C), 157.30 (C_q, 1C), 155.27 (C_q, 1C), 154.98 (C_q, 1C), 151.60 (C_q, 1C), 150.15 (C_t, 1C), 147.43 (C_q, 1C), 143.28 (C_q, 1C), 138.34 (C_t, 1C), 133.08 (C_{phenyl}, 2C), 128.22 (C_{phenyl}, 2C), 128.18 (C_{phenyl}, 2C), 121.96 (C_t, 1C), 121.73 (C_t, 1C), 120.65 (C_t, 1C), 119.63 (C_t, 1C), 118.76 (C_q, 1C) , 118.17 (C_t, 1C), 112.88 ($C_{q\ (CN)}$, 1C) , 112.53 (C_{phenyl}, 2C), 40.50 (C_{methyl}, 1C). In the ^{13}C-spectrum and in the DEPT-135 three signals less than expected were found probably due to coincident signals.

MS (EI$^+$, 70 eV): *m/z* [ion, intensity (%)] = 453.2 (M^+, 100), 409.1 (M^+-NMe_2, 5), 226.6 (M^{2+}, 8).

ESI-MS (MeOH, *positive* ion mode): *m/z* [ion, intensity (%)] = 454.3 ($M+H^+$), 476.3 ($M+Na^+$)

HRMS (ESI-ToF): *m/z* calcd. for $[C_{30}H_{24}N_5+H]^+$: 454.2026; found: 454.2018.

***N,N*-Dimethyl-4-(4′′-(4-nitrophenyl)-[2,2′:6′,2′′-terpyridin]-4-yl)aniline (184)**

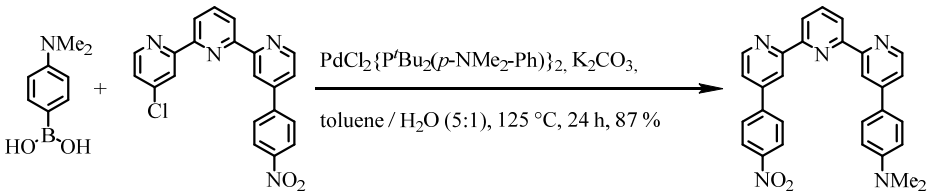

182 **184**

Compound **184** was prepared according to general procedure B described above. 4-Chloro-4′′-(4-nitrophenyl)-2,2′:6′,2′′-terpyridine (**182**) (58.3 mg, 150 µmol, 1.00 eq.) as the reactant, 4-(dimethylamino)phenylboronic acid (253 mg, 1.50 mmol, 10.0 eq.) as coupling partner, the catalyst $PdCl_2\{P^tBu_2(p\text{-}NMe_2\text{-}Ph)\}_2$ (5.31 mg, 7.50 µmol, 0.05 eq.) and the usual base K_2CO_3 (62.8 mg, 450 µmol, 3.00 eq.) were charged into a Schlenk tube under inert atmosphere. All reagents were mixed and suspended in previously degassed toluene (20 mL) and H_2O (4 mL). The reaction vessel was sealed and heated to 125 °C for 24 h. After completion the reaction mixture was allowed to cool down to room temperature and was subsequently diluted with DCM, brine and water. Now the reaction mixture was extracted with DCM (4 *x*). The organic phases were combined, dried over $MgSO_4$, filtered and residual solvent was evaporated under reduced pressure. The crude product was purified by FCC using EtOAc / *n*-hexane (1:1) as the solvent mixture to afford *N,N*-dimethyl-4-(4′′-(4-nitrophenyl)-[2,2′:6′,2′′-terpyridin]-4-yl)aniline (**184**) as the desired asymmetric product in an overall yield of 87% (61.8 mg, 131 µmol).

Analytical data 184:

^{1}H-NMR (400 MHz, $CDCl_3$, ppm, 25 °C): δ_H = 8.94 (d, $^4J_{H,H}$ = 1.1 Hz, 1H, *H3* / H3′′**), 8.82 – 8.79 (m, 2H, *H3* / H3′′* / H6* / H6′′**), 8.65 (d, , $^3J_{H,H}$ = 5.2 Hz, 1H, *H6* / H6′′**), 8.48 (dd, $^3J_{H,H}$ = 7.8 Hz, $^4J_{H,H}$ = 2.4 Hz, 2H, *H3′ / H5′*), 8.38 (d, $^3J_{H,H}$ = 8.5 Hz, 2H, H_{phenyl}), 7.99 (t, $^3J_{H,H}$ = 7.8 Hz, 1H, *H4′*), 7.94 (d, $^3J_{H,H}$ = 8.9 Hz, 2H, H_{phenyl}), 7.70 (d, $^3J_{H,H}$ = 8.9 Hz, 2H, H_{phenyl}), 7.56 (dd, $^3J_{H,H}$ = 5.1 Hz, $^4J_{H,H}$ = 1.8 Hz, 1H, *H5* / H5′′**), 7.51 (dd, $^3J_{H,H}$ = 5.1 Hz, $^4J_{H,H}$ = 1.9 Hz, 1H, *H5* / H5′′**), 6.81 (d, $^3J_{H,H}$ = 8.9 Hz, 2H, H_{phenyl}), 3.05 (s, 6H, H_{methyl}).

^{13}C-NMR (101 MHz, $CDCl_3$, ppm, 25 °C): δ_C = 157.63 (C_q, 1C), 156.54 (C_q, 1C), 156.06 (C_q, 1C), 154.82 (C_q, 1C), 151.42 (C_q, 1C), 150.26 (C_t, 1C), 149.80 (C_t, 1C), 149.23 (C_q, 1C), 148.42 (C_q, 1C), 146.92 (C_q, 1C), 145.31 (C_q, 1C), 138.30 (C_t, 1C), 128.36 (C_{phenyl}, 2C), 128.00 (C_{phenyl}, 2C), 125.58 (C_q, 1C), 124.58 (C_{phenyl}, 2C),

121.79 (C_t, 1C), 121.66 (C_t, 1C), 121.24 (C_t, 1C), 120.76 (C_t, 1C), 119.70 (C_t, 1C), 118.21 (C_t, 1C), 112.55 (C_{phenyl}, 2C), 40.53(C_{methyl}, 2C).

ESI-MS (MeOH, *positive* ion mode): *m/z* [ion, intensity (%)] = 474.2 ($M+H^+$, 40), 496.2 ($M+Na^+$, 100).

HRMS (ESI-ToF): *m/z* calcd. for $[C_{29}H_{23}N_5O_2+H]^+$: 474.1925; found: 474.1919, *m/z* calcd. for $[C_{29}H_{23}N_5O_2+Na]^+$: 496.1744; found: 496.1740.

4-(4-Methoxyphenyl)-4´´-(4-(trifluoromethyl)phenyl)-2,2´:6´,2´´-terpyridine (185)

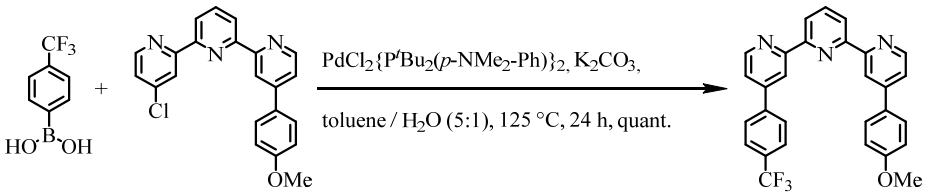

179 **185**

Compound **185** was prepared by an adaptation of representative procedure B described above. 4-Chloro-4´´-(4-methoxyphenyl)-2,2´:6´,2´´-terpyridine (**179**) (56.1 mg, 150 µmol, 1.00 eq.), 4-(trifluoromethyl)phenylboronic acid (285 mg, 1.50 mmol, 10.0 eq.), K_2CO_3 (62.8 mg, 450 µmol, 3.00 eq.), and $PdCl_2\{P^tBu_2(p\text{-}NMe_2\text{-}Ph)\}_2$ (5.31 mg, 7.50 µmol, 0.05 eq.) were charged into a Schlenk tube which was repeatedly evacuated and backfilled with inert gas prior to use. All reagents were mixed and suspended in previously degassed toluene (20 mL) and H_2O (4 mL). The reaction vessel was sealed and heated to 125 °C for 24 h. After completion the reaction mixture was allowed to cool down to room temperature and was subsequently diluted with DCM, brine and water. Now the reaction mixture was extracted with DCM (4 *x*). The organic phases were combined, dried over $MgSO_4$, filtered and residual solvent was evaporated under reduced pressure. The crude product was purified by FCC using an isocratic solvent mixture consisting of EtOAc / *n*-hexane (1:1) to afford 4-(4-methoxyphenyl)-4´´-(4-(trifluoromethyl)phenyl)-2,2´:6´,2´´-terpyridine (**185**) as the desired asymmetric product as a colorless solid in quantitative yield (72.5 mg, 150 µmol).

Analytical data 185:

^{1}H-NMR (400 MHz, $CDCl_3$, ppm, 25 °C): δ_H = 8.86 (d, $^4J_{H,H}$ = 1.0 Hz, 1H, *H3* / H3´´**), 8.79 (d, $^4J_{H,H}$ = 1.2 Hz, 1H, *H3* / H3´´**), 8.77 (d, $^3J_{H,H}$ = 5.1 Hz, 1H, *H6* / H6´´**), 8.69 (d, , $^3J_{H,H}$ = 5.1 Hz, 1H, *H6* / H6´´**), 8.48 (dd, $^3J_{H,H}$ = 7.9 Hz, $^4J_{H,H}$ = 1.3 Hz, 2H, *H3´ / H5´*), 7.98 (t, $^3J_{H,H}$ = 7.8 Hz, 1H, *H4´*), 7.87 (d, $^3J_{H,H}$ = 8.1 Hz, 2H, $H_{phenyl(pull)}$), 7.76 (d, $^3J_{H,H}$ = 8.2 Hz, 2H, $H_{phenyl(pull)}$), 7.71 (d, $^3J_{H,H}$ = 8.8 Hz, 2H, $H_{phenyl(push)}$), 7.53 (dd, $^3J_{H,H}$ = 5.1 Hz, $^4J_{H,H}$ = 1.8 Hz, 1H, *H5* / H5´´**), 7.50 (dd, $^3J_{H,H}$ = 5.1 Hz, $^4J_{H,H}$ = 1.9 Hz, 1H, *H5* / H5´´**), 7.01 (d, $^3J_{H,H}$ = 8.8 Hz, 2H, $H_{phenyl(push)}$), 3.87 (s, 3H, $H_{methoxy}$).

^{13}C-NMR (101 MHz, $CDCl_3$, ppm, 25 °C): δ_C = 160.85 (C_q, 1C), 157.36 (C_q, 1C), 156.82 (C_q, 1C), 155.84 (C_q, 1C), 155.23 (C_q, 1C), 150.11 (C_t, 1C), 149.87 (C_t, 1C), 148.90 (C_q, 1C), 147.95 (C_q, 1C), 142.47 (C_q, 1C), 138.25 (C_t, 1C), 131.25 (q,

$^{1}J_{C,F}$ = 32.7 Hz,-CF_3, 1C), 130.96 (C_q, 1C), 128.46 (C_{phenyl}, 2C), 127.79 (C_{phenyl}, 2C), 126.27 (q, $^{3}J_{C,F}$ = 3.7 Hz, C_{phenyl}, 2C), 121.85 (C_t, 1C), 121.74 (C_t, 1C), 121.47 (C_t, 1C), 121.39 (C_t, 1C), 119.59 (C_t, 1C) , 118.83 (C_t, 1C), 114.74 (C_{phenyl}, 2C), 55.59 ($C_{methoxy}$, 1C). In the ^{13}C-spectrum and in the DEPT-135 one signal less than expected was found probably due to coincident signals.

^{19}F NMR (376 MHz, $CDCl_3$, ppm, 25 °C): δ_F = –62.62 (3F).

ESI-MS (MeOH, *positive* ion mode): *m/z* [ion, intensity (%)] = 484.2 ($M+H^+$, 100).

HRMS (ESI-ToF): *m/z* calcd. for $[C_{29}H_{20}F_3N_3O+H]^+$: 484.1631; found: 484.1636.

4-(4´´-(4-Methoxyphenyl)-[2,2´:6´,2´´-terpyridin]-4-yl)benzonitrile (186)

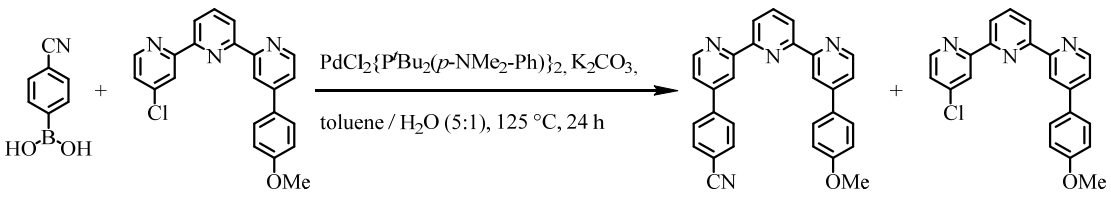

179 **186** (80 %) **179** (20 %)

Tpy derivative **186** was prepared according to the representative procedure B described above. 4-Chloro-4´´-(4-methoxyphenyl)-2,2´:6´,2´´-terpyridine (**179**) (43.0 mg, 115 µmol, 1.00 eq.), 4-(cyano)phenylboronic acid (230 mg, 1.50 mmol, 13.0 eq.), K_2CO_3 (62.8 mg, 450 µmol, 3.91 eq.), and t $PdCl_2\{P^tBu_2(p\text{-}NMe_2\text{-}Ph)\}_2$ (5.31 mg, 7.50 µmol, 0.07 eq.) were charged into a Schlenk tube which was three times evacuated and backfilled with inert gas prior to use. All reagents were mixed and suspended in previously degassed toluene (20 mL) and H_2O (4 mL). The reaction vessel was sealed and heated to 125 °C for 24 h. After completion the reaction mixture was allowed to cool down to room temperature and was subsequently diluted with DCM, brine and water. Now the reaction mixture was extracted with DCM (5 *x*). The organic phases were combined, dried over $MgSO_4$, filtered and residual solvent was evaporated under reduced pressure. The crude product was purified by FCC using EtOAc / *n*-hexane (1:1) as the solvent mixture to afford 4-(4´´-(4-methoxyphenyl)-[2,2´:6´,2´´-terpyridin]-4-yl)benzonitrile (**186**) as the desired asymmetric product in a yield of 80% (40.3 mg, 91.5 µmol). Apart from this the starting material **179** was reisolated in 20% (8.9 mg, 23.8 µmol).

Analytical data 186:

^{1}H-NMR (400 MHz, $CDCl_3$, ppm, 25 °C): δ_H = 8.85 (d, $^4J_{H,H}$ = 1.2 Hz, 1H, *H3* / H3´´**), 8.81 (dd, $^3J_{H,H}$ = 5.1 Hz, $^5J_{H,H}$ = 0.6 Hz, 1H, *H6* / H6´´**), 8.76 (d, $^4J_{H,H}$ = 1.9 Hz, $^5J_{H,H}$ = 0.8 Hz, 1H, *H3* / H3´´**), 8.72 (d, , $^3J_{H,H}$ = 5.1 Hz, 1H, *H6* / H6´´**), 8.50 (app. ddd, $^3J_{H,H}$ = 7.8 Hz, $^4J_{H,H}$ = 0.9 Hz, 2H, *H3´ / H5´*), 8.01 (t, $^3J_{H,H}$ = 7.8 Hz, 1H, *H4´*), 7.88 (d, $^3J_{H,H}$ = 8.5 Hz, 2H, $H_{phenyl(pull)}$), 7.81 (d, $^3J_{H,H}$ = 8.5 Hz, 2H, $H_{phenyl(pull)}$), 7.72 (d, $^3J_{H,H}$ = 8.8 Hz, 2H, $H_{phenyl(push)}$), 7.53 (app. dt, $^3J_{H,H}$ = 5.1 Hz, $^4J_{H,H}$ = 1.6 Hz, 2H, *H5 / H5´´*), 7.04 (d, $^3J_{H,H}$ = 8.8 Hz, 2H, $H_{phenyl(push)}$), 3.90 (s, 3H, $H_{methoxy}$).

^{13}C-NMR (101 MHz, $CDCl_3$, ppm, 25 °C): δ_C = 160.82 (C_q, 1C), 158.73 (C_q, 1C), 157.39 (C_q, 1C), 156.60 (C_q, 1C), 155.08 (C_q, 1C), 150.13 (C_t, 1C), 149.72 (C_t, 1C), 149.01 (C_q, 1C), 147.34 (C_q, 1C), 143.26 (C_q, 1C), 138.21 (C_t, 1C), 133.02 (C_{phenyl}, 2C),

130.82 (C_q, 1C), 128.41 (C_{phenyl}, 2C), 128.03 (C_{phenyl}, 2C), 121.85 (C_t, 1C), 121.67 (C_t, 1C), 121.52 (C_t, 1C), 121.42 (C_t, 1C), 119.32 (C_t, 1C), 118.75 (C_t, 1C), 118.62 (C_q, 1C), 114.68 (C_{phenyl}, 2C), 112.90 ($C_{q\ (CN)}$, 1C) 55.59 ($C_{methoxy}$, 1C).

ESI-MS (MeOH, *positive* ion mode): *m/z* [ion, intensity (%)] = 441.2 ($M+H^+$, 100), 463.2 ($M+Na^+$, 20).

HRMS (ESI-ToF): *m/z* calcd. for $[C_{29}H_{20}N_4O+H]^+$: 441.1710; found: 441.1716, *m/z* calcd. for $[C_{29}H_{20}N_4O+Na]^+$: 463.1529; found: 463.1529.

4-(4-Methoxyphenyl)-4´´-(4-nitrophenyl)-2,2´:6´,2´´-terpyridine (187)

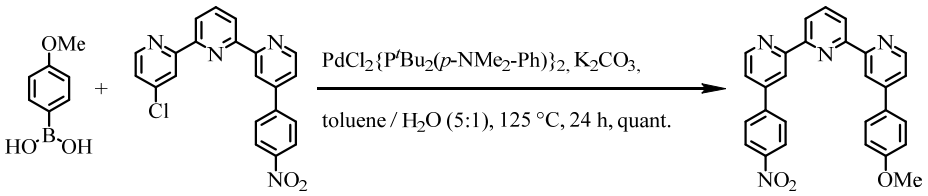

182 **187**

Compound **187** was prepared according to general procedure B described above. 4-Chloro-4´´-(4-nitrophenyl)-2,2´:6´,2´´-terpyridine (**182**) (46.7 mg, 120 µmol, 1.00 eq.), 4-(methoxy)-phenylboronic acid (186 mg, 1.20 mmol, 10.0 eq.), $PdCl_2\{P^tBu_2(p\text{-}NMe_2\text{-}Ph)\}_2$ (4.25 mg, 6.00 µmol, 0.05 eq.), and K_2CO_3 (50.3 mg, 360 µmol, 3.00 eq.) were charged into a Schlenk tube under inert atmosphere. All reagents were mixed and suspended in previously degassed toluene (20 mL) and H_2O (4 mL). The reaction vessel was sealed and heated to 125 °C for 24 h. After completion the reaction mixture was allowed to cool down to room temperature and was subsequently diluted with DCM, brine and water. Now the reaction mixture was extracted with DCM (4 *x*) and with EtOAc. The organic phases were combined, dried over $MgSO_4$, filtered and residual solvent was evaporated under reduced pressure. The crude product was purified by FCC using EtOAc / *n*-hexane (1:1) as the solvent mixture to afford the desired asymmetric product 4-(4-methoxyphenyl)-4´´-(4-nitrophenyl)-2,2´:6´,2´´-terpyridine (**187**) in quantitative yield (55.3 g, 120 µmol).

Analytical data 187:

^{1}H-NMR (400 MHz, $CDCl_3$, ppm, 25 °C): δ_H = 8.87 (d, $^4J_{H,H}$ = 1.2 Hz, 1H, *H3* / H3´´**), 8.81 (dd, , $^3J_{H,H}$ = 5.0 Hz, $^5J_{H,H}$ = 0.5 Hz, 1H, *H6* / H6´´**), 8.76 (d, $^4J_{H,H}$ = 1.2 Hz, 1H, *H3* / H3´´**), 8.70 (d, , $^3J_{H,H}$ = 5.1 Hz, 1H, *H6* / H6´´**), 8.50 (dd, $^3J_{H,H}$ = 7.8 Hz, $^4J_{H,H}$ = 1.4 Hz, 2H, *H3´ / H5´*), 8.36 (d, $^3J_{H,H}$ = 8.8 Hz, 2H, H_{phenyl}), 8.00 (t, $^3J_{H,H}$ = 7.8 Hz, 1H, *H4´*), 7.91 (d, $^3J_{H,H}$ = 8.9 Hz, 2H, H_{phenyl}), 7.71 (d, $^3J_{H,H}$ = 8.9 Hz, 2H, H_{phenyl}), 7.55 (dd, $^3J_{H,H}$ = 5.1 Hz, $^4J_{H,H}$ = 1.9 Hz, 1H, *H5* / H5´´**), 7.51 (dd, $^3J_{H,H}$ = 5.1 Hz, $^4J_{H,H}$ = 1.9 Hz, 1H, *H5* / H5´´**), 7.02 (d, $^3J_{H,H}$ = 8.8 Hz, 2H, H_{phenyl}), 3.89 (s, 3H, $H_{methoxy}$).
^{13}C-NMR (101 MHz, $CDCl_3$, ppm, 25 °C): δ_C = 160.79 (C_q, 1C), 157.41 (C_q, 1C), 156.63 (C_q, 1C), 155.79 (C_q, 1C), 154.89 (C_q, 1C), 150.15 (C_t, 1C), 149.80 (C_t, 1C), 148.85 (C_q, 1C), 148.31 (C_q, 1C), 146.88 (C_q, 1C), 145.11 (C_q, 1C), 138.20 (C_t, 1C), 130.81 (C_q, 1C), 128.35 (C_{phenyl}, 2C), 128.21 (C_{phenyl}, 2C), 124.45 (C_{phenyl}, 2C),

121.81 (C_t, 1C), 121.69 (C_t, 1C), 121.42 (C_t, 1C), 121.37 (C_t, 1C), 119.44 (C_t, 1C), 118.71 (C_t, 1C), 114.67 (C_{phenyl}, 2C), 55.57($C_{methoxy}$, 1C).

ESI-MS (MeOH, *positive* ion mode): *m/z* [ion, intensity (%)] = 461.2 ($M+H^+$, 40), 483.2 ($M+Na^+$, 100).

HRMS (ESI-ToF): *m/z* calcd. for $[C_{28}H_{20}N_4O_3+H]^+$: 461.1608; found: 461.1604, *m/z* calcd. for $[C_{28}H_{20}N_4O_3+Na]^+$: 483.1428; found: 483.1420.

(2-((4-Ethynylphenyl)thio)ethyl)trimethylsilane (149) (in two steps via 181)

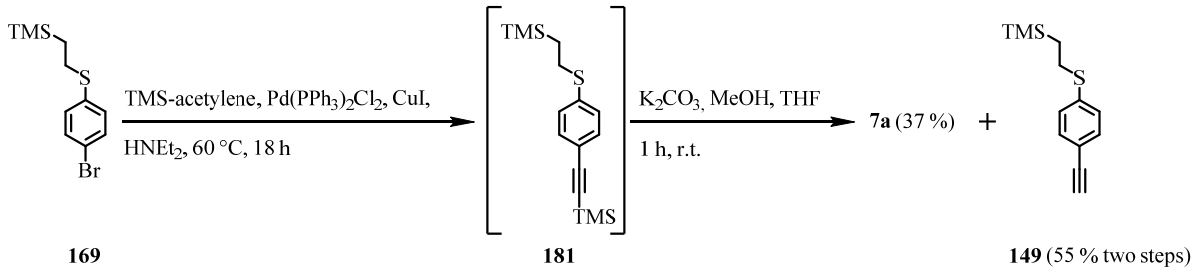

169 **181** **149** (55 % two steps)

149 was prepared in two steps by adapting a previously reported literature procedure.[537] 2-((4-Bromophenyl)thio)ethyltrimethylsilane (**169**) (810 mg, 2.80 mmol, 1.00 eq.), TMS-acetylene (58.9 mg, 0.31 mmol, 0.11 eq.), $Pd(PPh_3)_2Cl_2$ (199 mg, 0.28 mmol, 0.10 eq.) and CuI (810 mg, 2.80 mmol, 1.00 eq.) were charged into a Schlenk tube, dissolved in diethylamine ($HNEt_2$) (50 mL) and degassed for 30 min before the reaction vessel was sealed and heated to 60 °C overnight. Subsequently the reaction was allowed to cool down to room temperature before being quenched by the addition of water and dilution with DCM. Saturated NH_4Cl-solution and brine were added prior to repeated extraction of the mixture with DCM (4 *x*). The combined organic layers were dried over $MgSO_4$ and concentrated under reduced pressure to yield the crude product which was now purified by FCC using a gradient of solvents reaching from pure *n*-hexane to a mixture of *n*-hexane / EtOAc (17:3). The column yielded 821.4 mg of a mixture of **169** and **181**. In the second step 767 mg (at least 2.5 mmol) of the described mixture were charged into a round-bottomed flask and K_2CO_3 (873 mg, 6.25 mmol) was added. The reagents were dissolved in a 1:1 mixture of MeOH and THF (15 mL each) and the mixture was stirred for 1 h at room temperature, until the deprotection was finished (monitored by TLC). After DCM and brine were added to the reaction mixture the same was extracted with DCM (4 *x*). The combined organic layers were dried over $MgSO_4$ and concentrated to yield the crude product which was now purified by FCC using a gradient of solvents reaching from pure *n*-hexane to a mixture of *n*-hexane / DCM (9:1). Thus the desired product (2-((4-ethynylphenyl)thio)ethyl)trimethylsilane (**149**) was obtained quantitatively (338 mg, 1.44 mmol) from this reaction step. Apart from this the original starting material **169** was reisolated (283 mg, 0.98 mmol). Therefore the desired target compound **149** was isolated in an overall yield of 55% (362 mg, 1.54 mmol), whereas the starting material **169** was recovered in a yield of 37% (303 mg, 1.05 mmol).

Analytical data of 149:

^{1}H-NMR (400 MHz, $CDCl_3$, ppm, 25 °C): δ_H = 7.40 (d, $^{3}J_{H,H}$ = 8.4 Hz, 2H, *H_{phenyl}*), 7.21 (d, $^{3}J_{H,H}$ = 8.5 Hz, 2H, *H_{phenyl}*), 3.08 (s, 1H, *$H_{acetylene}$*), 2.97 (m, 2H, -*S*-***CH_2***-*CH_2*-*TMS*), 0.94 (m, 2H, -*S*-*CH_2*-***CH_2***–*TMS*), 0.06 (s, 9H, *H_{TMS}*).

^{13}C-NMR (101 MHz, $CDCl_3$, ppm, 25 °C): δ_C = 139.18 (C_q, 1C), 132.49 (C_t, 2C), 127.73 (C_t, 2C), 118.89 (C_q, 1C), 83.56 ($C_{acetylene}$, 1C), 77.43 ($C_{acetylene}$, 1C), 28.91 (C_{ethyl}, 1C), 16.70 (C_{ethyl}, 1C), -1.65 (C_{TMS}, 3C).

GCMS (EI^+, 70 eV): *m/z* [ion, intensity (%)] = 234.2 (M^+, 31), 206.1 (M^+-2 CH_2, 58), 191.1 (M^+-2 CH_2 –CH_3, 50).

4,4´´-Bis((4-((2-(trimethylsilyl)ethyl)thio)phenyl)ethynyl)-2,2´:6´,2´´-terpyridine (148)

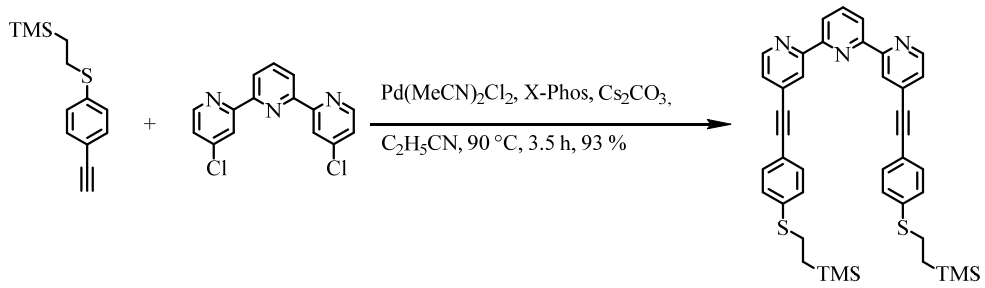

149 **47** **148**

148 was prepared by adapting a literature reported protocol.[538] 4,4´´-dichloro-2,2´:6´2´´-terpyridine **(47)** (60.4 mg, 200 µmol, 1.00 eq.), (2-((4-ethynylphenyl)thio)ethyl)trimethylsilane (**149**) (1.57 mg, 600 µmol, 3.00 eq.), the base Cs_2CO_3 (393 mg, 1.20 mmol, 6.00 eq.), the pre-catalyst $Pd(CH_3CN)_2Cl_2$ (35.4 mg, 6.00 µmol, 0.03 eq.) and the ligand 2-dicyclohexylphosphino-2′,4′,6′-triisopropylbiphenyl (*X-Phos)* (8.85 mg, 18.0 µmol, 0.09 eq.) were charged into a two-neck flask with reflux condenser and suspended in previously degassed propionitrile (10 mL). The reaction mixture was heated to reflux for 3.5 h until the reaction was finished according to TLC. Prior to workup the reaction mixture was allowed to cool down to room temperature and successively diluted with DCM and saturated NH_4Cl- solution. Now the reaction mixture was extracted with DCM (5 *x*) before the combined organic phases were dried over $MgSO_4$, filtered and concentrated under reduced pressure. Finally the crude product was further purified by FCC using EtOAc / *n*-hexane (3:17) as eluent to yield the disubstituted product 4,4´´-bis((4-((2-(trimethylsilyl)ethyl)thio)phenyl)ethynyl)-2,2´:6´,2´´-terpyridine (**148**) in a yield of 93% (129 mg, 185 µmol).

Analytical data of 148:

^{1}H-NMR (500 MHz, $CDCl_3$, ppm, 25 °C): δ_H = 8.70 (dd, $^4J_{H,H}$ = 1.6 Hz, $^5J_{H,H}$ = 0.8 Hz, 2H, *H3 / H3´´*), 8.68 (dd, $^3J_{H,H}$ = 5.0 Hz, $^4J_{H,H}$ = 0.6 Hz, 2H, *H6´ / H6´´*), 8.46 (d, $^3J_{H,H}$ = 7.8 Hz, 2H, *H3´ / H5´*), 7.98 (t, $^3J_{H,H}$ = 7.8 Hz, 1H, *H4´*), 7.51 (d, $^3J_{H,H}$ = 8.5 Hz, 4H, H_{phenyl}), 7.42 (dd, $^3J_{H,H}$ = 5.0 Hz, $^4J_{H,H}$ = 1.6 Hz, 2H, *H5 / H5´´*), 7.25 (d, $^3J_{H,H}$ = 8.3 Hz, 4H, H_{phenyl}), 3.01 (m, 4H, *–S–**CH₂**–CH₂–TMS*), 0.96 (m, 4H, *-S-CH₂-**CH₂**–TMS*), 0.06 (s, 18H, H_{TMS}).

^{13}C-NMR (126 MHz, $CDCl_3$, ppm, 25 °C): δ_C = 156.45 (C_q, 2C), 155.18 (C_q, 2C), 149.27 (C_t, 2C), 140.07 (C_q, 2C), 138.10 (C_t, 1C), 132.52 (C_q, 2C), 132.35 (C_{phenyl}, 4C),

127.59 (C_{phenyl}, 4C), 121.58 (C_t, 2C), 123.24 (C_t, 2C), 121.61 (C_t, 2C), 118.85 (C_q, 2C), 94.09 ($C_{acetylene}$, 2C), 87.67 ($C_{acetylene}$, 2C), 28.78 (C_{ethyl}, 2C), 16.66 (C_{ethyl}, 2C), -1.59 (C_t, 2C).

ESI-MS (MeOH, *positive* ion mode): *m/z* [ion, intensity (%)] = 698.5 ($M+H^+$, 100), 720.4 ($M+Na^+$, 10).

HRMS (ESI-ToF): *m/z* calcd. for $[C_{41}H_{43}N_3S_2Si_2+H]^+$: 698.2510; found: 698.2501.

_S,S´_-(([2,2´:6´,2´´-terpyridine]-4,4´´-diylbis(ethyne-2,1-diyl))bis(4,1-phenylene)) diethanethioate (146)

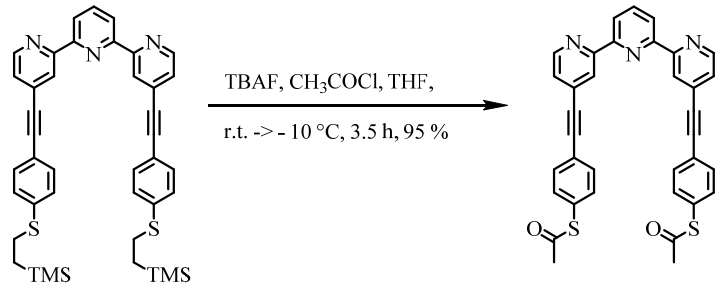

148 **146**

The acetyl-protected thiol **146** was prepared by the transprotection of the ethyl-TMS protected 4,4´´-bis((4-((2-(trimethylsilyl)ethyl)thio)phenyl)ethynyl)-2,2´:6´,2´´-terpyridine (**148**). An oven-dried round-bottom flask was charged with terpyridine precursor **148** (76.8 mg, 0.11 mmol, 1.00 eq.) and put under inert atmosphere. Subsequently **148** was dissolved in rigorously degassed THF (20 mL) as the solvent, before TBAF (1M in THF, 1.10 mL, 1.10 mmol, 10.0 eq.) was added which caused the former colorless solution to turn orange-red immediately. After 1.5 h of stirring the reaction mixture was cooled down to -10 °C prior to the dropwise addition of previously degassed acetyl chloride (1.74 g, 1.59 mL, 22.0 mmol, 200 eq.) to the red solution which subsequently turned colorless again followed by a bright yellow color. After further 2 h in the cooling bath the reaction was cautiously quenched by the addition of saturated $NaHCO_3$-solution. The reaction mixture was extracted with DCM (4 *x*), before the combined organic phases were dried over $MgSO_4$, filtered and concentrated under reduced pressure. Finally the resulting crude product was further purified by FCC using a solvent gradient ranging from EtOAc / *n*-hexane (1:3) via EtOAc / *n*-hexane (1:1) up to pure EtOAc to yield the desired disubstituted product *S,S´*-(([2,2´:6´,2´´-terpyridine]-4,4´´-diylbis-(ethyne-2,1-diyl))bis(4,1-phenylene)) diethanethioate (**146**) in an excellent yield of 95% (60.5 mg, 104 µmol).

Analytical data of 146:

^{1}H-NMR (400 MHz, $CDCl_3$, ppm, 25 °C): δ_H = 8.72 (dd, $^4J_{H,H}$ = 1.6 Hz, $^5J_{H,H}$ = 0.9 Hz, 2H, *H3 / H3´´*), 8.71 (dd, $^3J_{H,H}$ = 5.0 Hz, $^4J_{H,H}$ = 0.7 Hz, 2H, *H6´ / H6´´*), 8.48 (d, $^3J_{H,H}$ = 7.8 Hz, 2H, *H3´ / H5´*), 7.99 (t, $^3J_{H,H}$ = 7.8 Hz, 1H, *H4´*), 7.64 (d, $^3J_{H,H}$ = 8.4 Hz, 4H, H_{phenyl}), 7.44 (dd, $^3J_{H,H}$ = 4.9 Hz, $^4J_{H,H}$ = 1.6 Hz, 2H, *H5 / H5´´*), 7.43 (d, $^3J_{H,H}$ = 8.4 Hz, 4H, H_{phenyl}), 2.45 (s, 6H, H_{methyl}).

^{13}C-NMR (101 MHz, $CDCl_3$, ppm, 25 °C): δ_C = 193.27 ($C_{(C=O)}$, 2C), 156.53 (C_q, 2C), 155.13 (C_q, 2C), 149.36 (C_t, 2C), 138.17 (C_t, 1C), 134.47 (C_{phenyl}, 4C), 132.62 (C_{phenyl}, 4C), 132.13 (C_q, 2C), 129.41 (C_q, 2C), 125.68 (C_t, 2C), 123.54 (C_q, 2C), 123.35 (C_t, 2C), 121.69 (C_t, 2C), 93.19 ($C_{acetylene}$, 2C), 88.90 ($C_{acetylene}$, 2C), 30.49 (C_{methyl}, 2C).

ESI-MS (MeOH, *positive* ion mode): *m/z* [ion, intensity (%)] = 582.2 ($M+H^+$, 50), 291.6 ($M+2H^+$, 100).

HRMS (ESI-ToF): *m/z* calcd. for $[C_{35}H_{23}N_3O_2S_2+2H]^{2+}$: 291.5689; found: 291.5693, *m/z* calcd. for $[C_{35}H_{23}N_3O_2S_2+H]^+$: 582.1304; found: 582.1302.

Representative Procedure C (Complexation of previously herein, described terpyridine ligands with $FeCl_2$):

The described complexation was usually performed by dissolving the appropriate terpyridine ligand (2.0 - 2.2 eq.) in organic solvents (MeOH / EtOH / DCM) before $FeCl_2$ (1.0 eq.) was added. Usually an instantaneous color change occurred. After approximately one hour of stirring with or without mild heating (~50 °C) depending on the substrate the now deeply colored solution was diluted with the 5-fold amount of H_2O and afterwards it was stirred for some time (30 min to 5 h) before being extracted with some organic solvent (e. g. EtOAc, DCM) to get rid of excess ligand. Now the reaction mixture was liberated from any organic solvents under reduced pressure before excess saturated NH_4PF_6 – solution (15 – 50 eq.) was added. The addition of NH_4PF_6 resulted in the expected anion exchange and in the precipitation of the desired homoleptic $\{[Fe(tpy)_2]^{2+}[(PF_6)^-]_2\}$ – complexes. This precipitation was usually completed by storing the reaction mixture in the refrigerator overnight. The mixture was now filtered over a fine glass frit (porosity 4) (usually only by gravitation) and washed excessively with H_2O to eliminate excess NH_4PF_6. Finally the strongly colored residue was dissolved in acetone or MeCN, dried over $MgSO_4$, filtered and concentrated under reduced pressure and under high vacuum to yield the desired products.

{[Fe(*47*)$_2$]$^{2+}$[(PF$_6$)$^-$]$_2$} (189)

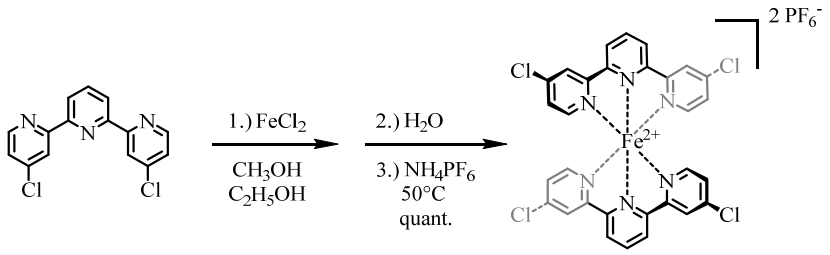

47 **189**

189 was prepared by adapting the representative procedure C. $FeCl_2$ (63.4 mg, 500 µmol, 1.00 eq.), the ligand 4,4´´-dichloro-2,2´:6´2´´-terpyridine (**47**) (350 mg, 1.10 mmol, 2.20 eq.), MeOH (10 mL), EtOH (10 mL), water (100 mL) and NH_4PF_6 (1.22 g, 7.50 mmol, 15.0 eq.) were used. The product complex **189** was isolated as a deep purple powder in quantitative yield (473 mg, 500 µmol), whereas the remaining excess ligand was recovered as well during the extraction. By applying a solvent diffusion technique using acetonitrile and hexane with an intermediate spacer layer of benzene it was possible to obtain single crystals of **189** suitable for x-ray analysis. The crystallographic information of compound **189** is discussed in chapter 9.2. Hereafter, only the further analytical data of target compound **189** are discussed.

Analytical data of 189

T$_M$: >300 °C.

^{1}H-NMR (400 MHz, acetone-d$_6$, ppm, 25 °C): δ_H = 9.32 (d, $^3J_{H,H}$ = 8.1 Hz, 4H, *H3´ / H5´*), 8.89 (m, 6H, *H4´ / H3 / H3´´*), 7.37 (d, $^3J_{H,H}$ = 6.1 Hz, 4H, *H6 / H6´´*), 7.29 (dd, $^3J_{H,H}$ = 6.1 Hz, $^4J_{H,H}$ = 2.2 Hz, 4H, *H5 / H5´´*).

^{13}C-NMR (101 MHz, acetone-d$_6$, ppm, 25 °C): δ_C = 161.21 (C$_q$, 4C), 160.55 (C$_q$, 4C), 155.66 (C$_t$, 4C), 148.27 (C$_q$, 4C), 140.27 (C$_t$, 2C), 129.04 (C$_t$, 4C), 126.52 (C$_t$, 4C), 125.83 (C$_t$, 4C).

MS (FAB$^+$): *m/z* [ion, intensity (%)] = 805.0 (M$^+$-PF$_6^-$, 23), 679.0 (M$^+$-2PF$_6^-$+F, 42), 660.0 (M$^+$-2PF$_6^-$, 42).

ESI-MS (MeCN, *positive* ion mode): *m/z* [ion, intensity (%)] = 330.1 (M^{2+}-2PF$_6^-$, 100).

HRMS (ESI-ToF): *m/z* calcd. for [C$_{30}$H$_{18}$Cl$_4$FeN$_6$]$^{2+}$: 328.9843; found: 328.9847.

UV/VIS (acetone): λ_{max} (ε) = 364 nm (7773 L·cm^{-1}·mol^{-1}), 556 nm (13693 L·cm^{-1}·mol^{-1}).

UV/VIS (MeCN): λ_{max} (ε) = 270 nm (32115 L·cm^{-1}·mol^{-1}), 281 nm (31265 L·cm^{-1}·mol^{-1}), 322 nm (52320 L·cm^{-1}·mol^{-1}), 365 nm (4860 L·cm^{-1}·mol^{-1}), 555 nm (10690 L·cm^{-1}·mol^{-1}).

{[Fe(*167a*)$_2$]$^{2+}$[(PF$_6$)$^-$]$_2$} (190)

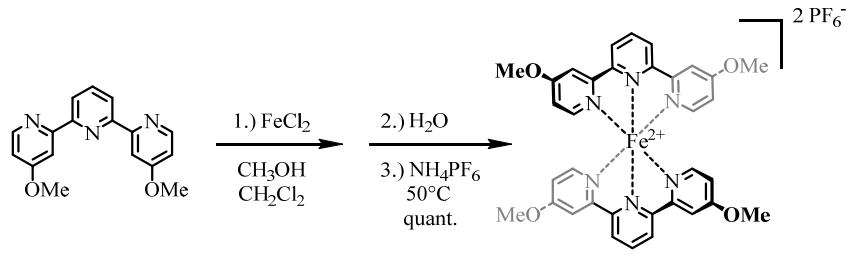

167a **190**

190 was prepared by adapting the representative procedure C. $FeCl_2$ (5.20 mg, 40.0 µmol, 1.00 eq.), 4,4′′-dimethoxy-2,2′:6′2′′-terpyridine **(167a)** (25.0 mg, 80.0 µmol, 2.00 eq.), MeOH (10 mL), DCM (10 mL), water (50 mL) and NH_4PF_6 (326 mg, 2.00 mmol, 50.0 eq.) were used. The product **190** was isolated as a deep purple powder in quantitative yield (38.2 mg, 40.0 µmol).

Analytical data of 190:

T$_M$: >300 °C.

^{1}H-NMR (500 MHz, acetone-d$_6$, ppm, 25 °C): δ_H = 9.24 (d, $^3J_{H,H}$ = 8.1 Hz, 4H, *H3′ / H5′*), 8.79 (t, $^3J_{H,H}$ = 8.1 Hz, 2H, *H4′*), 8.38 (d, $^3J_{H,H}$ = 2.7 Hz, 2H, *H3 / H3′′*), 7.07 (d, $^3J_{H,H}$ = 6.5 Hz, 4H, *H6 / H6′′*), 6.78 (dd, $^3J_{H,H}$ = 6.5 Hz, $^4J_{H,H}$ = 2.7 Hz, 4H, *H5 / H5′′*).

^{13}C-NMR (126 MHz, acetone-d$_6$, ppm, 25 °C): δ_C = 169.08 (C$_q$, 4C), 161.67 (C$_q$, 4C), 160.06 (C$_q$, 4C), 154.09 (C$_t$, 4C), 138.52 (C$_t$, 2C), 124.78 (C$_t$, 4C), 114.90 (C$_t$, 4C), 111.71 (C$_t$, 4C), 57.19 (C$_{methoxy}$, 4C).

^{19}F-NMR (376 MHz, acetone-d$_6$, ppm, 25 °C): δ_F = –72.44 (d, $^1J_{P,F}$ = 708.1 Hz, 12F).

^{31}P-NMR (162 MHz, acetone-d$_6$, ppm, 25 °C): δ_P = –144.25 (hept, $^1J_{P,F}$ = 707.9 Hz, 2P).

ESI-MS (MeCN, *positive* ion mode): *m/z* [ion, intensity (%)] = 786.9 (M^{2+}-PF$_6^-$, 16), 321.1 (M^{2+}-2PF$_6^-$, 100).

HRMS (ESI-ToF): *m/z* calcd. for [C$_{34}$H$_{30}$FeN$_6$O$_4$]$^{2+}$: 321.0834; found: 321.0839.

UV/VIS (acetone): λ_{max} (ε) = 365 nm (3557 L·cm^{-1}·mol^{-1}), 556 nm (9167 L·cm^{-1}·mol^{-1}).

UV/VIS (MeCN): λ_{max} (ε) = 269 nm (25442 L·cm^{-1}·mol^{-1}), 315 nm (37468 L·cm^{-1}·mol^{-1}), 365 nm (2924 L·cm^{-1}·mol^{-1}), 554 nm (8826 L·cm^{-1}·mol^{-1}).

{[Fe(*168a*)$_2$]$^{2+}$[(PF$_6$)$^-$]$_2$} (191)

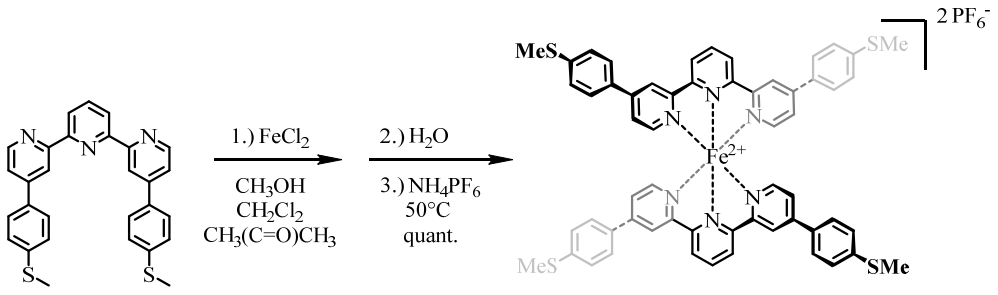

191 was prepared by adapting the representative procedure C. $FeCl_2$ (3.60 mg, 30.0 µmol, 1.00 eq.), the ligand 4,4´´-bis(4-(methylthio)phenyl)-2,2´:6´,2´´-terpyridine (**168a**) (30.0 mg, 60.0 µmol, 2.00 eq.), the solvents MeOH (10 mL), DCM (25 mL), acetone (15 mL) and water (50 mL) and finally NH_4PF_6 (205 mg, 1.26 mmol, 42.0 eq.) were used. **191** was isolated as a dark purple solid in quantitative yield (37.0 mg, 30.0 µmol). By applying a solvent diffusion technique using acetonitrile and hexane with an intermediate spacer layer of benzene it was additionally, possible to obtain single crystals of **191** suitable for x-ray structure determination. The crystallographic information of compound **191** are however discussed in detailed form in chapter 9.2. Thus hereafter, only the remaining analytical data of target compound **191** are discussed.

Analytical data of 191:

T$_M$: >300 °C.

^{1}H-NMR (400 MHz, acetone-d$_6$, ppm, 25 °C): δ_H = 9.49 (d, $^3J_{H,H}$ = 8.1 Hz, 4H, *H3´/H5´*), 9.17 (d, $^4J_{H,H}$ = 1.7 Hz, 4H, *H3/H3´´*), 8.93 (t, $^3J_{H,H}$ = 8.1 Hz, 2H, *H4´*), 7.79 (d, $^3J_{H,H}$ = 8.6 Hz, 8H, *H$_{phenyl}$*), 7.54 (dd, $^3J_{H,H}$ = 6.1 Hz, $^4J_{H,H}$ = 2.0 Hz, 4H, *H5 / H5´´)*, 7.46 (d, $^3J_{H,H}$ = 6.0 Hz, 4H, *H6 / H6´´*), 7.37 (d, $^3J_{H,H}$ = 8.7 Hz, 8H, *H$_{phenyl}$*), 2.52 (s, 12H, *H$_{methyl}$*).

^{13}C-NMR (101 MHz, acetone-d$_6$, ppm, 25 °C): δ_C = 161.64 (C$_q$, 4C), 159.59 (C$_q$, 4C), 154.05 (C$_t$, 4C), 150.91 (C$_q$, 4C), 144.12 (C$_q$, 4C), 139.11 (C$_t$, 2C), 132.11 (C$_q$, 4C), 128.48 (C$_{phenyl}$, 8C), 127.05 (C$_{phenyl}$, 8C), 125.09 (C$_t$, 4C), 121.77 (C$_t$, 4C), 14.79 (C$_{methyl}$, 4C). Note: Only 12 instead of the expected 13 signals can be seen in the ^{13}C-NMR spectrum which is most likely due to coincidence of two tertiary carbon signals at 125.09 ppm.

^{19}F-NMR (376 MHz, acetone-d$_6$, ppm, 25 °C): δ_F = -72.20 (d, $^1J_{P,F}$ = 707.2 Hz, 12F).

^{31}P-NMR (162 MHz, acetone-d$_6$, ppm, 25 °C): δ_P = –144.21 (hept, $^1J_{P,F}$ = 707.9 Hz, 2P).

MS (FAB$^+$): *m/z* [ion, intensity (%)] = 1155.4 (M^+-PF_6^-, 10), 1029.3 (M^+-$2PF_6^-$+F, 9), 1010.3 (M^+-$2PF_6^-$, 24), 504.9 (M^{2+}-$2PF_6^-$, 31).

ESI-MS (MeCN, *positive* ion mode): *m/z* [ion, intensity (%)] = 1155.2 (M^{2+}-PF_6^-, 3), 505.2 (M^{2+}-$2PF_6^-$, 100).

HRMS (ESI-ToF): *m/z* calcd. for $[C_{58}H_{46}FeN_6S_4]^{2+}$: 505.1003; found: 505.1014.

UV/VIS (acetone): λ_{max} (ε) = 355 nm (94420 $L \cdot cm^{-1} \cdot mol^{-1}$), 568 nm (20173 $L \cdot cm^{-1} \cdot mol^{-1}$).

UV/VIS (MeCN): λ_{max} (ε) = 268 nm (33685 $L \cdot cm^{-1} \cdot mol^{-1}$), 285 nm (41835 $L \cdot cm^{-1} \cdot mol^{-1}$), 350 nm (60830 $L \cdot cm^{-1} \cdot mol^{-1}$), 567 nm (11775 $L \cdot cm^{-1} \cdot mol^{-1}$), 631 nm (5165 $L \cdot cm^{-1} \cdot mol^{-1}$).

{[Fe(*171*)$_2$]$^{2+}$[(PF$_6$)$^-$]$_2$} (192)

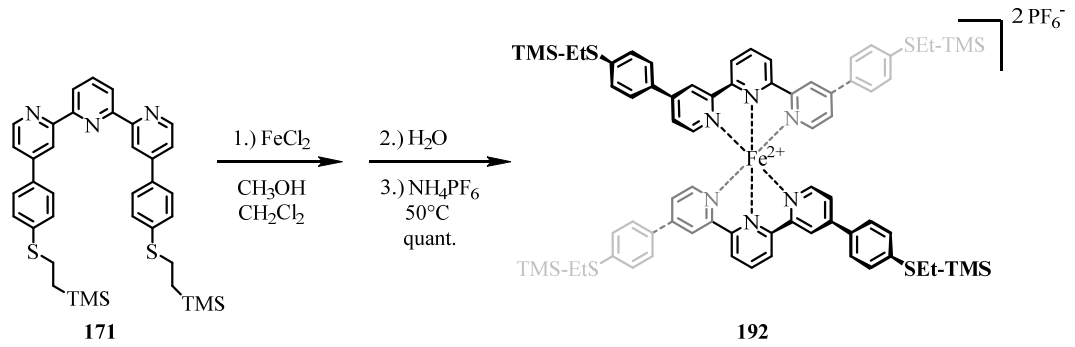

192 was prepared according to representative procedure C. The ligand 4,4′′-bis(4-((2-(trimethylsilyl)ethyl)thio)phenyl)-2,2′:6′,2′′-terpyridine (**171**) (75.3 mg, 110 µmol, 2.20 eq.) was dissolved in a mixture of MeOH (15 mL) and DCM (15 mL) before $FeCl_2$ (6.30 mg, 50.0 µmol, 1.00 eq.) was added. Additionally, water (75 mL) and NH_4PF_6 (359 mg, 2.20 mmol, 44.0 eq.) were used. The product **192** was isolated as a dark purple solid in quantitative yield (82.5 mg, 50.0 µmol).

Analytical data of 192:

T$_M$: >300 °C.

^{1}H-NMR (400 MHz, acetone-d$_6$, ppm, 25 °C): δ_H = 9.46 (d, $^3J_{H,H}$ = 8.1 Hz, 4H, *H3′/H5′*), 9.13 (d, $^4J_{H,H}$ = 1.6 Hz, 4H, *H3/H3′′*), 8.88 (t, $^3J_{H,H}$ = 8.1 Hz, 2H, *H4′*), 7.79 (d, $^3J_{H,H}$ = 8.6 Hz, 8H, *H$_{phenyl}$*), 7.53 (dd, $^3J_{H,H}$ = 6.1 Hz, $^4J_{H,H}$ = 1.9 Hz, 4H, *H5/H5′′*), 7.45 (d, $^3J_{H,H}$ = 6.0 Hz, 4H, *H6/H6′′*), 7.35 (d, $^3J_{H,H}$ = 8.6 Hz, 8H, *H$_{phenyl}$*), 3.06 (m, 8H, *H$_{ethyl}$*), 0.92 (m, 8H, *H$_{ethyl}$*), 0.04 (s, 36H, *TMS*).

^{13}C-NMR (101 MHz, acetone-d$_6$, ppm, 25 °C): δ_C = 161.43 (C$_q$, 4C), 159.50 (C$_q$, 4C), 153.96 (C$_t$, 4C), 150.68 (C$_q$, 4C), 142.95 (C$_q$, 4C), 139.07 (C$_t$, 2C), 132.38 (C$_q$, 4C), 128.44 (C$_{phenyl}$, 8C), 128.42 (C$_{phenyl}$, 8C), 125.07 (C$_t$, 4C), 124.99 (C$_t$, 4C), 121.63 (C$_t$, 4C), 28.53 (C$_{ethyl}$, 4C), 17.07 (C$_{ethyl}$, 4C), –1.69 (C$_{TMS}$, 12C).

^{19}F-NMR (376 MHz, acetone-d$_6$, ppm, 25 °C): δ_F = –72.26 (d, $^1J_{P,F}$ = 709.1 Hz, 12F).

ESI-MS (MeCN, *positive* ion mode): *m/z* [ion, intensity (%)] = 677.2 (M^{2+}-2PF$_6^-$, 100).

HRMS (ESI-ToF): *m/z* calcd. for [C$_{74}$H$_{86}$FeN$_6$S$_4$Si$_4$]$^{2+}$: 677.2108; found: 677.2126.

UV/VIS (acetone): λ_{max} (ε) = 361 nm (86567 L·cm^{-1}·mol^{-1}), 568 nm (18067 L·cm^{-1}·mol^{-1}).

UV/VIS (MeCN): λ_{max} (ε) = 269 nm (38945 L·cm^{-1}·mol^{-1}), 284 nm (46155 L·cm^{-1}·mol^{-1}), 354 nm (69000 L·cm^{-1}·mol^{-1}), 567 nm (14245 L·cm^{-1}·mol^{-1}), 631 nm (6340 L·cm^{-1}·mol^{-1}).

{[Fe(*131*)$_2$]$^{2+}$[(PF$_6$)$^-$]$_2$} (129)

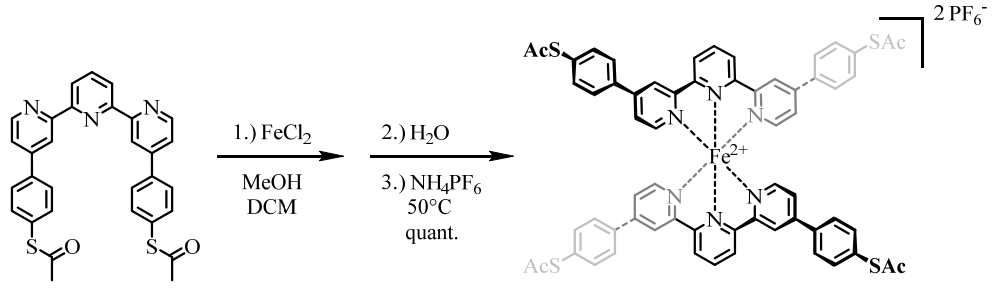

129 was prepared after the representative procedure C. $FeCl_2$ (6.30 mg, 50.0 µmol, 1.00 eq.), *S,S´*-([2,2´:6´,2´´-terpyridine]-4,4´´-diylbis(4,1-phenylene)) diethanethioate (**131**) (56.2 mg, 100 µmol, 2.00 eq.), MeOH (15 mL), DCM (15 mL), water (75 mL), and NH_4PF_6 (408 mg, 2.50 mmol, 50.0 eq.) were used. The product **129** was isolated as a dark purple solid in a yield of 99%(70.0 mg, 50.0 µmol).

Analytical data of 129:

T*$_M$*: >300 °C.

^{1}H-NMR (400 MHz, acetone-d$_6$, ppm, 25 °C): δ_H = 9.52 (d, $^3J_{H,H}$ = 7.9 Hz, 4H, *H3´ / H5´*), 9.22 (m, 4H, *H3 / H3´´*), 8.94 (t, $^3J_{H,H}$ = 7.7 Hz, 2H, *H4´*), 7.89 (d, $^3J_{H,H}$ = 8.2 Hz, 8H, H_{phenyl}), 7.58 (m, 8H, *H5 / H5´´ / H6 / H6´´)*, 7.54 (d, $^3J_{H,H}$ = 8.3 Hz, 8H, H_{phenyl}), 2.43 (s, 12H, H_{methyl}).

^{13}C-NMR (101 MHz, acetone-d$_6$, ppm, 25 °C): δ_C = 192.99 ($C_{C=O}$, 4C), 161.51 (C_q, 4C), 159.74 (C_q, 4C), 154.37 (C_t, 4C), 150.62 (C_q, 4C), 139.36 (C_t, 2C), 137.07 (C_q, 4C), 135.96 (C_{phenyl}, 8C), 132.23 (C_q, 4C), 128.89 (C_{phenyl}, 8C), 125.82 (C_t, 4C), 125.37 (C_t, 4C), 122.52 (C_t, 4C), 30.45 (C_{methyl}, 4C).

^{19}F-NMR (376 MHz, acetone-d$_6$, ppm, 25 °C): δ_F = –72.22 (d, $^1J_{P,F}$ = 707.5 Hz, 12F).

^{31}P-NMR (162 MHz, acetone-d$_6$, ppm, 25 °C): δ_P = -144.20 (hept, $^1J_{P,F}$ = 708 Hz, 2P).

ESI-MS (MeCN, *positive* ion mode): *m/z* [ion, intensity (%)] = 561.2 (M^{2+}-2PF_6^-, 100).

HRMS (ESI-ToF): *m/z* calcd. for $[C_{62}H_{46}FeN_6O_4S_4]^{2+}$: 561.0902; found: 561.0912.

UV/VIS (acetone): λ_{max} (ε) = 338 nm (81333 L·cm^{-1}·mol^{-1}), 380 nm (14600 L·cm^{-1}·mol^{-1}), 567 nm (11867 L·cm^{-1}·mol^{-1}).

UV/VIS (MeCN): λ_{max} (ε) = 276 nm (68550 L·cm^{-1}·mol^{-1}), 336 nm (83685 L·cm^{-1}·mol^{-1}), 379 nm (15880 L·cm^{-1}·mol^{-1}), 566 nm (13540 L·cm^{-1}·mol^{-1}), 626 nm (5965 L·cm^{-1}·mol^{-1}).

{[Fe(*177*)$_2$]$^{2+}$[(PF$_6$)$^-$]$_2$} (197)

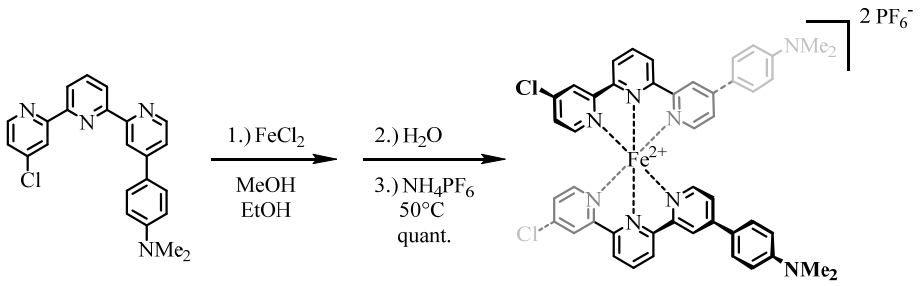

177 **197**

197 was prepared according to representative procedure C. $FeCl_2$ (8.88 mg, 70.0 µmol, 1.00 eq.), 4-(4′′-chloro-[2,2′:6′,2′′-terpyridin]-4-yl)-*N,N*-dimethylaniline (**177**) (61.0 mg, 158 µmol, 2.20 eq.), MeOH (10 mL), EtOH (10 mL), water (100 mL), and NH_4PF_6 (228 mg, 1.40 mmol, 20.0 eq.) were used. The product **197** was isolated as a dark purple solid in quantitative yield (79.0 mg, 71.0 µmol). The excess ligand was reisolated (12.0 mg, 31.0 µmol) as well.

Analytical data of 197:

^{1}H-NMR (400 MHz, acetone-d$_6$, ppm, 25 °C): δ_H = 9.43 (d, $^3J_{H,H}$ = 8.0 Hz, 2H, *H3′* / H5′**), 9.30 (d, $^3J_{H,H}$ = 8.0 Hz, 2H, *H3′* / H5′**), 9.02 (d, $^4J_{H,H}$ = 1.8 Hz, 2H, *H3* / H3′′**), 8.91 (d, $^4J_{H,H}$ = 2.1 Hz, 2H, *H3* / H3′′**), 8.86 (t, $^3J_{H,H}$ = 8.1 Hz, 2H, *H4′*), 7.75 (d, $^3J_{H,H}$ = 9.0 Hz, 4H, H_{phenyl}), 7.43 (dd, $^3J_{H,H}$ = 6.1 Hz, $^4J_{H,H}$ = 1.9 Hz, 2H, *H5*), 7.42 (d, $^3J_{H,H}$ = 6.2 Hz, 2H, *H6* / H6′′**), 7.30 (dd, $^3J_{H,H}$ = 6.1 Hz, $^4J_{H,H}$ = 2.2 Hz, 2H, *H5′*), 7.18 (d, $^3J_{H,H}$ = 6.1 Hz, 2H, *H6* / H6′′**), 6.78 (d, $^3J_{H,H}$ = 9.1 Hz, 4H, H_{phenyl}), 3.01 (s, 12H, H_{methyl}).

^{13}C-NMR (101 MHz, acetone-d$_6$, ppm, 25 °C): δ_C = 162.02 (C_q, 2C), 160.46 (C_q, 2C), 160.40 (C_q, 2C), 158.80 (C_q, 2C), 155.02 (C_t, 2C), 153.27 (C_t, 2C), 151.47 (C_q, 2C), 147.42 (C_q, 2C), 139.20 (C_t, 2C), 129.02 (C_{phenyl}, 4C), 128.37 (C_t, 2C), 125.41 (C_t, 2C), 125.15 (C_t, 2C), 123.63 (C_t, 2C), 121.92 (C_q, 2C), 120.44 (C_t, 2C), 113.10 (C_{phenyl}, 4C), 40.12 (C_{methyl}, 4C). In the ^{13}C-spectrum and in the DEPT-135 one signal less than expected was found probably due to coincident signals.

^{19}F-NMR (376 MHz, acetone-d$_6$, ppm, 25 °C): δ_F = –72.20 (d, $^1J_{P,F}$ = 709.3 Hz, 12F).

^{31}P-NMR (162 MHz, acetone-d$_6$, ppm, 25 °C): δ_P = -144.20 (hept, $^1J_{P,F}$ = 712.9 Hz, 2P).

MS (FAB$^+$): *m/z* [ion, intensity (%)] = 973.1 (M^{2+}-PF_6^-, 8), 414.1 (M^{2+}-2PF_6^-, 22).

ESI-MS (MeCN, *positive* ion mode): *m/z* [ion, intensity (%)] = 414.2 (M^{2+}-$2PF_6^-$, 100).

HRMS (ESI-ToF): *m/z* calcd. for $[C_{46}H_{38}Cl_2FeN_8]^{2+}$: 414.0968; found: 414.0971.

UV/VIS (MeCN): λ_{max} (ε) = 265 nm (41067 $L \cdot cm^{-1} \cdot mol^{-1}$), 283 nm (27247 $L \cdot cm^{-1} \cdot mol^{-1}$), 327 nm (58807 $L \cdot cm^{-1} \cdot mol^{-1}$), 393 nm (32720 $L \cdot cm^{-1} \cdot mol^{-1}$), 564 nm (13240 $L \cdot cm^{-1} \cdot mol^{-1}$).

{[Fe(*173*)$_2$]$^{2+}$[(PF$_6$)$^-$]$_2$} (198)

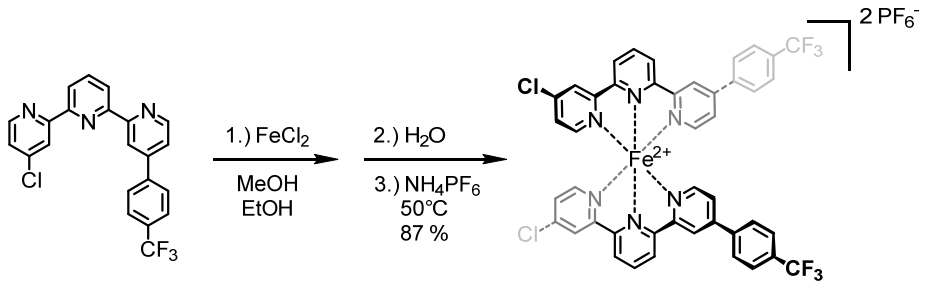

6f **8g**

198 was prepared by adapting the representative procedure C. $FeCl_2$ (13.3 mg, 105 µmol, 1.00 eq.), 4-chloro-4′′-(4-(trifluoromethyl)phenyl)-2,2′:6′,2′′-terpyridine (**173**) (95.1 mg, 231 µmol, 2.20 eq.), MeOH (15 mL), EtOH (10 mL), water (75 mL), and NH_4PF_6 (343 mg, 2.10 mmol, 20.0 eq.) were used. The product **198** was isolated as a dark purple solid in a yield of 87% (107 mg, 91.0 µmol). The excess ligand was reisolated completely (21.0 mg, 51.0 µmol).

Analytical data of 198:

^{1}H-NMR (400 MHz, acetone-d$_6$, ppm, 25 °C): δ_H = 9.48 (d, $^3J_{H,H}$ = 7.9 Hz, 2H, *H3′* / H5′**), 9.35 (d, $^3J_{H,H}$ = 7.9 Hz, 2H, *H3′* / H5′**), 9.22 (s, 2H, *H3* / H3′′**), 8.99 - 8.83 (m, 4H, *H3* / H3′′* / H4′*), 8.05 (d, $^3J_{H,H}$ = 7.9 Hz, 4H, H_{phenyl}), 7.85 (d, $^3J_{H,H}$ = 8.0 Hz, 4H, H_{phenyl}), 7.61 (d, $^3J_{H,H}$ = 5.1 Hz, 2H, *H5* / H5′′* / H6* / H6′′**), 7.54 (d, $^3J_{H,H}$ = 5.7 Hz, 2H, *H5* / H5′′* / H6* / H6′′**), 7.46 (d, $^3J_{H,H}$ = 6.0 Hz, 2H, *H5* / H5′′* / H6* / H6′′**), 7.32 (d, $^3J_{H,H}$ = 4.7 Hz, 2H, *H5* / H5′′* / H6* / H6′′**).

^{13}C-NMR (101 MHz, acetone-d$_6$, ppm, 25 °C): δ_C = 161.63 (C$_q$, 2C), 160.64 (C$_q$, 2C), 160.28 (C$_q$, 2C), 159.75 (C$_q$, 2C), 155.15 (C$_t$, 2C), 154.75 (C$_t$, 2C), 150.15 (C$_q$, 2C), 147.82 (C$_q$, 2C), 140.25 (C$_q$, 2C), 140.24 (C$_q$, 2C), 139.69 (C$_t$, 2C), 132.38 (q, ^{1}J = 33.1 Hz, 2C, -***C***F_3), 129.20 (C$_{phenyl}$, 4C), 128.62 (C$_t$, 2C), 127.14 (q, ^{3}J = 3.6 Hz, 4C, -*(**C**H)$_2$CCF$_3$*), 126.19 (C$_t$, 2C), 125.85 (C$_{phenyl}$, 4C), 125.39 (C$_t$, 2C), 122.83 (C$_t$, 2C). In the ^{13}C-spectrum and in the DEPT-135 one signal less than expected was found probably due to coincident signals.

^{19}F-NMR (376 MHz, acetone-d$_6$, ppm, 25 °C): δ_F = -63.36 (s, 6F, CF_3), -72.20 (d, $^1J_{P,F}$ = 708.3 Hz, 12F).

MS (FAB$^+$): *m/z* [ion, intensity (%)] = 1023.0 (M^{2+}-PF$_6^-$, 9), 439.0 (M^{2+}-2PF$_6^-$, 14).

ESI-MS (MeCN, *positive* ion mode): *m/z* [ion, intensity (%)] = 439.1 (M^{2+}-2PF_6^-, 100).

HRMS (ESI-ToF): *m/z* calcd. for $[C_{44}H_{26}Cl_2F_6FeN_6]^{2+}$: 439.0420; found: 439.0426.

UV/VIS (MeCN): λ_{max} (ε) = 272 nm (44415 $L \cdot cm^{-1} \cdot mol^{-1}$), 328 nm (53885 $L \cdot cm^{-1} \cdot mol^{-1}$), 372 nm (7115 $L \cdot cm^{-1} \cdot mol^{-1}$), 560 nm (11080 $L \cdot cm^{-1} \cdot mol^{-1}$), 614 nm (3285 $L \cdot cm^{-1} \cdot mol^{-1}$).

{[Fe(*174*)$_2$]$^{2+}$[(PF$_6$)$^-$]$_2$} (194)

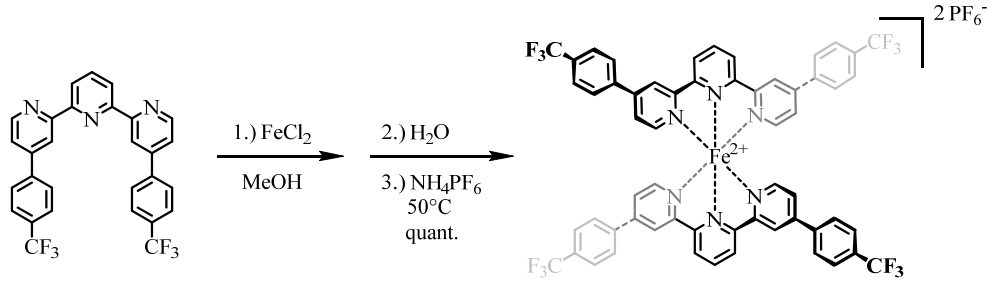

174 **194**

194 was prepared by adapting the representative procedure C. $FeCl_2$ (4.44 mg, 35.0 µmol, 1.00 eq.), 4,4′′-bis(4-(trifluoromethyl)phenyl)-2,2′:6′,2′′-terpyridine (**174**) (40.2 mg, 77.0 µmol, 2.20 eq.), MeOH (10 mL), water (50 mL), and NH_4PF_6 (250 mg, 1.53 mmol, 43.7 eq.) were used. The product **194** was yielded quantitatively as a dark purple solid (48.7 mg, 35.0 µmol).

Analytical data of 194:

^{19}F-NMR (376 MHz, acetone-d$_6$, ppm, 25 °C): δ_F = -63.36 (s, 12F, CF_3), -72.30 (d, $^1J_{P,F}$ = 708.1 Hz, 12F).

^{31}P-NMR (162 MHz, acetone-d$_6$, ppm, 25 °C): δ_P = -139.86 (hept, $^1J_{P,F}$ = 708.2 Hz, 2P).

MS (FAB$^+$): *m/z* [ion, intensity (%)] = 1243.0 (M^{2+}-PF_6^-, 7), 549.1 (M^{2+}-2PF_6^-, 8).

ESI-MS (MeCN, *positive* ion mode): *m/z* [ion, intensity (%)] = 549.3 (M^{2+}-2PF_6^-, 100).

HRMS (ESI-ToF): *m/z* calcd. for $[C_{58}H_{34}F_{12}FeN_6]^{2+}$: 549.0997; found: 549.1004.

UV/VIS (MeCN): λ_{max} (ε) = 270 nm (38353 L·cm^{-1}·mol^{-1}), 332 nm (26813 L·cm^{-1}·mol^{-1}), 377 nm (4427 L·cm^{-1}·mol^{-1}), 562 nm (5760 L·cm^{-1}·mol^{-1}), 619 nm (2153 L·cm^{-1}·mol^{-1}).

{[Fe(*147*)$_2$]$^{2+}$[(PF$_6$)$^-$]$_2$} (119)

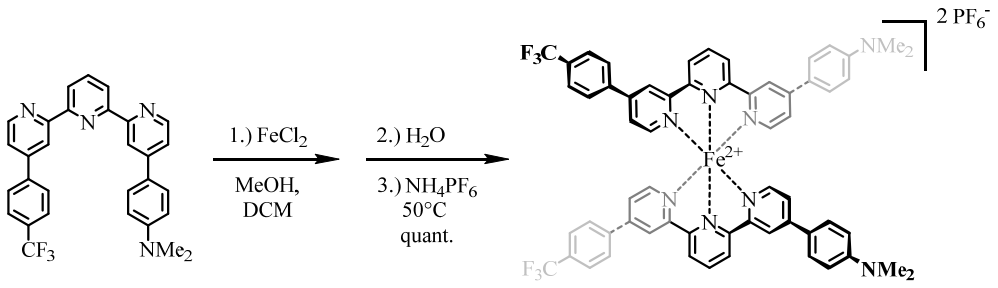

147 **119**

119 was prepared following representative procedure C. $FeCl_2$ (5.80 mg, 45.8 µmol, 1.00 eq.), the asymmetric ligand *N,N*-dimethyl-4-(4′′-(4-(trifluoromethyl)phenyl)-[2,2′:6′,2′′-terpyridin]-4-yl)aniline (**147**) (49.7 mg, 100 µmol, 2.18 eq.), MeOH (20 mL), DCM (20 mL), water (100 mL), and NH_4PF_6 (326 mg, 2.00 mmol, 43.7 eq.) were used. The product **119** was isolated as a dark purple solid in a quantitative yield (61.0 mg, 46.0 µmol).

Analytical data of 119:

^{1}H-NMR (400 MHz, acetone-d$_6$, ppm, 25 °C): δ_H = 9.47 (d, $^3J_{H,H}$ = 7.9 Hz, 4H, *H3′ / H5′*), 9.24 (s, 2H, *H3* / H3′′**), 9.07 (s, 2H, *H3* / H3′′**), 8.90 (t, $^3J_{H,H}$ = 7.9 Hz, 2H, *H4′*), 8.06 (d, $^3J_{H,H}$ = 7.9 Hz, 4H, H_{phenyl}), 7.85 (d, $^3J_{H,H}$ = 8.0 Hz, 4H, H_{phenyl}), 7.77 (d, $^3J_{H,H}$ = 8.6 Hz, 4H, H_{phenyl}), 7.67 – 7.53 (m, 4H, *H5* / H5′′* / H6* / H6′′**), 7.46 (d, $^3J_{H,H}$ = 5.6 Hz, 2H, *H5* / H5′′* / H6* / H6′′**), 7.27 (d, $^3J_{H,H}$ = 5.9 Hz, 2H, *H5* / H5′′* / H6* / H6′′**), 6.78 (d, $^3J_{H,H}$ = 8.6 Hz, 4H, H_{phenyl}), 3.01 (s, 12H, H_{methyl}).

^{13}C-NMR (101 MHz, acetone-d$_6$, ppm, 25 °C): δ_C = 161.84 (C_q, 2C), 161.27 (C_q, 2C), 160.01 (C_q, 2C), 158.93 (C_q, 2C), 154.52 (C_t, 2C), 153.28 (C_q, 2C), 153.18 (C_t, 2C), 151.44 (C_q, 2C), 149.75 (C_q, 2C), 140.38 (C_q, 2C), 139.02 (C_t, 2C), 132.29 (q, ^{1}J = 32.1 Hz, 2C, -***C***F_3), 129.18 (C_{phenyl}, 4C), 129.03 (C_{phenyl}, 4C), 127.11 (q, ^{3}J = 3.7 Hz, 4C, -*(**C**H)$_2$CCF$_3$*), 125.92 (C_t, 2C), 125.10 (C_t, 2C), 124.87 (C_t, 2C), 123.62 (C_t, 2C), 122.54 (C_t, 2C), 121.97 (C_q, 2C), 120.39 (C_t, 2C), 113.09 (C_{phenyl}, 4C), 40.11 (C_{methyl}, 4C). In the ^{13}C-spectrum and in the DEPT-135 one signal less than expected was found probably due to coincident signals.

^{19}F-NMR (376 MHz, acetone-d$_6$, ppm, 25 °C): δ_F = -63.32 (s, 6F, CF_3), -72.20 (d, $^1J_{P,F}$ = 708.6 Hz, 12F).

MS (FAB$^+$): *m/z* [ion, intensity (%)] = 1193.4 (M^{2+}-PF_6^-, 5), 523.9 (M^{2+}-2PF_6^-, 11).

ESI-MS (MeCN, *positive* ion mode): *m/z* [ion, intensity (%)] = 524.4 (M^{2+}-2PF_6^-, 100).

HRMS (ESI-ToF): *m/z* calcd. for $[C_{60}H_{46}F_6FeN_8]^{2+}$: 524.1545; found: 524.1554.

UV/VIS (MeCN): λ_{max} (ε) = 269 nm (44790 $L \cdot cm^{-1} \cdot mol^{-1}$), 331 nm (56190 $L \cdot cm^{-1} \cdot mol^{-1}$), 397 nm (34630 $L \cdot cm^{-1} \cdot mol^{-1}$), 569 nm (12670 $L \cdot cm^{-1} \cdot mol^{-1}$), 635 nm (5960 $L \cdot cm^{-1} \cdot mol^{-1}$).

{[Fe(*183*)$_2$]$^{2+}$[(PF$_6$)$^-$]$_2$} (120)

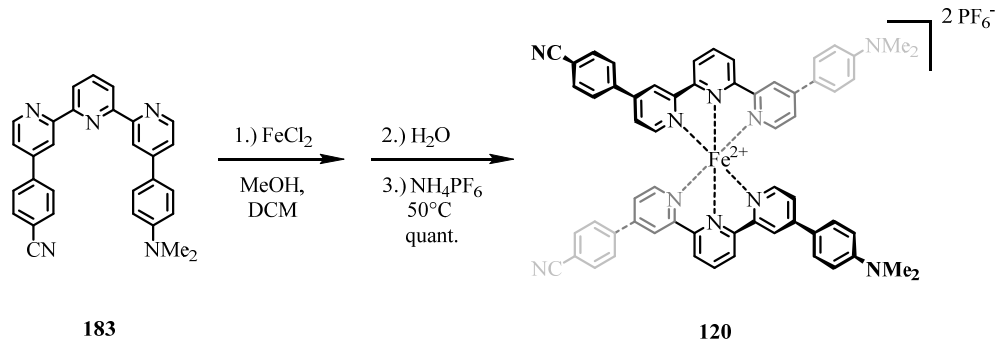

183 **120**

120 was prepared following representative procedure C. $FeCl_2$ (9.68 mg, 76.3 µmol, 1.00 eq.), 4-(4′′-(4-(dimethylamino)phenyl)-[2,2′:6′,2′′-terpyridin]-4-yl)benzonitrile (**183**) (76.2 mg, 168 µmol, 2.20 eq.), MeOH (20 mL), DCM (20 mL), water (100 mL), and NH_4PF_6 (548 mg, 3.36 mmol, 44.0 eq.) were used. The product **120** was isolated as a dark purple solid in quantitative yield (95.3 mg, 76.0 µmol).

Analytical data of 120:

^{1}H-NMR (400 MHz, acetone-d$_6$, ppm, 25 °C): δ_H = 9.47 (dd, $^3J_{H,H}$ = 8.0 Hz, $^4J_{H,H}$ = 3.3 Hz, 4H, *H3′ / H5′*), 9.24 (d, $^4J_{H,H}$ = 1.3 Hz, 2H, *H3* / H3′′**), 9.07 (d, $^4J_{H,H}$ = 1.8 Hz, 2H, *H3* / H3′′**), 8.89 (t, $^3J_{H,H}$ = 8.1 Hz, 2H, *H4′*), 8.04 (d, $^3J_{H,H}$ = 8.7 Hz, 4H, H_{phenyl}), 7.90 (d, $^3J_{H,H}$ = 8.6 Hz, 4H, H_{phenyl}), 7.76 (d, $^3J_{H,H}$ = 9.1 Hz, 4H, H_{phenyl}), 7.64 – 7.55 (m, 4H, *H5* / H5′′* / H6* / H6′′**), 7.46 (dd, $^3J_{H,H}$ = 6.2 Hz, $^4J_{H,H}$ = 2.0 Hz, 2H, *H5* / H5′′**), 7.27 (d, $^3J_{H,H}$ = 6.1 Hz, 2H, *H6* / H6′′**), 6.78 (d, $^3J_{H,H}$ = 9.1 Hz, 4H, H_{phenyl}), 3.01 (s, 12H, H_{methyl}).

^{13}C-NMR (101 MHz, acetone-d$_6$, ppm, 25 °C): δ_C = 161.84 (C_q, 2C), 161.24 (C_q, 2C), 160.08 (C_q, 2C), 158.90 (C_q, 2C), 154.59 (C_t, 2C), 153.30 (C_q, 2C), 153.16 (C_t, 2C), 151.47 (C_q, 2C), 149.38 (C_q, 2C), 140.72 (C_q, 2C), 139.05 (C_t, 2C), 133.98 (C_{phenyl}, 4C), 129.23 (C_{phenyl}, 4C), 129.04 (C_{phenyl}, 4C), 125.83 (C_t, 2C), 125.15 (C_t, 2C), 124.90 (C_t, 2C), 123.63 (C_t, 2C), 122.49 (C_t, 2C), 121.96 (C_q, 2C), 120.42 (C_t, 2C), 118.79 (C_q, 2C), 114.67 ($C_{(CN)}$, 2C), 113.09 (C_{phenyl}, 4C), 40.12 (C_{methyl}, 4C).

^{19}F-NMR (376 MHz, acetone-d$_6$, ppm, 25 °C): δ_F = -72.21 (d, $^1J_{P,F}$ = 708.2 Hz, 12F).

^{31}P-NMR (162 MHz, acetone-d$_6$, ppm, 25 °C): δ_P = -144.18 (hept, $^1J_{P,F}$ = 708.3 Hz, 2P).

MS (FAB$^+$): *m/z* [ion, intensity (%)] = 1107.2 (M^{2+}-PF_6^-, 5), 481.1 (M^{2+}-2PF_6^-, 9).

ESI-MS (MeCN, *positive* ion mode): *m/z* [ion, intensity (%)] = 481.4 (M^{2+}-2PF_6^-, 100).

HRMS (ESI-ToF): *m/z* calcd. for $[C_{60}H_{46}FeN_{10}]^{2+}$: 481.1623; found: 481.1631.

UV/VIS (MeCN): λ_{max} (ε) = 268 nm (48985 $L \cdot cm^{-1} \cdot mol^{-1}$), 333 nm (52165 $L \cdot cm^{-1} \cdot mol^{-1}$), 397 nm (30635 $L \cdot cm^{-1} \cdot mol^{-1}$), 571 nm (11150 $L \cdot cm^{-1} \cdot mol^{-1}$), 634 nm (59505 $L \cdot cm^{-1} \cdot mol^{-1}$).

{[Fe(147)(*131*)]$^{2+}$[(PF$_6$)$^-$]$_2$} (112)

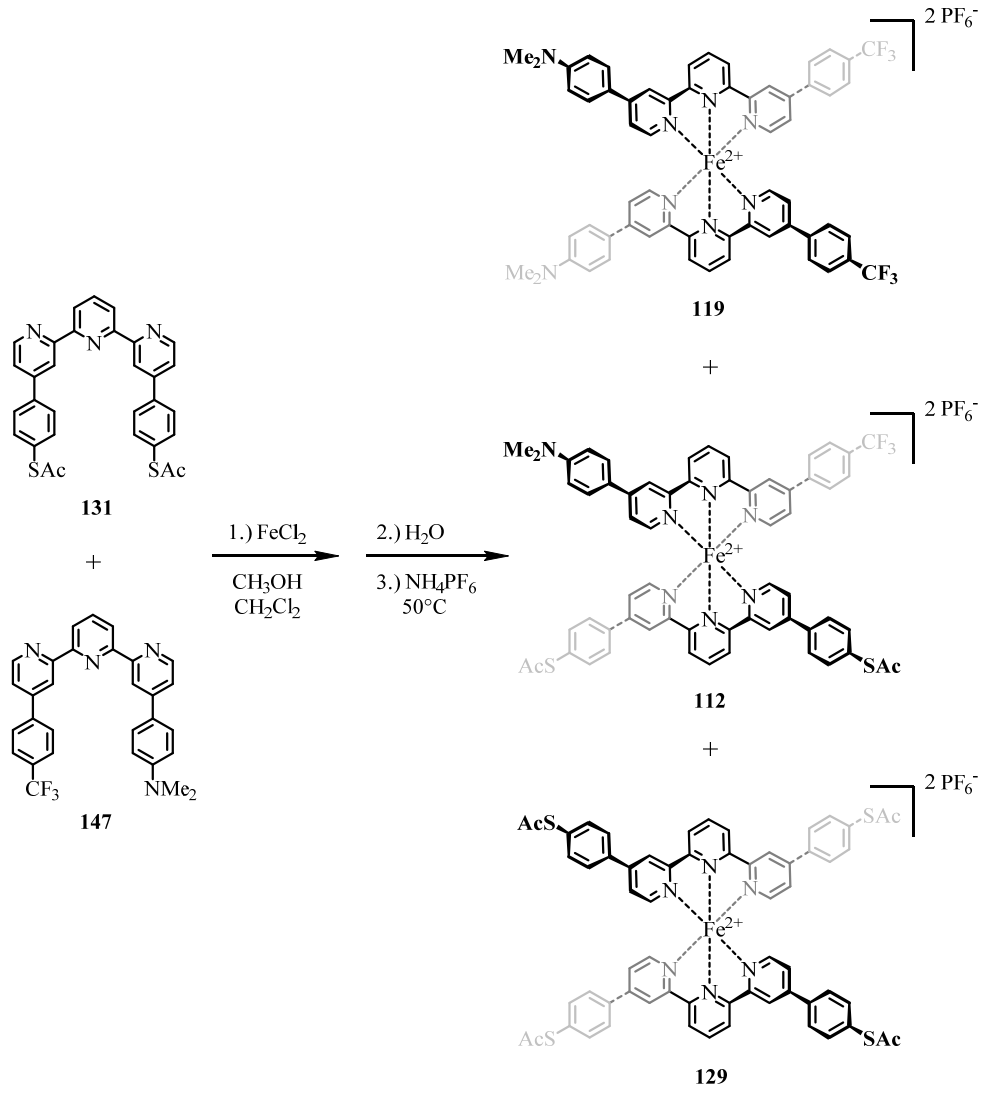

112 was prepared by a modification of the representative procedure C. In this case a statistic reaction had to be performed in which an equimolar amount of the terpyridine precursors was used. Thus the symmetric ligand *S,S´*-([2,2´:6´,2´´-terpyridine]-4,4´´-diylbis(4,1-phenylene)) diethanethioate (**131**) (66.7 mg, 125 µmol, 1.04 eq.) and the asymmetric ligand *N,N*-dimethyl-4-(4´´-(4-(trifluoromethyl)phenyl)-[2,2´:6´,2´´-terpyridin]-4-yl)aniline (**147**) (62.1 mg, 125 µmol, 1.04 eq.) were mixed with $FeCl_2$ (15.2 mg, 0.12 mmol, 1.00 eq.). The reagents were dissolved in MeOH (40 mL), DCM (40 mL), and water (200 mL) and for the final anion exchange NH_4PF_6 (979 mg, 6.00 mmol, 50.0 eq.) was used. The crude product turned out to be the expected statistical mixture of the three complexes **112**, **119** and **129**. To obtain the desired heteroleptic target complex **112** the crude mixture was subjected to purification via preparative reversed-phase HPLC using a solvent gradient ranging from H_2O / MeCN (60:40) up to H_2O / MeCN (40:60) at a flow rate of 20 mL/min yielding the desired product **112** as a

dark purple solid in a yield of 8% (13.0 mg, 9.00 µmol). The two expected homoleptic side products could be separated successfully from the desired heteroleptic target structure. As they have been synthesized separately otherwise they were not explicitly isolated in this context and thus their analytical data is also discussed at the place where their exclusive synthesis is discussed (namely complexes **119** and **129**). Hereafter, only the analytical data of target compound **112** are discussed.

Analytical data of 112:

^{1}H-NMR (600 MHz, acetone-d_6, ppm, 25 °C): δ_H = 9.53 (d, $^{3}J_{H,H}$ = 8.1 Hz, 1H, *H3´* / H5´**), 9.52 (d, $^{3}J_{H,H}$ = 8.1 Hz, 1H, *H3´* / H5´**), 9.50 – 9.47 (m, 2H, *H3´* / H5´**), 9.26 (dd, $^{3}J_{H,H}$ = 5.9 Hz, $^{4}J_{H,H}$ = 1.4 Hz, 1H, *H3$_{(asym)}$* / H3$_{(asym)}$´´**), 9.23 (dd, $^{3}J_{H,H}$ = 5.6 Hz, $^{4}J_{H,H}$ = 1.6 Hz, 2H, *H3$_{(sym)}$ / H3$_{(sym)}$´´*), 9.08 (dd, $^{3}J_{H,H}$ = 5.0 Hz, $^{4}J_{H,H}$ = 1.9 Hz, 1H, *H3$_{(asym)}$* / H3$_{(asym)}$´´**), 8.98 – 8.89 (m, 2H, *H4´*), 8.05 (d, $^{3}J_{H,H}$ = 8.4 Hz, 2H, *H$_{phenyl(push)}$*), 7.89 (d, $^{3}J_{H,H}$ = 8.3 Hz, 4H, *H$_{phenyl(sym)}$*), 7.86 (d, $^{3}J_{H,H}$ = 8.3 Hz, 2H, *H$_{phenyl(push)}$*), 7.76 (app. dd, $^{3}J_{H,H}$ = 9.1 Hz, $^{4}J_{H,H}$ = 1.7 Hz, 2H, *H$_{phenyl(pull)}$*), 7.63 - 7.55 (m, 6H, *H5* / H5´´* / H6* / H6´´**), 7.55 (d, $^{3}J_{H,H}$ = 8.7 Hz, 4H, *H$_{phenyl(sym)}$*), 7.46 (dd, $^{3}J_{H,H}$ = 6.2 Hz, $^{4}J_{H,H}$ = 2.0 Hz, 1H, *H5$_{(asym)}$* / H5$_{(asym)}$´´**), 7.30 - 7.26 (m, 1H, *H5$_{(asym)}$* / H5$_{(asym)}$´´* / H6$_{(asym)}$* / H6$_{(asym)}$´´**), 6.80 (d, $^{3}J_{H,H}$ = 9.1 Hz, 2H, *H$_{phenyl(pull)}$*), 3.03 (s, 6H, *H$_{methyl(NMe2)}$*), 2.43 (s, 6H, *H$_{methyl(SAc)}$*).

^{13}C-NMR (151 MHz, acetone-d_6, ppm, 25 °C): δ_C = 192.99 ($C_{C=O}$, 2C), 161.89 (C_q, 1C), 161.61 (C_q, 1C), 161.57 (C_q, 2C), 161.30 (C_q, 1C), 159.75 (C_q, 2C), 158.96 (C_q, 1C), 154.40 (C_t, 2C), 154.32 (C_t, 1C), 153.37 (C_q, 1C), 153.28 (C_t, 1C), 153.21 (C_q, 1C), 150.70 (C_q, 1C), 150.60 (C_q, 2C), 140.38 (C_q, 1C), 139.26 (C_t, 1C), 139.13 (C_t, 1C), 137.14 (C_q, 2C), 135.99 (C_{phenyl}, 4C), 132.25 (C_q, 2C), 129.20 (C_{phenyl}, 2C), 129.07 (C_{phenyl}, 2C), 128.91 (C_{phenyl}, 4C), 127.15 (q, ^{3}J = 3.2 Hz, 2C, *C$_{phenyl}$*), 125.97 (C_t, 1C), 125.83 (C_t, 2C), 125.37 (C_t, 2C), 125.26 (C_t, 1C), 125.21 (C_t, 1C), 123.65 (C_t, 1C), 122.72 (C_q, 1C), 122.63 (C_t, 1C), 122.57 (C_t, 2C), 122.48 (C_t, 1C), 120.54 (C_q, 1C), 113.11 (C_{phenyl}, 2C), 40.14 ($C_{methyl(NMe2)}$, 2C). 30.45 ($C_{methyl(SAc)}$, 2C). In the ^{13}C-spectrum and in the DEPT-135 one signal less than expected was found probably due to coincident signals.

^{19}F-NMR (376 MHz, acetone-d_6, ppm, 25 °C): δ_F = -63.37 (s, 3F, ***CF$_3$***), -72.42 (d, $^{1}J_{P,F}$ = 707.6 Hz, 12F, ***PF$_6$***).

^{31}P-NMR (162 MHz, acetone-d_6, ppm, 25 °C): δ_P = -144.23 (hept, $^{1}J_{P,F}$ = 708.3 Hz, 2P, ***PF$_6$***).

ESI-MS (MeCN, *positive* ion mode): *m/z* [ion, intensity (%)] = 542.7 (M^{2+}-2PF_6^-, 100).

ESI-MSMS (MeCN, *positive* ion mode (MSMS of *m/z* = 542.7): *m/z* [ion, intensity (%)] = 500.6 (M^{2+}-2((C=O)CH_3), 100), 521.6 (M^{2+}-((C=O)CH_3), 50), 542.6 (M^{2+}, 25).
HRMS (ESI-ToF): *m/z* calcd. for $[C_{61}H_{46}F_3FeN_7O_2S_2]^{2+}$: 542.6223; found: 542.6229.
UV/VIS (MeCN): λ_{max} (ε) = 273 nm (60010 $L \cdot cm^{-1} \cdot mol^{-1}$), 335 nm (75830 $L \cdot cm^{-1} \cdot mol^{-1}$), 386 nm (27940 $L \cdot cm^{-1} \cdot mol^{-1}$), 568 nm (14515 $L \cdot cm^{-1} \cdot mol^{-1}$), 628 nm (6470 $L \cdot cm^{-1} \cdot mol^{-1}$).

{[Fe(*183*)(*131*)]$^{2+}$[(PF$_6$)$^-$]$_2$} (114)

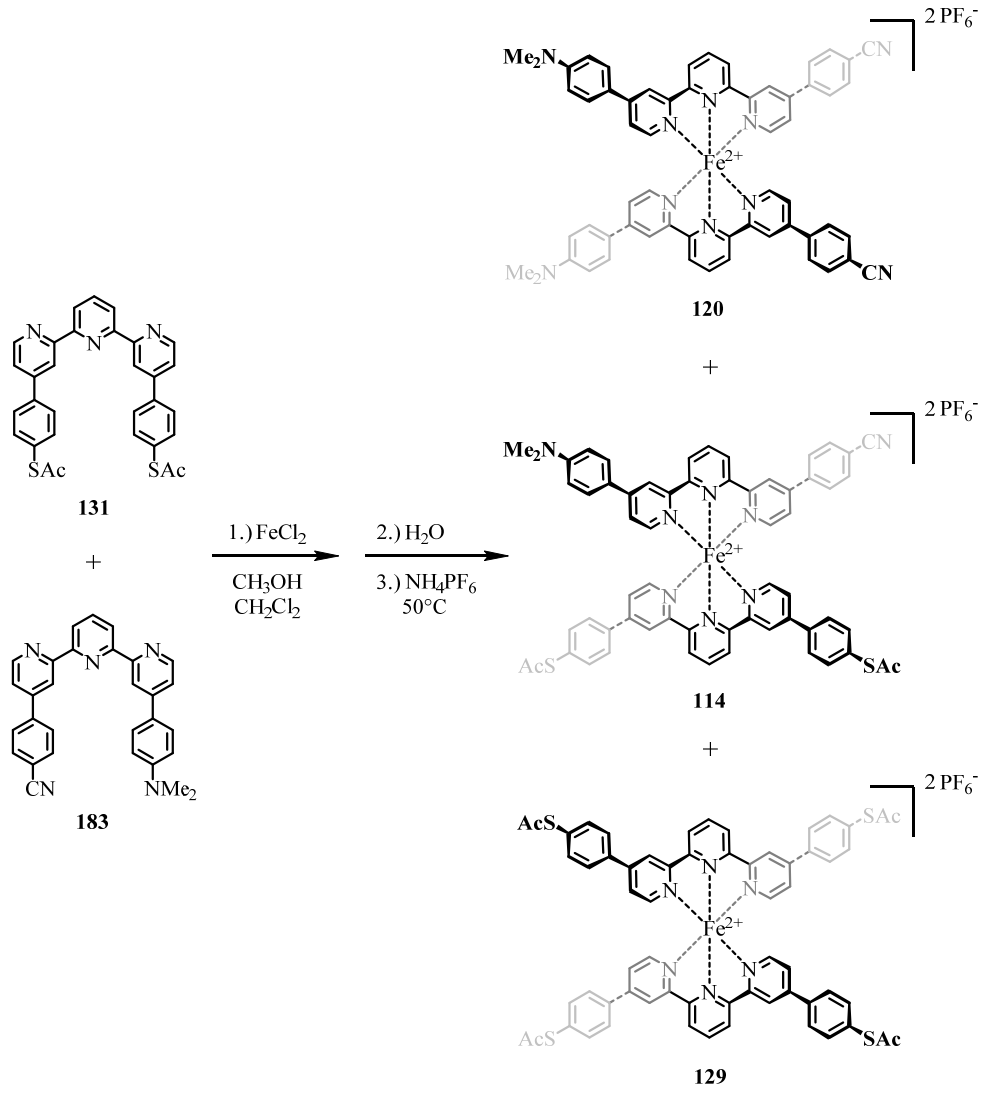

114 was prepared by a modification of the representative procedure C. In this case a statistic reaction had to be performed in which an equimolar amount of the terpyridine precursors was used. Thus the symmetric ligand *S,S′*-([2,2′:6′,2′′-terpyridine]-4,4′′-diylbis(4,1-phenylene)) diethanethioate (**131**) (61.4 mg, 115 µmol, 1.00 eq.) and the asymmetric ligand 4-(4′′-(4-(dimethylamino)phenyl)-[2,2′:6′,2′′-terpyridin]-4-yl)benzonitrile (**183**) (52.2 mg, 115 µmol, 1.00 eq.) were mixed with $FeCl_2$ (14.6 mg, 115 µmol, 1.00 eq.). The reagents were dissolved in MeOH (40 mL), DCM (40 mL), and water (200 mL), before NH_4PF_6 (937 mg, 5.75 mmol, 50.0 eq.) was added. As expected the statistical crude product contained the three complexes **114**, **120** and **129**. To obtain the desired heteroleptic target complex **114** the crude mixture purified via preparative reversed-phase HPLC using a solvent gradient ranging from H_2O / MeCN (60:40) to H_2O / MeCN (52:48) at a flow rate of 20 mL/min yielding the desired pure product **114** as a dark purple-reddish solid in a yield of 20% (30.1 mg, 23.0 µmol). The

two expected homoleptic side products could be separated successfully from the desired heteroleptic target structure. As they have been synthesized separately otherwise they were not explicitly isolated in this context and thus their analytical data is also discussed at the place where their exclusive synthesis is discussed (namely complexes **120** and **129**). Hereafter, only the analytical data of target compound **114** are discussed.

Analytical data of 114:

^{1}H-NMR (400 MHz, acetone-d_6, ppm, 25 °C): δ_H = 9.51 (d, $^{3}J_{H,H}$ = 7.7 Hz, 2H, *H3(sym)´ / H5(sym)´*), 9.55 – 9.45 (m, 2H, *H3(asym)´ / H5(asym)´*), 9.26 (s, 1H, *H3(asym)* / H3(asym)´´**), 9.22 (s, 2H, *H3(sym) / H3(sym)´´*), 9.08 (s, 1H, *H3(asym)* / H3(asym)´´**), 8.99 - 8.86 (m, 2H, *H4´*), 8.04 (d, $^{3}J_{H,H}$ = 8.4 Hz, 2H, $H_{phenyl(push)}$), 7.92 (d, $^{3}J_{H,H}$ = 8.6 Hz, 2H, $H_{phenyl(push)}$), 7.89 (d, $^{3}J_{H,H}$ = 8.4 Hz, 4H, $H_{phenyl(sym)}$), 7.77 (d, $^{3}J_{H,H}$ = 8.9 Hz, 2H, $H_{phenyl(pull)}$), 7.64 - 7.54 (m, 6H, *H5* / H5´´* / H6* / H6´´**), 7.55 (d, $^{3}J_{H,H}$ = 8.3 Hz, 4H, $H_{phenyl(sym)}$), 7.46 (d, $^{3}J_{H,H}$ = 6.0 Hz, 1H, *H5(asym)* / H5(asym)´´**), 7.28 (d, $^{3}J_{H,H}$ = 6.1 Hz, 1H, *H5(asym)* / H5(asym)´´* / H6(asym)* / H6(asym)´´**), 6.79 (d, $^{3}J_{H,H}$ = 8.9 Hz, 2H, $H_{phenyl(pull)}$), 3.02 (s, 6H, $H_{methyl(NMe2)}$), 2.43 (s, 6H, $H_{methyl(SAc)}$).

^{13}C-NMR (101 MHz, acetone-d_6, ppm, 25 °C): δ_C = 193.00 ($C_{C=O}$, 2C), 161.54 (C_q, 2C), 161.24 (C_q, 1C), 159.75 (C_q, 2C), 159.72 (C_q, 1C), 158.93 (C_q, 1C), 157.72 (C_q, 1C), 157.06 (C_q, 1C), 154.68 (C_t, 1C), 154.38 (C_t, 1C), 154.30 (C_t, 2C), 153.33 (C_q, 1C), 153.24 (C_t, 1C), 151.56 (C_q, 1C), 150.56 (C_q, 2C), 149.50 (C_q, 1C), 140.68 (C_q, 1C), 139.24 (C_t, 1C), 139.15 (C_t, 1C), 137.12 (C_q, 2C), 135.97 (C_{phenyl}, 4C), 134.00 (C_{phenyl}, 2C), 132.20 (C_q, 2C), 129.24 (C_{phenyl}, 2C), 129.06 (C_{phenyl}, 2C), 128.90 (C_{phenyl}, 4C), 125.87 (C_t, 1C), 125.80 (C_t, 2C), 125.27 (C_t, 2C), 123.64 (C_t, 1C), 122.62 (C_t, 1C), 122.53 (C_t, 1C), 122.45 (C_t, 2C), 121.89 (C_q, 1C), 120.51 (C_t, 1C), 118.78 (C_q, 1C), 114.73 ($C_{(CN)}$, 1C), 113.09 (C_{phenyl}, 2C), 40.13 ($C_{methyl(NMe2)}$, 2C). 30.45 ($C_{methyl(SAc)}$, 2C).

^{19}F-NMR (376 MHz, acetone-d_6, ppm, 25 °C): δ_F = -72.35 (d, $^{1}J_{P,F}$ = 708.1 Hz, 12F, ***PF_6***).

^{31}P-NMR (162 MHz, acetone-d_6, ppm, 25 °C): δ_P = -144.22 (hept, $^{1}J_{P,F}$ = 708.5 Hz, 2P, ***PF_6***).

ESI-MS (MeCN, *positive* ion mode): *m/z* [ion, intensity (%)] = 521.2 (M^{2+}-2PF_6^-, 100).

ESI-MSMS (MeCN, *positive* ion mode (MSMS of *m/z* = 521.2): *m/z* [ion, intensity (%)] = 479.2 (M^{2+}-2((C=O)CH_3), 100), 500.2 (M^{2+}-((C=O)CH_3), 50), 521.2 (M^{2+}, 20).

HRMS (ESI-ToF): *m/z* calcd. for $[C_{61}H_{46}FeN_8O_2S_2]^{2+}$: 521.1263; found: 521.1270.

UV/VIS (MeCN): λ_{max} (ε) = 275 nm (36972 L·cm^{-1}·mol^{-1}), 336 nm (43004 L·cm^{-1}·mol^{-1}), 387 nm (15262 L·cm^{-1}·mol^{-1}), 568 nm (8142 L·cm^{-1}·mol^{-1}), 629 nm (3740 L·cm^{-1}·mol^{-1}).

{[Fe(*172*)(*131*)]$^{2+}$[(PF$_6$)$^-$]$_2$} (121)

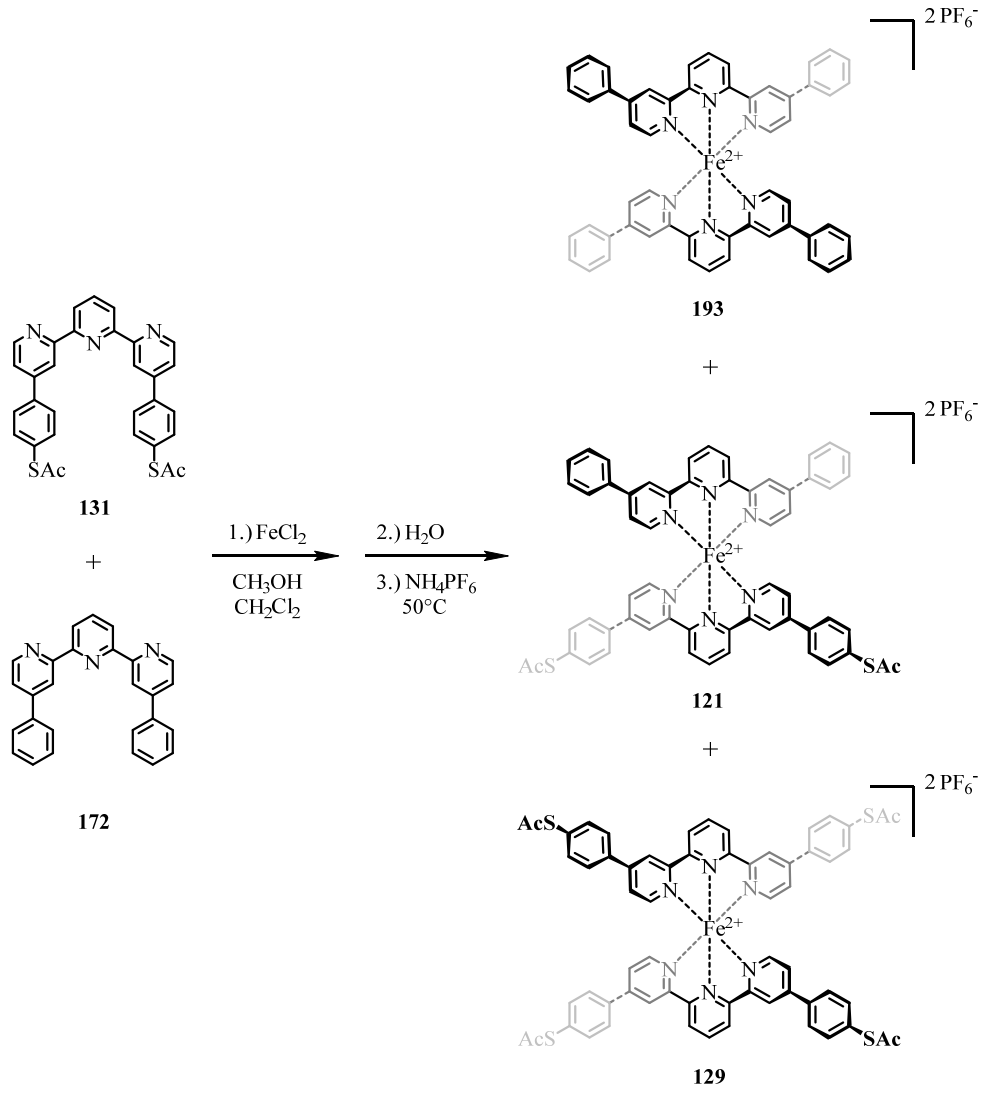

121 was prepared by a modification of the representative procedure C. In this case a statistic reaction had to be performed in which an equimolar amount of the terpyridine precursors was used. Thus 4,4′′-diphenyl-2,2′:6′,2′′-terpyridine (**172**) (46.3 mg, 120 µmol, 1.00 eq.) and *S,S′*-([2,2′:6′,2′′-terpyridine]-4,4′′-diylbis(4,1-phenylene)) diethanethioate (**131**) (64.0 mg, 120 µmol, 1.00 eq.) were mixed with $FeCl_2$ (15.2 mg, 120 µmol, 1.00 eq.). The reagents were dissolved in MeOH (40 mL), DCM (40 mL), and water (200 mL) prior to the addition of NH_4PF_6 (978 mg, 6.00 mmol, 50.0 eq.). The statistical crude product, as expected, contained a mixture of the three complexes **121**, **129** and **193**. To obtain the desired heteroleptic target complex **121** the crude mixture was subjected to purification via preparative reversed-phase HPLC using a solvent gradient ranging from H_2O / MeCN (60:40) to H_2O / MeCN (40:60) at a flow rate of 20 mL/min yielding the desired pure product **121** as a dark purple solid in a yield of 26% (38.7 mg, 31.0 µmol). The two expected homoleptic side products could be

separated successfully from the desired heteroleptic target structure. As they have been synthesized separately otherwise they were not explicitly isolated in this context and thus their analytical data is also discussed at the place where their exclusive synthesis is discussed (namely complexes **129** and **193**). Therefore hereafter, only the analytical data of target compound **121** are discussed.

Analytical data of 121:

^{1}H-NMR (400 MHz, CD_3CN, ppm, 25 °C): δ_H = 9.11 (d, $^{3}J_{H,H}$ = 8.1 Hz, 4H, *H3´/H5´*), 8.83 – 8.74 (m, 6H, *H3 / H3´´ / H4´*), 7.79 (d, $^{3}J_{H,H}$ = 8.5 Hz, 4H, $H_{thioacetylphenyl}$), 7.78 - 7.70 (m, 4H, H_{phenyl}), 7.56 (d, $^{3}J_{H,H}$ = 8.5 Hz, 4H, $H_{thioacetylphenyl}$), 7.57 - 7.49 (m, 4H, H_{phenyl}), 7.39 (dd, $^{3}J_{H,H}$ = 6.0 Hz, $^{4}J_{H,H}$ = 1.9 Hz,2H, *H5* / H5´´**), 7.37 (dd, $^{3}J_{H,H}$ = 6.0 Hz, $^{4}J_{H,H}$ = 2.0 Hz, 2H, *H5* / H5´´**), 7.19 (d, $^{3}J_{H,H}$ = 6.0 Hz, 2H, *H6* / H6´´**), 7.15 (d, $^{3}J_{H,H}$ = 6.0 Hz, 2H, *H6* / H6´´**), 2.41 (s, 6H, $H_{methyl(SAc)}$).
^{13}C-NMR (101 MHz, CD_3CN, ppm, 25 °C): δ_C = 194.29 ($C_{C=O}$, 2C), 161.41 (C_q, 2C), 161.40 (C_q, 2C), 159.45 (C_q, 2C), 159.35 (C_q, 2C), 154.22 (C_t, 2C), 154.10 (C_t, 2C), 151.82 (C_q, 2C), 150.73 (C_q, 2C), 139.15 (C_t, 1C), 139.12 (C_t, 1C), 137.37 (C_q, 2C), 136.37 (C_q, 2C), 136.27 (C_{phenyl}, 4C), 132.20 (C_q, 2C), 131.73 (C_q, 2C), 130.50 (C_{phenyl}, 4C), 129.14 (C_{phenyl}, 4C), 128.41 (C_{phenyl}, 4C), 125.83 (C_t, 2C), 125.76 (C_t, 2C), 125.11 (C_t, 2C), 125.08 (C_t, 2C), 122.75 (C_t, 2C), 122.66 (C_t, 2C), 30.73 ($C_{methyl(SAc)}$, 2C).
^{19}F-NMR (376 MHz, CD_3CN, ppm, 25 °C): δ_F = -72.89 (d, $^{1}J_{P,F}$ = 706.6 Hz, 12F, ***PF_6***).
^{31}P-NMR (162 MHz, CD_3CN, ppm, 25 °C): δ_P = -144.62 (hept, $^{1}J_{P,F}$ = 706.5 Hz, 2P, ***PF_6***).
ESI-MS (MeCN, *positive* ion mode): *m/z* [ion, intensity (%)] = 487.1 (M^{2+}-2PF_6^-, 100).
ESI-MSMS (MeCN, *positive* ion mode (MSMS of *m/z* = 487.1): *m/z* [ion, intensity (%)] = 445.1 (M^{2+}-2((C=O)CH_3), 100), 466.1 (M^{2+}-((C=O)CH_3), 90), 487.1 (M^{2+}, 50).
HRMS (ESI-ToF): *m/z* calcd. for $[C_{58}H_{42}FeN_6O_2S_2]^{2+}$: 487.1075; found: 487.1073.
UV/VIS (MeCN): λ_{max} (ε) = 273 nm (31538 L·cm^{-1}·mol^{-1}), 333 nm (35956 L·cm^{-1}·mol^{-1}), 564 nm (8392 L·cm^{-1}·mol^{-1}), 621 nm (4832 L·cm^{-1}·mol^{-1}).

{[Fe(*172*)$_2$]$^{2+}$[(PF$_6$)$^-$]$_2$} (193)

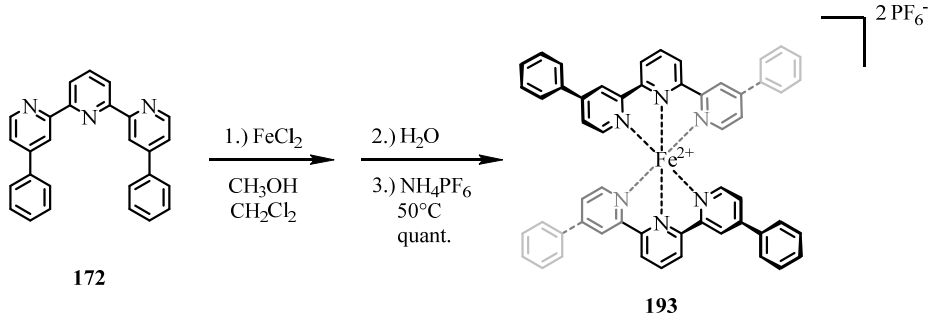

172 **193**

193 was prepared after the representative procedure C. $FeCl_2$ (3.80 mg, 30.0 µmol, 1.00 eq.), 4,4´´-diphenyl-2,2´:6´,2´´-terpyridine (**172**) (23.1 mg, 60.0 µmol, 2.00 eq.), MeOH (10 mL), DCM (10 mL), water (50 mL), and NH_4PF_6 (245 mg, 1.50 mmol, 50.0 eq.) were used. The desired product **193** was isolated as a dark purple solid in quantitative yield (33.5 mg, 30.0 µmol). By applying a solvent diffusion technique using acetonitrile and hexane with an intermediate spacer layer of benzene it was additionally, possible to obtain single crystals of **193** suitable for x-ray structure determination. The crystallographic information of compound **193** are discussed in detailed form in chapter 9.2. Thus hereafter, only the remaining analytical data of target compound **193** are discussed.

Analytical data of 193:

^{1}H-NMR (400 MHz, acetone-d6, ppm, 25 °C): δ_H = 9.52 (d, $^3J_{H,H}$ = 7.8 Hz, 4H, *H3´ / H5´*), 9.18 (s, 4H, *H3 / H3´´*), 8.94 (t, $^3J_{H,H}$ = 7.7 Hz, 2H, *H4´*), 7.86 - 7.80 (m, 8H, H_{phenyl}), 7.60 - 7.48 (m, 20H, *2H5 /2 H5´´ / 2H6 / 2H6´´ / 12*H_{phenyl}).

^{13}C-NMR (101 MHz, acetone-d6, ppm, 25 °C): δ_C = 161.61 (C_q, 4C), 159.65 (C_q, 4C), 154.23 (C_t, 4C), 151.64 (C_q, 4C), 139.26 (C_t, 2C), 136.26 (C_q, 4C), 131.58 (C_q, 4C), 130.37 (C_{phenyl}, 8C), 128.24 (C_{phenyl}, 8C), 125.75 (C_t, 4C), 125.24 (C_t, 4C), 122.40 (C_t, 4C).

^{19}F-NMR (376 MHz, acetone-d6, ppm, 25 °C): δ_F = -72.37 (d, $^1J_{P,F}$ = 707.6 Hz, 12F, ***PF$_6$***).

^{31}P-NMR (162 MHz, acetone-d6, ppm, 25 °C): δ_P = -144.21 (hept, $^1J_{P,F}$ = 708.0 Hz, 2P, ***P**F$_6$*).

ESI-MS (MeCN, *positive* ion mode): *m/z* [ion, intensity (%)] = 413.2 (M^{2+}-2PF_6^-, 100).

HRMS (ESI-ToF): *m/z* calcd. for $[C_{58}H_{42}FeN_6O_2S_2]^{2+}$: 413.1249; found: 413.1254

UV/VIS (MeCN): λ_{max} (ε) = 273 nm (69165 L·cm^{-1}·mol^{-1}), 332 nm (83255 L·cm^{-1}·mol^{-1}), 376 nm (13835 L·cm^{-1}·mol^{-1}), 563 nm (15240 L·cm^{-1}·mol^{-1}), 623 nm (5560 L·cm^{-1}·mol^{-1}).

{[Fe(*185*)(*131*)]$^{2+}$[(PF$_6$)$^-$]$_2$} (113)

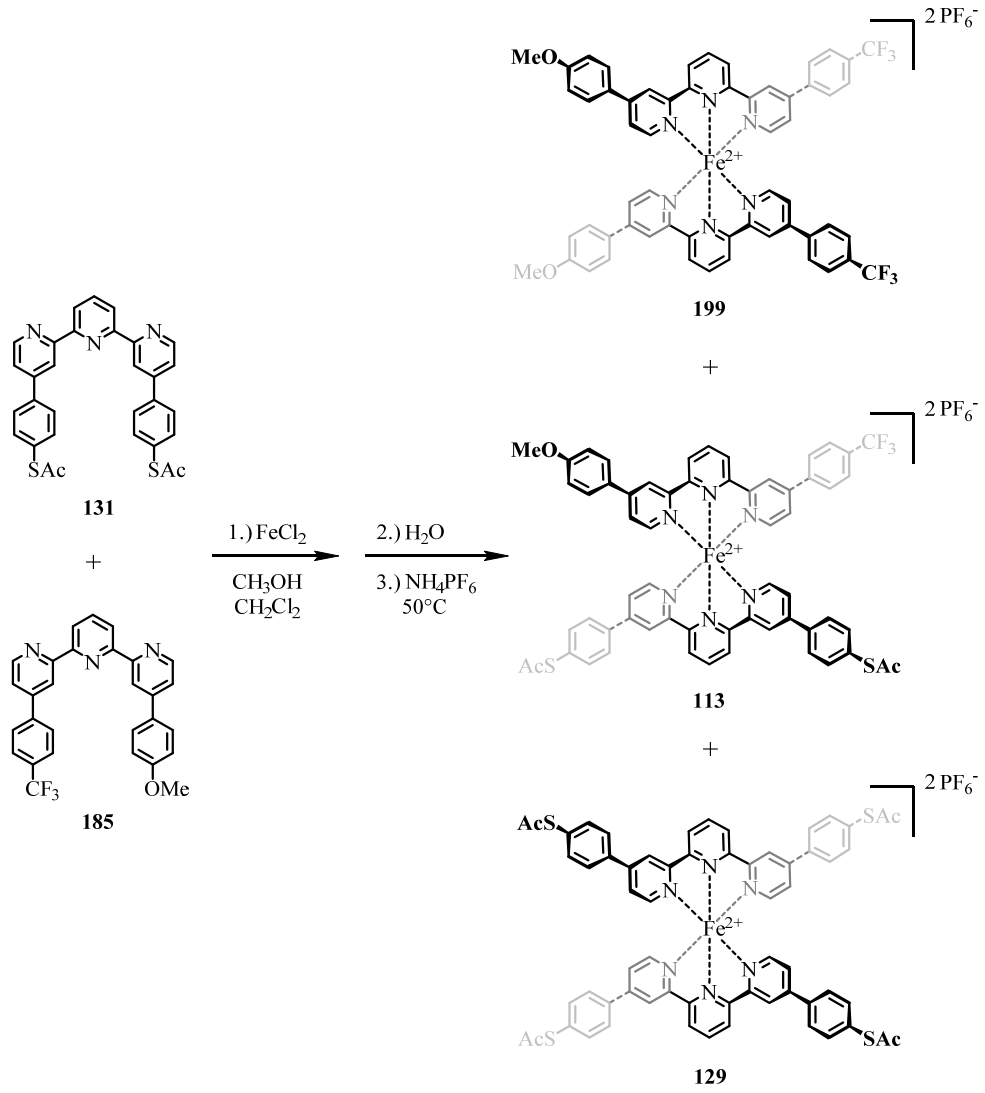

113 was prepared by a modification of the representative procedure C. In this case a statistic reaction had to be performed in which an equimolar amount of the terpyridine precursors was used. Therefore *S,S′*-([2,2′:6′,2′′-terpyridine]-4,4′′-diylbis(4,1-phenylene)) diethanethioate (**131**) (40.6 mg, 76.0 µmol, 1.00 eq.) 4-(4-methoxyphenyl)-4′′-(4-(trifluoromethyl)-phenyl)-2,2′:6′,2′′-terpyridine (**185**) (36.7 mg, 76.0 µmol, 1.00 eq.) were mixed with $FeCl_2$ (9.63 mg, 76.0 µmol, 1.00 eq.). The reagents were dissolved in MeOH (40 mL), DCM (40 mL), and water (200 mL), whereas NH_4PF_6 (619 mg, 3.80 mmol, 50.0 eq.) was used for the final anion exchange. The crude product, as expected, was isolated as a statistical mixture of the three complexes **113**, **129** and **199**. To obtain the desired heteroleptic target complex **113** the crude mixture was subjected to purification via preparative reversed-phase HPLC using a solvent gradient ranging from H_2O / MeCN (50:50) up to H_2O / MeCN (5:95) at a flow rate of 20 mL/min yielding the desired pure product **113** as a dark purple solid in a

yield of 15% (15.6 mg, 11.0 µmol). The two expected homoleptic side products could be separated successfully from the desired heteroleptic target structure. As complex **129** has been synthesized separately otherwise it is not explicitly isolated in this context and thus its analytical data is also discussed at the place where its exclusive synthesis is discussed. Since compound **199** was however not synthesized separately it was isolated in this experiment in a yield of 6% (5.50 mg, 4.00 µmol). Therefore hereafter, only the analytical data of target compound **113** and the ones from compound **199** are reported.

Analytical data of 113:

^{1}H-NMR (500 MHz, CD_3CN, ppm, 25 °C): δ_H = 9.10 (dd, $^{3}J_{H,H}$ = 8.2 Hz, $^{4}J_{H,H}$ = 1.0 Hz, 4H, *H3´ / H5´*), 8.82 – 8.74 (m, 6H, *H3 / H3´´ / H4´*), 7.90 (d, $^{3}J_{H,H}$ = 8.3 Hz, 2H, $H_{phenyl(push)}$), 7.83 (d, $^{3}J_{H,H}$ = 8.4 Hz, 2H, $H_{phenyl(push)}$), 7.78 (d, $^{3}J_{H,H}$ = 8.6 Hz, 4H, $H_{phenyl(sym)}$), 7.74 (d, $^{3}J_{H,H}$ = 9.0 Hz, 2H, $H_{phenyl(pull)}$), 7.56 (d, $^{3}J_{H,H}$ = 8.6 Hz, 4H, $H_{phenyl(sym)}$), 7.39 (app. ddd, $^{3}J_{H,H}$ = 6.1 Hz, $^{3}J_{H,H}$ = 4.6 Hz, $^{4}J_{H,H}$ = 2.0 Hz, 3H, $H5_{(sym)}$ / $H5_{(sym)}$´´ / $H5_{(asym)}$ * *or* $H5_{(asym)}$ ´´*), 7.33 (dd, $^{3}J_{H,H}$ = 6.1 Hz, $^{4}J_{H,H}$ = 2.0 Hz, 1H, $H5_{(asym)}$* / $H5_{(asym)}$´´*), 7.21 (d, $^{3}J_{H,H}$ = 6.0 Hz, 1H, $H6_{(asym)}$* / $H6_{(asym)}$´´*), 7.17 (d, $^{3}J_{H,H}$ = 6.0 Hz, 2H, $H6_{(sym)}$ / $H6_{(sym)}$´´), 7.08 (d, $^{3}J_{H,H}$ = 6.1 Hz, 1H, $H6_{(asym)}$* / $H6_{(asym)}$´´*), 7.08 (d, $^{3}J_{H,H}$ = 9.0 Hz, 2H, $H_{phenyl(pull)}$), 3.83 (s, 3H, $H_{methoxy}$), 2.41 (s, 6H, $H_{methyl(SAc)}$).

^{13}C-NMR (126 MHz, CD_3CN, ppm, 25 °C): δ_C = 194.28 ($C_{C=O}$, 2C), 163.02 (C_q, 1C), 161.51 (C_q, 1C), 161.36 (C_q, 2C), 161.18 (C_q, 1C), 159.63 (C_q, 1C), 159.42 (C_q, 2C), 159.05 (C_q, 1C), 154.43 (C_t, 1C), 154.20 (C_t, 2C), 153.76 (C_t, 1C), 151.31 (C_q, 1C), 150.72 (C_q, 2C), 150.12 (C_q, 1C), 140.35 (C_q, 1C), 139.15 (C_t, 1C), 139.13 (C_t, 1C), 137.34 (C_q, 2C), 136.26 ($C_{phenyl(sym)}$, 4C), 132.18 (C_q, 2C), 129.89 ($C_{phenyl(asym)}$, 2C), 129.29 ($C_{phenyl(asym)}$, 2C), 129.13 ($C_{phenyl(sym)}$, 4C), 128.17 (C_q, 1C), 127.25 (q, ^{3}J = 3.5 Hz, 2C, $C_{phenyl(asym)}$), 125.97 (C_t, 1C), 125.80 (C_t, 2C), 125.12 (C_t, 1C), 125.10 (C_t, 2C), 125.05 (C_t, 1C), 124.94 (C_t, 1C), 122.90 (C_t, 1C), 122.75 (C_t, 2C), 121.90 (C_t, 1C), 115.85 ($C_{phenyl(asym)}$, 2C), 56.34 ($C_{methoxy}$, 2C). 30.72 ($C_{methyl(SAc)}$, 2C). In the ^{13}C-spectrum two signals less than expected were found probably due to coincident signals and due to the fact that the CF_3-group cannot be seen properly.

^{19}F-NMR (376 MHz, CD_3CN, ppm, 25 °C): δ_F = -63.36 (s, 3F, CF_3), -72.85 (d, $^{1}J_{P,F}$ = 706.3 Hz, 12F, PF_6).

^{31}P-NMR (162 MHz, CD_3CN, ppm, 25 °C): δ_P = -144.62 (hept, $^{1}J_{P,F}$ = 705.7 Hz, 2P, PF_6).

ESI-MS (MeCN, *positive* ion mode): *m/z* [ion, intensity (%)] = 536.2 (M^{2+}-2PF_6^-, 100).

ESI-MSMS (MeCN, *positive* ion mode (MSMS of *m/z* = 536.2): *m/z* [ion, intensity (%)] = 494.1 (M^{2+}-2((C=O)CH_3), 100), 515.1 (M^{2+}-((C=O)CH_3), 50), 536.2 (M^{2+}, 5).
HRMS (ESI-ToF): *m/z* calcd. for $[C_{60}H_{43}F_3FeN_6O_3S_2]^{2+}$: 536.1065; found: 536.1066.
UV/VIS (MeCN): λ_{max} (ε) = 274 nm (58960 L·cm^{-1}·mol^{-1}), 336 nm (70255) L·cm^{-1}·mol^{-1}), 566 nm (11525) L·cm^{-1}·mol^{-1}), 627 nm (4845 L·cm^{-1}·mol^{-1}).

Analytical data of 199:

^{1}H-NMR (400 MHz, CD_3CN, ppm, 25 °C): δ_H = 9.10 (d, $^{3}J_{H,H}$ = 8.3 Hz, 4H, *H3´ / H5´*), 8.80 (d, $^{4}J_{H,H}$ = 1.6 Hz, 2H, *H3* / H3´´**), 8.77 (t, $^{3}J_{H,H}$ = 8.0 Hz, 2H, *H4´*), 8.74 (s, 2H, *H3* / H3´´**), 7.89 (d, $^{3}J_{H,H}$ = 8.4 Hz, 4H, $H_{phenyl(push)}$), 7.83 (d, $^{3}J_{H,H}$ = 8.4 Hz, 4H, $H_{phenyl(push)}$), 7.73 (d, $^{3}J_{H,H}$ = 9.0 Hz, 4H, $H_{phenyl(pull)}$), 7.38 (dd, $^{3}J_{H,H}$ = 6.0 Hz, $^{4}J_{H,H}$ = 2.0 Hz, 2H, *H5* / H5´´**), 7.33 (dd, $^{3}J_{H,H}$ = 6.1 Hz, $^{4}J_{H,H}$ = 2.0 Hz, 2H, *H5* / H5´´**), 7.20 (d, $^{3}J_{H,H}$ = 6.0 Hz, 2H, *H6* / H6´´**), 7.09 – 7.02 (m, 2H, *H6* / H6´´**), 7.05 (d, $^{3}J_{H,H}$ = 8.8 Hz, 4H, $H_{phenyl(pull)}$), 3.83 (s, 6H, $H_{methoxy}$).
^{13}C-NMR (101 MHz, CD_3CN, ppm, 25 °C): δ_C = 162.97 (C_q, 2C), 161.49 (C_q, 2C), 161.16 (C_q, 2C), 159.57 (C_q, 2C), 158.99 (C_q, 2C), 154.33 (C_t, 2C), 153.66 (C_t, 2C), 151.24 (C_q, 2C), 150.03 (C_q, 2C), 140.29 (C_q, 2C), 139.01 (C_t, 2C), 136.20 (C_t, 2C), 129.83 (C_{phenyl}, 4C), 129.22 (C_{phenyl}, 4C), 128.14 (C_q, 2C), 127.19 (q, ^{3}J = 3.8 Hz, 2C, $C_{phenyl(asym)}$), 125.90 (C_t, 2C), 125.01 (C_t, 2C), 124.93 (C_t, 2C), 124.88 (C_t, 2C), 122.80 (C_t, 2C), 121.81 (C_t, 2C), 115.79 (C_{phenyl}, 4C), 56.28 ($C_{methoxy}$, 2C). In the ^{13}C-spectrum one signal less than expected was found probably due to the fact that the CF_3-group cannot be seen properly.
^{19}F-NMR (376 MHz, CD_3CN, ppm, 25 °C): δ_F = -63.36 (s, 6F, ***CF$_3$***), -72.89 (d, $^{1}J_{P,F}$ = 706.7 Hz, 12F, ***PF$_6$***).
^{31}P-NMR (162 MHz, CD_3CN, ppm, 25 °C): δ_P = -144.62 (hept, $^{1}J_{P,F}$ = 705.1 Hz, 2P, ***P**F$_6$*).
ESI-MS (MeCN, *positive* ion mode): *m/z* [ion, intensity (%)] = 511.2 (M^{2+}-2PF_6^-, 100).
HRMS (ESI-ToF): *m/z* calcd. for $[C_{58}H_{40}F_6FeN_6O_2]^{2+}$: 511.1228; found: 511.1239.
UV/VIS (MeCN): λ_{max} (ε) = 271 nm (47740 L·cm^{-1}·mol^{-1}), 335 nm (51845 L·cm^{-1}·mol^{-1}), 566 nm (9745 L·cm^{-1}·mol^{-1}), 627 nm (4110 L·cm^{-1}·mol^{-1}).

{[Fe(*186*)(*131*)]$^{2+}$[(PF$_6$)$^-$]$_2$} (115)

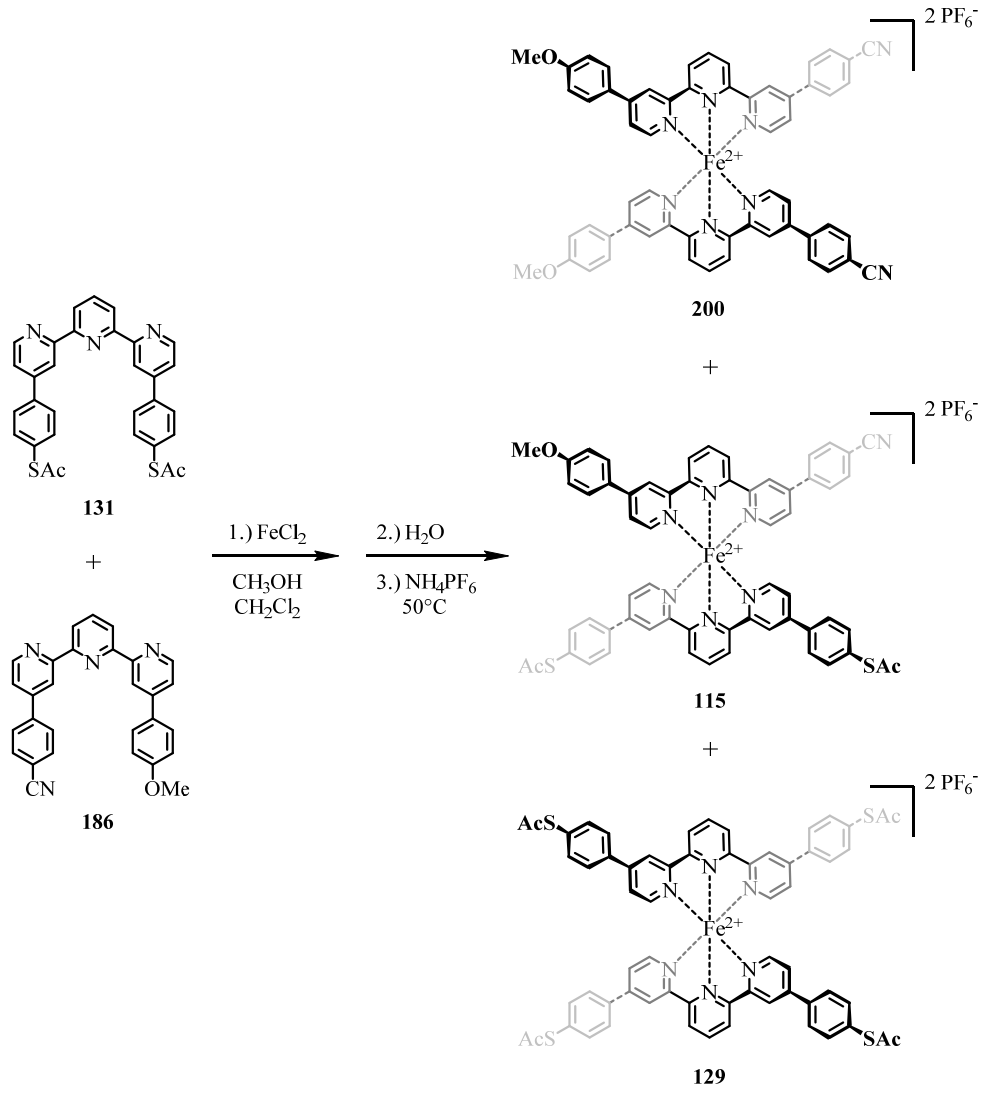

115 was prepared by a modification of the representative procedure C. In this case a statistic reaction had to be performed in which equimolar amounts of the terpyridine precursors were used. Thus 4-(4′′-(4-methoxyphenyl)-[2,2′:6′,2′′-terpyridin]-4-yl)benzonitrile (**186**) (30.8 mg, 70.0 µmol, 1.00 eq.), *S,S′*-([2,2′:6′,2′′-terpyridine]-4,4′′-diylbis(4,1-phenylene)) diethanethioate (**131**) (37.4 mg, 70.0 µmol, 1.00 eq.) and the asymmetric dipolar ligand were mixed with $FeCl_2$ (8.87 mg, 70.0 µmol, 1.00 eq.). The reagents were dissolved in MeOH (40 mL), DCM (40 mL), and water (200 mL), before NH_4PF_6 (571 mg, 3.50 mmol, 50.0 eq.) was added. The statistical crude, as expected, turned out to contain the product complexes **115**, **129** and **200**. In order to obtain the desired heteroleptic target complex **115** the crude mixture was subjected to purification via preparative reversed-phase HPLC using a solvent gradient ranging from H_2O / MeCN (60:40) up to H_2O / MeCN (40:60) at a flow rate of 20 mL/min yielding the desired pure product **115** as a dark purple solid in a yield of 13%

(12.0 mg, 9.00 µmol). The two expected homoleptic side products could be separated successfully from the desired heteroleptic target structure. Since complex **129** has been synthesized separately otherwise it is not explicitly isolated in this context and thus its analytical data is also shown at the place where its exclusive synthesis is discussed. Since compound **200** was however not synthesized separately, it was isolated in this experiment in a yield of 5% (4.00 mg, 3.00 µmol). Therefore hereafter, the analytical data of target compound **115** and the ones from compound **200** are reported.

Analytical data of 115:

^{1}H-NMR (500 MHz, CD_3CN, ppm, 25 °C): δ_H = 9.10 (d, $^3J_{H,H}$ = 8.1 Hz, 2H, *H3´* / H5´**), 9.10 (d, $^3J_{H,H}$ = 8.1 Hz, 2H, *H3´* / H5´**), 8.82 – 8.73 (m, 6H, *H3 / H3´´ / H4´*), 7.87 (app. d, $^3J_{H,H}$ = 0.6 Hz, 4H, $H_{phenyl(sym)}$), 7.79 (app. d, $^3J_{H,H}$ = 2.7 Hz, 2H, $H_{phenyl(push)}$), 7.77 (app. d, $^3J_{H,H}$ = 2.7 Hz, 2H, $H_{phenyl(push)}$), 7.74 (d, $^3J_{H,H}$ = 9.0 Hz, 2H, $H_{phenyl(pull)}$), 7.56 (app. dd, $^3J_{H,H}$ = 8.6 Hz, $^4J_{H,H}$ =1.2 Hz 4H, $H_{phenyl(sym)}$), 7.38 (app. dd, $^3J_{H,H}$ = 6.0 Hz, $^4J_{H,H}$ = 2.0 Hz, 3H, *H5(sym) / H5(sym)´´ / H5(asym) * or H5(asym) ´´**), 7.33 (dd, $^3J_{H,H}$ = 6.1 Hz, $^4J_{H,H}$ = 2.0 Hz, 1H, *H5(asym)* / H5(asym)´´**), 7.22 – 7.18 (m, 1H, *H6(asym)* / H6(asym)´´**), 7.16 (d, $^3J_{H,H}$ = 6.1 Hz, 2H, *H6(sym) / H6(sym)´*), 7.07 (d, $^3J_{H,H}$ = 6.4 Hz, 1H, *H6(asym)* / H6(asym)´´**), 7.05 (d, $^3J_{H,H}$ = 9.0 Hz, 2H, $H_{phenyl(pull)}$), 3.83 (s, 3H, $H_{methoxy}$), 2.41 (s, 6H, $H_{methyl(SAc)}$).

^{13}C-NMR (126 MHz, CD_3CN, ppm, 25 °C): δ_C = 194.20 ($C_{C=O}$, 2C), 162.95 (C_q, 1C), 161.45 (C_q, 1C), 161.27 (C_q, 2C), 161.07 (C_q, 1C), 159.63 (C_q, 1C), 159.33 (C_q, 2C), 158.96 (C_q, 1C), 154.43 (C_t, 1C), 154.13 (C_t, 2C), 153.67 (C_t, 1C), 151.26 (C_q, 1C), 150.66 (C_q, 2C), 149.67 (C_q, 1C), 140.68 (C_q, 1C), 139.08 (C_t, 2C, but 2 separate signals in DEPT-135 spectrum), 137.25 (C_q, 2C), 136.19 ($C_{phenyl(sym)}$, 4C), 134.13 ($C_{phenyl(asym)}$, 2C), 132.12 (C_q, 2C), 129.82 ($C_{phenyl(asym)}$, 2C), 129.22 ($C_{phenyl(asym)}$, 2C), 129.06 ($C_{phenyl(sym)}$, 4C), 128.09 (C_q, 1C), 125.80 (C_t, 1C), 125.73 (C_t, 2C), 125.06 (C_t, 1C), 125.04 (C_t, 2C), 124.99 (C_t, 1C), 124.88 (C_t, 1C), 122.75 (C_q, 1C), 122.71 (C_t, 1C), 122.68 (C_t, 2C), 121.84 (C_t, 1C), 115.78 ($C_{phenyl(asym)}$, 2C), 114.65 ($C_{(CN)}$, 1C), 56.27 ($C_{methoxy}$, 2C), 30.65 ($C_{methyl(SAc)}$, 2C).

ESI-MS (MeCN, *positive* ion mode): *m/z* [ion, intensity (%)] = 514.7 (M^{2+}-2PF_6^-, 100).

HRMS (ESI-ToF): *m/z* calcd. for $[C_{60}H_{43}FeN_7O_3S_2]^{2+}$: 514.6104; found: 514.6106.

UV/VIS (MeCN): λ_{max} (ε) = 281 nm (73400 L·cm^{-1}·mol^{-1}), 336 nm (81770 L·cm^{-1}·mol^{-1}), 566 nm (13615 L·cm^{-1}·mol^{-1}), 626 nm (6030 L·cm^{-1}·mol^{-1}).

Analytical data of 200:

^{1}H-NMR (400 MHz, CD_3CN, ppm, 25 °C): δ_H = 9.09 (d, $^{3}J_{H,H}$ = 8.1 Hz, 2H, *H3´* / H5´**), 9.08 (d, $^{3}J_{H,H}$ = 7.5 Hz, 2H, *H3´* / H5´**), 8.83 – 8.73 (m, 6H, *H3 / H3´´ / H4´*), 7.87 (app. d, $^{3}J_{H,H}$ = 1.7 Hz, 8H, $H_{phenyl(push)}$), 7.73 (d, $^{3}J_{H,H}$ = 9.0 Hz, 4H, $H_{phenyl(pull)}$), 7.36 (dd, $^{3}J_{H,H}$ = 6.0 Hz, $^{4}J_{H,H}$ = 2.0 Hz, 2H, *H5* / H5´´**), 7.32 (dd, $^{3}J_{H,H}$ = 6.1 Hz, $^{4}J_{H,H}$ = 2.0 Hz, 2H, *H5* / H5´´**), 7.19 (d, $^{3}J_{H,H}$ = 6.0 Hz, 2H, *H6 / H6´´*), 7.06 (d, $^{3}J_{H,H}$ = 6.0 Hz, 2H, *H6 / H6´´*), 7.05 (d, $^{3}J_{H,H}$ = 9.0 Hz, 4H, $H_{phenyl(pull)}$), 3.83 (s, 6H, $H_{methoxy}$).

^{13}C-NMR (101 MHz, CD_3CN, ppm, 25 °C): δ_C = 162.98 (C_q, 2C), 161.45 (C_q, 2C), 161.10 (C_q, 2C), 159.63 (C_q, 2C), 158.95 (C_q, 2C), 154.40 (C_t, 2C), 153.65 (C_t, 2C), 151.27 (C_q, 2C), 149.67 (C_q, 2C), 140.70 (C_q, 2C), 139.05 (C_t, 2C), 136.20 (C_q, 2C), 134.14 (C_{phenyl}, 4C), 129.82 (C_{phenyl}, 4C), 129.22 (C_{phenyl}, 4C), 125.81 (C_t, 2C), 125.04 (C_t, 2C), 124.96 (C_t, 2C), 124.89 (C_t, 2C), 122.73 (C_q, 2C), 121.83 (C_t, 1C), 115.80 (C_{phenyl}, 4C), 114.67 ($C_{(CN)}$, 2C), 56.29 ($C_{methoxy}$, 2C).

^{19}F-NMR (376 MHz, CD_3CN, ppm, 25 °C): δ_F = -72.90 (d, $^{1}J_{P,F}$ = 706.6 Hz, 12F, PF_6).

^{31}P-NMR (162 MHz, CD_3CN, ppm, 25 °C): δ_P = -144.63 (hept, $^{1}J_{P,F}$ = 705.8 Hz, 2P, PF_6).

ESI-MS (MeCN, *positive* ion mode): *m/z* [ion, intensity (%)] = 468.1 (M^{2+}-2PF_6^-, 100).

HRMS (ESI-ToF): *m/z* calcd. for $[C_{58}H_{40}FeN_8O_2]^{2+}$: 468.1307; found: 468.1315.

UV/VIS (MeCN): λ_{max} (ε) = 275 nm (58125 L·cm^{-1}·mol^{-1}), 336 nm (55680 L·cm^{-1}·mol^{-1}), 566 nm (10010 L·cm^{-1}·mol^{-1}), 625 nm (4285 L·cm^{-1}·mol^{-1}).

{[Fe(*178*)(*131*)]$^{2+}$[(PF$_6$)$^-$]$_2$} (123)

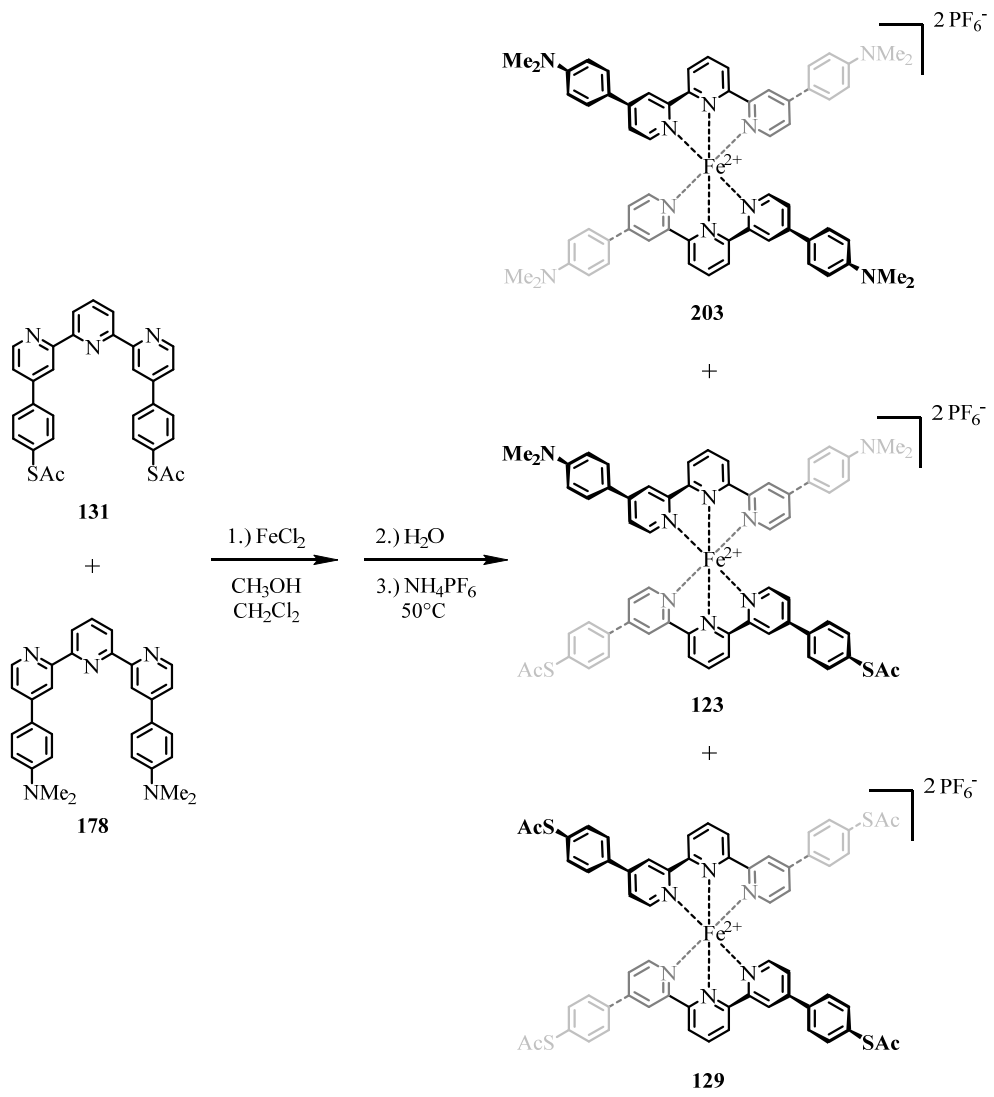

123 was prepared by a modification of the representative procedure C. In this case a statistic reaction had to be performed in which an equimolar amount of the terpyridine precursors was used. The thiolated ligand *S,S´*-([2,2´:6´,2´´-terpyridine]-4,4´´-diylbis(4,1-phenylene)) diethanethioate (**131**) (53.4 mg, 100 µmol, 1.00 eq.) and 4,4´-([2,2´:6´,2´´-terpyridine]-4,4´´-diyl)bis(*N,N*-dimethylaniline) (**178**) (47.2 mg, 100 µmol, 1.00 eq.) were mixed with $FeCl_2$ (12.7 mg, 100 µmol, 1.00 eq.). The reagents were suspended in MeOH (30 mL), DCM (60 mL), and water (200 mL) and for the final anion exchange NH_4PF_6 (815 mg, 5.00 mmol, 50.0 eq.) was used. The crude product contained the expectable statistical mixture of the three complexes **123**, **129** and **203**. To obtain the heteroleptic target complex **123** the crude mixture was subjected to purification via preparative reversed-phase HPLC using a solvent gradient ranging from H_2O / MeCN (60:40) up to H_2O / MeCN (40:60) at a flow rate of 20 mL/min yielding the product **123** as a dark purple solid in a yield of 6% (6.50 mg,

5.00 µmol). The two expected homoleptic side products could be separated successfully from the desired heteroleptic target structure. Thus hereafter, only the analytical data of target compound **123** are discussed.

Analytical data of 123:

^{1}H-NMR (400 MHz, CD_3CN, ppm, 25 °C): δ_H = 9.14 – 9.00 (m, 4H, *H3´ / H5´*), 8.82 - 8.64 (m, 6H, *H3 / H3´´ / H4´*), 7.78 (app. dd, $^3J_{H,H}$ = 8.6 Hz, $J_{H,H}$ = 2.2 Hz, 4H, $H_{thioacetylphenyl}$), 7.67 (app. dd, $^3J_{H,H}$ = 9.1 Hz, $J_{H,H}$ = 3.9Hz, 4H, $H_{dimethylaminophenyl}$), 7.56 (app. dd, $^3J_{H,H}$ = 8.6 Hz, $J_{H,H}$ = 2.7 Hz, 4H, $H_{thioacetylphenyl}$), 7.38 (app. td, $^3J_{H,H}$ = 6.2 Hz, $^4J_{H,H}$ = 2.0 Hz, 2H, $H5_{thioacetylphenyl}$ / $H5_{thioacetylphenyl´´}$), 7.26 (app. td, $^3J_{H,H}$ = 5.8 Hz, $^4J_{H,H}$ = 2.1 Hz, 2H, $H5_{dimethylaminophenyl}$ / $H5_{dimethylaminophenyl´´}$), 7.17 (app. t, $^3J_{H,H}$ = 5.6 Hz, 2H, $H6_{thioacetylphenyl}$ / $H6_{thioacetylphenyl´´}$), 6.93 (dd, $^3J_{H,H}$ = 6.1 Hz, $^4J_{H,H}$ = 3.1 Hz 2H, $H6_{dimethylaminophenyl}$ / $H6_{dimethylaminophenyl´´}$), 6.78 (dd, $^3J_{H,H}$ = 9.1 Hz, 4H, $H_{dimethylaminophenyl}$), 3.00 (s, 12H, $H_{methyl(NMe2)}$), 2.41 (s, 6H, $H_{methyl(SAc)}$). Due to bad solubility no proper 13C-spectrum was recorded.

ESI-MS (MeCN, *positive* ion mode): *m/z* [ion, intensity (%)] = 530.3 (M^{2+}-2PF_6^-, 100).

ESI-MSMS (MeCN, *positive* ion mode (MSMS of *m/z* = 530.3): *m/z* [ion, intensity (%)] = 488.2 (M^{2+}-2((C=O)CH_3), 100), 509.2 (M^{2+}-((C=O)CH_3), 60), 530.3 (M^{2+}, 60).

HRMS (ESI-ToF): *m/z* calcd. for $[C_{62}H_{52}FeN_8O_2S_2]^{2+}$: 530.1497; found: 530.1501.

UV/VIS (MeCN): λ_{max} (ε) = 272 nm (58125 L·cm^{-1}·mol^{-1}), 335 nm (71385 L·cm^{-1}·mol^{-1}), 389 nm (27810 L·cm^{-1}·mol^{-1}), 567 nm (14470 L·cm^{-1}·mol^{-1}), 625 nm (7095 L·cm^{-1}·mol^{-1}).

{[Fe(*184*)(*131*)]$^{2+}$[(PF$_6$)$^-$]$_2$} (116)

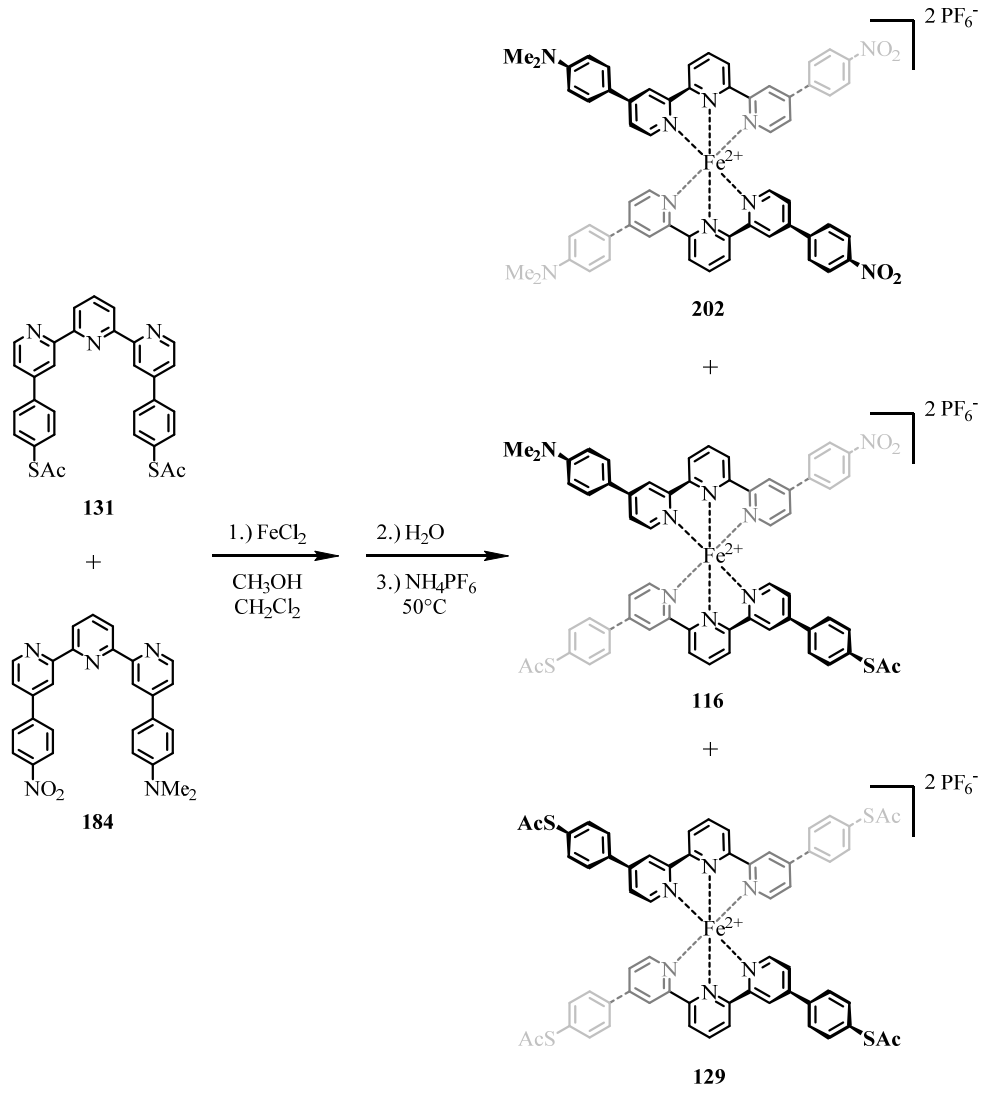

116 was prepared by a modification of the representative procedure C. In this case a statistic reaction had to be performed in which an equimolar amount of the terpyridine precursors was used. For the reaction *N,N*-dimethyl-4-(4′′-(4-nitrophenyl)-[2,2′:6′,2′′-terpyridin]-4-yl)-aniline (**184**) (47.4 mg, 100 µmol, 1.00 eq.) and *S,S′*-([2,2′:6′,2′′-terpyridine]-4,4′′-diylbis(4,1-phenylene)) diethanethioate (**131**) (53.4 mg, 100 µmol, 1.00 eq.) were mixed with $FeCl_2$ (12.7 mg, 100 µmol, 1.00 eq.). The reagents were dissolved in MeOH (40 mL), DCM (40 mL) and water (200 mL) and NH_4PF_6 (815 mg, 5.00 mmol, 50.0 eq.) was used for the final anion exchange. The crude product turned out to be the expected statistical mixture of the three complexes **116**, **129** and **202**. To obtain the desired heteroleptic target complex **116** the crude mixture was subjected to purification via preparative reversed-phase HPLC using a solvent gradient ranging from H_2O / MeCN (55:45) up to H_2O / MeCN (40:60) at a flow rate of 20 mL/min yielding the desired pure product **116** as a dark purple-reddish solid in

a yield of 18% (23.8 mg, 10.0 µmol). The two expected homoleptic side products could be separated successfully from the desired heteroleptic target structure. Hereafter, the complete analytical data of target compound **116** is discussed. However of the side product **202** only the ESI-MS and the HR-ESI-MS data have been collected.

Analytical data of 116:

^{1}H-NMR (400 MHz, CD_3CN, ppm, 25 °C): δ_H = 9.10 (d, $^{3}J_{H,H}$ = 8.1 Hz, 4H, *H3´ / H5´*), 8.83 - 8.69 (m, 6H, *H3 / H3´´ / H4´*), 8.32 (d, $^{3}J_{H,H}$ = 9.0 Hz, 2H, $H_{phenyl(push)}$), 7.92 (d, $^{3}J_{H,H}$ = 9.0 Hz, 2H, $H_{phenyl(push)}$), 7.78 (d, $^{3}J_{H,H}$ = 8.6 Hz, 4H, $H_{phenyl(sym)}$), 7.69 (d, $^{3}J_{H,H}$ = 9.1 Hz, 2H, $H_{phenyl(pull)}$), 7.56 (d, $^{3}J_{H,H}$ = 8.6 Hz, 4H, $H_{phenyl(sym)}$), 7.40 (dd, $^{3}J_{H,H}$ = 5.7 Hz, $^{4}J_{H,H}$ = 2.0 Hz, 1H, $H5_{(asym)}$*/ $H5_{(asym)}$´´*), 7.38 (dd, $^{3}J_{H,H}$ = 5.9 Hz, $^{4}J_{H,H}$ = 2.0 Hz, 2H, $H5_{(sym)}$ / $H5_{(sym)}$´´), 7.29 (dd, $^{3}J_{H,H}$ = 6.1 Hz, $^{4}J_{H,H}$ = 2.1 Hz, 1H, $H5_{(asym)}$*/ $H5_{(asym)}$´´*), 7.23 (d, $^{3}J_{H,H}$ = 6.0 Hz, 1H, $H6_{(asym)}$*/ $H6_{(asym)}$´´*), 7.17 (d, $^{3}J_{H,H}$ = 6.0 Hz, 2H, $H6_{(sym)}$ / $H6_{(sym)}$´´), 6.96 (d, $^{3}J_{H,H}$ = 6.1 Hz, 1H, $H6_{(asym)}$*/ $H6_{(asym)}$´´*), 6.79 (d, $^{3}J_{H,H}$ = 9.1 Hz, 2H, $H_{phenyl(pull)}$), 3.00 (s, 6H, $H_{methyl(NMe2)}$), 2.41 (s, 6H, $H_{methyl(SAc)}$).

^{13}C-NMR (101 MHz, CD_3CN, ppm, 25 °C): δ_C = 194.21 ($C_{C=O}$, 2C), 161.65 (C_q, 1C), 161.32 (C_q, 2C), 160.97 (C_q, 1C), 159.77 (C_q, 2C), 159.36 (C_q, 2C), 158.59 (C_q, 1C), 154.50 (C_t, 1C), 154.09 (C_t, 2C), 153.42 (C_q, 1C), 153.14 (C_q, 1C), 151.54 (C_q, 1C), 150.63 (C_q, 2C), 150.04 (C_q, 1C), 149.20 (C_q, 1C), 142.57 (C_q, 1C), 139.05 (C_t, 1C), 138.97 (C_t, 1C), 137.30 (C_q, 2C), 136.20 (C_{phenyl}, 4C), 132.13 (C_q, 2C), 129.74 (C_{phenyl}, 2C), 129.15 (C_{phenyl}, 2C), 129.06 (C_{phenyl}, 4C), 125.91 (C_t, 1C), 125.74 (C_t, 2C), 125.32 (C_{phenyl}, 2C), 125.00 (C_t, 2C), 124.82 (C_t, 1C), 123.60 (C_t, 1C), 122.87 (C_t, 1C), 122.65 (C_t, 2C), 121.82 (C_q, 1C), 120.71 (C_t, 1C), 113.15 (C_{phenyl}, 2C), 40.29 ($C_{methyl(NMe2)}$, 2C). 30.66 ($C_{methyl(SAc)}$, 2C). In the ^{13}C-spectrum one signal less than expected was found probably due to coincident signals.

^{19}F-NMR (376 MHz, CD_3CN, ppm, 25 °C): δ_F = -72.83 (d, $^{1}J_{P,F}$ = 706.7 Hz, 12F, PF_6).

^{31}P-NMR (162 MHz, CD_3CN, ppm, 25 °C): δ_P = -144.61 (hept, $^{1}J_{P,F}$ = 706.6 Hz, 2P, PF_6).

ESI-MS (MeCN, *positive* ion mode): *m/z* [ion, intensity (%)] = 531.2 (M^{2+}-2PF_6^-, 100).

ESI-MSMS (MeCN, *positive* ion mode (MSMS of *m/z* = 531.2): *m/z* [ion, intensity (%)] = 489.2 (M^{2+}-2((C=O)CH_3), 75), 510.2 (M^{2+}-((C=O)CH_3), 75), 531.2 (M^{2+}, 100).

HRMS (ESI-ToF): *m/z* calcd. for $[C_{60}H_{46}FeN_8O_4S_2]^{2+}$: 531.1212; found: 531.1219.

UV/VIS (MeCN): λ_{max} (ε) = 283 nm (64465 $L \cdot cm^{-1} \cdot mol^{-1}$), 335 nm (76100 $L \cdot cm^{-1} \cdot mol^{-1}$), 389 nm (25825 $L \cdot cm^{-1} \cdot mol^{-1}$), 569 nm (14290 $L \cdot cm^{-1} \cdot mol^{-1}$), 625 nm (6910 $L \cdot cm^{-1} \cdot mol^{-1}$).

Analytical data of 202:

ESI-MS (MeCN, *positive* ion mode): *m/z* [ion, intensity (%)] = 501.2 (M^{2+}-2PF_6^-, 100).
HRMS (ESI-ToF): *m/z* calcd. for $[C_{58}H_{46}FeN_{10}O_4]^{2+}$: 501.1522; found: 501.1526.

{[Fe(*176*)(*131*)]$^{2+}$[(PF$_6$)$^-$]$_2$} (126)

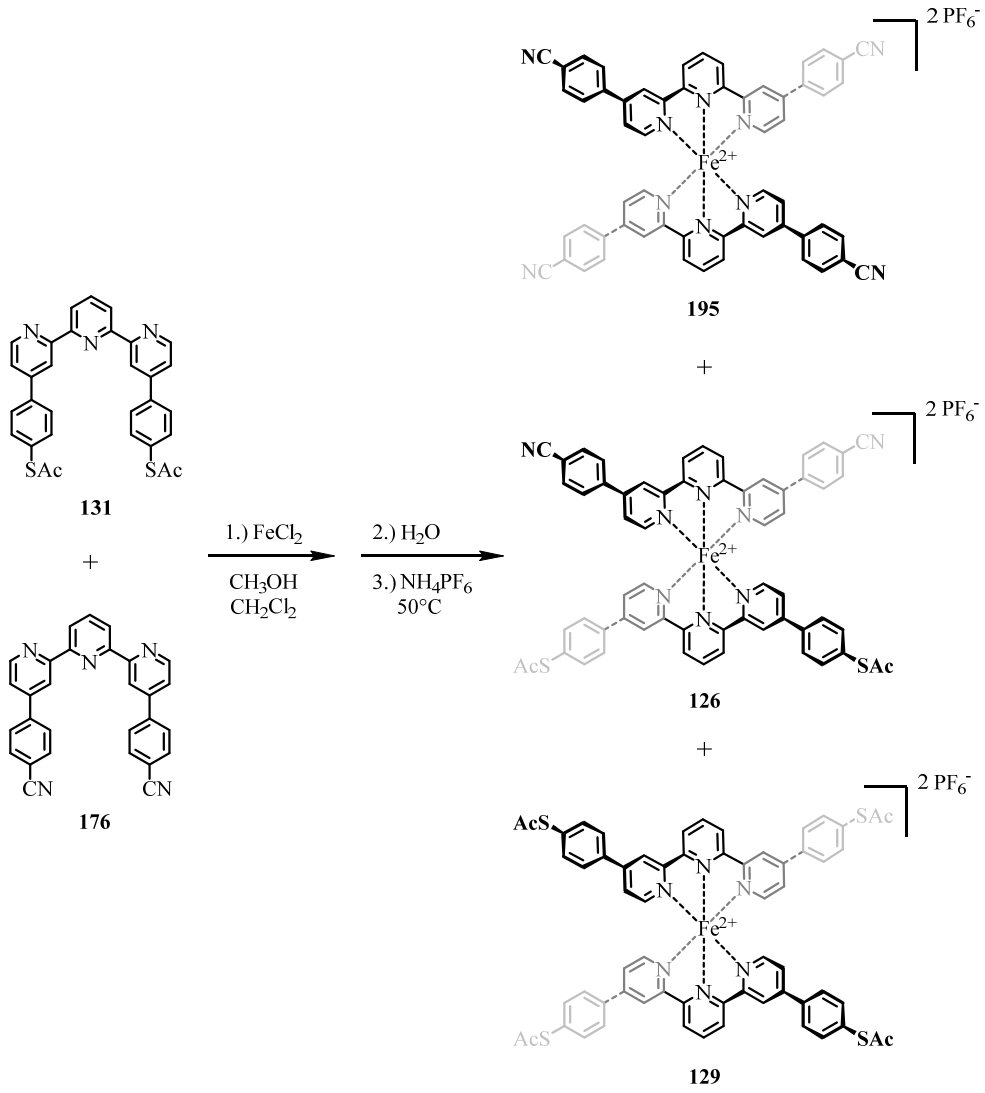

126 was prepared by a modification of the representative procedure C. In this case a statistic reaction had to be performed in which an equimolar amount of the terpyridine precursors was used. Thus the thiolated ligand *S,S´*-([2,2´:6´,2´´-terpyridine]-4,4´´-diylbis(4,1-phenylene)) diethanethioate (**131**) (26.7 mg, 50.0 µmol, 1.00 eq.) and 4,4´-([2,2´:6´,2´´-terpyridine]-4,4´´-diyl)dibenzonitrile (**176**) (21.8 mg, 50.0 µmol, 1.00 eq.) were mixed with $FeCl_2$ (6.34 mg, 50.0 µmol, 1.00 eq.). The reagents were suspended in MeOH (20 mL), DCM (20 mL), and water (100 mL) and NH_4PF_6 (407 mg, 2.50 mmol, 50.0 eq.) was used for the anion exchange. The crude product revealed the expected statistical mixture of the three complexes **126**, **129** and **195**. To obtain the desired heteroleptic target complex **126** the crude mixture was subjected to purification via preparative reversed-phase HPLC using a solvent gradient ranging from H_2O / MeCN (55:45) up to H_2O / MeCN (40:60) at a flow rate of 20 mL/min yielding the desired pure product **126** as a dark purple solid in a yield of 43% (28.2 mg,

21.0 µmol). The two expected homoleptic side products **129** and **195** could be separated successfully from the desired heteroleptic target structure and were isolated in a yield of 24% (**129**, 16.6 mg, 12.0 µmol) and 33% (**195**, 20.3 mg, 17.0 µmol), respectively. As the analytical data of compound **129** is already presented at the place where its exclusive synthesis is discussed only the analytical data of target compound **126** and the second side product **195** are listed hereafter.

Analytical data of 126:

^{1}H-NMR (400 MHz, CD_3CN, ppm, 25 °C): δ_H = 9.10 (d, $^{3}J_{H,H}$ = 8.0 Hz, 4H, *H3´ / H5´*), 8.87 - 8.73 (m, 6H, *H3 / H3´´ / H4´*), 7.87 (s, 8H, $H_{cyanophenyl}$), 7.78 (d, $^{3}J_{H,H}$ = 8.5 Hz, 4H, $H_{thioacetylphenyl}$), 7.56 (d, $^{3}J_{H,H}$ = 8.5 Hz, 4H, $H_{thioacetylphenyl}$), 7.38 (app. dt, $^{3}J_{H,H}$ = 5.8 Hz, $^{4}J_{H,H}$ = 1.4 Hz, 4H, *H5 / H5´´*), 7.22 (d, $^{3}J_{H,H}$ = 6.0 Hz, 2H, $H6_{cyanophenyl}$ / $H6_{cyanophenyl´´}$), 7.17 (d, $^{3}J_{H,H}$ = 6.0 Hz, 2H, $H6_{thioacetylphenyl}$ / $H6_{thioacetylphenyl´´}$), 2.41 (s, 6H, $H_{methyl(SAc)}$).
^{13}C-NMR (101 MHz, CD_3CN, ppm, 25 °C): δ_C = 194.19 ($C_{C=O}$, 2C), 161.22 (C_q, 2C), 159.53 (C_q, 2C), 159.32 (C_q, 2C), 154.42 (C_t, 2C), 154.22 (C_t, 2C), 150.75 (C_q, 2C), 149.81 (C_q, 2C), 140.67 (C_q, 2C), 140.64 (C_q, 2C), 139.31 (C_t, 1C), 139.21 (C_t, 1C), 137.22 (C_q, 2C), 136.19 (C_{phenyl}, 4C), 134.14 (C_{phenyl}, 4C), 132.17 (C_q, 2C), 129.24 (C_{phenyl}, 4C), 129.06 (C_{phenyl}, 4C), 125.94 (C_t, 2C), 125.77 (C_t, 2C), 125.26 (C_t, 2C), 125.15 (C_t, 2C), 122.81 (C_t, 2C), 122.75 (C_t, 2C), 119.08 (C_q, 2C), 114.68 ($C_{(CN)}$, 2C), 30.65 ($C_{methyl(SAc)}$, 2C).
^{19}F-NMR (376 MHz, CD_3CN, ppm, 25 °C): δ_F = -72.77 (d, $^{1}J_{P,F}$ = 706.7 Hz, 12F, PF_6).
^{31}P-NMR (162 MHz, CD_3CN, ppm, 25 °C): δ_P = -144.61 (hept, $^{1}J_{P,F}$ = 706.7 Hz, 2P, PF_6).
ESI-MS (MeCN, *positive* ion mode): *m/z* [ion, intensity (%)] = 512.1 (M^{2+}-2PF_6^-, 100).
ESI-MSMS (MeCN, *positive* ion mode (MSMS of *m/z* = 512.1): *m/z* [ion, intensity (%)] = 470.1 (M^{2+}-2((C=O)CH_3), 100), 491.1 (M^{2+}-((C=O)CH_3), 40), 512.1 (M^{2+}, 20).
HRMS (ESI-ToF): *m/z* calcd. for $[C_{60}H_{40}FeN_8O_2S_2]^{2+}$: 512.1028; found: 512.1038.
UV/VIS (MeCN): λ_{max} (ε) = 277 nm (89755 L·cm^{-1}·mol^{-1}), 336 nm (92405 L·cm^{-1}·mol^{-1}), 382 nm (18910 L·cm^{-1}·mol^{-1}), 564 nm (16690 L·cm^{-1}·mol^{-1}), 625 nm (7780 L·cm^{-1}·mol^{-1}).
Analytical data of 195:

^{1}H-NMR (400 MHz, CD_3CN, ppm, 25 °C): δ_H = 9.11 (d, $^{3}J_{H,H}$ = 8.1 Hz, 4H, *H3´ / H5´*), 8.88 - 8.73 (m, 6H, *H3 / H3´´ / H4´*), 7.86 (s, 16H, H_{phenyl}), 7.38 (dd, $^{3}J_{H,H}$ = 6.0 Hz, $^{4}J_{H,H}$ = 2.0 Hz, 4H, *H5 / H5´´*), 7.21 (d, $^{3}J_{H,H}$ = 5.9 Hz, 4H, *H6 / H6´´*).

^{13}C-NMR (101 MHz, CD_3CN, ppm, 25 °C): δ_C = 161.16 (C_q, 4C), 159.50 (C_q, 4C), 154.47 (C_t, 4C), 149.86 (C_q, 4C), 140.65 (C_q, 4C), 139.36 (C_t, 2C), 134.15 (C_{phenyl}, 8C), 129.23 (C_{phenyl}, 8C), 125.95 (C_t, 4C), 125.31 (C_t, 4C), 122.84 (C_t, 4C), 119.08 (C_q, 4C), 114.69 ($C_{(CN)}$, 4C).

^{19}F-NMR (376 MHz, CD_3CN, ppm, 25 °C): δ_F = -72.71 (d, $^1J_{P,F}$ = 706.8 Hz, 12F, ***PF_6***).

^{31}P-NMR (162 MHz, CD_3CN, ppm, 25 °C): δ_P = -144.60 (hept, $^1J_{P,F}$ = 706.9 Hz, 2P, ***PF_6***).

ESI-MS (MeCN, *positive* ion mode): *m/z* [ion, intensity (%)] = 463.2 (M^{2+}-2PF_6^-, 100).

HRMS (ESI-ToF): *m/z* calcd. for $[C_{58}H_{34}FeN_{10}]^{2+}$: 463.1154; found: 463.1161.

UV/VIS (MeCN): λ_{max} (ε) = 275 nm (111867 L·cm^{-1}·mol^{-1}), 336 nm (92800 L·cm^{-1}·mol^{-1}), 384 nm (17773 L·cm^{-1}·mol^{-1}), 567 nm (17000 L·cm^{-1}·mol^{-1}), 625 nm (7813 L·cm^{-1}·mol^{-1}).

{[Fe(*174*)(*131*)]$^{2+}$[(PF$_6$)$^-$]$_2$} (125)

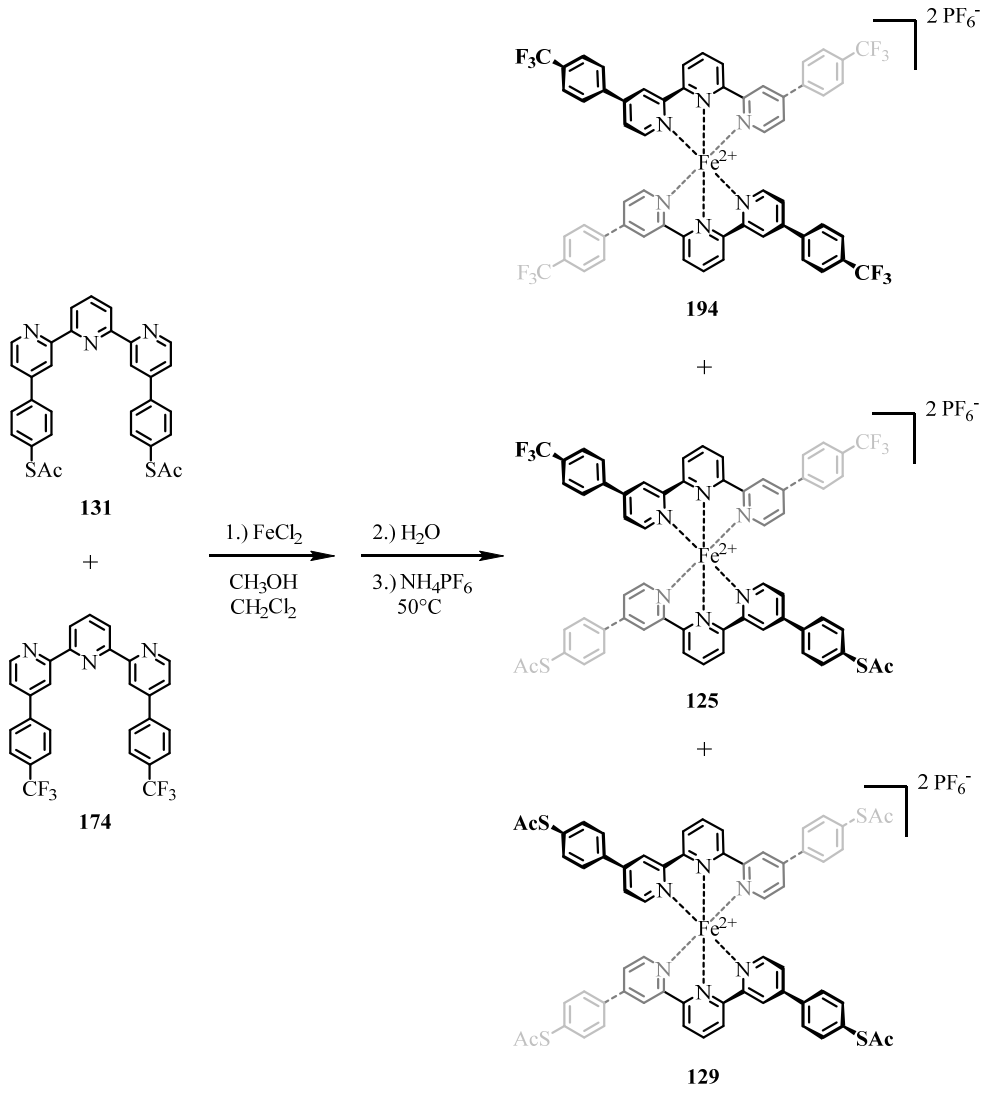

125 was prepared by a modification of the representative procedure C. In this case a statistic reaction had to be performed in which an equimolar amount of the terpyridine precursors was used. Therefore *S,S´*-([2,2´:6´,2´´-terpyridine]-4,4´´-diylbis(4,1-phenylene)) diethanethioate (**131**) (21.3 mg, 40.0 µmol, 1.00 eq.) and 4,4´´-bis(4-(trifluoromethyl)phenyl-2,2´:6´,2´´-terpyridine (**174**) (20.9 mg, 40.0 µmol, 1.00 eq.) were mixed with $FeCl_2$ (5.07 mg, 40.0 µmol, 1.00 eq.). The reagents were suspended in MeOH (20 mL), DCM (20 mL), and water (100 mL) and for the final anion exchange NH_4PF_6 (326 mg, 2.00 mmol, 50.0 eq.) was added. As expected the crude product turned out to be a statistical mixture of the three complexes **125**, **129** and **194**. To obtain the desired heteroleptic target complex **125** the crude mixture was subjected to purification via preparative reversed-phase HPLC using a solvent gradient ranging from H_2O / MeCN (55:45) up to H_2O / MeCN (40:60) at a flow rate of 20 mL/min yielding the desired pure product **125** as a dark purple solid in a yield of

31% (17.1 mg, 12.0 µmol). The two expected homoleptic side products **129** and **194** could be separated successfully from the desired heteroleptic target structure. As their exclusive synthesis together with their analytical data is discussed at the corresponding section they were not explicitly isolated or characterized in this context. Thus hereafter, only the analytical data of complex **125** are discussed.

Analytical data of 125:

^{1}H-NMR (400 MHz, CD_3CN, ppm, 25 °C): δ_H = 9.12 (d, $^{3}J_{H,H}$ = 8.1 Hz, 2H, *H3´* / H5´**), 9.11 (d, $^{3}J_{H,H}$ = 8.1 Hz, 2H, *H3´* / H5´**), 8.87 - 8.72 (m, 6H, *H3 / H3´´ / H4´*), 7.90 (d, $^{3}J_{H,H}$ = 8.3 Hz, 4H, $H_{trifluoromethylphenyl}$), 7.84 (d, $^{3}J_{H,H}$ = 8.3 Hz, 4H, $H_{trifluoromethylphenyl}$), 7.79 (d, $^{3}J_{H,H}$ = 8.5 Hz, 4H, $H_{thioacetylphenyl}$), 7.57 (d, $^{3}J_{H,H}$ = 8.5 Hz, 4H, $H_{thioacetylphenyl}$), 7.40 (app. dt, $^{3}J_{H,H}$ = 5.9 Hz, $^{4}J_{H,H}$ = 1.9 Hz, 4H, *H5 / H5´´*), 7.22 (d, $^{3}J_{H,H}$ = 5.9 Hz, 2H, $H6_{trifluoromethylphenyl}$ / $H6_{trifluoromethylphenyl´´}$), 7.18 (d, $^{3}J_{H,H}$ = 6.0 Hz, 2H, $H6_{thioacetylphenyl}$ / $H6_{thioacetylphenyl´´}$), 2.41 (s, 6H, $H_{methyl(SAc)}$).

^{13}C-NMR (101 MHz, CD_3CN, ppm, 25 °C): δ_C = 194.21 ($C_{C=O}$, 2C), 161.27 (C_q, 2C), 161.26 (C_q, 2C), 159.49 (C_q, 2C), 159.36 (C_q, 2C), 154.36 (C_t, 2C), 154.22 (C_t, 2C), 150.77 (C_q, 2C), 150.19 (C_q, 2C), 140.25 (C_q, 2C), 139.27 (C_t, 1C), 139.20 (C_t, 1C), 137.25 (C_q, 2C), 136.21 ($C_{thioacetylphenyl}$, 4C), 132.39 (q, ^{1}J = 32.6 Hz, 2C, -***C***F_3), 132.18 (C_q, 2C), 129.25 (C_{phenyl}, 4C), 129.07 (C_{phenyl}, 4C), 127.21 (q, ^{3}J = 3.8 Hz, 4C, -*(**C**H)$_2$CCF$_3$*), 126.42 (C_q, 2C), 126.02 (C_t, 2C), 125.78 (C_t, 2C), 125.23 (C_t, 2C), 125.13 (C_t, 2C), 122.90 (C_t, 2C), 122.76 (C_t, 2C), 30.66 ($C_{methyl(SAc)}$, 2C).

^{19}F-NMR (376 MHz, CD_3CN, ppm, 25 °C): δ_F = -63.37 (s, 6F, C**F$_3$**), -72.83 (d, $^{1}J_{P,F}$ = 706.7 Hz, 12F, *P**F$_6$***).

^{31}P-NMR (162 MHz, CD_3CN, ppm, 25 °C): δ_P = -144.61 (hept, $^{1}J_{P,F}$ = 706.6 Hz, 2P, ***P**F$_6$*).

ESI-MS (MeCN, *positive* ion mode): *m/z* [ion, intensity (%)] = 555.3 (M^{2+}-2PF_6^-, 100).

ESI-MSMS (MeCN, *positive* ion mode (MSMS of *m/z* = 555.3): *m/z* [ion, intensity (%)] = 513.3 (M^{2+}-2((C=O)CH_3), 100), 534.3 (M^{2+}-((C=O)CH_3), 50), 555.3 (M^{2+}, 45).

HRMS (ESI-ToF): *m/z* calcd. for $[C_{60}H_{40}FeN_8O_2S_2]^{2+}$: 555.0949; found: 555.0955.

UV/VIS (MeCN): λ_{max} (ε) = 273 nm (70520 L·cm^{-1}·mol^{-1}), 334 nm (82980 L·cm^{-1}·mol^{-1}), 379 nm (15105 L·cm^{-1}·mol^{-1}), 566 nm (14400 L·cm^{-1}·mol^{-1}), 625 nm (6070 L·cm^{-1}·mol^{-1}).

{[Fe(*187*)(*131*)]$^{2+}$[(PF$_6$)$^-$]$_2$} (117)

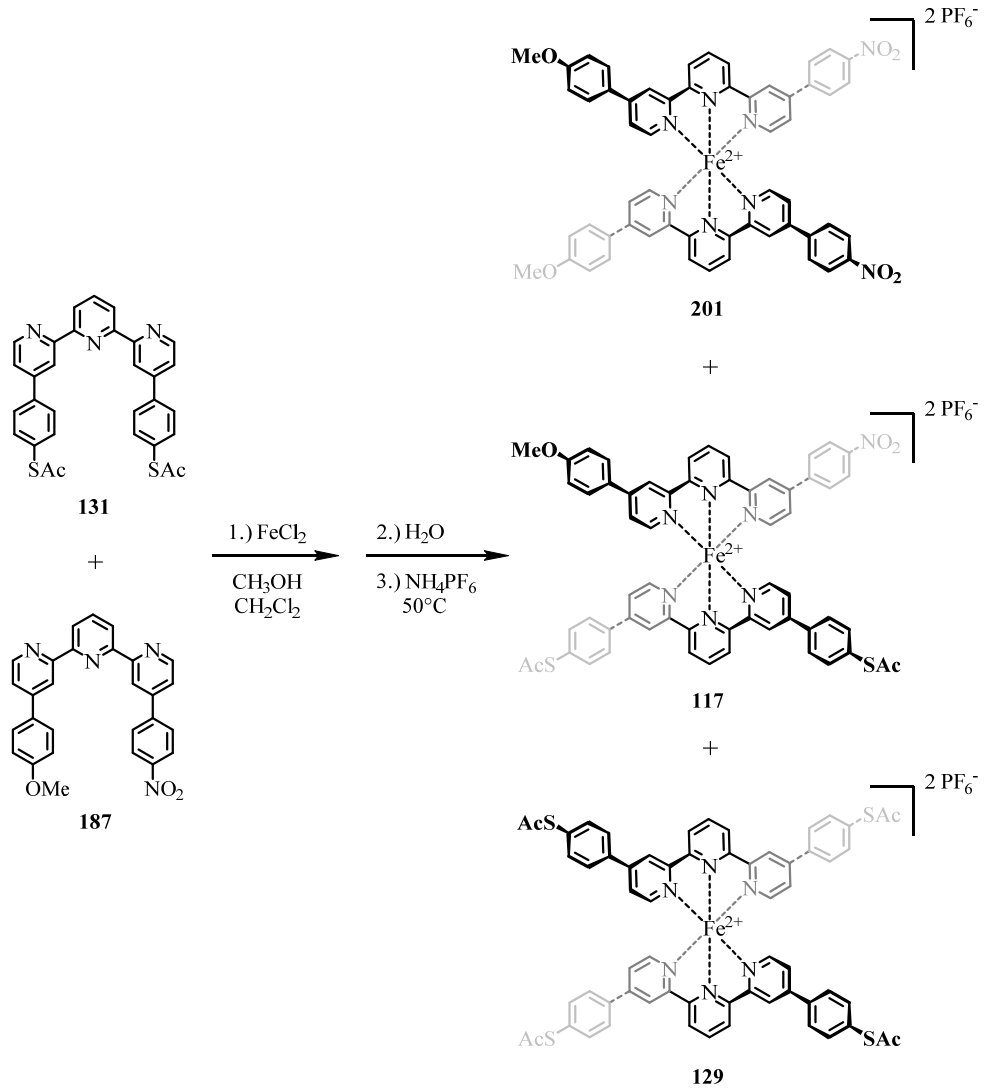

117 was prepared by a modification of the representative procedure C. In this case a statistic reaction utilizing equimolar amounts of the terpyridine precursors was used. Thus thiolated *S,S′*-([2,2′:6′,2′′-terpyridine]-4,4′′-diylbis(4,1-phenylene)) diethanethioate (**131**) (26.7 mg, 50.0 µmol, 1.00 eq.) and the asymmetric ligand 4-(4-methoxyphenyl)-4′′-(4-nitrophenyl)-2,2′:6′,2′′-terpyridine (**187**) (23.0 mg, 50.0 µmol, 1.00 eq.) were mixed with $FeCl_2$ (6.34 mg, 50.0 µmol, 1.00 eq.). The reagents were dissolved in MeOH (20 mL), DCM (20 mL) and water (100 mL) and NH_4PF_6 (408 mg, 2.50 mmol, 50.0 eq.) was used for the final anion exchange. The statistical crude product mixture contained the three complexes **117**, **129** and **201** as expected. To obtain the desired heteroleptic target complex **117** the crude mixture was subjected to purification via preparative reversed-phase HPLC using a solvent gradient ranging from H_2O / MeCN 55:45) up to H_2O / MeCN (40:60) at a flow rate of 20 mL/min

yielding the desired pure product **117** as a dark purple-reddish solid in a yield of 34% (22.5 mg, 17.0 µmol). The two expected homoleptic side products could be separated successfully from the desired heteroleptic target structure and the homoleptic side product **201** was isolated in a yield of 15% (9.20 mg, 7.00 µmol). Hereafter, the complete analytical data of target compound **117** and the side product **201** are discussed. The data of complex **129** have been listed at the place where their exclusive synthesis is discussed.

Analytical data of 117:

^{1}H-NMR (400 MHz, CD_3CN, ppm, 25 °C): δ_H = 9.11 (d, $^{3}J_{H,H}$ = 8.1 Hz, 2H, *H3´* / H5´**), 9.10 (d, $^{3}J_{H,H}$ = 8.1 Hz, 2H, *H3´* / H5´**), 8.84 - 8.74 (m, 6H, *H3 / H3´´ / H4´*), 8.32 (d, $^{3}J_{H,H}$ = 8.9 Hz, 2H, $H_{phenyl(push)}$), 7.92 (d, $^{3}J_{H,H}$ = 8.9 Hz, 2H, $H_{phenyl(push)}$), 7.78 (d, $^{3}J_{H,H}$ = 8.5 Hz, 4H, $H_{phenyl(sym)}$), 7.74 (d, $^{3}J_{H,H}$ = 8.9 Hz, 2H, $H_{phenyl(pull)}$), 7.56 (d, $^{3}J_{H,H}$ = 8.5 Hz, 4H, $H_{phenyl(sym)}$), 7.41 (dd, $^{3}J_{H,H}$ = 6.1 Hz, $^{4}J_{H,H}$ = 2.0 Hz, 1H, *H5$_{(asym)}$* / H5$_{(asym)}$´´**), 7.38 (dd, $^{3}J_{H,H}$ = 6.0 Hz, $^{4}J_{H,H}$ = 1.9 Hz, 2H, *H5$_{(sym)}$ / H5$_{(sym)}$´´*), 7.34 (dd, $^{3}J_{H,H}$ = 6.0 Hz, $^{4}J_{H,H}$ = 1.9 Hz, 1H, *H5$_{(asym)}$* / H5$_{(asym)}$´´**), 7.23 (d, $^{3}J_{H,H}$ = 5.9 Hz, 1H, *H6$_{(asym)}$* / H6$_{(asym)}$´´**), 7.17 (d, $^{3}J_{H,H}$ = 6.0 Hz, 2H, *H6$_{(sym)}$ / H6$_{(sym)}$´´*), 7.08 (d, $^{3}J_{H,H}$ = 6.0 Hz, 1H, *H6$_{(asym)}$* / H6$_{(asym)}$´´**), 7.05 (d, $^{3}J_{H,H}$ = 8.9 Hz, 2H, $H_{phenyl(pull)}$), 3.83 (s, 3H, $H_{methoxy}$), 2.41 (s, 6H, $H_{methyl(SAc)}$).

^{13}C-NMR (101 MHz, CD_3CN, ppm, 25 °C): δ_C = 194.21 ($C_{C=O}$, 2C), 162.99 (C_q, 1C), 161.49 (C_q, 1C), 161.30 (C_q, 2C), 161.08 (C_q, 1C), 159.71 (C_q, 1C), 159.36 (C_q, 2C), 158.97 (C_q, 1C), 154.50 (C_t, 1C), 154.16 (C_t, 2C), 153.69 (C_t, 1C), 151.30 (C_q, 1C), 150.69 (C_q, 2C), 150.05 (C_q, 1C), 149.29 (C_q, 1C), 142.55 (C_q, 1C), 139.13 (C_t, 2C), 137.27 (C_q, 2C), 136.20 (C_{phenyl}, 4C), 132.16 (C_q, 2C), 129.84 (C_{phenyl}, 2C), 129.75 (C_{phenyl}, 2C), 129.07 (C_{phenyl}, 4C), 128.12 (C_q, 1C), 125.99 (C_t, 1C), 125.76 (C_t, 2C), 125.32 (C_{phenyl}, 2C), 125.13 (C_t, 1C), 125.07 (C_t, 2C), 124.92 (C_t, 1C), 122.91 (C_t, 1C), 122.70 (C_t, 2C), 121.86 (C_t, 1C), 115.81 (C_{phenyl}, 2C), 56.29 ($C_{methoxy}$, 1C), 30.66 ($C_{methyl(SAc)}$, 2C). In the ^{13}C-spectrum one signal less than expected was found probably due to coincident C4´-signals at δ_C = 139.13 ppm.

^{19}F-NMR (376 MHz, CD_3CN, ppm, 25 °C): δ_F = -72.81 (d, $^{1}J_{P,F}$ = 706.7 Hz, 12F, ***PF_6***).

^{31}P-NMR (162 MHz, CD_3CN, ppm, 25 °C): δ_P = -144.61 (hept, $^{1}J_{P,F}$ = 706.6 Hz, 2P, ***P***F_6).

ESI-MS (MeCN, *positive* ion mode): *m/z* [ion, intensity (%)] = 524.9 (M^{2+}-2PF_6^-, 100).

ESI-MSMS (MeCN, *positive* ion mode (MSMS of *m/z* = 524.9): *m/z* [ion, intensity (%)] = 482.8 (M^{2+}-2((C=O)CH_3), 10), 503.8 (M^{2+}-((C=O)CH_3), 20), 524.9 (M^{2+}, 100).

HRMS (ESI-ToF): *m/z* calcd. for $[C_{59}H_{43}FeN_7O_5S_2]^{2+}$: 524.6053; found: 524.6062.
UV/VIS (MeCN): λ_{max} (ε) = 281 nm (72330 $L \cdot cm^{-1} \cdot mol^{-1}$), 338 nm (78415 $L \cdot cm^{-1} \cdot mol^{-1}$), 566 nm (14410 $L \cdot cm^{-1} \cdot mol^{-1}$), 626 nm (6790 $L \cdot cm^{-1} \cdot mol^{-1}$).

Analytical data of 201:

^{1}H-NMR (400 MHz, CD_3CN, ppm, 25 °C): δ_H = 9.11 (d, $^{3}J_{H,H}$ = 8.1 Hz, 4H, *H3´ / H5´*), 8.81 (d, $^{4}J_{H,H}$ = 1.6 Hz, 2H, *H3* / H3´´**), 8.77 (t, $^{3}J_{H,H}$ = 8.1 Hz, 2H, *H4´*), 8.74 (d, $^{4}J_{H,H}$ = 1.8 Hz, 2H, *H3* / H3´´**), 8.33 (d, $^{3}J_{H,H}$ = 9.0 Hz, 4H, $H_{phenyl(push)}$), 7.92 (d, $^{3}J_{H,H}$ = 9.0 Hz, 4H, $H_{phenyl(push)}$), 7.73 (d, $^{3}J_{H,H}$ = 9.0 Hz, 4H, $H_{phenyl(pull)}$), 7.40 (dd, $^{3}J_{H,H}$ = 6.0 Hz, $^{4}J_{H,H}$ = 2.0 Hz, 2H, $H5_{(asym)}$* / $H5_{(asym)}$´´*), 7.33 (dd, $^{3}J_{H,H}$ = 6.10 Hz, $^{4}J_{H,H}$ = 2.0 Hz, 2H, $H5_{(asym)}$* / $H5_{(asym)}$´´*), 7.22 (d, $^{3}J_{H,H}$ = 6.0 Hz, 2H, $H6_{(asym)}$* / $H6_{(asym)}$´´*), 7.08 (d, $^{3}J_{H,H}$ = 6.1 Hz, 2H, $H6_{(asym)}$* / $H6_{(asym)}$´´*), 7.05 (d, $^{3}J_{H,H}$ = 9.0 Hz, 4H, $H_{phenyl(pull)}$), 3.83 (s, 6H, $H_{methoxy}$).
^{13}C-NMR (101 MHz, CD_3CN, ppm, 25 °C): δ_C = 162.99 (C_q, 2C), 161.50 (C_q, 2C), 161.09 (C_q, 2C), 159.69 (C_q, 2C), 158.96 (C_q, 2C), 154.48 (C_t, 2C), 153.67 (C_t, 2C), 151.30 (C_q, 2C), 150.06 (C_q, 2C), 149.28 (C_q, 2C), 142.56 (C_q, 2C), 139.10 (C_t, 2C), 137.27 (C_q, 2C), 129.84 (C_{phenyl}, 4C), 129.75 (C_{phenyl}, 4C), 128.13 (C_q, 2C), 125.99 (C_t, 2C), 125.32 (C_{phenyl}, 4C), 125.10 (C_t, 2C), 124.99 (C_t, 2C), 124.92 (C_t, 2C), 122.90 (C_t, 2C), 121.84 (C_t, 2C), 115.81 (C_{phenyl}, 4C), 56.29 ($C_{methoxy}$, 2C).
^{19}F-NMR (376 MHz, CD_3CN, ppm, 25 °C): δ_F = -72.84 (d, $^{1}J_{P,F}$ = 706.3 Hz, 12F, PF_6).
^{31}P-NMR (162 MHz, CD_3CN, ppm, 25 °C): δ_P = -144.61 (hept, $^{1}J_{P,F}$ = 706.5 Hz, 2P, PF_6).
ESI-MS (MeCN, *positive* ion mode): *m/z* [ion, intensity (%)] = 488.3 (M^{2+}-2PF_6^-, 100).
HRMS (ESI-ToF): *m/z* calcd. for $[C_{59}H_{43}FeN_7O_5S_2]^{2+}$: 488.1205; found: 488.1213.
UV/VIS (MeCN): λ_{max} (ε) = 283 nm (68245 $L \cdot cm^{-1} \cdot mol^{-1}$), 334 nm (64195 $L \cdot cm^{-1} \cdot mol^{-1}$), 568 nm (12235 $L \cdot cm^{-1} \cdot mol^{-1}$), 629 nm (5695 $L \cdot cm^{-1} \cdot mol^{-1}$).

{[Fe(*180*)(*131*)]$^{2+}$[(PF$_6$)$^-$]$_2$} (124)

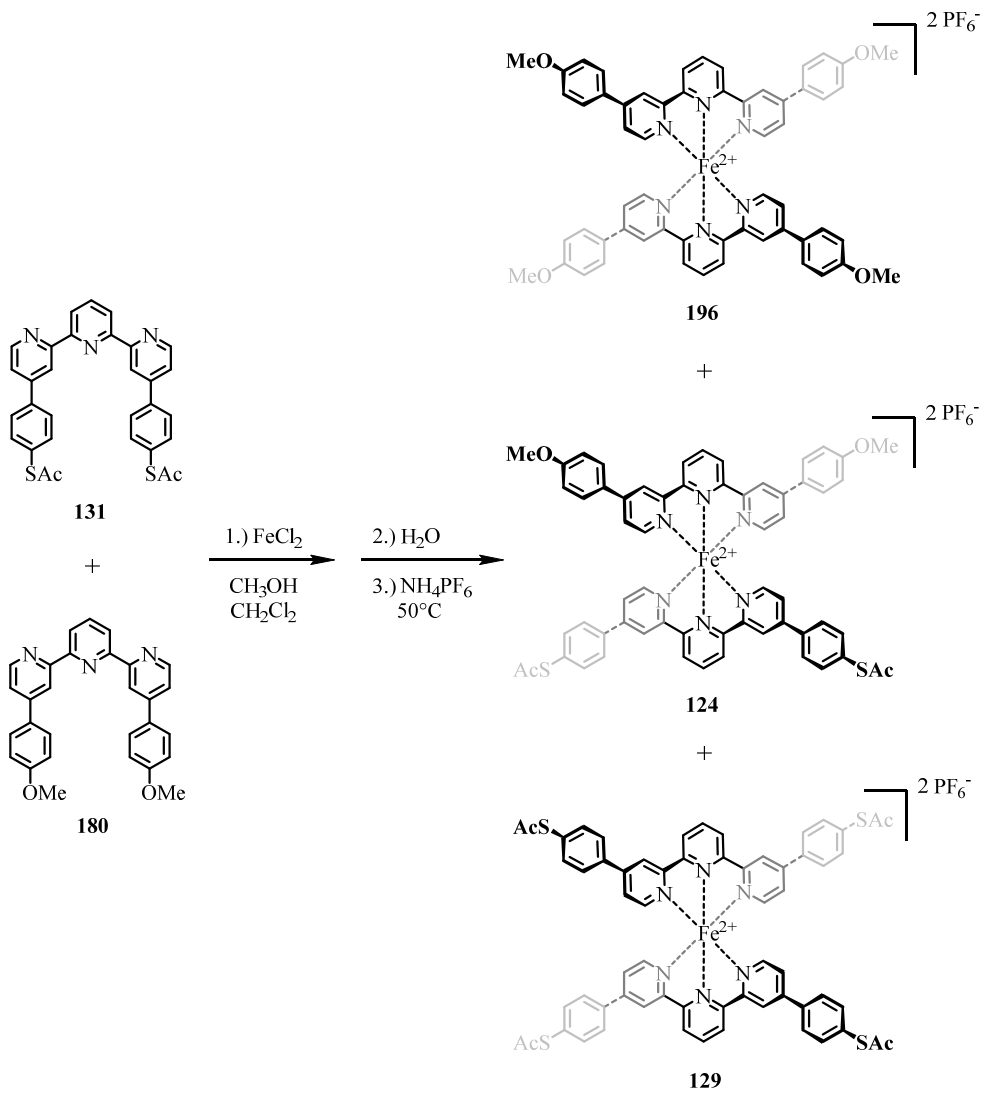

124 was prepared by modifying the representative procedure C. Herein, a statistic reaction had to be performed in which equimolar amounts of the terpyridine precursors were used. Thus *S,S´*-([2,2´:6´,2´´-terpyridine]-4,4´´-diylbis(4,1-phenylene)) diethanethioate (**131**) (16.0 mg, 30.0 µmol, 1.00 eq.) and 4,4´´-bis(4-methoxyphenyl)-2,2´:6´,2´´-terpyridine (**180**) (13.4 mg, 30.0 µmol, 1.00 eq.) were mixed with $FeCl_2$ (3.80 mg, 30.0 µmol, 1.00 eq.). The reagents were suspended in MeOH (20 mL), DCM (20 mL), and water (100 mL) and for the final anion exchange NH_4PF_6 (245 mg, 1.50 mmol, 50.0 eq.) was used. As expected the crude product turned out to be a statistical mixture of the three complexes **124**, **129** and **196**. To obtain the desired heteroleptic target complex **124** the crude mixture was subjected to purification by preparative reversed-phase HPLC using a solvent gradient ranging from H_2O / MeCN (50:50) up to H_2O / MeCN (40:60) at a flow rate of 20 mL/min yielding the product **124** as a dark purple solid in a yield of 26% (10.2 mg, 8.00 µmol). The two expected

homoleptic side products **129** and **196** could be separated successfully from the desired heteroleptic target structure. As **129** has been synthesized and characterized separately only the homoleptic compound **196** was isolated in a yield of 22% (9.10 mg, 6.00 µmol) in this context and hence only the analytical data of **124** and **196** are listed hereafter.

Analytical data of 124:

^{1}H-NMR (400 MHz, CD_3CN, ppm, 25 °C): δ_H = 9.09 (d, $^{3}J_{H,H}$ = 8.1 Hz, 4H, *H3´ / H5´*), 8.79 (d, $^{4}J_{H,H}$ = 1.5 Hz, 2H, *H3* / H3´´**), 8.76 (t, $^{3}J_{H,H}$ = 8.0 Hz, 2H, *H4´*), 8.74 (d, $^{4}J_{H,H}$ = 1.9 Hz, 2H, *H3* / H3´´**), 7.78 (d, $^{3}J_{H,H}$ = 8.6 Hz, 4H, $H_{thioacetylphenyl}$), 7.73 (d, $^{3}J_{H,H}$ = 9.0 Hz, 4H, $H_{methoxyphenyl}$), 7.56 (d, $^{3}J_{H,H}$ = 8.6 Hz, 4H, $H_{thioacetylphenyl}$), 7.38 (dd, $^{3}J_{H,H}$ = 6.0 Hz, $^{4}J_{H,H}$ = 2.0 Hz, 2H, $H5_{(thioligand)}$ / $H5_{(thioligand)}$´´), 7.32 (dd, $^{3}J_{H,H}$ = 6.1 Hz, $^{4}J_{H,H}$ = 2.0 Hz, 2H, $H5_{(methoxyligand)}$ / $H5_{(methoxyligand)}$´´), 7.17 (d, $^{3}J_{H,H}$ = 6.0 Hz, 2H, $H6_{(thioligand)}$ / $H6_{(thioligand)}$´´), 7.06 (d, $^{3}J_{H,H}$ = 5.8 Hz, 2H, $H6_{(methoxyligand)}$ / $H6_{(methoxyligand)}$´´), 7.05 (d, $^{3}J_{H,H}$ = 9.0 Hz, 4H, $H_{methoxyphenyl}$), 3.83 (s, 6H, $H_{methoxy}$).

^{13}C-NMR (101 MHz, CD_3CN, ppm, 25 °C): δ_C = 194.22 ($C_{C=O}$, 2C), 162.97 (C_q, 2C), 161.38 (C_q, 2C), 161.36 (C_q, 2C), 159.38 (C_q, 2C), 159.09 (C_q, 2C), 154.06 (C_t, 2C), 153.72 (C_t, 2C), 151.18 (C_q, 2C), 150.60 (C_q, 2C), 139.01 (C_t, 1C), 138.88 (C_t, 1C), 137.32 (C_q, 2C), 136.20 (C_{phenyl}, 4C), 132.12 (C_q, 2C), 129.82 (C_{phenyl}, 4C), 129.07 (C_{phenyl}, 4C), 128.16 (C_q, 2C), 125.73 (C_t, 2C), 124.96 (C_t, 2C), 124.82 (C_t, 2C), 124.82 (C_t, 2C), 122.62 (C_t, 2C), 121.80 (C_t, 2C), 115.81 (C_{phenyl}, 4C), 56.29 ($C_{methoxy}$, 2C), 30.66 ($C_{methyl(SAc)}$, 2C).

^{19}F-NMR (376 MHz, CD_3CN, ppm, 25 °C): δ_F = -72.88 (d, $^{1}J_{P,F}$ = 706.7 Hz, 12F, ***PF_6***).

^{31}P-NMR (162 MHz, CD_3CN, ppm, 25 °C): δ_P = -144.62 (hept, $^{1}J_{P,F}$ = 706.5 Hz, 2P, ***PF_6***).

ESI-MS (MeCN, *positive* ion mode): *m/z* [ion, intensity (%)] = 517.3 (M^{2+}-2PF_6^-, 100).

ESI-MSMS (MeCN, *positive* ion mode (MSMS of *m/z* = 517.3): *m/z* [ion, intensity (%)] = 475.3 (M^{2+}-2((C=O)CH_3), 100), 496.3 (M^{2+}-((C=O)CH_3), 70), 517.3 (M^{2+}, 30).

HRMS (ESI-ToF): *m/z* calcd. for $[C_{60}H_{46}FeN_6O_4S_2]^{2+}$: 517.1181; found: 517.1189.

UV/VIS (MeCN): λ_{max} (ε) = 278 nm (80533 L·cm^{-1}·mol^{-1}), 337 nm (103633 L·cm^{-1}·mol^{-1}), 566 nm (16493 L·cm^{-1}·mol^{-1}), 626 nm (6767 L·cm^{-1}·mol^{-1}).

Analytical data of 196:

^{1}H-NMR (400 MHz, CD_3CN, ppm, 25 °C): δ_H = 9.08 (d, $^{3}J_{H,H}$ = 8.1 Hz, 4H, *H3´/H5´*), 8.74 (t, $^{3}J_{H,H}$ = 8.1 Hz, 2H, *H4´*), 8.73 (d, $^{4}J_{H,H}$ = 1.6 Hz, 4H, *H3 / H3´´*), 7.73 (d, $^{3}J_{H,H}$ = 9.0 Hz, 8H, H_{phenyl}), 7.31 (dd, $^{3}J_{H,H}$ = 6.1 Hz, $^{4}J_{H,H}$ = 2.0 Hz, 4H, *H5 / H5´´*), 7.05 (d, $^{3}J_{H,H}$ = 5.9 Hz, 4H, *H6 / H6´´*), 7.05 (d, $^{3}J_{H,H}$ = 9.0 Hz, 8H, H_{phenyl}), 3.83 (s, 12H, $H_{methoxy}$).

^{13}C-NMR (101 MHz, CD_3CN, ppm, 25 °C): δ_C = 162.93 (C_q, 4C), 161.44 (C_q, 4C), 159.11 (C_q, 4C), 153.62 (C_t, 4C), 151.06 (C_q, 4C), 138.73 (C_t, 2C), 129.81 (C_{phenyl}, 8C), 128.23 (C_q, 4C), 124.78 (C_t, 4C), 124.70 (C_t, 4C), 121.71 (C_t, 4C), 115.79 (C_{phenyl}, 8C), 56.28 ($C_{methoxy}$, 4C).

^{19}F-NMR (376 MHz, CD_3CN, ppm, 25 °C): δ_F = -72.88 (d, $^{1}J_{P,F}$ = 706.6 Hz, 12F, PF_6).

^{31}P-NMR (162 MHz, CD_3CN, ppm, 25 °C): δ_P = -144.61 (hept, $^{1}J_{P,F}$ = 706.5 Hz, 2P, PF_6).

ESI-MS (MeCN, *positive* ion mode): *m/z* [ion, intensity (%)] = 473.3 (M^{2+}-2PF_6^-, 100).

HRMS (ESI-ToF): *m/z* calcd. for $[C_{58}H_{46}FeN_6O_4]^{2+}$: 473.1460; found: 473.1469.

UV/VIS (MeCN): λ_{max} (ε) = 280 nm (58080 $L \cdot cm^{-1} \cdot mol^{-1}$), 336 nm (78560 $L \cdot cm^{-1} \cdot mol^{-1}$), 565 nm (13575 $L \cdot cm^{-1} \cdot mol^{-1}$), 630 nm (5340 $L \cdot cm^{-1} \cdot mol^{-1}$).

{[Fe(*11*)(*131*)]$^{2+}$[(PF$_6$)$^-$]$_2$} (122)

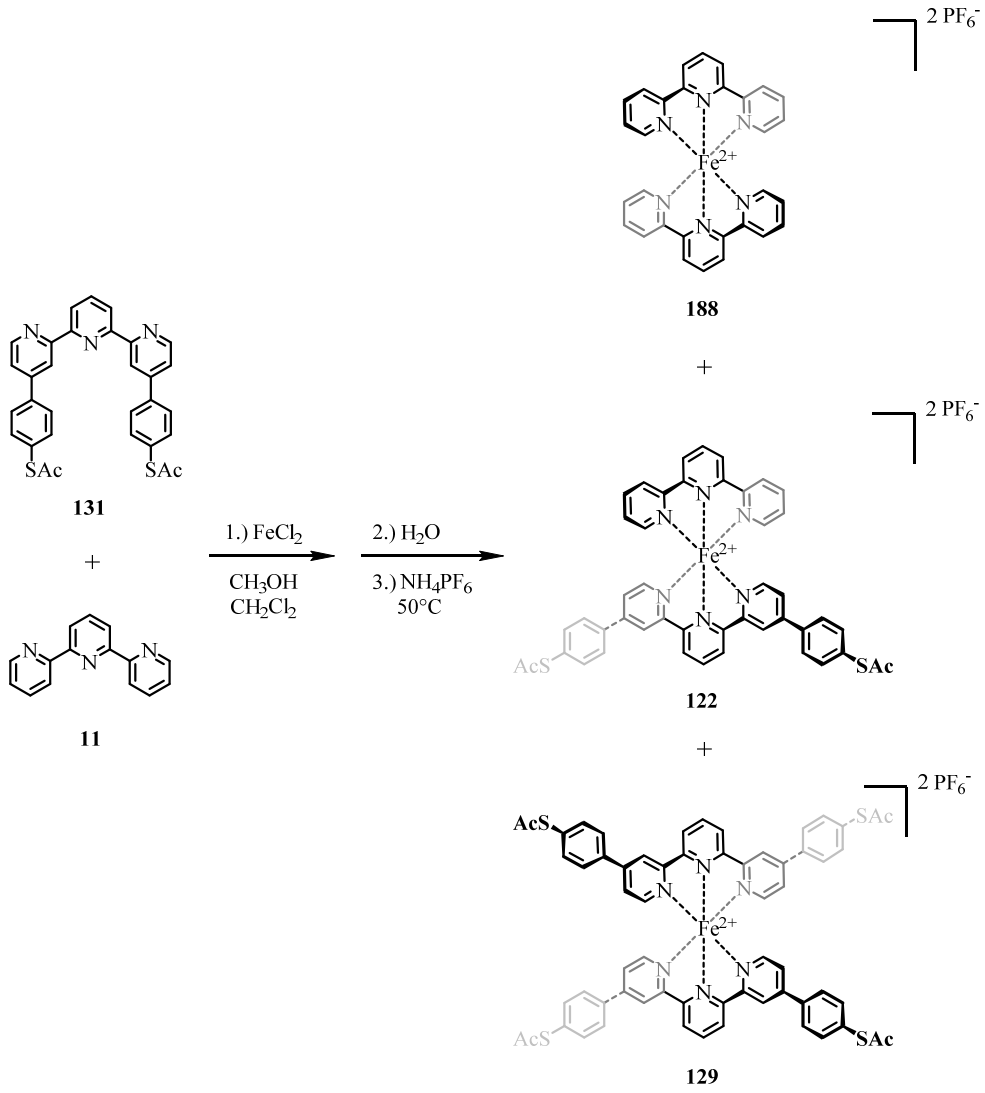

122 was prepared by a modification of the representative procedure C. In this case a statistic reaction had to be performed in which an equimolar amount of the terpyridine precursors was used. Thus 2,2′:6′,2′′-terpyridine (**11**) (19.0 mg, 80.0 µmol, 1.00 eq.) and *S,S′*-([2,2′:6′,2′′-ter-pyridine]-4,4′′-diylbis(4,1-phenylene)) diethanethioate (**131**) (42.7 mg, 80.0 µmol, 1.00 eq.) were mixed with $FeCl_2$ (10.1 mg, 80.0 µmol, 1.00 eq.). The reagents were suspended in MeOH (40 mL), DCM (40 mL), and water (200 mL) and NH_4PF_6 (652 mg, 4.00 mmol, 50.0 eq.) was used for the final anion exchange. As expected the crude product turned out to be a statistical mixture of the three complexes **122**, **129** and **188**. To obtain the desired heteroleptic target complex **122** the crude mixture was subjected to purification by preparative reversed-phase HPLC using a solvent gradient ranging from H_2O / MeCN (50:50) up to H_2O / MeCN (5:95) at a flow rate of 20 mL/min yielding the product **122** as a dark purple solid in a yield of 10% (8.50 mg, 8.00 µmol). The two expected homoleptic side products **129**

and **188** could be separated successfully from the desired heteroleptic target structure. As **129** has been synthesized and characterized separately only the analytical data of **122** are listed hereafter.

Analytical data of 122:

^{1}H-NMR (400 MHz, CD_3CN, ppm, 25 °C): δ_H = 9.07 (d, $^{3}J_{H,H}$ = 8.1 Hz, 2H, *H3$_{thioacetylphenyl}$´ / H5$_{thioacetylphenyl}$´*), 8.93 (d, $^{3}J_{H,H}$ = 8.1 Hz, 2H, *H3$_{terpy}$´ / H5$_{terpy}$´*), 8.77 (d, $^{4}J_{H,H}$ = 1.9 Hz, 2H, *H3$_{thioacetylphenyl}$ / H3$_{thioacetylphenyl}$´´*), 8.71 (app. dd, $^{3}J_{H,H}$ = 16.6 Hz, $^{3}J_{H,H}$ = 8.3 Hz, 2H, *H4´*), 8.49 (d, $^{3}J_{H,H}$ = 8.0 Hz, 2H, *H3$_{terpy}$ / H3$_{terpy}$´´*), 7.90 (ddd, $^{3}J_{H,H}$ = 8.1 Hz, $^{3}J_{H,H}$ = 6.4 Hz, $^{4}J_{H,H}$ = 2.6 Hz, 2H, *H4$_{terpy}$ / H4$_{terpy}$´´*), 7.77 (d, $^{3}J_{H,H}$ = 8.6 Hz, 4H, *H$_{thioacetylphenyl}$*), 7.57 (d, $^{3}J_{H,H}$ = 8.6 Hz, 4H, *H$_{thioacetylphenyl}$*), 7.34 (dd, $^{3}J_{H,H}$ = 6.0 Hz, $^{4}J_{H,H}$ = 2.0 Hz, 2H, *H5$_{(thioligand)}$ / H5$_{(thioligand)}$´´*), 7.15 – 7.07 (m, 6H, *H5$_{terpy}$ / H5$_{terpy}$´´ / H6 / H6´´*), 2.42 (s, 6H, *H$_{methyl}$*).

^{13}C-NMR (101 MHz, CD_3CN, ppm, 25 °C): δ_C = 194.22 ($C_{C=O}$, 2C), 161.34 (C_q, 2C), 161.19 (C_q, 2C), 159.34 (C_q, 2C), 158.80 (C_q, 2C), 154.15 (C_t, 2C), 154.08 (C_t, 2C), 150.65 (C_q, 2C), 139.85 (C_t, 2C), 139.08 (C_t, 1C), 139.04 (C_t, 1C), 136.20 (C_{phenyl}, 4C), 132.12 (C_q, 2C), 129.06 (C_{phenyl}, 4C), 128.42 (C_t, 2C), 125.71 (C_t, 2C), 124.96 (C_t, 2C), 124.78 (C_t, 2C), 124.78 (C_t, 2C), 122.84 (C_q, 2C), 122.70 (C_t, 2C), 30.66 ($C_{methyl(SAc)}$, 2C).

^{19}F-NMR (376 MHz, CD_3CN, ppm, 25 °C): δ_F = -72.87 (d, $^{1}J_{P,F}$ = 706.6 Hz, 12F, ***P*F$_6$**).

^{31}P-NMR (162 MHz, CD_3CN, ppm, 25 °C): δ_P = -144.62 (hept, $^{1}J_{P,F}$ = 706.4 Hz, 2P, ***P*F$_6$**).

ESI-MS (MeCN, *positive* ion mode): *m/z* [ion, intensity (%)] = 411.3 (M^{2+}-2PF_6^-, 100).

ESI-MSMS (MeCN, *positive* ion mode (MSMS of *m/z* = 411.3): *m/z* [ion, intensity (%)] = 369.3 (M^{2+}-2((C=O)CH_3), 100), 390.2 (M^{2+}-((C=O)CH_3), 60), 411.3 (M^{2+}, 20).

HRMS (ESI-ToF): *m/z* calcd. for $[C_{46}H_{34}FeN_6O_4S_2]^{2+}$: 411.0762; found: 411.0769.

UV/VIS (MeCN): λ_{max} (ε) = 274 nm (60810 L·cm^{-1}·mol^{-1}), 335 nm (64490 L·cm^{-1}·mol^{-1}), 374 nm (10550 L·cm^{-1}·mol^{-1}), 558 nm (13170 L·cm^{-1}·mol^{-1}).

{[Fe(*146*)(*147*)]$^{2+}$[(PF$_6$)$^-$]$_2$} (118)

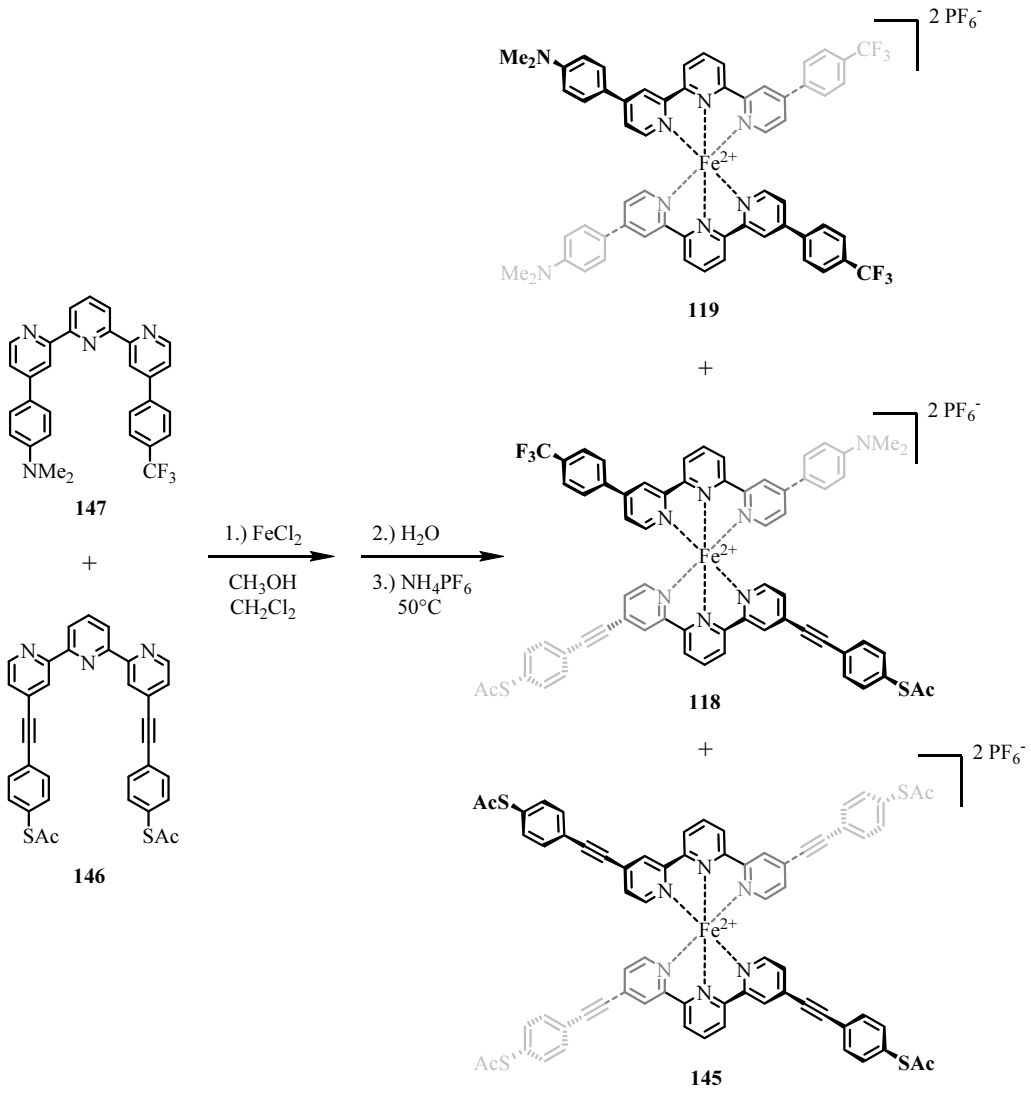

118 was prepared by a modification of the representative procedure C. In this case a statistic reaction had to be performed in which an equimolar amount of the terpyridine precursors was used. Thus *S,S′*-(([2,2′:6′,2′′-terpyridine]-4,4′′-diylbis(ethyne-2,1-diyl))bis(4,1-phenylene)) diethanethioate (**146**) (29.1 mg, 50.0 µmol, 1.00 eq.) and *N,N*-dimethyl-4-(4′′-(4-(trifluoro-methyl)phenyl)-[2,2′:6′,2′′-terpyridin]-4-yl)aniline (**147**) (24.8 mg, 50.0 µmol, 1.00 eq.) were mixed with $FeCl_2$ (6.34 mg, 50.0 µmol, 1.00 eq.). The reagents were suspended in MeOH (20 mL), DCM (20 mL), and water (100 mL) and for the final anion exchange NH_4PF_6 (407 mg, 2.50 mmol, 50.0 eq.) was used. As expected the crude product turned out to be a statistical mixture of the three complexes **118**, **119** and **145**. To obtain the desired heteroleptic target complex **118** the crude mixture was subjected to purification by preparative reversed-phase HPLC using a solvent gradient ranging from H_2O / MeCN (50:50) up to H_2O / MeCN (5:95) at a flow rate of 20 mL/min yielding the product **118** as a dark purple

solid in a yield of 19% (13.2 mg, 9.00 µmol). The two expected homoleptic side products **119** and **145** could be separated successfully from the desired heteroleptic target structure. As **119** has been synthesized and characterized separately only the homoleptic compound **145** was isolated in a yield of 8% (5.70 mg, 4.00 µmol) in this context and hence only the analytical data of **118** and **145** are listed hereafter.

Analytical data of 118:

^{1}H-NMR (400 MHz, CD_3CN, ppm, 25 °C): δ_H = 9.07 (d, $^{3}J_{H,H}$ = 8.1 Hz, 2H, *H3(asym)´ / H5(asym)´*), 8.95 (d, $^{3}J_{H,H}$ = 8.1 Hz, 2H, *H3(sym)´ / H5(sym)´*), 8.78 (d, $^{4}J_{H,H}$ = 1.6 Hz, 1H, *H3(asym)* / H3(asym)´´**), 8.75 (t, $^{3}J_{H,H}$ = 7.7 Hz, 1H, *H4(sym)´*), 8.73 (t, $^{3}J_{H,H}$ = 7.8 Hz, 1H, *H4(asym)´*), 8.69 (d, $^{4}J_{H,H}$ = 1.9 Hz, 1H, *H3(asym)* / H3(asym)´´**), 8.62 (d, $^{4}J_{H,H}$ = 1.1 Hz, 2H, *H3(sym) / H3(sym)´´*), 7.90 (d, $^{3}J_{H,H}$ = 8.4 Hz, 2H, *H phenyl(push)*), 7.84 (d, $^{3}J_{H,H}$ = 8.5 Hz, 2H, *H phenyl(push)*), 7.69 (d, $^{3}J_{H,H}$ = 9.1 Hz, 2H, *H phenyl(pull)*), 7.60 (d, $^{3}J_{H,H}$ = 8.5 Hz, 4H, *H phenyl(sym)*), 7.48 (d, $^{3}J_{H,H}$ = 8.5 Hz, 4H, *H phenyl(sym)*), 7.37 (dd, $^{3}J_{H,H}$ = 6.0 Hz, $^{4}J_{H,H}$ = 2.0 Hz, 1H, *H5(asym)* / H5(asym)´´**), 7.28 (dd, $^{3}J_{H,H}$ = 6.1 Hz, $^{4}J_{H,H}$ = 2.0 Hz, 1H, *H5(asym)* / H5(asym)´´**), 7.17 (dd, $^{3}J_{H,H}$ = 5.9 Hz, $^{4}J_{H,H}$ = 1.7 Hz, 2H, *H5(sym) / H5(sym)´´*), 7.12 (app. d, $^{3}J_{H,H}$ = 6.0 Hz, 3H, *H6(sym) / H6(sym)´´ / H6(asym)* or H6(asym)´´**), 6.89 (d, $^{3}J_{H,H}$ = 6.1 Hz, 1H, *H6(asym)* / H6(asym)´´**), 6.80 (d, $^{3}J_{H,H}$ = 9.1 Hz, 2H, *H phenyl(pull)*), 3.01 (s, 6H, *H methyl(NMe2)*), 2.41 (s, 6H, *H methyl(SAc)*).

^{13}C-NMR (101 MHz, CD_3CN, ppm, 25 °C): δ_C = 193.98 ($C_{C=O}$, 2C), 161.50 (C_q, 1C), 160.92 (C_q, 2C), 160.87 (C_q, 1C), 159.45 (C_q, 1C), 159.05 (C_q, 2C), 158.44 (C_q, 1C), 154.49 (C_t, 1C), 154.02 (C_t, 2C), 153.42 (C_q, 1C), 153.28 (C_t, 1C), 151.57 (C_q, 1C), 150.08 (C_q, 1C), 140.31 (C_q, 1C), 139.31 (C_t, 1C), 139.01 (C_t, 1C), 135.68 ($C_{phenyl(sym)}$, 4C), 134.08 (C_q, 2C), 133.48 ($C_{phenyl(sym)}$, 4C), 131.89 (C_q, 2C), 129.42 (C_t, 2C), 129.22 ($C_{phenyl(asym)}$, 2C), 129.15 ($C_{phenyl(asym)}$, 2C), 127.21 (app d, ^{3}J = 3.7 Hz, 2C, *C trifluoromethylphenyl*), 126.28 (C_t, 2C), 125.89 (C_t, 1C), 125.14 (C_t, 2C), 124.91 (C_t, 1C), 124.76 (C_t, 2C), 123.60 (C_t, 1C), 122.92 (C_q, 2C), 122.84 (C_t, 1C), 121.83 (C_q, 1C), 120.74 (C_t, 1C), 113.15 ($C_{phenyl(asym)}$, 2C), 97.92 ($C_{acetylene}$, 2C), 87.25 ($C_{acetylene}$, 2C), 40.29 ($C_{methyl(NMe2)}$, 2C), 30.66 ($C_{methyl(SAc)}$, 2C). In the ^{13}C-spectrum two signals less than expected were found probably due to coincident signals and to the fact that the CF_3-group cannot be seen properly.

^{19}F-NMR (376 MHz, CD_3CN, ppm, 25 °C): δ_F = -63.36 (s, 3F, C**F$_3$**), -72.87 (d, $^{1}J_{P,F}$ = 706.6 Hz, 12F, ***PF$_6$***).

^{31}P-NMR (162 MHz, CD_3CN, ppm, 25 °C): δ_P = -144.61 (hept, $^{1}J_{P,F}$ = 706.5 Hz, 2P, ***P***F_6).

ESI-MS (MeCN, *positive* ion mode): *m/z* [ion, intensity (%)] = 566.9 (M^{2+}-2PF_6^-, 100).
ESI-MSMS (MeCN, *positive* ion mode (MSMS of *m/z = 567.3*): *m/z* [ion, intensity (%)] = 525.3 (M^{2+}-2((C=O)CH_3), 65), 546.3 (M^{2+}-((C=O)CH_3), 100), 567.3 (M^{2+}, 60).
HRMS (ESI-ToF): *m/z* calcd. for $[C_{65}H_{46}F_3FeN_7O_2S_2]^{2+}$: 566.6223; found: 566.6233.
UV/VIS (MeCN): λ_{max} (ε) = 271 nm (67035 L·cm^{-1}·mol^{-1}), 344 nm (84165 L·cm^{-1}·mol^{-1}), 391 nm (30595 L·cm^{-1}·mol^{-1}), 573 nm (14470 L·cm^{-1}·mol^{-1}).

Analytical data of 145:

^{1}H-NMR (400 MHz, CD_3CN, ppm, 25 °C): δ_H = 8.94 (d, $^3J_{H,H}$ = 8.1 Hz, 4H, *H3´ / H5´*), 8.74 (t, $^3J_{H,H}$ = 8.0 Hz, 1H, *H4´*), 8.61 (d, $^4J_{H,H}$ = 1.0 Hz, 2H, *H3 / H3´*), 7.61 (d, $^3J_{H,H}$ = 8.5 Hz, 8H, H_{phenyl}), 7.49 (d, $^3J_{H,H}$ = 8.5 Hz, 8H, H_{phenyl}), 7.17 (dd, $^3J_{H,H}$ = 5.9 Hz, $^4J_{H,H}$ = 1.5 Hz, 4H, *H5 / H5´*), 7.05 (d, $^3J_{H,H}$ = 5.9 Hz, 4H, *H6 / H6´*), 2.41 (s, 12H, H_{methyl}).
^{13}C-NMR (101 MHz, CD_3CN, ppm, 25 °C): δ_C = 193.97 ($C_{C=O}$, 4C), 160.74 (C_q, 4C), 158.86 (C_q, 4C), 154.27 (C_t, 4C), 139.51 (C_t, 2C), 135.69 (C_{phenyl}, 8C), 134.29 (C_q, 4C), 133.50 (C_{phenyl}, 8C), 131.94 (C_q, 4C), 129.52 (C_t, 4C), 126.41 (C_t, 4C), 125.22 (C_t, 4C), 122.89 (C_q, 4C), 98.04 ($C_{acetylene}$, 4C), 87.19 ($C_{acetylene}$, 4C), 30.66 (C_{methyl}, 4C).
^{19}F-NMR (376 MHz, CD_3CN, ppm, 25 °C): δ_F = -72.87 (d, $^1J_{P,F}$ = 706.7 Hz, 12F, ***PF_6***).
^{31}P-NMR (162 MHz, CD_3CN, ppm, 25 °C): δ_P = -144.62 (hept, $^1J_{P,F}$ = 706.4 Hz, 2P, ***PF_6***).
ESI-MS (MeCN, *positive* ion mode): *m/z* [ion, intensity (%)] = 609.4 (M^{2+}-2PF_6^-, 100).
ESI-MSMS (MeCN, *positive* ion mode (MSMS of *m/z = 609.4*): *m/z* [ion, intensity (%)] = 525.4 (M^{2+}-4((C=O)CH_3), 50), 546.3 (M^{2+}-3((C=O)CH_3), 70), 567.3 (M^{2+}-2((C=O)CH_3), 75), 588.4 (M^{2+}-((C=O)CH_3), 100), 609.8 (M^{2+}, 20).
HRMS (ESI-ToF): *m/z* calcd. for $[C_{70}H_{46}FeN_6O_4S_4]^{2+}$: 609.0902; found: 609.0908.
UV/VIS (MeCN): λ_{max} (ε) = 274 nm (76740 L·cm^{-1}·mol^{-1}), 345 nm (129560 L·cm^{-1}·mol^{-1}), 386 nm (23653 L·cm^{-1}·mol^{-1}), 572 nm (15347 L·cm^{-1}·mol^{-1}), 633 nm (8573 L·cm^{-1}·mol^{-1}).

{[Ru(*131*)(*147*)]$^{2+}$[(PF$_6$)$^-$]$_2$} (127)

127 was prepared following two different routes. **Route A** utilizes a literature-known[539–542] step-by-step introduction of the terpyridine ligands to the Ru(III) source via the intermediate product **{[Ru(*147*)]$^{3+}$[Cl$^-$]$_3$} (204)** followed by an in-situ reduction of this intermediate to Ru(II) to yield the desired heteroleptic Ru(II)-bis-terpyridine complex **127**. **Route B** is inspired by adapting a literature-reported procedure[539] according to the representative procedure C used for the Fe(II) complexes throughout this work. Instead of the step-by-step introduction of the ligands in this case a statistic reaction had to be performed in which an equimolar amount of the terpyridine precursors **131** and **147** was used to form a statistical mixture including the complexes **127**, **205** and **206**.

Route A:

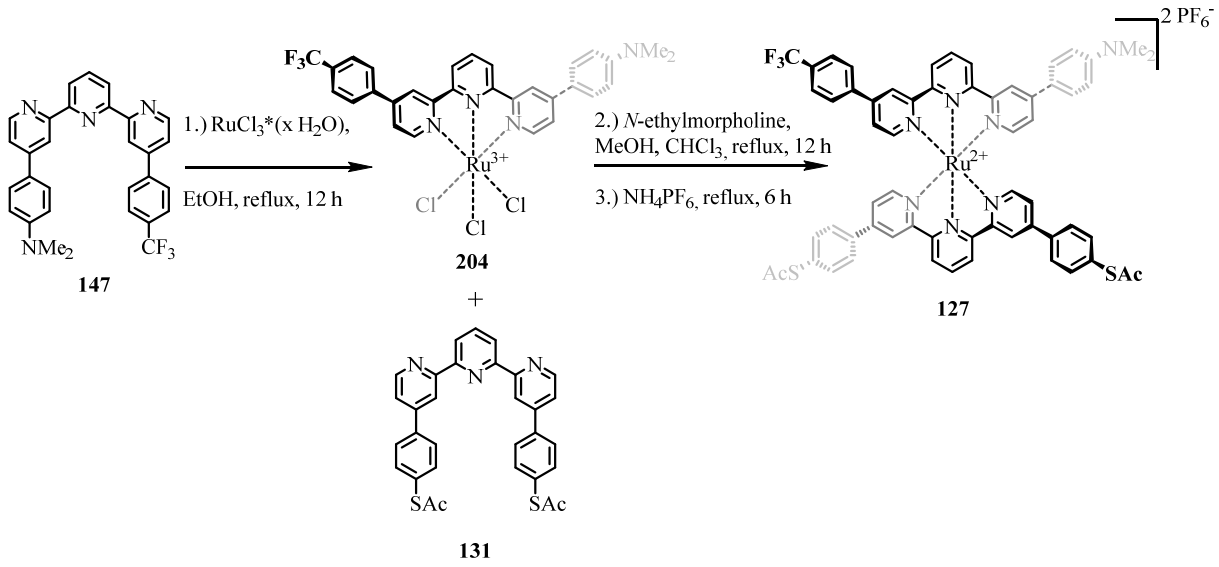

To prepare the desired target compound **127** first of all the intermediate Ru(III)-monoterpyridine complex **{[Ru(*147*)]$^{3+}$[Cl$^-$]$_3$} (204)** had to be prepared. This was achieved by suspending the corresponding terpyridine ligand *N,N*-dimethyl-4-(4′′-(4-(trifluoromethyl)-phenyl)-[2,2′:6′,2′′-terpyridin]-4-yl)aniline (**147**) (49.7 mg, 100 µmol, 1.00 eq.) and $RuCl_3$ (23.9 mg, 115 µmol, 1.15 eq.) in EtOH (10 mL) and refluxing the mixture for 12 h. After cooling down to room temperature the reaction mixture was filtered over a frit (porosity grade 4) and washed with cold EtOH before being dried in vacuo and used for the next step without further purification. In the following reaction step the isolated crude intermediate **204** (35.2 mg, 50.0 µmol, 1.00 eq.) was mixed with an excess of *S,S′*-([2,2′:6′,2′′-terpy-ridine]-4,4′′-diylbis(4,1-phenylene)) diethanethioate (**131**) (53.4 mg, 100 µmol, 2.00 eq.) and

suspended in MeOH (20 mL) and $CHCl_3$ (20 mL) before *N*-ethylmorpholine (297 mg, 330 µl, 2.50 mmol, 50.0 eq.) was added and the whole mixture was refluxed for 12 h. Subsequently NH_4PF_6 (81.5 mg, 0.50 mmol, 10.0 eq.) dissolved in water (20 mL) was added for the final anion exchange. After removal of the organic solvents under reduced pressure the precipitated solid was filtered from the aqueous phase, washed with more water, dissolved in MeCN, dried over $MgSO_4$, filtered and finally the remaining organic solvents were removed in vacuo prior to drying of the crude product in high vacuum. Since the crude product contained unreduced Ru(III) species and some homoleptic side products the desired heteroleptic target complex **127** was obtained by purification of the crude mixture via preparative reversed-phase HPLC using a solvent gradient ranging from H_2O / MeCN (50:50) up to H_2O / MeCN (5:95) at a flow rate of 20 mL/min yielding the product **127** as a deep red solid in a yield of 30% (21.0 mg, 15.0 µmol). The analytical data basically equal the ones obtained by the preparation of complex **127** via route B. Thus the data will be listed after the description of preparative **route B** below.

Route B:

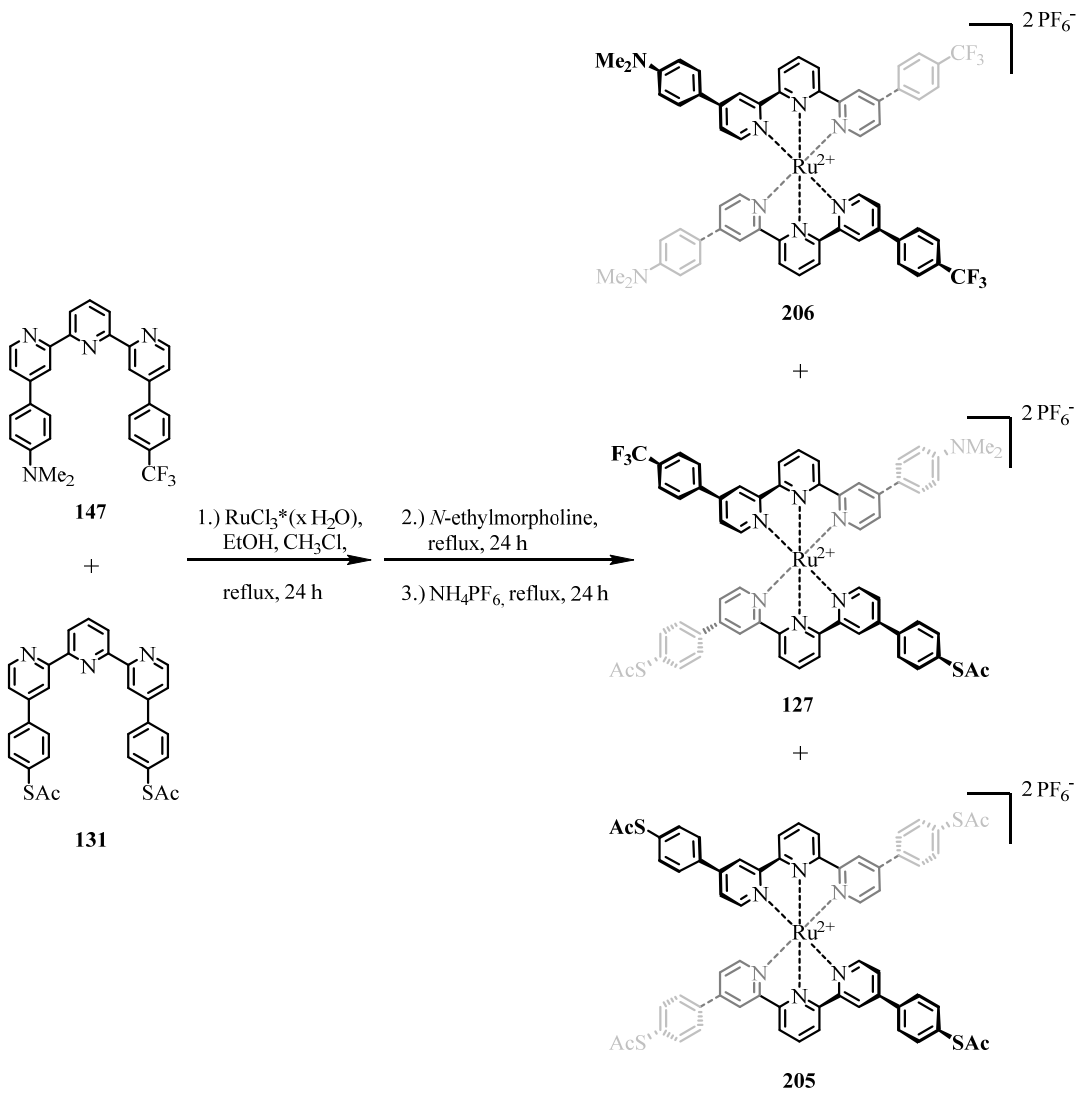

On this route **127** was prepared by adapting a literature known procedure[539] to representative procedure C. Instead of the step-by-step introduction of the ligands which turned out to be troublesome due to solubility issues in this case a statistic reaction was performed in which an equimolar amount of the terpyridine precursors was used avoiding the otherwise used excess of one ligand to favor the complexation. Thus *S,S´*-([2,2´:6´,2´´-terpyridine]-4,4´´-diylbis(4,1-phenylene)) diethanethioate (**131**) (40.0 mg, 75.0 µmol, 1.00 eq.) and *N,N*-dimethyl-4-(4´´-(4-(trifluoromethyl)phenyl)-[2,2´:6´,2´´-terpyridin]-4-yl)aniline (**147**) (37.2 mg, 75.0 µmol, 1.00 eq.) were dissolved in EtOH (100 mL) and $CHCl_3$ (100 mL) before $RuCl_3$ (17.9 mg, 86.3 µmol, 1.15 eq.) was added and the mixture was refluxed for 24 h After *N*-ethyl-morpholine (445 mg, 495 µl, 3.75 mmol, 50.0 eq.) has been added the mixture was refluxed for additional 24 h. Subsequently NH_4PF_6 (611 mg, 3.75 mmol, 50.0 eq.) dissolved in water (100 mL) was added for the final anion exchange and the mixture was refluxed for another

24 h. After workup according to the general procedure C the brownish-red crude product was yielded which turned out to be a statistical mixture of the three complexes **127**, **205** and **206** as it was expected. To obtain the desired heteroleptic target complex **127** the crude mixture was subjected to purification by preparative reversed-phase HPLC using a solvent gradient ranging from H_2O / MeCN (50:50) up to H_2O / MeCN (5:95) at a flow rate of 20 mL/min yielding the product **127** as a deep red solid in a yield of 16% (16.6 mg, 12.0 µmol). The two expected homoleptic side products **205** and **206** could be separated successfully from the desired heteroleptic target structure.

Analytical data of 127:

^{1}H-NMR (400 MHz, CD_3CN, ppm, 25 °C): δ_H = 8.95 (app. dd, $^{3}J_{H,H}$ = 8.1 Hz, $^{3}J_{H,H}$ = 3.5 Hz, 4H, *H3´ / H5´*), 8.80 (app. d, 3H, *H3$_{(sym)}$ / H3$_{(sym)}$´´ / H3$_{(asym)}$* or H3$_{(asym)}$´´**), 8.70 (d, $^{4}J_{H,H}$ = 2.0 Hz, 1H, *H3$_{(asym)}$* / H3$_{(asym)}$´´**), 8.49 (t, $^{3}J_{H,H}$ = 8.1 Hz, 1H, *H4´**), 8.49 (t, $^{3}J_{H,H}$ = 8.1 Hz, 1H, *H4´**), 7.94 (d, $^{3}J_{H,H}$ = 8.3 Hz, 2H, *H$_{phenyl(push)}$*), 7.85 (d, $^{3}J_{H,H}$ = 8.2 Hz, 2H, *H$_{phenyl(push)}$*), 7.83 (d, $^{3}J_{H,H}$ = 8.5 Hz, 4H, *H$_{phenyl(sym)}$*), 7.72 (d, $^{3}J_{H,H}$ = 9.1 Hz, 2H, *H$_{phenyl(pull)}$*), 7.58 (d, $^{3}J_{H,H}$ = 8.6 Hz, 4H, *H$_{phenyl(sym)}$*), 7.50 - 7.42 (m, 6H, *H5$_{(sym)}$ / H5$_{(sym)}$´´ / H6$_{(sym)}$ / H6$_{(sym)}$´´ / H5$_{(asym)}$* or H5$_{(sym)}$´´* / H6$_{(asym)}$* / H6$_{(asym)}$´´**), 7.37 (dd, $^{3}J_{H,H}$ = 6.1 Hz, $^{4}J_{H,H}$ = 2.1 Hz, 1H, *H5$_{(asym)}$* or H5$_{(asym)}$´´**), 7.23 (d, $^{3}J_{H,H}$ = 6.1 Hz, 1H, *H6$_{(asym)}$* or H6$_{(asym)}$´´**), 6.81 (d, $^{3}J_{H,H}$ = 9.1 Hz, 2H, *H$_{phenyl(pull)}$*), 3.01 (s, 6H, *H$_{methyl(NMe2)}$*), 2.42 (s, 6H, *H$_{methyl(SAc)}$*).

^{13}C-NMR (101 MHz, CD_3CN, ppm, 25 °C): δ_C = 194.26 ($C_{C=O}$, 2C), 159.77 (C_q, 1C), 159.57 (C_q, 2C), 158.88 (C_q, 1C), 157.05 (C_q, 1C), 156.80 (C_q, 1C), 156.52 (C_q, 2C), 156.26 (C_q, 1C), 153.64 (C_t, 1C), 153.40 (C_t, 2C), 152.68 (C_t, 1C), 152.59 (C_q, 1C), 150.80 (C_q, 1C), 149.81 (C_q, 2C), 149.16 (C_q, 1C), 137.44 (C_q, 2C), 136.85 (C_t, 1C), 136.71 (C_t, 1C), 136.21 ($C_{phenyl(sym)}$, 4C), 132.07 (C_q, 2C), 129.98 (C_q, 1C), 129.28 ($C_{phenyl(asym)}$, 2C), 129.23 ($C_{phenyl(asym)}$, 2C), 129.13 ($C_{phenyl(sym)}$, 4C), 127.19 (app d, ^{3}J = 3.5 Hz, 2C, *C$_{trifluoromethylphenyl}$*), 126.01 (C_t, 1C), 125.86 (C_t, 2C), 125.10 (C_t, 2C), 125.03 (C_t, 1C), 124.97 (C_t, 1C), 124.87 (C_t, 1C), 123.42 (C_t, 2C), 123.24 (C_t, 2C), 122.03 (C_q, 1C), 121.18 (C_t, 1C), 113.18 ($C_{phenyl(asym)}$, 2C), 40.31 ($C_{methyl(NMe2)}$, 2C), 30.67 ($C_{methyl(SAc)}$, 2C). In the ^{13}C-spectrum one signal less than expected was found probably due to the fact that the CF_3-group cannot be seen.

^{19}F-NMR (376 MHz, CD_3CN, ppm, 25 °C): δ_F = -63.34 (s, 3F, C**F$_3$**), -72.88 (d, $^{1}J_{P,F}$ = 706.5 Hz, 12F, *P**F$_6$***).

^{31}P-NMR (162 MHz, CD_3CN, ppm, 25 °C): δ_P = -144.62 (hept, $^1J_{P,F}$ = 706.5 Hz, 2P, ***P**F*$_6$).
ESI-MS (MeCN, *positive* ion mode): *m/z* [ion, intensity (%)] = 565.8 (M^{2+}-2PF_6^-, 100).
ESI-MSMS (MeCN, *positive* ion mode (MSMS of *m/z = 565.8*): *m/z* [ion, intensity (%)] = 523.7 (M^{2+}-2((C=O)CH_3), 100), 544.8 (M^{2+}-((C=O)CH_3), 90), 565.8 (M^{2+}, 25).
HRMS (ESI-ToF): *m/z* calcd. for $[C_{61}H_{46}F_3N_7O_2RuS_2]^{2+}$: 565.6077; found: 565.6083.
UV/VIS (MeCN): λ_{max} (ε) = 270 nm (70413 $L \cdot cm^{-1} \cdot mol^{-1}$), 329 nm (103893 $L \cdot cm^{-1} \cdot mol^{-1}$), 363 nm (38313 $L \cdot cm^{-1} \cdot mol^{-1}$), 490 nm (27993 $L \cdot cm^{-1} \cdot mol^{-1}$).

4-phenyl-4´´-(4-((2-(trimethylsilyl)ethyl)thio)phenyl)-2,2´:6´,2´´-terpyridine (211)

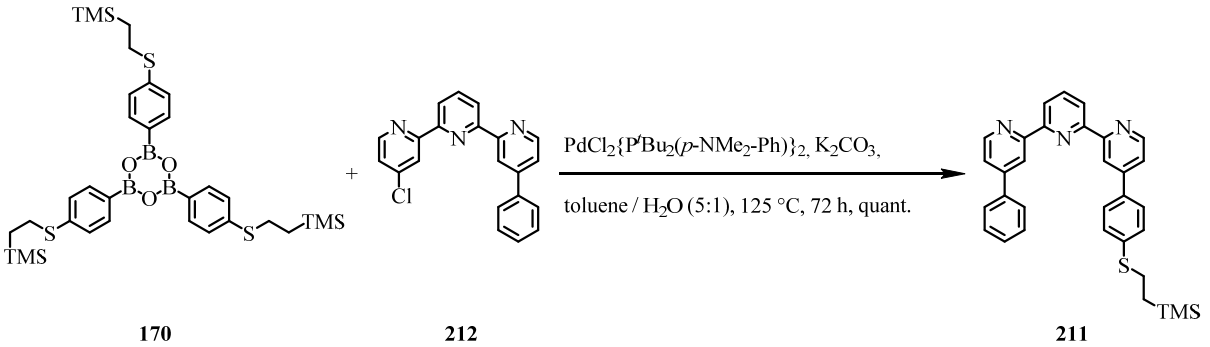

170 **212** **211**

Compound **211** was prepared according to general procedure B described above. 4-chloro-4´´-phenyl-2,2´:6´,2´´-terpyridine **212** (34.4 mg, 100 µmol, 1.00 eq.), 2,4,6-Tris(4-(2-(trimethylsilyl)ethyl)thiophenyl)-1,3,5,2,4,6-trioxatriborinane (**170**) (142 mg, 0.20 mmol, 2.00 eq.) as the borylation agent, $PdCl_2\{P^tBu_2(p\text{-}NMe_2\text{-}Ph)\}_2$ (7.08 mg, 10.0 µmol, 0.10 eq.) and K_2CO_3 (83.8 mg, 600 µmol, 6.00 eq.) were charged into a Schlenk tube under inert atmosphere. All reagents were mixed and suspended in previously degassed toluene (25 mL) and H_2O (5 mL). The reaction vessel was sealed and heated up 125 °C for 72 h. After completion the reaction mixture was allowed to cool down to room temperature and was subsequently diluted with DCM, brine and water. Now the reaction mixture was extracted with DCM (5 *x*). The organic phases were combined, dried over $MgSO_4$, filtered and residual solvent was evaporated under reduced pressure. The crude product was purified by FCC using a gradient of solvents ranging from EtOAc / *n*-hexane (1:3) up to EtOAc / *n*-hexane (1:1) to afford the desired asymmetric product 4-phenyl-4´´-(4-((2-(trimethylsilyl)ethyl)thio)phenyl)-2,2´:6´,2´´-terpyridine (**211**) in quantitative yield (52.0 g, 100 µmol).

Analytical data 211:

^{1}H-NMR (400 MHz, $CDCl_3$, ppm, 25 °C): δ_H = 8.89 (d, $^4J_{H,H}$ = 1.1 Hz, 1H, *H3* / H3´´**), 8.87 (d, $^4J_{H,H}$ = 1.2 Hz, 1H, *H3* / H3´´**), 8.75 (dd, , $^3J_{H,H}$ = 5.1 Hz, $^5J_{H,H}$ = 0.4 Hz, 1H, *H6* / H6´´**), 8.73 (dd, , $^3J_{H,H}$ = 5.1 Hz, $^5J_{H,H}$ = 0.5 Hz, 1H, *H6* / H6´´**), 8.50 (dd, $^3J_{H,H}$ = 7.7 Hz, $^4J_{H,H}$ = 1.0 Hz, 2H, *H3´ / H5´*), 8.00 (t, $^3J_{H,H}$ = 7.8 Hz, 1H, *H4´*), 7.80 (d, $^3J_{H,H}$ = 8.4 Hz, 2H, H_{phenyl}), 7.72 (d, $^3J_{H,H}$ = 8.4 Hz, 2H, H_{phenyl}), 7.57 (dd, $^3J_{H,H}$ = 5.1 Hz, $^4J_{H,H}$ = 1.8 Hz, 1H, *H5* / H5´´**), 7.56 – 7.45 (m, 4H *H5* / H5´´* / 3*H_{phenyl}), 7.41 (d, $^3J_{H,H}$ = 8.4 Hz, 2H, H_{phenyl}), 3.13 – 2.93 (m, 2H, *–S–**CH$_2$**–CH$_2$–TMS*), 1.07 - 0.91 (m, 2H, *-S-CH$_2$-**CH$_2$**–TMS*), 0.08 (s, 9H, $H_{methyl\ (TMS)}$).

^{13}C-NMR (101 MHz, $CDCl_3$, ppm, 25 °C): δ_C = 156.90 (C_q, 1C), 156.88 (C_q, 1C), 155.48 (C_q, 1C), 155.46 (C_q, 1C), 149.79 (C_t, 1C), 149.77 (C_t, 1C), 149.28 (C_q, 1C), 148.54 (C_q, 1C), 139.40 (C_q, 1C), 138.66 (C_q, 1C), 138.10 (C_t, 1C), 135.46 (C_q, 1C), 129.24 (C_{phenyl}, 3C), 128.72 (C_{phenyl}, 2C), 127.49 (C_{phenyl}, 2C), 127.24 (C_{phenyl}, 2C), 121.79 (C_t, 1C), 121.44 (C_t, 1C), 121.43 (C_t, 1C), 121.31 (C_t, 1C), 119.34 (C_t, 1C), 118.87 (C_t, 1C), 29.20 (C_{ethyl}, 1C), 16.86 (C_{ethyl}, 1C), -1.59 (C_{TMS}, 3C).

ESI-MS (MeOH, *positive* ion mode): *m/z* [ion, intensity (%)] = 518.3 ($M+H^+$, 100), 259.6 ($M+2H^+$, 15).

HRMS (ESI-ToF): *m/z* calcd. for $[C_{32}H_{31}N_3SSi+H]^+$: 518.2081; found: 518.2087.

_S_-(4-(4′′-phenyl-[2,2′:6′,2′′-terpyridin]-4-yl)phenyl) ethanethioate (210)

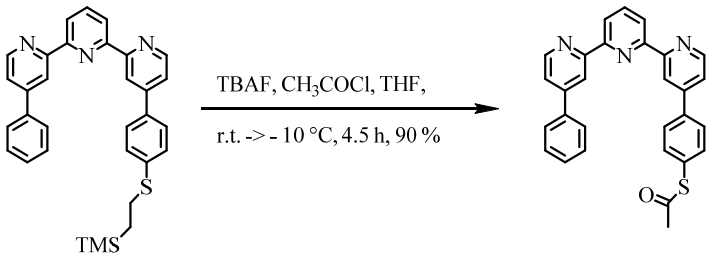

The acetyl-protected thiol **210** was prepared by transprotection of the ethyl-TMS-protected thiol 4-phenyl-4′′-(4-((2-(trimethylsilyl)ethyl)thio)phenyl)-2,2′:6′,2′′-terpyridine (**211**). An oven-dried round-bottom flask was charged with terpyridine precursor **211** (104 mg, 0.20 mmol, 1.00 eq.) and put under inert atmosphere. Subsequently **211** was dissolved in rigorously degassed THF (30 mL), before TBAF (1M in THF, 2.50 mL, 2.50 mmol, 12.5 eq.) was added which caused the former pale yellow solution to turn bright orange immediately. After 1.5 h the reaction was cooled down to -10 °C and previously degassed acetyl chloride (3.97 g, 3.60 mL, 50.0 mmol, 250 eq.) was added dropwise to the orange solution which subsequently turned colorless again followed by a bright yellow color. After further 2 h in the cooling bath the reaction was cautiously quenched by the addition of saturated $NaHCO_3$ -solution. Due to the base-lability of the acetyl protection group the reaction mixture was extracted quickly first with DCM (3 *x*) and then with EtOAc (1 *x*), before the combined organic phases were dried over $MgSO_4$, filtered and concentrated under reduced pressure. Finally the resulting crude product was further purified by FCC using a gradient ranging from EtOAc / *n*-hexane (1:1) to pure EtOAc to yield the desired disubstituted, poorly soluble product *S*-(4-(4′′-phenyl-[2,2′:6′,2′′-terpyridin]-4-yl)phenyl) ethanethioate **210** in a very good yield of 90% (92.8 mg, 179 µmol).

Analytical data 210:

^{1}H-NMR (500 MHz, $CDCl_3$, ppm, 25 °C): δ_H = 8.86 (dd, $^4J_{H,H}$ = 1.8 Hz, $^5J_{H,H}$ = 0.6 Hz, 1H, *H3* / H3′′**), 8.86 (dd, $^4J_{H,H}$ = 1.9 Hz, $^5J_{H,H}$ = 0.7 Hz, 1H, *H3* / H3′′**), 8.76 (dd, $^3J_{H,H}$ = 5.2 Hz, $^5J_{H,H}$ = 0.8 Hz, 1H, *H6* / H6′′**), 8.75 (dd, , $^3J_{H,H}$ = 5.2 Hz, $^5J_{H,H}$ = 0.6 Hz, 1H, *H6* / H6′′**), 8.50 (dd, $^3J_{H,H}$ = 7.8 Hz, $^4J_{H,H}$ = 1.6 Hz, 2H, *H3′ / H5′*), 8.00 (t, $^3J_{H,H}$ = 7.8 Hz, 1H, *H4′*), 7.81 (d, $^3J_{H,H}$ = 8.5 Hz, 2H, H_{phenyl}), 7.78 (d, $^3J_{H,H}$ = 8.1 Hz, 2H, H_{phenyl}), 7.55 (d, $^3J_{H,H}$ = 8.5 Hz, 2H, H_{phenyl}), 7.60 – 7.43 (m, 5H *H5* / H5′′* / 3*H_{phenyl}), 2.47 (s, 3H, H_{methyl}).

^{13}C-NMR (126 MHz, $CDCl_3$, ppm, 25 °C): δ_C = 193.65 ($C_{(C=O)}$, 1C), 157.08 (C_q, 1C), 156.86 (C_q, 1C), 155.60 (C_q, 1C), 155.37 (C_q, 1C), 149.91 (C_t, 1C), 149.79 (C_t, 1C), 149.33 (C_q, 1C), 148.25 (C_q, 1C), 139.72 (C_q, 1C), 138.62 (C_q, 1C), 138.13 (C_t, 1C), 135.12 (C_{phenyl}, 2C), 129.28 (C_{phenyl}, 2C), 129.26 (C_t, 1C), 129.13 (C_q, 1C), 127.98 (C_{phenyl}, 2C), 127.23 (C_{phenyl}, 2C), 121.84 (C_t, 1C), 121.75 (C_t, 1C), 121.55 (C_t, 1C), 121.46 (C_t, 1C), 119.35 (C_t, 1C), 119.30 (C_t, 1C), 30.48 (C_{methyl}, 1C).

ESI-MS (MeOH, *positive* ion mode): *m/z* [ion, intensity (%)] = 460.2 ($M+H^+$, 100), 482.2 ($M+Na^+$, 45), 941.3 ($2M+Na^+$).

HRMS (ESI-ToF): *m/z* calcd. for $[C_{29}H_{21}N_3OS+Na]^+$: 482.1298; found: 482.1298, *m/z* calcd. for $[C_{58}H_{42}N_6O_2S_2+Na]^+$: 941.2703; found: 941.2703.

{[Fe(*210*)$_2$]$^{2+}$[(PF$_6$)$^-$]$_2$} (208)

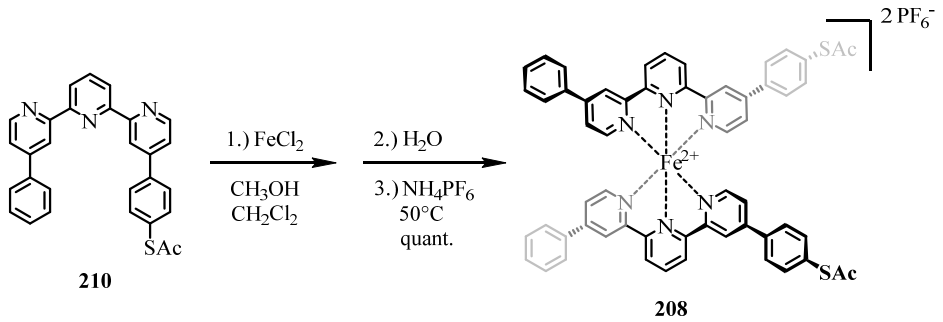

208 was prepared after the representative procedure C. $FeCl_2$ (2.92 mg, 23.0 µmol, 1.00 eq.), *S*-(4-(4′′-phenyl-[2,2′:6′,2′′-terpyridin]-4-yl)phenyl) ethanethioate (**210**) (21.1 mg, 46.0 µmol, 2.00 eq.), MeOH (10 mL), DCM (10 mL), water (90 mL), and NH_4PF_6 (187 mg, 1.15 mmol, 50.0 eq.) were used. The desired product **208** was isolated as a dark purple solid in quantitative yield (29.2 mg, 23.0 µmol).

Analytical data of 208:

^{1}H-NMR (500 MHz, CD_3CN, ppm, 25 °C): δ_H = 9.12 (d, $^3J_{H,H}$ = 8.1 Hz, 4H, *H3′ / H5′*), 8.81 (d, $^4J_{H,H}$ = 1.6 Hz, 2H, *H3* / H3′′**), 8.80 (d, $^4J_{H,H}$ = 1.9 Hz, 2H, *H3* / H3′′**), 8.77 (app. d, $^3J_{H,H}$ = 8.0 Hz, 2H, *H4′*), 7.79 (d, $^3J_{H,H}$ = 8.6 Hz, 4H, *H$_{thioacetylphenyl}$)*, 7.74 (dd, $^3J_{H,H}$ = 7.7 Hz, $^4J_{H,H}$ = 1.9 Hz, 4H, *H$_{phenyl}$)*, 7.55 (d, $^3J_{H,H}$ = 8.6 Hz, 4H, *H$_{thioacetylphenyl}$)*, 7.53 – 7.50 (m, 6H, *H$_{phenyl}$*), 7.38 (app. td, $^3J_{H,H}$ = 5.8 Hz, $^4J_{H,H}$ = 1.9 Hz, 4H, *H5 / H5′′)*, 7.19 (d, $^3J_{H,H}$ = 6.0 Hz, 2H, *H6* / H6′′*)*, 7.16 (d, $^3J_{H,H}$ = 6.0 Hz, 2H, *H6* / H6′′*)*, 2.41 (s, 6H, *H$_{methyl}$)*.

^{13}C-NMR (126 MHz, CD_3CN, ppm, 25 °C): δ_C = 194.20 ($C_{C=O}$, 2C), 161.35 (C_q, 2C), 161.25 (C_q, 2C), 159.39 (C_q, 2C), 159.22 (C_q, 2C), 154.15 (C_t, 2C), 153.99 (C_t, 2C), 151.71 (C_q, 2C), 150.59 (C_q, 2C), 139.05 (C_t, 2C), 137.26 (C_q, 2C), 136.27 (C_q, 2C), 136.17 (C_{phenyl}, 4C), 132.08 (C_q, 2C), 131.63 (C_q, 2C), 130.40 (C_{phenyl}, 4C), 129.05 (C_{phenyl}, 4C), 128.32 (C_{phenyl}, 4C), 125.70 (C_t, 2C), 125.69 (C_t, 2C), 125.02 (C_t, 2C), 122.66 (C_t, 2C), 122.56 (C_t, 2C), 30.64 ($C_{methyl(SAc)}$, 2C).). In the ^{13}C-spectrum and in the DEPT-135 one signal less than expected was found probably due to coincident signals. However the assignment of the listed NMR-signals was done by correlating appropriate 2D-NMR data like, ^{1}H,^{1}H-COSY, ^{1}H,^{13}C-HMQC and ^{1}H,^{13}C-HMBC.

ESI-MS (MeCN, *positive* ion mode): *m/z* [ion, intensity (%)] = 487.0 (M^{2+}-2PF_6^-, 100).

ESI-MSMS (MeCN, *positive* ion mode (MSMS of *m/z* = 487.0): *m/z* [ion, intensity (%)] = 445.0 (M^{2+}-2((C=O)CH_3), 100), 465.9 (M^{2+}-((C=O)CH_3), 65), 487.0 (M^{2+}, 35).
HRMS (ESI-ToF): *m/z* calcd. for $[C_{58}H_{42}FeN_6O_2S_2]^{2+}$: 487.1075; found: 487.1082.
UV/VIS (MeCN): λ_{max} (ε) = 276 nm (65390 $L \cdot cm^{-1} \cdot mol^{-1}$), 334 nm (80930 $L \cdot cm^{-1} \cdot mol^{-1}$), 377 nm (13605 $L \cdot cm^{-1} \cdot mol^{-1}$), 565 nm (13500 $L \cdot cm^{-1} \cdot mol^{-1}$), 626 nm (5365 $L \cdot cm^{-1} \cdot mol^{-1}$).

{[Ru(*210*)$_2$]$^{2+}$[(PF$_6$)$^-$]$_2$} (209)

209 was prepared by following the literature-inspired[539–542] adaptation of representative procedure C. In this reaction the intermediately formed **{[Ru(*210*)]$^{3+}$[Cl$^-$]$_3$} (214)** is however not isolated but directly converted to the target compound **209** in the following step utilizing a one-pot strategy.

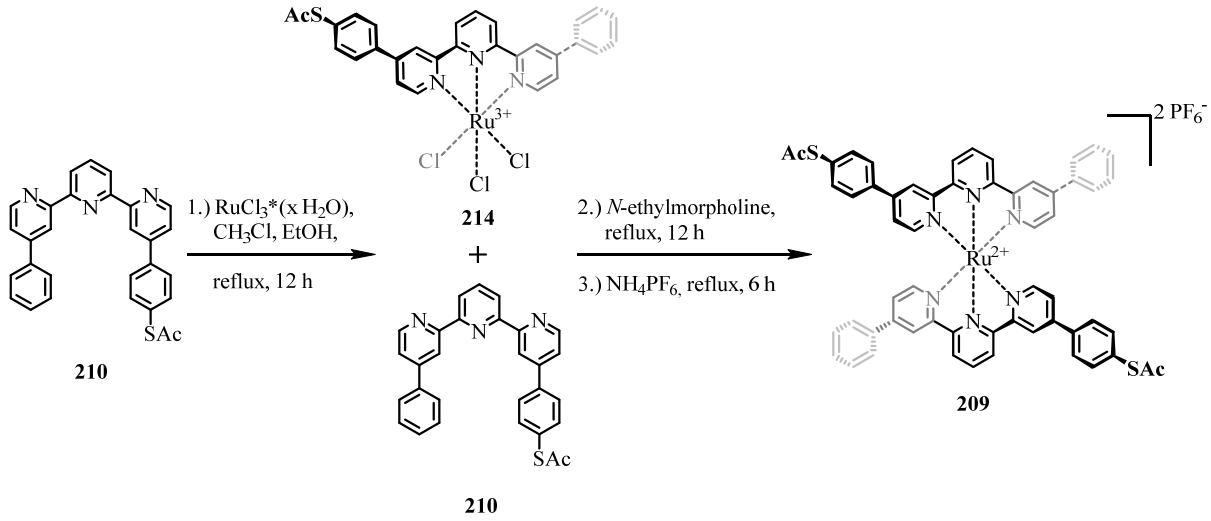

To prepare the desired target compound **209**, $RuCl_3$ (6.22 mg, 30.0 µmol, 1.00 eq.) and *S*-(4-(4′′-phenyl-[2,2′:6′,2′′-terpyridin]-4-yl)phenyl) ethanethioate (**210**) (27.6 mg, 60.0 µmol, 2.00 eq.) were dissolved in a mixture of EtOH (100 mL) and $CHCl_3$ (100 mL) before being refluxed for 12 h. Now *N*-ethylmorpholine (175 mg, 194 µl, 1.50 mmol, 50.0 eq.) was added and the whole mixture was refluxed for further 12 h prior to the addition of NH_4PF_6 (245 mg, 1.50 mmol, 50.0 eq.) dissolved in water (100 mL). After removal of the organic solvents under reduced pressure the precipitated solid was filtered from the aqueous phase, washed with water, dissolved in MeCN, dried over $MgSO_4$, filtered and finally the remaining organic solvents were removed in vacuo prior to drying of the crude product at the high vacuum. Since the crude product still contained unreduced Ru(III) species and unreacted ligand the desired homoleptic target complex **209** was obtained by purification of the crude mixture via preparative reversed-phase HPLC using a solvent gradient ranging from H_2O / MeCN (50:50) up to H_2O / MeCN (5:95) at a flow rate of 20 mL/min yielding the product **209** as a deep red solid in a yield of 18% (5.4 mg, 5.00 µmol).

Analytical data of 209:

^{1}H-NMR (400 MHz, CD_3CN, ppm, 25 °C): δ_H = 8.96 (dd, $^{3}J_{H,H}$ = 8.2 Hz, $^{4}J_{H,H}$ = 1.9 Hz, 4H, *H3´ / H5´*), 8.80 (dd, $^{4}J_{H,H}$ = 1.9 Hz, $^{5}J_{H,H}$ = 0.9 Hz, 2H, *H3* / H3´´**), 8.79 (dd, $^{4}J_{H,H}$ = 2.1 Hz, $^{5}J_{H,H}$ = 0.8 Hz, 2H, *H3* / H3´´**), 8.50 (t, $^{3}J_{H,H}$ = 8.2 Hz, 2H, *H4´*), 7.83 (d, $^{3}J_{H,H}$ = 8.6 Hz, 4H, $H_{thioacetylphenyl}$), 7.78 (dd, $^{3}J_{H,H}$ = 7.7 Hz, $^{3}J_{H,H}$ = 1.9 Hz, 4H, H_{phenyl}), 7.58 (d, $^{3}J_{H,H}$ = 8.6 Hz, 4H, $H_{thioacetylphenyl}$), 7.56 - 7.52 (m, 6H, H_{phenyl}), 7.50 - 7.39 (m, 8H, *H5 / H5´´ / H6 / H6´´*), 2.42 (s, 6H, $H_{methyl(SAc)}$).

^{13}C-NMR (101 MHz, CD_3CN, ppm, 25 °C): δ_C = 194.24 ($C_{C=O}$, 2C), 159.58 (C_q, 2C), 159.44 (C_q, 2C), 156.55 (C_q, 2C), 156.47 (C_q, 2C), 153.49 (C_t, 2C), 153.38 (C_t, 2C), 150.49 (C_q, 2C), 149.86 (C_q, 2C), 137.41 (C_q, 2C), 136.85 (C_t, 2C), 136.42 (C_q, 2C), 136.21 ($C_{thioacetylphenyl}$, 4C), 132.08 (C_q, 2C), 131.61 (C_t, 2C), 130.43 (C_{phenyl}, 4C), 129.13 ($C_{thioacetylphenyl}$, 4C), 128.41 (C_{phenyl}, 4C), 125.84 (C_t, 2C), 125.76 (C_t, 2C), 125.13 (C_t, 2C), 123.27 (C_t, 2C), 123.15 (C_t, 2C), 30.66 ($C_{methyl(SAc)}$, 2C). In the ^{13}C-spectrum and in the DEPT-135 probably due to coincidence one signal less than expected was found.

^{19}F-NMR (376 MHz, CD_3CN, ppm, 25 °C): δ_F = -72.91 (d, $^{1}J_{P,F}$ = 706.6 Hz, 12F, PF_6).

^{31}P-NMR (162 MHz, CD_3CN, ppm, 25 °C): δ_P = -144.62 (hept, $^{1}J_{P,F}$ = 706.4 Hz, 2P, PF_6).

ESI-MS (MeCN, *positive* ion mode): *m/z* [ion, intensity (%)] = 510.1 (M^{2+}-2PF_6^-, 100).

ESI-MSMS (MeCN, *positive* ion mode (MSMS of *m/z = 510.1*): *m/z* [ion, intensity (%)] = 468.1 (M^{2+}-2((C=O)CH_3), 5), 489.1 (M^{2+}-((C=O)CH_3), 65), 510.1 (M^{2+}, 100).

HRMS (ESI-ToF): *m/z* calcd. for $[C_{61}H_{46}F_3N_7O_2RuS_2]^{2+}$: 510.0929; found: 510.0938.

UV/VIS (MeCN): λ_{max} (ε) = 274 nm (72350 L·cm^{-1}·mol^{-1}), 325 nm (90100 L·cm^{-1}·mol^{-1}), 487 nm (15550 L·cm^{-1}·mol^{-1}).

7.2.2 Light Switchable Iron-Terpyridine-Azobenzene Macrocycles

4-Chloro-4´´-(*p*-tolyl)-2,2´:6´,2´´-terpyridine (225)

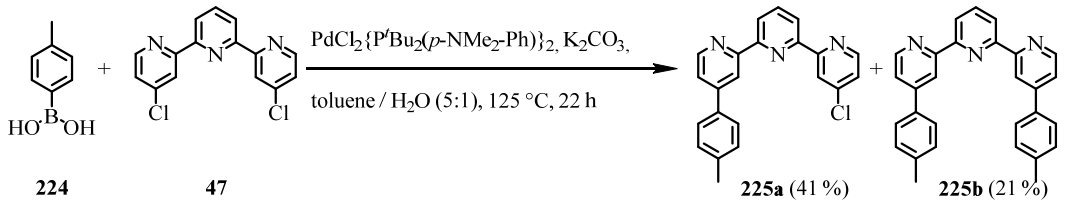

224 **47** **225a** (41 %) **225b** (21 %)

225 was prepared applying the representative procedure B described above. 4,4´´-Dichloro-2,2´:6´2´´-terpyridine (**47**) (151 mg, 0.50 mmol, 1.00 eq.), *p*-tolylboronic acid (56.1 mg, 0.40 mmol, 0.80 eq.), $PdCl_2\{P^tBu_2(p\text{-}NMe_2\text{-}Ph)\}_2$ (17.9 mg, 25.0 µmol, 0.05 eq.) and K_2CO_3 (175 mg, 1.25 mmol, 2.50 eq.) were charged into a Schlenk tube and suspended in degassed toluene (30 mL) and H_2O (6 mL). The reaction vessel was sealed and heated to 125 °C for 22 h. After completion the reaction mixture was allowed to cool down to room temperature and was subsequently diluted with DCM, water and brine. Now the reaction mixture was extracted with DCM (4 *x*) and with EtOAc (1 *x*). The combined organic layers were dried over $MgSO_4$, filtered and residual solvent was removed under reduced pressure. The crude product was purified via FCC using a gradient of solvent mixtures from EtOAc / *n*-hexane (1:3) up to EtOAc / *n*-hexane (1:1). Under these conditions two main products could be isolated. Apart from the undesired disubstituted side product 4,4´´-bis(*p*-tolyl)-2,2´:6´,2´´-terpyridine (**225b**), which was obtained in a yield of 21% (42.4 mg, 103 µmol), mainly the monosubstituted target compound 4-Chloro-4´´-(*p*-tolyl)-2,2´:6´,2´´-terpyridine (**225a**) was isolated in a yield of 41% (72.4 mg, 202 µmol). By applying a solvent diffusion technique using dichloromethane and hexane with an intermediate spacer layer of benzene it was additionally, possible to obtain single crystals of **225b** suitable for x-ray structure determination. The crystallographic information of compound **225b** is however discussed in detailed form in section 9.2. Thus hereafter, only the remaining analytical data of both compounds **225a** and **225b** are listed below.

Analytical data 225a:

^{1}H-NMR (400 MHz, $CDCl_3$, ppm, 25 °C): δ_H = 8.78 (d, $^4J_{H,H}$ = 1.1 Hz, 1H, *H3* / H3´´**), 8.73 (dd, $^3J_{H,H}$ = 5.2 Hz, $^5J_{H,H}$ = 0.6 Hz, 1H, *H6* / H6´´**), 8.61 (d, $^4J_{H,H}$ = 1.8 Hz, 1H, *H3* / H3´´**), 8.59 (d, $^3J_{H,H}$ = 5.2 Hz, 1H, *H6* / H6´´**), 8.53 (dd, $^3J_{H,H}$ = 7.8 Hz,

$^{4}J_{H,H}$ = 0.9 Hz, 1H, *H3´* / H5´**), 8.46 (dd, $^{3}J_{H,H}$ = 7.8 Hz, $^{4}J_{H,H}$ = 1.0 Hz, 1H, *H3´* / H5´**), 7.99 (t, $^{3}J_{H,H}$ = 7.9 Hz, 1H, *H4´*), 7.70 (d, $^{3}J_{H,H}$ = 8.1 Hz, 2H, H_{phenyl}), 7.56 (dd, $^{3}J_{H,H}$ = 5.1 Hz, $^{4}J_{H,H}$ = 1.8 Hz, 1H, *H5* / H5´´**), 7.36 (d, $^{3}J_{H,H}$ = 7.9 Hz, 2H, H_{phenyl}), 7.34 (dd, $^{3}J_{H,H}$ = 5.3 Hz, $^{4}J_{H,H}$ = 2.1 Hz, 1H, *H5* / H5´´**), 2.45 (s, 3H, H_{methyl}).

^{13}C NMR (101 MHz, $CDCl_3$, ppm, 25 °C): δ_C = 157.88 (C_q, 1C), 156.43 (C_q, 1C), 155.65 (C_q, 1C), 154.33 (C_q, 1C), 150.13 (C_t, 1C), 149.72 (C_q, 1C), 149.57 (C_t, 1C), 145.26 (C_q, 1C), 139.45 (C_q, 1C), 138.18 (C_t, 1C), 135.69 (C_t, 1C), 130.05 (C_{phenyl}, 2C), 127.21 (C_{phenyl}, 2C), 124.06 (C_t, 1C), 122.10 (C_t, 1C), 121.89 (C_t, 1C), 121.67 (C_t, 1C), 121.59 (C_t, 1C), 119.13 (C_t, 1C), 21.41 (C_{methyl}, 1C).

ESI-MS (MeOH, *positive* ion mode): *m/z* [ion, intensity (%)] = 358.1 ($M+H^+$, 100), 380.1 ($M+Na^+$, 80).

HRMS (ESI-ToF): *m/z* calcd. for $[C_{22}H_{16}ClN_3+H]^+$: 358.1106; found: 358.1109, *m/z* calcd. for $[C_{22}H_{16}ClN_3+Na]^+$: 380.0925; found: 380.0928, *m/z* calcd. for $[C_{44}H_{32}Cl_2N_6+Na]^+$: 737.1958; found: 737.1961.

Analytical data 225b:

^{1}H-NMR (400 MHz, $CDCl_3$, ppm, 25 °C): δ_H = 8.87 (d, $^{4}J_{H,H}$ = 1.3 Hz, 2H, *H3 / H3´*), 8.74 (dd, $^{3}J_{H,H}$ = 5.1 Hz, $^{5}J_{H,H}$ = 0.4 Hz 2H, *H6 / H6´*), 8.51 (d, $^{3}J_{H,H}$ = 7.8 Hz, 2H, *H3´ / H5´*), 8.01 (t, $^{3}J_{H,H}$ = 7.9 Hz, 1H, *H4´*), 7.71 (d, $^{3}J_{H,H}$ = 8.1 Hz, 4H, H_{phenyl}), 7.58 (dd, $^{3}J_{H,H}$ = 5.1 Hz, $^{4}J_{H,H}$ = 1.9 Hz, 2H, *H5 / H5´*), 7.34 (d, $^{3}J_{H,H}$ = 7.9 Hz, 4H, H_{phenyl}), 2.45 (s, 6H, H_{methyl}).

^{13}C NMR (101 MHz, $CDCl_3$, ppm, 25 °C): δ_C = 156.72 (C_q, 2C), 155.43 (C_q, 2C), 149.57 (C_t, 2C), 149.41 (C_q, 2C), 139.40 (C_q, 2C), 138.14 (C_t, 2C), 135.64 (C_q, 2C), 130.00 (C_{phenyl}, 4C), 127.12 (C_{phenyl}, 4C), 121.61 (C_t, 1C), 121.54 (C_t, 1C), 119.19 (C_t, 1C), 21.44 (C_{methyl}, 2C).

ESI-MS (MeOH, *positive* ion mode): *m/z* [ion, intensity (%)] = 414.3 ($M+H^+$, 100).

HRMS (ESI-ToF): *m/z* calcd. for $[C_{29}H_{23}N_3+H]^+$: 414.1965; found: 414.1967.

4-Phenyl-4′′-(*p*-tolyl)-2,2′:6′,2′′-terpyridine (223)

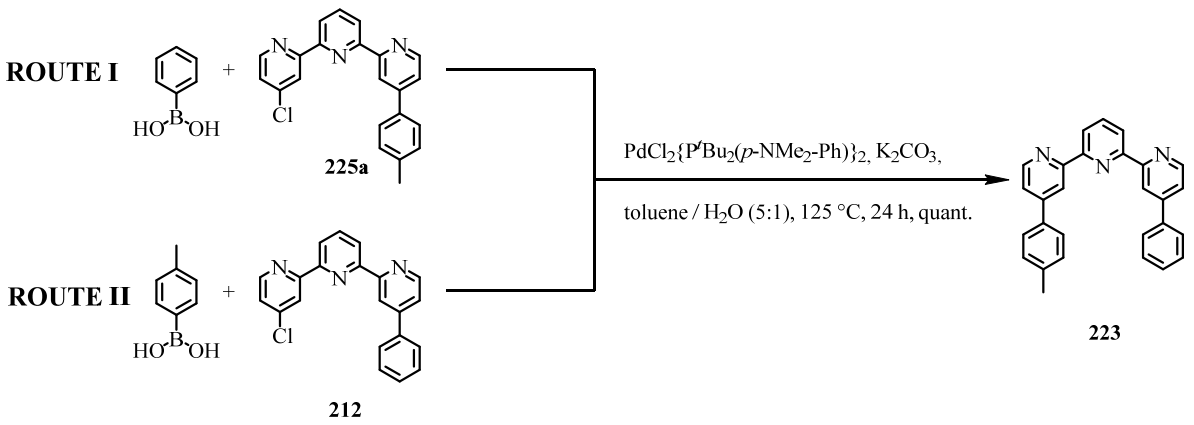

The preparation of **223** was pursued by following two different strategies. On **route I** the target compound 4-Phenyl-4′′-(*p*-tolyl)-2,2′:6′,2′′-terpyridine (**223**) was prepared starting from 4-Chloro-4′′-(*p*-tolyl)-2,2′:6′,2′′-terpyridine (**225a**), whereas on **route II** the target compound **223** was synthesized from 4-chloro-4′′-phenyl-2,2′:6′,2′′-terpyridine (**212**) by applying the representative procedure B in both cases. The different procedures are described below, whereas the analytical results described afterwards.

Route I: 4-Chloro-4′′-(*p*-tolyl)-2,2′:6′,2′′-terpyridine (**225a**) (53.7 mg, 0.15 mmol, 1.00 eq.), phenylboronic acid (189 mg, 1.50 mmol, 10.0 eq.), K_2CO_3 (62.8 mg, 0.45 mmol, 3.00 eq.), and $PdCl_2\{P^tBu_2(p\text{-}NMe_2\text{-}Ph)\}_2$ (5.36 mg, 7.50 µmol, 0.05 eq.) were charged into a Schlenk tube and suspended in degassed toluene (15 mL) and H_2O (3 mL). The reaction vessel was sealed and heated to 125 °C for 24 h. After completion the reaction mixture was allowed to cool down to room temperature and was subsequently diluted with DCM, water and brine. Now the reaction mixture was extracted with DCM (4 *x*) and with EtOAc (1 *x*). The combined organic layers were dried over $MgSO_4$, filtered and residual solvent was removed under reduced pressure. The crude product was purified via FCC using a gradient of solvent mixtures from EtOAc / *n*-hexane (1:3) to EtOAc / *n*-hexane (1:1). Under these conditions the desired target compound 4-Phenyl-4′′-(*p*-tolyl)-2,2′:6′,2′′-terpyridine (**223**) was isolated in quantitative yield (60.1 mg, 0.15 mmol).

Route II: 4-chloro-4′′-phenyl-2,2′:6′,2′′-terpyridine (**212**) (241 mg, 0.70 mmol, 1.00 eq.), *p*-tolylboronic acid (981 mg, 7.00 mmol, 10.0 eq.), K_2CO_3 (293 mg, 2.10 mmol, 3.00 eq.), and $PdCl_2\{P^tBu_2(p\text{-}NMe_2\text{-}Ph)\}_2$ (25.0 mg, 35.0 µmol, 0.05 eq.) were charged into a Schlenk tube and suspended in degassed toluene (15 mL) and H_2O (3 mL). The reaction vessel was

sealed and heated to 125 °C for 24 h. After completion the reaction mixture was allowed to cool down to room temperature and was subsequently diluted with DCM, water and brine. Now the reaction mixture was extracted with DCM (5 *x*) before the combined organic layers were dried over $MgSO_4$, filtered and residual solvent was removed under reduced pressure. The crude product was purified via FCC using a gradient of solvent mixtures ranging from EtOAc / *n*-hexane (1:3) to EtOAc / *n*-hexane (1:1). Under these conditions the desired target compound 4-Phenyl-4´´-(*p*-tolyl)-2,2´:6´,2´´-terpyridine (**223**) was isolated in quantitative yield (280 mg, 0.70 mmol).

Analytical data 223:

^{1}H-NMR (400 MHz, $CDCl_3$, ppm, 25 °C): δ_H = 8.90 (d, $^{4}J_{H,H}$ = 1.2 Hz, 1H, *H3* / H3´´**), 8.88 (d, $^{4}J_{H,H}$ = 1.2 Hz, 1H, *H3* / H3´´**), 8.75 (d, $^{3}J_{H,H}$ = 5.1 Hz, 1H, *H6* / H6´´**), 8.73 (d, $^{3}J_{H,H}$ = 5.1 Hz, 1H, *H6* / H6´´**), 8.51 (d, $^{3}J_{H,H}$ = 7.9 Hz, 2H, *H3´* / H5´**), 7.99 (t, $^{3}J_{H,H}$ = 7.8 Hz, 1H, *H4´*), 7.80 (d, $^{3}J_{H,H}$ = 8.3 Hz, 2H, H_{phenyl}), 7.70 (d, $^{3}J_{H,H}$ = 8.1 Hz, 2H, H_{phenyl}), 7.62 – 7.44 (m, 5H, *H5* / H5´´* / 3* H_{phenyl}), 7.31 (d, $^{3}J_{H,H}$ = 7.9 Hz, 2H, H_{phenyl}), 2.44 (s, 3H, H_{methyl}).

^{13}C NMR (101 MHz, $CDCl_3$, ppm, 25 °C): δ_C = 156.89 (C_q, 1C), 156.77 (C_q, 1C), 155.52 (C_q, 1C), 155.45 (C_q, 1C), 149.74 (C_t, 1C), 149.66 (C_t, 1C), 149.30 (C_q, 1C), 149.22 (C_q, 1C), 139.36 (C_q, 1C), 138.64 (C_q, 1C), 138.10 (C_t, 1C), 135.62 (C_q, 1C), 129.96 (C_{phenyl}, 2C), 129.24 (C_{phenyl}, 2C), 129.22 (C_t, 1C), 127.24 (C_{phenyl}, 2C), 127.05 (C_{phenyl}, 2C), 121.77 (C_t, 1C), 121.54 (C_t, 1C), 121.45 (C_t, 1C), 121.40 (C_t, 1C), 119.35 (C_t, 1C), 119.08 (C_t, 1C), 21.41 (C_{methyl}, 1C).

ESI-MS (MeOH, *positive* ion mode): *m/z* [ion, intensity (%)] = 400.2 ($M+H^+$, 50), 422.2 ($M+Na^+$, 100).

HRMS (ESI-ToF): *m/z* calcd. for $[C_{28}H_{21}N_3+H]^+$: 400.1808; found: 400.1809, *m/z* calcd. for $[C_{28}H_{21}N_3+Na]^+$: 422.1628; found: 422.1626, *m/z* calcd. for $[C_{56}H_{42}N_6+Na]^+$: 821.3363; found: 821.3369.

4-Phenyl-4′′-(4-(bromomethyl)phenyl)-2,2′:6′,2′′-terpyridine (220)

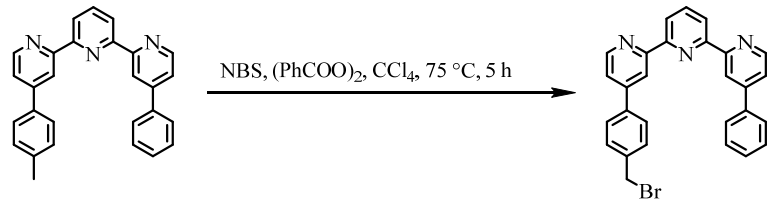

223 **220**

The desired compound 4-Phenyl-4′′-(4-(bromomethyl)phenyl)-2,2′:6′,2′′-terpyridine (**220**) was prepared by radical side chain bromination of precursor **223** based on a reported literature procedure.[554,555] Therefore 4-Phenyl-4′′-(*p*-tolyl)-2,2′:6′,2′′-terpyridine (**223**) (200 mg, 0.50 mmol, 1.00 eq.), the brominating agent *N*-bromosuccinimide (NBS) (108 mg, 0.60 mmol, 1.20 eq.) and the radical initiator dibenzoyl peroxide (31.2 mg, 125 µmol, 0.25 eq.) were dissolved in previously degassed tetrachloromethane (CCl_4) (30 mL) and heated to 75 °C for about 5 h until the reaction progress stopped (monitoring by TLC). Now the reaction mixture was allowed to cool down to room temperature and was stirred in an ice-water bath for 30 min prior to dilution with DCM, brine and aqueous saturated $Na_2S_2O_3$-solution. The resulting mixture was repeatedly extracted with DCM (4 *x*) before the combined organic layers were dried over $MgSO_4$, filtered and residual solvent was removed under reduced pressure. The crude product was purified via FCC using a solvent mixture of EtOAc / *n*-hexane (1:3). Apart from the reisolation of unreacted starting material **223** in a yield of 16% (33.1 mg, 82.9 µmol) mainly the desired target compound 4-Phenyl-4′′-(4-(bromomethyl)phenyl)-2,2′:6′,2′′-terpyridine (**220**) was isolated in a yield of 84% (200 mg, 418 µmol).

Analytical data 220:

^{1}H-NMR (400 MHz, $CDCl_3$, ppm, 25 °C): δ_H = 8.87 (d, $^4J_{H,H}$ = 1.3 Hz, 1H, *H3* / H3′′**), 8.86 (d, $^4J_{H,H}$ = 1.2 Hz, 1H, *H3* / H3′′**), 8.75 (d, $^3J_{H,H}$ = 4.7 Hz, 2H, *H6* / H6′′**), 8.50 (dd, $^3J_{H,H}$ = 7.8 Hz, $^4J_{H,H}$ = 1.5 Hz, 1H, *H3′* / H5′**), 8.00 (t, $^3J_{H,H}$ = 7.8 Hz, 1H, *H4′*), 7.79 (d, $^3J_{H,H}$ = 7.8 Hz, 2H, H_{phenyl}), 7.76 (d, $^3J_{H,H}$ = 8.2 Hz, 2H, H_{phenyl}), 7.56 (dd, $^3J_{H,H}$ = 5.2 Hz, $^4J_{H,H}$ = 1.9 Hz, 2H, *H5* / H5′′**), 7.55 – 7.48 (m, 5H, H_{phenyl}), 4.57 (s, 2H, $H_{methylene}$).

^{13}C NMR (101 MHz, $CDCl_3$, ppm, 25 °C): δ_C = 157.01 (C_q, 1C), 156.88 (C_q, 1C), 155.54 (C_q, 1C), 155.39 (C_q, 1C), 149.86 (C_t, 1C), 149.80 (C_t, 1C), 149.27 (C_q, 1C), 148.46 (C_q, 1C), 138.86 (C_q, 1C), 138.76 (C_q, 1C), 138.65 (C_q, 1C), 138.12 (C_t, 1C),

129.92 (C_{phenyl}, 2C), 129.26 (C_{phenyl}, 3C), 127.67 (C_{phenyl}, 2C), 127.23 (C_{phenyl}, 2C), 121.80 (C_t, 1C), 121.64 (C_t, 1C), 121.49 (C_t, 1C), 121.42 (C_t, 1C), 119.33 (C_t, 1C), 119.25 (C_t, 1C), 32.96 ($C_{methylene}$, 1C).

ESI-MS (MeCN, *positive* ion mode): *m/z* [ion, intensity (%)] = 478.1 ($M+H^+$, 90), 500.1 ($M+Na^+$, 100).

HRMS (ESI-ToF): *m/z* calcd. for $[C_{28}H_{20}BrN_3+H]^+$: 478.0913; found: 478.0910,

1-Bromo-4-(4-nitrobenzyl)benzene (246)

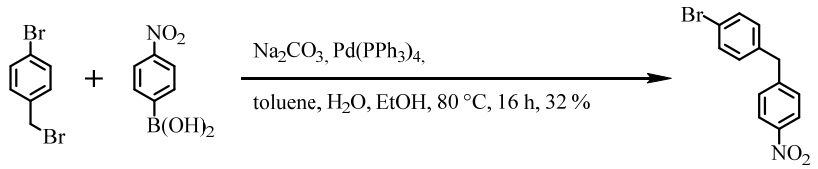

245 **246**

1-Bromo-4-(4-nitrobenzyl)benzene (**246**) was prepared inspired by previously reported literature procedure.[555,560] 4-Bromobenzyl bromide (**245**) (1.53 g, 6.00 mmol, 1.00 eq.), 4-nitrophenylboronic acid (1.00 g, 6.00 mmol, 1.00 eq.), Na_2CO_3 (700 mg, 6.60 mmol, 1.10 eq.), and $Pd(PPh_3)_4$ (208 mg, 0.18 mmol, 0.03 eq.) were charged into a Schlenk tube, put under inert atmosphere and dissolved in the previously degassed solvents toluene (12 mL), water (10 mL) and ethanol (10 mL). before the reaction was sealed and heated to 80 °C for 16 h. After the reaction was allowed to cool down it was diluted with brine and DCM and extracted with DCM (3 *x*). prior to pre-drying of the recombined organic fractions over $MgSO_4$, filtration and evaporation of residual organic solvents under reduced pressure. Finally the resulting crude product was purified by repeated FCC using a solvent mixture of EtOAc / *n*-hexane (1:19) to yield the desired product **246** in a yield of 32% (559 mg, 1.91 mmol) in form of light yellow crystals.

Analytical data of 246:

^{1}H-NMR (400 MHz, $CDCl_3$, ppm, 25 °C): δ_H = 8.13 (d, $^3J_{H,H}$ = 8.8 Hz, 2H, *H3´ / H5´*), 7.43 (d, $^3J_{H,H}$ = 8.4 Hz, 2H, *H2 / H6*), 7.31 (d, $^3J_{H,H}$ = 8.8 Hz, 2H, *H2´ / H6´*), 7.05 (d, $^3J_{H,H}$ = 8.5 Hz, 2H, *H3 / H5*), 4.03 (s, 2H, $H_{methylene}$). The connectivity of the protons was assigned via 2D-NMR (HMBC, NOESY).

^{13}C-NMR (101 MHz, $CDCl_3$, ppm, 25 °C): δ_C = 148.19 (C_q, 1C), 146.70 (C_q, 1C), 138.27 (C_q, 1C), 131.96 (C_{phenyl}, 2C), 130.76 (C_{phenyl}, 2C), 129.69 (C_{phenyl}, 2C), 123.89 (C_{phenyl}, 2C), 41.11 ($C_{methylene}$, 1C).

GCMS (EI$^+$, 70 eV): *m/z* [ion, intensity (%)] = 291 (M^+, 30), 212 (M^+-Br, 30) 165 (M^+-Br-NO_2, 100).

4,4,5,5-Tetramethyl-2-(4-(4-nitrobenzyl)phenyl)-1,3,2-dioxaborolane (247)

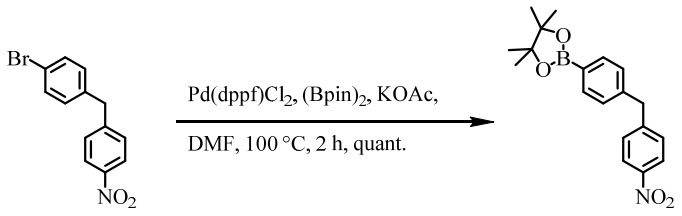

246 **247**

4,4,5,5-tetramethyl-2-(4-(4-nitrobenzyl)phenyl)-1,3,2-dioxaborolane (**247**) was prepared via a Miyaura borylation reaction of bromide **246** by a previously reported literature procedure.[561] 1-Bromo-4-(4-nitrobenzyl)benzene (**246**) (292 mg, 1.00 mmol, 1.00 eq.), bis(pinacolato)diboron ($(Bpin)_2$) (279 mg, 1.10 mmol, 1.10 eq.), $Pd(dppf)Cl_2$ (58.5 mg, 0.08 mmol, 0.08 eq.), and KOAc (297 mg, 3.00 mmol, 3.00 eq.) were charged into a Schlenk tube, put under inert atmosphere and dissolved in dry DMF (15 mL). The solution was degassed for 30 min prior to being heated to 100 °C for 15 h. After cooling down to room temperature the reaction mixture was diluted with TBME (200 mL) and filtered through a plug of celite. Subsequently water and brine were added to the mixture and after separation of the phases the aqueous phase was extracted with DCM (2 *x*). The dark brown, oily crude product was purified by FCC using EtOAc to quantitatively yield the desired product 4,4,5,5-tetramethyl-2-(4-(4-nitrobenzyl)-phenyl)-1,3,2-dioxaborolane (**247**) together with some rests of unreacted $(Bpin)_2$ yielding 519 mg of the described product mixture.

Analytical data of 247:

^{1}H-NMR (400 MHz, $CDCl_3$, ppm, 25 °C): δ_H = 8.11 (d, $^{3}J_{H,H}$ = 8.7 Hz, 2H, *H3´ / H5´*), 7.76 (d, $^{3}J_{H,H}$ = 8.0 Hz, 2H, *H2 / H6*), 7.30 (d, $^{3}J_{H,H}$ = 8.7 Hz, 2H, *H2´ / H6´*), 7.17 (d, $^{3}J_{H,H}$ = 8.7.9 Hz, 2H, *H3 / H5*), 4.06 (s, 2H, $H_{methylene}$), 1.32(s, 12H, H_{methyl}).
^{13}C-NMR (101 MHz, $CDCl_3$, ppm, 25 °C): δ_C = 148.66 (C_q, 1C), 146.59 (C_q, 1C), 142.40 (C_q, 1C), 135.38 (C_{phenyl}, 2C), 129.70 (C_{phenyl}, 2C), 128.46 (C_{phenyl}, 2C), 123.78 (C_{phenyl}, 2C), 83.54 (C_q, 2C), 41.93 ($C_{methylene}$, 1C), 25.08 (C_{methyl}, 4C).
Note: The carbon-atom bound to the boron cannot be seen in the ^{13}C-NMR spectrum.
^{11}B-NMR (128 MHz, $CDCl_3$, ppm, 25 °C): δ_B = 30.45 (1B).

4-(4-(4-nitrobenzyl)phenyl)-4′′-phenyl-2,2′:6′,2′′-terpyridine (248)

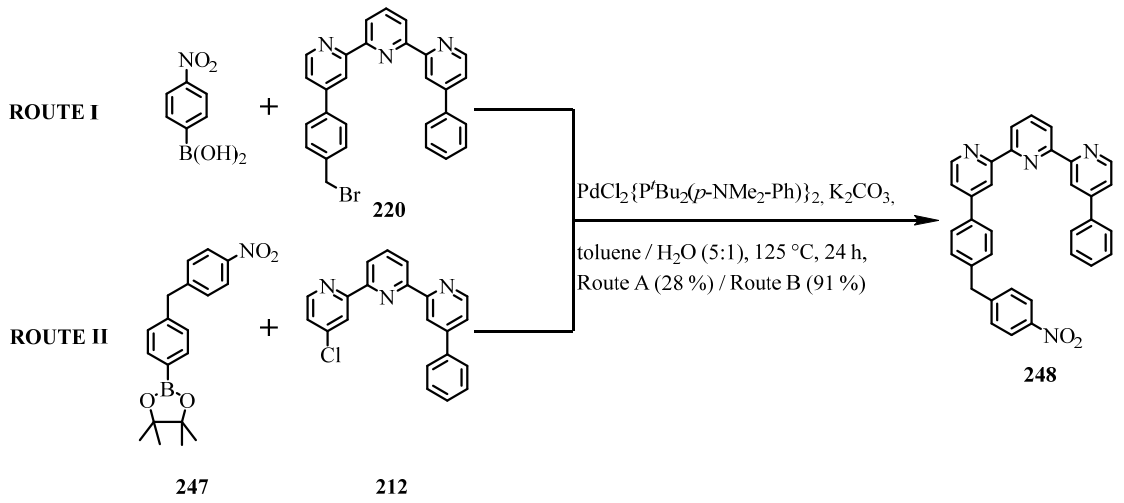

For the preparation of 4-(4-(4-nitrobenzyl)phenyl)-4′′-phenyl-2,2′:6′,2′′-terpyridine (**248**) two different strategies were applied. On **route I** the target compound **248** was prepared starting from 4-Phenyl-4′′-(4-(bromomethyl)phenyl)-2,2′:6′,2′′-terpyridine (**220**),whereas on **route II** 4-chloro-4′′-phenyl-2,2′:6′,2′′-terpyridine (**212**) serves as the starting material. In both cases representative procedure B has been applied. The different procedures are described separately below, whereas the common analytical results are listed afterwards

Route I: On this route 4-Phenyl-4′′-(4-(bromomethyl)phenyl)-2,2′:6′,2′′-terpyridine (**220**) (35.9 mg, 75.0 µmol, 1.00 eq.), 4-nitrophenylboronic acid (125 mg, 0.75 mmol, 10.0 eq.), K_2CO_3 (31.4 mg, 225 µmol, 3.00 eq.), and $PdCl_2\{P^tBu_2(p\text{-}NMe_2\text{-}Ph)\}_2$ (2.66 mg, 3.75 µmol, 0.05 eq.) were charged into a Schlenk tube and suspended in previously degassed toluene (20 mL) and H_2O (4 mL). The reaction vessel was sealed and heated to 125 °C for 24 h. After completion the reaction mixture was allowed to cool down to room temperature and was subsequently diluted with DCM, water and brine. Now the reaction mixture was extracted with DCM (4 *x*) and with EtOAc (2 *x*). The combined organic layers were dried over $MgSO_4$, filtered and residual solvent was removed under reduced pressure. The crude product was purified via FCC using a gradient of solvent mixtures ranging from EtOAc / *n*-hexane (1:3) up to EtOAc / *n*-hexane (1:1) to obtain the desired target compound 4-(4-(4-nitrobenzyl)phenyl)-4′′-phenyl-2,2′:6′,2′′-terpyridine (**248**) in a poor yield of 28% (11.0 mg, 21.1 µmol).

Route II: 4-chloro-4´´-phenyl-2,2´:6´,2´´-terpyridine (**212**) (29.0 mg, 0.08 mmol, 1.00 eq.), 4,4,5,5-tetramethyl-2-(4-(4-nitrobenzyl)phenyl)-1,3,2-dioxaborolane (**247**) (136 mg, 0.40 mmol, 5.00 eq.), K_2CO_3 (33.5 mg, 0.24 mmol, 3.00 eq.), and $PdCl_2\{P^tBu_2(p\text{-}NMe_2\text{-}Ph)\}_2$ (2.86 mg, 4.00 µmol, 0.05 eq.) were charged into a Schlenk tube and suspended in degassed toluene (15 mL) and H_2O (3 mL). The reaction vessel was sealed and heated to 125 °C for 24 h. After completion the reaction mixture was allowed to cool down to room temperature and was subsequently diluted with DCM, water and brine. Now the reaction mixture was extracted with DCM (4 *x*) and EtOAc (2 *x*) before the combined organic layers were dried over $MgSO_4$, filtered and residual solvent was removed under reduced pressure. The crude product was purified via FCC using a gradient of solvent mixtures ranging from EtOAc / *n*-hexane (1:3) to EtOAc / *n*-hexane (1:1) to obtain the desired target compound 4-(4-(4-nitrobenzyl)phenyl)-4´´-phenyl-2,2´:6´,2´´-terpyridine (**248**) in a yield of 91% (38.0 mg, 73,0 µmol).

Analytical data of 248:

^{1}H-NMR (400 MHz, $CDCl_3$, ppm, 25 °C): δ_H = 8.86 (s, 2H, *H3* / H3´´* / H6* / H6´´**), 8.75 8.71 (m, 2H, *H3* / H3´´* / H6* / H6´´**), 8.50 (d, $^3J_{H,H}$ = 7.8 Hz, 2H, *H3´ / H5´*), 8.17 (d, $^3J_{H,H}$ = 8.7 Hz, 2H, H_{phenyl}), 7.98 (t, $^3J_{H,H}$ = 7.8 Hz, 1H, *H4´*), 7.79 - 7.74 (m, 2H, H_{phenyl}), 7.72 (d, $^3J_{H,H}$ = 8.2 Hz, 2H, H_{phenyl}), 7.54 (dd, $^3J_{H,H}$ = 5.1 Hz, $^4J_{H,H}$ = 1.8 Hz, 1H, *H5* / H5´´**), 7.52 (dd, $^3J_{H,H}$ = 5.1 Hz, $^4J_{H,H}$ = 1.8 Hz, 1H, *H5* / H5´´**), 7.45 (app. dd, $^3J_{H,H}$ = 5.1 Hz, $^4J_{H,H}$ = 1.9 Hz, 3H, H_{phenyl}), 7.36 (d, $^3J_{H,H}$ = 8,7 Hz, 2H, H_{phenyl}), 7.29 (d, $^3J_{H,H}$ = 8.2 Hz, 2H, H_{phenyl}), 4.13 (s, 2H, $H_{methylene}$).

^{13}C NMR (101 MHz, $CDCl_3$, ppm, 25 °C): δ_C = 156.88 (C_q, 1C), 156.84 (C_q, 1C), 155.46 (C_q, 1C), 155.38 (C_q, 1C), 149.78 (C_t, 1C), 149.13 (C_q, 1C), 148.63 (C_q, 1C), 148.41 (C_q, 1C), 146.73 (C_q, 1C), 140.38 (C_q, 1C), 138.58 (C_q, 1C), 138.05 (C_t, 1C), 137.11 (C_q, 1C), 129.81 (C_{phenyl}, 2C), 129.77 (C_{phenyl}, 2C), 129.15 (C_{phenyl}, 2C), 127.59 (C_{phenyl}, 2C), 127.16 (C_{phenyl}, 2C), 123.93 (C_{phenyl}, 2C), 121.73 (C_t, 1C), 121.51 (C_t, 1C), 121.42 (C_t, 1C), 121.35 (C_t, 1C), 119.21 (C_t, 1C), 119.13 (C_t, 1C), 41.45 ($C_{methylene}$, 1C). In the ^{13}C-spectrum and in the DEPT-135 two signals less than expected were found most likely due to coincident signals.

ESI-MS (MeCN, *positive* ion mode): *m/z* [ion, intensity (%)] = 521.1 ($M+H^+$, 80), 543.2 ($M+Na^+$, 100).

HRMS (ESI-ToF): *m/z* calcd. for $[C_{34}H_{24}N_4O_2+H]^+$: 521.1972; found: 521.1975, *m/z* calcd. for $[C_{34}H_{24}N_4O_2+H]^+$: 543.1791; found: 543.1786

4-(4-((4-Nitrophenoxy)methyl)phenyl)-4′′-phenyl-2,2′:6′,2′′-terpyridine (243)

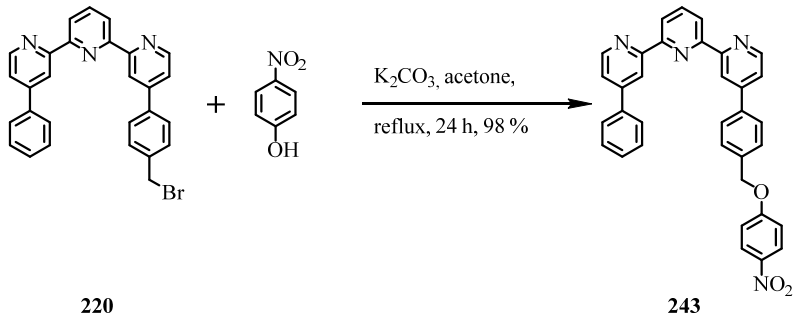

220 **243**

4-(4-((4-nitrophenoxy)methyl)phenyl)-4′′-phenyl-2,2′:6′,2′′-terpyridine (**243**) was prepared via a S_N2-reaction inspired by a previously reported literature procedure.[556] Thus 4-Phenyl-4′′-(4-(bromomethyl)phenyl)-2,2′:6′,2′′-terpyridine (**220**) (47.8 mg, 0.10 mmol, 1.00 eq.), 4-nitrophenol (71 mg, 0.50 mmol, 5.00 eq.), and K_2CO_3 (69.8 mg, 0.50 mmol, 1.50 eq.) were charged into a Schlenk tube, put under inert atmosphere and dissolved in dry acetone (30 mL), before the reaction was sealed and heated to reflux for 24 h. After the reaction was allowed to cool down to room temperature the solvent was evaporated under reduced pressure. The resulting crude product was purified by FCC using *n*-hexane / EtOAc (1:1) as the solvent mixture of to obtain the off-white product 4-(4-((4-nitrophenoxy)methyl)phenyl)-4′′-phenyl-2,2′:6′,2′′-terpyridine (**243**) in a yield of 98% (52.7 mg, 98.2 µmol).

Analytical data of 243:

^{1}H-NMR (400 MHz, $CDCl_3$, ppm, 25 °C): δ_H = 8.87 (d, $^4J_{H,H}$ = 1.3 Hz, 1H, *H3* / H3′′**), 8.86 (d, $^4J_{H,H}$ = 1.4 Hz, 1H, *H3* / H3′′**), 8.77 (dd, $^3J_{H,H}$ = 3.0 Hz, $^5J_{H,H}$ = 0.5 Hz, 1H, *H6* / H6′′**), 8.76 (dd, $^3J_{H,H}$ = 3.1 Hz, $^5J_{H,H}$ = 0.5 Hz, 1H, *H6* / H6′′**), 8.51 (d, $^3J_{H,H}$ = 7.9 Hz, 2H, *H3′ / H5′*), 8.23 (d, $^3J_{H,H}$ = 9.2 Hz, 2H, H_{phenyl}), 8.01 (t, $^3J_{H,H}$ = 7.8 Hz, 1H *H4′*), 7.83 (d, $^3J_{H,H}$ =8.2 Hz, 2H, H_{phenyl}), 7.79 (app. dd, $^3J_{H,H}$ = 8.3 Hz, $^4J_{H,H}$ = 1.6 Hz, 2H, H_{phenyl}), 7.61 – 7.53 (m, 4H, *H5 / H5′′ / 2*H_{phenyl}), 7.56 – 7.42 (m, 3H, H_{phenyl}), 7.06 (d, $^3J_{H,H}$ = 9.2 Hz, 2H, H_{phenyl}), 5.24 (s, 2H, $H_{methylene}$).

^{13}C-NMR (101 MHz, $CDCl_3$, ppm, 25 °C): δ_C = 163.65 (C_q, 1C), 157.06 (C_q, 1C), 156.92 (C_q, 1C), 155.62 (C_q, 1C), 155.46 (C_q, 1C), 149.89 (C_t, 1C), 149.84 (C_t, 1C), 149.32 (C_q, 1C), 148.63 (C_q, 1C), 141.96 (C_q, 1C), 138.94 (C_q, 1C), 138.71 (C_q, 1C), 138.16 (C_t, 1C), 136.58 (C_q, 1C), 129.23 (C_{phenyl}, 2C), 129.21 (C_t, 1C), 128.28 (C_{phenyl}, 2C), 127.71 (C_{phenyl}, 2C), 127.27 (C_{phenyl}, 2C), 126.14 (C_{phenyl}, 2C), 121.88 (C_t, 1C),

121.74 (C_t, 1C), 121.59 (C_t, 1C), 121.50 (C_t, 1C), 119.35 (C_t, 1C), 119.30 (C_t, 1C), 115.01 (C_{phenyl}, 2C), 70.35($C_{methylene}$, 1C).

ESI-MS (MeCN, *positive* ion mode): *m/z* [ion] = 537.2 ($M+H^+$), 559.2 ($M+Na^+$).

HRMS (ESI-ToF): *m/z* calcd. for $[C_{34}H_{24}N_4O_3+H]^+$: 537.1921 ; found: 537.1925.

(*E*)-4,4′-(diazene-1,2-diyl)diphenol (219)

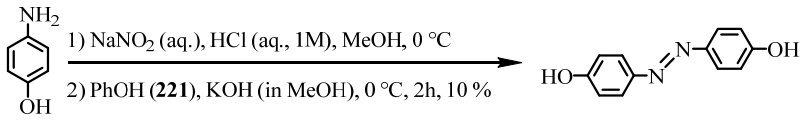

222 **219**

To prepare (*E*)-4,4′-(diazene-1,2-diyl)diphenol **219**, 4-hydroxyaniline (**222**) (6.39 g, 58.0 mmol, 1.0 eq.) was dissolved in aq. HCl (1M, 100 mL) and cooled to 0 °C. Sodium nitrite ($NaNO_2$) (4.08 g, 58,0 mmol, 1.00 eq.) was dissolved in water (20 mL) and added dropwise to the solution of 4-hydroxyaniline (**222**) which turned purple upon the addition. The reaction mixture was diluted with pre-cooled MeOH (200 mL). In another flask phenol (**221**) (5.51 g, 58.0 mmol, 1.00 eq.) and KOH (6.53 g, 116 mmol, 2.00 eq.) were dissolved in MeOH (40 mL) and cooled to 0 °C. At this temperature the phenolate solution was added dropwise to the reaction mixture which turned red upon addition. The reaction was stirred for 2h at 0 °C before it was stopped by the addition of aqueous HCl (1M). The mixture was acidified to pH 7 prior to dilution with DCM. After separation of the layers the aqueous phase was acidified down to pH 1 by addition of aq. HCl (3M). The water phase was extracted with DCM prior to combination of the organic layers, drying over $MgSO_4$ and evaporation of organic solvent under reduced pressure. The crude product was purified by repeated (3 *x*) FCC using cyclohexane / EtOAc (1:1) as the solvent mixture. The still impure product was further purified by recrystallization from acetic acid. The filter cake yielded in a first filtration was a black solid. However after cooling of the mother liquor, a second orange solid could be filtered off. Both residues showed to be pure and were combined yielding the desired product (*E*)-4,4′-(diazene-1,2-diyl)diphenol **219** in a yield of 10% (1.21 g, 5.65 mmol) as an orange or black solid.

Analytical data of 219:

^{1}H-NMR (400 MHz, DMSO-d_6, ppm, 25 °C): δ_H = 10.11 (s, 2H), 7.74 – 7.68 (m, 4H), 6.93 - 6.88 (m, 4H).

^{13}C-NMR (101 MHz, DMSO-d_6, ppm, 25 °C): δ_C = 159.9 (C_q, 2C), 145.2 (C_q, 2C), 124.1 (C_t, 4C), 115.7 (C_t, 4C).

ESI-MS (MeCN, *positive* ion mode): *m/z* [ion] = 215.0 ($M+H^+$).

HRMS (ESI-ToF): *m/z* calcd. for $[C_{12}H_{10}N_2O_2+H]^+$: 215.0815; found: 215.0813.

{[Fe(*243*)$_2$]$^{2+}$[(PF$_6$)$^-$]$_2$} (244)

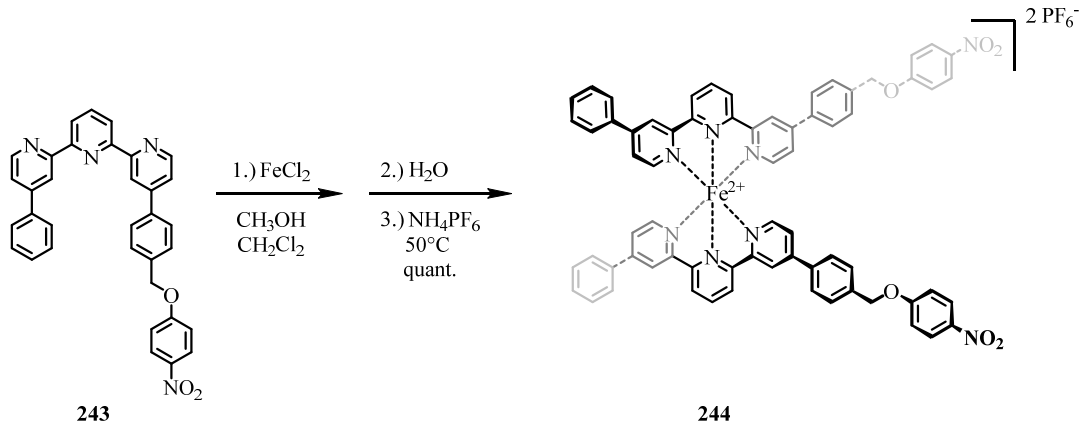

243 **244**

244 was prepared by adapting the representative procedure C. Thus 4-(4-((4-nitrophenoxy)-methyl)phenyl)-4´´-phenyl-2,2´:6´,2´´-terpyridine (**243**) (21.5 mg, 40.0 µmol, 2.00 eq.), $FeCl_2$ (2.54 mg, 20.0 µmol, 1.00 eq.), MeOH (50 mL), DCM (50 mL), water (200 mL), and NH_4PF_6 (163 mg, 1.00 mmol, 50.0 eq.) were used. The product **244** was isolated as a dark purple solid in quantitative yield (22.6 mg, 20.0 µmol).

Analytical data of 244:

^{1}H-NMR (400 MHz, CD_3CN, ppm, 25 °C): δ_H = 9.10 (dd, $^3J_{H,H}$ = 8.1 Hz, $^4J_{H,H}$ = 1.4 Hz, 4H, *H3´ / H5´*), 8.78 (d, $^4J_{H,H}$ = 1.2 Hz, 4H, *H3 / H3´´*), 8.76 (t, $^3J_{H,H}$ = 8.0 Hz, 2H, *H4´*), 8.18 (d, $^3J_{H,H}$ = 9.3 Hz, 4H, H_{phenyl}), 7.77 (d, $^3J_{H,H}$ = 8.4 Hz, 4H, H_{phenyl}), 7.77 - 7.70 (m, 4H, H_{phenyl}), 7.60 (d, $^3J_{H,H}$ = 8.2 Hz, 4H, H_{phenyl}), 7.52 (app. dd, $^3J_{H,H}$ = 5.2 Hz, $^4J_{H,H}$ = 2.0 Hz, 6H, H_{phenyl}), 7.37 (app. dt, $^3J_{H,H}$ = 6.0 Hz, $^4J_{H,H}$ = 1.9 Hz, 4H, *H5* / H5´´* / H6* / H6´´**), 7.16 (dd, $^3J_{H,H}$ = 6.0 Hz, $^4J_{H,H}$ = 2.0 Hz, 4H, *H5* / H5´´* / H6* / H6´´**), 7.11 (d, $^3J_{H,H}$ = 9.3 Hz, 4H, H_{phenyl}), 5.25 (s, 4H, $H_{methylene}$).

^{13}C-NMR (101 MHz, CD_3CN, ppm, 25 °C): δ_C = 164.63 (C_q, 2C), 161.38 (C_q, 2C), 161.33 (C_q, 2C), 159.32 (C_q, 2C), 159.26 (C_q, 2C), 154.04 (C_t, 2C), 154.00 (C_t, 2C), 151.72 (C_q, 2C), 151.13 (C_q, 2C), 142.76 (C_q, 2C), 139.93 (C_q, 2C), 139.01 (C_t, 2C), 136.30 (C_q, 2C), 136.18 (C_q, 2C), 132.27 (C_t, 2C), 131.65 (C_t, 2C), 130.43 (C_{phenyl}, 4C), 129.58 (C_{phenyl}, 4C), 128.65 (C_{phenyl}, 4C), 128.33 (C_{phenyl}, 4C), 126.85 (C_{phenyl}, 4C), 125.69 (C_t, 2C), 125.63 (C_t, 2C), 124.96 (C_t, 2C), 122.55 (C_t, 2C), 122.52 (C_t, 2C), 116.04 (C_{phenyl}, 4C), 70.73 ($C_{methylene}$, 2C).

^{19}F-NMR (376 MHz, CD_3CN, ppm, 25 °C): δ_F = –72.77 (d, $^1J_{P,F}$ = 706.7 Hz, 12F).

^{31}P-NMR (162 MHz, CD_3CN, ppm, 25 °C): δ_P = -144.58 (hept, $^1J_{P,F}$ = 706.7 Hz, 2P).

ESI-MS (MeCN, *positive* ion mode): *m/z* [ion, intensity (%)] = 564.4 (M^{2+}-2PF_6^-, 100).

HRMS (ESI-ToF): *m/z* calcd. for $[C_{68}H_{48}FeN_8O_6]^{2+}$: 564.1519; found: 564.1527.

UV/VIS (MeCN): λ_{max} (ε) = 275 nm (58775 $L \cdot cm^{-1} \cdot mol^{-1}$), 334 nm (65845 $L \cdot cm^{-1} \cdot mol^{-1}$), 375 nm (9245 $L \cdot cm^{-1} \cdot mol^{-1}$), 564 nm (8790 $L \cdot cm^{-1} \cdot mol^{-1}$).

(*E*)-1,2-bis(4-((4-(4′′-phenyl-[2,2′:6′,2′′-terpyridin]-4-yl)benzyl)oxy)phenyl)-diazene (218a)

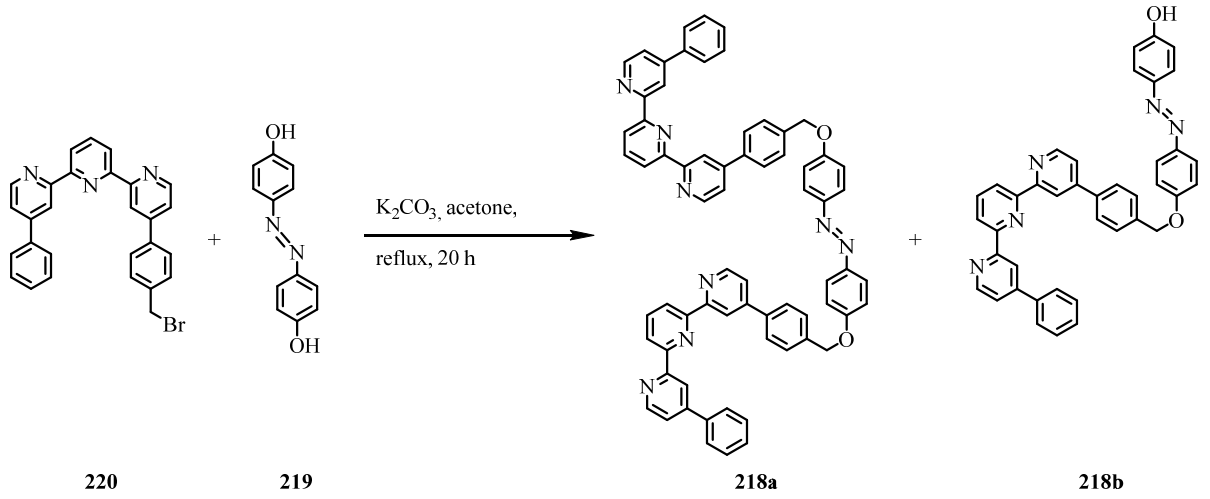

220 **219** **218a** **218b**

(*E*)-1,2-bis(4-((4-(4′′-phenyl-[2,2′:6′,2′′-terpyridin]-4-yl)benzyl)oxy)phenyl)diazene (**218a**) was prepared via a S_N2-reaction inspired by a previously reported literature procedure.[556] Thus (*E*)-4,4′-(diazene-1,2-diyl)diphenol (**219**) (10.7 mg, 0.05 mmol, 1.00 eq.), 4-Phenyl-4′′-(4-(bromomethyl)phenyl)-2,2′:6′,2′′-terpyridine (**220**) (52.6 mg, 0.11 mmol, 2.20 eq), and K_2CO_3 (18.1 mg, 0.13 mmol, 2.60 eq.) were charged into a Schlenk tube, put under inert atmosphere and dissolved in dry acetone (15 mL), before the reaction was sealed and heated to reflux for 20 h. After the reaction was allowed to cool down to room temperature it was diluted with DCM and water and extracted with DCM (3 *x*), before drying over $MgSO_4$, filtration and evaporation of residual solvent. The still yellow aqueous phase was liberated from remaining acetone and the resulting yellow solid was filtered off and fully crystallized by cooling the solution down in an ice bath. After drying at the high vacuum the yellow precipitate from the aqueous phase was characterized as the desired product (*E*)-1,2-bis(4-((4-(4′′-phenyl-[2,2′:6′,2′′-terpyridin]-4-yl)benzyl)oxy)phenyl)diazene (**218a**) via HR-ESI-MS techniques, although no NMR-characterization was possible due to the very limited solubility of **218a.** In the organic phases also traces of monosubstituted side product (*E*)-4-((4-((4-(4′′-phenyl-[2,2′:6′,2′′-terpyridin]-4-yl)benzyl)-oxy)phenyl)diazenyl)phenol (**218b**) could be found. Compounds **218a** and **218b** were both clearly characterized by HR-ESI-MS as shown below, however the limited solubility prevented any NMR analysis.

Analytical data of 218a:

ESI-MS (THF, *positive* ion mode): *m/z* [ion] = 1009.4 ($M+H^+$).
HRMS (ESI-ToF): *m/z* calcd. for $[C_{68}H_{48}N_8O_2+H]^+$: 1009.3973; found: 1009.3987.

Analytical data of 218b:

ESI-MS (THF, *positive* ion mode): *m/z* [ion] = 612.3 ($M+H^+$).
HRMS (ESI-ToF): *m/z* calcd. for $[C_{40}H_{29}N_5O_2+H]^+$: 612.2391; found: 612.2395

{[Fe(*218a*)]$^{2+}$[(PF$_6$)$^-$]$_2$} (215)

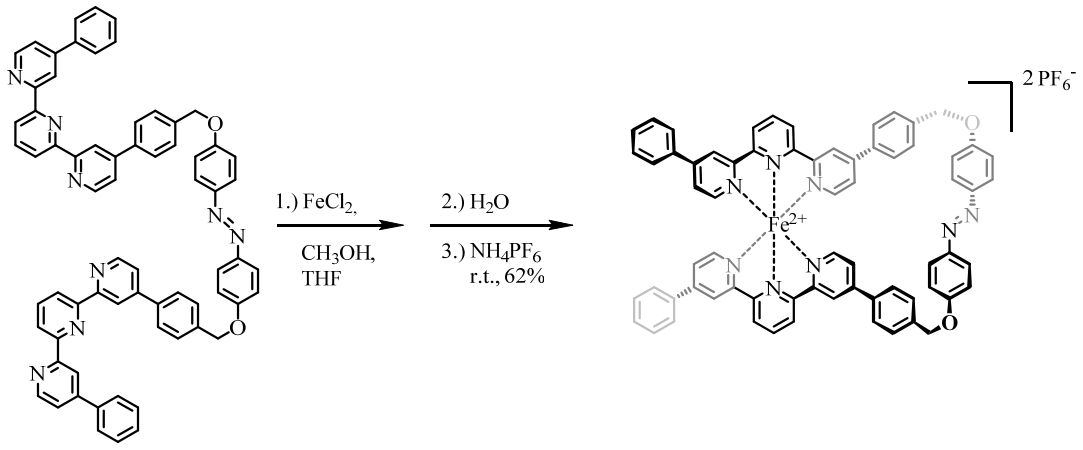

218a **215**

215 was prepared by a modification of the representative procedure C. The ligand (*E*)-1,2-bis-(4-((4-(4´´-phenyl-[2,2´:6´,2´´-terpyridin]-4-yl)benzyl)oxy)phenyl)diazene (**218a**) (40.4 mg, 40.0 µmol, 1.00 eq.) was suspended in a mixture of MeOH (500 mL) and THF (500 mL) first. Now $FeCl_2$ (5.07 mg, 40.0 µmol, 1.00 eq.) was dissolved in MeOH (50 mL) and added dropwise to the ligand´s solution over 2 h via syringe pump. After an additional hour of stirring, NH_4PF_6 (326 mg, 2.00 mmol, 50.0 eq.) and water (500 mL) were added to the reddish solution, which turned slightly purple upon the addition of water. After another hour of stirring the organic solvents were evaporated from the solution under reduced pressure yielding a dark purple precipitate in the aqueous phase. The precipitate was filtered off and excessively washed with water to get rid of excess NH_4PF_6 before it was dried to yield the crude product **215**. This was now subjected to purification via preparative reversed-phase HPLC using a solvent gradient ranging from H_2O / MeCN (35:65) up to H_2O / MeCN (20:80) at a flow rate of 20 mL/min yielding the desired pure product **215** in a yield of 62% (25.8 mg, 24.2 µmol) as a dark purple solid. The product could be comprehensively characterized as the *trans*-isomer (*E*)-**215** of the target compound. By UV-irradiation at λ = 365 nm also the corresponding *cis*-isomer (*Z*)-**215** could be formed and cleanly characterized. The divergent data of both isomeric forms are listed separately in the analytical section below.

Analytical data of (*E*)-215:

^{1}H-NMR (500 MHz, CD_3CN, ppm, 25 °C): δ_H = 9.06 (dd, $^3J_{H,H}$ = 8.1 Hz, $^4J_{H,H}$ = 0.6 Hz, 2H, *H3´*), 9.03 (dd, $^3J_{H,H}$ = 8.2 Hz, $^4J_{H,H}$ = 0.7 Hz, 2H, *H5´*), 8.76 (dd, $^4J_{H,H}$ = 2.1 Hz, $^5J_{H,H}$ = 0.7 Hz, 2H, *H3´´*), 8.72 (t, $^3J_{H,H}$ = 8.0 Hz, 2H, *H4´*), 8.71 (d, $^4J_{H,H}$ = 1.4 Hz, 2H, *H3*),

7.76 – 7.70 (m, 4H, *H2$_{phenyl}$*), 7.63 (d, $^{3}J_{H,H}$ = 8.6 Hz, 4H, *H2$_{tolyl}$*), 7.54 – 7.50 (m, 6H, *H3$_{phenyl}$ / H3$_{phenyl}$*), 7.46 (d, $^{3}J_{H,H}$ = 9.1 Hz, 4H, *H2$_{phenyl(azo)}$*), 7.40 (d, $^{3}J_{H,H}$ = 8.6 Hz, 4H, *H3$_{tolyl}$*), 7.35 (dd, $^{3}J_{H,H}$ = 6.0 Hz, $^{4}J_{H,H}$ = 2.0 Hz, 2H, *H5´´)*, 7.18 (dd, $^{3}J_{H,H}$ = 5.5 Hz, $^{4}J_{H,H}$ = 0.4 Hz, 2H, *H5)*, 7.18 – 7.16 (m, 2H, *H6´´*), 6.90 (d, $^{3}J_{H,H}$ = 9.0 Hz, 4H, *H3$_{phenyl(azo)}$*), 6.92 - 6.87 (m, 2H, *H6*), 5.41 (d, $^{2}J_{H,H}$ = 2.9 Hz 4H, *H$_{methylene}$*).

^{13}C-NMR (101 MHz, CD_3CN, ppm, 25 °C): δ_C = 161.35 (C_q, 2C, *C2´*), 161.34 (C_q, 2C, *C6´*), 160.21 (C_q, 2C, *C2*), 159.31 (C_q, 2C, *C2´´*), 159.13 ($C_{azophenyl}$, 2C, *C4*), 154.13 (C_t, 2C, *C6´´*), 153.62 (C_t, 2C, *C6*), 151.68 (C_q, 2C, *C4´´*), 149.87 (C_q, 2C, *C4*), 147.65 ($C_{azophenyl}$, 2C, *C1*), 140.80 (C_{tolyl}, 2C, *C4*), 138.86 (C_t, 2C, *C4´*), 136.34 (C_{phenyl}, 2C, *C1*), 134.55 (C_{tolyl}, 2C, *C1*), 131.63 (C_{phenyl}, 2C, *C4*), 131.00 (C_{tolyl}, 4C, *C3*), 130.41 (C_{phenyl}, 4C, *C3*), 128.32 (C_{phenyl}, 4C, *C2*), 127.54 (C_{tolyl}, 4C, *C2*), 125.64 (C_t, 2C, *C5´´*), 125.02 (C_t, 2C, *C5*), 124.83 (C_t, 2C, *C5´*), 124.69 (C_t, 2C, *C3´*), 124.27 ($C_{azophenyl}$, 4C, *C2*), 122.53 (C_t, 2C, *C3´´*), 121.31 (C_t, 2C, *C3*), 119.89 ($C_{azophenyl}$, 4C, *C3*), 71.13 ($C_{methylene}$, 2C). The unambiguous assignment of the listed NMR-signals was done by correlating the appropriate 2D-NMR data, namely, ^{1}H,^{1}H-COSY, ^{1}H,^{13}C-HMQC, ^{1}H,^{13}C-HSQC and ^{1}H,^{13}C-HMBC.

^{19}F-NMR (376 MHz, CD_3CN, ppm, 25 °C): δ_F = –72.88 (d, $^{1}J_{P,F}$ = 705.5 Hz, 12F).

^{31}P-NMR (162 MHz, CD_3CN, ppm, 25 °C): δ_P = -144.61 (hept, $^{1}J_{P,F}$ = 706.5 Hz, 2P).

ESI-MS (MeCN, *positive* ion mode): *m/z* [ion, intensity (%)] = 532.4 (M^{2+}-2PF_6^-, 100).

HRMS (ESI-ToF): *m/z* calcd. for $[C_{68}H_{48}FeN_8O_2]^{2+}$: 532.1620; found: 532.1630.

UV/VIS (MeCN): λ_{max} (ε) = 273 nm (54140 L·cm^{-1}·mol^{-1}), 334 nm (65476 L·cm^{-1}·mol^{-1}), 365 nm (19168 L·cm^{-1}·mol^{-1}), 565 nm (9024 L·cm^{-1}·mol^{-1}).

Analytical data of (*Z*)-215:

^{1}H-NMR (600 MHz, CD_3CN, ppm, 25 °C): δ_H = 9.09 (dd, $^{3}J_{H,H}$ = 8.1 Hz, $^{4}J_{H,H}$ = 0.7 Hz, 2H, *H3´* / H5´**), 9.03 (d, $^{3}J_{H,H}$ = 8.2 Hz, 2H, *H3´* / H5´**), 8.80 (d, $^{4}J_{H,H}$ = 1.5 Hz, 2H, *H3´´*), 8.72 (t, $^{3}J_{H,H}$ = 8.1 Hz, 2H, *H4´*), 8.66 (d, $^{4}J_{H,H}$ = 1.7 Hz, 2H, *H3*), 7.76 (dd, $^{3}J_{H,H}$ = 8.0 Hz, $^{4}J_{H,H}$ = 1.8 Hz, 4H, *H2$_{phenyl}$*), 7.65 (d, $^{3}J_{H,H}$ = 8.4 Hz, 4H, *H2$_{tolyl}$*), 7.55 – 7.51 (m, 6H, *H3$_{phenyl}$ / H4$_{phenyl}$*), 7.48 (d, $^{3}J_{H,H}$ = 8.5 Hz, 4H, *H3$_{tolyl}$*), 7.41 (dd, $^{3}J_{H,H}$ = 6.0 Hz, $^{4}J_{H,H}$ = 2.0 Hz, 2H, *H5´´)*, 7.38 (dd, $^{3}J_{H,H}$ = 6.0 Hz, $^{5}J_{H,H}$ = 0.4 Hz, 2H, *H6´´)*, 7.16 (dd, $^{3}J_{H,H}$ = 6.1 Hz, $^{4}J_{H,H}$ = 2.0 Hz, 2H, *H5)*, 6.84 (d, $^{3}J_{H,H}$ = 6.1 Hz, 2H, *H6)*, 6.80 (d, $^{3}J_{H,H}$ = 9.1 Hz, 4H, *H2$_{phenyl(azo)}$*), 6.73 (d, $^{3}J_{H,H}$ = 9.1 Hz, 4H, *H3$_{phenyl(azo)}$*), 5.20 (d, $^{2}J_{H,H}$ = 15.9 Hz 4H, *H$_{methylene}$*).

^{13}C-NMR (151 MHz, CD_3CN, ppm, 25 °C): δ_C = 161.4 (C_q, 2C, *C2´*), 161.3 (C_q, 2C, *C6´*), 159.3 (C_q, 2C, *C2´´*), 159.2 (C_q, 2C, *C2*), 158.6 ($C_{azophenyl}$, 2C, *C4*), 154.4 (C_t, 2C, *C6´´*),

152.9 (C_t, 2C, *C6*), 151.4 (C_q, 2C, *C4´´*), 150.6 (C_q, 2C, *C4*), 148.2 ($C_{azophenyl}$, 2C, *C1*), 141.6 (C_{tolyl}, 2C, *C4*), 138.7 (C_t, 2C, *C4´*), 136.1 (C_{phenyl}, 2C, *C1*), 135.3 (C_{tolyl}, 2C, *C1*), 131.4 (C_{phenyl}, 2C, *C4*), 130.2 (C_{phenyl}, 4C, *C3*), 128.4 (C_{tolyl}, 8C, *C2 / C3*), 128.1 (C_{phenyl}, 4C, *C2*), 125.3 (C_t, 2C, *C5´´*), 125.2 (C_t, 2C, *C5*), 124.6 (C_t, 4C, *C3´ / C5´*), 122.8 ($C_{azophenyl}$, 4C, *C2*), 122.4 (C_t, 2C, *C3´´*), 121.9 (C_t, 2C, *C3*), 116.7 ($C_{azophenyl}$, 4C, *C3*), 70.6 ($C_{methylene}$, 2C). The unambiguous assignment of the listed NMR-signals was done by correlating the appropriate 2D-NMR, namely, ^{1}H,^{1}H-COSY, ^{1}H,^{13}C-HMQC, ^{1}H,^{13}C-HSQC, ^{1}H,^{13}C-HMBC and ^{1}H,^{1}H-NOESY.

(*E*)-1-(6-bromopyridin-2-yl)-3-phenylprop-2-en-1-one (234)

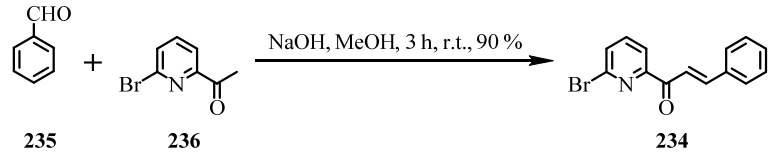

235 **236** **234**

The target compound (*E*)-1-(6-bromopyridin-2-yl)-3-phenylprop-2-en-1-one (**234**) was prepared inspired by a previously reported literature procedure.[558,559] At first a methanolic solution (600 mL) of benzaldehyde (**235**) (5.41 g, 5.18 mL, 50.0 mmol, 1.00 eq.) was prepared. Subsequently 2-acetyl-6-bromopyridine (**236**) (10.0 g, 50.0 mmol, 1.00 eq.) and aqueous NaOH (2%, 110 mL, 55.0 mmol, 1.10 eq.) were added and the reaction mixture was stirred at room temperature for 3 h. The off-white precipitate formed during the reaction was filtered off and sequentially washed with water and MeOH three times each. After leaving the filtrate overnight the solution was filtered again to yield a second product fraction. After rigorous drying at high vacuum (*E*)-1-(6-bromopyridin-2-yl)-3-phenylprop-2-en-1-one (**234**) could be isolated as the desired product in a yield of 90% (13.0 g, 45.1 mmol).

Analytical data of 234:

^{1}H-NMR (400 MHz, $CDCl_3$, ppm, 25 °C): δ_H = 8.20 (d, $^{3}J_{H,H}$ = 16.0 Hz, 1H, *COC**H**=CH*), 8.15 (d, $^{3}J_{H,H}$ = 7.4 Hz, 1H, *H3$_{(pyr)}$*), 7.95 (d, $^{3}J_{H,H}$ = 16.0 Hz, 1H, *COCH=C**H***), 7.77 - 7.71 (m, 3H, *H4*$_{(pyr)}$ or H5*$_{(pyr)}$ / 2 H$_{phenyl}$*), 7.68 (d, $^{3}J_{H,H}$ = 7.7 Hz, 1H, *H4*$_{(pyr)}$ / H5*$_{(pyr)}$*), 7.46 – 7.41 (m, 3H, *3 H$_{phenyl}$*).

^{13}C-NMR (101 MHz, $CDCl_3$, ppm, 25 °C): δ_C = 187.98 ($C_{(C=O)}$, 1C), 155.16 (C_q, 1C), 145.78 (C_t, 1C), 141.45 (C_q, 1C), 139.43 (C_t, 1C), 135.07 (C_q, 1C), 131.70 (C_t, 1C), 130.98 (C_t, 1C), 129.13 (C_{phenyl}, 2C), 129.13 (C_{phenyl}, 2C), 121.93 (C_t, 1C), 120.38 (C_t, 1C).

GCMS (EI$^+$, 70 eV): *m/z* [ion, intensity (%)] = 286.9 (M^+, 39).

ESI-MS (MeOH, *positive* ion mode): *m/z* [ion] = 288.1 ($M+H^+$), 310.1 ($M+Na^+$).

HRMS (ESI-ToF): *m/z* calcd. for $[C_{14}H_{10}BrNO+H]^+$: 288.0019; found: 288.0020, *m/z* calcd. for $[C_{14}H_{10}BrNO+Na]^+$: 309.9838; found: 308.9839.

6′-Bromo-4,6-diphenyl-2,2′-bipyridine (232)

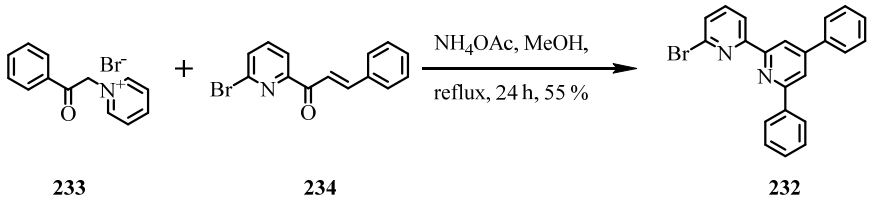

233 **234** **232**

The target compound 6′-bromo-4,6-diphenyl-2,2′-bipyridine (**232**) was prepared inspired by a previously reported literature procedure.[558,559] First of all a methanolic solution (600 mL) of (*E*)-1-(6-bromopyridin-2-yl)-3-phenylprop-2-en-1-one (**234**) (8.61 g, 29.0 mmol, 1.00 eq.) was prepared. Subsequently 1-(2-oxo-2-phenylethyl)pyridin-1-ium bromide (**233**) (8.23 g, 29.0 mmol, 1.00 eq.) and NH_4OAc (68.4 g, 870 mmol, 30.0 eq.) were added and the reaction mixture was heated to reflux for 24 h. Upon cooling down to room temperature and in the fridge afterwards a colorless precipitate appeared which was filtered off and sequentially washed with water and MeOH three times each. The obtained crude product was further purified by FCC using a mixture of EtOAc / *n*-hexane (1:9) as the solvent to obtain the desired product After leaving the filtrate overnight the solution was filtered again to yield a second product 6′-bromo-4,6-diphenyl-2,2′-bipyridine (**232**) in a yield of 55% (6.16 g, 15.9 mmol)**.** By applying a solvent diffusion technique using dichloromethane and *n*-hexane with an intermediate spacer layer of benzene it was additionally, possible to obtain single crystals of **232** suitable for x-ray structure determination. The crystallographic information of compound **232** are discussed in detailed form in section 9.2. Thus hereafter, only the remaining analytical data of target compound **232** are listed.

Analytical data of 232:

^{1}H-NMR (400 MHz, $CDCl_3$, ppm, 25 °C): δ_H = 8.64 (dd, $^3J_{H,H}$ = 7.7 Hz, $^4J_{H,H}$ = 0.9 Hz, 1H), 8.60 (d, $^4J_{H,H}$ = 1.5 Hz, 1H), 8.19 (dd, $^3J_{H,H}$ = 8.3 Hz, $^4J_{H,H}$ = 1.3 Hz, 2H), 7.98 (d, $^3J_{H,H}$ = 1.6 Hz, 1H), 7.80 (dd, $^3J_{H,H}$ = 8.2 Hz, $^4J_{H,H}$ = 1.3 Hz, 2H), 7.70 (t, $^3J_{H,H}$ = 7.8 Hz, 1H), 7.57 – 7.51 (m, 5H), 7.51 – 7.46 (m, 5H).

^{13}C-NMR (101 MHz, $CDCl_3$, ppm, 25 °C): δ_C = 157.70 (C_q, 1C), 157.29 (C_q, 1C), 154.75 (C_q, 1C), 150.59 (C_q, 1C), 141.63 (C_q, 1C), 139.34 (C_q, 1C), 139.26 (C_t, 1C), 138.70 (C_q, 1C), 129.32 (C_t, 1C), 129.22 (C_t, 1C), 129.18 (C_{phenyl}, 2C), 128.89 (C_{phenyl}, 2C),

128.16 (C_t, 1C), 127.41 (C_{phenyl}, 2C), 127.18 (C_{phenyl}, 2C), 120.29 (C_t, 1C), 119.15 (C_t, 1C), 118.02 (C_t, 1C).

GCMS (EI$^+$, 70 eV): *m/z* [ion, intensity (%)] = 386.0 (M^+, 100), 307.1 (M^+-Br, 51).

ESI-MS (MeOH, *positive* ion mode): *m/z* [ion] = 387.2 ($M+H^+$, 100), 409.2 ($M+Na^+$, 15).

HRMS (ESI-ToF): *m/z* calcd. for $[C_{22}H_{15}BrN_2+H]^+$: 387.0491; found: 387.0497.

6′-Iodo-4,6-diphenyl-2,2′-bipyridine (231)

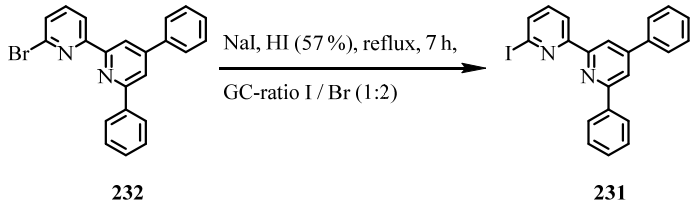

232 **231**

A mixture of 6′-bromo-4,6-diphenyl-2,2′-bipyridine (**232**) (5.81 g, 15.0 mmol, 1.00 eq.) and NaI (3.15 g, 21.0 mmol, 1.40 eq.) was charged into a two-neck round-bottom flask and suspended in aqueous HI (57%, 40.4 g, 23.7 mL, 180 mmol, 12.0 eq.) before being refluxed for 7 h under nitrogen atmosphere. For the workup the reaction mixture was carefully poured onto pre-cooled aqueous NaOH- solution (40%, 7.20 g, 18.0 mL, 180 mmol, 12.0 eq.) and ice. Afterwards the quenched reaction mixture was extracted with DCM (8 *x* 100 mL). The combined organic extracts were subsequently washed with water and saturated aqueous $Na_2S_2O_3$- solution prior to drying of the combined organic phases over $MgSO_4$, filtration and evaporation of residual solvent under reduced pressure. Unfortunately neither by FCC nor by recrystallization the desired product 6′-iodo-4,6-diphenyl-2,2′-bipyridine (**231**) could be purely isolated. Instead 6.13 g of a mixture of the starting material 6′-bromo-4,6-diphenyl-2,2′-bipyridine (**232**) and the iodo-derivative **231** was isolated in an approximate I / Br– ratio of 1:2 according to GCMS-analysis.

Analytical data of 231:

GCMS (EI$^+$, 70 eV): *m/z* [ion, intensity (%)] = 433.9 (M^+, 72), 307.1 (M^+-I, 100).
ESI-MS (MeOH, *positive* ion mode): *m/z* [ion] = 435.1 ($M+H^+$, 100).
HRMS (ESI-ToF): *m/z* calcd. for $[C_{22}H_{15}IN_2+H]^+$: 435.0353; found: 435.0354.

4′′-chloro-4,6-diphenyl-2,2′:6′,2′′-terpyridine (230)

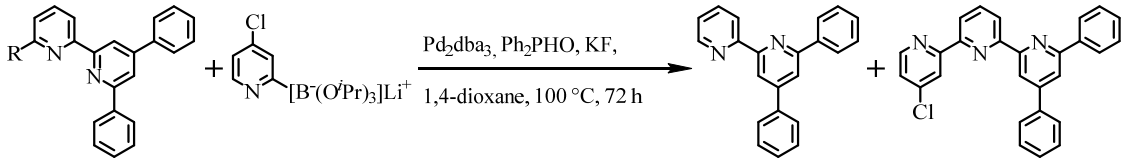

232: R = Br **140** **237** **230**
231: R = I

The target compound 4′′-chloro-4,6-diphenyl-2,2′:6′,2′′-terpyridine (**230**) was prepared in a Suzuki-Miyaura cross-coupling reaction following a procedure similar to that one of the preparation of compound **47**. For this procedure a Schlenk tube was charged with the 1:2-mixture of the bromo- and the iodo compound **232** and **231** (calculated fractions: 3.80 g / 2.13 g, 9.80 mmol / 4.90 mmol, 2.00 eq. / 1.00 eq.). To this mixture the coupling partner tri*iso*propyl-2-(4-chloropyridyl) borate (**140**) (15.1 g, 49.0 mmol, 10.0 eq.), Pd_2dba_3 (808 mg, 882 µmol, 0.18 eq.), diphenylphosphine oxide (1.10 g, 5.29 mmol, 1.08 eq.), and KF (5.75 g, 98.0 mmol, 20.0 eq.) were added. All those reagents were evacuated and the flask was put under inert atmosphere three times, before the mixture was dissolved in previously degassed 1,4-dioxane (100 mL), sealed pressure safe and heated to 100 °C for 72 h. After diluting the reaction mixture with EtOAc it was filtered through a plug of silica gel. Concentration of the solvent under reduced pressure yielded the crude product, which was now subjected to flash column chromatography on silica gel using a gradient of EtOAc / *n*-hexane (15:85 to 25:75) as the eluent. Unfortunately the desired product 4′′-chloro-4,6-diphenyl-2,2′:6′,2′′-terpyridine (**230**) could not be isolated purely but only in a mixture (2.20 g) with the dehalogenated side product 4,6-diphenyl-2,2′-bipyridine (**237**). Both compounds could be unambiguously identified by mass spectroscopy. As the side product **237** is separated from the reaction mixture after the next step its analytical details are listed there. Only the mass spectroscopic details of 4,6-diphenyl-2,2′-bipyridine (**237**) and 4′′-chloro-4,6-diphenyl-2,2′:6′,2′′-terpyridine (**230**) are listed directly hereafter.

Analytical data of 230:

GCMS (EI$^+$, 70 eV): *m/z* [ion, intensity (%)] = 419.1 (M^+, 100), 230.0 (M^+-Bipy-Cl, 22).
ESI-MS (MeCN, *positive* ion mode): *m/z* [ion] = 420.3 ($M+H^+$, 100).
HRMS (ESI-ToF): *m/z* calcd. for $[C_{27}H_{18}ClN_3+H]^+$: 420.1262; found: 420.1268.

Analytical data of 237:

GCMS (EI$^+$, 70 eV): *m/z* [ion, intensity (%)] = 308.1 (M^+, 100), 230.1 (M^+-pyridyl, 30).
ESI-MS (MeCN, *positive* ion mode): *m/z* [ion] = 309.3 ($M+H^+$, 100).
HRMS (ESI-ToF): *m/z* calcd. for $[C_{22}H_{16}N_2+H]^+$: 309.1386; found: 309.1388.

4,6-Diphenyl-4´´-(*p*-tolyl)-2,2´:6´,2´´-terpyridine (229)

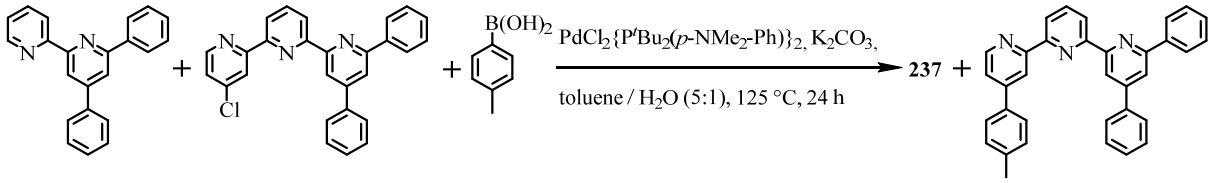

237 **230** **224** **229**

The target compound 4,6-diphenyl-4´´-(*p*-tolyl)-2,2´:6´,2´´-terpyridine (**229**) was prepared from a mixture of compounds **230** and **237** in a Suzuki-Miyaura cross-coupling reaction following representative procedure B. A Schlenk tube was charged with 525 mg of the mixture of 4,6-diphenyl-2,2´-bipyridine (**237**), which was postulated to be inert towards the reaction conditions, and 4´´-chloro-4,6-diphenyl-2,2´:6´,2´´-terpyridine (**230**). Now *p*-tolyl-boronic acid (**224**) (1.05 g, 7.50 mmol), $PdCl_2\{P^tBu_2(p\text{-}NMe_2\text{-}Ph)\}_2$ (26.8 mg, 37.5 µmol), and K_2CO_3 (314 mg, 2.25 mmol) were added and the mixture was suspended in previously degassed toluene (75 mL) and H_2O (15 mL). The reaction vessel was sealed and heated to 125 °C for 24 h. The resulting reaction mixture was allowed to cool down to room temperature and was subsequently diluted with DCM and water. Now the reaction mixture was extracted with DCM (4 *x*) followed by extraction of the combined organic phases with brine (2 *x*). The organics were dried over $MgSO_4$, filtered and residual solvent was evaporated under reduced pressure. The crude product was purified by FCC using a solvent mixture of EtOAc / *n*-hexane (3:17) to afford the desired product 4,6-diphenyl-4´´-(*p*-tolyl)-2,2´:6´,2´´-terpyridine (**229**) (247 mg, 0.52 mmol) and the dehalogenated side-product 4,6-diphenyl-2,2´-bipyridine (**237**) (300 mg, 0.97 mmol), which was carried through from the starting material. For both compounds the analytical data is listed below.

Analytical data 229:

^{1}H-NMR (400 MHz, $CDCl_3$, ppm, 25 °C): δ_H = 8.91 (d, $^4J_{H,H}$ = 1.2 Hz, 1H, *H3´´*), 8.86 (d, $^4J_{H,H}$ = 1.5 Hz, 1H, *H3*), 8.75 (d, $^3J_{H,H}$ = 5.1 Hz, 1H, *H6´´*), 8.73 (dd, $^3J_{H,H}$ = 7.8 Hz, $^5J_{H,H}$ = 1.0 Hz, 1H, *H3´* / H5´**), 8.53 (dd, $^3J_{H,H}$ = 7.8 Hz, $^5J_{H,H}$ = 0.8 Hz, 1H, *H3´* / H5´**), 8.25 (dd, $^3J_{H,H}$ = 8.5 Hz, $^4J_{H,H}$ = 1.4 Hz, 2H, H_{phenyl}), 8.02 (t, $^3J_{H,H}$ = 7.8 Hz, 1H, *H4´´*), 8.01 (d, $^4J_{H,H}$ = 1.5 Hz, 1H, *H5*), 7.86 (dd, $^3J_{H,H}$ = 8.6 Hz, $^4J_{H,H}$ = 1.3 Hz, 2H, H_{phenyl}), 7.72 (d, $^3J_{H,H}$ = 8.1 Hz, 2H, H_{phenyl}), 7.60 – 7.44 (m, 7H, *H5´´ / 6* H_{phenyl}), 7.33 (d, $^3J_{H,H}$ = 7.9 Hz, 2H, H_{phenyl}), 2.45 (s, 3H, H_{methyl}).

^{13}C NMR (101 MHz, $CDCl_3$, ppm, 25 °C): δ_C = 157.29 (C_q, 1C), 156.74 (C_q, 1C), 156.51 (C_q, 1C), 155.73 (C_q, 1C), 155.25 (C_q, 1C), 150.18 (C_q, 1C), 149.36 (C_t, 1C), 139.60 (C_q, 1C), 139.42 (C_q, 1C), 139.15 (C_q, 1C), 138.02 (C_t, 1C), 135.60 (C_q, 1C), 129.99 (C_{phenyl}, 2C), 129.23 (C_{phenyl}, 3C), 129.14 (C_t, 1C), 128.90 (C_{phenyl}, 2C), 127.35 (C_{phenyl}, 2C), 127.24 (C_{phenyl}, 2C), 127.09 (C_{phenyl}, 2C), 121.71 (C_t, 1C), 121.54 (C_t, 1C), 121.48 (C_t, 1C), 119.15 (C_t, 1C), 118.64 (C_t, 1C), 117.82 (C_t, 1C), 21.43 (C_{methyl}, 1C). In the ^{13}C-spectrum and in the DEPT-135 one signal less than expected was found most likely due to coincident signals.

GCMS (EI$^+$, 70 eV): *m/z* [ion, intensity (%)] = 476.4 (M^+, 100).

ESI-MS (MeOH, *positive* ion mode): *m/z* [ion, intensity (%)] = 476.3 ($M+H^+$, 100), 498.3 ($M+Na^+$, 10).

HRMS (ESI-ToF): *m/z* calcd. for $[C_{34}H_{25}N_3+H]^+$: 476.2121; found: 476.2128

Analytical data 237:

^{1}H-NMR (400 MHz, $CDCl_3$, ppm, 25 °C): δ_H = 8.78 – 8.72 (m, 3H), 8.27 (d, $^3J_{H,H}$ = 7.1 Hz, 2H), 7.99 (d, $^4J_{H,H}$ = 1.5 Hz, 1H), 7.87 – 7.78 (m, 3H), 7.60 – 7.44 (m, 6H), 7.30 (ddd, $^3J_{H,H}$ = 7.4 Hz, $^4J_{H,H}$ = 4.8 Hz, $^5J_{H,H}$ = 1.1 Hz, 1H).

^{13}C-NMR (101 MHz, $CDCl_3$, ppm, 25 °C): δ_C = 156.93 (C_q, 1C), 156.21 (C_q, 1C), 156.14 (C_q, 1C), 150.03 (C_q, 1C), 148.94 (C_t, 1C), 139.36 (C_q, 1C), 138.59 (C_q, 1C), 136.70 (C_t, 1C), 129.00 (C_t, 1C), 128.92 (C_{phenyl}, 2C), 128.91 (C_t, 1C), 128.66 (C_{phenyl}, 2C), 127.14 (C_{phenyl}, 2C), 127.02 (C_{phenyl}, 2C), 123.70 (C_t, 1C), 121.40 (C_t, 1C), 118.28 (C_t, 1C), 117.41 (C_t, 1C).

GCMS (EI$^+$, 70 eV): *m/z* [ion, intensity (%)] = 308.1 (M^+, 100), 230.1 (M^+-pyridyl, 30).

ESI-MS (MeCN, *positive* ion mode): *m/z* [ion] = 309.3 ($M+H^+$, 100).

HRMS (ESI-ToF): *m/z* calcd. for $[C_{22}H_{16}N_2+H]^+$: 309.1386; found: 309.1388.

4´´-(4-(bromomethyl)phenyl)-4,6-diphenyl-2,2´:6´,2´´-terpyridine (228)

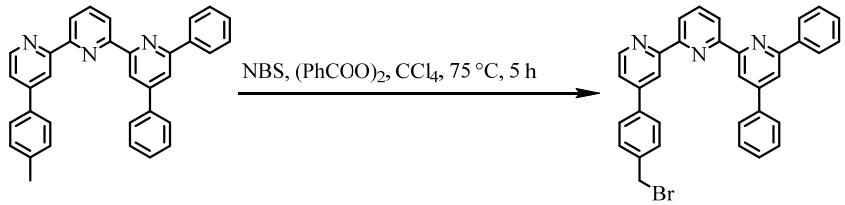

229 **228**

The desired 4´´-(4-(bromomethyl)phenyl)-4,6-diphenyl-2,2´:6´,2´´-terpyridine (**228**) was prepared by radical side chain bromination of precursor **229** based on a reported literature procedure.[554,555] Therefore 4,6-diphenyl-4´´-(*p*-tolyl)-2,2´:6´,2´´-terpyridine (**229**) (214 mg, 0.45 mmol, 1.00 eq.), NBS (97.1 mg, 0.54 mmol, 1.20 eq.), and dibenzoyl peroxide (28.1 mg, 113 µmol, 0.25 eq.) were dissolved in previously degassed CCl_4 (30 mL) and heated to 75 °C for about 5 h until the reaction progress stopped (monitoring by TLC). Now the reaction mixture was allowed to cool to room temperature and was stirred in an ice-water bath for 30 min prior to dilution with DCM, brine and aqueous saturated $Na_2S_2O_3$-solution. The resulting mixture was repeatedly extracted with DCM (4 *x*) before the combined organic layers were dried over $MgSO_4$, filtered and residual solvent was removed under reduced pressure. The crude product was purified via FCC using a gradient of solvent mixtures ranging from of EtOAc / *n*-hexane (3:17) up to EtOAc / *n*-hexane (1:3). Apart from the reisolation of unreacted starting material **229** in a yield of 17% (35.4 mg, 74.4 µmol) mainly the desired target compound 4´´-(4-(bromomethyl)phenyl)-4,6-diphenyl-2,2´:6´,2´´-terpyridine (**228**) was isolated in a yield of 82% (206 mg, 371 µmol).

Analytical data 228:

^{1}H-NMR (400 MHz, $CDCl_3$, ppm, 25 °C): δ_H = 8.88 (d, $^4J_{H,H}$ = 1.1 Hz, 1H, *H3´´*), 8.82 (d, $^4J_{H,H}$ = 1.5 Hz, 1H, *H3*), 8.75 (dd, $^3J_{H,H}$ = 5.1 Hz, $^5J_{H,H}$ = 0.4 Hz 1H, *H6´´*), 8.72 (dd, $^3J_{H,H}$ = 7.8 Hz, $^5J_{H,H}$ = 0.9 Hz, 1H, *H3´** / *H5´**), 8.51 (dd, $^3J_{H,H}$ = 7.8 Hz, $^5J_{H,H}$ = 0.7 Hz, 1H, *H3´** / *H5´**), 8.24 (dd, $^3J_{H,H}$ = 8.4 Hz, $^4J_{H,H}$ = 1.3 Hz, 2H, H_{phenyl}), 8.01 (t, $^3J_{H,H}$ = 7.8 Hz, 1H, *H4´*), 8.00 (d, $^4J_{H,H}$ = 1.5 Hz, 1H, *H5*), 7.84 (dd, $^3J_{H,H}$ = 8.1 Hz, $^4J_{H,H}$ = 1.3 Hz, 2H, H_{phenyl}), 7.76 (d, $^3J_{H,H}$ = 8.2 Hz, 2H, H_{phenyl}), 7.61 – 7.46 (m, 9H, *H5´´ / 8 H_{phenyl}*), 4.57 (s, 3H, $H_{methylene}$).

^{13}C NMR (101 MHz, $CDCl_3$, ppm, 25 °C): δ_C = 157.26 (C_q, 1C), 156.89 (C_q, 1C), 156.41 (C_q, 1C), 155.73 (C_q, 1C), 155.02 (C_q, 1C), 150.15 (C_q, 1C), 149.64 (C_t, 1C),

138.61 (C_q, 1C), 139.54 (C_q, 1C), 139.10 (C_q, 1C), 138.91 (C_q, 1C), 138.66 (C_q, 1C), 138.03 (C_t, 1C), 129.93 (C_{phenyl}, 2C), 129.24 (C_{phenyl}, 3C), 129.19 (C_t, 1C), 128.89 (C_{phenyl}, 2C), 127.68 (C_{phenyl}, 2C), 127.32 (C_{phenyl}, 2C), 127.22 (C_{phenyl}, 2C), 121.79 (C_t, 1C), 121.62 (C_t, 1C), 121.47 (C_t, 1C), 119.31 (C_t, 1C), 118.63 (C_t, 1C), 117.78 (C_t, 1C), 32.97 ($C_{methylene}$, 1C). In the ^{13}C-spectrum and in the DEPT-135 one signal less than expected was found most likely due to coincident signals.

ESI-MS (MeCN, *positive* ion mode): *m/z* [ion, intensity (%)] = 554.2 ($M+H^+$, 100), 576.2 ($M+Na^+$, 15).

HRMS (ESI-ToF): *m/z* calcd. for $[C_{34}H_{24}BrN_3+H]^+$: 554.1226; found: 544.1226.

(*E*)-4,6-diphenyl-4′′-(4-((4-((4-(4′′-phenyl-[2,2′:6′,2′′-terpyridin]-4-yl)benzyl)oxy)-phenyl)diazenyl)phenoxy)methyl)phenyl)-2,2′:6′,2′′-terpyridine (226)

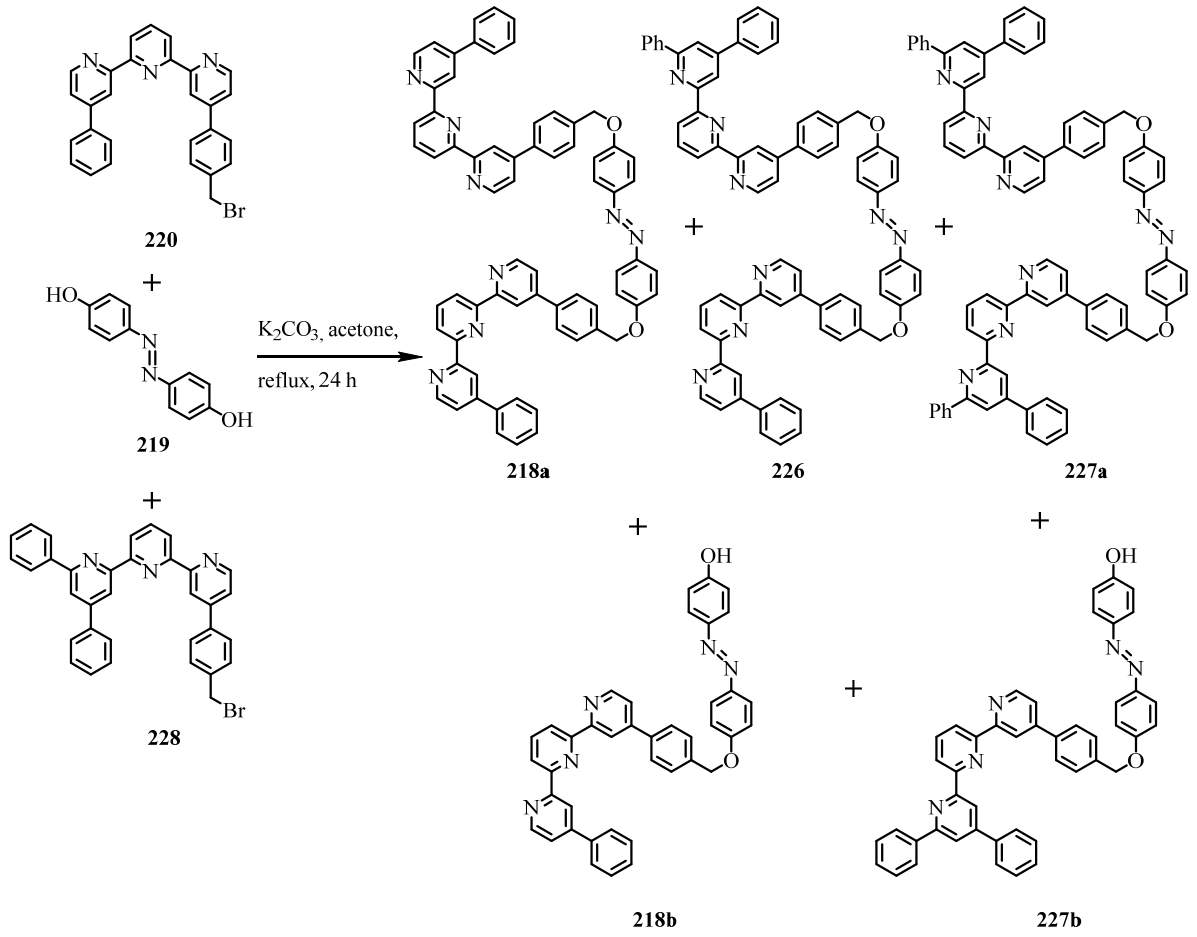

Compound **226** was prepared via a statistical twofold S_N2-reaction inspired by a previously reported literature procedure.[556] Therefore (*E*)-4,4′-(diazene-1,2-diyl)diphenol **219** (10.7 mg, 0.05 mmol, 1.00 eq.), the ligands 4-(4-(bromomethyl)phenyl)-4′′-phenyl-2,2′:6′,2′′-terpyridine (**220**) (23.9 mg, 0.05 mmol, 1.00 eq) and 4′′-(4-(bromomethyl)phenyl)-4,6-diphenyl-2,2′:6′,2′′-terpyridine (**228**) (27.7 mg, 0.05 mmol, 1.00 eq), and K_2CO_3 (18.1 mg, 0.13 mmol, 2.60 eq.) were charged into a Schlenk tube, put under inert atmosphere and dissolved in dry acetone (100 mL), before the reaction was sealed and heated to reflux for 24 h. After the reaction was allowed to cool down to room temperature it was diluted with DCM and water and extracted with DCM (5 *x*), before drying over $MgSO_4$, filtration and evaporation of residual solvent. The product showed to be highly insoluble and the crude product contained all five compounds to be expected from this statistical reaction, which could be proven by ESI-MS as shown in the analytical data listed below. By washing the residue with MeOH, DCM and EtOAc **218b** and **227b** could be eliminated from the mixture, so that only **218a**,

226 and **227a** remained in the crude product. The disubstituted compounds **218a**, **226** and **227a** could be verified by HR-ESI-MS as shown below.

Analytical data of 218a:

ESI-MS (THF, *positive* ion mode): *m/z* [ion] = 1009.8 ($M+H^+$).
HRMS (ESI-ToF): *m/z* calcd. for $[C_{68}H_{48}N_8O_2+H]^+$: 1009.3973; found: 1009.3961, *m/z* calcd. for $[C_{68}H_{48}N_8O_2+2H]^{2+}$: 505.2023; found: 505.2021.

Analytical data of 227a:

ESI-MS (THF, *positive* ion mode): *m/z* [ion] = 1161.9 ($M+H^+$).
HRMS (ESI-ToF): *m/z* calcd. for $[C_{80}H_{56}N_8O_2+H]^+$: 1161.4599; found: 1161.4586, *m/z* calcd. for $[C_{80}H_{56}N_8O_2+2H]^{2+}$: 581.2336; found: 581.2332.

Analytical data of 226:

ESI-MS (THF, *positive* ion mode): *m/z* [ion] = 1085.9 ($M+H^+$), 543.5($M+2H^+$).
HRMS (ESI-ToF): *m/z* calcd. for $[C_{74}H_{52}N_8O_2+H]^+$: 1085.4286; found: 1085.4273, *m/z* calcd. for $[C_{74}H_{52}N_8O_2+2H]^{2+}$: 543.2179; found: 543.2179.

Analytical data of 218b:

ESI-MS (THF, *positive* ion mode): *m/z* [ion] = 612.5 ($M+H^+$).

Analytical data of 227b:

ESI-MS (THF, *positive* ion mode): *m/z* [ion] = 688.65 ($M+H^+$).

{[Fe(*226*)]$^{2+}$[(PF$_6$)$^-$]$_2$} (216)

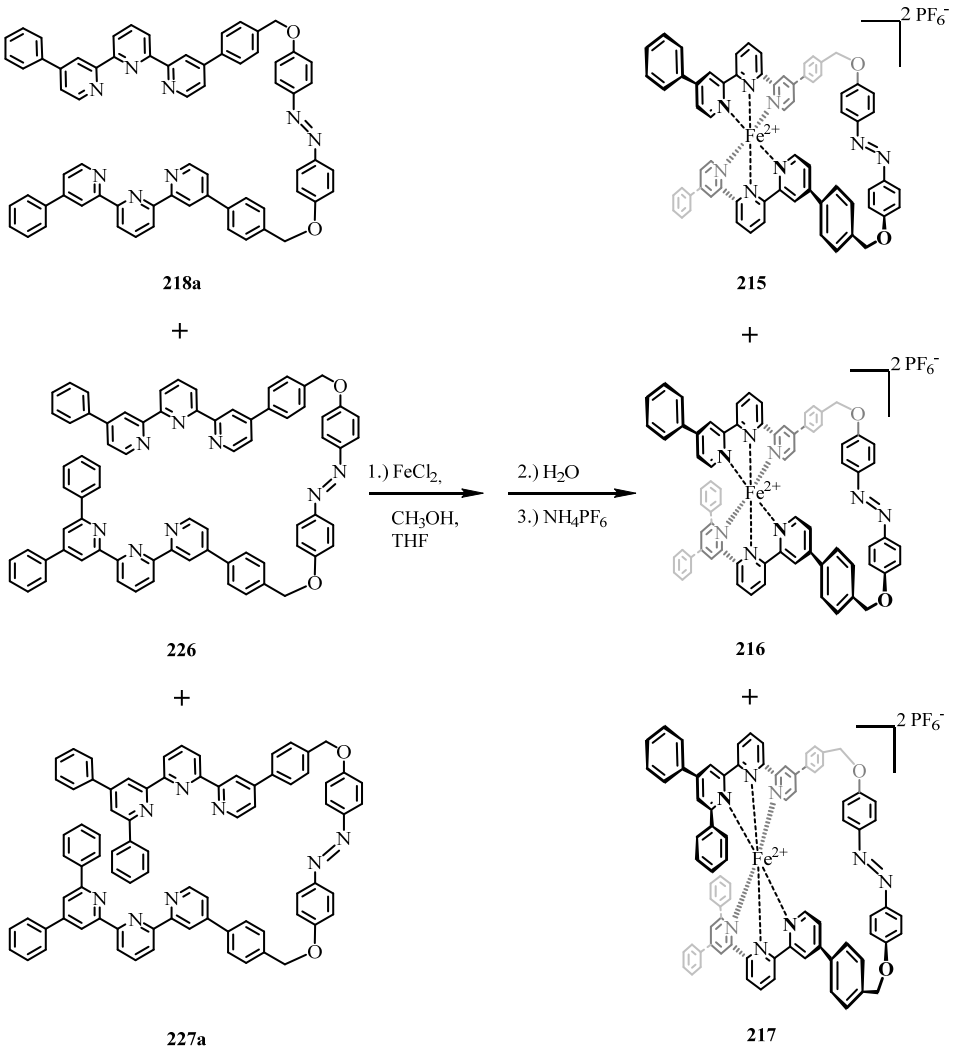

The preparation of **216** was attempted by a modification of the representative procedure C. The reaction was performed by suspending the inseparable mixture of the three azo-ligands (*E*)-1,2-bis-(4-((4-(4′′-phenyl-[2,2′:6′,2′′-terpyridin]-4-yl)benzyl)oxy)phenyl)diazene (**218a**), (*E*)-4,6-diphe-nyl-4′′-(4-((4-((4-((4-(4′′-phenyl-[2,2′:6′,2′′-terpyridin]-4-yl)benzyl)oxy)-phenyl)diazenyl)phenoxy)methyl)phenyl)-2,2′:6′,2′′-terpyridine (**226**), and (*E*)-1,2-bis(4-((4-(4′′,6′′-diphenyl-[2,2′:6′,2′′-terpyridin]-4-yl)benzyl)oxy)phenyl)diazene (**227a**), in a mixture of MeOH (600 mL) and THF (600 mL). Now $FeCl_2$ (6,34 mg, 50.0 µmol) was dissolved in MeOH (50 mL) and added dropwise to the ligand's solution over 3 h via syringe pump. After an additional hour of stirring NH_4PF_6 (408 mg, 2.50 mmol) and water (600 mL) were added to the solution, which turned slightly purple upon the addition of water. After 20h of stirring, the organic solvents were evaporated from the solution under reduced pressure yielding a dark purple precipitate in the aqueous phase. The precipitate was filtered off and excessively washed with water, before it was dried to yield the crude product mixture containing the

metalloazobenzenophanes **215**, **216**, and **217**, as proven by ESI-MS analysis. This mixture was now subjected to purification via preparative reversed-phase HPLC yielding the pure macrocycle **215**, as a dark purple solid. Furthermore, instead of the expected monomeric macrocycle **216** the species was isolated in its dimeric form **238**, containing two metal centers and two ligands, instead of the expected one each.

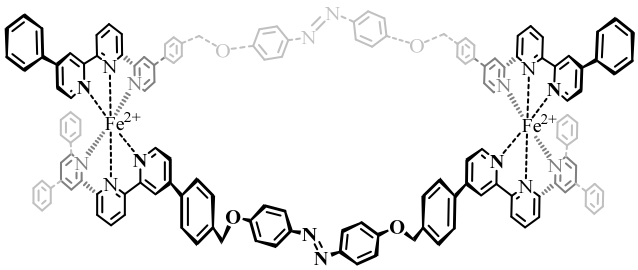

238

The repeated investigation of the isolated dimeric metalloazobenzenophane **238** via HR-ESI-MS revealed, that the dimeric macrocycle **238** forms an isomerization equilibrium with the monomeric metalloazobenzenophane **216**. Therefore no clean NMR-spectroscopic characterization or further optical switching experiments of either one of the two named species were possible. Since the purely isolated macrocycle **215** has been discussed above only the accessible mass-spectroscopic data obtained for the monomeric metalloazobenzeno-phane **216** and its dimeric form **238**, respectively, are listed hereafter.

Analytical data of 216:

ESI-MS (MeCN, *positive* ion mode): *m/z* [ion, intensity (%)] = 570.4 (M^{2+}-2PF_6^-, 100).
HRMS (ESI-ToF): *m/z* calcd. for $[C_{74}H_{52}FeN_8O_2]^{2+}$: 570.1777; found: 570.1787.

Analytical data of 238:

ESI-MS (MeCN, *positive* ion mode): *m/z* [ion, intensity (%)] = 570.7 (M^{4+}-4PF_6^-, 100), 798.6 (M^{3+}-4PF_6^-+$F_3CCO_2^-$, 100).
HRMS (ESI-ToF): *m/z* calcd. for $[C_{148}H_{104}Fe_2N_{16}O_4]^{4+}$: 570.1777; found: 570.1787; *m/z* calcd. for $[C_{150}H_{104}F_3Fe_2N_{16}O_6]^{3+}$: 797.8987; found: 797.9003.

{[Fe(*220*)$_2$]$^{2+}$[(PF$_6$)$^-$]$_2$} (239)

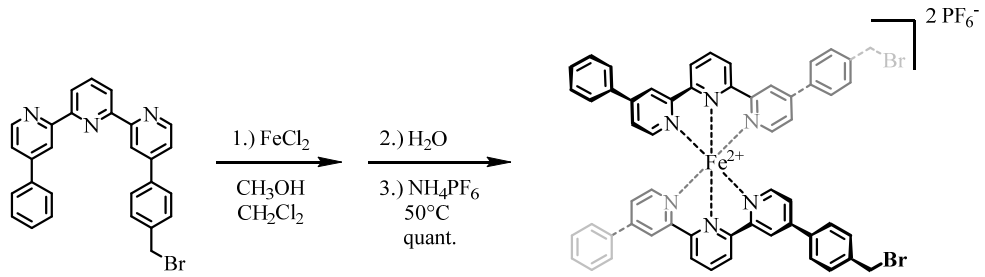

220 **239**

239 was prepared according to the representative procedure C. The established iron(II) source $FeCl_2$ (0.35 mg, 2.75 µmol, 1.00 eq.), the ligand 4-(4-(bromomethyl)phenyl)-4´´-phenyl-2,2´:6´,2´´-terpyridine (**220**) (2.63 mg, 5.50 µmol, 1.00 eq.), the solvents MeOH (10 mL), DCM (10 mL) and water (100 mL) and for the final anion exchange NH_4PF_6 (44.8 mg, 275 µmol, 50.0 eq.) were used. The product **239** was isolated as a dark purple solid in quantitative yield (2.78 mg, 2.75 µmol).

Analytical data of 239:

^{1}H-NMR (500 MHz, CD_3CN, ppm, 25 °C): δ_H = 9.09 (4H, *H3´ / H5´*), 8.78 (4H, *H3 / H3´´*), 8.76 (2H, *H4´*), 7.74 (4H, H_{phenyl}), 7.72 (4H, H_{phenyl}), 7.56 (4H, H_{phenyl}), 7.52 (4H, H_{phenyl}), 7.51 (2H, H_{phenyl}), 7.36 (2H, *H5*), 7.35 (2H, *H5´´*), 7.15 (2H, *H6*), 7.14 (2H, *H6´´*), 4.62 (4H, $H_{methylene}$). The assignment of the listed NMR-signals was done by correlating appropriate 2D-NMR data like, ^{1}H,^{1}H-COSY, ^{1}H,^{13}C-HMQC and ^{1}H,^{13}C-HMBC.

^{13}C-NMR (126 MHz, $CDCl_3$, ppm, 25 °C): δ_C = 161.7 (C_q, 4C), 159.6 (C_q, 4C), 154.4 (C_t, 4C), 152.0 (C_q, 2C), 151.3 (C_q, 2C), 142.3 (C_q, 2C), 139.4 (C_t, 2C), 136.6 (C_q, 4C), 131.9 (C_{phenyl}, 2C), 131.4 (C_{phenyl}, 4C), 130.7 (C_{phenyl}, 8C), 129.7 (C_t, 6C), 125.9 (C_t, 4C), 125.2 (C_t, 4C), 129.7 (C_t, 6C), 122.9 (C_t, 2C), 33.9 ($C_{methylene}$, 2C).

HRMS (ESI-ToF): *m/z* calcd. for $[C_{56}H_{40}Br_2FeN_6]^{2+}$: 505.0510; found: 505.0517.

{[Fe(*220*)(*228*)]$^{2+}$[(PF$_6$)$^-$]$_2$} (240)

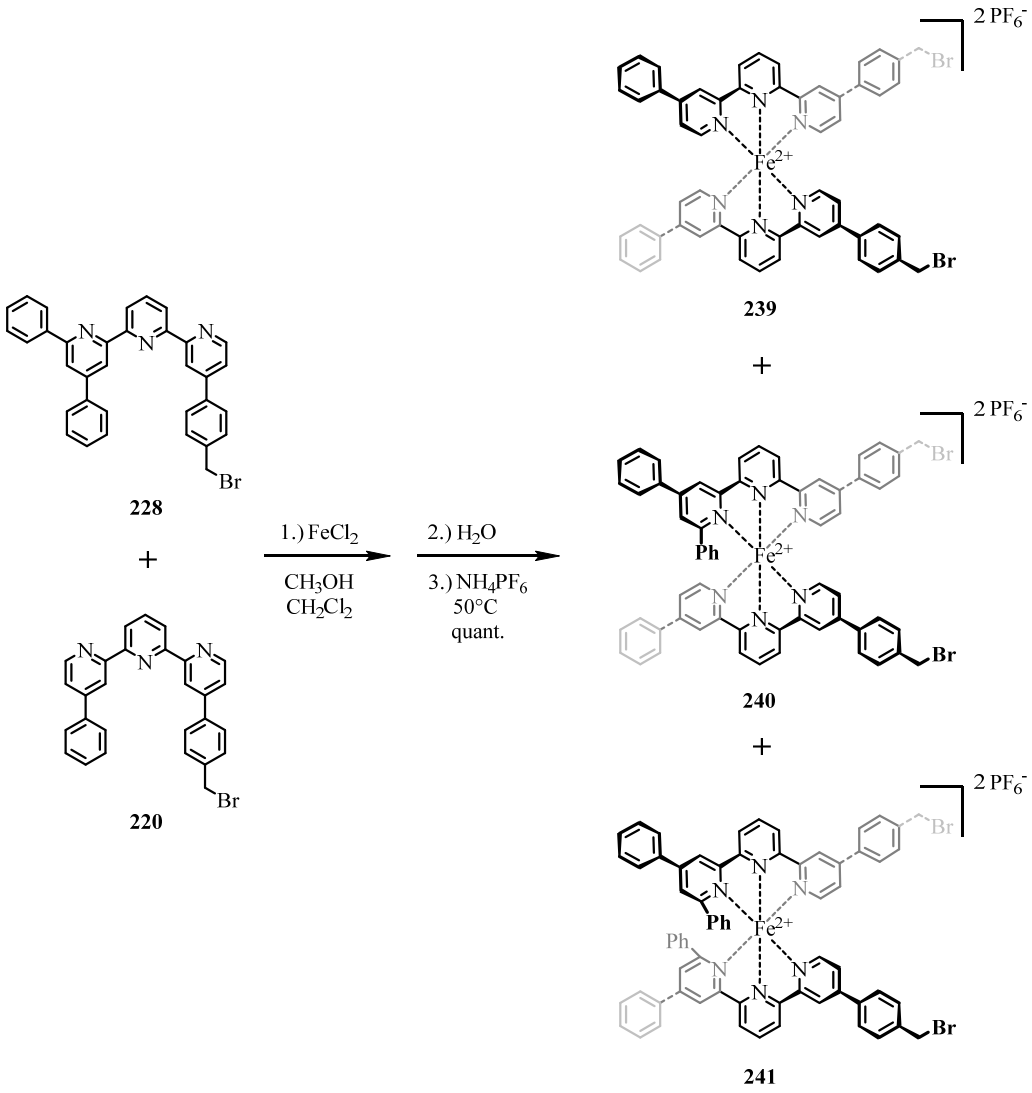

240 was prepared by a modification of the general procedure C. In this case a statistic reaction had to be performed in which equimolar amounts of 4′′-(4-(bromo-methyl)phenyl)-4,6-di-phenyl-2,2′:6′,2′′-terpyridine (**228**) (55.4 mg, 0.10 mmol, 1.00 eq.) and 4-(4-(bromomethyl)-phenyl)-4′′-phenyl-2,2′:6′,2′′-terpyridine (**220**) (47.8 mg, 0.10 mmol, 1.00 eq.) were mixed with $FeCl_2$ (12.7 mg, 0.10 mmol, 1.00 eq.). The reagents were dissolved in MeOH (50 mL), DCM (50 mL), and water (100 mL), before NH_4PF_6 (815 mg, 5.00 mmol, 50.0 eq.) was added. The crude product mixture was isolated as a dark purple solid and subjected to purification via preparative reversed-phase HPLC using a solvent gradient ranging from H_2O / MeCN (50:50) up to H_2O / MeCN (25:75) at a flow rate of 20 mL/min yielding the desired purified product **240** as a dark purple solid in a yield of 20% (26.9 mg, 19.5 µmol). The two expected homoleptic side products could be separated successfully from the desired heteroleptic target structure. The analytical data of these two complexes **239** and **241** is

however discussed separately at the place where their exclusive synthesis is discussed. Thus, hereafter, only analytical data of target compound **240** are listed.

Analytical data of 240:

^{1}H-NMR (500 MHz, CD_3CN, ppm, 25 °C): δ_H = 9.33 (d, $^3J_{H,H}$ = 8.1 Hz, 1H, *H3´(220)* or *H5´(220)*), 9.05 (d, $^3J_{H,H}$ = 8.1 Hz, 1H, *H3´(220)* or *H5´(220)*), 8.95 (d, $^4J_{H,H}$ = 2.1 Hz, 1H, *H3(228)*), 8.81 (t, $^3J_{H,H}$ = 8.1 Hz, 1H, *H4´(220)*), 8.68 (dd, $^4J_{H,H}$ = 3.1 Hz, $^5J_{H,H}$ = 1.8 Hz, 2H, *H3(220) / H3´´(220)*), 8.65 (d, $^3J_{H,H}$ = 7.9 Hz, 2H, *H3´(228) / H5´(228)*), 8.62 (d, $^4J_{H,H}$ = 2.0 Hz, 1H, *H3´´(228)*), 8.34 (t, $^3J_{H,H}$ = 8.0 Hz, 1H, *H4´(228)*), 7.84 – 7.80 (m, 5H, H_{phenyl}), 7.79 (app. s, 1H, H_{phenyl}), 7.61 (d, $^3J_{H,H}$ = 8.5 Hz, 4H, H_{tolyl}), 7.57 – 7.50 (m, 9H, H_{phenyl}), 7.49 – 7.46 (m, 3H, *H5(220) / H5´´(220)* and *H6(220)* or *H6´´(220)*), 7.34 – 7.28 (m, 1H, *H6(220)* or *H6´´(220)*), 7.20 (d, $^4J_{H,H}$ = 2.0 Hz, 1H, *H5(228)*), 7.17 (dd, $^3J_{H,H}$ = 6.2 Hz, $^4J_{H,H}$ = 2.0 Hz, 1H, *H5´´(228)*), 7.10 (app. t, $^3J_{H,H}$ = 7.8 Hz 2H, H_{phenyl}), 6.15 (app. s, 2H, H_{phenyl}), 5.70 (d, $^3J_{H,H}$ = 6.2 Hz, 1H, *H6´´(228)*), 4.64 (s, 2H, $H_{methylene}$), 4.58 (s, 2H, $H_{methylene}$). The assignment of the listed ^{1}H-NMR-signals was done by correlating the appropriate 2D-NMR, namely, ^{1}H,^{1}H-COSY, ^{1}H,^{13}C-HMQC and ^{1}H,^{13}C-HMBC.

ESI-MS (MeCN, *positive* ion mode): *m/z* [ion, intensity (%)] = 544.3 (M^{2+}-2PF_6^-, 100).

HRMS (ESI-ToF): *m/z* calcd. for $[C_{62}H_{44}Br_2FeN_6]^{2+}$: 543.0667; found: 543.0674.

UV/VIS (MeCN): λ_{max} (ε) = 275 nm (69550 L·cm^{-1}·mol^{-1}), 334 nm (62840 L·cm^{-1}·mol^{-1}), 376 nm (10440 L·cm^{-1}·mol^{-1}), 564 nm (9990 L·cm^{-1}·mol^{-1}).

{[Fe(*228*)$_2$]$^{2+}$[(PF$_6$)$^-$]$_2$} (241)

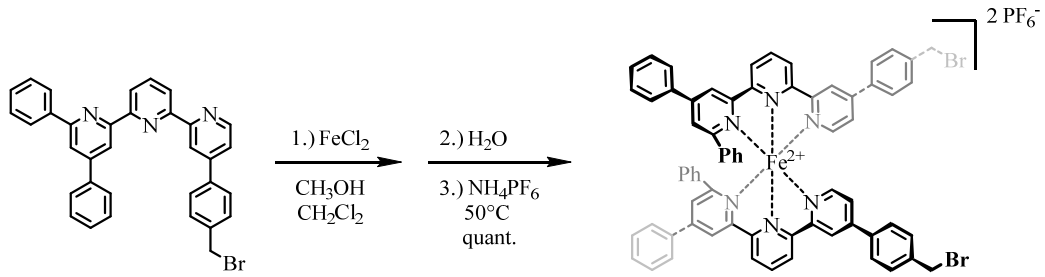

228 **241**

241 was prepared according to the representative procedure C. $FeCl_2$ (2.28 mg, 18.0 µmol, 1.00 eq.), 4′′-(4-(bromomethyl)phenyl)-4,6-di-phenyl-2,2′:6′,2′′-terpyridine **228** (20.0 mg, 36.0 µmol, 2.00 eq.), MeOH (50 mL), DCM (50 mL), water (100 mL), and NH_4PF_6 (147 mg, 0.90 mmol, 50.0 eq.) were used. The product **241** was isolated as a dark purple solid in quantitative yield (26.3 mg, 30.1 µmol). Unexpectedly, the complex exhibited distinct paramagnetic behavior as can be seen from the very unique NMR-data shown below.

Analytical data of 241:

^{1}H-NMR (500 MHz, CD_3CN, ppm, 25 °C): δ_H = 74 (very broad), 39.2 (br. s), 34.1 (br. s), 30.9 (br. s), 29.0 (br. s), 27.2 (br. s), 25.1 (br. s), 9.57 (s, 4H, *H$_{phenyl}$)*, 8.90 (d, $^3J_{H,H}$ = 7.6 Hz, 4H, *H$_{phenyl}$)*, 8.30 (app. t, $^3J_{H,H}$ = 7.3 Hz, 4H, *H$_{phenyl}$)*, 8.18 (app. t, $^3J_{H,H}$ = 7.4 Hz, 2H, *H$_{phenyl}$)*, 7.09 (d, $^3J_{H,H}$ = 7.6 Hz, 4H, *H$_{phenyl}$)*, 4.12 (s, 4H, *H$_{methylene}$*), 3.52 (br. s, 2H), 0.29 (br. s, 2H), -12.0 (very broad).

ESI-MS (MeCN, *positive* ion mode): *m/z* [ion, intensity (%)] = 581.3 (M^{2+}-2PF_6^-, 100).

HRMS (ESI-ToF): *m/z* calcd. for $[C_{68}H_{48}Br_2FeN_6]^{2+}$: 581.0823; found: 581.0830.

UV/VIS (MeCN): λ_{max} (ε) = 273 nm (69155 L·cm^{-1}·mol^{-1}), 341 nm (51325 L·cm^{-1}·mol^{-1}), 563 nm (5115 L·cm^{-1}·mol^{-1}).

{[Fe(*229*)$_2$]$^{2+}$[(PF$_6$)$^-$]$_2$} (242)

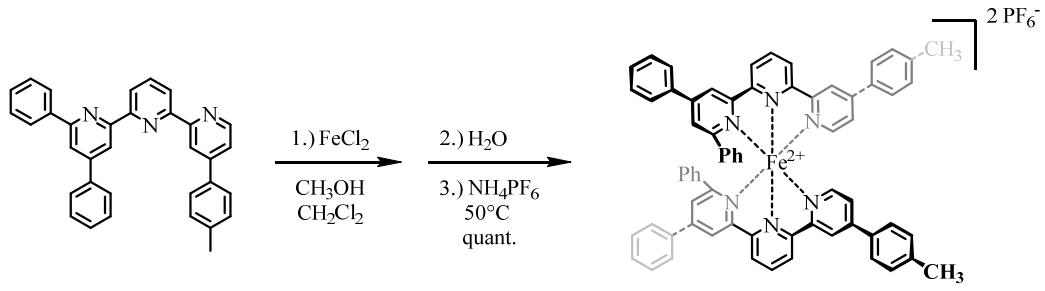

229 **242**

242 was prepared by a modification of the representative procedure C. $FeCl_2$ (7.61 mg, 60.0 µmol, 1.00 eq.), 4,6-diphenyl-4′′-(*p*-tolyl)-2,2′:6′,2′′-terpyridine (**229**) (28.5 mg, 60.0 µmol, 1.00 eq.), MeOH (50 mL), DCM (50 mL), water (100 mL) and NH_4PF_6 (489 mg, 3.00 mmol, 50.0 eq.) were used. The product **242** was isolated as a dark purple solid in quantitative yield (39.1 mg, 30.1 µmol). Unexpectedly, the complex exhibited distinct paramagnetic behavior as can be seen from the very unique NMR-data shown below.

Analytical data of 242:

^{1}H-NMR (400 MHz, CD_3CN, ppm, 25 °C): δ_H = 70 (very broad), 38.0 (br. s), 33.4 (br. s), 30.0 (br. s), 28.5 (br. s), 27.2 (br. s), 24.9 (br. s), 9.53 (d, $^3J_{H,H}$ = 5.6 Hz, 4H, *H$_{phenyl}$)*, 8.82 (d, $^3J_{H,H}$ = 7.2 Hz, 4H, *H$_{phenyl}$)*, 8.27 (app. t, $^3J_{H,H}$ = 6.9 Hz, 4H, *H$_{phenyl}$)*, 8.19 (app. t, $^3J_{H,H}$ = 7.2 Hz, 2H, *H$_{phenyl}$)*, 6.94 (d, $^3J_{H,H}$ = 7.2 Hz, 4H, *H$_{phenyl}$)*, 3.64 (br. s, 2H), 1.42 (s, 6H, *H$_{methyl}$*), 0.45 (br. s, 2H), -10.9 (very broad).

^{13}C-NMR (101 MHz, CD_3CN, ppm, 25 °C): δ_C = 137.92 (C_q), 137.01 (C_q), 135.63 (C_t), 133.03 (C_t), 131.53 (C_q), 130.59 (C_t), 130.00 (C_t), 117.37 (C_t), 23.63 (C_{methyl}, 2C).

^{19}F-NMR (376 MHz, CD_3CN, ppm, 25 °C): δ_F = –72.66 (d, $^1J_{P,F}$ = 706.8 Hz, 12F).

^{31}P-NMR (162 MHz, CD_3CN, ppm, 25 °C): δ_P = -144.52 (hept, $^1J_{P,F}$ = 706.8 Hz, 2P).

ESI-MS (MeCN, *positive* ion mode): *m/z* [ion, intensity (%)] = 503.4 (M^{2+}-2PF_6^-, 100).

HRMS (ESI-ToF): *m/z* calcd. for $[C_{68}H_{50}FeN_6]^{2+}$: 503.1719; found: 503.1724.

UV/VIS (MeCN): λ_{max} (ε) = 286 nm (58490 L·cm^{-1}·mol^{-1}), 341 nm (47340 L·cm^{-1}·mol^{-1}), 563 nm (3920 L·cm^{-1}·mol^{-1}).

(*E*)-1,2-bis(4-((4-(4′′,6′′-diphenyl-[2,2′:6′,2′′-terpyridin]-4-yl)benzyl)oxy)phenyl)diazene (227a)

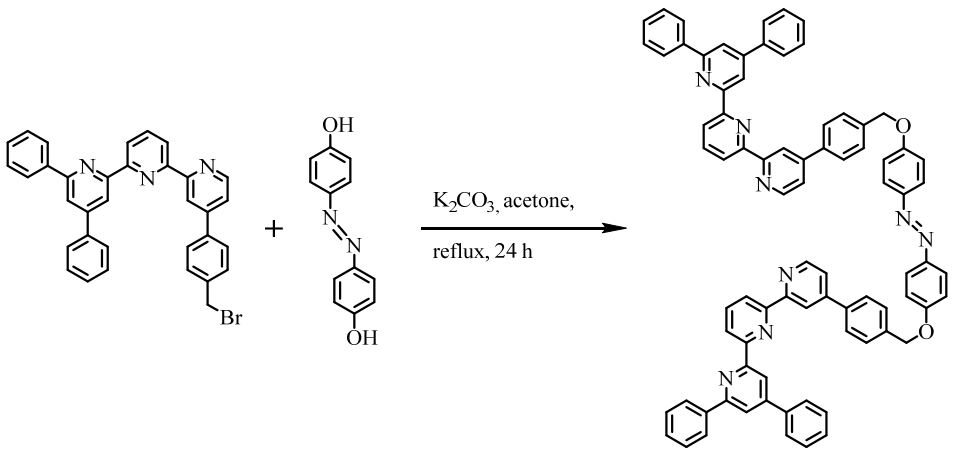

228 **219** **227a**

The desired product (*E*)-1,2-bis(4-((4-(4′′,6′′-diphenyl-[2,2′:6′,2′′-terpyridin]-4-yl)benzyl)-oxy)phenyl)-diazene (**227a**) was prepared via a S_N2-reaction inspired by a previously reported literature procedure.[556] Thus (*E*)-4,4′-(diazene-1,2-diyl)diphenol (**219**) (30.0 mg, 0.14 mmol, 1.00 eq.), 4′′-(4-(bromomethyl)phenyl)-4,6-diphenyl-2,2′:6′,2′′-terpyridine (**228**) (180 mg, 0.31 mmol, 2.20 eq), and K_2CO_3 (50.8 mg, 0.36 mmol, 2.60 eq.) were charged into a Schlenk tube, put under inert atmosphere and dissolved in dry acetone (60 mL), before the reaction was sealed and heated to reflux for 24 h. After the reaction was allowed to cool down to room temperature the solvent was removed under reduced pressure. Now DCM and water were added to the residue and the resulting suspension was with DCM (4 *x*), before drying over $MgSO_4$, filtration and evaporation of residual solvent. The still pale yellow aqueous phase contained a solid which was filtered off and dried at the high vacuum. Due to insolubility of the crude product no NMR-spectroscopic characterization was possible, but HR-ESI-MS spectroscopy revealed that the solid contained the desired target compound (*E*)-1,2-bis(4-((4-(4′′,6′′-diphenyl-[2,2′:6′,2′′-terpyridin]-4-yl)benzyl)oxy)phenyl)diazene (**227a**).

Analytical data of 227a:

ESI-MS (THF, *positive* ion mode): *m/z* [ion] = 1161.7 ($M+H^+$).
HRMS (ESI-ToF): *m/z* calcd. for $[C_{80}H_{56}N_8O_2+H]^+$: 1161.4599; found: 1161.4601.

2-Bromo-6-phenylpyridine (246)

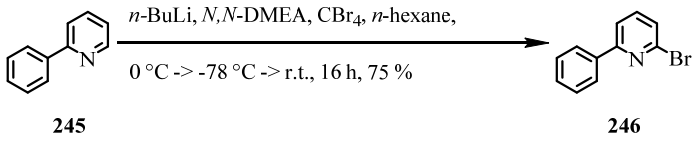

245 **246**

246 was prepared in adaption of a reported literature procedure.[566] Therefore *n*-BuLi (1.6M in hexanes, 75.0 mL, 120 mmol, 6.00 eq.) was added dropwise to a solution of *N,N*-dimethyl-ethanolamine (6.05 mL, 60.0 mmol, 3.00 eq.) dissolved in *n*-hexane (45 mL) at 0 °C. After 30 min of stirring a solution of 2-phenylpyridine (**245**) (3.23 g, 2.98 mL, 20.0 mmol, 1.00 eq.) in *n*-hexane (30 mL) was added dropwise to the reaction mixture at 0 °C. After the addition the mixture was stirred for an additional hour before being cooled down to -78 °C. Now CBr_4 (23.45 g, 70.0 mmol, 3.50 eq.) dissolved in *n*-hexane (45 mL) was added slowly at -78 °C and after the addition the reaction mixture was kept at this temperature for another hour before being allowed to warm up to room temperature overnight. The reaction was stopped after 16 h by the addition of water at 0 °C. After diluting the reaction mixture with DCM the crude product was extracted repeatedly with DCM and EtOAc, whereas the resulting organic phases were washed with saturated $Na_2S_2O_3$- solution and brine prior to pre-drying of the recombined organic fractions over $MgSO_4$, filtration and evaporation of residual organic solvents under reduced pressure. Finally the resulting crude product was purified via repeated FCC using a solvent gradient from pure *n*-hexane up to EtOAc / *n*-hexane (1:19) to yield the desired product **246** in a yield of 75% (3.52 g, 75.1 mmol) as a light yellow solidifying oil.

Analytical data of 246:

^{1}H-NMR (400 MHz, $CDCl_3$, ppm, 25 °C): δ_H = 7.99 (dd, $^3J_{H,H}$ = 8.2 Hz, $^4J_{H,H}$ = 1.5 Hz, 2H), 7.68 (dd, $^3J_{H,H}$ = 7.7 Hz, $^4J_{H,H}$ = 0.8 Hz, 1H),7.59 (t, $^3J_{H,H}$ = 7.7 Hz 1H), 7.51 – 7.43 (m, 1H), 7.41 (dd, $^3J_{H,H}$ = 7.8 Hz, $^4J_{H,H}$ = 0.8 Hz, 1H).

^{13}C-NMR (101 MHz, $CDCl_3$, ppm, 25 °C): δ_C = 158.74 (C_q, 1C), 142.30 (C_q, 1C), 139.12 (C_t, 1C), 137.77 (C_q, 1C), 129.77 (C_t, 1C), 128.95 (C_t, 1C), 127.12 (C_t, 1C), 126.46 (C_t, 1C), 119.13 (C_t, 1C).

GCMS (EI$^+$, 70 eV): *m/z* [ion, intensity (%)] = 234.9 (M^+, 37), 154.1 (M^+-Br, 100).

ESI-MS (MeCN, *positive* ion mode): *m/z* [ion] = 235.9 ($M+H^+$).

HRMS (ESI-ToF): *m/z* calcd. for $[C_{11}H_9BrN+H]^+$: 233.9913 ; found: 233.9911.

Lithium tri*iso*propyl 2-(6-phenylpyridyl) borate (247)

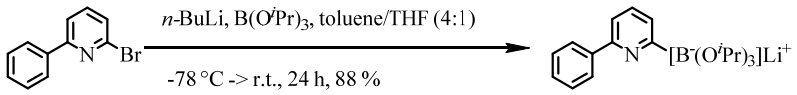

246 **247**

247 was prepared according to general procedure A. 2-Bromo-6-phenylpyridine (**246**) (5.15 g, 22.0 mmol, 1.00 eq.), tri*iso*propylborate (4.64 g, 5.71 mL, 24.2 mmol, 1.10 eq.), *n*-BuLi (1.6M in hexanes, 15.1 mL, 24.2 mmol, 1.10 eq.), toluene (100 mL) and THF (25 mL) were used to obtain the desired product **247** as an off-white powder in a yield of 88% (6.72 g, 19.3 mmol).

Analytical data of 247:

^{1}H-NMR (400 MHz, CD_3OD, ppm, 25 °C): δ_H = 7.79 (d, $^{3}J_{H,H}$ = 7.2 Hz, 2H), 7.67 (t, $^{3}J_{H,H}$ = 7.7 Hz, 1H), 7.51 (dd, $^{3}J_{H,H}$ = 7.5 Hz, $^{4}J_{H,H}$ = 1.1 Hz, 1H), 7.48 – 7.32 (m, 4H), 3.93 (hept, $^{3}J_{H,H}$ = 6.1 Hz, 3H, –*C**H**(CH$_3$)$_2$*), 1.15 (d, $^{3}J_{H,H}$ = 6.2 Hz, 18H, –*CH(C**H**$_3$)$_2$*).
^{13}C-NMR (101 MHz, CD_3OD, ppm, 25 °C): δ_C = 158.28 (C_q, 1C), 143.10 (C_q, 1C), 136.27 (C_t, 1C), 129.69 (C_t, 2C), 129.14 (C_t, 1C), 128.57 (C_t, 2C), 127.21 (C_t, 1C), 120.35 (C_t, 1C), 64.68 ($C_{isopropyl}$, 3C), 25.32 (C_{methyl}, 18C).
Note: The carbon-atom bound to the boron cannot be seen in the ^{13}C-NMR spectrum.
^{11}B-NMR (128 MHz, CD_3OD, ppm, 25 °C): 2.96 (s, 1B).

6′′-Phenyl-4-(*p*-tolyl)-2,2′:6′,2′′-terpyridine (248) via intermediate 4-chloro-6′′-phenyl-2,2′:6′,2′′-terpyridine (249)

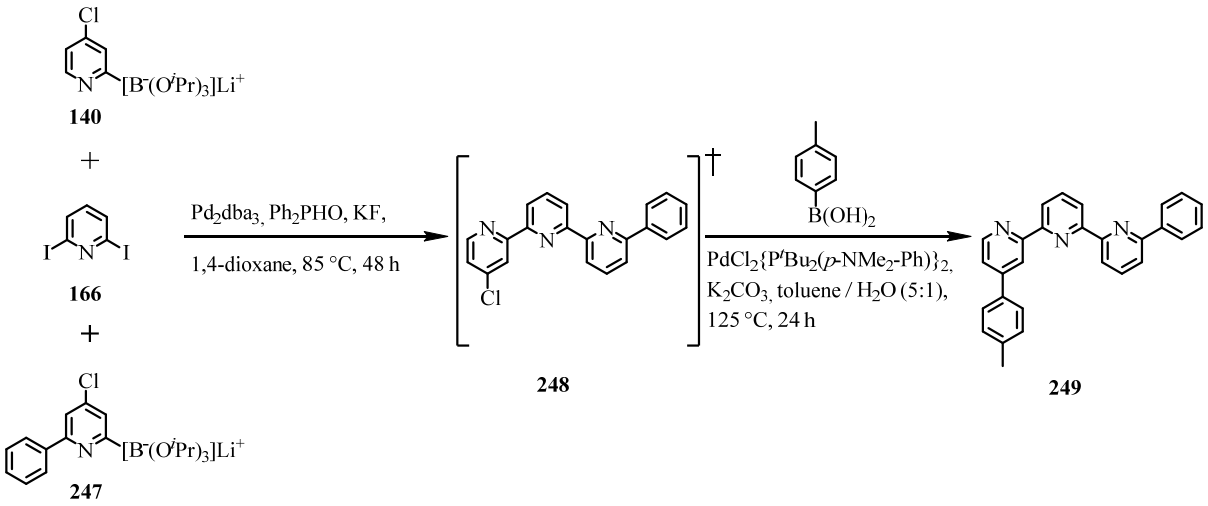

The desired target compound 6′′-phenyl-4-(p-tolyl)-2,2′:6′,2′′-terpyridine **249** was prepared in a sequence of two consecutive Suzuki-Miyaura cross-coupling reactions via the intermediate 4-chloro-6′′-phenyl-2,2′:6′,2′′-terpyridine (**248**) which could not be purely isolated. The procedures of the two cross-couplings are however described separately below.

Preparation of 4-chloro-6′′-phenyl-2,2′:6′,2′′-terpyridine (248):

246 was prepared in a statistical reaction similar to the preparation of compound **47**. A Schlenk tube was charged with 2,6-diiodopyridine (**166**) (2.98 g, 9.00 mmol, 1.00 eq.) and mixed with a twofold excess of the two required coupling partners, namely, lithium tri*iso*-propyl 2-(4-chloropyridyl) borate (**140**) (5.54 g, 18.0 mmol, 2.00 eq.) and lithium tri*iso*propyl 2-(6-phenylpyridyl) borate (**247**) (6.29 g, 18.0 mmol, 2.00 eq.), together with KF (3.17 g, 54.0 mmol, 6.00 eq.), Pd_2dba_3 (494 mg, 0.54 mmol, 0.06 eq.) and diphenylphosphine oxide (675 mg, 3.24 mmol, 0.36 eq.). All those reagents were evacuated and the flask was put under inert atmosphere three times. The mixture was dissolved in previously degassed 1,4-dioxane (120 mL) before the reaction vessel was sealed. Now the reaction was heated to 85 °C for 48 h. After dilution with EtOAc the reaction mixture was filtered through a plug of silica gel to get rid of insoluble side products. Concentration of residual solvent yielded the crude product which was subjected to repeated FCC on silica gel using solvent mixtures of EtOAc and *n*-hexane with varying solvent ratios in the range of 1:9 up to a ratio of 1:3. However the desired product 4-chloro-6′′-phenyl-2,2′:6′,2′′-terpyridine (**248**) could never be

isolated in a pure fashion, but always together with inseparable side products of the statistical coupling reaction.

Analytical data of 248

ESI-MS (MeCN, *positive* ion mode): *m/z* [ion, intensity (%)] = 344.1 ($M+H^+$), 366.2 ($M+Na^+$),.
HRMS (ESI-ToF): *m/z* calcd. for $[C_{21}H_{14}ClN_3+H]^+$: 344.0949; found: 344.0950.

Preparation of 6´´-phenyl-4-(*p*-tolyl)-2,2´:6´,2´´-terpyridine (249):

The product **249** was prepared from the mixture containing 4-chloro-6´´-phenyl-2,2´:6´,2´´-terpyridine (**248**). Therefore a Schlenk tube was charged with **248** (68.8 mg, 0.20 mmol, 1.00 eq.), *p*-tolylboronic acid (**224**) (280 mg, 2.00 mmol, 10.0 eq.), K_2CO_3 (83.8 mg, 0.60 mmol, 3.00 eq.), and $PdCl_2\{P^tBu_2(p\text{-}NMe_2\text{-}Ph)\}_2$ (7.15 mg, 10.0 µmol, 0.05 eq.). All reagents were mixed and suspended in previously degassed toluene (25 mL) and H_2O (5 mL). The reaction vessel was sealed and heated to 125 °C for 24 h. After completion the reaction mixture was allowed to cool to room temperature and was subsequently diluted with DCM, brine and water. Now the reaction mixture was extracted with DCM (4 *x*). The organic phases were combined, dried over $MgSO_4$, filtered and residual solvent was evaporated under reduced pressure. Subsequently the crude product was purified by repeated FCC using a gradient of solvent mixtures ranging from EtOAc / *n*-hexane (3:17) up to EtOAc / *n*-hexane (1:3). As the regular FCC did not yield pure **249** the obtained crude product was further purified by semi-preparative HPLC using a *Reprospher 100 SI, 5 µm* column (250 mm *x* 16 mm) a with varying mixtures of EtOAc and *n*-hexane as the eluent to finally give the desired asymmetric product 6´´-phenyl-4-(p-tolyl)-2,2´:6´,2´´-terpyridine **249** in a yield of 21% (16.7 mg, 42.0 µmol).

Analytical data of 249:

^{1}H-NMR (500 MHz, $CDCl_3$, ppm, 25 °C): δ_H = 9.19 (d, $^{4}J_{H,H}$ = 0.8 Hz, 1H, *H3*), 8.85 (d, $^{3}J_{H,H}$ = 5.0 Hz, 1H), 8.81 (d, $^{3}J_{H,H}$ = 5.2 Hz, 1H), 8.45 (d, $^{3}J_{H,H}$ = 7.7 Hz, 1H, *H3´* / H5´**), 8.19 (dd, $^{3}J_{H,H}$ = 8.1 Hz, $^{4}J_{H,H}$ = 1.6 Hz, 2H, H_{phenyl}), 8.13 (d, $^{4}J_{H,H}$ = 0.6 Hz, 1H), 8.05 (dd, $^{3}J_{H,H}$ = 5.1 Hz, $^{4}J_{H,H}$ = 1.6 Hz, 1H), 7.93 (t, $^{3}J_{H,H}$ = 7.8 Hz, 1H, *H4´*), 7.81 (d, $^{3}J_{H,H}$ = 7.5 Hz, 1H, *H3´* / H5´**), 7.64 (d, $^{3}J_{H,H}$ = 8.1 Hz, 2H, H_{phenyl}), 7.58 (dd, $^{3}J_{H,H}$ = 5.1 Hz, $^{4}J_{H,H}$ = 1.6 Hz, 1H, *H5*), 7.52 (app. t, $^{3}J_{H,H}$ = 7.4 Hz, 2H, H_{phenyl}), 7.46 (d, $^{3}J_{H,H}$ = 7.3 Hz, 1H), 7.34 (d, $^{3}J_{H,H}$ = 7.9 Hz, 2H, H_{phenyl}), 2.45 (s, 3H, H_{methyl}).

^{13}C NMR (101 MHz, $CDCl_3$, ppm, 25 °C): δ_C = 157.04 (C_q, 1C), 156.76 (C_q, 1C), 155.73 (C_q, 1C), 155.58 (C_q, 1C), 150.55 (C_t, 1C), 149.78 (C_q, 1C), 149.66 (C_t, 1C), 148.15 (C_q, 1C), 139.72 (C_q, 1C), 139.45 (C_q, 1C), 137.91 (C_t, 1C), 135.15 (C_q, 1C), 130.11 (C_{phenyl}, 2C), 129.17 (C_t, 1C), 128.88 (C_{phenyl}, 2C), 127.73 (C_t, 1C), 127.21 (C_{phenyl}, 2C), 127.11 (C_{phenyl}, 2C), 121.76 (C_t, 1C), 120.74 (C_t, 1C), 119.88 (C_t, 1C), 119.33 (C_t, 1C), 119.12 (C_t, 1C), 21.41 (C_{methyl}, 1C).

ESI-MS (MeOH, *positive* ion mode): *m/z* [ion, intensity (%)] = 400.2 ($M+H^+$, 100), 422.2 ($M+Na^+$, 10).

HRMS (ESI-ToF): *m/z* calcd. for $[C_{28}H_{21}N_3+H]^+$: 400.1808; found: 400.1813

4-(4-(Bromomethyl)phenyl)-6′′-phenyl-2,2′:6′,2′′-terpyridine (250)

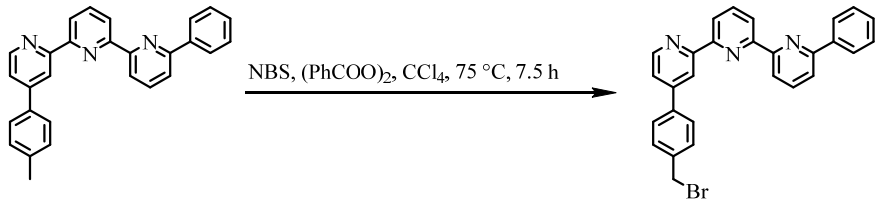

249 **250**

The desired compound 4-(4-(bromomethyl)phenyl)-6′′-phenyl-2,2′:6′,2′′-terpyridine (**250**) was prepared by radical side chain bromination of precursor **249** based on a reported literature procedure.[553,554] 6′′-phenyl-4-(p-tolyl)-2,2′:6′,2′′-terpyridine (**249**) (14.0 mg, 35.0 µmol, 1.00 eq.), NBS (7.55 mg, 42.0 µmol, 1.20 eq.), and dibenzoyl peroxide (2.19 mg, 8.75 µmol, 0.25 eq.) were dissolved in previously degassed CCl_4 (15 mL) and heated to 75 °C for 7.5 h until the reaction progress stopped (monitoring by TLC). Now the reaction mixture was allowed to cool to room temperature and was stirred in an ice-water bath for 30 min prior to dilution with DCM, brine and aqueous saturated $Na_2S_2O_3$-solution. The resulting mixture was repeatedly extracted with DCM (5 *x*) before the combined organic layers were dried over $MgSO_4$, filtered and residual solvent was removed under reduced pressure. The crude product was purified via FCC using a solvent mixture of EtOAc / *n*-hexane (1:3) yielding 22% (3.00 mg, 8.00 µmol) of the starting material **249** and 78% (13.1 mg, 27.0 µmol) of the desired target compound 4-(4-(bromomethyl)phenyl)-6′′-phenyl-2,2′:6′,2′′-terpyridine (**250**).

Analytical data 250:

^{1}H-NMR (400 MHz, $CDCl_3$, ppm, 25 °C): δ_H = 9.23 (d, $^3J_{H,H}$ = 3.7 Hz, 1H), 8.85 (dd, $^3J_{H,H}$ = 7.8 Hz, $^3J_{H,H}$ = 5.0 Hz 2H), 8.52 (t, $^3J_{H,H}$ = 6.6 Hz, 1H), 8.18 (dd, $^3J_{H,H}$ = 8.4 Hz, $^4J_{H,H}$ = 1.3 Hz 2H, H_{phenyl}), 8.14 (d, $^4J_{H,H}$ = 1.6 Hz, 1H), 8.11 (s, 1H) 7.95 (t, $^3J_{H,H}$ = 7.8 Hz, 1H, *H4′*), 7.83 (dd, $^3J_{H,H}$ = 7.8 Hz, $^4J_{H,H}$ = 2.2 Hz, 1H, *H3′* / H5′**), 7.72 (d, $^3J_{H,H}$ = 8.2 Hz, 2H, H_{phenyl}), 7.62 - 7.50 (m, 5H), 7.51 (d, $^3J_{H,H}$ = 7.0 Hz, 1H), 4.57 (s, 2H, $H_{methylene}$).

ESI-MS (MeCN, *positive* ion mode): *m/z* [ion, intensity (%)] = 478.1 ($M+H^+$, 100).

HRMS (ESI-ToF): *m/z* calcd. for $[C_{28}H_{20}BrN_3+H]^+$: 478.0913; found: 478.0915

8 Bibliography

[1] W. A. Reinerth, L. J. Ii, T. P. Burgin, C. Zhou, C. J. Muller, M. R. Deshpande, M. A. Reed, J. M. Tour, *Nanotechnology* **1998**, *9*, 246.
[2] J. M. Tour, *Acc. Chem. Res.* **2000**, *33*, 791–804.
[3] A. R. Pease, J. O. Jeppesen, J. F. Stoddart, Y. Luo, C. P. Collier, J. R. Heath, *Acc. Chem. Res.* **2001**, *34*, 433–444.
[4] N. Weibel, S. Grunder, M. Mayor, *Org. Biomol. Chem.* **2007**, *5*, 2343–2353.
[5] K. Nørgaard, T. Bjørnholm, *Chem. Commun.* **2005**, 1812–1823.
[6] S. Kubatkin, A. Danilov, M. Hjort, J. Cornil, J.-L. Brédas, N. Stuhr-Hansen, P. Hedegård, T. Bjørnholm, *Nature* **2003**, *425*, 698–701.
[7] K. Moth-Poulsen, T. Bjørnholm, *Nat. Nanotechnol.* **2009**, *4*, 551–556.
[8] R. L. McCreery, A. J. Bergren, *Adv. Mater.* **2009**, *21*, 4303–4322.
[9] G. E. Moore, *IEEE Solid-State Circuits Soc. Newsl.* **2006**, *11*, 33–35.
[10] N. Robertson, C. A. McGowan, *Chem. Soc. Rev.* **2003**, *32*, 96–103.
[11] J. J. L. Morton, D. R. McCamey, M. A. Eriksson, S. A. Lyon, *Nature* **2011**, *479*, 345–353.
[12] I. L. Markov, *Nature* **2014**, *512*, 147–154.
[13] H. Iwai, in *2nd Int. Workshop Electron Devices Semicond. Technol. 2009 IEDST 09*, **2009**, pp. 1–4.
[14] R. P. Feynman, "Engineering and Science, Volume 23:5, February 1960," can be found under http://resolver.caltech.edu/CaltechES:23.5.0, **1960**.
[15] X. D. Cui, A. Primak, X. Zarate, J. Tomfohr, O. F. Sankey, A. L. Moore, T. A. Moore, D. Gust, G. Harris, S. M. Lindsay, *Science* **2001**, *294*, 571–574.
[16] J. Park, A. N. Pasupathy, J. I. Goldsmith, C. Chang, Y. Yaish, J. R. Petta, M. Rinkoski, J. P. Sethna, H. D. Abruña, P. L. McEuen, et al., *Nature* **2002**, *417*, 722–725.
[17] T. Dadosh, Y. Gordin, R. Krahne, I. Khivrich, D. Mahalu, V. Frydman, J. Sperling, A. Yacoby, I. Bar-Joseph, *Nature* **2005**, *436*, 677–680.
[18] L. Venkataraman, J. E. Klare, C. Nuckolls, M. S. Hybertsen, M. L. Steigerwald, *Nature* **2006**, *442*, 904–907.
[19] J. Repp, G. Meyer, S. Paavilainen, F. E. Olsson, M. Persson, *Science* **2006**, *312*, 1196–1199.
[20] G. Binnig, H. Rohrer, *Ibm J. Res. Dev.* **1986**, *30*, 355–369.
[21] **2014**.
[22] G. Binnig, H. Rohrer, *Angew. Chem. Int. Ed. Engl.* **1987**, *26*, 606–614.
[23] I. Ekvall, E. Wahlström, D. Claesson, H. Olin, E. Olsson, *Meas. Sci. Technol.* **1999**, *10*, 11.
[24] M. Bowker, P. R. Davies, *Scanning Tunneling Microscopy in Surface Science*, **2009**.
[25] E. L. Wolf, *Principles of Electron Tunneling Spectroscopy: Second Edition*, Oxford University Press, **2012**.
[26] G. K. Binnig, *Method and Atomic Force Microscope for Imaging Surfaces with Atomic Resolution*, **1990**, CA1270132 (A1).
[27] M. C. Petty, *Molecular Electronics: From Principles to Practice*, John Wiley & Sons, **2007**.
[28] G. Haugstad, *Atomic Force Microscopy: Understanding Basic Modes and Advanced Applications*, John Wiley & Sons, **2012**.
[29] "The Department of Chemistry at State University of New York, Potsdam N.Y.," can be found under http://www2.potsdam.edu/hepelmr/AFM3.htm, **2014**.
[30] J. Moreland, J. W. Ekin, *J. Appl. Phys.* **1985**, *58*, 3888–3895.
[31] C. J. Muller, J. M. van Ruitenbeek, L. J. de Jongh, *Phys. Rev. Lett.* **1992**, *69*, 140–143.
[32] N. Agraït, A. L. Yeyati, J. M. van Ruitenbeek, *Phys. Rep.* **2003**, *377*, 81–279.
[33] E. Lörtscher, J. W. Ciszek, J. Tour, H. Riel, *Small* **2006**, *2*, 973–977.
[34] R. Turanský, M. Konôpka, N. L. Doltsinis, I. Štich, D. Marx, *Phys. Chem. Chem. Phys.* **2010**, *12*, 13922–13932.
[35] R. Landauer, *IBM J. Res. Dev.* **1957**, *1*, 223–231.
[36] C. W. J. Beenakker, H. van Houten, in *Solid State Phys.* (Ed.: Henry Ehrenreich and David Turnbull), Academic Press, **1991**, pp. 1–228.

[37] D. A. Wharam, T. J. Thornton, R. Newbury, M. Pepper, H. Ahmed, J. E. F. Frost, D. G. Hasko, D. C. Peacock, D. A. Ritchie, G. a. C. Jones, *J. Phys. C Solid State Phys.* **1988**, *21*, L209.
[38] B. J. van Wees, H. van Houten, C. W. J. Beenakker, J. G. Williamson, L. P. Kouwenhoven, D. van der Marel, C. T. Foxon, *Phys. Rev. Lett.* **1988**, *60*, 848–850.
[39] S. Wu, Electrical Conductance of Single Conjugated Oligomers, University of Basel, **2010**.
[40] C. Jia, X. Guo, *Chem. Soc. Rev.* **2013**, *42*, 5642–5660.
[41] A. Nitzan, M. A. Ratner, *Science* **2003**, *300*, 1384–1389.
[42] K. Yokota, M. Taniguchi, T. Kawai, *J. Am. Chem. Soc.* **2007**, *129*, 5818–5819.
[43] C. D. Bain, G. M. Whitesides, *Angew. Chem. Int. Ed. Engl.* **1989**, *28*, 506–512.
[44] F. Chen, X. Li, J. Hihath, Z. Huang, N. Tao, *J. Am. Chem. Soc.* **2006**, *128*, 15874–15881.
[45] R. Huber, M. T. González, S. Wu, M. Langer, S. Grunder, V. Horhoiu, M. Mayor, M. R. Bryce, C. Wang, R. Jitchati, et al., *J. Am. Chem. Soc.* **2008**, *130*, 1080–1084.
[46] S. Wu, M. T. González, R. Huber, S. Grunder, M. Mayor, C. Schönenberger, M. Calame, *Nat. Nanotechnol.* **2008**, *3*, 569–574.
[47] Y. Ie, T. Hirose, H. Nakamura, M. Kiguchi, N. Takagi, M. Kawai, Y. Aso, *J. Am. Chem. Soc.* **2011**, *133*, 3014–3022.
[48] M. Kamenetska, S. Y. Quek, A. C. Whalley, M. L. Steigerwald, H. J. Choi, S. G. Louie, C. Nuckolls, M. S. Hybertsen, J. B. Neaton, L. Venkataraman, *J. Am. Chem. Soc.* **2010**, *132*, 6817–6821.
[49] S. Y. Quek, M. Kamenetska, M. L. Steigerwald, H. J. Choi, S. G. Louie, M. S. Hybertsen, J. B. Neaton, L. Venkataraman, *Nat. Nanotechnol.* **2009**, *4*, 230–234.
[50] Y. S. Park, A. C. Whalley, M. Kamenetska, M. L. Steigerwald, M. S. Hybertsen, C. Nuckolls, L. Venkataraman, *J. Am. Chem. Soc.* **2007**, *129*, 15768–15769.
[51] R. Parameswaran, J. R. Widawsky, H. Vázquez, Y. S. Park, B. M. Boardman, C. Nuckolls, M. L. Steigerwald, M. S. Hybertsen, L. Venkataraman, *J. Phys. Chem. Lett.* **2010**, *1*, 2114–2119.
[52] M. Kamenetska, M. Koentopp, A. C. Whalley, Y. S. Park, M. L. Steigerwald, C. Nuckolls, M. S. Hybertsen, L. Venkataraman, *Phys. Rev. Lett.* **2009**, *102*, 126803.
[53] L. Venkataraman, J. E. Klare, I. W. Tam, C. Nuckolls, M. S. Hybertsen, M. L. Steigerwald, *Nano Lett.* **2006**, *6*, 458–462.
[54] A. Mishchenko, L. A. Zotti, D. Vonlanthen, M. Bürkle, F. Pauly, J. C. Cuevas, M. Mayor, T. Wandlowski, *J. Am. Chem. Soc.* **2011**, *133*, 184–187.
[55] L. A. Zotti, T. Kirchner, J.-C. Cuevas, F. Pauly, T. Huhn, E. Scheer, A. Erbe, *Small* **2010**, *6*, 1529–1535.
[56] Kim, J. M. Beebe, Y. Jun, X.-Y. Zhu, C. D. Frisbie, *J. Am. Chem. Soc.* **2006**, *128*, 4970–4971.
[57] C.-H. Ko, M.-J. Huang, M.-D. Fu, C. Chen, *J. Am. Chem. Soc.* **2010**, *132*, 756–764.
[58] L. Patrone, S. Palacin, J. P. Bourgoin, *Appl. Surf. Sci.* **2003**, *212–213*, 446–451.
[59] S. Yasuda, S. Yoshida, J. Sasaki, Y. Okutsu, T. Nakamura, A. Taninaka, O. Takeuchi, H. Shigekawa, *J. Am. Chem. Soc.* **2006**, *128*, 7746–7747.
[60] L. Patrone, S. Palacin, J. Charlier, F. Armand, J. P. Bourgoin, H. Tang, S. Gauthier, *Phys. Rev. Lett.* **2003**, *91*, 096802.
[61] D. Gao, F. Scholz, H.-G. Nothofer, W. E. Ford, U. Scherf, J. M. Wessels, A. Yasuda, F. von Wrochem, *J. Am. Chem. Soc.* **2011**, *133*, 5921–5930.
[62] M. Carrara, F. Nüesch, L. Zuppiroli, *Synth. Met.* **2001**, *121*, 1633–1634.
[63] C. A. Martin, D. Ding, J. K. Sørensen, T. Bjørnholm, J. M. van Ruitenbeek, H. S. J. van der Zant, *J. Am. Chem. Soc.* **2008**, *130*, 13198–13199.
[64] H. Park, J. Park, A. K. L. Lim, E. H. Anderson, A. P. Alivisatos, P. L. McEuen, *Nature* **2000**, *407*, 57–60.
[65] Z.-L. Cheng, R. Skouta, H. Vazquez, J. R. Widawsky, S. Schneebeli, W. Chen, M. S. Hybertsen, R. Breslow, L. Venkataraman, *Nat. Nanotechnol.* **2011**, *6*, 353–357.
[66] M. B. Nielsen, Ed. , *Organic Synthesis and Molecular Engineering*, John Wiley & Sons, Inc., **2013**.
[67] M. Frei, S. V. Aradhya, M. S. Hybertsen, L. Venkataraman, *J. Am. Chem. Soc.* **2012**, *134*, 4003–4006.
[68] D. R. Jones, A. Troisi, *J. Phys. Chem. C* **2007**, *111*, 14567–14573.
[69] F. Pauly, J. Viljas, J. Cuevas, *Phys. Rev. B Condens. Matter Mater. Phys.* **2008**, *78*, DOI 10.1103/PhysRevB.78.035315.

[70] M. Dell'Angela, G. Kladnik, A. Cossaro, A. Verdini, M. Kamenetska, I. Tamblyn, S. Y. Quek, J. B. Neaton, D. Cvetko, A. Morgante, et al., *Nano Lett.* **2010**, *10*, 2470–2474.
[71] A. Bagrets, A. Arnold, F. Evers, *J. Am. Chem. Soc.* **2008**, *130*, 9013–9018.
[72] M. Mayor, H. B. Weber, J. Reichert, M. Elbing, C. von Hänisch, D. Beckmann, M. Fischer, *Angew. Chem. Int. Ed.* **2003**, *42*, 5834–5838.
[73] A. Salomon, D. Cahen, S. Lindsay, J. Tomfohr, V. b. Engelkes, C. d. Frisbie, *Adv. Mater.* **2003**, *15*, 1881–1890.
[74] V. Kaliginedi, P. Moreno-García, H. Valkenier, W. Hong, V. M. García-Suárez, P. Buiter, J. L. H. Otten, J. C. Hummelen, C. J. Lambert, T. Wandlowski, *J. Am. Chem. Soc.* **2012**, *134*, 5262–5275.
[75] D. Vonlanthen, A. Mishchenko, M. Elbing, M. Neuburger, T. Wandlowski, M. Mayor, *Angew. Chem. Int. Ed.* **2009**, *48*, 8886–8890.
[76] J. R. Heath, M. A. Ratner, *Phys. Today* **2003**, *56*, 43–49.
[77] A. Erbe, S. Verleger, *Acta Phys Pol. A* **2009**, 455–461.
[78] W. G. van der Wiel, S. D. Franceschi, T. Fujisawa, J. M. Elzerman, S. Tarucha, L. P. Kouwenhoven, *Science* **2000**, *289*, 2105–2108.
[79] J. Kondo, *Prog. Theor. Phys.* **1964**, *32*, 37–49.
[80] L. I. Glatman, M. E. Raikh, *JETP Lett.* **1988**, *47*, 452–455.
[81] T. K. Ng, P. A. Lee, *Phys. Rev. Lett.* **1988**, *61*, 1768–1771.
[82] W. Liang, M. P. Shores, M. Bockrath, J. R. Long, H. Park, *Nature* **2002**, *417*, 725–729.
[83] L. H. Yu, D. Natelson, *Nano Lett.* **2004**, *4*, 79–83.
[84] A. N. Pasupathy, R. C. Bialczak, J. Martinek, J. E. Grose, L. A. K. Donev, P. L. McEuen, D. C. Ralph, *Science* **2004**, *306*, 86–89.
[85] Y. Zhang, S. Kahle, T. Herden, C. Stroh, M. Mayor, U. Schlickum, M. Ternes, P. Wahl, K. Kern, *Nat. Commun.* **2013**, *4*, DOI 10.1038/ncomms3110.
[86] E. A. Osorio, T. Bjørnholm, J.-M. Lehn, M. Ruben, H. S. J. van der Zant, *J. Phys. Condens. Matter* **2008**, *20*, 374121.
[87] J. J. Parks, A. R. Champagne, G. R. Hutchison, S. Flores-Torres, H. D. Abruña, D. C. Ralph, *Phys. Rev. Lett.* **2007**, *99*, 026601.
[88] D. Goldhaber Gordon, J. Göres, M. Kastner, H. Shtrikman, D. Mahalu, U. Meirav, *Phys. Rev. Lett.* **1998**, *81*, 5225–5228.
[89] J. Nygård, D. H. Cobden, P. E. Lindelof, *Nature* **2000**, *408*, 342–346.
[90] M. Buitelaar, A. Bachtold, T. Nussbaumer, M. Iqbal, C. Schönenberger, *Phys. Rev. Lett.* **2002**, *88*, DOI 10.1103/PhysRevLett.88.156801.
[91] L. H. Yu, Z. K. Keane, J. W. Ciszek, L. Cheng, J. M. Tour, T. Baruah, M. R. Pederson, D. Natelson, *Phys. Rev. Lett.* **2005**, *95*, 256803.
[92] N. Fuentes, A. Martín-Lasanta, L. Á. de Cienfuegos, M. Ribagorda, A. Parra, J. M. Cuerva, *Nanoscale* **2011**, *3*, 4003–4014.
[93] L. Cui, B. Liu, D. Vonlanthen, M. Mayor, Y. Fu, J.-F. Li, T. Wandlowski, *J. Am. Chem. Soc.* **2011**, *133*, 7332–7335.
[94] A. Mishchenko, D. Vonlanthen, V. Meded, M. Bürkle, C. Li, I. V. Pobelov, A. Bagrets, J. K. Viljas, F. Pauly, F. Evers, et al., *Nano Lett.* **2010**, *10*, 156–163.
[95] A. J. Kronemeijer, H. B. Akkerman, T. Kudernac, B. J. van Wees, B. L. Feringa, P. W. M. Blom, B. de Boer, *Adv. Mater.* **2008**, *20*, 1467–1473.
[96] J. He, F. Chen, P. A. Liddell, J. Andréasson, S. D. Straight, D. Gust, T. A. Moore, A. L. Moore, J. Li, O. F. Sankey, et al., *Nanotechnology* **2005**, *16*, 695.
[97] D. Dulić, S. J. van der Molen, T. Kudernac, H. T. Jonkman, J. J. D. de Jong, T. N. Bowden, J. van Esch, B. L. Feringa, B. J. van Wees, *Phys. Rev. Lett.* **2003**, *91*, 207402.
[98] N. Katsonis, T. Kudernac, M. Walko, S. J. van der Molen, B. J. van Wees, B. L. Feringa, *Adv. Mater.* **2006**, *18*, 1397–1400.
[99] S. J. van der Molen, J. Liao, T. Kudernac, J. S. Agustsson, L. Bernard, M. Calame, B. J. van Wees, B. L. Feringa, C. Schönenberger, *Nano Lett.* **2009**, *9*, 76–80.
[100] S. Yasuda, T. Nakamura, M. Matsumoto, H. Shigekawa, *J. Am. Chem. Soc.* **2003**, *125*, 16430–16433.
[101] J. M. Mativetsky, G. Pace, M. Elbing, M. A. Rampi, M. Mayor, P. Samorì, *J. Am. Chem. Soc.* **2008**, *130*, 9192–9193.

[102] K. Smaali, S. Lenfant, S. Karpe, M. Oçafrain, P. Blanchard, D. Deresmes, S. Godey, A. Rochefort, J. Roncali, D. Vuillaume, *ACS Nano* **2010**, *4*, 2411–2421.
[103] D. I. Gittins, D. Bethell, D. J. Schiffrin, R. J. Nichols, *Nature* **2000**, *408*, 67–69.
[104] Z. Li, I. Pobelov, B. Han, T. Wandlowski, A. Błaszczyk, M. Mayor, *Nanotechnology* **2007**, *18*, 044018.
[105] I. V. Pobelov, Z. Li, T. Wandlowski, *J. Am. Chem. Soc.* **2008**, *130*, 16045–16054.
[106] E. Leary, S. J. Higgins, H. van Zalinge, W. Haiss, R. J. Nichols, S. Nygaard, J. O. Jeppesen, J. Ulstrup, *J. Am. Chem. Soc.* **2008**, *130*, 12204–12205.
[107] Y. Zhou, H. Wu, L. Qu, D. Zhang, D. Zhu, *J. Phys. Chem. B* **2006**, *110*, 15676–15679.
[108] J. Liao, J. S. Agustsson, S. Wu, C. Schönenberger, M. Calame, Y. Leroux, M. Mayor, O. Jeannin, Y.-F. Ran, S.-X. Liu, et al., *Nano Lett.* **2010**, *10*, 759–764.
[109] E. H. van Dijk, D. J. T. Myles, M. H. van der Veen, J. C. Hummelen, *Org. Lett.* **2006**, *8*, 2333–2336.
[110] S. Tsoi, I. Griva, S. A. Trammell, A. S. Blum, J. M. Schnur, N. Lebedev, *ACS Nano* **2008**, *2*, 1289–1295.
[111] C. P. Collier, G. Mattersteig, E. W. Wong, Y. Luo, K. Beverly, J. Sampaio, F. M. Raymo, J. F. Stoddart, J. R. Heath, *Science* **2000**, *289*, 1172–1175.
[112] S. S. Jang, Y. H. Jang, Y.-H. Kim, W. A. Goddard, A. H. Flood, B. W. Laursen, H.-R. Tseng, J. F. Stoddart, J. O. Jeppesen, J. W. Choi, et al., *J. Am. Chem. Soc.* **2005**, *127*, 1563–1575.
[113] T. Ye, A. S. Kumar, S. Saha, T. Takami, T. J. Huang, J. F. Stoddart, P. S. Weiss, *ACS Nano* **2010**, *4*, 3697–3701.
[114] Y. Luo, C. P. Collier, J. O. Jeppesen, K. A. Nielsen, E. DeIonno, G. Ho, J. Perkins, H.-R. Tseng, T. Yamamoto, J. F. Stoddart, et al., *ChemPhysChem* **2002**, *3*, 519–525.
[115] J. E. Green, J. Wook Choi, A. Boukai, Y. Bunimovich, E. Johnston-Halperin, E. DeIonno, Y. Luo, B. A. Sheriff, K. Xu, Y. Shik Shin, et al., *Nature* **2007**, *445*, 414–417.
[116] Y. Chen, G.-Y. Jung, D. A. A. Ohlberg, X. Li, D. R. Stewart, J. O. Jeppesen, K. A. Nielsen, J. F. Stoddart, R. S. Williams, *Nanotechnology* **2003**, *14*, 462.
[117] M.-M. Russew, S. Hecht, *Adv. Mater.* **2010**, *22*, 3348–3360.
[118] T. Kudernac, N. Katsonis, W. R. Browne, B. L. Feringa, *J. Mater. Chem.* **2009**, *19*, 7168–7177.
[119] E. Lörtscher, J. W. Ciszek, J. Tour, H. Riel, *Small* **2006**, *2*, 973–977.
[120] A. C. Whalley, M. L. Steigerwald, X. Guo, C. Nuckolls, *J. Am. Chem. Soc.* **2007**, *129*, 12590–12591.
[121] P. Ahonen, T. Laaksonen, D. J. Schiffrin, K. Kontturi, *Phys. Chem. Chem. Phys.* **2007**, *9*, 4898–4901.
[122] G. Pace, V. Ferri, C. Grave, M. Elbing, C. von Hänisch, M. Zharnikov, M. Mayor, M. A. Rampi, P. Samorì, *Proc. Natl. Acad. Sci.* **2007**, *104*, 9937–9942.
[123] V. Ferri, M. Elbing, G. Pace, M. D. Dickey, M. Zharnikov, P. Samorì, M. Mayor, M. A. Rampi, *Angew. Chem. Int. Ed.* **2008**, *47*, 3407–3409.
[124] I. Diez-Perez, J. Hihath, T. Hines, Z.-S. Wang, G. Zhou, K. Müllen, N. Tao, *Nat. Nanotechnol.* **2011**, *6*, 226–231.
[125] K. Konstas, S. J. Langford, M. J. Latter, *Int. J. Mol. Sci.* **2010**, *11*, 2453–2472.
[126] L. Cambi, L. Szegö, *Berichte Dtsch. Chem. Ges. B Ser.* **1931**, *64*, 2591–2598.
[127] L. Cambi, L. Szegö, *Berichte Dtsch. Chem. Ges. B Ser.* **1933**, *66*, 656–661.
[128] L. Cambi, L. Malatesta, *Berichte Dtsch. Chem. Ges. B Ser.* **1937**, *70*, 2067–2078.
[129] L. G. Vanquickenborne, L. Haspeslagh, *Inorg. Chem.* **1982**, *21*, 2448–2454.
[130] S. Sugano, Y. Tanabe, H. Kamimura, *Multiplets of Transition-Metal Ions in Crystals*, Academic Press, New York, **1970**.
[131] P. Gütlich, A. Hauser, H. Spiering, *Angew. Chem. Int. Ed. Engl.* **1994**, *33*, 2024–2054.
[132] J. A. Real, A. B. Gaspar, M. C. Muñoz, *Dalton Trans.* **2005**, 2062–2079.
[133] S. Thies, C. Bornholdt, F. Köhler, F. D. Sönnichsen, C. Näther, F. Tuczek, R. Herges, *Chem. – Eur. J.* **2010**, *16*, 10074–10083.
[134] M. Pápai, G. Vankó, C. de Graaf, T. Rozgonyi, *J. Chem. Theory Comput.* **2013**, *9*, 509–519.
[135] A. Hauser, *J. Chem. Phys.* **1991**, *94*, 2741–2748.
[136] M. A. Hoselton, L. J. Wilson, R. S. Drago, *J. Am. Chem. Soc.* **1975**, *97*, 1722–1729.
[137] B. A. Katz, C. E. Strouse, *J. Am. Chem. Soc.* **1979**, *101*, 6214–6221.
[138] M. Mikami-Kido, Y. Saito, *Acta Crystallogr. B* **1982**, *38*, 452–455.

[139] L. Wiehl, G. Kiel, C. P. Koehler, H. Spiering, P. Guetlich, *Inorg. Chem.* **1986**, *25*, 1565–1571.
[140] T. Granier, B. Gallois, J. Gaultier, J. A. Real, J. Zarembowitch, *Inorg. Chem.* **1993**, *32*, 5305–5312.
[141] P. Gütlich, A. B. Gaspar, Y. Garcia, V. Ksenofontov, *Comptes Rendus Chim.* **2007**, *10*, 21–36.
[142] P. Gütlich, V. Ksenofontov, A. B. Gaspar, *Coord. Chem. Rev.* **2005**, *249*, 1811–1829.
[143] V. Ksenofontov, A. B. Gaspar, G. Levchenko, B. Fitzsimmons, P. Gütlich, *J. Phys. Chem. B* **2004**, *108*, 7723–7727.
[144] K. Madeja, E. König, *J. Inorg. Nucl. Chem.* **1963**, *25*, 377–385.
[145] D. C. Fisher, H. G. Drickamer, *J. Chem. Phys.* **1971**, *54*, 4825–4837.
[146] D. M. Adams, G. J. Long, A. D. Williams, *Inorg. Chem.* **1982**, *21*, 1049–1053.
[147] J. Pebler, *Inorg. Chem.* **1983**, *22*, 4125–4128.
[148] S. Usha, R. Srinivasan, C. N. R. Rao, *Chem. Phys.* **1985**, *100*, 447–455.
[149] P. Gütlich, A. B. Gaspar, V. Ksenofontov, Y. Garcia, *J. Phys. Condens. Matter* **2004**, *16*, S1087.
[150] J. J. McGravey, I. Lawthers, *J. Chem. Soc. Chem. Commun.* **1982**, 906–907.
[151] S. Decurtins, P. Gütlich, C. P. Köhler, H. Spiering, A. Hauser, *Chem. Phys. Lett.* **1984**, *105*, 1–4.
[152] P. Gütlich, *Z. Für Anorg. Allg. Chem.* **2012**, *638*, 15–43.
[153] C. Roux, J. Zarembowitch, B. Gallois, T. Granier, R. Claude, *Inorg. Chem.* **1994**, *33*, 2273–2279.
[154] M.-L. Boillot, C. Roux, J.-P. Audière, A. Dausse, J. Zarembowitch, *Inorg. Chem.* **1996**, *35*, 3975–3980.
[155] M.-L. Boillot, A. Sour, P. Delhaès, C. Mingotaud, H. Soyer, *Coord. Chem. Rev.* **1999**, *190–192*, 47–59.
[156] J. J. Parks, A. R. Champagne, T. A. Costi, W. W. Shum, A. N. Pasupathy, E. Neuscamman, S. Flores-Torres, P. S. Cornaglia, A. A. Aligia, C. A. Balseiro, et al., *Science* **2010**, *328*, 1370–1373.
[157] F. Prins, M. Monrabal-Capilla, E. A. Osorio, E. Coronado, H. S. J. van der Zant, *Adv. Mater.* **2011**, *23*, 1545–1549.
[158] S. Wagner, F. Kisslinger, S. Ballmann, F. Schramm, R. Chandrasekar, T. Bodenstein, O. Fuhr, D. Secker, K. Fink, M. Ruben, et al., *Nat. Nanotechnol.* **2013**, *8*, 575–579.
[159] G. T. Morgan, F. H. Burstall, *J. Chem. Soc. Resumed* **1932**, 20–30.
[160] G. Morgan, F. H. Burstall, *J. Chem. Soc. Resumed* **1937**, 1649–1655.
[161] J. M. Lehn, *Science* **1993**, *260*, 1762–1763.
[162] J.-M. Lehn, *Angew. Chem. Int. Ed. Engl.* **1988**, *27*, 89–112.
[163] C. J. Pedersen, *Angew. Chem. Int. Ed. Engl.* **1988**, *27*, 1021–1027.
[164] D. J. Cram, *Angew. Chem. Int. Ed. Engl.* **1988**, *27*, 1009–1020.
[165] A. Wild, A. Winter, F. Schlütter, U. S. Schubert, *Chem. Soc. Rev.* **2011**, *40*, 1459–1511.
[166] R. Shunmugam, G. J. Gabriel, K. A. Aamer, G. N. Tew, *Macromol. Rapid Commun.* **2010**, *31*, 784–793.
[167] E. C. Constable, *Chem. Soc. Rev.* **2007**, *36*, 246–253.
[168] M. W. Cooke, G. S. Hanan, *Chem. Soc. Rev.* **2007**, *36*, 1466–1476.
[169] D. G. Kurth, M. Higuchi, *Soft Matter* **2006**, *2*, 915–927.
[170] E. A. Medlycott, G. S. Hanan, *Chem. Soc. Rev.* **2005**, *34*, 133–142.
[171] P. R. Andres, U. S. Schubert, *Adv. Mater.* **2004**, *16*, 1043–1068.
[172] M. Heller, U. S. Schubert, *Eur. J. Org. Chem.* **2003**, *2003*, 947–961.
[173] A. E. Tschitschibabin, *J. Für Prakt. Chem.* **1924**, *107*, 122–128.
[174] C. Hollins, *The Synthesis of Nitrogen Ring Compounds Containing a Single Hetero-Atom [nitrogen]*, Van Nostrand, New York, **1924**.
[175] F. Kröhnke, *Synthesis* **1976**, *1976*, 1–24.
[176] K. T. Potts, D. A. Usifer, A. Guadalupe, H. D. Abruna, *J. Am. Chem. Soc.* **1987**, *109*, 3961–3967.
[177] F. Kröhnke, *Angew. Chem. Int. Ed. Engl.* **1963**, *2*, 225–238.
[178] E. C. Constable, J. Lewis, *Polyhedron* **1982**, *1*, 303–306.
[179] G. R. Newkome, D. C. Hager, G. E. Kiefer, *J. Org. Chem.* **1986**, *51*, 850–853.
[180] D. C. Owsley, J. M. Nelke, J. J. Bloomfield, *J. Org. Chem.* **1973**, *38*, 901–903.

[181] K. T. Potts, P. Ralli, G. Theodoridis, P. Winslow, *Org. Synth.* **1986**, *64*, 189.
[182] D. L. Jameson, L. E. Guise, *Tetrahedron Lett.* **1991**, *32*, 1999–2002.
[183] G. R. Pabst, J. Sauer, *Tetrahedron* **1999**, *55*, 5067–5088.
[184] J. C. Adrian Jr., L. Hassib, N. De Kimpe, M. Keppens, *Tetrahedron* **1998**, *54*, 2365–2370.
[185] I. Sasaki, J. C. Daran, G. G. A. Balavoine, *Synthesis* **1999**, *1999*, 815–820.
[186] R.-A. Fallahpour, E. C. Constable, *J. Chem. Soc. [Perkin 1]* **1997**, 2263–2264.
[187] R.-A. Fallahpour, M. Neuburger, M. Zehnder, *Polyhedron* **1999**, *18*, 2445–2454.
[188] Y. Tohda, M. Eiraku, T. Nakagawa, Y. Usami, M. Ariga, T. Kawashima, K. Tani, H. Watanabe, Y. Mori, *Bull. Chem. Soc. Jpn.* **1990**, *63*, 2820–2827.
[189] J. Uenishi, T. Tanaka, S. Wakabayashi, S. Oae, H. Tsukube, *Tetrahedron Lett.* **1990**, *31*, 4625–4628.
[190] J. E. Parks, B. E. Wagner, R. H. Holm, *J. Organomet. Chem.* **1973**, *56*, 53–66.
[191] A. Suzuki, *Angew. Chem. Int. Ed.* **2011**, *50*, 6722–6737.
[192] R. Heck, **2010**.
[193] E. Negishi, *Angew. Chem. Int. Ed.* **2011**, *50*, 6738–6764.
[194] R. F. Heck, *Acc. Chem. Res.* **1979**, *12*, 146–151.
[195] S. Bräse, A. D. Meijere, in *Met.-Catalyzed Cross-Coupling React.* (Eds.: A. de Meijere, F. Diederich), Wiley-VCH Verlag GmbH, **2004**, pp. 217–315.
[196] R. F. Heck, J. P. Nolley, *J. Org. Chem.* **1972**, *37*, 2320–2322.
[197] T. Mizoroki, K. Mori, A. Ozaki, *Bull. Chem. Soc. Jpn.* **1971**, *44*, 581–581.
[198] R. J. P. Corriu, J. P. Masse, *J. Chem. Soc. Chem. Commun.* **1972**, 144a–144a.
[199] K. Tamao, K. Sumitani, M. Kumada, *J. Am. Chem. Soc.* **1972**, *94*, 4374–4376.
[200] T. Hayashi, M. Konishi, Y. Kobori, M. Kumada, T. Higuchi, K. Hirotsu, *J. Am. Chem. Soc.* **1984**, *106*, 158–163.
[201] E.-I. Negishi, X. Zeng, Z. Tan, M. Qian, Q. Hu, Z. Huang, in *Met.-Catalyzed Cross-Coupling React.* (Eds.: A. de Meijere, F. Diederich), Wiley-VCH Verlag GmbH, **2004**, pp. 815–889.
[202] E. Negishi, in *Handb. Organopalladium Chem. Org. Synth.* (Ed.: E. Negishi), John Wiley & Sons, Inc., **2002**, pp. 229–247.
[203] A. O. King, N. Okukado, E. Negishi, *J. Chem. Soc. Chem. Commun.* **1977**, 683–684.
[204] L. Kurti, B. Czako, *Strategic Applications of Named Reactions in Organic Synthesis*, Elsevier, **2005**.
[205] K. Sonogashira, *J. Organomet. Chem.* **2002**, *653*, 46–49.
[206] N. M. Jenny, M. Mayor, T. R. Eaton, *Eur. J. Org. Chem.* **2011**, *2011*, 4965–4983.
[207] J. A. Marsden, M. M. Haley, in *Met.-Catalyzed Cross-Coupling React.* (Eds.: A. de Meijere, F. Diederich), Wiley-VCH Verlag GmbH, **2004**, pp. 317–394.
[208] Y. Hatanaka, T. Hiyama, *J. Org. Chem.* **1988**, *53*, 918–920.
[209] Y. Hatanaka, T. Hiyama, *Synlett* **1991**, *1991*, 845–853.
[210] S. E. Denmark, R. F. Sweis, in *Met.-Catalyzed Cross-Coupling React.* (Eds.: A. de Meijere, F. Diederich), Wiley-VCH Verlag GmbH, **2004**, pp. 163–216.
[211] N. Miyaura, A. Suzuki, *Chem. Rev.* **1995**, *95*, 2457–2483.
[212] N. Miyaura, in *Met.-Catalyzed Cross-Coupling React.* (Eds.: A. de Meijere, F. Diederich), Wiley-VCH Verlag GmbH, **2004**, pp. 41–123.
[213] N. Miyaura, A. Suzuki, *J. Chem. Soc. Chem. Commun.* **1979**, 866–867.
[214] N. Miyaura, K. Yamada, A. Suzuki, *Tetrahedron Lett.* **1979**, *20*, 3437–3440.
[215] J. K. Stille, *Angew. Chem. Int. Ed. Engl.* **1986**, *25*, 508–524.
[216] V. Farina, V. Krishnamurthy, W. J. Scott, in *Org. React.*, John Wiley & Sons, Inc., **2004**.
[217] T. N. Mitchell, in *Met.-Catalyzed Cross-Coupling React.* (Eds.: A. de Meijere, F. Diederich), Wiley-VCH Verlag GmbH, **2004**, pp. 125–161.
[218] D. J. Cárdenas, J.-P. Sauvage, *Synlett* **1996**, *1996*, 916–918.
[219] R.-A. Fallahpour, *Synthesis* **2000**, *2000*, 1138–1142.
[220] R.-A. Fallahpour, *Synthesis* **1999**, *1999*, 1051–1055.
[221] R.-A. Fallahpour, M. Neuburger, M. Zehnder, *New J. Chem.* **1999**, *23*, 53–61.
[222] G. Ulrich, S. Bedel, C. Picard, P. Tisnès, *Tetrahedron Lett.* **2001**, *42*, 6113–6115.
[223] M. Heller, U. S. Schubert, *J. Org. Chem.* **2002**, *67*, 8269–8272.
[224] M. Heller, U. S. Schubert, *Synlett* **2002**, *2002*, 0751–0754.
[225] R.-A. Fallahpour, *Synthesis* **2000**, *2000*, 1665–1667.

[226] R.-A. Fallahpour, M. Neuburger, *Eur. J. Org. Chem.* **2001**, *2001*, 1853–1856.
[227] U. S. Schubert, C. Eschbaumer, *Org. Lett.* **1999**, *1*, 1027–1029.
[228] U. Lehmann, O. Henze, A. D. Schlüter, *Chem. – Eur. J.* **1999**, *5*, 854–859.
[229] F. Louërat, P. C. Gros, *Tetrahedron Lett.* **2010**, *51*, 3558–3560.
[230] S. A. Savage, A. P. Smith, C. L. Fraser, *J. Org. Chem.* **1998**, *63*, 10048–10051.
[231] M. Chavarot, Z. Pikramenou, *Tetrahedron Lett.* **1999**, *40*, 6865–6868.
[232] D. Venkataraman, Y. Du, S. R. Wilson, K. A. Hirsch, P. Zhang, J. S. Moore, *J. Chem. Educ.* **1997**, *74*, 915.
[233] C. Mugemana, P. Guillet, S. Hoeppener, U. S. Schubert, C.-A. Fustin, J.-F. Gohy, *Chem. Commun.* **2010**, *46*, 1296–1298.
[234] J. P. Sauvage, J. P. Collin, J. C. Chambron, S. Guillerez, C. Coudret, V. Balzani, F. Barigelletti, L. De Cola, L. Flamigni, *Chem. Rev.* **1994**, *94*, 993–1019.
[235] S. Campagna, F. Puntoriero, F. Nastasi, G. Bergamini, V. Balzani, in *Photochem. Photophysics Coord. Compd. I* (Eds.: V. Balzani, S. Campagna), Springer Berlin Heidelberg, **2007**, pp. 117–214.
[236] M. T. Indelli, C. Chiorboli, F. Scandola, in *Photochem. Photophysics Coord. Compd. I* (Eds.: V. Balzani, S. Campagna), Springer Berlin Heidelberg, **2007**, pp. 215–255.
[237] J. Paul, S. Spey, H. Adams, J. A. Thomas, *Inorganica Chim. Acta* **2004**, *357*, 2827–2832.
[238] J. A. G. Williams, A. J. Wilkinson, V. L. Whittle, *Dalton Trans.* **2008**, 2081–2099.
[239] B. O'Regan, M. Grätzel, *Nature* **1991**, *353*, 737–740.
[240] P. Péchy, T. Renouard, S. M. Zakeeruddin, R. Humphry-Baker, P. Comte, P. Liska, L. Cevey, E. Costa, V. Shklover, L. Spiccia, et al., *J. Am. Chem. Soc.* **2001**, *123*, 1613–1624.
[241] O. Kohle, S. Ruile, M. Grätzel, *Inorg. Chem.* **1996**, *35*, 4779–4787.
[242] J. Bandara, H. Weerasinghe, *Sol. Energy Mater. Sol. Cells* **2006**, *90*, 864–871.
[243] M. K. Nazeeruddin, P. Péchy, M. Grätzel, *Chem. Commun.* **1997**, 1705–1706.
[244] Y. Chiba, A. Islam, Y. Watanabe, R. Komiya, N. Koide, L. Han, *Jpn. J. Appl. Phys.* **2006**, *45*, L638.
[245] T. W. Hamann, R. A. Jensen, A. B. F. Martinson, H. V. Ryswyk, J. T. Hupp, *Energy Environ. Sci.* **2008**, *1*, 66–78.
[246] A. Hepp, G. Ulrich, R. Schmechel, H. von Seggern, R. Ziessel, *Synth. Met.* **2004**, *146*, 11–15.
[247] S.-H. Hwang, P. Wang, C. N. Moorefield, J.-C. Jung, J.-Y. Kim, S.-W. Lee, G. R. Newkome, *Macromol. Rapid Commun.* **2006**, *27*, 1809–1813.
[248] M. Ichikawa, K. Wakabayashi, S. Hayashi, N. Yokoyama, T. Koyama, Y. Taniguchi, *Org. Electron.* **2010**, *11*, 1966–1973.
[249] M. Ichikawa, T. Yamamoto, H.-G. Jeon, K. Kase, S. Hayashi, M. Nagaoka, N. Yokoyama, *J. Mater. Chem.* **2012**, *22*, 6765–6773.
[250] J. Kuwabara, T. Namekawa, M. Haga, T. Kanbara, *Dalton Trans.* **2011**, *41*, 44–46.
[251] Y.-Y. Chen, Y.-T. Tao, H.-C. Lin, *Macromolecules* **2006**, *39*, 8559–8566.
[252] Y.-Y. Chen, H.-C. Lin, *J. Polym. Sci. Part Polym. Chem.* **2007**, *45*, 3243–3255.
[253] A. Winter, C. Friebe, M. Chiper, M. D. Hager, U. S. Schubert, *J. Polym. Sci. Part Polym. Chem.* **2009**, *47*, 4083–4098.
[254] H. J. Bolink, L. Cappelli, E. Coronado, P. Gaviña, *Inorg. Chem.* **2005**, *44*, 5966–5968.
[255] E. C. Constable, C. E. Housecroft, G. E. Schneider, J. A. Zampese, H. J. Bolink, A. Pertegás, C. Roldan-Carmona, *Dalton Trans.* **2014**, *43*, 4653–4667.
[256] F. D. Angelis, S. Fantacci, A. Sgamelotti, F. Cariati, D. Roberto, F. Tessore, R. Ugo, *Dalton Trans.* **2006**, 852–859.
[257] H. T. Uyeda, Y. Zhao, K. Wostyn, I. Asselberghs, K. Clays, A. Persoons, M. J. Therien, *J. Am. Chem. Soc.* **2002**, *124*, 13806–13813.
[258] F. Tessore, D. Roberto, R. Ugo, M. Pizzotti, S. Quici, M. Cavazzini, S. Bruni, F. De Angelis, *Inorg. Chem.* **2005**, *44*, 8967–8978.
[259] D. Roberto, F. Tessore, R. Ugo, S. Bruni, A. Manfredi, S. Quici, *Chem. Commun.* **2002**, 846–847.
[260] S. Qu, C. Du, Y. Song, Y. Wang, Y. Gao, S. Liu, Y. Li, D. Zhu, *Chem. Phys. Lett.* **2002**, *356*, 403–408.
[261] A. Scarpaci, C. Monnereau, N. Hergué, E. Blart, S. Legoupy, F. Odobel, A. Gorfo, J. Pérez-Moreno, K. Clays, I. Asselberghs, *Dalton Trans.* **2009**, 4538–4546.

[262] F. Dumur, C. R. Mayer, K. Hoang-Thi, I. Ledoux-Rak, F. Miomandre, G. Clavier, E. Dumas, R. Méallet-Renault, M. Frigoli, J. Zyss, et al., *Inorg. Chem.* **2009**, *48*, 8120–8133.
[263] J.-M. Lehn, *Supramolecular Chemistry - Concepts and Perspectives*, Wiley-VCH: Weinheim, Weinheim, **1995**.
[264] U. S. Schubert, A. Winter, G. R. Newkome, in *Terpyridine-Based Mater.*, Wiley-VCH Verlag GmbH & Co. KGaA, **2011**, pp. 129–197.
[265] M. Schmittel, P. Mal, *Chem. Commun.* **2008**, 960–962.
[266] S. Bonnet, J.-P. Collin, M. Koizumi, P. Mobian, J.-P. Sauvage, *Adv. Mater.* **2006**, *18*, 1239–1250.
[267] G. R. Newkome, P. Wang, C. N. Moorefield, T. J. Cho, P. P. Mohapatra, S. Li, S.-H. Hwang, O. Lukoyanova, L. Echegoyen, J. A. Palagallo, et al., *Science* **2006**, *312*, 1782–1785.
[268] E. C. Constable, R. W. Handel, C. E. Housecroft, A. Farràn Morales, B. Ventura, L. Flamigni, F. Barigelletti, *Chem. – Eur. J.* **2005**, *11*, 4024–4034.
[269] E. C. Constable, C. E. Housecroft, M. Cattalini, D. Phillips, *New J. Chem.* **1998**, *22*, 193–200.
[270] D. J. Cárdenas, J.-P. Collin, P. Gaviña, J.-P. Sauvage, A. D. Cian, J. Fischer, N. Armaroli, L. Flamigni, V. Vicinelli, V. Balzani, *J. Am. Chem. Soc.* **1999**, *121*, 5481–5488.
[271] D. J. Cárdenas, P. Gaviña, J.-P. Sauvage, *Chem. Commun.* **1996**, 1915–1916.
[272] D. J. Cárdenas, P. Gaviña, J.-P. Sauvage, *J. Am. Chem. Soc.* **1997**, *119*, 2656–2664.
[273] M. C. Jimenez-Molero, C. Dietrich-Buchecker, J.-P. Sauvage, *Chem. – Eur. J.* **2002**, *8*, 1456–1466.
[274] U. S. Schubert, C. Eschbaumer, *Angew. Chem. Int. Ed.* **2002**, *41*, 2892–2926.
[275] H. Hofmeier, U. S. Schubert, *Chem. Commun.* **2005**, 2423–2432.
[276] J.-F. Gohy, *Coord. Chem. Rev.* **2009**, *253*, 2214–2225.
[277] Y. Zhang, C. B. Murphy, W. E. Jones, *Macromolecules* **2002**, *35*, 630–636.
[278] Y. Cui, Q. Chen, D.-D. Zhang, J. Cao, B.-H. Han, *J. Polym. Sci. Part Polym. Chem.* **2010**, *48*, 1310–1316.
[279] P. Wang, C. N. Moorefield, G. R. Newkome, *Angew. Chem. Int. Ed.* **2005**, *44*, 1679–1683.
[280] K. T. Potts, M. Keshavarz-K, F. S. Tham, H. D. Abruna, C. Arana, *Inorg. Chem.* **1993**, *32*, 4436–4449.
[281] K. T. Potts, M. Keshavarz-K, F. S. Tham, H. D. Abruna, C. Arana, *Inorg. Chem.* **1993**, *32*, 4450–4456.
[282] K. T. Potts, M. Keshavarz-K, F. S. Tham, K. A. G. Raiford, C. Arana, H. D. Abruna, *Inorg. Chem.* **1993**, *32*, 5477–5484.
[283] M. D. Hager, P. Greil, C. Leyens, S. van der Zwaag, U. S. Schubert, *Adv. Mater.* **2010**, *22*, 5424–5430.
[284] H. Hofmeier, U. S. Schubert, *Chem. Soc. Rev.* **2004**, *33*, 373–399.
[285] U. Mansfeld, M. D. Hager, R. Hoogenboom, C. Ott, A. Winter, U. S. Schubert, *Chem. Commun.* **2009**, 3386–3388.
[286] B. G. G. Lohmeijer, U. S. Schubert, *J. Polym. Sci. Part Polym. Chem.* **2005**, *43*, 6331–6344.
[287] C.-A. Fustin, P. Guillet, U. S. Schubert, J.-F. Gohy, *Adv. Mater.* **2007**, *19*, 1665–1673.
[288] J.-F. Gohy, C. Ott, S. Hoeppener, U. S. Schubert, *Chem. Commun.* **2009**, 6038–6040.
[289] M. Chiper, D. Fournier, R. Hoogenboom, U. S. Schubert, *Macromol. Rapid Commun.* **2008**, *29*, 1640–1647.
[290] H. Hofmeier, U. S. Schubert, *Macromol. Chem. Phys.* **2003**, *204*, 1391–1397.
[291] S. J. Lippard, *Acc. Chem. Res.* **1978**, *11*, 211–217.
[292] I. Eryazici, C. N. Moorefield, G. R. Newkome, *Chem. Rev.* **2008**, *108*, 1834–1895.
[293] P. M. van Vliet, S. M. S. Toekimin, J. G. Haasnoot, J. Reedijk, O. Nováková, O. Vrána, V. Brabec, *Inorganica Chim. Acta* **1995**, *231*, 57–64.
[294] J. R. Peterson, T. A. Smith, P. Thordarson, *Chem. Commun.* **2007**, 1899–1901.
[295] H. Bertrand, S. Bombard, D. Monchaud, E. Talbot, A. Guédin, J.-L. Mergny, R. Grünert, P. J. Bednarski, M.-P. Teulade-Fichou, *Org. Biomol. Chem.* **2009**, *7*, 2864–2871.
[296] Y.-C. Lo, T.-P. Ko, W.-C. Su, T.-L. Su, A. H.-J. Wang, *J. Inorg. Biochem.* **2009**, *103*, 1082–1092.
[297] P. Wu, E. L.-M. Wong, D.-L. Ma, G. S.-M. Tong, K.-M. Ng, C.-M. Che, *Chem. – Eur. J.* **2009**, *15*, 3652–3656.

[298] K. W. Jennette, S. J. Lippard, G. A. Vassiliades, W. R. Bauer, *Proc. Natl. Acad. Sci.* **1974**, *71*, 3839–3843.
[299] J. R. Peterson, T. A. Smith, P. Thordarson, *Org. Biomol. Chem.* **2009**, *8*, 151–162.
[300] A. Anthonysamy, S. Balasubramanian, V. Shanmugaiah, N. Mathivanan, *Dalton Trans.* **2008**, 2136–2143.
[301] K. K.-W. Lo, C.-K. Chung, D. C.-M. Ng, N. Zhu, *New J. Chem.* **2002**, *26*, 81–88.
[302] E. C. Long, J. K. Barton, *Acc. Chem. Res.* **1990**, *23*, 271–273.
[303] X. Piao, Y. Zou, J. Wu, C. Li, T. Yi, *Org. Lett.* **2009**, *11*, 3818–3821.
[304] B. Tang, F. Yu, P. Li, L. Tong, X. Duan, T. Xie, X. Wang, *J. Am. Chem. Soc.* **2009**, *131*, 3016–3023.
[305] Y. Gao, J. Wu, Y. Li, P. Sun, H. Zhou, J. Yang, S. Zhang, B. Jin, Y. Tian, *J. Am. Chem. Soc.* **2009**, *131*, 5208–5213.
[306] P. J. Bond, R. Langridge, K. W. Jennette, S. J. Lippard, *Proc. Natl. Acad. Sci.* **1975**, *72*, 4825–4829.
[307] W. B. Pratt, R. W. Ruddon, *The Anticancer Drugs*, Oxford University Press, New York, **1979**.
[308] O. Novakova, J. Kasparkova, O. Vrana, P. M. van Vliet, J. Reedijk, V. Brabec, *Biochemistry (Mosc.)* **1995**, *34*, 12369–12378.
[309] Y. Gao, J. Wu, Q. Zhao, L. Zheng, H. Zhou, S. Zhang, J. Yang, Y. Tian, *New J. Chem.* **2009**, *33*, 607–611.
[310] T.-Y. Dong, C. Huang, C.-P. Chen, M.-C. Lin, *J. Organomet. Chem.* **2007**, *692*, 5147–5155.
[311] Y.-T. Chan, S. Li, C. N. Moorefield, P. Wang, C. D. Shreiner, G. R. Newkome, *Chem. – Eur. J.* **2010**, *16*, 4164–4168.
[312] M. Alvaro, C. Aprile, B. Ferrer, F. Sastre, H. García, *Dalton Trans.* **2009**, 7437–7444.
[313] V. Duffort, R. Thouvenot, C. Afonso, G. Izzet, A. Proust, *Chem. Commun.* **2009**, 6062–6064.
[314] Y. Pan, B. Tong, J. Shi, W. Zhao, J. Shen, J. Zhi, Y. Dong, *J. Phys. Chem. C* **2010**, *114*, 8040–8047.
[315] T. Salditt, U. S. Schubert, *Rev. Mol. Biotechnol.* **2002**, *90*, 55–70.
[316] N. Tuccitto, I. Delfanti, V. Torrisi, F. Scandola, C. Chiorboli, V. Stepanenko, F. Würthner, A. Licciardello, *Phys. Chem. Chem. Phys.* **2009**, *11*, 4033–4038.
[317] N. Tuccitto, V. Ferri, M. Cavazzini, S. Quici, G. Zhavnerko, A. Licciardello, M. A. Rampi, *Nat. Mater.* **2009**, *8*, 41–46.
[318] N. Tuccitto, V. Torrisi, M. Cavazzini, T. Morotti, F. Puntoriero, S. Quici, S. Campagna, A. Licciardello, *ChemPhysChem* **2007**, *8*, 227–230.
[319] M. Utsuno, F. Toshimitsu, S. Kume, H. Nishihara, *Macromol. Symp.* **2008**, *270*, 153–160.
[320] A. Auditore, N. Tuccitto, G. Marzanni, S. Quici, F. Puntoriero, S. Campagna, A. Licciardello, C*hem. Commun.* **2003**, 2494–2495.
[321] T. Kurita, Y. Nishimori, F. Toshimitsu, S. Muratsugu, S. Kume, H. Nishihara, *J. Am. Chem. Soc.* **2010**, *132*, 4524–4525.
[322] D. J. Díaz, S. Bernhard, G. D. Storrier, H. D. Abruña, *J. Phys. Chem. B* **2001**, *105*, 8746–8754.
[323] C. Haensch, M. Chiper, C. Ulbricht, A. Winter, S. Hoeppener, U. S. Schubert, *Langmuir* **2008**, *24*, 12981–12985.
[324] H. L. Smith, R. L. Usala, E. W. McQueen, J. I. Goldsmith, *Langmuir* **2010**, *26*, 3342–3349.
[325] W. Kubo, M. Nagao, Y. Otsuka, T. Homma, H. Miyata, *Langmuir* **2009**, *25*, 13340–13343.
[326] F. Ullmann, in *Berichte Dtsch. Chem. Ges.*, **1901**, pp. 2174–2185.
[327] P. E. Fanta, *Chem. Rev.* **1964**, *64*, 613–632.
[328] P. E. Fanta, *Synthesis* **1974**, *1974*, 9–21.
[329] M. Sainsbury, *Tetrahedron* **1980**, *36*, 3327–3359.
[330] G. Bringmann, R. Walter, R. Weirich, *Angew. Chem. Int. Ed. Engl.* **1990**, *29*, 977–991.
[331] K. Tamao, K. Sumitani, Y. Kiso, M. Zembayashi, A. Fujioka, S. Kodama, I. Nakajima, A. Minato, M. Kumada, *Bull. Chem. Soc. Jpn.* **1976**, *49*, 1958–1969.
[332] M. Kumada, *Pure Appl. Chem.* **1980**, *52*, DOI 10.1351/pac198052030669.
[333] N. Miyaura, in *Adv. Met.-Org. Chem.* (Ed.: Lanny S. Liebeskind), JAI, **1998**, pp. 187–243.
[334] N. Miyaura, in *Cross-Coupling React.* (Ed.: P.N. Miyaura), Springer Berlin Heidelberg, **2002**, pp. 11–59.
[335] A. Suzuki, in *Met.-Catalyzed Cross-Coupling React.* (Eds.: F. Diederich, P.J. Stang), Wiley-VCH Verlag GmbH, **1998**, pp. 48–97.

[336] A. Suzuki, *J. Organomet. Chem.* **1999**, *576*, 147–168.
[337] S. Kotha, K. Lahiri, D. Kashinath, *Tetrahedron* **2002**, *58*, 9633–9695.
[338] J. Hassan, M. Sévignon, C. Gozzi, E. Schulz, M. Lemaire, *Chem. Rev.* **2002**, *102*, 1359–1470.
[339] S. P. Stanforth, *Tetrahedron* **1998**, *54*, 263–303.
[340] A. F. Littke, G. C. Fu, *Angew. Chem. Int. Ed.* **2002**, *41*, 4176–4211.
[341] S. R. Chemler, D. Trauner, S. J. Danishefsky, *Angew. Chem. Int. Ed.* **2001**, *40*, 4544–4568.
[342] G. J. Irvine, M. J. G. Lesley, T. B. Marder, N. C. Norman, C. R. Rice, E. G. Robins, W. R. Roper, G. R. Whittell, L. J. Wright, *Chem. Rev.* **1998**, *98*, 2685–2722.
[343] T. Ishiyama, N. Miyaura, *J. Organomet. Chem.* **2000**, *611*, 392–402.
[344] V. V. Grushin, H. Alper, *Chem. Rev.* **1994**, *94*, 1047–1062.
[345] V. V. Grushin, H. Alper, in *Act. Unreactive Bonds Org. Synth.* (Eds.: P.S. Murai, H. Alper, R.A. Gossage, V.V. Grushin, M. Hidai, Y. Ito, W.D. Jones, F. Kakiuchi, G. van Koten, Y.-S. Lin, et al.), Springer Berlin Heidelberg, **1999**, pp. 193–226.
[346] J. Krause, G. Cestaric, K.-J. Haack, K. Seevogel, W. Storm, K.-R. Pörschke, *J. Am. Chem. Soc.* **1999**, *121*, 9807–9823.
[347] A. F. Littke, C. Dai, G. C. Fu, *J. Am. Chem. Soc.* **2000**, *122*, 4020–4028.
[348] A. F. Littke, G. C. Fu, *Angew. Chem. Int. Ed.* **1998**, *37*, 3387–3388.
[349] T. Yoshida, S. Otsuka, *J. Am. Chem. Soc.* **1977**, *99*, 2134–2140.
[350] M. Portnoy, D. Milstein, *Organometallics* **1993**, *12*, 1665–1673.
[351] A. Zapf, A. Ehrentraut, M. Beller, *Angew. Chem. Int. Ed.* **2000**, *39*, 4153–4155.
[352] J. P. Wolfe, R. A. Singer, B. H. Yang, S. L. Buchwald, *J. Am. Chem. Soc.* **1999**, *121*, 9550–9561.
[353] D. W. Old, J. P. Wolfe, S. L. Buchwald, *J. Am. Chem. Soc.* **1998**, *120*, 9722–9723.
[354] N. Kataoka, Q. Shelby, J. P. Stambuli, J. F. Hartwig, *J. Org. Chem.* **2002**, *67*, 5553–5566.
[355] M. G. Andreu, A. Zapf, M. Beller, *Chem. Commun.* **2000**, 2475–2476.
[356] X. Bei, H. W. Turner, W. H. Weinberg, A. S. Guram, J. L. Petersen, *J. Org. Chem.* **1999**, *64*, 6797–6803.
[357] G. Y. Li, *Angew. Chem. Int. Ed.* **2001**, *40*, 1513–1516.
[358] G. Y. Li, *J. Org. Chem.* **2002**, *67*, 3643–3650.
[359] A. C. Hillier, G. A. Grasa, M. S. Viciu, H. M. Lee, C. Yang, S. P. Nolan, *J. Organomet. Chem.* **2002**, *653*, 69–82.
[360] A. Fürstner, G. Seidel, *Org. Lett.* **2002**, *4*, 541–543.
[361] K. Selvakumar, A. Zapf, A. Spannenberg, M. Beller, *Chem. – Eur. J.* **2002**, *8*, 3901–3906.
[362] M. B. Andrus, C. Song, *Org. Lett.* **2001**, *3*, 3761–3764.
[363] G. A. Grasa, M. S. Viciu, J. Huang, C. Zhang, M. L. Trudell, S. P. Nolan, *Organometallics* **2002**, *21*, 2866–2873.
[364] C. Zhang, J. Huang, M. L. Trudell, S. P. Nolan, *J. Org. Chem.* **1999**, *64*, 3804–3805.
[365] N. A. Bumagin, V. V. Bykov, *Tetrahedron* **1997**, *53*, 14437–14450.
[366] N. Miyaura, T. Ishiyama, H. Sasaki, M. Ishikawa, M. Sato, A. Suzuki, *J. Am. Chem. Soc.* **1989**, *111*, 314–321.
[367] T. Ishiyama, N. Miyaura, A. Suzkuki, *Org. Synth.* **1993**, *71*, 89.
[368] Y. Kobayashi, R. Mizojiri, *Tetrahedron Lett.* **1996**, *37*, 8531–8534.
[369] G. Zou, J. R. Falck, *Tetrahedron Lett.* **2001**, *42*, 5817–5819.
[370] H. Nakai, S. Ogo, Y. Watanabe, *Organometallics* **2002**, *21*, 1674–1678.
[371] K. Matos, J. A. Soderquist, *J. Org. Chem.* **1998**, *63*, 461–470.
[372] N. Miyaura, K. Yamada, H. Suginome, A. Suzuki, *J. Am. Chem. Soc.* **1985**, *107*, 972–980.
[373] T. Ishiyama, M. Murata, N. Miyaura, *J. Org. Chem.* **1995**, *60*, 7508–7510.
[374] A. Gillie, J. K. Stille, *J. Am. Chem. Soc.* **1980**, *102*, 4933–4941.
[375] F. Ozawa, T. Hidaka, T. Yamamoto, A. Yamamoto, *J. Organomet. Chem.* **1987**, *330*, 253–263.
[376] F. Ozawa, T. Ito, Y. Nakamura, A. Yamamoto, *Bull. Chem. Soc. Jpn.* **1981**, *54*, 1868–1880.
[377] F. Ozawa, T. Ito, A. Yamamoto, *J. Am. Chem. Soc.* **1980**, *102*, 6457–6463.
[378] F. Ozawa, K. Kurihara, M. Fujimori, T. Hidaka, T. Toyoshima, A. Yamamoto, *Organometallics* **1989**, *8*, 180–188.
[379] F. Ozawa, K. Kurihara, T. Yamamoto, A. Yamamoto, *Bull. Chem. Soc. Jpn.* **1985**, *58*, 399–400.
[380] F. Ozawa, A. Yamamoto, *Nippon Kagaku Kaishi* **1987**, *1987*, 773–784.

[381] A. Yamamoto, *Organotransition Metal Chemistry: Fundamental Concepts and Applications*, Wiley-Interscience, New York, **1986**.
[382] G. B. Smith, G. C. Dezeny, D. L. Hughes, A. O. King, T. R. Verhoeven, *J. Org. Chem.* **1994**, *59*, 8151–8156.
[383] W. C. Shieh, J. A. Carlson, *J. Org. Chem.* **1992**, *57*, 379–381.
[384] T. Watanabe, N. Miyaura, A. Suzuki, *Synlett* **1992**, *1992*, 207–210.
[385] J. C. Anderson, H. Namli, C. A. Roberts, *Tetrahedron* **1997**, *53*, 15123–15134.
[386] R. M. Smith, A. E. Martell, *Critical Stability Constants. Volume 4, Volume 4,* Plenum Press, New York; London, **1989**.
[387] R. A. Batey, T. D. Quach, *Tetrahedron Lett.* **2001**, *42*, 9099–9103.
[388] S. W. Wright, D. L. Hageman, L. D. McClure, *J. Org. Chem.* **1994**, *59*, 6095–6097.
[389] D. K. Morita, J. K. Stille, J. R. Norton, *J. Am. Chem. Soc.* **1995**, *117*, 8576–8581.
[390] K. C. Kong, C. H. Cheng, *J. Am. Chem. Soc.* **1991**, *113*, 6313–6315.
[391] D. F. O'Keefe, M. C. Dannock, S. M. Marcuccio, *Tetrahedron Lett.* **1992**, *33*, 6679–6680.
[392] F. E. Goodson, T. I. Wallow, B. M. Novak, *J. Am. Chem. Soc.* **1997**, *119*, 12441–12453.
[393] F. E. Goodson, T. I. Wallow, B. M. Novak, *Macromolecules* **1998**, *31*, 2047–2056.
[394] V. V. Grushin, *Organometallics* **2000**, *19*, 1888–1900.
[395] M. H. Kowalski, R. J. Hinkle, P. J. Stang, *J. Org. Chem.* **1989**, *54*, 2783–2784.
[396] C.-C. Huang, J.-P. Duan, M.-Y. Wu, F.-L. Liao, S.-L. Wang, C.-H. Cheng, *Organometallics* **1998**, *17*, 676–682.
[397] A. L. Casado, P. Espinet, *J. Am. Chem. Soc.* **1998**, *120*, 8978–8985.
[398] R. A. Widenhoefer, H. A. Zhong, S. L. Buchwald, *J. Am. Chem. Soc.* **1997**, *119*, 6787–6795.
[399] H. G. Kuivila, J. F. Reuwer, J. A. Mangravite, *J. Am. Chem. Soc.* **1964**, *86*, 2666–2670.
[400] H. G. Kuivila, K. V. Nahabedian, *J. Am. Chem. Soc.* **1961**, *83*, 2164–2166.
[401] H. G. Kuivila, K. V. Nahabedian, *J. Am. Chem. Soc.* **1961**, *83*, 2159–2163.
[402] K. V. Nahabedian, H. G. Kuivila, *J. Am. Chem. Soc.* **1961**, *83*, 2167–2174.
[403] H. C. Brown, G. A. Molander, *J. Org. Chem.* **1986**, *51*, 4512–4514.
[404] A. Bouillon, J.-C. Lancelot, J. Sopkova de Oliveira Santos, V. Collot, P. R. Bovy, S. Rault, *Tetrahedron* **2003**, *59*, 10043–10049.
[405] H. Matondo, M. Baboulène, I. Rico-Lattes, *Appl. Organomet. Chem.* **2003**, *17*, 239–243.
[406] H. Matondo, S. Souirti, M. Baboulène, *Synth. Commun.* **2003**, *33*, 795–800.
[407] K. L. Billingsley, S. L. Buchwald, *Angew. Chem.* **2008**, *120*, 4773–4776.
[408] G. R. Dick, D. M. Knapp, E. P. Gillis, M. D. Burke, *Org. Lett.* **2010**, *12*, 2314–2317.
[409] G. R. Dick, E. M. Woerly, M. D. Burke, *Angew. Chem. Int. Ed.* **2012**, *51*, 2667–2672.
[410] P. B. Hodgson, F. H. Salingue, *Tetrahedron Lett.* **2004**, *45*, 685–687.
[411] Y. Yamamoto, M. Takizawa, X.-Q. Yu, N. Miyaura, *Angew. Chem. Int. Ed.* **2008**, *47*, 928–931.
[412] C.-J. Yao, L.-Z. Sui, H.-Y. Xie, W.-J. Xiao, Y.-W. Zhong, J. Yao, *Inorg. Chem.* **2010**, *49*, 8347–8350.
[413] D. M. Knapp, E. P. Gillis, M. D. Burke, *J. Am. Chem. Soc.* **2009**, *131*, 6961–6963.
[414] B. T. O'Neill, D. Yohannes, M. W. Bundesmann, E. P. Arnold, *Org. Lett.* **2000**, *2*, 4201–4204.
[415] G. D. Harzmann, M. Neuburger, M. Mayor, *Eur. J. Inorg. Chem.* **2013**, *2013*, 3334–3347.
[416] Y.-Q. Fang, G. S. Hanan, *Synlett* **2003**, 0852–0854.
[417] C. R. Woods, M. Benaglia, S. Toyota, K. Hardcastle, J. S. Siegel, *Angew. Chem. Int. Ed.* **2001**, *40*, 749–751.
[418] T.-T.-T. Nguyen, D. Türp, D. Wang, B. Nölscher, F. Laquai, K. Müllen, *J. Am. Chem. Soc.* **2011**, *133*, 11194–11204.
[419] M. Kawamoto, T. Aoki, T. Wada, *Chem. Commun.* **2007**, 930–932.
[420] E. Wagner-Wysiecka, T. Rzymowski, M. S. Fonari, R. Kulmaczewski, E. Luboch, *Tetrahedron* **2011**, *67*, 1862–1872.
[421] S. Malek-Ahmadi, A. Abdolmaleki, *Chin. Chem. Lett.* **2011**, *22*, 439–442.
[422] K. Tanaka, S. Fukuoka, H. Miyanishi, H. Takahashi, *Tetrahedron Lett.* **2010**, *51*, 2693–2696.
[423] H.-S. Tang, N. Zhu, V. W.-W. Yam, *Organometallics* **2007**, *26*, 22–25.
[424] Y.-T. Shen, L. Guan, X.-Y. Zhu, Q.-D. Zeng, C. Wang, *J. Am. Chem. Soc.* **2009**, *131*, 6174–6180.
[425] S. Shinkai, T. Minami, Y. Kusano, O. Manabe, *J. Am. Chem. Soc.* **1983**, *105*, 1851–1856.
[426] M. Yamamura, Y. Okazaki, T. Nabeshima, *Chem. Commun.* **2012**, *48*, 5724–5726.

[427] R. Reuter, H. A. Wegner, *Chem. Commun.* **2012**, *49*, 146–148.
[428] A. Khan, S. Hecht, *Chem. – Eur. J.* **2006**, *12*, 4764–4774.
[429] K. Kinbara, T. Muraoka, T. Aida, *Org. Biomol. Chem.* **2008**, *6*, 1871–1876.
[430] M. C. Basheer, Y. Oka, M. Mathews, N. Tamaoki, *Chem. – Eur. J.* **2010**, *16*, 3489–3496.
[431] E. Merino, M. Ribagorda, *Beilstein J. Org. Chem.* **2012**, *8*, 1071–1090.
[432] M. Mathews, N. Tamaoki, *J. Am. Chem. Soc.* **2008**, *130*, 11409–11416.
[433] T. Muraoka, K. Kinbara, T. Aida, *Nature* **2006**, *440*, 512–515.
[434] T. Muraoka, K. Kinbara, A. Wakamiya, S. Yamaguchi, T. Aida, *Chem. – Eur. J.* **2007**, *13*, 1724–1730.
[435] Y. Norikane, N. Tamaoki, *Org. Lett.* **2004**, *6*, 2595–2598.
[436] E. Karp, C. S. Pecinovsky, M. J. McNevin, D. L. Gin, D. K. Schwartz, *Langmuir* **2007**, *23*, 7923–7927.
[437] E. Mitscherlich, *Ann. Pharm.* **1834**, *12*, 311–314.
[438] G. P. Moss, P. A. S. Smith, D. Tavernier, *Pure Appl. Chem.* **1995**, *67*, DOI 10.1351/pac199567081307.
[439] G. S. Hartley, *Nature* **1937**, *140*, 281.
[440] J. M. Robertson, *J. Chem. Soc. Resumed* **1939**, 232–236.
[441] H. Zollinger, *Color Chemistry: Syntheses, Properties, and Applications of Organic Dyes and Pigments*, Wiley, **2003**.
[442] K. Hunger, *Industrial Dyes: Chemistry, Properties, Applications*, John Wiley & Sons, **2007**.
[443] E. Merino, *Chem. Soc. Rev.* **2011**, *40*, 3835–3853.
[444] K. Hunger, P. Mischke, W. Rieper, in *Ullmanns Encycl. Ind. Chem.*, Wiley-VCH Verlag GmbH & Co. KGaA, **2000**.
[445] K. Haghbeen, E. W. Tan, *J. Org. Chem.* **1998**, *63*, 4503–4505.
[446] J. L. Hartwell, L. F. Fieser, *Org. Synth.* **1936**, *16*, 12.
[447] H. T. Clarke, W. R. Kirner, *Org. Synth.* **1922**, *2*, 47.
[448] E. Haselbach, *Helv. Chim. Acta* **1970**, *53*, 1526–1543.
[449] W. A. Velema, M. van der Toorn, W. Szymanski, B. L. Feringa, *J. Med. Chem.* **2013**, *56*, 4456–4464.
[450] M. H. Davey, V. Y. Lee, R. D. Miller, T. J. Marks, *J. Org. Chem.* **1999**, *64*, 4976–4979.
[451] O. Wallach, L. Belli, *Berichte Dtsch. Chem. Ges.* **1880**, *13*, 525–527.
[452] Z. Wang, in *Compr. Org. Name React. Reag.*, John Wiley & Sons, Inc., **2010**.
[453] E. Buncel, *Acc. Chem. Res.* **1975**, *8*, 132–139.
[454] I. Shimao, S. Oae, *Bull. Chem. Soc. Jpn.* **1983**, *56*, 643–644.
[455] L. Gattermann, H. Rüdt, *Berichte Dtsch. Chem. Ges.* **1894**, *27*, 2293–2297.
[456] M. Müri, K. C. Schuermann, L. De Cola, M. Mayor, *Eur. J. Org. Chem.* **2009**, *2009*, 2562–2575.
[457] N. Tamaoki, K. Ogata, K. Koseki, T. Yamaoka, *Tetrahedron* **1990**, *46*, 5931–5942.
[458] R. O. Hutchins, D. W. Lamson, L. Rua, C. Milewski, B. Maryanoff, *J. Org. Chem.* **1971**, *36*, 803–806.
[459] H. E. Bigelow, D. B. Robinson, *Org. Synth.* **1942**, *22*, 28.
[460] W. Wei, T. Tomohiro, M. Kodaka, H. Okuno, *J. Org. Chem.* **2000**, *65*, 8979–8987.
[461] C. Karunakaran, P. N. Palanisamy, *J. Mol. Catal. Chem.* **2001**, *172*, 9–17.
[462] R. Reuter, H. A. Wegner, *Chem. – Eur. J.* **2011**, *17*, 2987–2995.
[463] B. Ortiz, P. Villanueva, F. Walls, *J. Org. Chem.* **1972**, *37*, 2748–2750.
[464] M. Hedayatullah, J. Pierre Dechatre, L. Denivelle, *Tetrahedron Lett.* **1975**, *16*, 2039–2042.
[465] C. F. Billera, T. B. Dunn, D. A. Barry, P. S. Engel, *J. Org. Chem.* **1998**, *63*, 9763–9768.
[466] D. A. Blackadder, C. Hinshelwood, *J. Chem. Soc. Resumed* **1957**, 2904–2906.
[467] J. A. Hyatt, *Tetrahedron Lett.* **1977**, *18*, 141–142.
[468] Y.-K. Lim, K.-S. Lee, C.-G. Cho, *Org. Lett.* **2003**, *5*, 979–982.
[469] H.-M. Kang, J.-W. Jung, C.-G. Cho, *J. Org. Chem.* **2007**, *72*, 679–682.
[470] G. H. Brown, *Photochromism*, Wiley-Interscience, **1971**.
[471] H. Rau, in *Photochem. Photophysics*, CRC Press, **1989**, pp. 119–142.
[472] G. S. Kumar, D. C. Neckers, *Chem. Rev.* **1989**, *89*, 1915–1925.
[473] A. A. Beharry, G. A. Woolley, *Chem. Soc. Rev.* **2011**, *40*, 4422–4437.

[474] F. P. Nicoletta, D. Cupelli, P. Formoso, G. De Filpo, V. Colella, A. Gugliuzza, *Membranes* **2012**, *2*, 134–197.
[475] H. Rau, *Angew. Chem. Int. Ed. Engl.* **1973**, *12*, 224–235.
[476] E. Müller, *Neuere Anschauungen Der Organischen Chemie - Organische Chemie Für Fortgeschrittene*, **n.d.**
[477] G. S. Hartley, *J. Chem. Soc. Resumed* **1938**, 633–642.
[478] M. Tsuda, K. Kuratani, *Bull. Chem. Soc. Jpn.* **1964**, *37*, 1284–1288.
[479] H. Rau, in *Photochromism Mol. Syst.*, Elsevier, Amsterdam, **1990**, pp. 165–193.
[480] Z. Sekkat, W. Knoll, *Photoreactive Organic Thin Films*, Academic Press, **2002**.
[481] B. Marcandalli, L. P.-D. Liddo, C. D. Fede, I. R. Bellobono, *J. Chem. Soc. Perkin Trans. 2* **1984**, 589–593.
[482] H. M. D. Bandara, S. C. Burdette, *Chem. Soc. Rev.* **2012**, *41*, 1809–1825.
[483] H. Kessler, D. Leibfritz, *Tetrahedron Lett.* **1970**, *11*, 1423–1426.
[484] N. Nishimura, T. Tanaka, M. Asano, Y. Sueishi, *J. Chem. Soc. Perkin Trans. 2* **1986**, 1839–1845.
[485] D. Gegiou, K. A. Muszkat, E. Fischer, *J. Am. Chem. Soc.* **1968**, *90*, 12–18.
[486] T. Asano, T. Yano, T. Okada, *J. Am. Chem. Soc.* **1982**, *104*, 4900–4904.
[487] S. Malkin, E. Fischer, *J. Phys. Chem.* **1962**, *66*, 2482–2486.
[488] C.-W. Chang, Y.-C. Lu, T.-T. Wang, E. W.-G. Diau, *J. Am. Chem. Soc.* **2004**, *126*, 10109–10118.
[489] N. Tamai, H. Miyasaka, *Chem. Rev.* **2000**, *100*, 1875–1890.
[490] H. Rau, E. Lueddecke, *J. Am. Chem. Soc.* **1982**, *104*, 1616–1620.
[491] C. R. Crecca, A. E. Roitberg, *J. Phys. Chem. A* **2006**, *110*, 8188–8203.
[492] J. L. Magee, W. Shand, H. Eyring, *J. Am. Chem. Soc.* **1941**, *63*, 677–688.
[493] D. Y. Curtin, E. J. Grubbs, C. G. McCarty, *J. Am. Chem. Soc.* **1966**, *88*, 2775–2786.
[494] E. Wei-Guang Diau, *J. Phys. Chem. A* **2004**, *108*, 950–956.
[495] J. Griffiths, *Chem. Soc. Rev.* **1972**, *1*, 481–493.
[496] D. Röttger, H. Rau, *J. Photochem. Photobiol. Chem.* **1996**, *101*, 205–214.
[497] Y. Norikane, R. Katoh, N. Tamaoki, *Chem. Commun.* **2008**, 1898–1900.
[498] S. A. Nagamani, Y. Norikane, N. Tamaoki, *J. Org. Chem.* **2005**, *70*, 9304–9313.
[499] K. Ziegler, H. Eberle, H. Ohlinger, *Justus Liebigs Ann. Chem.* **1933**, *504*, 94–130.
[500] J.-F. Ayme, J. E. Beves, D. A. Leigh, R. T. McBurney, K. Rissanen, D. Schultz, *Nat. Chem.* **2012**, *4*, 15–20.
[501] J.-F. Ayme, J. E. Beves, D. A. Leigh, R. T. McBurney, K. Rissanen, D. Schultz, *J. Am. Chem. Soc.* **2012**, *134*, 9488–9497.
[502] P. E. Barran, H. L. Cole, S. M. Goldup, D. A. Leigh, P. R. McGonigal, M. D. Symes, J. Wu, M. Zengerle, *Angew. Chem. Int. Ed.* **2011**, *50*, 12280–12284.
[503] J. E. Beves, C. J. Campbell, D. A. Leigh, R. G. Pritchard, *Angew. Chem. Int. Ed.* **2013**, *52*, 6464–6467.
[504] J. A. Bravo, F. M. Raymo, J. F. Stoddart, A. J. P. White, D. J. Williams, *Eur. J. Org. Chem.* **1998**, *1998*, 2565–2571.
[505] K. S. Chichak, S. J. Cantrill, A. R. Pease, S.-H. Chiu, G. W. V. Cave, J. L. Atwood, J. F. Stoddart, *Science* **2004**, *304*, 1308–1312.
[506] W. R. Dichtel, O. Š. Miljanić, J. M. Spruell, J. R. Heath, J. F. Stoddart, *J. Am. Chem. Soc.* **2006**, *128*, 10388–10390.
[507] A. R. Williams, B. H. Northrop, T. Chang, J. F. Stoddart, A. J. P. White, D. J. Williams, *Angew. Chem. Int. Ed.* **2006**, *45*, 6665–6669.
[508] M. C. O'Sullivan, J. K. Sprafke, D. V. Kondratuk, C. Rinfray, T. D. W. Claridge, A. Saywell, M. O. Blunt, J. N. O'Shea, P. H. Beton, M. Malfois, et al., *Nature* **2011**, *469*, 72–75.
[509] J. K. Sprafke, D. V. Kondratuk, M. Wykes, A. L. Thompson, M. Hoffmann, R. Drevinskas, W.-H. Chen, C. K. Yong, J. Kärnbratt, J. E. Bullock, et al., *J. Am. Chem. Soc.* **2011**, *133*, 17262–17273.
[510] P. Liu, P. Neuhaus, D. V. Kondratuk, T. S. Balaban, H. L. Anderson, *Angew. Chem. Int. Ed.* **2014**, *53*, 7770–7773.
[511] M. J. Langton, J. D. Matichak, A. L. Thompson, H. L. Anderson, *Chem. Sci.* **2011**, *2*, 1897–1901.

[512] D. V. Kondratuk, L. M. A. Perdigao, M. C. O'Sullivan, S. Svatek, G. Smith, J. N. O'Shea, P. H. Beton, H. L. Anderson, *Angew. Chem. Int. Ed.* **2012**, *51*, 6696–6699.
[513] D. V. Kondratuk, J. K. Sprafke, M. C. O'Sullivan, L. M. A. Perdigao, A. Saywell, M. Malfois, J. N. O'Shea, P. H. Beton, A. L. Thompson, H. L. Anderson, *Chem. – Eur. J.* **2014**, *20*, 12826–12834.
[514] D. Gräf, H. Nitsch, D. Ufermann, G. Sawitzki, H. Patzelt, H. Rau, *Angew. Chem. Int. Ed. Engl.* **1982**, *21*, 373–374.
[515] H.-W. Losensky, H. Spelthann, A. Ehlen, F. Vögtle, J. Bargon, *Angew. Chem.* **1988**, *100*, 1225–1227.
[516] F. Vögtle, W. M. Müller, U. Müller, M. Bauer, K. Rissanen, *Angew. Chem.* **1993**, *105*, 1356–1358.
[517] Y. Norikane, K. Kitamoto, N. Tamaoki, *J. Org. Chem.* **2003**, *68*, 8291–8304.
[518] Y. Norikane, K. Kitamoto, N. Tamaoki, *Org. Lett.* **2002**, *4*, 3907–3910.
[519] Y. Norikane, N. Tamaoki, *Eur. J. Org. Chem.* **2006**, *2006*, 1296–1302.
[520] N. Tamaoki, K. Koseki, T. Yamaoka, *Angew. Chem. Int. Ed. Engl.* **1990**, *29*, 105–106.
[521] N. Tamaoki, K. Koseki, T. Yamaoka, *Tetrahedron Lett.* **1990**, *31*, 3309–3312.
[522] E. Tauer, R. Machinek, *Liebigs Ann.* **1996**, *1996*, 1213–1216.
[523] T. Muraoka, K. Kinbara, Y. Kobayashi, T. Aida, *J. Am. Chem. Soc.* **2003**, *125*, 5612–5613.
[524] T. Muraoka, K. Kinbara, T. Aida, *Chem. Commun.* **2007**, 1441–1443.
[525] C. S. Pecinovsky, E. S. Hatakeyama, D. L. Gin, *Adv. Mater.* **2008**, *20*, 174–178.
[526] B. L. Feringa, W. R. Browne, *Molecular Switches*, John Wiley & Sons, **2011**.
[527] S. Grunder, R. Huber, V. Horhoiu, M. T. González, C. Schönenberger, M. Calame, M. Mayor, *J. Org. Chem.* **2007**, *72*, 8337–8344.
[528] S. Grunder, R. Huber, S. Wu, C. Schönenberger, M. Calame, M. Mayor, *Eur. J. Org. Chem.* **2010**, *2010*, 833–845.
[529] J. Sauer, D. K. Heldmann, G. R. Pabst, *Eur. J. Org. Chem.* **1999**, *1999*, 313–321.
[530] W. Baker, R. F. Curtis, M. G. Edwards, *J. Chem. Soc. Resumed* **1951**, 83–87.
[531] B. X. Colasson, C. Dietrich-Buchecker, J.-P. Sauvage, *Synlett* **2002**, *2002*, 0271–0272.
[532] G. R. Newkome, J. M. Roper, *J. Organomet. Chem.* **1980**, *186*, 147–153.
[533] A. S. Guram, A. O. King, J. G. Allen, X. Wang, L. B. Schenkel, J. Chan, E. E. Bunel, M. M. Faul, R. D. Larsen, M. J. Martinelli, et al., *Org. Lett.* **2006**, *8*, 1787–1789.
[534] A. Błaszczyk, M. Elbing, M. Mayor, *Org. Biomol. Chem.* **2004**, *2*, 2722–2724.
[535] J. M. Tour, L. Jones, D. L. Pearson, J. J. S. Lamba, T. P. Burgin, G. M. Whitesides, D. L. Allara, A. N. Parikh, S. Atre, *J. Am. Chem. Soc.* **1995**, *117*, 9529–9534.
[536] N. Crivillers, E. Orgiu, F. Reinders, M. Mayor, P. Samorì, *Adv. Mater.* **2011**, *23*, 1447–1452.
[537] C. J. Yu, Y. Chong, J. F. Kayyem, M. Gozin, *J Org Chem* **1999**, *64*, 2070–2079.
[538] D. Gelman, S. L. Buchwald, *Angew. Chem. Int. Ed.* **2003**, *42*, 5993–5996.
[539] G. R. Newkome, T. J. Cho, C. N. Moorefield, R. Cush, P. S. Russo, L. A. Godínez, M. J. Saunders, P. Mohapatra, *Chem. – Eur. J.* **2002**, *8*, 2946–2954.
[540] K. Heinze, K. Hempel, S. Tschierlei, M. Schmitt, J. Popp, S. Rau, *Eur. J. Inorg. Chem.* **2009**, *2009*, 3119–3126.
[541] M. Maestri, N. Armaroli, V. Balzani, E. C. Constable, A. M. W. C. Thompson, *Inorg. Chem.* **1995**, *34*, 2759–2767.
[542] R. Siebert, A. Winter, B. Dietzek, U. S. Schubert, J. Popp, *Macromol. Rapid Commun.* **2010**, *31*, 883–888.
[543] J. M. Rao, D. J. Macero, M. C. Hughes, *Inorganica Chim. Acta* **1980**, *41*, 221–226.
[544] P. S. Braterman, J. I. Song, R. D. Peacock, *Inorg. Chem.* **1992**, *31*, 555–559.
[545] U. S. Schubert, A. Winter, G. R. Newkome, *Terpyridine-Based Materials*, Wiley-VCH, Weinheim, **2011**.
[546] N. Kaveevivitchai, L. Kohler, R. Zong, M. El Ojaimi, N. Mehta, R. P. Thummel, *Inorg. Chem.* **2013**, *52*, 10615–10622.
[547] J. P. Sauvage, J. P. Collin, J. C. Chambron, S. Guillerez, C. Coudret, V. Balzani, F. Barigelletti, L. De Cola, L. Flamigni, *Chem. Rev.* **1994**, *94*, 993–1019.
[548] D. Aravena, E. Ruiz, *J. Am. Chem. Soc.* **2012**, *134*, 777–779.
[549] C. Hamann, R. Woltmann, I.-P. Hong, N. Hauptmann, S. Karan, R. Berndt, *Rev. Sci. Instrum.* **2011**, *82*, 033903.

[550] J. V. Barth, H. Brune, G. Ertl, R. J. Behm, *Phys. Rev. B* **1990**, *42*, 9307–9318.
[551] F. Reinert, G. Nicolay, *Appl. Phys. A* **2004**, *78*, 817–821.
[552] U. Fano, *Phys. Rev.* **1961**, *124*, 1866–1878.
[553] V. Meded, A. Bagrets, K. Fink, R. Chandrasekar, M. Ruben, F. Evers, A. Bernand-Mantel, J. S. Seldenthuis, A. Beukman, H. S. J. van der Zant, *Phys. Rev. B* **2011**, *83*, 245415.
[554] G. A. Holloway, H. M. Hügel, M. A. Rizzacasa, *J. Org. Chem.* **2003**, *68*, 2200–2204.
[555] S.-W. Kang, C. M. Gothard, S. Maitra, Atia-tul-Wahab, J. S. Nowick, *J. Am. Chem. Soc.* **2007**, *129*, 1486–1487.
[556] D. M. Junge, D. V. McGrath, *Chem. Commun.* **1997**, 857–858.
[557] E. C. Constable, G. Baum, E. Bill, R. Dyson, R. van Eldik, D. Fenske, S. Kaderli, D. Morris, A. Neubrand, M. Neuburger, et al., *Chem. – Eur. J.* **1999**, *5*, 498–508.
[558] R. R. Pal, M. Higuchi, D. G. Kurth, *Org. Lett.* **2009**, *11*, 3562–3565.
[559] F. S. Han, M. Higuchi, D. G. Kurth, *J. Am. Chem. Soc.* **2008**, *130*, 2073–2081.
[560] T. Fuchigami, T. Haradahira, N. Fujimoto, Y. Nojiri, T. Mukai, F. Yamamoto, T. Okauchi, J. Maeda, K. Suzuki, T. Suhara, et al., *Bioorg. Med. Chem.* **2009**, *17*, 5665–5675.
[561] T. Ishiyama, M. Murata, N. Miyaura, *J. Org. Chem.* **1995**, *60*, 7508–7510.
[562] Burgdorf, Beier, Gleitz, Charon, Cravo, *MERCK PATENT GMBH; WO2009046784 (A1); 2009*, **n.d.**, WO2009046784 (A1).
[563] T. L. Draper, T. R. Bailey, *Synlett* **1995**, *1995*, 157,158.
[564] M. C. Haberecht, J. M. Schnorr, E. V. Andreitchenko, C. G. C. Jr, M. Wagner, K. Müllen, *Angew. Chem. Int. Ed.* **2008**, *47*, 1662–1667.
[565] S. Grunder, R. Huber, S. Wu, C. Schönenberger, M. Calame, M. Mayor, *Eur. J. Org. Chem.* **2010**, *2010*, 833–845.
[566] L. Vandromme, H.-U. Reißig, S. Gröper, J. P. Rabe, *Eur. J. Org. Chem.* **2008**, *2008*, 2049–2055.

9 Appendix

9.1 Spectral Data of Target Structures

9.1.1 NMR

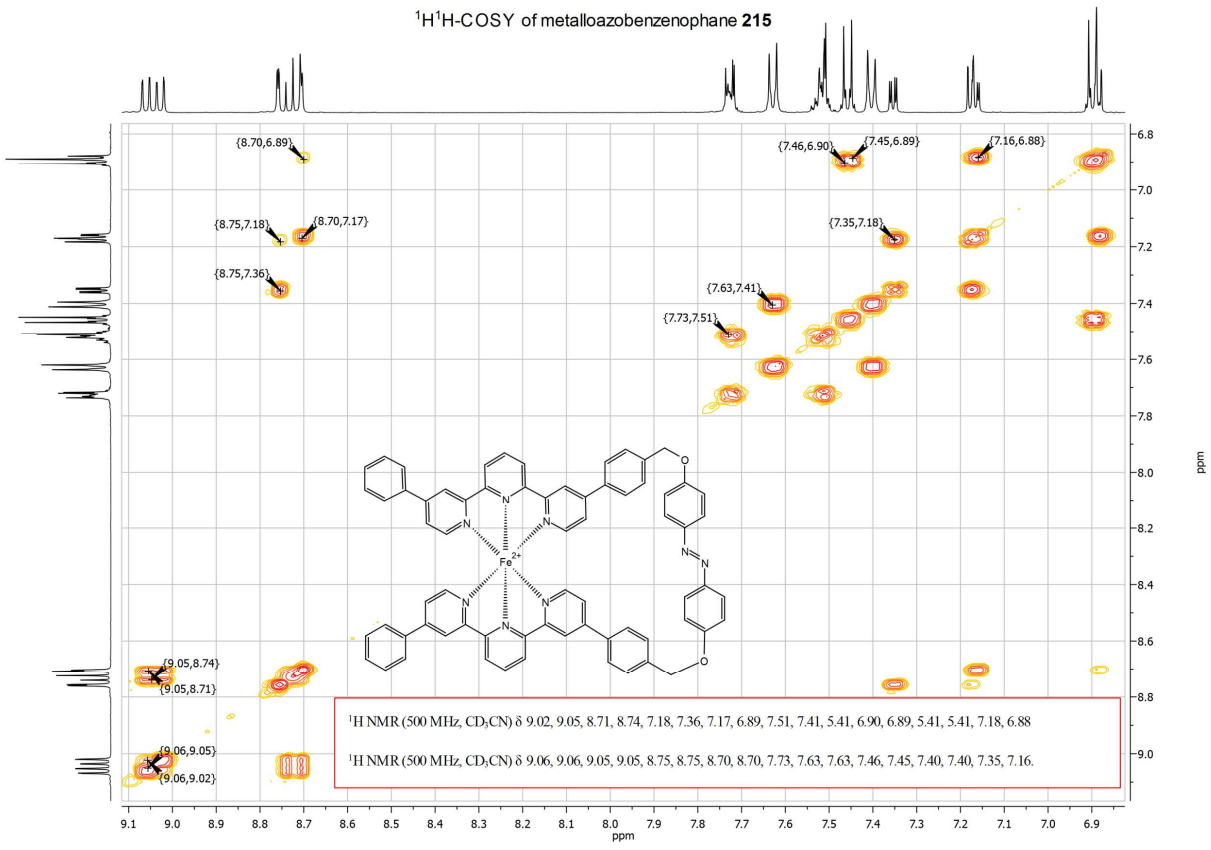

Figure 113: ^{1}H^{1}H-COSY NMR spectrum of metalloazobenzenophane **215**.

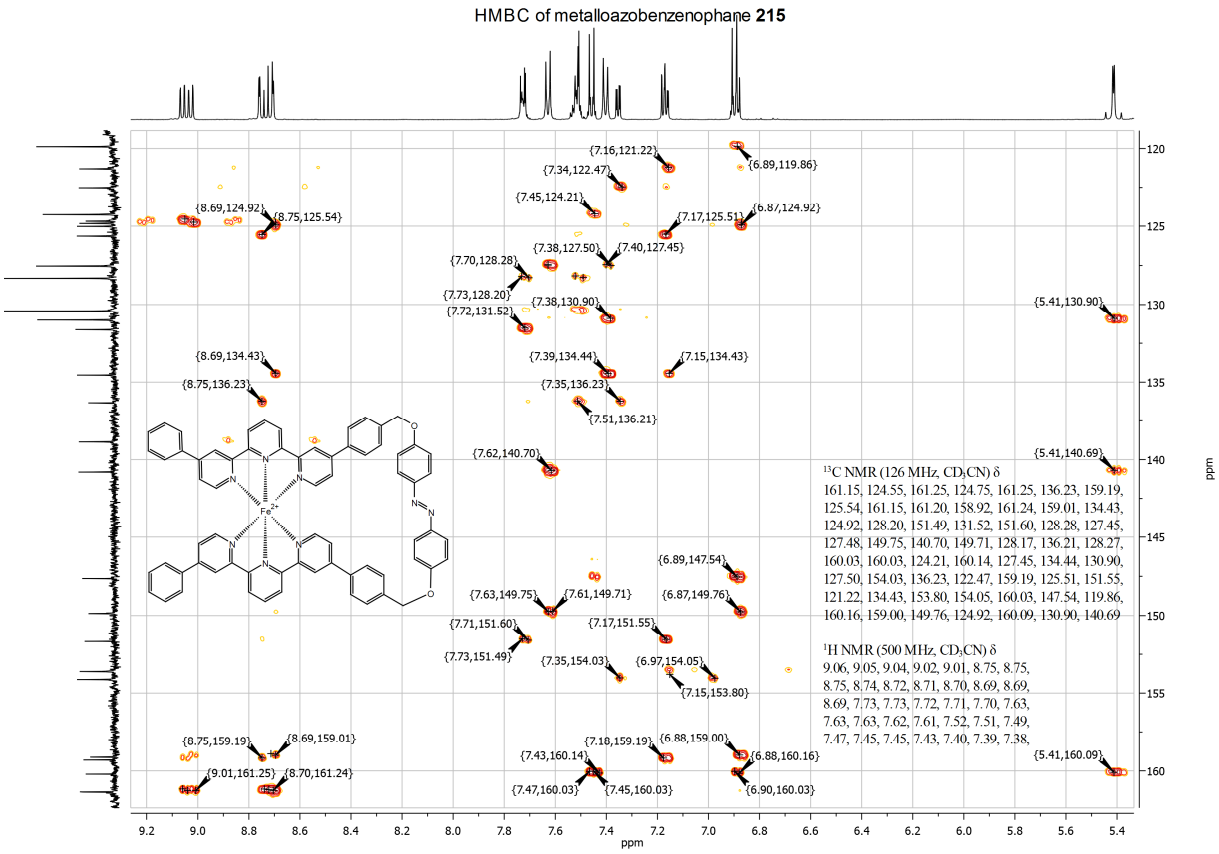

Figure 114: HMBC NMR spectrum of metalloazobenzenophane **215**.

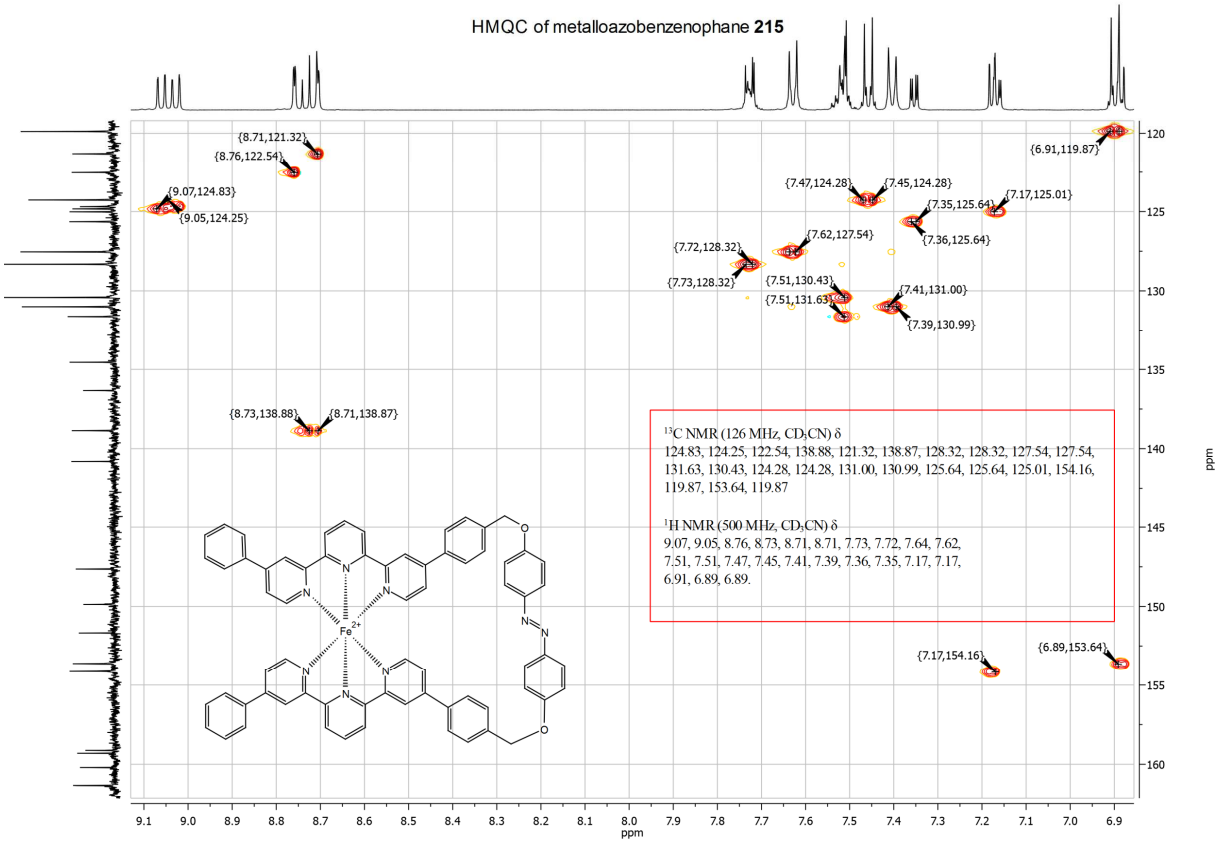

Figure 115: HMQC NMR spectrum of metalloazobenzenophane **215**.

9.1.2 HR-ESI-MS

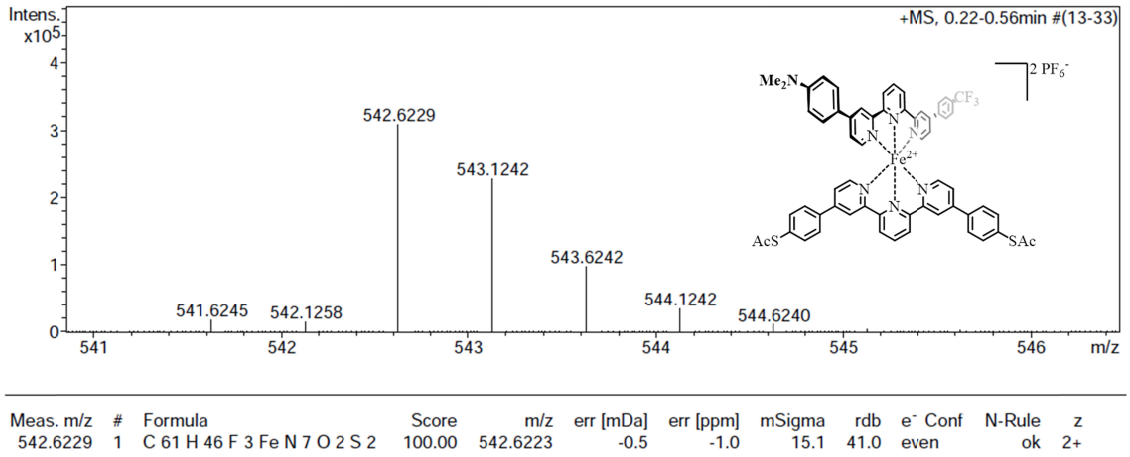

Meas. m/z	#	Formula	Score	m/z	err [mDa]	err [ppm]	mSigma	rdb	e⁻ Conf	N-Rule	z
542.6229	1	C 61 H 46 F 3 Fe N 7 O 2 S 2	100.00	542.6223	-0.5	-1.0	15.1	41.0	even	ok	2+

Figure 116: HR-ESI-MS of dipolar, heteroleptic Fe(II)-bis(tpy) target complex **112**.

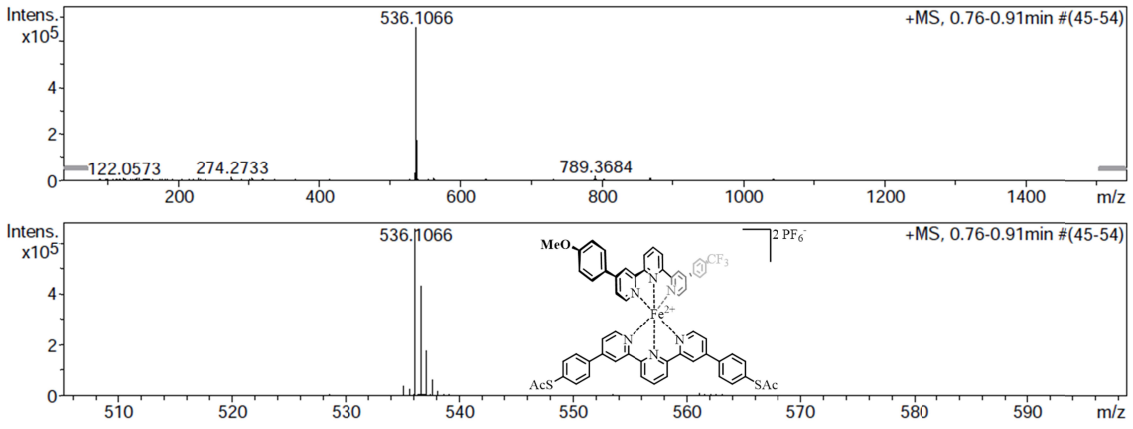

Meas. m/z	#	Formula	Score	m/z	err [mDa]	err [ppm]	mSigma	rdb	e⁻ Conf	N-Rule	z
536.1066	1	C 60 H 43 F 3 Fe N 6 O 3 S 2	100.00	536.1065	-0.1	-0.1	33.9	41.0	even	ok	2+

Figure 117: HR-ESI-MS of dipolar, heteroleptic Fe(II)-bis(tpy) target complex **113**.

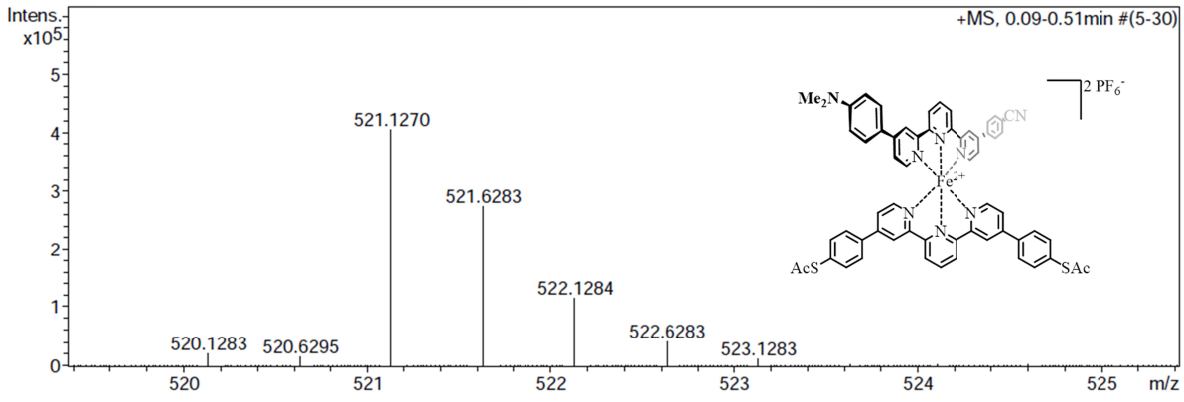

Meas. m/z	#	Formula	Score	m/z	err [mDa]	err [ppm]	mSigma	rdb	e⁻ Conf	N-Rule	z
521.1270	1	C 61 H 46 Fe N 8 O 2 S 2	100.00	521.1263	-0.7	-1.4	31.7	43.0	even	ok	2+

Figure 118: HR-ESI-MS of dipolar, heteroleptic Fe(II)-bis(tpy) target complex **114**.

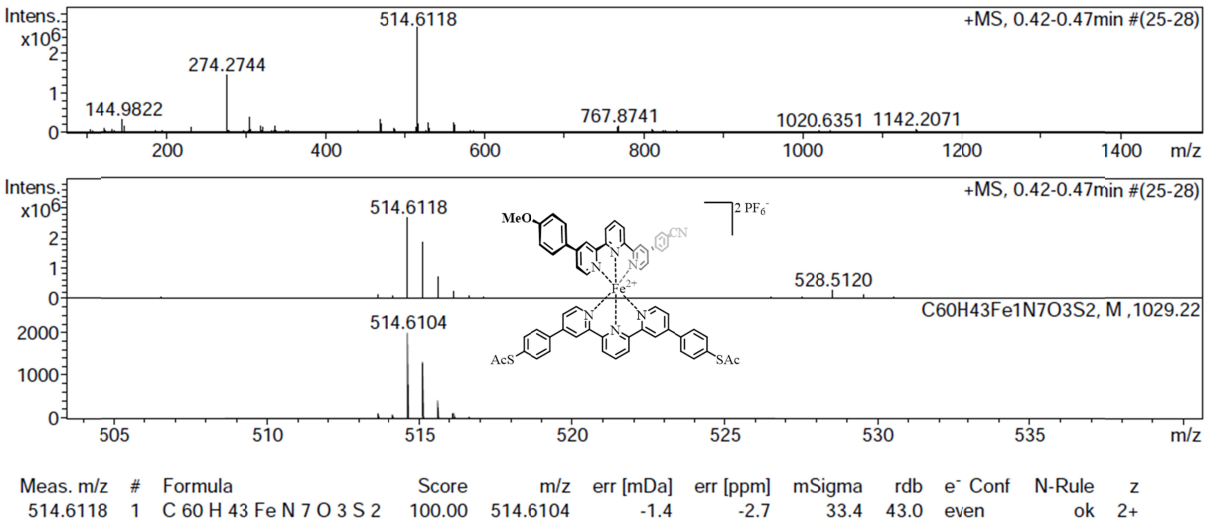

Meas. m/z	#	Formula	Score	m/z	err [mDa]	err [ppm]	mSigma	rdb	e⁻ Conf	N-Rule	z
514.6118	1	C 60 H 43 Fe N 7 O 3 S 2	100.00	514.6104	-1.4	-2.7	33.4	43.0	even	ok	2+

Figure 119: HR-ESI-MS of dipolar, heteroleptic Fe(II)-bis(tpy) target complex **115**.

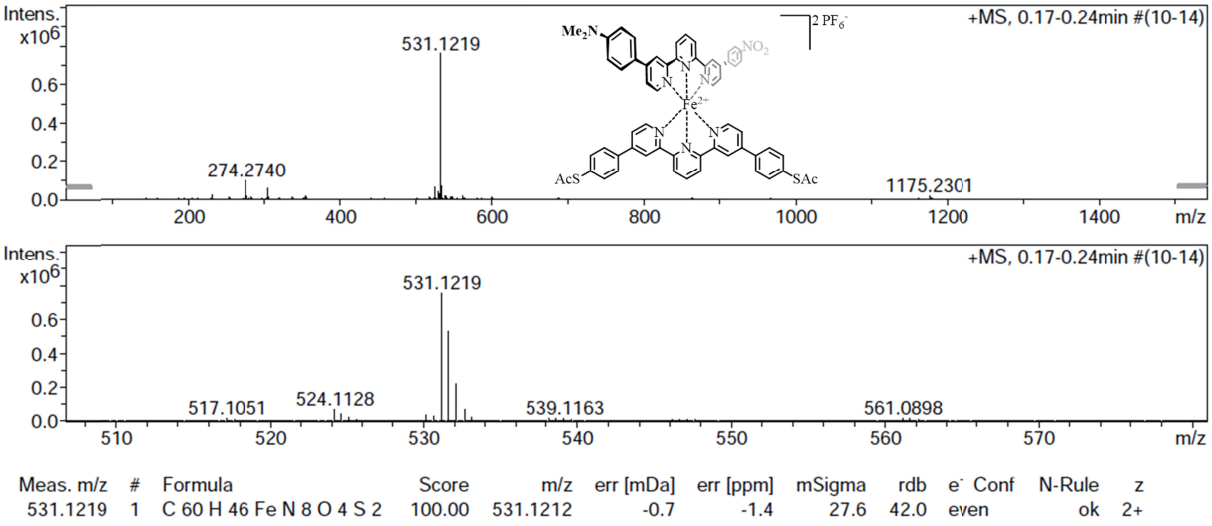

Meas. m/z	#	Formula	Score	m/z	err [mDa]	err [ppm]	mSigma	rdb	e⁻ Conf	N-Rule	z
531.1219	1	C 60 H 46 Fe N 8 O 4 S 2	100.00	531.1212	-0.7	-1.4	27.6	42.0	even	ok	2+

Figure 120: HR-ESI-MS of dipolar, heteroleptic Fe(II)-bis(tpy) target complex **116**.

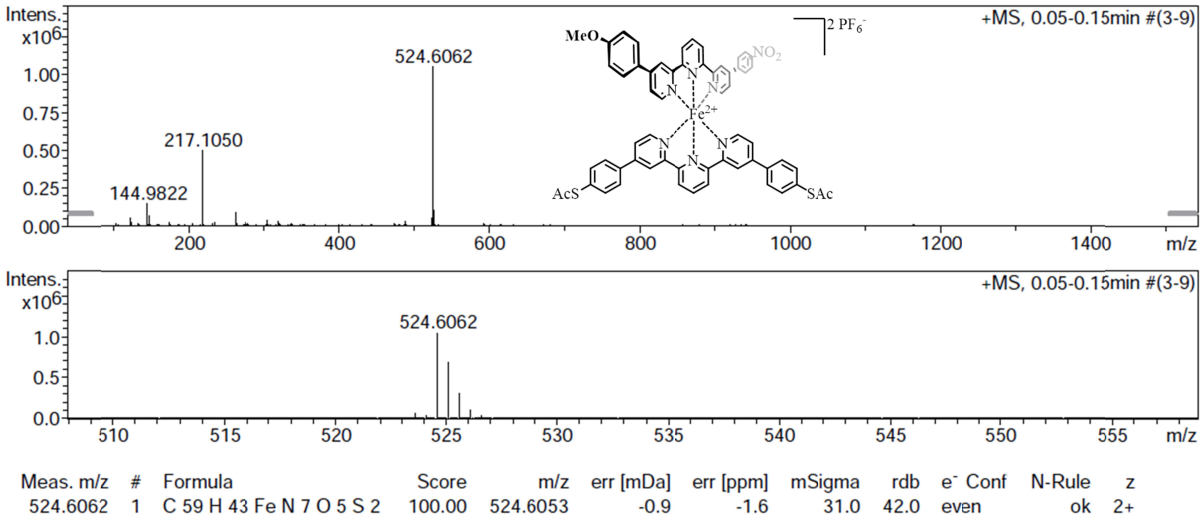

Meas. m/z	#	Formula	Score	m/z	err [mDa]	err [ppm]	mSigma	rdb	e⁻ Conf	N-Rule	z
524.6062	1	C 59 H 43 Fe N 7 O 5 S 2	100.00	524.6053	-0.9	-1.6	31.0	42.0	even	ok	2+

Figure 121: HR-ESI-MS of dipolar, heteroleptic Fe(II)-bis(tpy) target complex **117**.

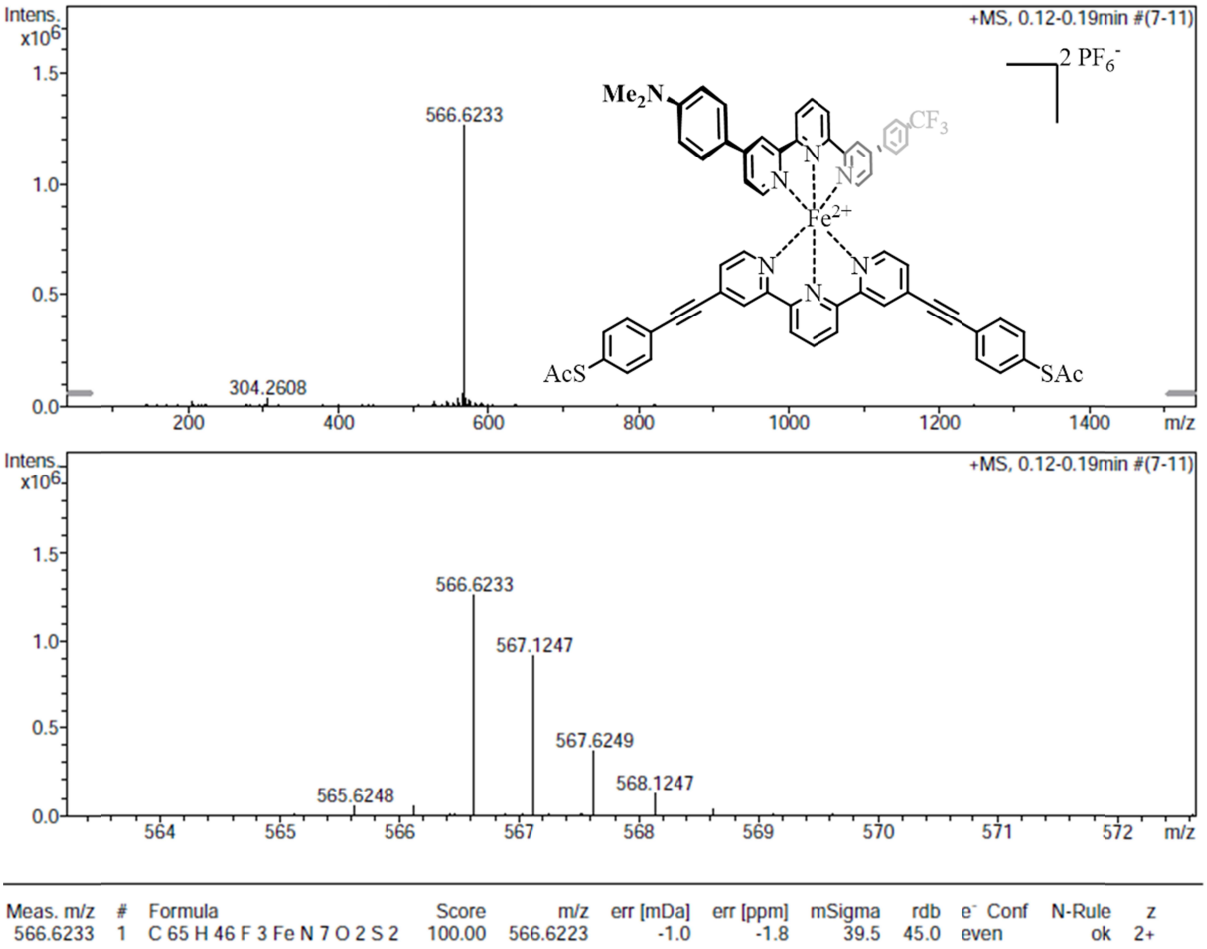

Meas. m/z	#	Formula	Score	m/z	err [mDa]	err [ppm]	mSigma	rdb	e⁻ Conf	N-Rule	z
566.6233	1	C 65 H 46 F 3 Fe N 7 O 2 S 2	100.00	566.6223	-1.0	-1.8	39.5	45.0	even	ok	2+

Figure 122: HR-ESI-MS of elongated, dipolar, heteroleptic Fe(II)-bis(tpy) target complex **118**.

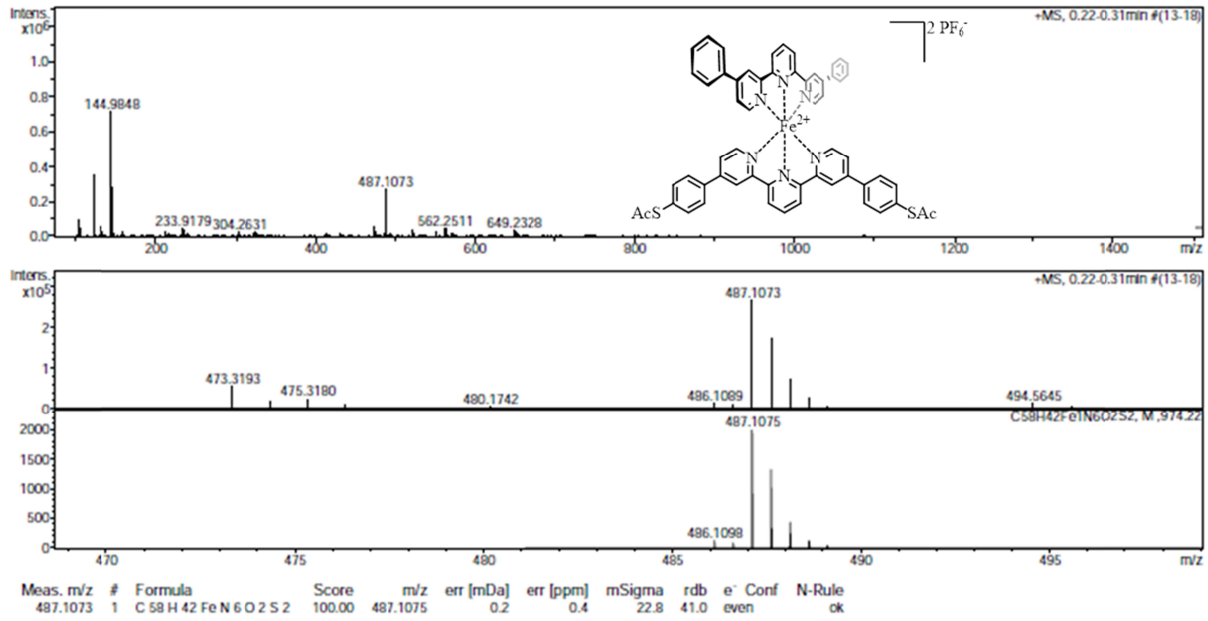

Meas. m/z	#	Formula	Score	m/z	err [mDa]	err [ppm]	mSigma	rdb	e⁻ Conf	N-Rule
487.1073	1	C 58 H 42 Fe N 6 O 2 S 2	100.00	487.1075	0.2	0.4	22.8	41.0	even	ok

Figure 123: HR-ESI-MS of non-dipolar, heteroleptic Fe(II)-bis(tpy) reference complex **121**.

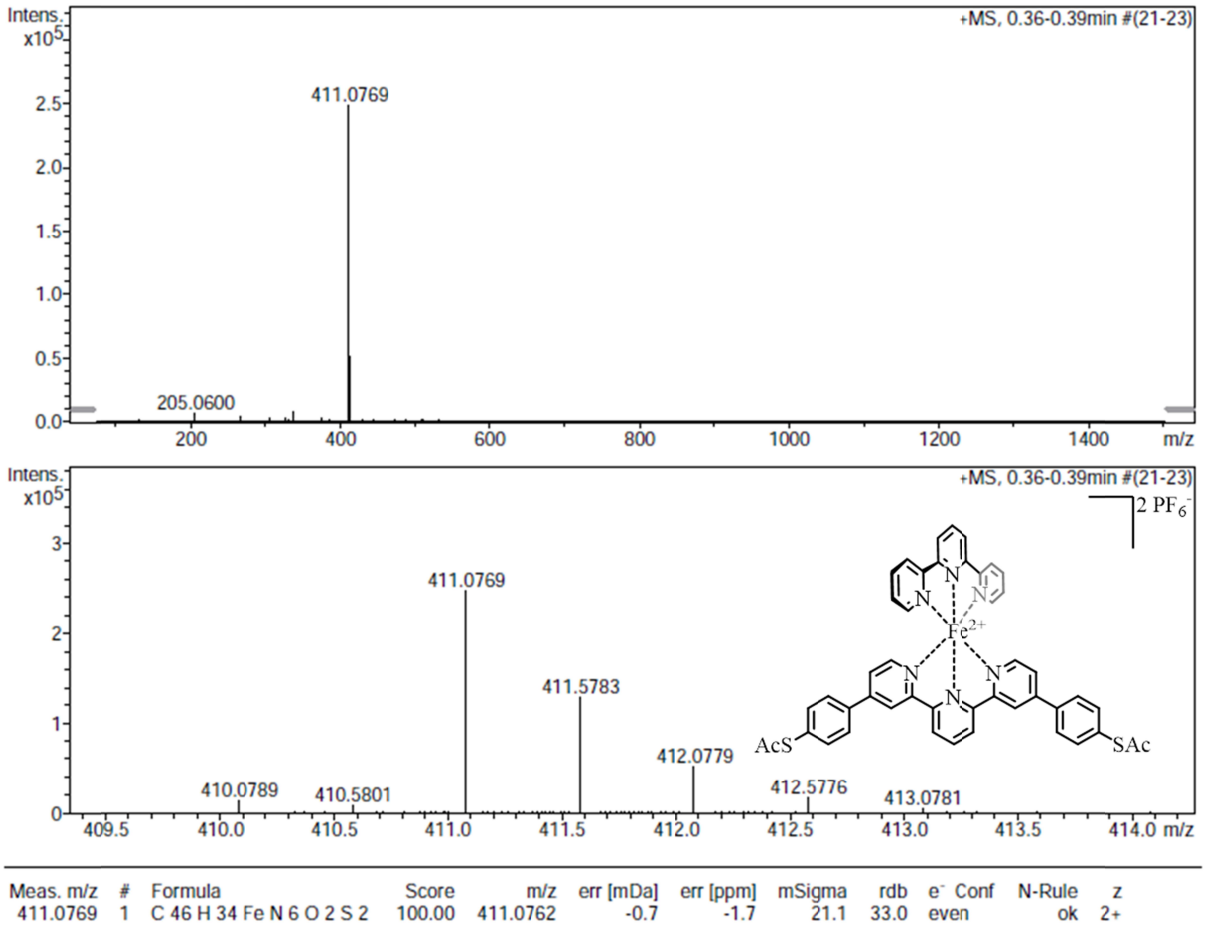

Figure 124: HR-ESI-MS of non-dipolar, heteroleptic Fe(II)-bis(tpy) reference complex **122**.

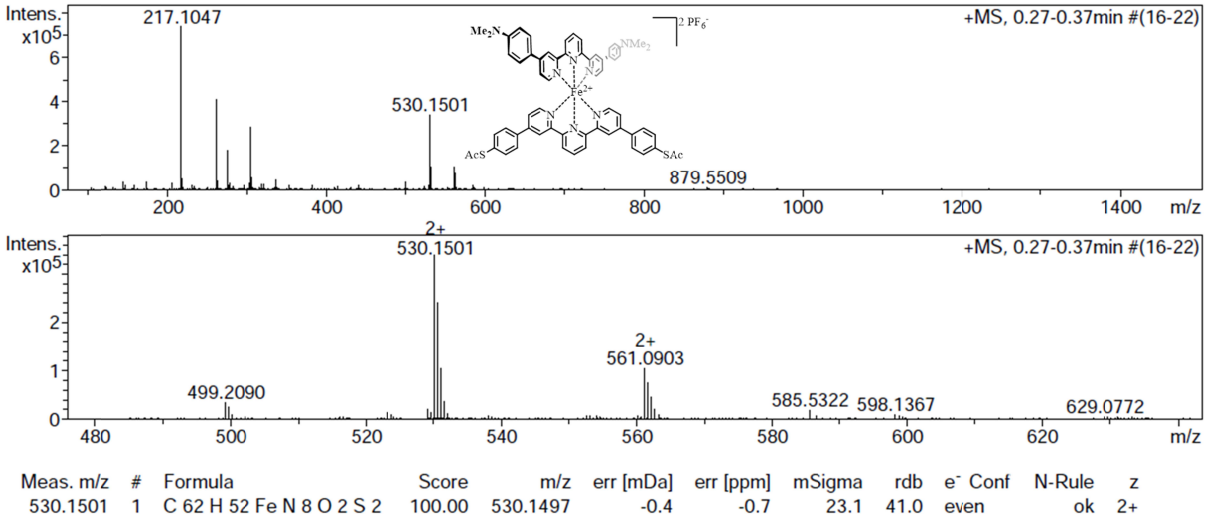

Figure 125: HR-ESI-MS of non-dipolar, heteroleptic Fe(II)-bis(tpy) reference complex **123**.

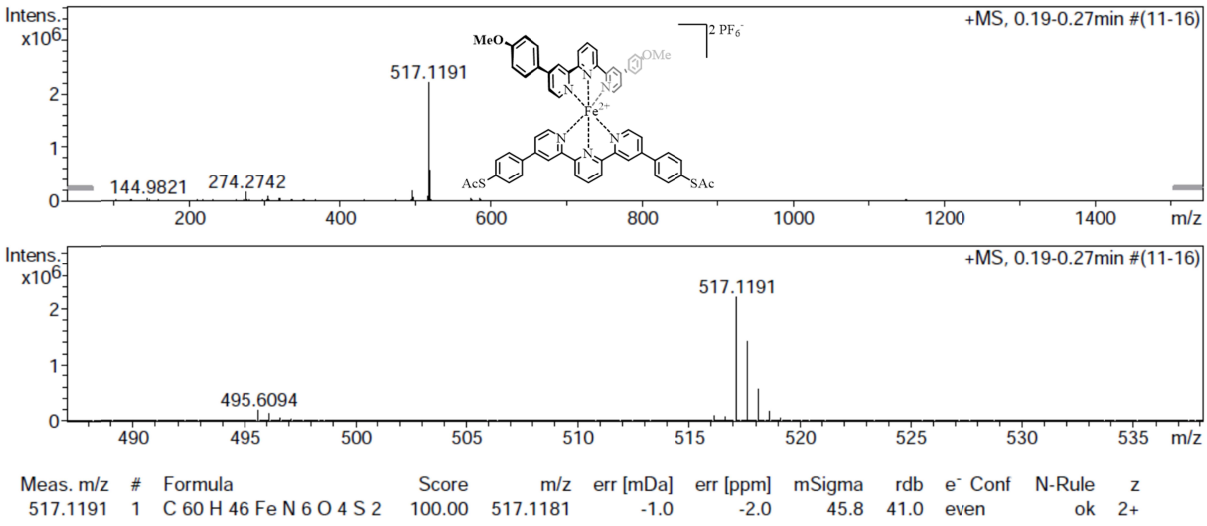

Meas. m/z	#	Formula	Score	m/z	err [mDa]	err [ppm]	mSigma	rdb	e⁻ Conf	N-Rule	z
517.1191	1	C 60 H 46 Fe N 6 O 4 S 2	100.00	517.1181	-1.0	-2.0	45.8	41.0	even	ok	2+

Figure 126: HR-ESI-MS of non-dipolar, heteroleptic Fe(II)-bis(tpy) reference complex **124**.

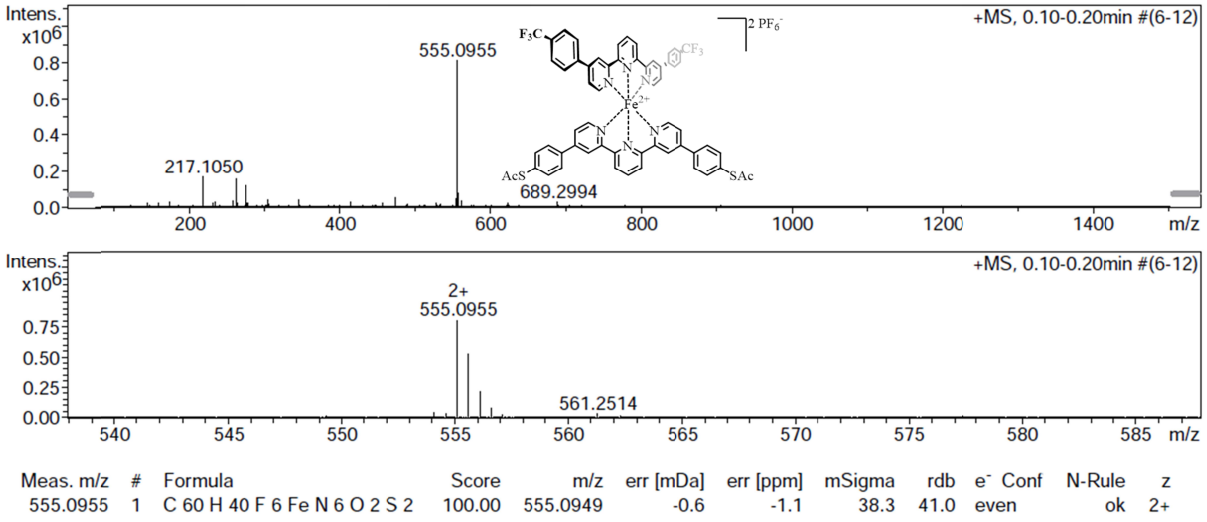

Meas. m/z	#	Formula	Score	m/z	err [mDa]	err [ppm]	mSigma	rdb	e⁻ Conf	N-Rule	z
555.0955	1	C 60 H 40 F 6 Fe N 6 O 2 S 2	100.00	555.0949	-0.6	-1.1	38.3	41.0	even	ok	2+

Figure 127: HR-ESI-MS of non-dipolar, heteroleptic Fe(II)-bis(tpy) reference complex **125**.

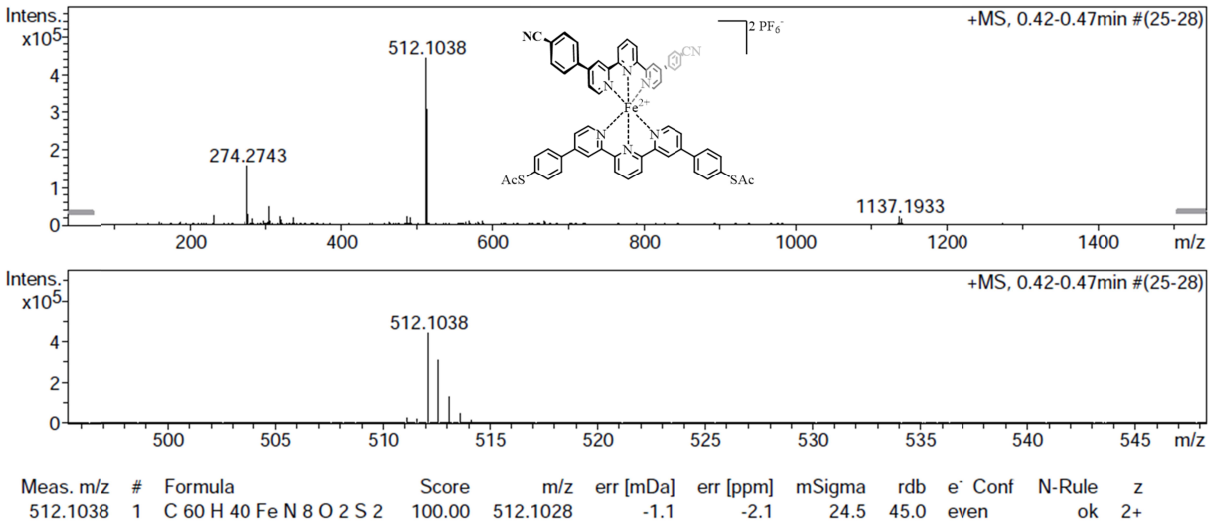

Meas. m/z	#	Formula	Score	m/z	err [mDa]	err [ppm]	mSigma	rdb	e⁻ Conf	N-Rule	z
512.1038	1	C 60 H 40 Fe N 8 O 2 S 2	100.00	512.1028	-1.1	-2.1	24.5	45.0	even	ok	2+

Figure 128: HR-ESI-MS of non-dipolar, heteroleptic Fe(II)-bis(tpy) reference complex **126**.

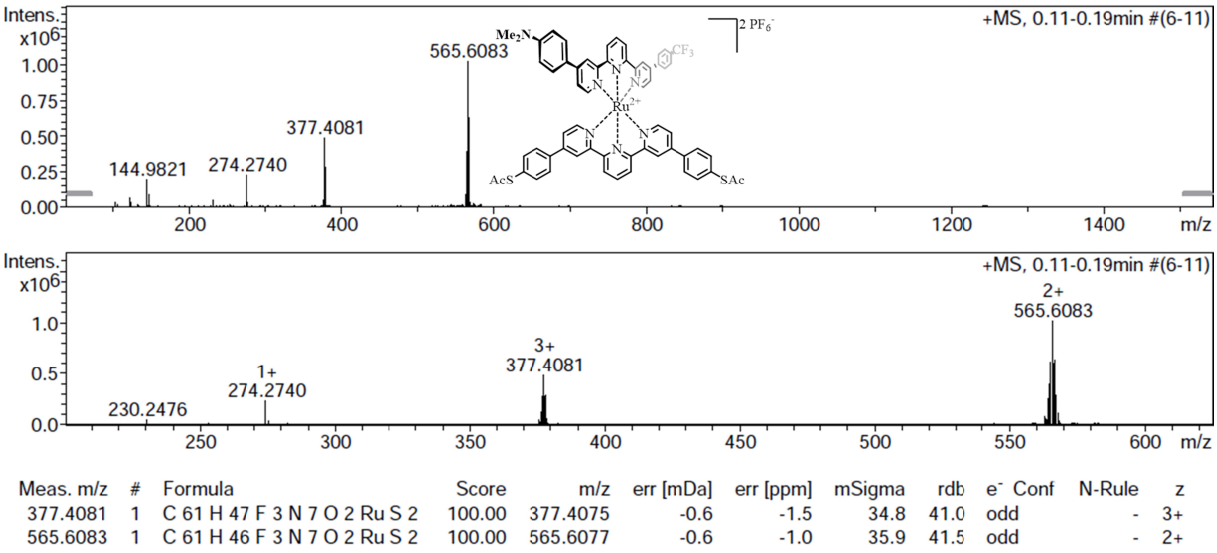

Meas. m/z	#	Formula	Score	m/z	err [mDa]	err [ppm]	mSigma	rdb	e⁻ Conf	N-Rule	z
377.4081	1	C 61 H 47 F 3 N 7 O 2 Ru S 2	100.00	377.4075	-0.6	-1.5	34.8	41.0	odd	-	3+
565.6083	1	C 61 H 46 F 3 N 7 O 2 Ru S 2	100.00	565.6077	-0.6	-1.0	35.9	41.5	odd	-	2+

Figure 129: HR-ESI-MS of dipolar, heteroleptic Ru(II)-bis(tpy) target complex **127**.

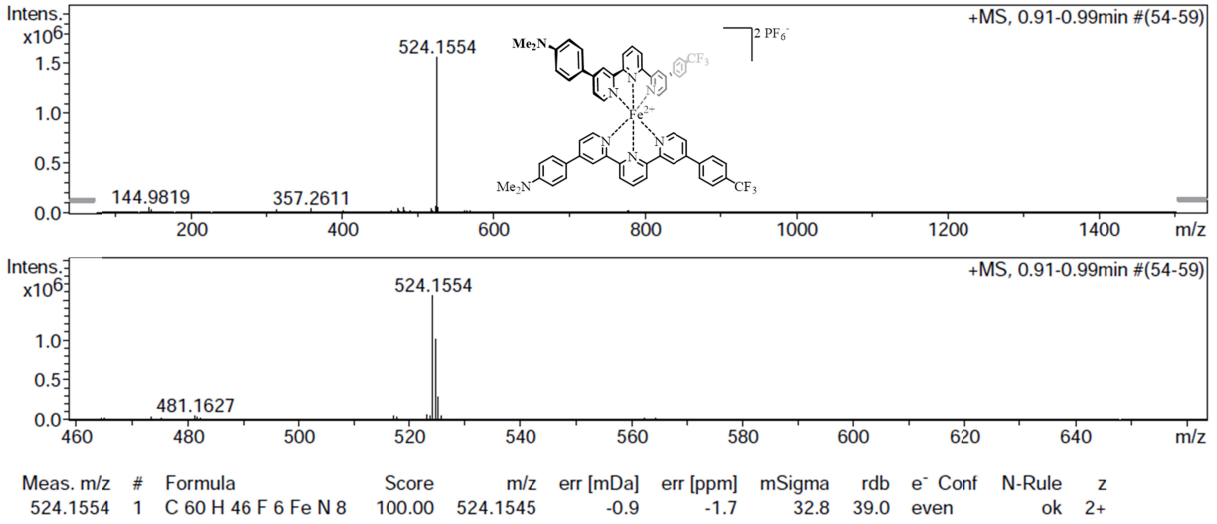

Meas. m/z	#	Formula	Score	m/z	err [mDa]	err [ppm]	mSigma	rdb	e⁻ Conf	N-Rule	z
524.1554	1	C 60 H 46 F 6 Fe N 8	100.00	524.1545	-0.9	-1.7	32.8	39.0	even	ok	2+

Figure 130: HR-ESI-MS of dipolar, homoleptic Fe(II)-bis(tpy) target complex **119**.

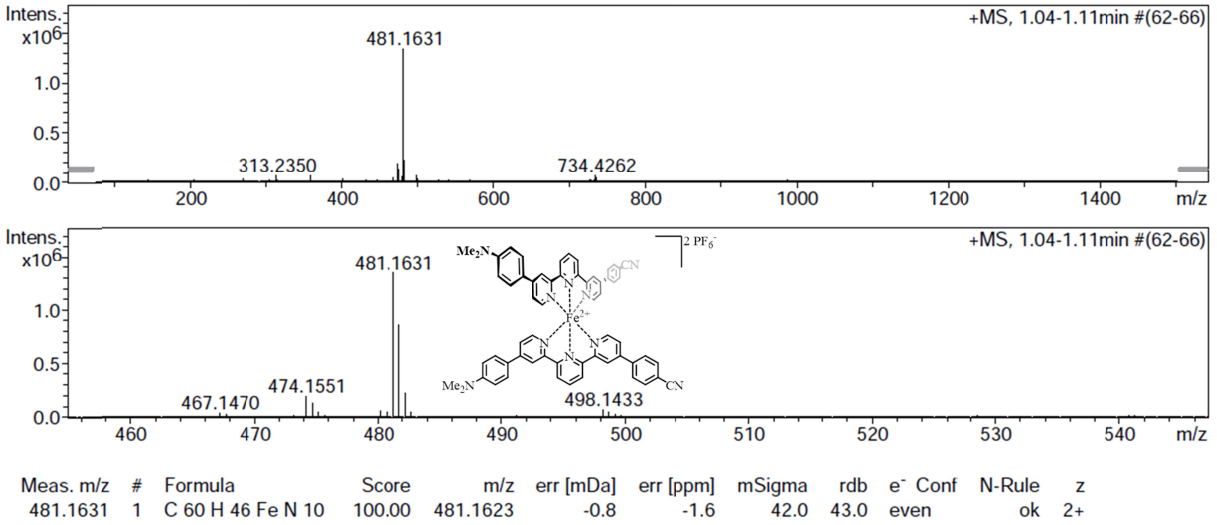

Meas. m/z	#	Formula	Score	m/z	err [mDa]	err [ppm]	mSigma	rdb	e⁻ Conf	N-Rule	z
481.1631	1	C 60 H 46 Fe N 10	100.00	481.1623	-0.8	-1.6	42.0	43.0	even	ok	2+

Figure 131: HR-ESI-MS of dipolar, homoleptic Fe(II)-bis(tpy) target complex **120**.

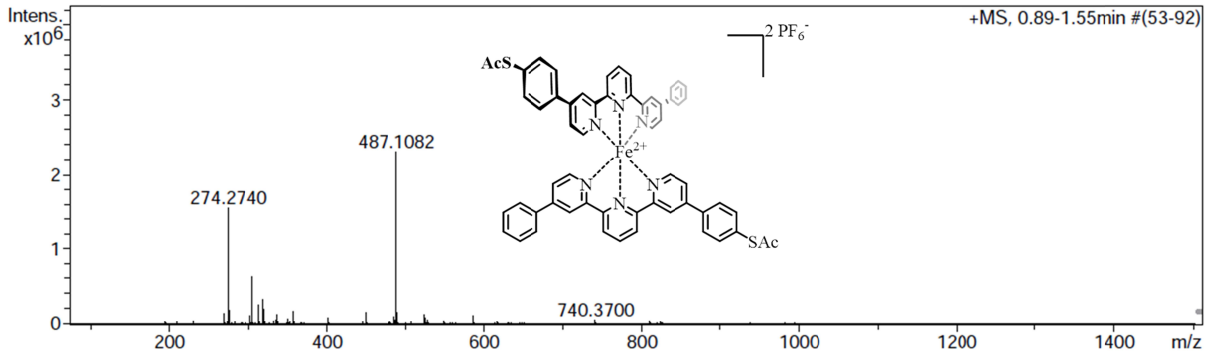

Meas. m/z	#	Formula	Score	m/z	err [mDa]	err [ppm]	mSigma	rdb	e⁻ Conf	N-Rule	z
487.1082	1	C 58 H 42 Fe N 6 O 2 S 2	100.00	487.1075	-0.6	-1.3	50.4	41.0	even	ok	2+

Figure 132: HR-ESI-MS of homoleptic Fe(II)-bis(tpy) target complex **208**.

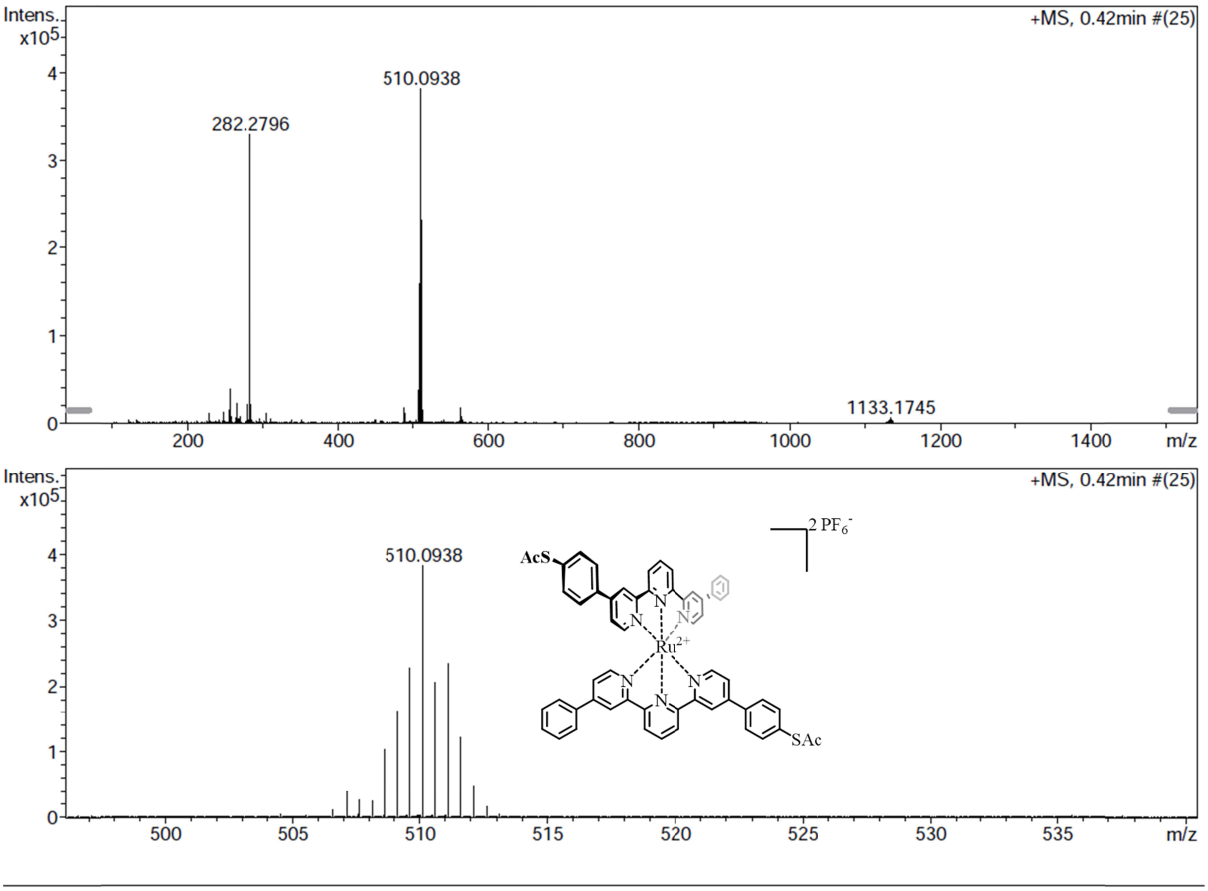

Meas. m/z	#	Formula	Score	m/z	err [mDa]	err [ppm]	mSigma	rdb	e⁻ Conf	N-Rule	z
510.0938	1	C 58 H 42 N 6 O 2 Ru S 2	100.00	510.0929	-1.0	-1.9	24.5	41.5	odd	-	2+

Figure 133: HR-ESI-MS of homoleptic Fe(II)-bis(tpy) target complex **209**.

9.2 Crystallographic Data

In this section at first the crystallographic data that are related to the x-ray structures, which have been discussed within the main text of this thesis, are depicted (Table 11 – 14). Subsequently those crystal structures, which have not been addressed in the main text, are displayed (Figure 134), followed by a listing of the corresponding crystallographic details thereafter, (Table 15).

Table 11: Comparison of the crystallographic data of the tpy ligands **47**, **168a**, **171**, and **131**.

Compound	47	168a	171	131
Formula	$C_{15}H_9Cl_2N_3$	$C_{29}H_{23}N_3S_2$	$C_{37}H_{43}N_3S_2\,Si_2$	$C_{31}H_{23}N_3O_2\,S_2$
Formula weight [g*mol^{-1}]	302.16	477.65	650.07	533.67
***T* [K]**	123	100	123	123
***λ* [Å]**	0.71073	0.71073	0.71073	0.71073
Crystal system	Orthorhombic	Monoclinic	Orthorhombic	Orthorhombic
Space group	$P2_12_12$	$P2_1$	$P2_12_12_1$	Pbcn
***a* [Å]**	3.8017(3)	5.2750(11)	5.8138(5)	9.647(2)
***b* [Å]**	19.9376(14)	16.552(3)	15.4607(13)	27.080(6)
***c* [Å]**	8.6668(6)	13.227(3)	39.588(3)	19.971(4)
***α* [°]**	90	90	90	90
***β* [°]**	90	94.04(3)	90	90
***γ* [°]**	90	90	90	90
***V* [Å^3]**	656.92(8)	1152.0(4)	3558.3(5)	5217.2(20)
Z	2	2	4	8
***D$_{calcd}$* [g*cm^{-3}]**	1.528	1.377	1.213	1.359
F(000)	308	500	1384	2224
***μ* [mm^{-1}]**	0.485	0.255	0.247	0.239
***θ* range [°]**	2.350 – 35.650	1.974 – 25.027	1.671 – 28.404	1.817 – 27.485
Reflns measured	2978	3745	8752	5991
Reflns used	2352	3402	4052	5972
Parameters	95	308	444	349
R1	0.0278	0.0872	0.0883	0.1120
wR2	0.0389	0.0883	0.1184	0.2995
Goodness of fit on F^2	1.0249	0.9486	1.0887	0.8315

Table 12: Comparison of the crystallographic data of the tpy ligands **47**, **177**, and **178**.

Compound	47	177	178
Formula	$C_{15}H_9Cl_2N_3$	$C_{23}H_{19}ClN_4$	$C_{31}H_{29}N_5$
Formula weight [g*mol^{-1}]	302.16	386.88	471.60
***T* [K]**	123	100	123
λ [Å]	0.71073	0.71073	0.71073
Crystal system	Orthorhombic	Monoclinic	triclinic
Space group	$P2_12_12$	$P2_1$	P-1
***a* [Å]**	3.8017(3)	11.368(2)	9.6044(7)
***b* [Å]**	19.9376(14)	6.0090(12)	19.3428(19)
***c* [Å]**	8.6668(6)	27.582(6)	25.868(2)
α [°]	90	90	90
β [°]	90	92.35(3)	90
γ [°]	90	90	75.770(6)
***V* [Å^3]**	656.92(8)	1882.5(7)	4658.2(7)
Z	2	4	8
D_{calcd} [g*cm^{-3}]	1.528	1.365	1.345
F(000)	308	808	2000
μ [mm^{-1}]	0.485	0.219	0.630
θ range [°]	2.350 – 35.650	0.739 – 25.025	8.569 – 68.535
Reflns measured	2978	6172	14134
Reflns used	2352	5210	4994
Parameters	95	506	1297
R1	0.0278	0.0605	0.1592
wR2	0.0389	0.0784	0.2636
Goodness of fit on F^2	1.0249	1.0415	1.1071

Table 13: Comparison of the crystallographic data of the tpy ligands **147** and **183**.

Compound	147*	183
Formula	$C_{30.25}F_3N_{3.5}$*	$C_{30}H_{23}N_5$
Formula weight [g*mol^{-1}]	469.35*	453.55
***T* [K]**	293	100
***λ* [Å]**	0.71073	1.54178
Crystal system	Monoclinic	Monoclinic
Space group	$P2_1/C$	$P2_1/n$
***a* [Å]**	16.5663(5)	9.6648(4)
***b* [Å]**	27.0908(9)	18.5307(8)
***c* [Å]**	22.1942(7)	26.4344(10)
***α* [°]**	90	90
***β* [°]**	108.214(2)	98.679(3)
***γ* [°]**	90	90
***V* [Å^3]**	9461.6(5)	4680.1(3)
Z	16	8
***D$_{calcd}$* [g*cm^{-3}]**	1.318	1.287
F(000)	3728	1904
***μ* [mm^{-1}]**	0.097	0.611
***θ* range [°]**	1.787 – 25.027	2.923 – 66.593
Reflns measured	16684	8133
Reflns used	7492	8094
Parameters	589	631
R1	0.2618	0.0582
wR2	0.2852	0.1969
Goodness of fit on F^2	0.3698*	0.9968

*The crystals obtained for compound **147** are of very poor quality and therefore the acquired crystallographic data have to be treated as preliminary results, although nevertheless xthe structure can be classified as confirmed.

Table 14: Comparison of the crystallographic data of the homoleptic Fe(II)-bis(tpy) complexes **189**, **191**, and **193**

Compound	189	191	193
Formula	$C_{30}H_{18}Cl_4F_{12}Fe_1N_6P_2$	$C_{413}H_{357}F_{72}Fe_6N_{45}P_{12}S_{24}$	$C_{66}H_{62}F_{12}Fe_1N_6O_4P_2$
Formula weight [g*mol^{-1}]	950.09	8794.90	1349.03
***T* [K]**	123	123	123
***λ* [Å]**	0.71073	0.71073	1.54178
Crystal system	Tetragonal	Monoclinic	monoclinic
Space group	P-42$_1$c	C 2/c	P2$_1$/c
***a* [Å]**	9.8570(7)	53.859(2)	12.0575(5)
***b* [Å]**	9.8570(7)	23.7430(8)	21.9097(8)
***c* [Å]**	18.7609(16)	40.4577(17)	23.8830(9)
***α* [°]**	90	90	90
***β* [°]**	90	127.658(3)	94.131(2)
***γ* [°]**	90	90	90
***V* [Å^3]**	1822.8(2)	40958(3)	6292.9(4)
Z	2	4	4
***D$_{calcd}$* [g*cm^{-3}]**	1.731	1.426	1.424
F(000)	944	18072	2784
***μ* [mm^{-1}]**	0.890	0.471	3.176
***θ* range [°]**	2.923 – 30.057	1.442 – 28.290	2.740 – 68.218
Reflns measured	2677	50747	11397
Reflns used	1333	50590	10865
Parameters	128	2611	820
R1	0.0527	0.0923	0.0351
wR2	0.1006	0.2742	0.0393
Goodness of fit on F^2	1.1944	1.2254	1.1000

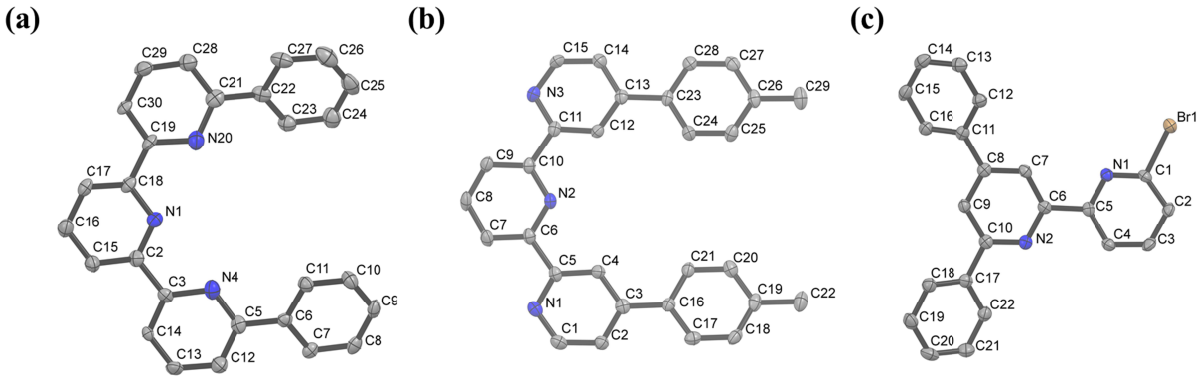

Figure 134: (a+b) ORTEP plots of the solid state structures of the two symmetric, non-dipolar tpy ligands **172**, and **225b**. **(c)** ORTEP plot of the solid state structure of bpy core precursor **232**. For all displayed structures the ellipsoids are plotted at 50% probability level and the hydrogen atoms were omitted for clarity reasons.

Table 15: Comparison of the crystallographic data of the ligands **172** and **225b**, and of the bpy derivative **232**.

Compound	172	225b	232
Formula	$C_{108}H_{76}N_{12}$	$C_{29}H_{23}N_3$	$C_{22}H_{15}1BrN_2$
Formula weight [g*mol^{-1}]	1541.87	413.52	387.28
***T* [K]**	123	123	123
***λ* [Å]**	1.54178	1.54178	01.54178
Crystal system	Monoclinic	Monoclinic	Monoclinic
Space group	Cc	$P2_1/c$	$P2_1/c$
***a* [Å]**	25.0456(18)	25.0650(9)	11.8991(10)
***b* [Å]**	9.9814(7)	11.5028(4)	20.6106(18)
***c* [Å]**	31.960(2)	15.4368(5)	13.9109(13)
***α* [°]**	90	90	90
***β* [°]**	101.638(5)	107.770(2)	90.832(6)
***γ* [°]**	90	90	90
***V* [Å^3]**	7825.5(5)	4238.4(3)	3411.3(5)
Z	4	8	8
***D*$_{calcd}$ [g*cm^{-3}]**	1.309	1.296	1.508
F(000)	3232	1744	1568
***μ* [mm^{-1}]**	0.605	0.593	3.315
***θ* range [°]**	3.603 – 66.891	1.851 – 69.579	3.715 – 68.278
Reflns measured	11333	7735	6097
Reflns used	11270	563.6	5227
Parameters	1081	577	451
R1	0.0719	0.0560	0.0438
wR2	0.2515	0.0969	0.0692
Goodness of fit on F^2	0.9926	1.1066	1.0720

9.3 Contributions

The mechanically controllable break junction measurements have been performed by Riccardo Frisenda in the group of Prof. Dr. Herre van der Zant at the Technical University of Delft.

All described STM measurements have been performed by Thomas Knaak at the Christian-Albrechts-Universität zu Kiel.

The X-ray crystallographic measurements have been performed by Dr. Markus Neuburger or by Dr. Alessandro Prescimone at the University of Basel.

All EI, FAB, and HR-ESI-TOF mass spectra were recorded by Dr. Heinz Nadig at the University of Basel.

Elemental analyses were measured either by Werner Kirsch or Sylvie Mittelheisser at the University of Basel.

The ^{1}H-NMR studies for the isomerization studies of the metalloazobenzenophanes and the more sophisticated 2D-NMR measurements have been performed by PD Dr. Daniel Häussinger, Heiko Gsellinger, or Kaspar Zimmermann.